Technical Report
TR-16-12
May 2017

Retrieval and post-test examination of packages 4 and 5 of the MiniCan field experiment

Andrew Gordon
Lena Sjögren
Claes Taxén
Adam Johannes Johansson

SVENSK KÄRNBRÄNSLEHANTERING AB

SWEDISH NUCLEAR FUEL
AND WASTE MANAGEMENT CO

Box 3091, SE-169 03 Solna
Phone +46 8 459 84 00
skb.se

SVENSK KÄRNBRÄNSLEHANTERING

ISSN 1404-0344
SKB TR-16-12
ID 1555086
May 2017

Retrieval and post-test examination of packages 4 and 5 of the MiniCan field experiment

Andrew Gordon, Lena Sjögren, Claes Taxén
Swerea KIMAB

Adam Johannes Johansson, Svensk Kärnbränslehantering AB

Abstract

MiniCan is an *in situ* or field test of certain aspects of corrosion in the KBS-3 concept for deep geological disposal of spent nuclear fuel in bentonite embedded copper-cast iron canisters. The experiment is performed by the Swedish Nuclear Fuel and Waste Management Company (SKB) at a depth of circa 450 m in the Äspö Hard Rock Laboratory (HRL). The experiment was started in late 2006 and consisted of five experimental packages. The packages differ in several design aspects, but most importantly regarding the presence and target density of the bentonite clay surrounding the copper-cast iron canisters. This report covers the retrieval and examination of two packages, MiniCan 4 embedded in high density bentonite with a target density of 2 000 kg/cm^3 and MiniCan 5 with no bentonite present.

The MiniCan packages 4 and 5 were retrieved during September and October 2015 and samples were taken inside an inert gas glovebox at the Äspö HRL, before being packed into sealed, nitrogen filled, sample holders and taken to Swerea KIMAB's laboratories in Kista, Sweden for spectroscopic and microscopic analyses.

The main conclusion from the examination is that the corrosion in the MiniCan 5 experiment was more extensive than in MiniCan 4, as evidenced from the iron electrodes, sandwich specimens and the copper and iron mass loss samples. The effect of having compact bentonite clay surrounding the samples seems to have been to limit corrosion on all components except for the cast iron insert near the machined defect through the copper canister. This suggests that the high density bentonite has the effect of restricting microbiologically influenced corrosion (MIC), however, the reduced mass flow may also have had an influence.

The bentonite present in MiniCan 4 made it difficult to analyse the surfaces of the samples, with many analysis techniques detecting the bentonite clay that remained after sampling. The samples from MiniCan 4 appeared visually intact and relatively unaffected by corrosion compared to those from MiniCan 5. The exceptions to this were the iron mass loss sample, iron electrodes and the sample taken from the cast iron insert near the ∅ 1 mm defect in the copper canister, which had corroded, albeit less than those from MiniCan 5.

Extensive iron corrosion was detected on the sandwich specimen and iron electrodes of MiniCan 5 as well as on the iron insert around the holes in the copper shell of both MiniCan 4 and 5. The detection of sulphate reducing bacteria (SRB), iron sulphide and the morphology of the corrosion damage on the sandwich specimen of MiniCan 5 suggests microbiologically influenced corrosion (MIC) may have occurred. Galvanic effects have also possibly accelerated the corrosion of the iron component of the sandwich specimens from MiniCan 5 as well as the iron insert samples taken from near the holes in the copper shell of both MiniCan 4 and 5. The large difference in iron corrosion rate between Minican 4 and 5 however indicates microbiologically influenced corrosion as having a major role.

It was attempted to preserve the surface deposits from the exposure conditions to analysis in the laboratory, by performing the sampling in an inert atmosphere and sealing the samples in nitrogen filled transparent sample holders. This technique appears to have worked, and Raman analysis was carried out on the samples whilst they were preserved without air-exposure. Subsequent analyses carried out on the samples after the sample holders were opened to the atmosphere suggest that the surface deposits altered, and more oxides of copper and iron, as well as sulphates instead of sulphides were detected.

A wide array of elements were detected in the SEM/EDS analyses of the surfaces, and these reflect the chemistry of the materials of construction as well as the groundwater chemistry and the bentonite clay (in the case of MiniCan 4). The main corrosion products found were cuprite and sulphide (iron or mixed iron and copper sulphides) on copper surfaces, sulphides and magnetite on iron, as well as green rust or iron(II) chloride on the outer surfaces of the cast iron insert.

The stress corrosion cracking (SCC) specimens exposed in MiniCan 4 were subjected to microscopy and metallographic examination to investigate their condition after exposure. The U-bend specimens did not appear damaged by the exposure, but did include some defects in the form of porosity in the bulk material. The wedge open loaded (WOL) specimens were examined with SEM and no signs of crack propagation from the original pre-crack were found, albeit smaller cracks were found emanating perpendicular from the original pre-crack.

Sammanfattning

MiniCan är ett så kallat *in situ*- eller fältförsök, avsett att belysa vissa aspekter av korrosion i KBS-3 konceptet för geologisk djupförvaring av använt kärnbränsle, i vilket kopparkapslar med en segjärnsinsats omgärdas av bentonitlera. Experimentet utförs av Svensk Kärnbränslehantering AB (SKB) i Äspölaboratoriet på ett djup av ca 450 m. Experimentet startades i slutet av 2006 och bestod från början av fem försökspaket. Dessa skiljer sig åt i flera avseenden men framför allt när det gäller närvaron och densiteten hos den bentonitlera som omger miniatyrkapslarna av koppar och segjärn. Denna rapport redovisar återtag och analyser av två försökspaket; MiniCan 4, där kapseln var inbäddad i bentonitlera av hög densitet (måldensitet 2 000 kg/cm^3) och MiniCan 5 som saknade bentonitlera.

Försökspaketen MiniCan 4 och 5 återtogs under september och oktober 2015 och provtagning utfördes inuti en handskbox med inert gas (kvävgas) vid Äspölabroratoriet innan de packades i förseglade kvävefyllda provhållare och skickades till Swerea KIMABs laboratorier i Kista för spektroskopiska och mikroskopiska analyser.

Den viktigaste slutsatsen från undersökningen är att korrosionen i MiniCan 5 var mer omfattande än i MiniCan 4, vilket framgår av järnelektroder, sandwichkomponeneter av koppar och järn, samt massförlustprover av koppar eller järn. Närvaron av kompakt bentonitlera som omger proverna verkar ha begränsat korrosionen av alla komponenter med undantag för gjutjärnsinsatsen innanför hålet genom kopparkapseln. Detta indikerar att bentonitlera med hög densitet kan begränsa mikrobiologiskt influerad korrosion (MIC), men även det reducerade vattenflödet kan ha bidragit till att begränsa korrosionen.

Den bentonit som finns i MiniCan 4 gjorde det svårt att analysera provernas ytor, flera analystekniker detekterade bara bentonit. Proverna från MiniCan 4 hade vid visuell inspektion behållit sin form och storlek och verkade relativt opåverkade av korrosion jämfört med motsvarande prover från MiniCan 5. Undantagen var massförlustproverna av järn, järnelektroderna och segjärnssatsen nära det millimeterstora hålet i kopparkapseln som hade korroderat, om än mindre än motsvarande prover i MiniCan 5.

Omfattande järnkorrosion observerades på sandwichprover och järnelektroder i MiniCan 5, samt på järninsatsen runt hålet i kopparkapseln i både MiniCan 4 och 5. Detektionen av sulfatreducerande bakterier (SRB), utfälld järnsulfid, samt korrosionsmorfologin på sandwichprovet i MiniCan 5 indikerar att mikrobiologiskt influerad korrosion (MIC) kan ha skett. Galvaniska effekter har möjligen påskyndat korrosionen av järnkomponenten i sandwichproverna från MiniCan 5 liksom de järninsatsprover som tagits från nära hålen i kopparkapseln på både MiniCan 4 och 5. Den stora skillnaden i korrosionshastighet mellan Minican 4 och 5 tyder på att mikrobiell aktivitet kan ha spelat en viktig roll.

Stor vikt lades vid att bevara de ytbeläggningar och korrosionsprodukter som bildats under exponeringsförhållandena i Äspölaboratoriet fram till dess att provernas ytor kunde analyseras i laboratorium. Detta gjordes genom att utföra provtagningen i en inert atmosfär och försegla proverna i kvävefyllda transparenta provhållare. Denna teknik verkar ha fungerat väl och Ramanspektroskopi kunde utföras på proven innan dessa exponerades för luft. Andra analyser som utfördes på proverna efter det att provhållarna öppnades för atmosfären tyder på att ytornas kemiska sammansättning förändrades, och mer oxider av koppar och järn, samt sulfater i stället för sulfider, detekterades.

Ett stort antal grundämnen detekterades i SEM/EDS-analyser av ytorna, vilket speglar såväl konstruktionsmaterialens sammansättning, som grundvattenkemin och närvaron av bentonitlera (i MiniCan 4). De huvudsakliga korrosionsprodukterna på koppar var kuprit och sulfid (koppar- och/eller järnsulfider). På järnkomponenternas ytor detekterades sulfider och magnetit, samt grön rost eller järn(II)klorid på segjärninsatsen.

De spänningskorrosionsprover som fanns i MiniCan 4 analyserades med metallografiska metoder. U-böjproverna verkade inte skadade av exponeringen, men innehöll defekter i form av porositet i bulkmaterialet. De förspräckta proverna (sk wedge open loaded, WOL) undersöktes med svepelektronmikroskopi (SEM) och uppvisade inga tecken på att den ursprungliga sprickan vuxit under exponeringen. Däremot observerades ett antal mindre sprickor omkring den ursprungliga sprickan.

Contents

1 Introduction

MiniCan is an *in situ* or field test of certain aspects of corrosion in the KBS-3 concept for deep geological disposal of spent nuclear fuel in bentonite embedded copper-cast iron canisters. The experiment is being performed by the Swedish Nuclear Fuel and Waste Management Company (SKB) at a depth of circa 450 m in the Äspö HRL. The experiment was started in late 2006 and consisted of five experimental packages from the beginning. The packages differ in several design aspects, but most importantly regarding the presence and target density of the bentonite clay surrounding the copper-cast iron canisters. In the MiniCan experiments, the copper-cast iron canisters are mounted inside a stainless steel cage, which holds the bentonite clay in place in the water-filled bore holes. This is in contrast to the design of the KBS-3 repository, in which the copper-cast iron canisters are fixed in the boreholes by bentonite clay filling the space between canister and rock.

In packages 1–3 the canister was surrounded by low density clay made from pellets, however, a steel filter was present between the canister and the clay, so that the clay was not in direct contact with the canister. In package 4 the canister was embedded in high density clay made from prefabricated blocks in direct contact with the copper surface, thus restricting water flow to the surface of the canister and associated samples. In package 5, there was no clay present in the experiment, meaning that the canister and samples were directly exposed to the ground water in the bore hole. On top of the copper-cast iron canister, inside the steel cage, various electrodes and coupons were installed on a nylon rack. In all packages, the copper canister has one or two holes (1 mm in diameter) to mimic defects in the copper shell. Due to a change of the welding technique, this aspect is no longer regarded as being of great importance in the safety assessment of the KBS-3 concept, but nevertheless it remains an important design feature of the MiniCan experiment since the contact with ground water allows corrosion of the cast iron insert. Further details of the design of the MiniCan experiment are given in Smart and Rance (2009) and shall not be discussed in more detail here.

The first package in the MiniCan series to be retrieved was package 3. This was done in 2011 and the results of the post-test examination are presented in Smart et al. (2012, 2013), Hallbeck et al. (2011) and Aggarwal et al. (2015). During analysis it appeared that microbial activity had influenced the corrosion of cast iron components in this particular package with low density bentonite.

In order to better understand the observations in package 3 and the corrosion in the MiniCan series in general, it was decided to retrieve packages 4 and 5, since these differ from package 3 in certain interesting aspects as mentioned above. Water analyses and on-line potential measurements in the MiniCan series have been reported elsewhere (Smart et al. 2011, 2015). The retrieval of MiniCan packages 4 and 5 took place in September and October 2015. Immediately after retrieval, samples for spectroscopic and microscopic examination were prepared at the Äspö HRL before being transferred to Swerea KIMAB's laboratories in Stockholm. Spectroscopic analyses of corrosion products, metallographic examination of metal surfaces and evaluation of corrosion rates by mass loss are detailed in this report. Results from microbiological analysis of water and clay, and microbial sampling of various surfaces in the experiments, are presented in a separate report (Hallbeck et al. 2017).

2 Retrieval of MiniCan 4 and 5

The decision to start with the retrieval of MiniCan 5 was based upon the assumption that MiniCan 4 could cause more problems during disassembly due to the presence of the high density bentonite, in which the copper canister was embedded. The bentonite was anticipated to have swelled due to uptake of groundwater and would therefore have made a tight seal between the copper canister and the stainless steel cage, making it difficult to remove the copper canister. MiniCan 5 had no bentonite clay present in the experiment, so withdrawal of the copper canister would be relatively simple by comparison and provide valuable experience as to the best way to handle and prepare the samples.

2.1 MiniCan 5 retrieval and sampling

28th September–2nd October 2015

Personnel from Swerea KIMAB travelled to Äspö HRL on the 28th September 2015 where work was already underway to remove MiniCan 5 from its borehole by SKB personnel. As with MiniCan 3 that was retrieved in 2011 (Smart et al. 2012), the MiniCan assembly was removed directly into a water-filled container which was flanged onto the borehole opening. The water in the container was ground water taken from a nearby source and purged with nitrogen from early morning. This was in order to maintain a low oxygen environment around the experimental materials. Images of the retrieval can be seen in Figure 2-1.

Once the experimental package contained by the stainless steel cage was withdrawn from the borehole it was placed in a stainless steel transfer flask which had been submerged in the transfer tank and purged with nitrogen.

Figure 2-1. *a) top-left: water-filler container connected to borehole; b) top-right: SKB personnel removing the MiniCan assembly; c) bottom-left: the MiniCan assembly remained under water at all times during removal; d) bottom-right: a sealed transfer flask was used to keep the MiniCan assembly oxygen-free until it was placed inside the glovebox.*

The transfer flask was then transported to the surface part of the Äspö HRL and placed inside an inert-gas glovebox, along with all necessary equipment and materials for dismantling and sample preparation. The glovebox was then sealed and purged with nitrogen gas. When the oxygen concentration inside the glovebox reached 50 ppm a copper-oxide reactor was used to remove the remaining oxygen more efficiently down to 0.1 ppm. This was achieved the morning after the retrieval on the 29th of September.

The transfer flask was opened and the MiniCan assembly was removed with the use of the in-built crane in the glovebox by attaching a lifting eye to the stainless steel cage. At this point, staff from Microbial Analytics AB (Micans) took microbiological samples from the outside of the stainless steel cage. The cage was then lowered and the lid was removed. The nylon rack which housed several coupons, electrodes, and other samples was removed and placed in a container with ground water. All cables from the electrodes were then identified and the potentials of the electrodes and coupons were measured against a Ag/AgCl reference electrode. The cables to electrodes and coupons were then cut and the items transferred to the attached smaller glovebox for packaging.

Inside the smaller glovebox, the electrodes, coupons and other loose test specimens were placed in their respective sample holders which were sealed. The design of the sample holders can be seen in Appendix 1 Sample holders. The sample holders consisted of a PMMA (poly methyl methacrylate, also known as acrylic glass) box which then had a microscope glass lid fastened in place using epoxy-based adhesive. The O_2 permeability of the sample holders was considered during the planning phase of the project and after submerging the design in water for several days with no signs of leakage it was deemed acceptable for this work.

The copper canister was then lifted out of the steel cage, again using the in-built crane in the glovebox, see Figure 2-2. Green deposits on the inside of the stainless steel cage were sampled, transferred to the small glove box and packaged in a sample holder. The diameter of the canister was measured at three locations using a calliper. Thereafter the canister was placed by a circle saw, installed in the glove-box, ready to be sectioned into samples. The location of one of the holes in the canister was identified and marked before cutting of the canister began but the second hole was missed and subsequently cut through when sectioning the copper canister. Groundwater was used to cool the material during cut-ting. The copper canister and its iron insert were sectioned as shown in Section 2.3 and in Appendix 2 Sample preparation. The samples of canister that were to be analysed for hydrogen content were cut first and removed from the glovebox via the sluice gate and placed in liquid nitrogen. All subsequent samples were then cut from the canister and cast iron insert, and moved over to the smaller glovebox to be placed in their sample holders.

Figure 2-2. *MiniCan 5 being lifted out of the stainless steel cage. The black deposit on the right hand side in the photograph was the bottom of the MiniCan, positioned downwards in the borehole.*

It was intended to also take samples from the stainless steel cage, but due to the (lack of) strength of the circle saw, unsuitable vice attachment and lack of suitable saw blades it was not possible to perform this task inside the glovebox. The steel cage was kept in the glovebox until it was opened, and transferred to Swerea KIMAB in one piece.

All samples transferred to the small glovebox were sealed in their sample holders, reserve samples taken were packaged in plastic clad aluminium foil bags; the bags were heat sealed inside the glovebox.

The sawing produced a lot of metal dust and the glovebox was intermittently cleaned internally using the in-built vacuum cleaner. It was noticed that metal chips from the cutting operations were collected in and around the gloves. The chips were (partly) removed by shaking and by using the vacuum cleaner (with an extension) and special care was then taken when using the gloves. It was noted that the iron chips/swarf did not rust although some of them were wet or even lying in droplets of ground water on the bench inside the glove box. This observation implied that there were no leaks in the gloves, which could have led to oxygen concentrations above the set limits inside the large glovebox.

The oxygen concentration was measured in the smaller glovebox, and found to be low throughout the sampling. Conditions in the large glovebox were damp during and after sawing operations. Due to the damp conditions, or perhaps due to the presence of metal dust/particles, the oxygen sensor in the large box did not function properly during most of the time after sawing. In order to reduce humidity and to ensure low oxygen levels, the large glovebox was intermittently purged with nitrogen. Also, three extra fans were placed inside the box to ensure circulation, which makes the purging and reduction of the oxygen level more efficient. It was concluded that the oxygen level was low enough throughout the sampling operations because of lack of red rust observed on the iron chips from sawing the cast iron insert. As soon as the glove-box was turned off and opened, the iron chips turned rust-red within an hour.

2.2 MiniCan 4 sampling

26–28th October 2015

The MiniCan assembly was withdrawn from its borehole on October 26th, placed in the transport flask and moved to the surface part of the Äspö HRL where it was placed inside the glovebox. All required tools and consumables had previously been placed inside the glovebox. To prevent the collection of metal chips from the cutting operations in and around the gloves, adhesive tape was applied around the rim of all gloves inside the box. The glovebox was then sealed, purged of air and filled with nitrogen.

In preparation for the sectioning of the canister and iron insert, the circle saw had been heavily modified between the MiniCan 5 and MiniCan 4 sampling. The vice attachment was re-designed to accommodate both the larger stainless steel cage and the smaller copper canister and iron insert components. Furthermore a new saw had been installed on the plinth, beside the original saw, see Figure 2-3.

Figure 2-3. *The modified circle saw assembly, with two saws installed on the customised base.*

The transfer flask was opened and the SCC specimens (U-bend and WOL samples) were removed, transferred to the smaller glove box and placed in their samples holders. Potential measurements were performed between each cable protruding from the copper canister (two bundles of cables, each cable identified by a number and its colour) and a reference electrode placed in the ground water in the transfer flask. The cage was then lifted out of the transfer flask and microbiological samples were taken from the outside of the cage.

The lid was removed from the cage and it was clear that the bentonite had swelled due to contact with the ground water as was expected, see Figure 2-4. The densities measured were a bit lower than the target density of 2.000 g/cm^3, meaning that slight expansion has occurred. This made it very difficult to remove the copper canister from the stainless steel cage due to the friction between the canister, bentonite and the cage. Firstly, a drill was used to drill out some of the bentonite with care not to disrupt the canister. Then the cage was turned upside down and the bottom removed. Microbiological samples were taken from the bentonite at this point, before the drilling procedure was repeated. The cage was then turned the right way up again and an attempt was made to pull the canister out, but without success.

The decision was taken to cut through the stainless steel cage at a point above the top edge of the copper canister, taking care to only cut through the stainless steel cage. There were some difficulties with this task as the electrical fuse for the glovebox tripped which required the help of an electrician which caused some delay in the dismantling procedure. As during the MiniCan 5 sampling, whilst carrying out the cutting operation the oxygen level in the larger glove box could not be controlled after starting of the saw, probably due to the damp conditions or from the presence of metal dust near the sensor. Therefore control of the larger chamber was turned off and it was intermittently re-purged with nitrogen. Just as during the previous dismantling of MiniCan 5, it was noted that the iron swarf and particles lying on the bench and floor of the box did not undergo rusting, despite the wet conditions. This was taken as an indicator of low oxygen conditions.

After cutting through the stainless steel and removing the top ring of the steel cage, the bentonite was removed by hand from the area above the canister and further microbiological samples were taken from this area. Plastic hand tools and ground water were used to remove coupons, electrodes and other samples from the surrounding bentonite clay. The samples were gently washed with groundwater in order to remove the bentonite whilst avoiding removing any surface film. After this the samples were moved to the smaller chamber of the glove-box and placed in their samples holders.

Figure 2-4. *The high-density bentonite as seen upon opening the MiniCan 4 assembly.*

After removing the bentonite from the top of the canister, a drill was used to remove as much bentonite as possible that remained between the canister and the cage, see Figure 2-5. The bentonite clay filling the space between the copper-cast iron canister and the stainless steel cage was sampled at several points for the purposes of microbial analyses, evaluation of the clay density, and chemical characterisation. Samples for microbial analysis were taken by staff from Micans. Samples for determination of clay density and water ratio were taken by SKB personnel and the analyses were made immediately at the Bentonite Laboratory at Äspö. Samples of bentonite for chemical characterization were taken by Swerea KIMAB and placed in plastic sample holders.

The remaining cage/canister assembly was then lifted back into the transfer flask which still contained ground water. The cage/canister assembly was lifted up and down repeatedly to wet the clay in the ground water and a hand tool was used to gently knock the cage downwards releasing the copper canister. A chisel was then used to remove as much as possible of the bentonite from the outside of the canister, see Figure 2-6. The remaining bentonite was now relatively easy to remove and came off in lumps/flakes as shown in Figure 2-6. Density samples were again taken from the bentonite. In total, the bentonite clay was sampled at ten positions around and along the copper canister. The measured wet densities were between 1.902 and 1.959 g/cm^3 with a mean value of 1.931 g/cm^3. The water ratio for the same samples varied between 0.30 and 0.37.

The location of the hole in the canister was identified and marked before cutting of the canister and iron insert began. Groundwater was used to cool the material during cutting, primarily whilst taking samples for hydrogen analyses. As with MiniCan 5 the hydrogen content samples were removed first and placed directly in liquid nitrogen. The remaining samples were sectioned as shown in Section 2.3 and in Appendix 2 Sample preparation.

All samples were gently washed using groundwater, left to dry for a short period and then moved to the smaller chamber to be placed in their respective sample holders. While this was being done, the larger box was purged with air to prepare it for opening and cleaning. Due to the malfunction of the oxygen sensor in the larger box, the safety lock would not allow opening of the door to the box, which made cleaning very difficult and time consuming. Some cleaning could be made through the holes for the gloves, which had been removed when an oxygen level of 20 per cent was confirmed by an external device. During the time between air purging and cleaning, it was noticed that remaining iron chips quickly rusted (i.e. became red). Eventually, the safety lock was removed (luckily screwed to the outside of the glove box) and the door could be opened. The smaller glovebox, in which all samples from MiniCan 4 and 5 were kept in air tight sample holders, was left in operation with an oxygen level of maximum a few ppm, as verified daily by SKB staff at Äspö HRL.

Figure 2-5. *The stainless steel cage was cut open and the bentonite was removed as much as possible by use of hand tools.*

Figure 2-6. *Removal of the final layers of bentonite surrounding MiniCan 4.*

2.3 Sectioning of samples

Samples from the copper canister were cut according to Figure 2-7. A detailed description of how the copper canister and its iron insert were sectioned can be seen in Appendix 2 Sample preparation.

2.4 Sample overview

The term “sample” refers to all metal objects positioned outside of the canister, parts of the copper canister and of the cast iron insert as well as water samples and bentonite samples. All samples were provided with identity numbers according to Table 2-1.

Samples that were positioned outside of the copper MiniCan canister (see Figure 2-8) are termed as *external* samples in this report. These were the copper and iron electrodes, the copper and iron mass loss samples, the copper iron sandwich specimen, the platinised titanium counter electrode, the gold and platinum electrodes, and the silver electrodes. The external samples are given in the white fields of Table 2-1. Parts of the copper canister shell and the iron insert are found in the blue fields of Table 2-1 while other sample types are given in the grey fields of the table.

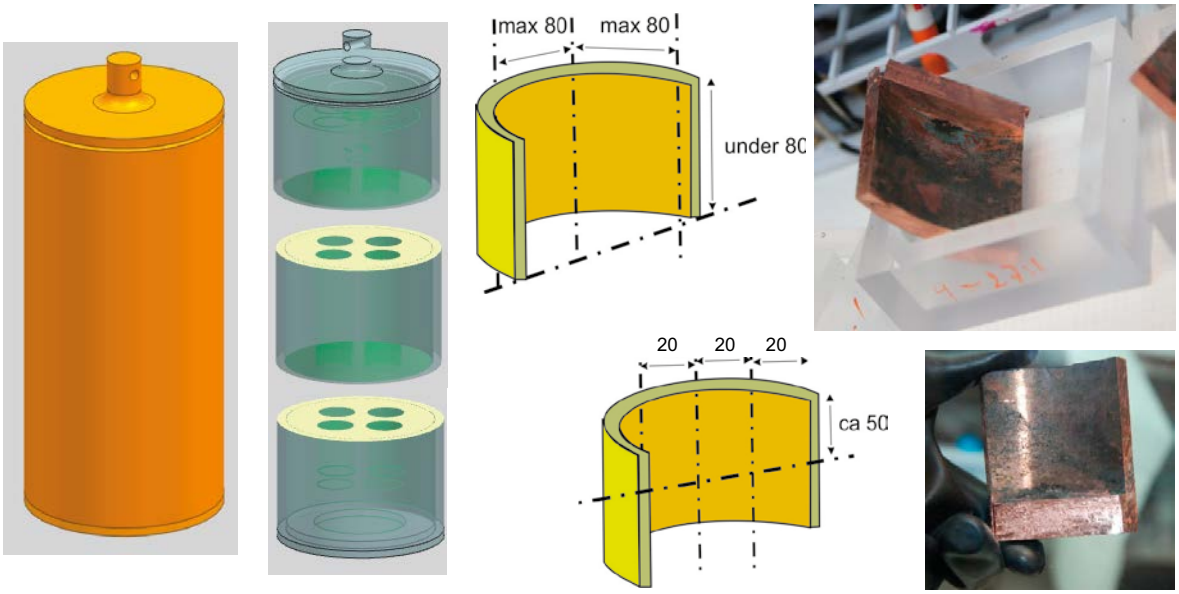

Figure 2-7. *Principal cutting scheme for copper samples.*

Figure 2-8. *Removal of the "external" samples from inside the MiniCan 5 assembly.*

Table 2-1. MiniCan 4 and MiniCan 5 – identification of all samples.

Sample	Sample-ID MiniCan 4 M4-	Sample-ID MiniCan 5 M5-
U-bend specimens	1:1, 2:1	
Copper WOL	3:1, 4:1	
Copper electrodes ×2	5:1, 6:1	5:1, 6:1
Copper weight loss coupons	7:1	7:1
Copper wire	8:1	8:1**
Iron electrodes ×2	9:1, 10:1	9:1, 10:1
Iron weight loss coupons	11:1	11:1
Any loose corrosion products	12:1, 13:1	
Green products from outside SS cage		12:1
Copper-iron sandwich specimen, copper outside up		14:1
Copper-iron sandwich specimen, copper part	14:1	
Copper-iron sandwich specimen, iron part	15:1	
Corrosion products from iron sandwich		13:1
Pt wire	16:1	16:1
Au wire	17:1	17:1
Ag/AgCl electrode ×2 (not found in the high density bentonite)	18:1, 19:1	
Ag Ø20 disc		18:1
Ø20 disc (found on glove-box floor, not analyzed)		19:1
Pt/Ti-net	20:1	20:1
Bentonite, different positions	40:1–51:1	
Bentonite, different positions	60:1–62:1	
Water from inside canister	–	Water MiniCan5
Wall of copper canister for H-analyses	21:1, 22:1, 23:1	21:1, 22:1, 23:1
Inner surface of copper canister	24:1	24:1
	24:2**	24:2**, 24:3**
Outer surface of copper canister	25:1	25:1
	25:2**	25:2
Welds in copper shell	26:1	26:1
	26:2	26:2**
Surfaces around holes in copper shell*	27:1	27:1
Bentonite with corrosion products at hole	28:1	–
Bentonite with corrosion products, from copper surface	28:2	
Corrosion products from outside of copper canister	–	35:1
Outer surface of cast iron insert	29:1	29:1
Inner surface of cast iron insert	29:2	29:2
Outer or inner surface of cast iron insert	29:3**	
Surfaces of cast iron insert at positions of hole(s) through copper shell*	30:1	30:1, 31:1
Stainless steel cage	–	Complete outer cage
	–	Complete inner cage

* Minican 5 had two defects near top weld facing up and down; Minican 4 had one defect near top weld facing down.

** In aluminium foil bag.

3 Analysis techniques

The first surface analysis method to be employed on the samples was Raman spectroscopy, which could be carried out without exposure of the samples to air whilst they were contained in the sealed sample holders. The instrument used was a Horiba Labram HR 800 with an objective lens of working distance 35 mm and laser wavelength of 532 nm. This is significant as the first attempt to use a laser of 785 nm wavelength and 20 mm working distance objective were not successful, and only analyses of the sample holder material could be obtained using this set-up. This was due to the working distance of the lens rather than the wavelength of the laser; however, it was seen that the shorter wavelength also gave clearer spectra when tested with the 35 mm objective so therefore it was decided to use this set-up for the analyses. The Raman analysis was the only method of analysis carried out before the samples were removed from their samples holders and exposed to air.

After the Raman spectroscopy the surfaces were analysed with FTIR, using a Perkin-Elmer Spotlight 200 FTIR microscopy system, with cut-off of 550 cm^{-1}. This means that some oxides and sulphides could not be detected with this instrument; however Raman and IR spectroscopy are complementary. FTIR analysis was carried out as soon as possible after the sample holders were opened, which means that the samples had been exposed to air for a period of several minutes to several hours prior to FTIR analysis.

SEM/EDS were subsequently carried out using a JEOL 7000F field emission instrument equipped with EDS and finally XRD analyses were performed using a Bruker D8 Discover instrument.

Supplementary analyses using GDOES, LAICPMS and XPS techniques were carried out for selected samples. In GDOES, glow-discharge optical emission spectroscopy, a plasma gas is used to melt the top 5 μm of the sample, analysing the elemental composition of the resulting gas. The instrument used for this was a LECO GDS 850 A. LAICPMS, laser ablation inductively coupled mass spectroscopy, uses laser radiation to sputter a sample, analysing the resulting gas for its elemental composition. XPS, x-ray photoelectron spectroscopy, was performed with a PHI 550 spectrometer using mono-chromatic Al-Kα radiation (1 468.8 eV) providing information on the molecular chemistry of the top 1 nm of the surface.

Analysis of the composition of water was performed by induced coupled plasma mass spectroscopy (ICP-MS), a method analysing the elemental composition of the sample. Elements such as Cl and S, expected as anions, are not readily analysed by the method. Accuracy of the results is ± 30 % as the method used is semi-quantitative.

The overall procedure of surface examination was thus such that Raman was applied while the specimens were still inside the air-tight sample holders, while other analyses were made after some period of air-exposure. In the results section a “short period” means that the samples were exposed to air for minutes or hours, while “extended period” means that the samples were exposed for days. Further technical details for each analysis method are given in the Appendices 6 (XPS, GDOES, LAICPMS), 7 (Raman), 8 (FTIR), 9 (XRD), and 10 (SEM/EDS).

4 Results

In this chapter results will be presented per sample. The results of each analysis method are presented and observations discussed. The samples can be divided into three groups:

1) SCC specimens mounted in the boreholes but outside the experimental packages contained by the steel cages.
2) Electrodes and coupons mounted on a plastic rack inside the steel cage above the copper canister (depicted in Figure 2-8).
3) Samples taken from the MiniCan copper canisters and cast iron inserts of the two packages.

Only a summary of the results is given in the sections below, with full analysis details given in the appendices:

Appendix 3 SCC samples.

Appendix 4 Mass loss.

Appendix 5 Hydrogen content analysis.

Appendix 6 XPS GDOES LAICPMS analyses.

Appendix 7 Raman analysis.

Appendix 8 FTIR analysis.

Appendix 9 XRD analysis.

Appendix 10 SEM/EDS analysis.

Appendix 11 Water sample analysis.

Appendix 12 Electrode potential measurements.

4.1 Water chemistry

Analysis of water chemistry was carried out on a sample of water collected from the inside of MiniCan 5 whilst it was being sectioned. The main constituents of the sample were Ca (4 g/l), Na (3 g/l), Fe (200 µg/l), Sr (70 mg/l) and Mg (50 mg/l). The concentration of iron in this sample was one magnitude higher than the concentration of dissolved Fe^{2+} in the support cage. Elements such as Cl and S, expected as anions, are not readily analysed by the method used (ICP-MS). All other elements analysed were lower by at least one order of magnitude. Full analysis results can be found in Appendix 11 Water sample analysis. Water analysis results obtained by SKB in 2007, 2008 and 2010 can be found in Smart et al. (2015).

4.2 Copper canister dimensions

Outer diameter dimensions of the copper canisters were taken immediately after they had been withdrawn from the stainless steel cage inside the glovebox, described also in Appendix 2 Sample preparation. The measurements were performed using calibrated callipers, with readings taken to the nearest 0.05 mm. The measurements of the diameter at the top (corresponding to the height position of the hole in the copper canister), middle and bottom of the canisters are given below in Table 4-1, and indicate that no change had occurred during the exposure, with the original diameter equal to 145 ± 0.5 mm as given in Smart and Rance (2009).

Table 4-1 - Measurements taken of the copper canisters immediately after withdrawal from the stainless steel cage. Nominal dimensions for the diameter were 145 ± 0.5 mm.

Position of measurement	MiniCan 4 Ø, mm	MiniCan 5 Ø, mm
Top	145.00	145.00
Middle	145.05	144.90
Bottom	145.00	145.00

4.3 Electrode potential

Electrode potential measurements were performed to make comparisons with the on-line measurements (Smart et al. 2015) possible. For MiniCan 5, electrode potentials were measured inside the glovebox, with all electrodes placed in a container of groundwater and vs. an Ag/AgCl reference electrode while for MiniCan 4 the measurements were performed with the electrodes still embedded in bentonite soaked in groundwater in the transport flask. It was not possible to identify the cables for MiniCan 4, so that although some measurements were taken it is unclear which electrode they refer to. Measurements were taken for MiniCan 5 and the cables were identifiable. Table 4-2 shows the potentials that were measured for the various electrodes present in the MiniCan 5 exposure. The potentials in the table have been converted to potential vs standard hydrogen electron (SHE) and compared with reported results from on-line measurements (Smart et al. 2015). In general it can be seen that the iron electrodes had a more negative potential than the copper electrodes, and that the "Silvion" reference electrodes, Ag/AgCl (seawater), differed significantly to the Ag/AgCl (3M KCl) reference electrodes used to take the measurements. The redox potential measured is lower than reported from the on-line measurement, indicating even less oxidative conditions after removal from the borehole. The measurements from MiniCan 4 were not as reliable, with many unstable readings, most likely due to the presence of the high density bentonite surrounding the electrodes. Full details can be found in Appendix 12 Electrode potential measurements.

Table 4-2. Electrode potential measurements from MiniCan 5 taken after the samples had been removed from the MiniCan assembly but remained in the glovebox.

MiniCan 5	Description	Potential vs. Ag/AgCl, 3M, expressed vs. SHE (mV)	MiniCan 5 on-line 2012–2013 (Smart et al. 2015), potential vs. Silvion expressed vs. SHE (mV)
"Cu1" vs. Ref A	Cu-electrode	−212	−320
"Cu2" vs. Ref A	Cu-electrode	−361	
"Fe1"vs Ref A	Fe-electrode	−424	−430
"Fe2"vs Ref A	Fe-electrode	−424	
"Eh" vs Ref A	Mixed metal oxide electrode	−447	−370
"Ag 2" vs Ref A	Ag-electrode	−192	
Silvion Ref vs. Ref A	MiniCan 5 ref	−159	
Silvion Ref vs. Ref B	MiniCan 5 ref	−159	

4.4 SCC U-bend and WOL specimens in the boreholes

This section presents the results from examination of U-bend (M4 1:1, M4 2:1) and WOL (M4 3:1 and M4 4:1) specimens mounted in the bore hole of MiniCan 4. U-bend specimens in their sample holders are shown in Figure 4-1.

Visual inspection of the SCC samples did not reveal any distinguishing factors except for the presence of a black surface deposit contained mainly to the inner surfaces and crevices. In particular the U-bend samples appeared very clean on their outer surfaces, which may have been a result of handling during the sample withdrawal and packing into sample holders, however, no deposit was observed during removal of the specimens from the bore hole.

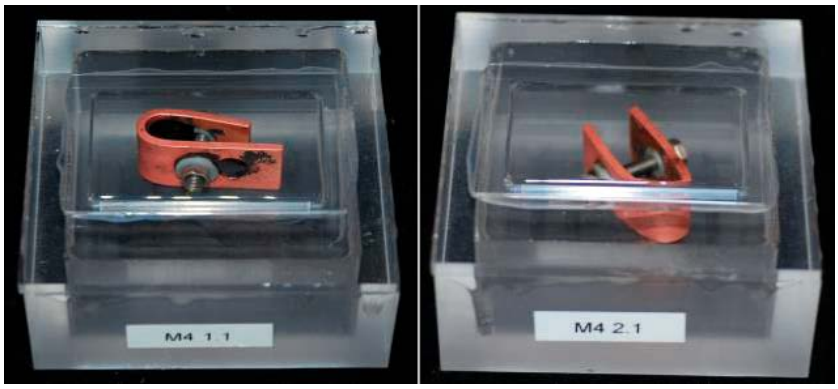

Figure 4-1. *Copper U-bend specimens M4 1:1 and M4 2:1.*

Raman analysis of the SCC samples did not produce any useful information; the spectra obtained detected only fluorescence of the samples rather than any surface compounds. This makes it difficult to obtain meaningful results from the Raman analysis as the signal is dominated by the fluorescence which by its nature is several orders of magnitude stronger than signals from small amounts of any specific compounds or adsorbates present on the surface. Figure 4-2 and Figure 4-3 show the spectra obtained for samples M4 1:1 (U-bend) and M4 4:1 (WOL), which show only the fluorescence - seen as an increase in signal intensity with a wave-like form (right hand side of Figure 4-2) – most probably from cuprite, detected in the analysis.

Optical microscope inspection of the U-bend samples did not reveal any areas of cracking or corrosion. The only physical attribute of note was the uneven surface caused by the deformation of the sample during bending, resulting in the "orange peel" appearance as noted in Smart et al. (2012).

The U-bends were sectioned as shown in Figure 4-4 and polished to a 1 µm finish before being examined under the optical microscope again. Several areas with pores were observed as shown in Figure 4-5.

SEM/EDS analysis of the porous areas detected increased amounts of O and Si compared to the surrounding areas which were Cu. The cause of the porosity is unclear at the time of writing, it could be related to material production and handling, but it seems unlikely to be corrosion-related due to the absence of sulphur and/or chlorine in or near the pores, as well as the absence of material loss at the surface of the sample.

The pre-crack of WOL specimen M4 3:1 is shown in Figure 4-6. The crack was created by fatigue cracking the material to the nominal length of 1.5 mm (Smart et al. 2013, Aggarwal et al. 2015). However, since the cracking method had an uncertainty of a few hundreds of µm, this can be set as an upper limit of any crack growth that might have occurred during the circa nine years of exposure in the MiniCan experiment. A definitive observation of crack growth would thus require that the crack was at least 2 mm, which has not been observed in any WOL specimens from previous MiniCan reports (Smart et al. 2013, Aggarwal et al. 2015).

It was decided to polish the surface perpendicular to the pre-crack and carry out inspection under a microscope before breaking open the WOL sample. This way, any crack elongation could be detected prior to destructive testing.

SEM/EDS investigation of the WOL samples detected presence of small amounts of sulphur at the crack tip in the surface oxide. It was observed that there were some smaller cracks that seemingly emanated from the main crack into the cold deformation area of the parent material on either side of the pre-crack, see Figure 4-7. These smaller cracks were notable as some of them were seen to be travelling perpendicular to the direction of the pre-crack (i.e. parallel to the load applied when fatiguing the specimens) and had more branches. These features are consistent with SCC but it is not possible to say if these smaller cracks are due to SCC in this instance or if they occurred during the original fatiguing of the samples. The presence of only O and Si in the smaller cracks but no S or Cl as found from the EDS analyses implies corrosion has not played a part in the cracking during the exposure. Full details of the SEM/EDS analyses can be seen in Appendix 3 SCC samples.

MiniCan 4

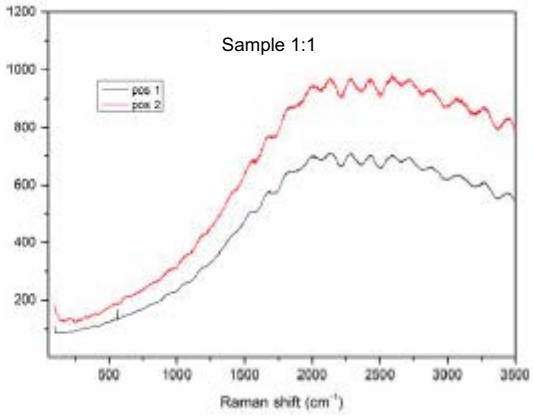

Figure 4-2. *Raman spectra for U-bend sample M4 1:1.*

4:1

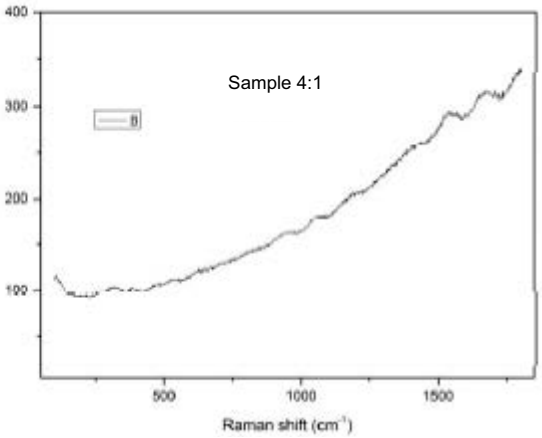

Figure 4-3. *Raman spectrum for WOL sample M4 4:1.*

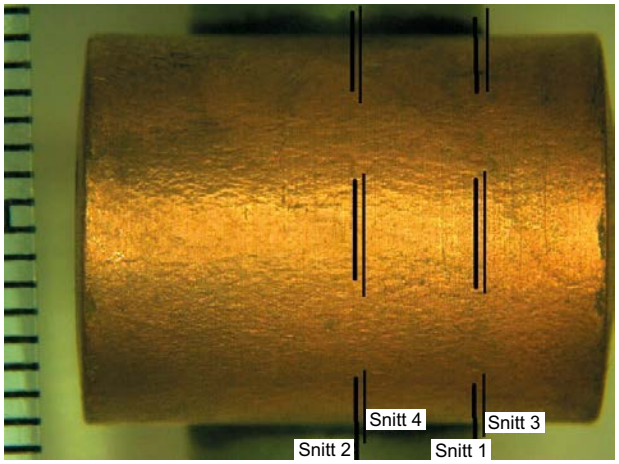

Figure 4-4. *U-bend sample M4 1.1 as seen through a microscope looking directly onto bent area of sample, indicating where the sample was sectioned and analysed using microscopy.*

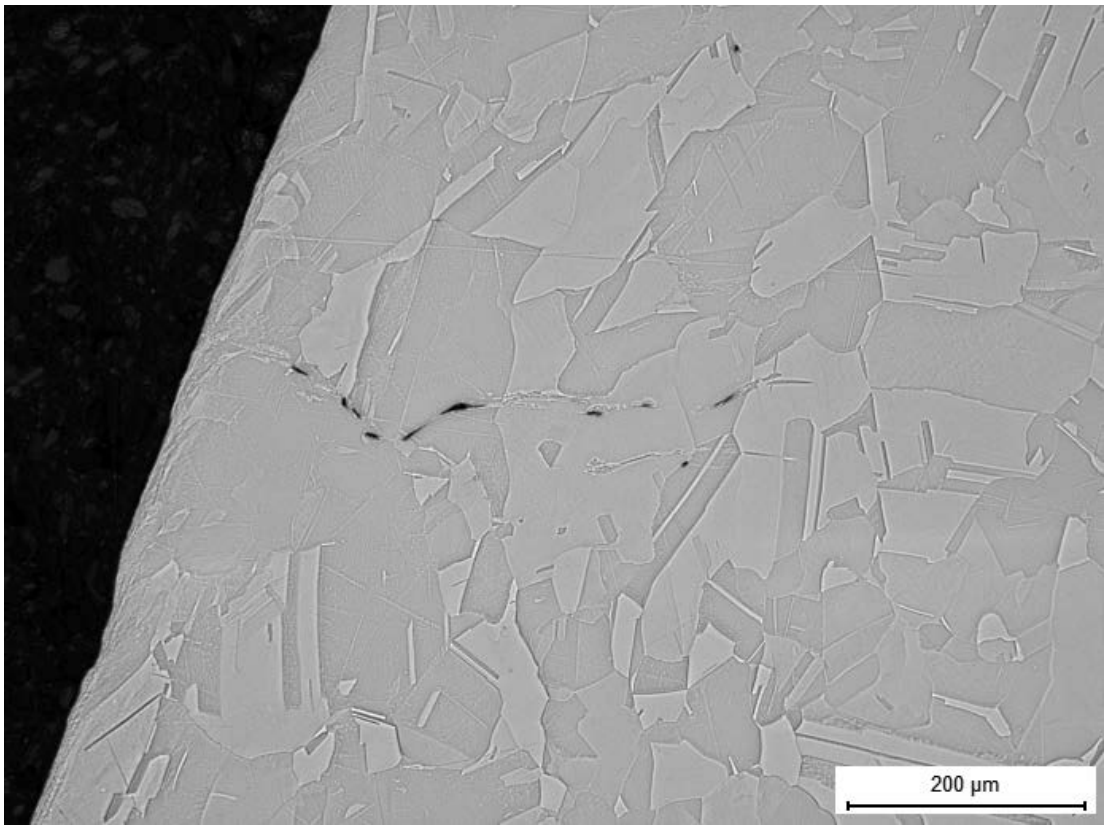

Figure 4-5. *U-bend sample M4 1.1 had an area of cold deformation near the surface, but also present were pores which appeared to be aligned along the grain boundaries.*

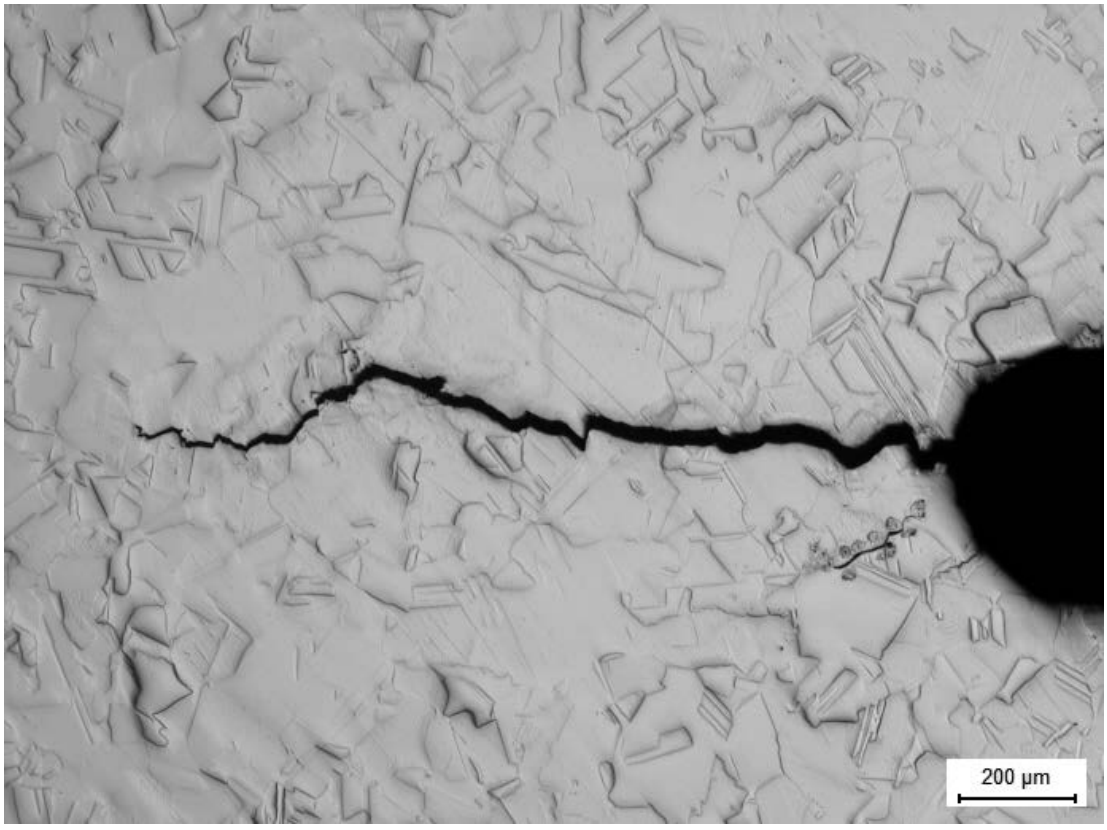

Figure 4-6. *Micrograph of the sample M4 3.1 showing the pre-crack from the notch, and smaller cracks in the vicinity of the notch as well as further along the main crack.*

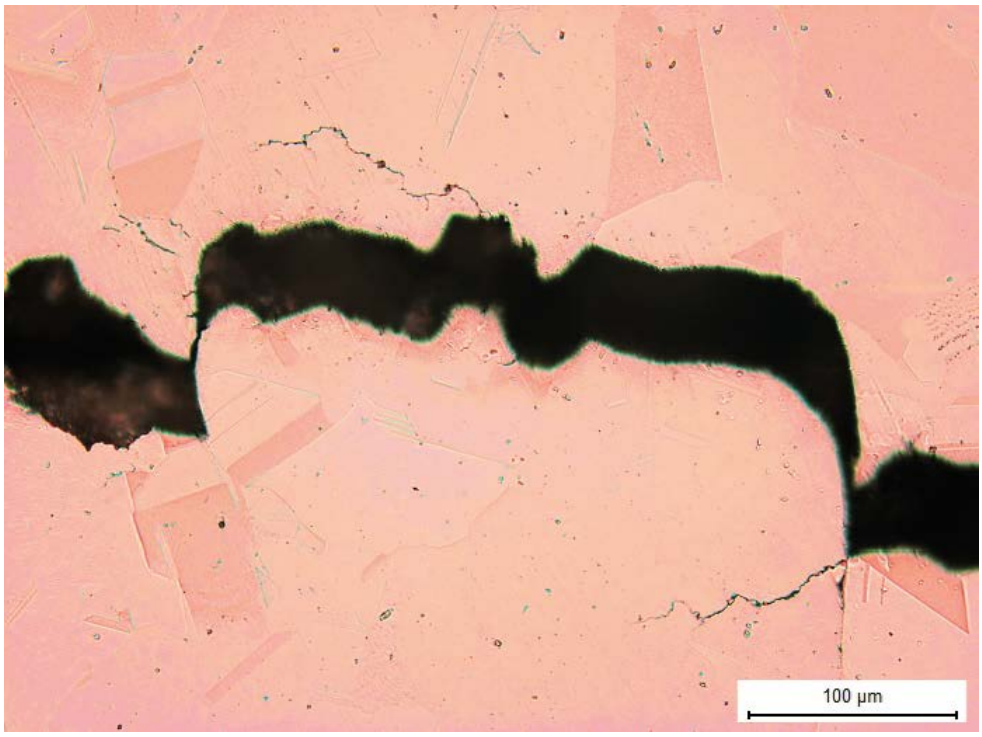

Figure 4-7. *Middle part of pre-crack of WOL sample M4 4:1, showing smaller cracks emanating perpendicular to the direction of the main crack.*

In order to fully utilise the samples it was decided to carry out further investigation using TEM on a FIB (Focused Ion Beam) prepared sample taken directly from the crack tip in the through-thickness direction of the material. The intention was to see if there was any evidence of accumulation of sulphur near or in the grain boundaries. In addition, it was also decided to look for the presence of phosphorus in these areas, which has been investigated earlier (Thuvander 2015).The TEM investigation also involved sampling a piece of canister material from the wall of the MiniCan 4 canister, from near to the exposed outer surface as a comparison to the WOL sample.

TEM examination of the FIB-prepared samples from WOL M4 3:1 showed an accumulation of sulphur in the surface oxide at the crack tip (see Figure 4-8), and that the pre-crack had propagated along grain boundaries in the material. It should be noted though, that in the other WOL specimen of MiniCan 4, sulphur was analysed and detected not only at the crack tip but along 50 µm of the crack, indicating no systematic variation in the sulphur content of the surface film (Figure 70, Appendix 3). The concentration of sulphur in the canister wall was low (<0.1 at%) and consistent throughout the samples except for one sulphur-rich particle found at a grain boundary.

The sample taken from the canister wall, prepared by electrolytic polishing had sulphur-rich particles in the surface oxide as well as at the grain boundary of the sample. The source of these particles may be the sample preparation rather than the exposure conditions or original material chemistry, as indicated by the fact that similar low levels of S were detected both at the surface of the base material as at the grain boundary in Figure 4-9.

The concentration of phosphorus was found to be increased at some positions in the grain boundaries, and the concentration of phosphorus was below or close to the detection limit (0.1 at%) in a large part of the grain boundaries and in the matrix, see Figure 4-9.

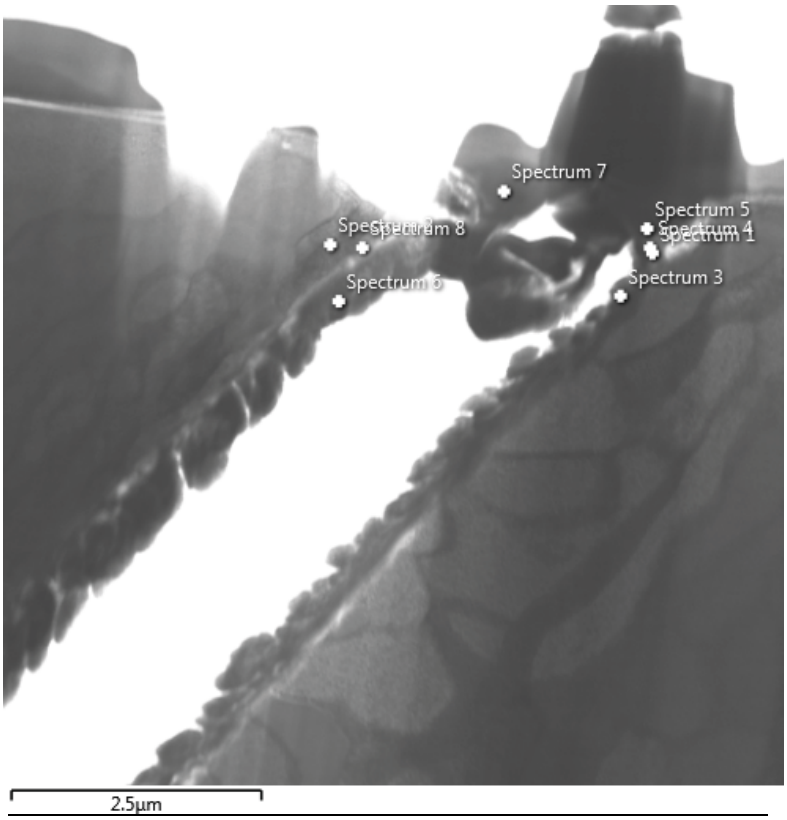

Spectrumat%	O	P	S	Cu	Pt	Total
Spectrum 1	28.98	0.00	5.94	36.54	28.54	100.00
Spectrum 2	7.00	0.01	0.00	92.99	0.00	10 0.00
Spectrum 3	13.02	0.00	9.52	50.52	26.93	100.00
Spectrum 4	25.71	0.00	1.48	29.90	42.91	100.00
Spectrum 5	9.46	0.00	0.78	31.49	58.27	100.00
Spectrum 6	13.54	0.13	0.00	86.33	0.00	100.00
Spectrum 7	9.25	0.00	1.53	31.52	57.69	100.00
Spectrum 8	12.56	0 .11	0.64	86.64	0.05	100.00

Note: The platinum originates from the platinum coating applied for protection before ion beam milling.

Figure 4-8. *FIB prepared sample of WOL sample M4 3:1 examined in TEM. Surface oxide can be seen here on the fracture surfaces of the crack tip. The image shows the view looking along the crack direction with the fracture surfaces on either side.*

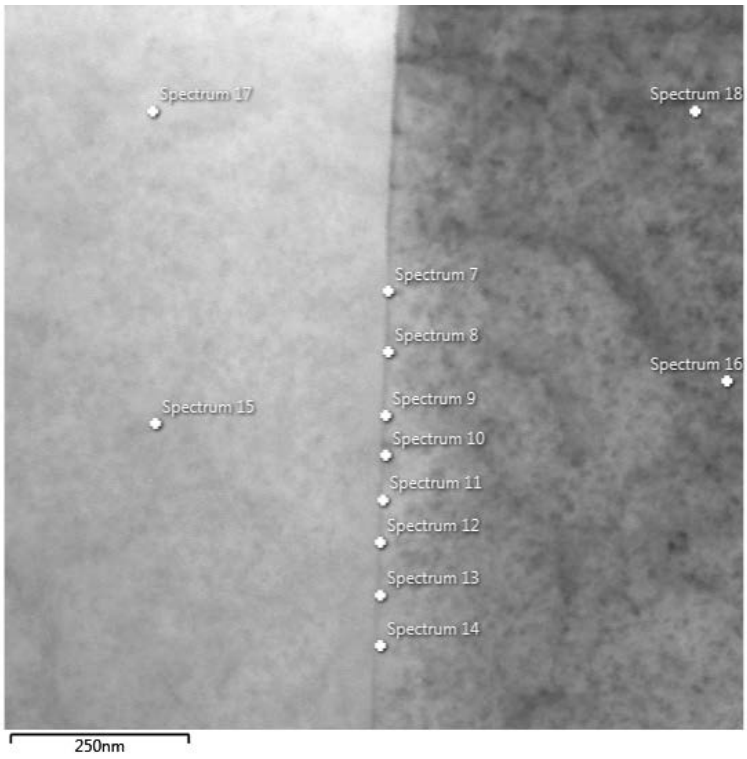

Spectrum at%	P	S	Cu	Total
Spectrum 7	0.00	0.00	100.00	100.00
Spectrum 8	0.23	0.00	99.77	100.00
Spectrum 9	0.06	0.07	99.87	100.00
Spectrum 10	0.00	0.00	100.00	100.00
Spectrum 11	0.18	0.03	99.79	100.00
Spectrum 12	0.16	0.00	99.84	100.00
Spectrum 13	0.09	0.05	99.86	100.00
Spectrum 14	0.01	0.04	99.94	100.00
Spectrum 15	0.00	0.09	99. 91	100.00
Spectrum 16	0.00	0.00	100.00	100.00
Spectrum 17	0.00	0.04	99.96	100.00
Spectrum 18	0.07	0.07	99.86	100.00

Figure 4-9. *Element concentrations at%, at grain boundary of a FIB-prepared TEM specimen from WOL sample M4 3:1, (spectra 7–14), and in grain area (spectra 15–18). Only the elements Cu, P and S are selected. Average values: Grain boundary: phosphorus 0.186 at%; Grain area: phosphorus 0.021 at%.*

After the TEM investigation the WOL sample M4 3:1 was opened by tensile load in order to examine the fracture faces of the pre-cracked area. The SEM investigation revealed that the fracture surfaces showed features consistent with fatigue failure as was expected. The interface between the fatigue fracture and the ductile failure from the tensile load was easily seen, but there were no areas which suggested that the crack had propagated during exposure due to SCC. In fact the crack tip appeared to be in an area of trans-granular fracture which is more associated with fatigue than SCC. The reason why the crack tip was trans-granular whilst the remainder of the crack appeared to have propagated inter-granular is not clear. Figure 4-10 shows the EDS results of the analysis on the fracture surface of the pre-crack, with a wider array of elements being detected nearer the opening of the crack near the notch (shown at the top of the image) which could be due to that the opening is wider than the further along the crack. It was decided to save the second WOL sample M4 4:1 so that it was not investigated by TEM nor was it opened.

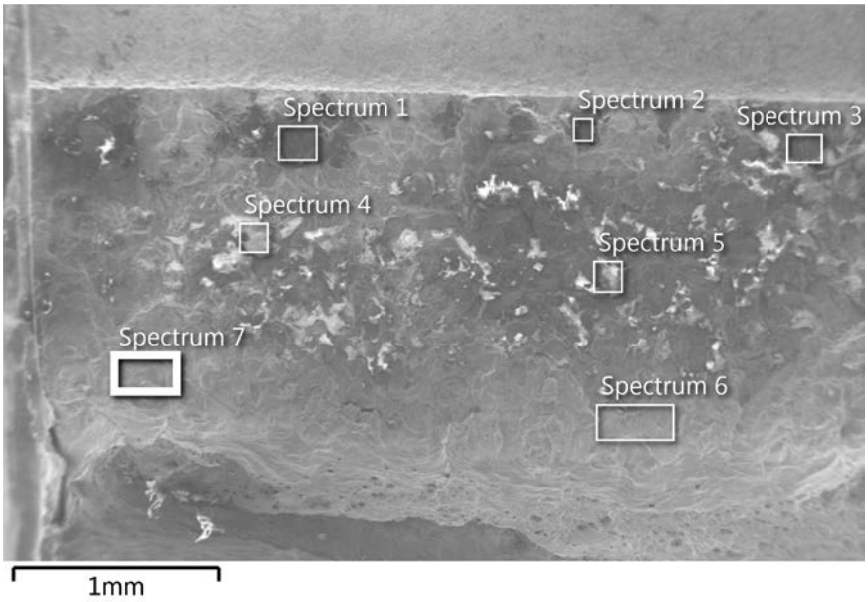

Spectrum Wt%	O	Mg	Al	Si	S	Ca	Cu	Total
Spectrum 1	53.20	1.22	5.91	19.75	1.45	1.70	16.77	100.00
Spectrum 2	43.62		1.99	33.33	0.91	0.93	19.21	100.00
Spectrum 3	47.37	0.73	2.26	27.97	0.65	2.28	18.75	100.00
Spectrum 4	46.87			35.46			17.67	100.00
Spectrum 5	42.07			30.82		1.27	25.84	100.00
Spectrum 6	13.28			4.21			82.52	100.00
Spectrum 7	10.06				0.63		89.31	100.00

Figure 4-10. *EDS analysis of fracture face of WOL sample M4 3:1. Elements associated with bentonite were detected along with copper and oxygen.*

4.5 Electrodes and coupons inside the steel cage

4.5.1 Copper electrodes

This section presents results from the examination of copper electrodes mounted on the nylon racks in the steel cages of MiniCan 4 (M4 5:1, M4 6:1) and MiniCan 5 (M5 5:1 and M5 6:1).

A common feature of the external samples removed from the MiniCan 4 experiment was that they were covered with a layer of bentonite. This was reflected in the Raman analyses of these samples. The visual appearance of these samples however was one of an uncorroded sample only slightly covered in surface deposits, especially when compared to the similar samples taken from the MiniCan 5 experiment; see Figure 4-11 and Figure 4-12. Samples from MiniCan 5 were entirely covered with a black deposit.

Raman analysis of M4 5:1 and M4 6:1 detected sulphide and cuprite, see Figure 4-13. Peaks from CuS and Cu_2S cannot be distinguished from one another and iron sulphides as well as mixed sulphides have similar peaks, see appendix 7, thus these are presented as “sulphide”. The results were somewhat similar to those obtained from the SCC samples, where fluorescence from cuprite was detected, but for the copper electrodes sulphide was also present.

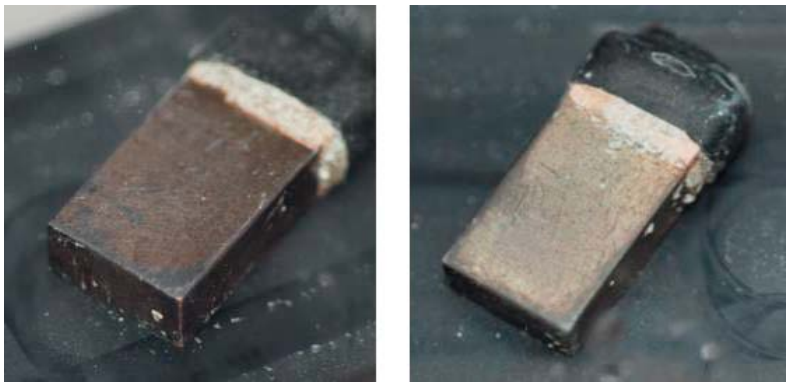

Figure 4-11. M4 5:1 and M4 6:1 copper electrodes after removal from the MiniCan 4 experiment.

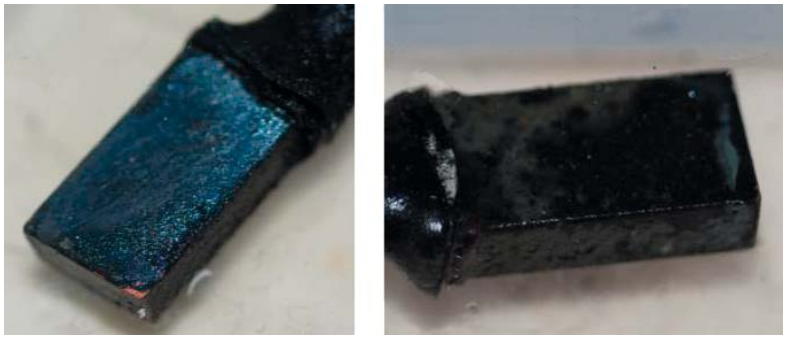

Figure 4-12. M5 5:1 and M5 6:1 copper electrodes after removal from the MiniCan 5 experiment.

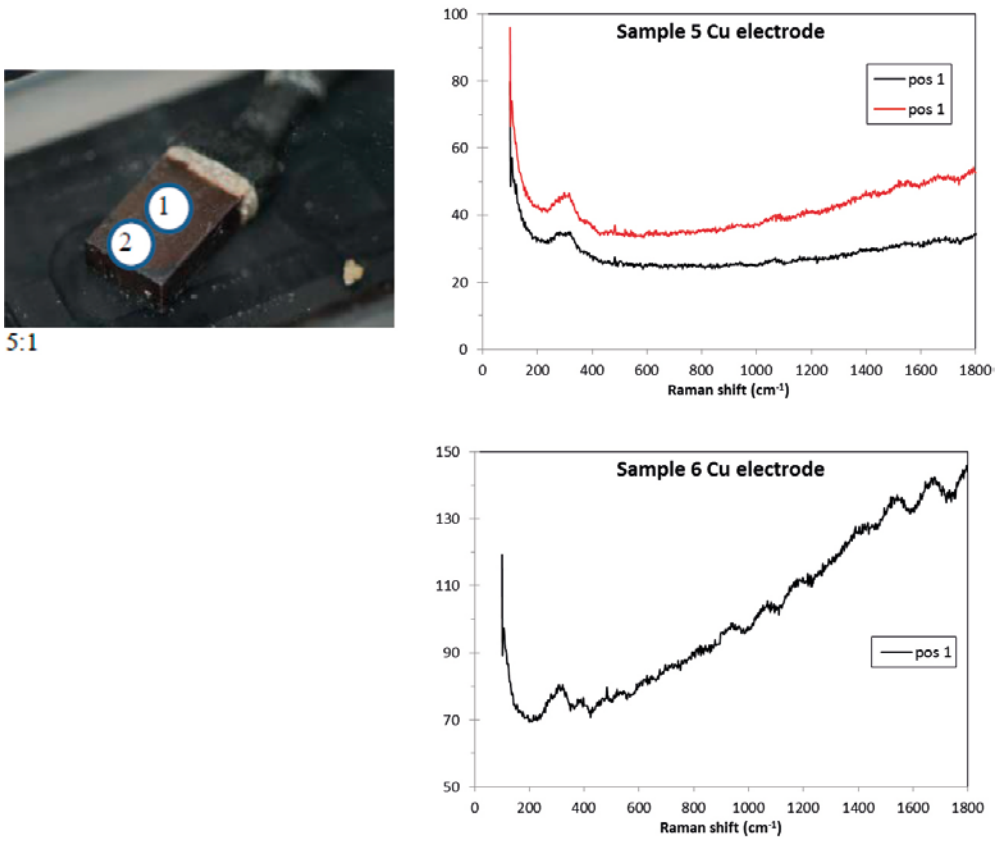

Figure 4-13. Raman spectra for M4 5:1 and M4 6:1 copper electrodes, showing peaks for sulphide as well as cuprite fluorescence.

Sample M5 5:1 was measured at four points on the surface, as shown in Figure 4-14. All points had a double peak at 240–320 cm^{-1}. Point 1 had a strong sulphate peak at 1 000 cm^{-1}. All points had fluorescence from cuprite. Cuprite may also have contributed to the peaks in the area between 250 and 320 cm^{-1} but with inverted relative intensity of the peaks (see discussion of reference spectra in Appendix 7). Another alternative is mixed sulphides, but not sulphate at this wave number. Sample M5 6:1 was measured at three points on the surface. Fluorescence dominates all points, but sulphate was detected (1 000 cm^{-1}) and the peaks at 200–400 cm^{-1} could be a mixture of copper oxide and iron oxide.

FTIR analyses of the copper electrodes from MiniCan 4 detected mainly bentonite with some carbonate and adsorbed sulphate and hydroxo-groups. Analyses from MiniCan 5 detected the presence of carbonate and hydroxy-groups, and possibly also sulphite and sulphate; sulphite would be an intermediary oxidation product of sulphide after brief exposure to oxygen prior to FTIR analyses.

SEM/EDS analyses showed that the samples from MiniCan 4 had deposits containing higher amounts of Si and less Fe than the MiniCan 5 samples, as can be expected due to the presence of bentonite and the lower extent of iron corrosion observed in MiniCan 4. The surface deposits on the MiniCan 5 samples were mainly comprised of Fe, O, S and Ca.

XRD analyses of the MiniCan 4 samples detected Cu, CuO, $CuSiO_3$, and $Ca_2SiO_3Cl_2$. The silicates are most likely from bentonite not completely washed off. XRD of MiniCan 5 samples detected Cu, CuO, Cu_2O, Cu_4O_3, NaCl, and SiO_2. SiO_2 is most likely from glass particles depositing on the surface after opening of the sample holder.

From the analysis results it would appear that the surfaces of the copper electrodes from the MiniCan 4 experiment were mainly copper oxide and sulphide with a layer of bentonite covering them. However the MiniCan 5 copper electrodes were clearly covered in a black deposit most likely emanating from the corrosion of iron from nearby samples. The detection of sulphides in Raman and SEM/EDS analyses suggests that iron sulphide has deposited out on the copper electrode surfaces from nearby corroding iron surfaces.

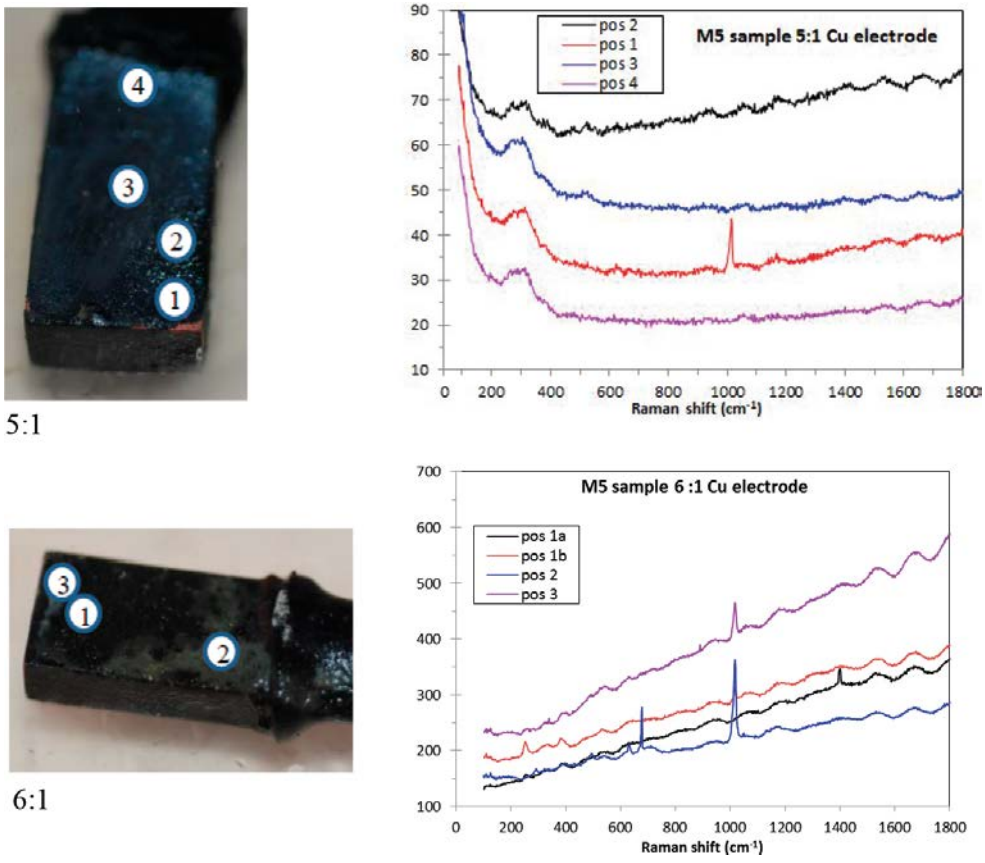

Figure 4-14. *Raman spectra for M5 5:1 and M5 6:1 copper electrodes with peaks for sulphate and sulphides (likely including iron sulphide) and cuprite detected on M5 5:1, and sulphate and a possible mix of copper and iron oxide on M6 6:1.*

Table 4-3. Summary of analysis of Cu electrodes in MiniCan 4 (M4 5:1 and M4 6:1)*.

Exposure to air before analyses	Method	M4 5:1 copper electrode	M4 6:1 copper electrode
None	Raman	Sulphide, Cu_2O	Sulphide, Cu_2O
Short period	FTIR	Bentonite, OH, OH/H_2O, H_2O, SO_4^{2-}, CO_3^{2-}	Bentonite, OH, OH/H_2O, H_2O, SO_4^{2-}, CO_3^{2-}
Extended period	SEM/EDS	C, O, Na, Mg, Al, Si, S, Cl, Ca, Fe, Cu	C, O, Na, Mg, Al, Si, S, Cl, K, Ca, Fe, Cu
Extended period	XRD	Cu	Cu, CuO, $CuSiO_3$, $Ca_2SiO_3Cl_2$
Likely compounds on surfaces before exposure to air		Sulphides including iron sulphides, cuprite, chloride, silicates etc. from bentonite, cuprite, chloride	

* The overall procedure was such that Raman was applied while the specimens were still inside the air-tight sample holders, while other analyses were made after some period of air-exposure. Here, “short period” means that the samples were exposed to air for minutes or hours, while “extended period” means that the samples were exposed for days.

Table 4-4. Summary of analysis of Cu electrodes in MiniCan 5 (M5 5:1 and M5 6:1).

Exposure to air before analyses	Method	M5 5:1 copper electrode	M5 6:1 copper electrode
None	Raman	Sulphide, Cu_2O, SO_4^{2-}	Cu oxide (incl. Cu_2O), Fe oxide, SO_4^{2-}
Short period	FTIR	H_2O/OH, CO_3^{2-}, SO_3^{2-}, SO_4^{2-}	H_2O/OH, CO_3^{2-}, possibly SO_4^{2-}
Extended period	SEM/EDS	C, O, Na, Al, Si, S, Cl, Ca, Cr, Fe, Ni, Cu	C, O, Na, Mg, Al, Si, S, Cl, K, Ca, Cr, Fe, Ni, Cu, Sn
Extended period	XRD	Cu, NaCl, CuO, Cu_2O	Cu, NaCl, CuO, Cu_4O_3, SiO_2
Likely compounds on surfaces before exposure to air		Sulphides including iron sulphide, cuprite, chloride	

4.5.2 Iron electrodes

This section presents results from the examination of iron electrodes mounted on the nylon rack inside the steel cage of MiniCan 4 (M4 9:1, M4 10:1) and MiniCan 5 (M5 9:1 and M5 10:1). Unlike the copper electrodes from the MiniCan 4 experiment, the iron electrodes in MiniCan 4 appeared corroded, with material loss particularly on sample M4 9:1. The iron electrodes from MiniCan 5 were completely covered with a black deposit, similar to the copper electrodes but seemingly much thicker. Photos of the electrodes are shown in Figure 4-15 and Figure 4-16.

Raman analyses of the iron electrodes from MiniCan 4 detected mainly fluorescence and calcite ($CaCO_3$) detected on M4 10:1. The analyses for M5 9:1 were similar to troilite (FeS). Sample M5 10:1 had peaks for troilite and sulphate, see Figure 4-17.

FTIR on MiniCan 4 samples detected mainly bentonite, with Fe-O functional groups found on sample 9 and OH, OH/H_2O, $FeSO_4 \cdot H_2O$ and bentonite on sample 10. Samples from MiniCan 5 had peaks for CO_3^{2-}, OH/H_2O, Fe-OH, FeOOH, Si-O (possibly from glass fragments).

SEM/EDS analyses found a mixture of mainly C, O and Si on the MiniCan 4 samples, most likely from the bentonite. On the MiniCan 5 samples Fe, C and O were the main elements found with smaller amounts of S, Si and Cl. It should be noted that the MiniCan 5 samples underwent a drastic change of appearance when the sealed sample holders were opened after the Raman analyses were completed and before any other analyses took place. Figure 4-18 shows the change in colour of M5 9:1 which occurred after just a few minutes exposure to air. This change can also be seen as a difference in the results between the Raman analyses (applied before exposure to air) and the other methods (applied after exposure to air), such as XRD for example (Table 4-6).

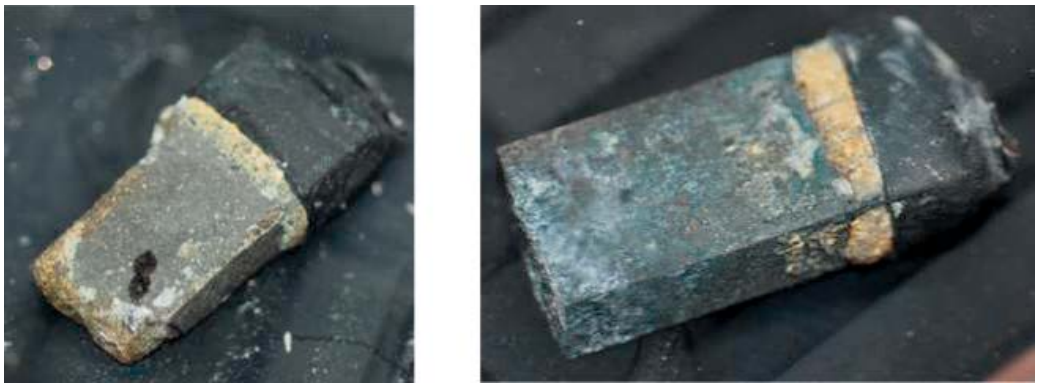

Figure 4-15. *M4 9:1 and M4 10:1 iron electrodes after removal from the MiniCan 4 experiment.*

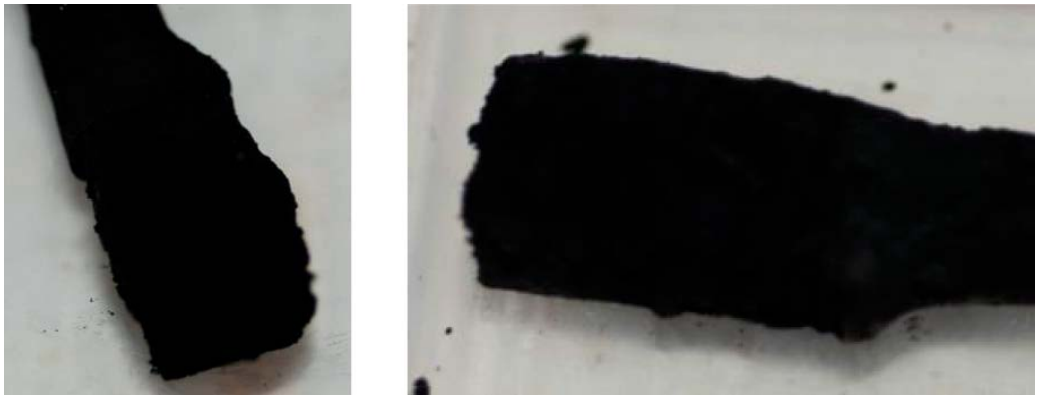

Figure 4-16. *M5 9:1 and M5 10:1 iron electrodes after removal from the MiniCan 5 experiment.*

XRD analysis detected SiO_2 and Fe on M4 9:1 and Fe, silicates, and SiO_2 on M4 10:1, and iron oxide hydroxides (rust) on M5 9:1 and M5 10:1. Results from the analyses of the iron electrodes are summarized in Table 4-5 and Table 4-6.

Table 4-5. Analysis summary of iron electrodes M4 9:1 and M4 10:1.

Exposure to air before analyses	Method	M4 9:1 iron electrode	M4 10:1 iron electrode
None	Raman	Bentonite fluorescence, possibly sulphide	$CaCO_3$, fluorescence
Short period	FTIR	Bentonite, Fe-O	Bentonite, OH, OH/H_2O, SO_4^{2-}
Extended period	SEM/EDS	C, O, Na, Mg, Al, Si, P, S, Cl, K, Ca, Ti, Fe, Ni, Cu	C, O, Na, Mg, Al, Si, S, Cl, K, Ca, Fe, W
Extended period	XRD	SiO_2, Fe	Fe, silicates SiO_2
Likely compounds on surfaces before exposure to air		Bentonite, iron oxides and sulphides, chloride	Bentonite, carbonate, sulphide, chloride

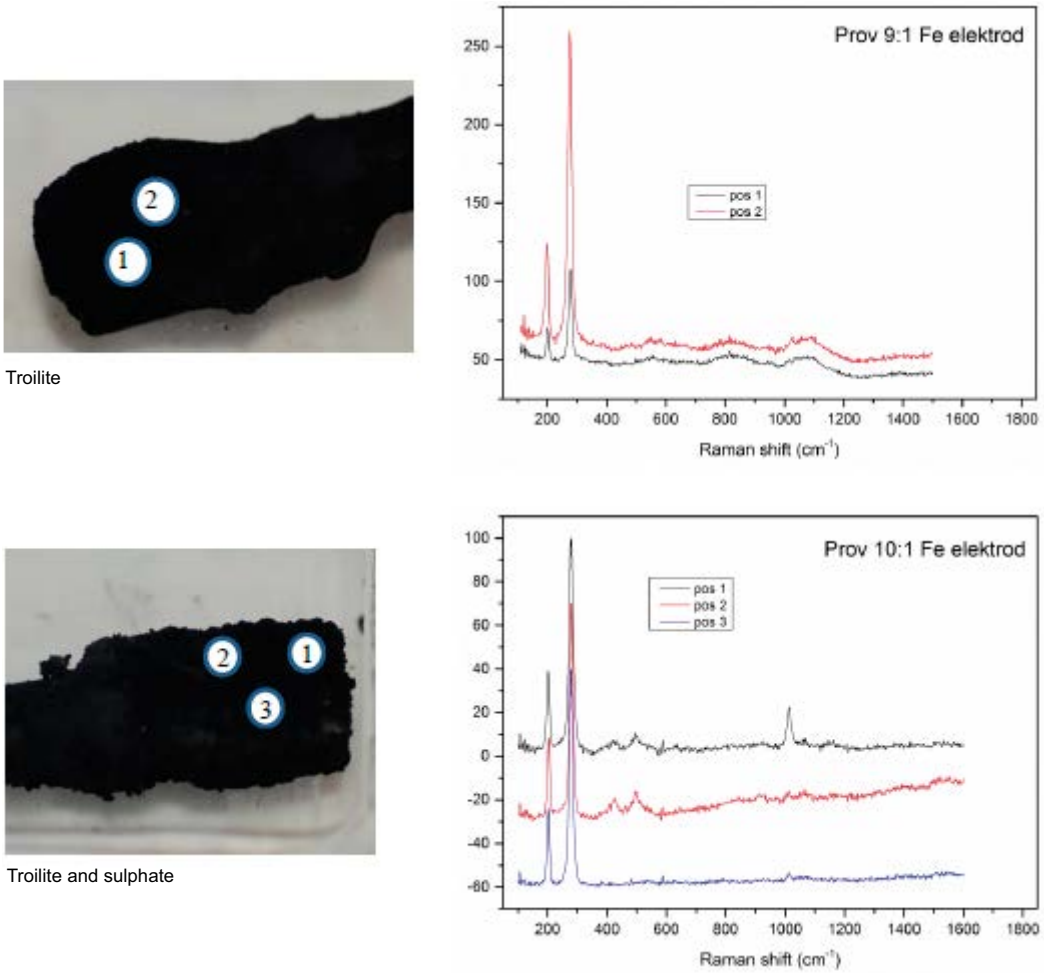

Figure 4-17. *Raman spectra for M5 9:1 with peaks for troilite FeS and for M5 10:1 with peaks for troilite and sulphate.*

Table 4-6. Analysis summary of iron electrodes M5 9:1 and M5 10:1.

Exposure to air before analyses	Method	M5 9:1 iron electrode	M5 10:1 iron electrode
None	Raman	FeS	FeS, sulphate
Short period	FTIR	SO_4^{2-}, H_2O	CO_3^{2-}, OH-/H_2O, Fe-OH, possibly FeOOH, possibly Si-O
Extended period	SEM/EDS	C, O, Na, Mg, Al, Si, S, Cl, Ca, Fe	C, O, Na, Mg, Al, Si, S, Cl, Ca, Cr, Fe, Ni
Extended period	XRD	Iron oxide/hydroxide	Iron oxide/hydroxide
Likely compounds on surfaces before exposure to air		FeS, chloride	FeS, sulphate, chloride

As seen in Figure 4-18, the appearance of the iron electrodes quickly changed after exposure to air. The black surface deposit changed rapidly to a red-brown colour with large cracks on the surface. There was also moisture seen to emanate from the sample surface when it was placed in another plastic container, suggesting the sample had remained wet whilst inside its sealed holder.

After removal of the surface deposits it could be seen that the MiniCan 5 electrodes had lost approximately 2.5 mm of material, see Figure 4-19. Electrode 9:1 from MiniCan 4 had lost approximately 1 mm from the edges, whilst 10:1 retained its original dimensions at the mm scale, see Figure 4-15.

Figure 4-18. *Sample M5 9:1 iron electrode before and after a few minutes of exposure to air after the sealed sample holder was opened.*

Figure 4-19. *Appearance of iron electrodes M5 9:1 (left hand side) and M5 10:1 from MiniCan 5 after removal of loose corrosion products. The uncorroded areas near the electrical connection were protected by heat shrink during the exposure period.*

4.5.3 Copper and iron mass loss specimens

This section presents results from spectroscopic, microscopic and gravimetric analysis of mass loss coupons mounted on the nylon racks of MiniCan 4 (M4 7:1, M4 11:1) and MiniCan 5 (M5 7:1, M5 11:1).

The mass loss samples from MiniCan 5 appeared to be covered with a black deposit immediately after removal from the experiment. This was in contrast to the similar samples retrieved from MiniCan 4. Also of note was the difference in appearance of samples M4 11:1 and M5 11:1, the iron mass loss specimens, which were both covered in surface deposits but M5 11:1 appeared to be corroded and the surface deposit was voluminous whilst M4 11:1 had a thin surface deposit with the underlying iron surfaces appearing relatively intact, see Figure 4-20 and Figure 4-21.

Raman analysis of M4 7:1 detected sulphide and cuprite, and M4 11:1 detected calcite and sulphide, carbon was found on both samples. There was also fluorescence from the bentonite on the surface as with other MiniCan 4 samples. Sample M5 7:1 had peaks at 250–320 cm^{-1} which could be cuprite or sulphide, and analysis on M5 11:1 detected iron oxide resembling FeO, carbon, and FeS.

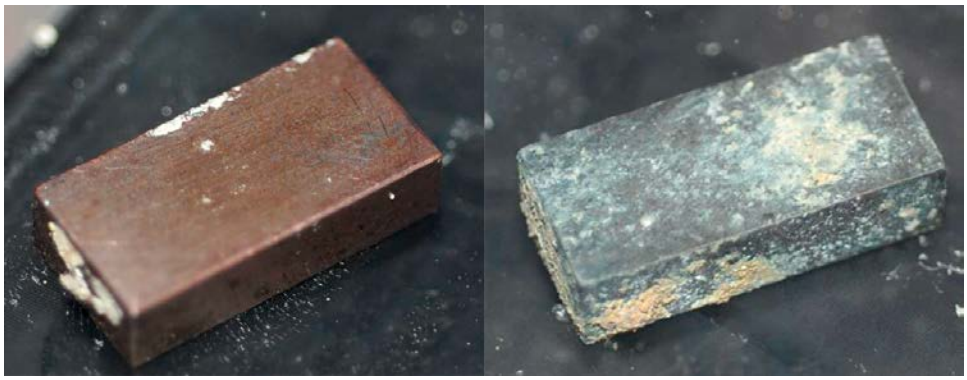

Figure 4-20. *M4 7:1 and M4 11:1 copper (left) and iron (right) mass loss samples after removal from the MiniCan 4 experiment.*

Figure 4-21. *M5 7:1 and M5 11:1 copper (left) and iron (right) mass loss samples after removal from the MiniCan 5 experiment.*

FTIR analyses of MiniCan 4 samples detected only bentonite. Analysis on M5 7:1 detected sulphite, sulphate, and carbonate varying over the sample surface. Sulphate and sulphite was detected on M5 11:1 but as discussed above, since sulphite is not present in the ground water, it is probably the result of post-test air exposure of sulphides formed at the surface during ground water exposure.

SEM/EDS analyses on the MiniCan 4 samples detected mainly bentonite. Analysis of M5 7:1 detected mainly Cu, Si, O, Cl, and S. On M5 11:1 Fe, Ni, Si, Ca, Cu, Cr, O, and S was detected.

XRD analysis on M4 7:1 detected Cu and SiO_2, and on M4 11:1 Fe, SiO_2 and silicates were found. XRD on M5 7:1 detected Cu, NaCl, SiO_2, CuO, and Cu_4O_3. Iron oxide hydroxides (rust) were detected on M5 11:1 as well as SiO_2, the latter likely from glass particles from the sample holder. Results from the analyses of the mass loss samples are summarized in Table 4-7 and Table 4-8.

Table 4-7. Analysis summary of copper and iron mass loss samples M4 7:1 and M4 11:1.

Exposure to air before analyses	Method	M4 7:1 Cu coupon	M4 11:1 Fe coupon
None	Raman	Sulphide, Cu_2O, C	$CaCO_3$, sulphide, C, fluorescence
Short period	FTIR	Bentonite	Bentonite
Extended period	SEM/EDS	C, O, Na, Mg, Al, Si, S, Cl, K, Ca, Fe, Cu	C, O, Na, Mg, Al, Si, S, Cl, K, Ca, Cr, Fe, Ni
Extended period	XRD	Cu, SiO_2	Fe, SiO_2, silicates, SiO_2
Likely compounds on surfaces before exposure to air		Sulphides including iron sulphides, cuprite, carbon, bentonite	Iron sulphide, carbonate, carbon, bentonite

Table 4-8. Analysis summary of copper and iron mass loss samples M5 7:1 and M5 11:1.

Exposure to air before analyses	Method	M5 7:1 Cu coupon	M5 11:1 Fe coupon
None	Raman	C, Cu_2O, sulphide	Iron oxide (possibly FeO), C, FeS
Short period	FTIR	SO_3^{2-}, SO_4^{2-}, CO_3^{2-}, H_2O, H_2O/OH	SO_3^{2-}, SO_4^{2-}, H_2O
Extended period	SEM/EDS	C, O, Na, Al, Mg, Si, S, Cl, Ca, Cr, Fe, Ni, Cu	C, O, Na, Mg, Al, Si, S, Cl, Ca, Cr, Fe, Ni, Cu
Extended period	XRD	Cu, NaCl, SiO_2, CuO, Cu_4O_3	Iron oxy hydroxides (rust), Fe, $Ca_{1.8}Al_2O_{4.8}$, SiO_2
Likely compounds on surfaces before exposure to air		Carbon, sulphides including iron sulphides, chloride	FeS, iron oxide, carbon, chloride

Mass loss analysis was carried out on the copper samples M4 7:1 and M5 7:1 according to the method described in SS-EN ISO 8407:2014 *Removal of corrosion products from corrosion samples*. This method is similar to that used in the post-test examination of MiniCan 3 (Smart et al. 2012) and involves repeated pickling steps to remove all corrosion products from the samples until only the base material remains. The difference in masses from the start of experiment to after the complete removal of corrosion products allows the determination of an average corrosion rate for the period of exposure.

The copper mass loss specimen in MiniCan 5 M5 (M5 7:1) had corroded by an average rate of 0.11 µm/y, which is very similar to the corrosion rate determined gravimetrically for copper in MiniCan 3 (0.15 µm/y) (Smart et al. 2012). For the copper mass loss specimen of MiniCan 4 (M4 7:1), embedded in compact bentonite clay, the average corrosion rate was 0.02 µm/y, i.e. one order of magnitude lower than for both MiniCan 3 and 5.

The mass loss analysis of the iron samples M4 11:1 and M5 11:1 gave average corrosion rates of 2.1 µm/y and 3.2 µm/y respectively. These are quite different to the corrosion rate given in the analysis of MiniCan 3 (Smart et al. 2012), where the iron mass loss sample had an estimated corrosion rate of at least 500 µm/y. There are clear differences between the appearances of the iron mass loss samples after exposure of MiniCan 3 as compared to MiniCan 4 and 5. Although the samples from MiniCan 4 and 5 had clearly corroded as shown in Figure 4-22, the sample from MiniCan 3 was reported to have completely corroded, leaving only the graphite and corrosion products behind. The corroded surfaces on the samples from MiniCan 4 and 5 had a pitted appearance, with most mass loss mainly confined to one end of each sample, see Figure 4-22 and Figure 4-23 below. Full details of the mass loss analysis are given in Appendix 4 Mass loss.

Figure 4-22. *Iron mass loss samples M4 11:1 and M5 11:1 after pickling.*

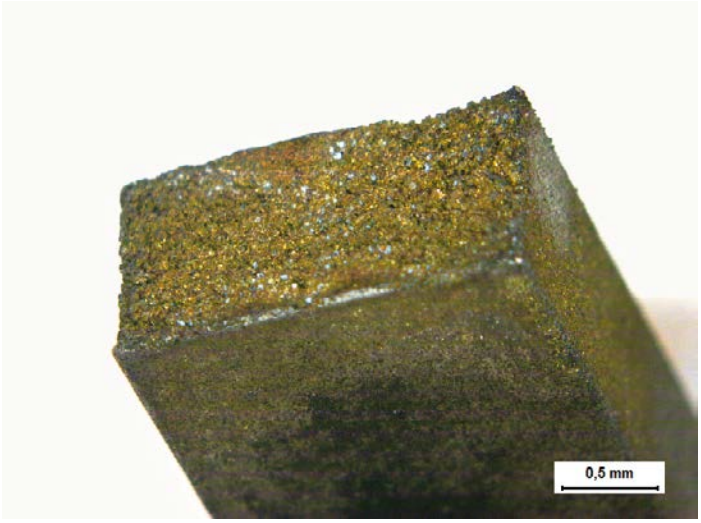

Figure 4-23. *Sample M5 11:1 with corrosion on the end of the sample.*

Both iron mass loss samples showed signs of material loss, particularly on one end (see Figure 4-23). The appearance of the material loss was that of selective corrosion, which is typical of cast iron corrosion, whereby the iron corrodes in preference to the graphite in the microstructure. SEM analysis of the iron mass loss sample M4 11:1 shows the typical nodules of graphite found in ductile iron and locations where the iron has corroded and the graphite has been removed from the surface see Figure 4-24.

4.5.4 Copper-Iron sandwich specimen

In this section the examination of copper-iron sandwich specimens of MiniCan 4 (M4 14:1, M4 15:1) and MiniCan 5 (M5 14:1) is presented. The copper-iron sandwich specimen from MiniCan 4 was separated into its respective copper and iron halves in the glovebox and packed into two separate sample holders whilst the sandwich specimen from the MiniCan 5, that could not be separated whilst in the glovebox, was packed into one sample holder which is why it is denoted as only M5 14:1 (Figure 4-26). Corrosion products from the iron half of the sandwich were collected as sample M5 13:1, see Section 4.7.7.

As can be seen in Figure 4-25, the sandwich specimen from MiniCan 4 appeared relatively unaffected by corrosion but was partially covered with bentonite clay. The sandwich specimen from MiniCan 5 however, had a thick black surface deposit. Once the sample holder was open to the atmosphere outside of the glovebox the black deposit changed to a red-brown colour on the outer surface with a thinner, less voluminous, black deposit underneath nearer the surface of the copper component. The external and inner surfaces of M5 14:1 can be seen in Figure 4-28 and Figure 4-29.

Figure 4-27 shows the appearance of the sample directly after removal from the steel cage of the MiniCan 5 assembly, with a thick black deposit covering the entire sandwich specimen as well as the other iron specimens, and spreading out over the adjacent nylon support table. It is noteworthy that the rest of the support table did not have this deposit, suggesting that it originates from the iron specimens and not from any other of the samples nearby. The distribution of the deposit could also be related to how the support table was positioned in the borehole, with the deposits settling out towards the lowest point.

Raman analysis on M4 14:1 detected cuprite fluorescence and M4 15:1 with remaining bentonite, fluorescence and carbon. Raman analysis on M5 14:1 (exposed to air) detected Fe_3O_4 and sulphides on both the copper and iron components.

FTIR analyses of MiniCan 4 samples detected mainly bentonite as well as OH/H_2O, H_2O, SO_4^{2-} and C-H on M4 14:1, and CO_3^{2-}, SO_4^{2-} and C-H on M4 15:1. M5 14:1 had SO_3^{2-}, CO_3^{2-}, H_2O, and OH^- detected.

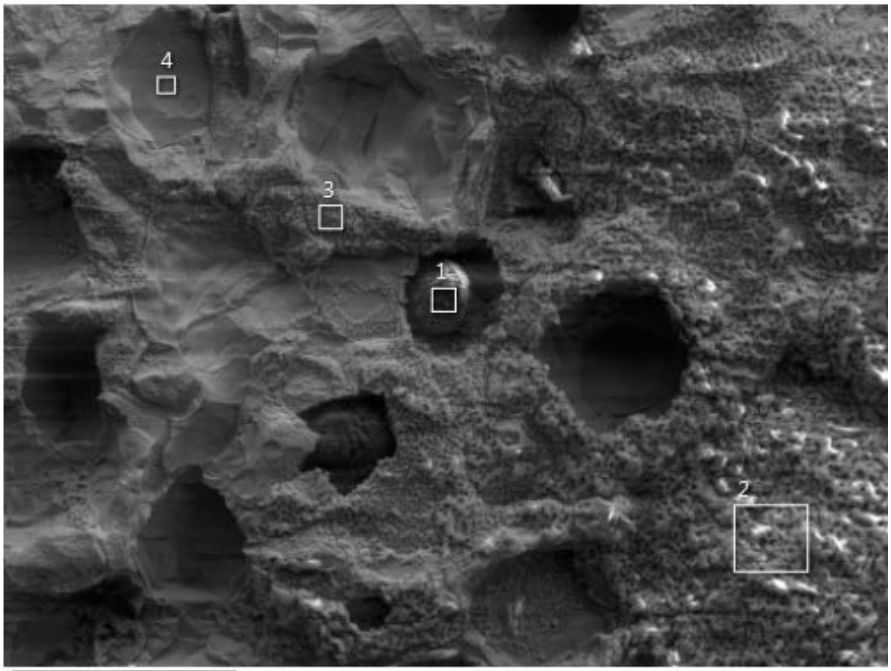

Element (Wt%)	1	2	3	4
C	93.33	5.77	3.91	1.87
O	4.05	29.56	22.01	1.84
Na	0.06	2.03	1.77	0.09
Mg	0.14		0.04	0.10
Al		0.06	0.04	
Si	0.07	1.58	2.08	2.11
P		0.12		
S	0.11	0.44	0.26	0.26
Cl	0.09	1.01	0.57	0.03
Ca	0.09		0.09	
Fe	2.07	59.43	69.23	93.69
Total:	100.00	10 0.00	100.00	100.00

Figure 4-24. *Corroded area of iron mass loss sample M4 11:1 from SEM analysis. A nodule of graphite can be seen at point 1. Points 2 and 3 consisted of mainly Fe and O, whilst point 4 was mainly Fe.*

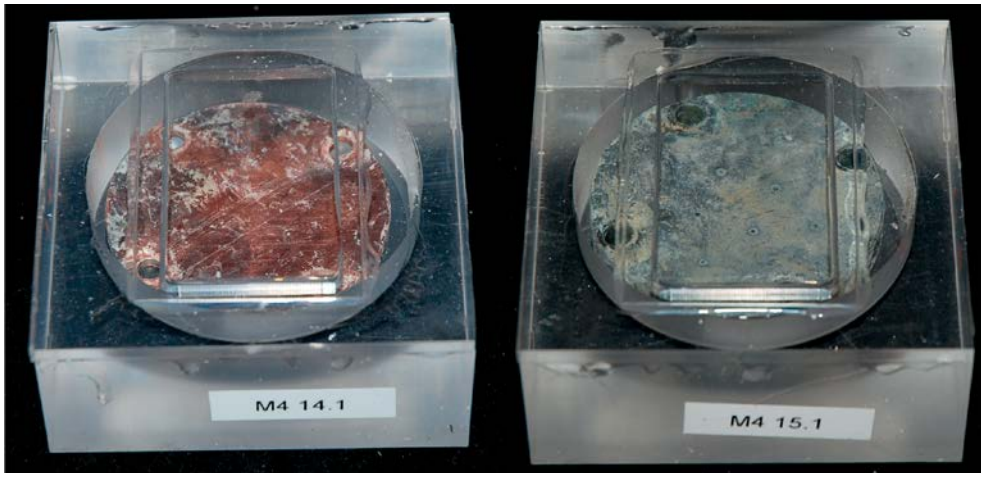

Figure 4-25. *Copper (M4 14:1) and iron (M4 15:1) parts of the sandwich specimen after removal from MiniCan 4.*

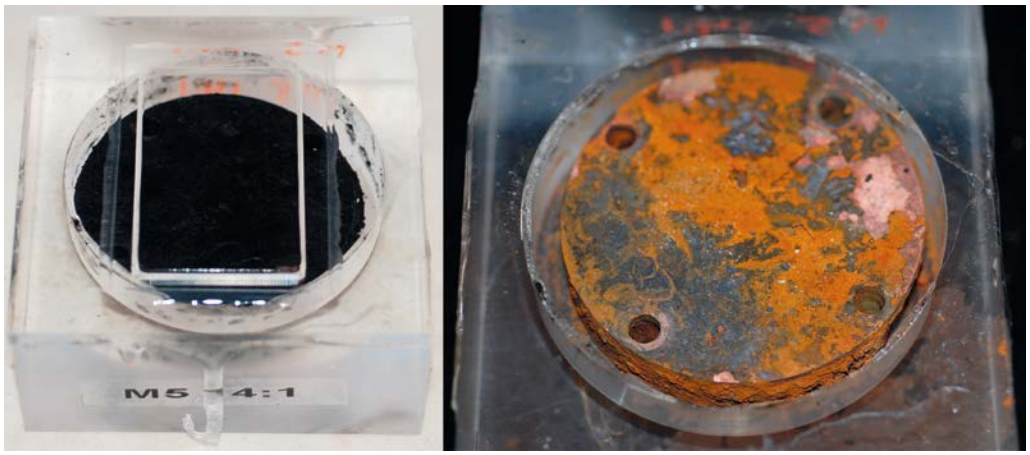

Figure 4-26. *M5 14:1 directly after removal from MiniCan 5, and shortly after the lid on the sample holder accidently came loose. Only the copper half can be seen in the photograph, but with iron corrosion products on the surface.*

Figure 4-27. *Copper-Iron sandwich sample M5 14:1 seen on the left hand side of the figure, directly after withdrawal from the MiniCan assembly. The outer surfaces are covered in a thick black deposit which also covers the adjacent areas of the support table.*

XRD analyses on M4 14:1 detected Cu and SiO_2 and Fe and SiO_2 on M4 15:1. Analysis of M5 14:1 was not possible due to the amorphous nature of the deposit.

SEM/EDS on the MiniCan 4 samples detected mainly bentonite. Analysis on the copper component of M5 14:1 detected mainly Fe and O on the orange deposit, and mainly Cu and S on the thinner black deposit.

The analyses suggest that oxides and sulphides/sulphates of Cu and Fe were present on the MiniCan 5 sample surfaces, with some water, carbonates as well as some Si and Cl. Sulphates may be oxidation products of sulphide. Summarized results from the analysis are given in Table 4-9 and Table 4-10.

Table 4-9. Analysis summary of copper-iron sandwich specimens M4 14:1 and M4 15:1.

Exposure to air before analyses	Method	M4 14:1 Cu component	M4 15:1 Fe component
None	Raman	Cu_2O fluorescence	C, fluorescence
Short period	FTIR	Bentonite, OH/H_2O, H_2O, SO_4^{2-}, C-H	CO_3^{2-}, SO_4^{2-}, C-H
Extended period	SEM/EDS	C, O, Na, Mg, Al, Si, S, Cl, K, Ca, Fe, Cu	C, O, Na, Mg, Al, Si, S, Cl, K, Ca, Fe
Extended period	XRD	Cu, SiO_2	SiO_2, Fe
Likely compounds on surfaces before exposure to air		Cuprite, bentonite, iron sulphides, chloride	Carbon, bentonite, iron sulphide, chloride

Table 4-10. Analysis summary of copper-iron sandwich specimens M5 14:1 (sample holder lid accidentally opened before Raman analyses).

Exposure to air before analyses	Method	M5 14:1 Cu component	M5 14:1 Fe component
Extended period	Raman	Fe_3O_4, sulphides	Fe_3O_4, sulphides
Extended period	FTIR	SO_3^{2-}, CO_3^{2-}, H_2O, OH^-	–
Extended period	SEM/EDS	C, O, Na, Mg, Al, Si, S, Cl, Ca, Cr, Fe, Ni, Cu	–
Possible compounds identified on surface *after* exposure to air		Magnetite, sulphides, chloride	Magnetite, sulphide, presumably also chloride

According to Smart and Rance (2009) the cast iron component had been machined to create a crevice of varying width with the copper component, varying from nominally 0 mm to 0.03 mm in 0.01 mm increments at 10 mm intervals from the circumference in towards the centre of the circular components. In addition to this $9 \times \varnothing 1$ mm holes had been drilled through the iron component (visible in Figure 4-31). This sample was denoted as a crevice-expansion sample, and was designed to test the combined effects of crevice corrosion as well as any expansive effects of iron corrosion coupled to copper.

No visible corrosion could be seen on the samples from MiniCan 4, and the surface analyses did not detect any of the corrosion products as found on M5 14:1. Due to the presence of visible corrosion products on sample M5 14:1 it was not immediately possible to ascertain if crevice corrosion had occurred between the iron and copper components of the sandwich. After removal of the corrosion products by pickling, the inner surface of the iron component was inspected in a microscope. In general, the inner surface displayed extensive corrosion at the surfaces adjacent to the $\varnothing 1$ mm holes, see Figure 4-33.

Crevice corrosion occurs in small gaps where local conditions can develop (anodic sites) which differ to those immediately outside the crevice (cathodic sites). The threat of crevice corrosion in anaerobic conditions should be small due to the lack of oxygen. According to Smart et al. (2005) the corrosion rate of iron coupled to copper in anaerobic groundwater conditions is similar to that of uncoupled iron in similar exposure conditions. Without oxygen, the cathode reaction is water reduction and hydrogen evolution, which by its nature leads to a slower corrosion reaction than oxygen reduction.

Corrosion at the edge of the iron component of MiniCan 5 was also found, mainly on one side, with another area of material loss on the opposite edge (see Figure 4-28). The use of polymeric bolts to hold the samples together may have resulted in slightly uneven contact between the mating surfaces, therefore creating crevices at certain locations around the circumference of the sample. If this occurred it could explain why there has been corrosion at two distinct areas on the iron sample rather than around the whole circumference. The corrosion can be seen in Figure 4-30 on the right hand side, at approximately the 7 o'clock and 11 o'clock positions of the sample.

It was clear though that the external surface of the iron component of M5 14:1 had suffered significant material loss compared to the iron mass loss sample M5 11:1. Measurements carried out with calibrated callipers suggest approximately 3 mm of material had corroded from the diameter of the sample during the exposure. After pickling it was clear that the corrosion was in the form of wide and deep pits on the outer surfaces. The morphology of these pits is similar to those seen for under-deposit corrosion and when MIC occurs on metal surfaces. This is in agreement with the results of the microbial analyses report for MiniCan 4 and 5 (Hallbeck et al. 2017) where SRB colonies on the surface of the specimen are reported. An estimation of the maximum corrosion rate over the exposure period gives 3 mm / 8.81 years = ~340 µm/year.

Figure 4-28. *External surfaces of sample M5 14:1 sandwich specimen, copper on the left, iron on the right. The external surfaces of both components were covered with a thick deposit consisting mainly of iron corrosion products. The iron specimen had significant material loss after the exposure, seen here at the 6 o'clock and 10 o'clock positions.*

Figure 4-29. *Inner surfaces or sample M5 14:1 sandwich specimen, copper on the left, iron on the right. The internal surfaces of the components were covered with iron corrosion products. The iron component had significant material loss as seen on the bottom left hand corner of the iron specimen to the right. The shiny area on the bottom right of the copper sample is the mating surface to the corroded area of the iron sample.*

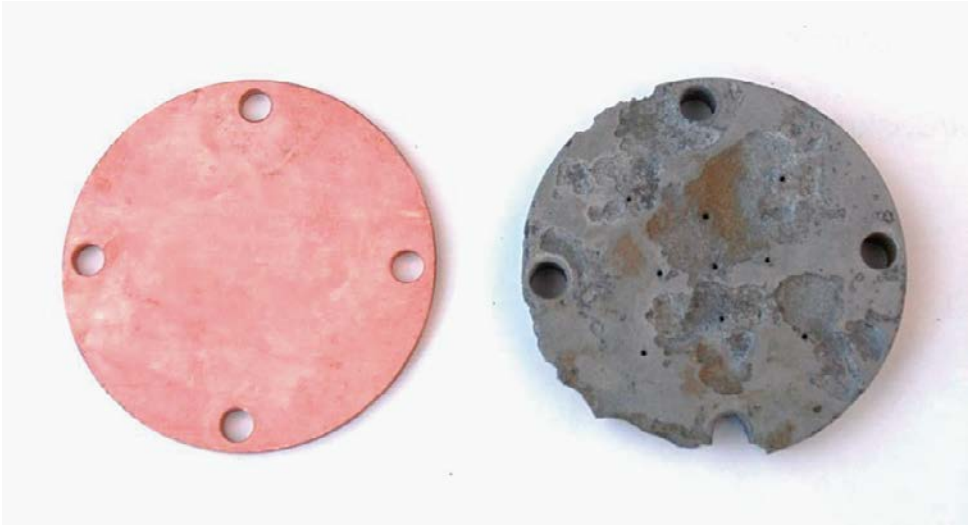

Figure 4-30. *External surfaces of sample M5 14:1 sandwich specimen after corrosion products have been removed by pickling. The copper component appeared intact whilst the iron component was heavily corroded in localised areas. The main wide pits on the outer surface ranged from 1–3 mm in depth, and the mass loss from the edges was up to 3 mm measuring across the circumference.*

Figure 4-31. *The inner surfaces of M5 14:1 sandwich specimen after pickling. The copper component is visibly uncorroded, whilst the iron component does not appear to be as corroded compared to the outer surface. The edges of the iron component are corroded however, and these correspond to contact points with the copper component when assembled.*

Figure 4-32. *Detail of iron component M5 14:1 after pickling. The wide pits shown here on the outer surface range from 1 -3 mm in depth.*

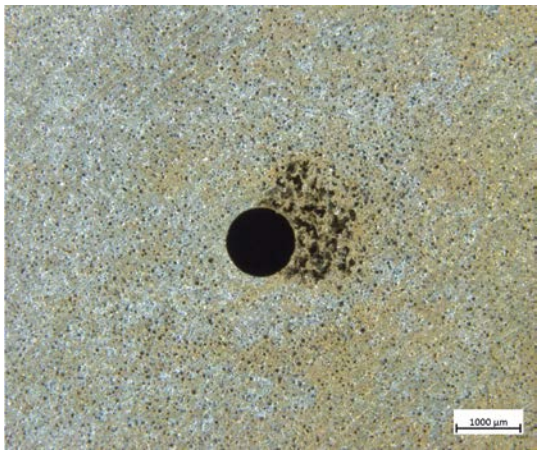

Figure 4-33. *Corrosion found around the ∅ 1 mm holes on the inner surface of the cast iron component of the sandwich specimen from MiniCan 5 (M5 14:1).*

4.5.5 Pt, Au, Ag/AgCl electrodes and Pt/Ti counter electrode

In this section the examination of various electrodes mounted in the MiniCan assemblies is presented. The electrodes are Pt from MiniCan 4 (M4 16:1), Au from MiniCan 4 (M4 17:1), Pt/Ti counter electrode from MiniCan 4 (M4 20:1), Pt from MiniCan 5 (M5 16:1), Au from MiniCan 5 (M5 17:1), Ag/AgCl from MiniCan 5 (M5 18:1), and Pt/Ti counter electrode from MiniCan 5 (M5 20:1).

Figure 4-34 to Figure 4-37 show the appearance of the measurement electrodes after removal from MiniCan 4 and 5. The Ag/AgCl electrodes could not be found amongst the dense bentonite clay of MiniCan 4. One of the Ag/AgCl electrodes was lost during the dismantling and sampling of MiniCan 5. Raman analyses detected only fluorescence for MiniCan 4 samples, and sulphide, carbon and iron oxide on the MiniCan 5 samples. No other analyses were carried out on these samples. See Table 4-11 for a summary of the results.

Table 4-11. Analysis summary of Pt, Au, Ag/AgCl electrodes and Pt/Ti counter electrode.

Exposure to air before analyses	Method	M4 samples	M5 samples
None	Raman	Fluorescence	Sulphide, carbon, iron oxide
Likely compounds on surfaces before exposure to air		Bentonite	Iron sulphide, iron oxide, carbon

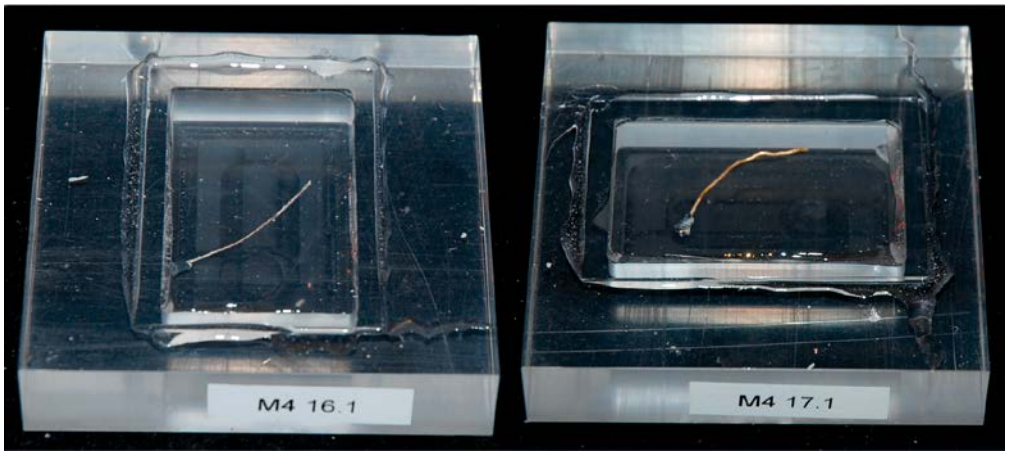

Figure 4-34. *M4 16:1 and 17:1, Pt and Au electrodes.*

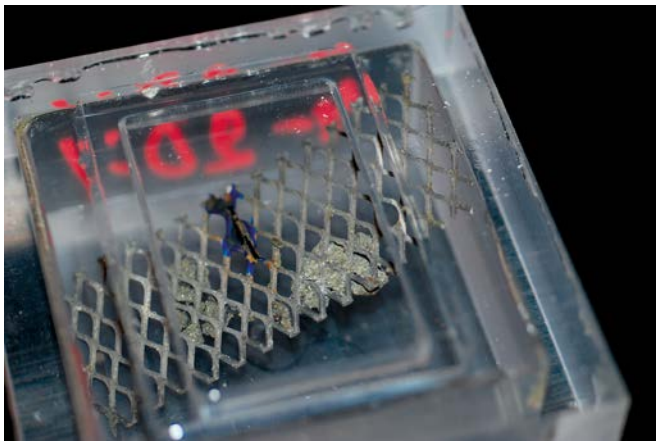

Figure 4-35. *M4 20:1 Pt/Ti counter electrode.*

Figure 4-36. *M5 16:1 and 17:1 Pt and Au electrodes.*

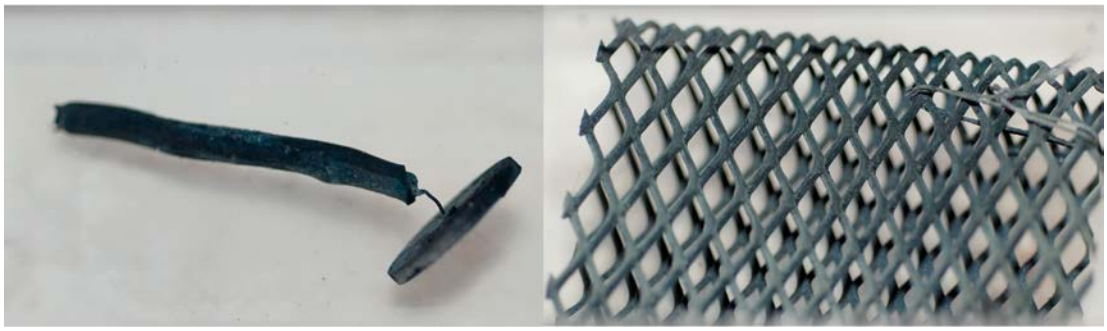

Figure 4-37. *M5 18:1 and 20:1 Ag/AgCl electrode and detail of the Pt/Ti counter electrode.*

4.6 Hydrogen content of copper canister

This section presents measurements of the hydrogen content in samples of the copper canister in MiniCan 4 (M4 21:1, M4 22:1, M4 23:1) and MiniCan 5 (M5 21:1, M5 22:1, M5 23:1).

Samples from the copper canisters were taken with the aim of investigating the hydrogen content at different positions through the wall thickness of the canisters. Sampling was carried out by cutting samples from the canister whilst it was inside the glovebox, and the samples were then placed directly into liquid nitrogen in order to preserve any hydrogen that was contained within the material. The risk of hydrogen diffusing out of the copper during cutting operations due to high temperatures was identified as a risk during the planning phase. As a precaution an infra-red thermometer was used to monitor the surface temperature of the samples as they were cut in the glovebox, and the highest temperature measured was 120 °C for MiniCan 5 before groundwater was used to cool the sample during cutting, then 50 °C was the highest temperature measured. The highest temperature measured during cutting samples from MiniCan 4 was 30 °C.

The samples were transferred to Swerea KIMAB for analysis, still in liquid nitrogen, after completion of the sampling for each experiment. In order to carry out the analysis it was necessary to first extract a smaller sample from each of the sections cut from the canister and then slice this sample into four further samples (each sample had a thickness of 1.2 mm and a mass of circa 1 g) which represented different positions through the 7.5 mm wall thickness of the canister – outer wall, middle 1, middle 2 and inner wall of canister (see Figure 4-38). Each sample was also taken in double to produce a larger dataset for evaluation.

A liquid cooled circular saw of type Struers Accutom 50 was used to prepare the samples. Using a Leco Rhen 602 instrument the slices were analysed for hydrogen content using melt-extraction, the results of which can be seen in Figure 4-39 and Figure 4-40. Tabulated results can be found in Appendix 5 Hydrogen content analysis.

The results of the tests show that there was variation in hydrogen content through the thickness of the canister wall. Sample 21:1 - 2 (Middle 1) from MiniCan 4 had an anomalous result, and this was deemed to be due to a surface deposit that was visually noted on the sample prior to analysis, that was almost certainly due to handling during sampling.

There was a slight tendency for higher hydrogen content from the samples positioned towards the inner and outer surfaces of the canister wall with the samples analysed from MiniCan 5. This pattern was not as clear for the samples analysed from MiniCan 4. However, the amount of hydrogen measured in the tests is deemed to be representative to reference material tested previously of approximately 0.6 ppm (Martinsson et al. 2013) (unexposed canister material) but higher than that detected of approximately 0.4 ppm in Taxén et al. (2012) (exposed canister material, different conditions to MiniCan). In both of these previous studies the analysis technique was the same to this work; however the exposure conditions were not identical. For MiniCan 4 the average (mean) hydrogen content measured was 0.76 ppm with a minimum value of 0.58 ppm and maximum value of 1.37 ppm measured. For MiniCan 5 the average hydrogen content measured was 0.87 ppm with a minimum value of 0.60 ppm and maximum value of 1.78 ppm measured.

For reference, analyses of hydrogen content from MiniCan 3 gave results of 0.54 ppm for the outer surface and 0.59 ppm for the inner surface (Smart et al. 2012), although the analysis technique differed from this work. Hydrogen on the surface may to some extent be included in the results even if measures were taken to remove surface hydrogen.

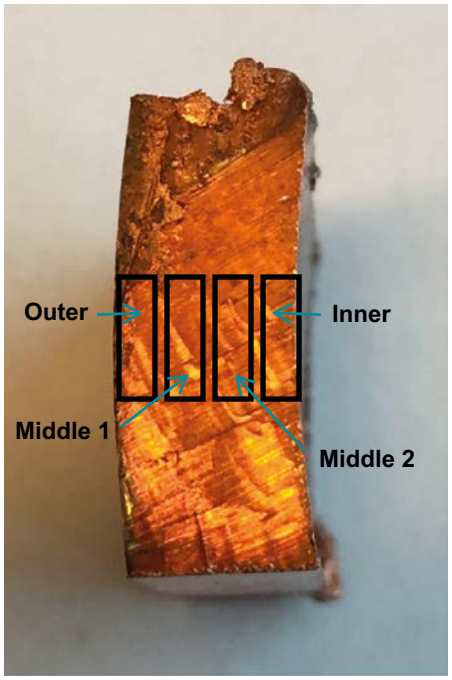

Figure 4-38. *Sampling of copper canister wall for measurement of hydrogen content. Four 1.2 mm thick samples each weighing approximately 1 g were taken from the samples of the canister.*

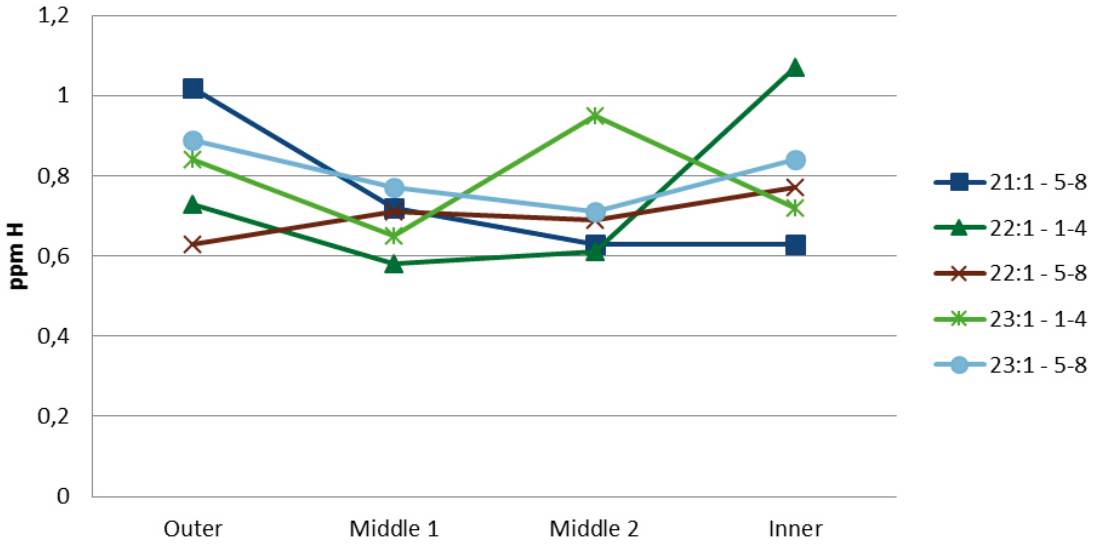

Figure 4-39. *Hydrogen content results from MiniCan 4 copper canister samples. Samples 21:1:1–4 are not shown in this figure as 21:1–2 gave an anomalous result. They can however be seen in Appendix 5 Hydrogen content analysis.*

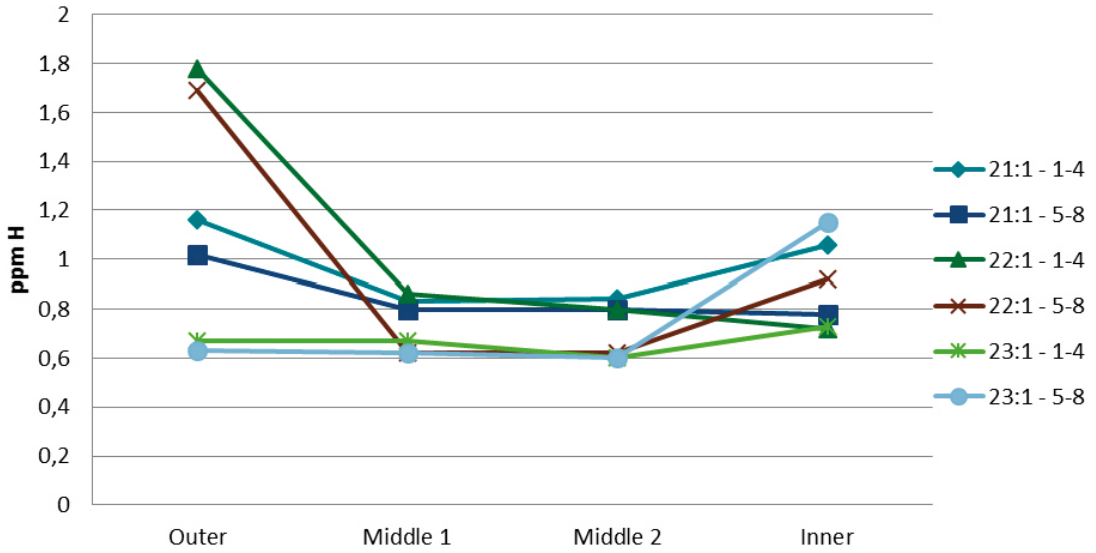

Figure 4-40. *Hydrogen content results of MiniCan 5 copper canister samples.*

4.7 Samples from MiniCan copper canisters and cast iron inserts

4.7.1 Inner surface of copper canister

This section contains results from examination of the inner surfaces of the copper canisters in MiniCan 4 (M4 24:1) and MiniCan 5 (M5 24:1), see photos in Figure 4-41 and Figure 4-42.

The inner surfaces of the copper canister from both MiniCan 4 and 5 appeared to have a black deposit partially covering the surface. The deposit seemed to be relatively thin and tightly adhered to the surface. Raman analysis detected only fluorescence from cuprite for MiniCan 4 and peaks for magnetite and fluorescence from cuprite for MiniCan 5, see Figure 4-43.

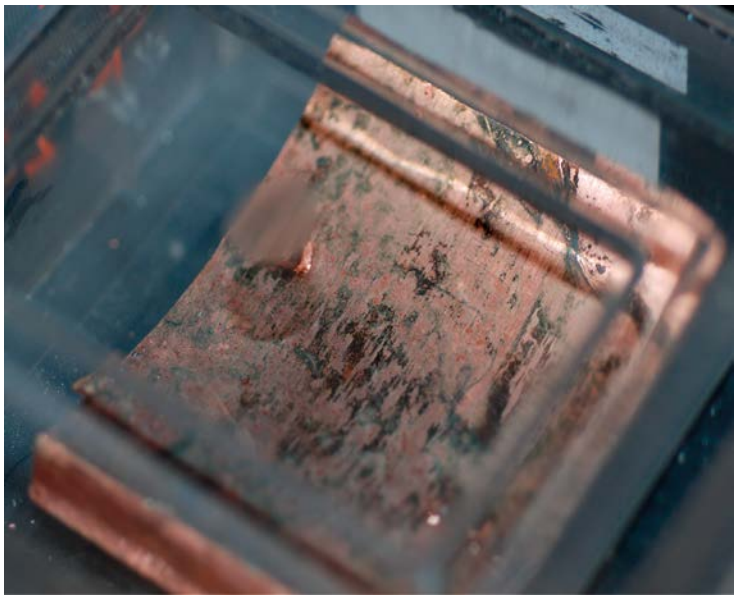

Figure 4-41. *Inner canister surface sample M4 24:1 contained in its sample holder.*

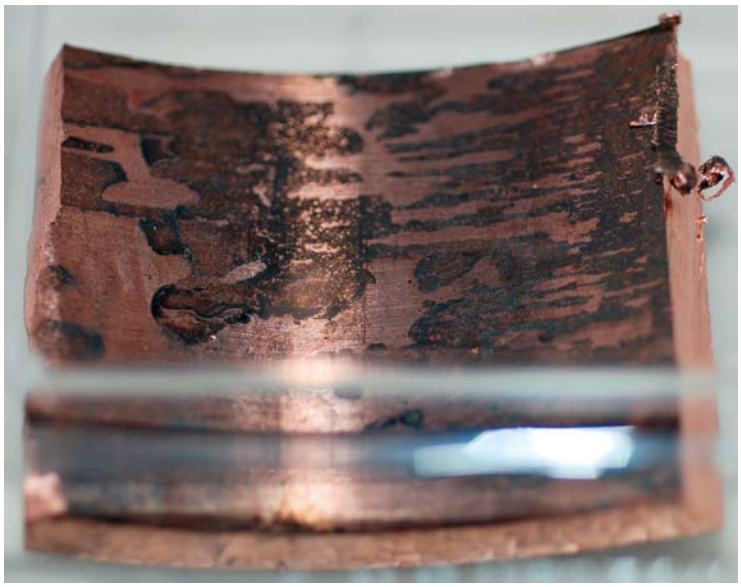

Figure 4-42. *Inner canister surface sample M5 24:1 contained in its sample holder.*

FTIR analysis detected SO_3^{2-} and/or Si-O, OH and C-H on M4 24:1 and SO_3^{2-}, possibly Si-O, CO_3^{2-}, H_2O/OH, C-H on M5 24:1. XRD analysis of M4 24:1 detected Cu, SiO_2, and of M5 24:1 detected Cu and Cu_2O. SEM/EDS analysis detected on M4 24:1 C, Cu, Fe, Si, O, Cl and on M5 24:1 Cu, Fe, O, Cl, C. XPS analysis was carried out on M5 24:1 as well as M5 25:1 (see Section 4.7.2), and from these analyses copper species of both valence states (I) and (II) including oxides, chlorides and hydroxide, as well as Ca, C, S and Si were detected. The analysis method characterises the top 1 nm of the sample surface, and showed that M5 25:1 was more oxidised than M4 24:1. Further details are given in Appendix 6 XPS GDOES LAICPMS analyses. A summary of the results from the analyses is given in Table 4-12.

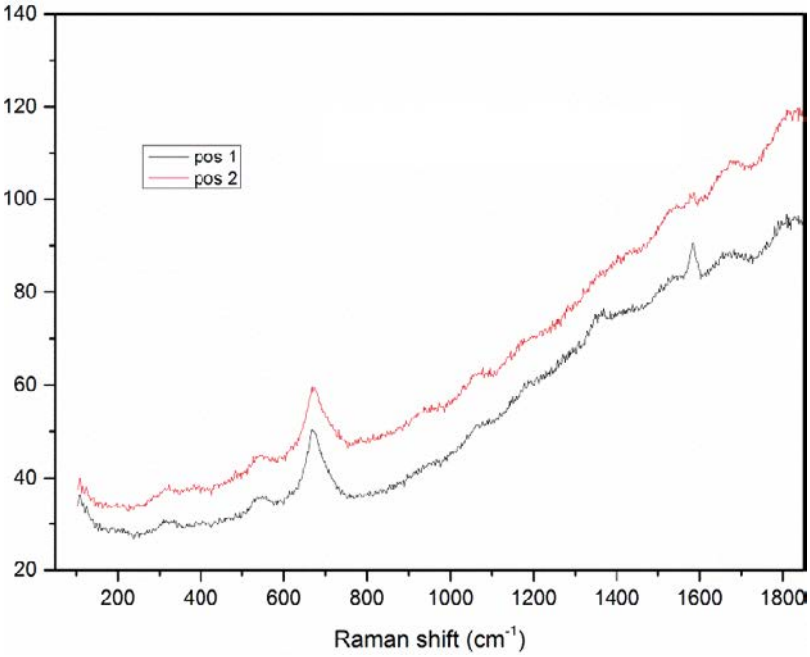

Figure 4-43. *Raman spectra from M5 24:1.*

Table 4-12. Analysis summary of the Cu canister inside M4 24:1 and M5 24:1.

Exposure to air before analyses	Method	M4 24:1 Cu canister inside	M5 24:1 Cu canister inside
None	Raman	Cu_2O fluorescence	Fe_3O_4, Cu_2O fluorescence
Short period	FTIR	Si-O/SO_3^{2-}, OH, C-H	SO_3^{2-}, Si-O, CO_3^{2-}, H_2O/OH, C-H,
Extended period	SEM/EDS	C, O, Na, Mg, Al, Si, S, Cl, Ca, Fe, Cu	C, O, Na, Al, Si, S, Cl, Ca, Cr, Fe, Cu
Extended period	XRD	Cu, SiO_2	Cu, Cu_2O
Extended period	XPS	–	Cu, Cu(I) and Cu(II) species, $Cu(OH)_2$, $CuCl_2$, possibly CuCl, copper oxides, Ca, C, S, SiO_2
Likely compounds on surfaces before exposure to air		Cuprite, iron sulphide, chloride	Magnetite, cuprite, iron sulphide, copper chloride

4.7.2 Outer surface of copper canister

This section contains results from the examination of the outer surfaces of the copper canisters of MiniCan 4 (M4 25:1) and MiniCan 5 (M5 25:1).

There was a marked difference in appearance between the outer surfaces of MiniCan 4 and 5, with MiniCan 5 having a thin black surface deposit asymmetrically distributed towards one side of the canister (presumably the downward side in the bore hole, see Figure 2-2), while MiniCan 4 seemed rather clean except for the layer of bentonite that remained after sampling (Figure 2-6). See Figure 4-44 and Figure 4-45 for photos of the samples. SEM analysis of cross sectioned samples showed no distinct areas of corrosion on MiniCan 4, and very little corrosion on MiniCan 5, see Figure 4-47 and Figure 4-48.

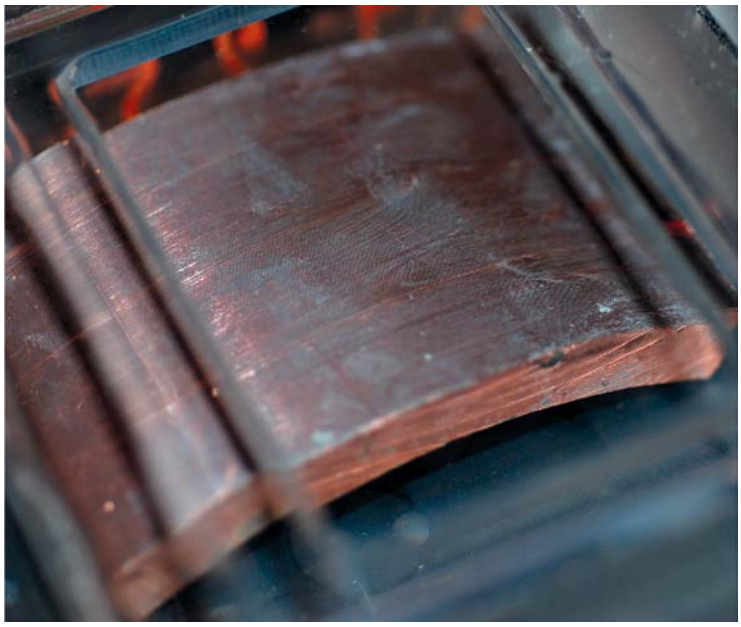

Figure 4-44. *Canister outer surface sample M4 25:1 contained in its sample holder.*

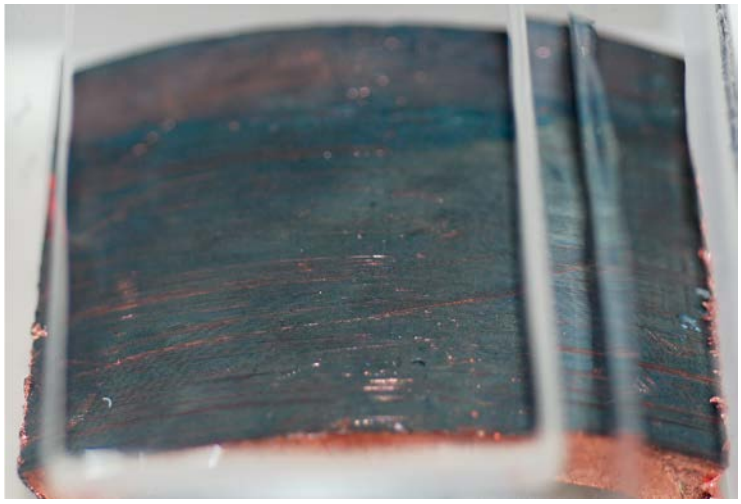

Figure 4-45. *Canister outer surface sample M5 25:1 contained in its sample holder.*

Raman analysis of the sample surfaces detected mainly fluorescence from cuprite, but also sulphide on MiniCan 4 and carbon on MiniCan 5, Figure 4-46. FTIR analysis detected Bentonite, OH/H_2O, C-H, SO_4^{2-} on M4 25:1 and SO_3^{2-} (possibly Si-O groups), CO_3^{2-}, H_2O/OH, C-H on M5 25:1.

XRD analysis detected Cu, CuO on M4 25:1 and on M5 25:1 Cu, $Cu(OH)_2 \cdot H_2O$, NaCl, CuO. SEM/EDS analysis detected Cu, Fe, Si, Na, Al, O, Cl on M4 25:1 and on M5 25:1 Cu, Fe, Ca, Ti, O, Cl.

As mentioned above for sample M4 25:1, XPS analysis on M5 25:1 detected Cu, copper species of both valence states (I) and (II) including oxides, chlorides and hydroxide , as well as Ca, C, S and Si on the surface. GDOES and LAICPMS analyses were also carried out and detected O, S, Fe, C, N, Si, Cr, P, Na, Al and Cu, Fe, Si, Ca, Cl, S, Na, Mg respectively. See Appendix 6 XPS GDOES LAICPMS analyses for more details. A summary of results obtained is shown in Table 4-13.

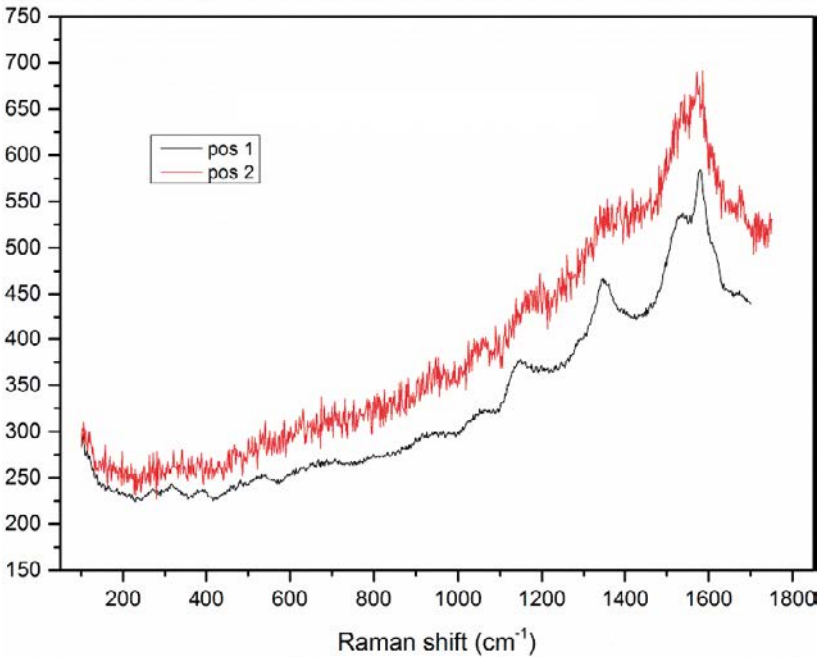

Figure 4-46. *Raman analysis of outer canister surface sample M5 25:1 with peaks for carbon and fluorescence from cuprite.*

Table 4-13. Analysis summary of the of the Cu canister outside, M4 25:1 and M5 25:1.

Exposure to air before analyses	Method	M4 25:1 Cu canister outside	M5 25:1 Cu canister outside
None	Raman	Sulphide, Cu_2O fluorescence	C, Cu_2O
Short period	FTIR	Bentonite, OH/H_2O, C-H, SO_4^{2-}	SO_3^{2-}, CO_3^{2-}, H_2O/OH, C-H, Si-O
Extended period	SEM/EDS	C, O, Na, Mg, Al, Si, P, S, Cl, Ca, Ti, Mn, Fe, Cu	C, O, Na, Al, Si, S, Cl, Ca, Ti, Cr, Fe, Cu
Extended period	XRD	Cu, CuO	Cu, $Cu(OH)_2.H_2O$, NaCl, CuO
Extended period	GDOES	–	O, S, Fe, C, N, Si, Cr, P, Na, Al
Extended period	LAICPMS	Cu, Si, Al, Ca, Cl	Cu, Fe, Si, Ca, Cl, S, Na, Mg
Extended period	XPS	–	Cu, Cu(I) and Cu(II) species, $Cu(OH)_2$, CuCl and/or $CuCl_2$, copper oxides, Ca, C, Cl, SiO_2
Likely compounds on surfaces before exposure to air		Sulphides, including iron sulphide, bentonite, cuprite	Sulphides including iron sulphide, cuprite, carbon, copper chloride

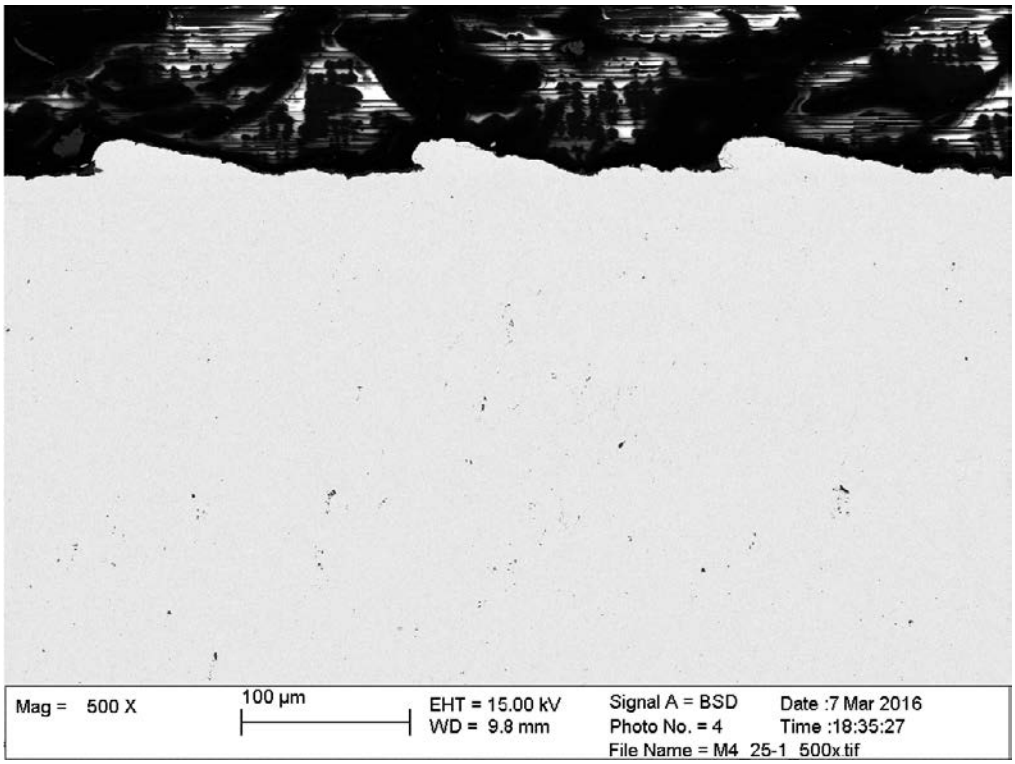

Figure 4-47. *Cross section of outer surface of copper canister from MiniCan 4 (M4 25:1) showing the machining marks. Frequently occurring pits of a few µm depth can also be seen.*

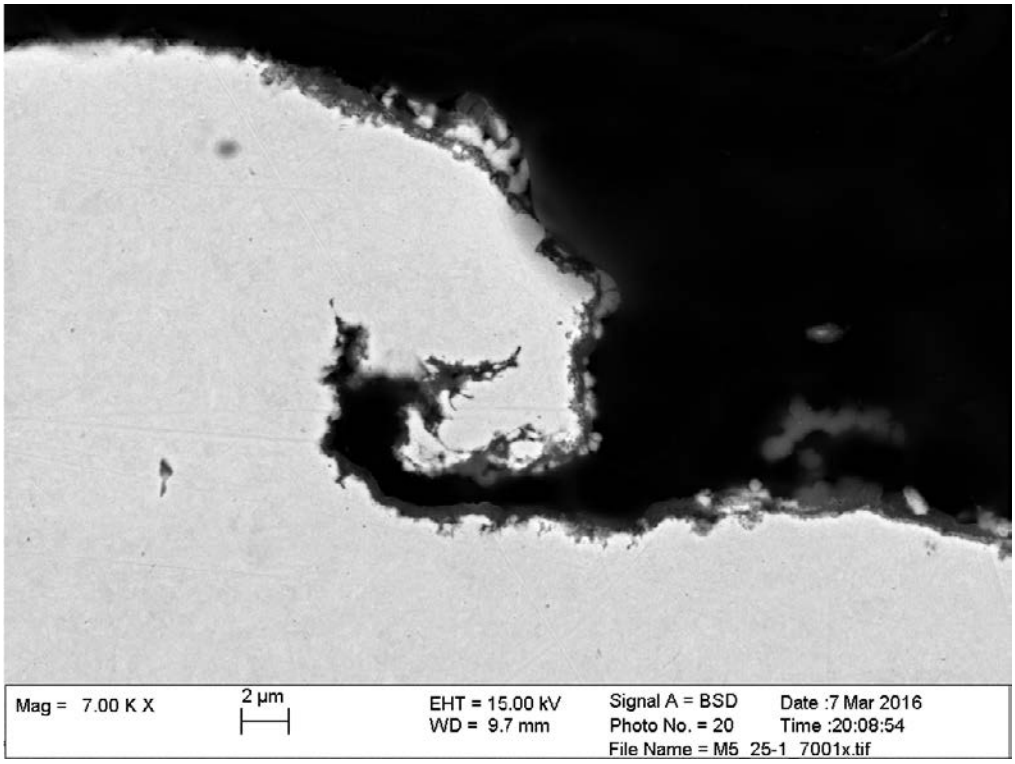

Figure 4-48. *Cross section of outer surface of copper canister from MiniCan 5 (M5 25:1) showing one of the machining marks. Some pits could be found on the surface of the sample with depths of approximately 2 µm, the surface did appear rougher than that of M4 25:1 and the machining marks were not as distinct. Further details can be found in Appendix 10 SEM/EDS analysis.*

4.7.3 Welds on copper canister

This section concerns samples containing the EB (electron beam) weld in the copper canisters of MiniCan 4 (M4 26:1) and MiniCan 5 (M5 26:1). Photos are included in Figure 4-49 and Figure 4-50.

The surfaces of the weld samples were similar to those of the outer surface of the copper canisters, with M4 26:1 having a layer of bentonite over the whole surface, whilst M5 26:1 had a thin black deposit on the surface. Raman analysis detected peaks for carbon and possible calcite or sulphate for MiniCan 5, but only fluorescence from cuprite for MiniCan 4. SEM analysis of cross sectioned samples detected very few pits on MiniCan 4, and very little corrosion on MiniCan 5, see Figure 4-52 and Figure 4-48.

Figure 4-49. *Top weld of copper canister sample M4 26:1.*

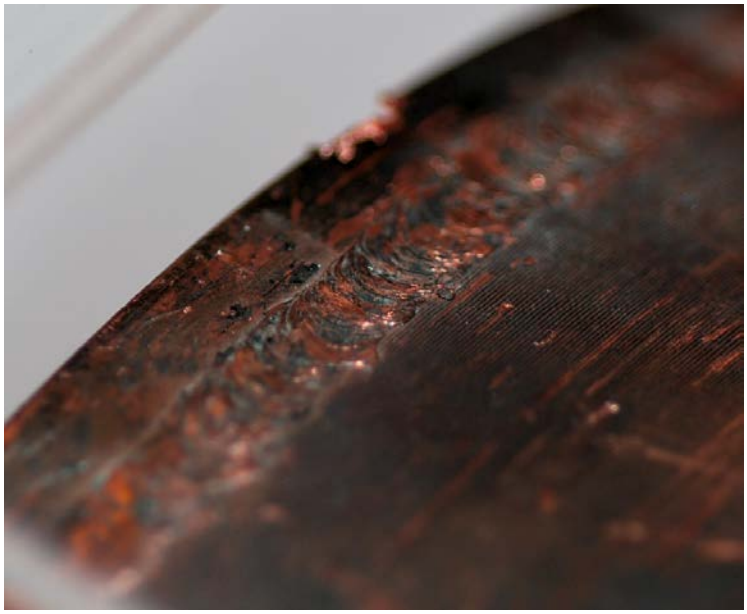

Figure 4-50. *Top weld of copper canister sample M5 26:1.*

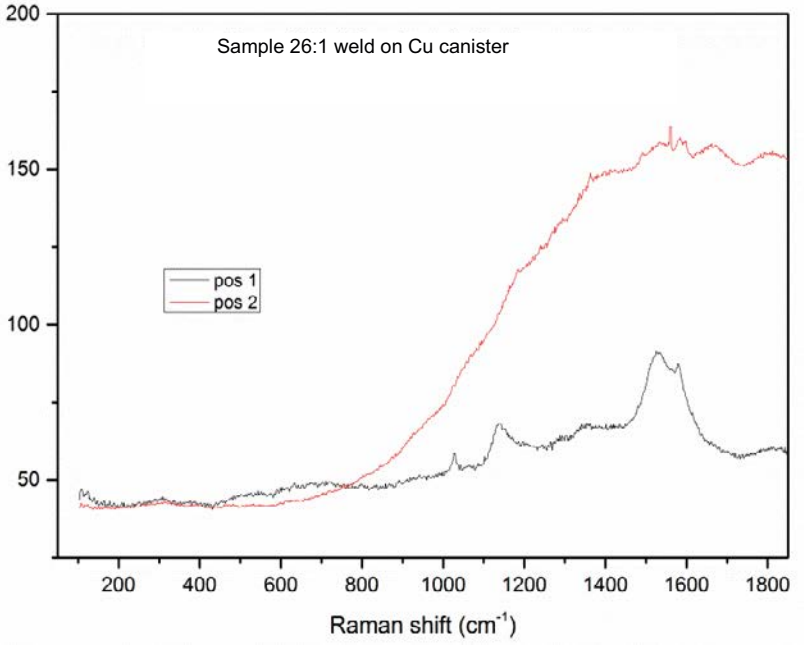

Figure 4-51. *Raman spectra for sample canister weld sample M5 26:1 showing peaks for carbon, and possible calcite or sulphate from position 1, as well as cuprite fluorescence from position 2.*

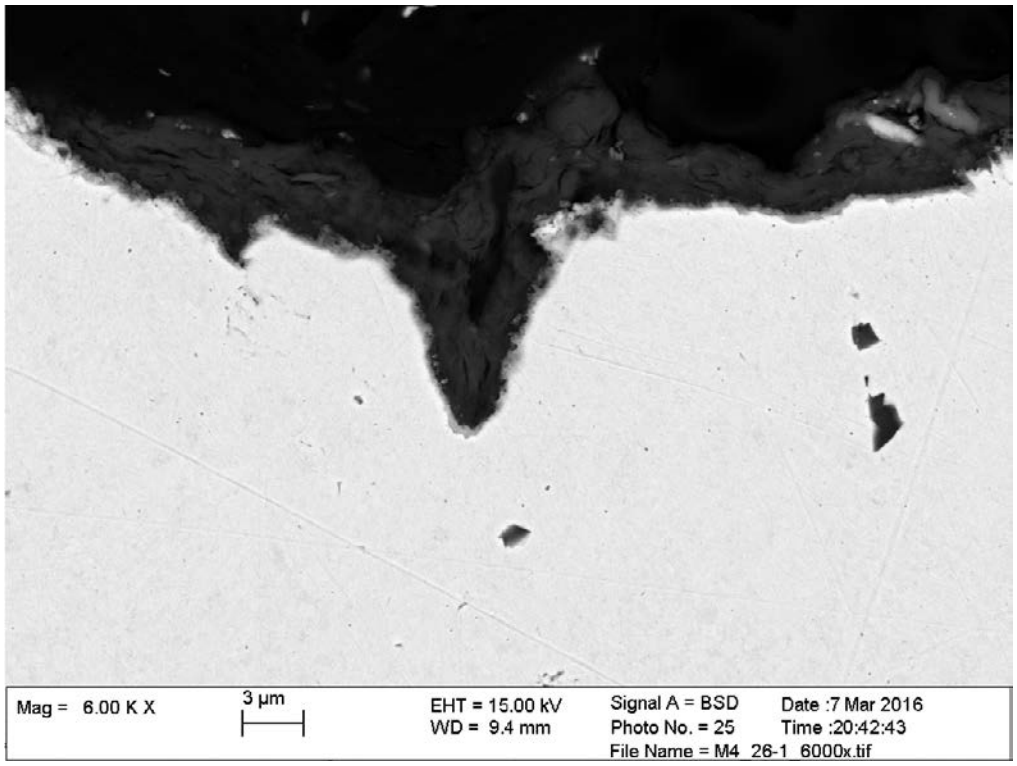

Figure 4-52. *Cross section of weld sample from MiniCan 4 (M4 26:1) displaying a pit with a depth of ca 5 µm, containing Cu, O, Si and C.*

FTIR analysis of M4 26:1 detected Bentonite, OH/H_2O, C-H, SO_4^{2-}, Si-O and of M5 26:1 detected SO_4^{2-}, CO_3^{2-}, H_2O/OH. XRD detected Cu and SiO2 on M4 26:1 and only Cu on M5 26:1. SEM/EDS analysis detected Cu, Fe, Si, Ca, Al, O, S, Cl, on M4 26:1 and Cu, Fe, Si, Al, Cr, O on M5 26:1. Results from the analysis are summarized in Table 4-14.

Table 4-14. Analysis summary of Cu canister EB weld, M4 26:1 and M5 26:1.

Exposure to air before analyses	Method	M4 26:1 Cu EB weld	M5 26:1 Cu EB weld
None	Raman	Fluorescence	C, $CaCO_3$, SO_4^{2-}, Cu_2O
Short period	FTIR	Bentonite, OH/H_2O, C-H, SO_4^{2-}	SO_4^{2-}, CO_3^{2-}, H_2O/OH
Extended period	SEM/EDS	C, O, Na, Mg, Al, Si, S, Cl, Ca, Ti, Fe, Cu	C, O, Na, Al, Si, S, Cl, K, Ca, Ti, Cr, Fe, Ni, Cu
	XRD	Cu, SiO_2	Cu
Likely compounds on surfaces before exposure to air		Bentonite, sulphate, chloride, iron sulphide	Calcite, sulphate, cuprite, chloride, iron sulphide, carbon

4.7.4 Surfaces near holes in copper canister

This section concerns samples containing the pin holes in the copper canisters of MiniCan 4 (M4 27:1) and MiniCan 5 (M5 27:1), se photos in Figure 4-53 and Figure 4-54.

The inner surfaces of the copper canister at the positions of the ∅1 mm holes had a surface deposit that was green and black in colour. The deposit seemingly emanated from the hole and had precipitated approximately 2 cm around the hole, but it is not known exactly how far the deposit spread over the rest of the inner canister surface.

Figure 4-53. *Sample M4 27:1 hole through copper canister, inner surface. The hole is located at edge between perpendicular surfaces as marked by the red circle.*

Figure 4-5. *Sample M5 27:1 hole through copper canister at top of MiniCan 5.*

MiniCan 4 had only one hole, near the top weld facing downwards in the borehole, whilst MiniCan 5 had two holes, both positioned at the top weld, one facing up and one facing down in the borehole. However, one of the holes on MiniCan 5 was mistakenly cut through during the sampling process. It is not certain which hole was successfully sampled, but it seems that it was the downward facing hole from the appearance of the outer surface of the sample which was black in colour.

Raman analysis of the surface deposit near the hole was difficult due to the geometry of the sample, and on both samples only carbon and cuprite fluorescence were detected. FTIR analysis of M4 27:1 detected only Si-O from bentonite or possible loose glass particles, and detected H_2O/OH, H_2O, SO_3^{2-}, C-H, Si-O on M5 27:1.

XRD analysis detected on M4 27:1 Cu and CuO, and detected Cu and Cu_2O on M5 27:1. SEM/EDS analysis detected Fe (high amounts) and O, with smaller amounts of Si and Al in the deposit on M4 27:1, and Fe, O, and Si on M5 27:1. A summary of results from the analysis is shown in Table 4-15.

Table 4-15. Analysis summary of Cu canister at pin-hole, M4 27:1 and M5 27:1.

Exposure to air before analyses	Method	M4 27:1 Cu canister pin-hole	M5 27:1 Cu canister pin-hole
None	Raman	C, fluorescence	Cu_2O fluorescence
Short period	FTIR	Bentonite	H_2O/OH, H_2O, SO_3^{2-}, C-H, possibly Si-O
Extended period	SEM/EDS	C, O, Na, Mg, Al, Si, S, Cl, K, Ca, Ti, Fe, Cu	C, O, Na, Si, S, Cl, Ca, Fe, Cu
Extended period	XRD	Cu, CuO	Cu, Cu_2O
Likely compounds on surfaces before exposure to air		Bentonite, carbon, iron sulphide, chloride	Cuprite, iron sulphide

4.7.5 Outer surfaces of cast iron insert

In this section, samples from the outer surfaces of the cast iron inserts from MiniCan 4 (M4 29:1, M4 29:2) and MiniCan 5 (M5 29:1) are examined. The iron insert of MiniCan 5 was vibrant green when still wet with groundwater but quickly turned greenish black with some reddish features upon drying, see Figure 4-55.

After drying, the appearance of the cast iron insert samples of MiniCan 4 and MiniCan 5 did not differ as much as when wet, see photos in Figure 4-56 and Figure 4-57. In general, the sample from MiniCan 4 had a thin layer of bentonite on it due to the handling inside the glovebox during the sampling procedure. Although the iron surfaces were black/greenish black and remained so in the sample holders. Once the iron samples were exposed to oxygen they quickly changed in appearance to a red/brown rust colour on some areas.

Raman analysis on M4 29:1 only detected carbon and fluorescence, most probably from iron oxide or bentonite. The Raman spectra obtained from MiniCan 5 however detected peaks for magnetite and carbon. FTIR analysis on M4 29:1 detected OH/H_2O, H_2O, SO_3^{2-}, SO_4^{2-}, CO_3^{2-}, Si-O, Fe-$SO_4 \cdot xH_2O$, and on M5 29:1 H_2O/OH, H_2O, SO_3^{2-}, SO_4^{2-}.

XRD analysis detected Fe and Fe_2O_3, on M4 29:1, and Fe, FeO(OH), $FeCl_3 \cdot 6H_2O$, Fe_3O_4, Fe_2O_3, and SiO_2 on M5 29:1. SEM/EDS analysis on M4 29:1 detected Fe, Si, Ca, Al, O, Cl, C and on M5 29:1 Fe, O, Cl, C.

The green colour suggests green rust, (Fe(II, III) double hydroxyl-salt with chloride, sulphate or carbonate). Another possibility is iron chloride $FeCl_2$. No obvious Raman peaks for green rust were found however, which may either be too weak or the product is instead iron(II) chloride $FeCl_2$, the first stage in the oxidation of iron. Presence of iron(II) chloride is supported by iron(III) chloride identified by XRD performed after oxidation in air. Summarized results from the analyses are found in Table 4-16.

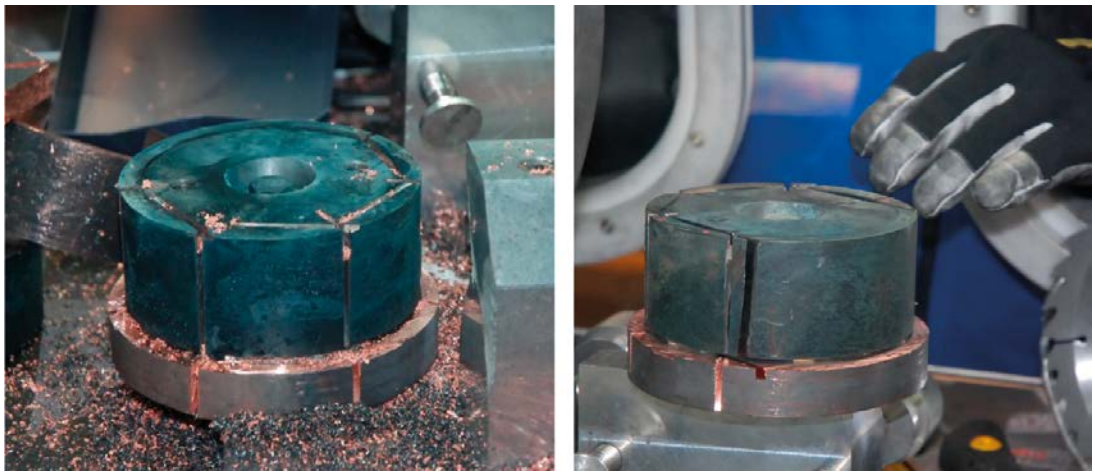

Figure 4-55. *Cast iron insert of MiniCan 5 during sampling, still wet to the left, after a few hours in the large chamber to the right.*

Figure 4-56. *Sample M4 29:1 outer surface of cast iron insert.*

Figure 4-57. *Sample M5 29:1 outer surface of cast iron insert.*

Table 4-16. Analysis summary of cast iron insert, M4 29:1.

Exposure to air before analyses	Method	M4 29:1 iron insert	M5 29:1 iron insert
None	Inspection	Shiny black steel lid, black iron insert	Green steel lid, green cast iron insert
None	Raman	C, fluorescence	Fe_3O_4, C
Short period	FTIR	OH/H_2O, H_2O, SO_3^{2-}, SO_4^{2-}, CO_3^{2-}, Si-O	H_2O/OH, H_2O, SO_3^{2-}, SO_4^{2-}
Extended period	SEM/EDS	C, O, Na, Mg, Al, Si, S, Cl, K, Ca, Ti, Fe	C, O, Mg, Al, Si, S, Cl, Ca, Fe
Extended period	XRD	Fe, Fe_2O_3	Fe, FeO(OH), $FeCl_3 \cdot 6H_2O$, Fe_3O_4, Fe_2O_3, SiO_2
Likely compounds on surfaces before exposure to air		Bentonite, carbon, chloride, iron corrosion products	Green rust and/or $FeCl_2$, magnetite, carbon, chloride

4.7.6 Cast iron insert at positions of holes through copper canister

Photos showing the area near the pin-hole through the copper canisters are shown in Figure 4-58 for MiniCan 4 (M4 30:1), after exposure to air, and in Figure 4-59 and Figure 4-60 for MiniCan 5, before (M5 30:1) and after (M5 31:1) exposure to air. When still wet this area appeared black, turning green when allowed to dry inside the glove box.

The cast iron samples taken from near the holes penetrating the copper canister had distinct areas of material loss corresponding to where the holes would have been. The material loss was in the form of a pit between 3 and 5 mm wide with graduated sides. Corrosion depths were measured with a microscope, and the corrosion on M4 30:1 had a maximum depth of 0.77 mm measured diagonally in from the edge of the insert, whilst the corrosion on sample M5 31:1 had a depth of 0.87 mm measured diagonally in from the edge. Sample M5 30:1 was trapped inside the XPS instrument after analysis so it was not possible to measure the corrosion depth.

Whilst it is not an accurate method to judge corrosion rates from such measurements, it is possible to estimate that a material loss of 0.8 mm over the exposure period (~9 years) equates to a penetration of approximately 90 µm/y. This is much larger than the corrosion rate seen from the iron mass loss samples, suggesting that accelerated corrosion has occurred at these locations.

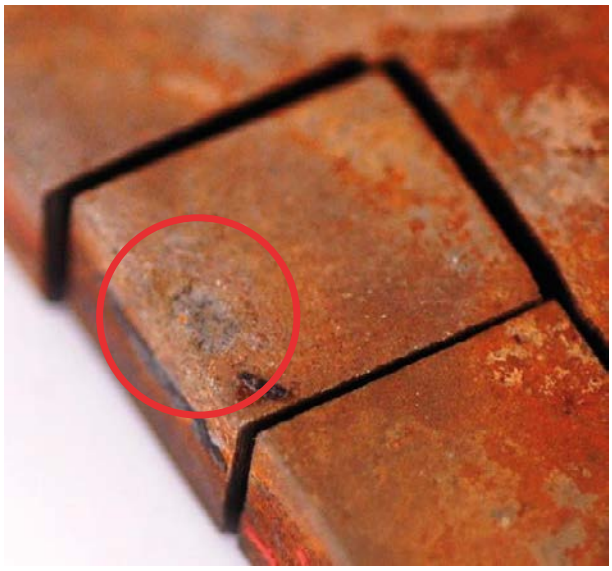

Figure 4-58. *Cast iron insert sample M4 30:1 after removal from the sample holder and after further sampling had taken place to cut out the corroded area, encircled, for analysis.*

Figure 4-59. *Cast iron insert sample M5 30:1 inside its sample holder with the corroded area encircled.*

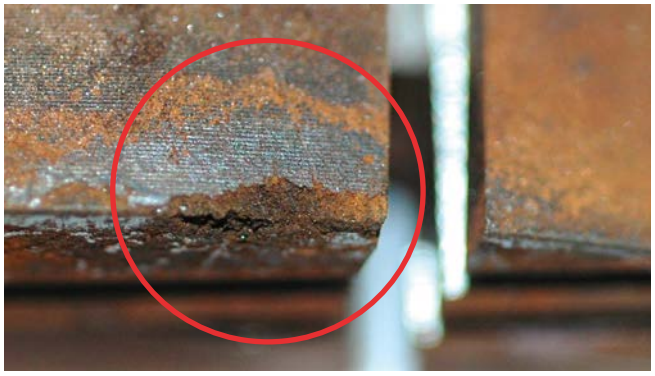

Figure 4-60. *Cast iron insert sample M5 31:1 after removal from the sample holder. The cut to the right hand side of the visible corrosion loss, shows where the saw had cut through the copper canister and into the cast iron insert during sampling in the glovebox. The corrosion extends over the edge of the cast iron insert.*

Raman analysis of the corroded areas detected peaks for amorphous carbon, graphite and possibly iron oxide. FTIR analysis of M4 30:1 detected OH/H_2O, H_2O and SO_4^{2-}, likely from $FeSO_4 \cdot xH_2O$ and FeOOH. For M5 30:1 H_2O/OH, H_2O, SO_3^{2-} and/or SO_4^{2-} was detected and for M5 31:1 H_2O, SO_4^{2-} and/or SO_3^{2-}, possibly $FeSO_3 \cdot H_2O$, possibly also β-FeOOH.

XRD analysis on M4 30:1 detected Fe, NaCl, SiO_2, Na_2SiO_3, and on M5 31:1 Fe, FeO(OH). SEM/EDS analysis on M4 29:1 detected Fe, Si, Al, Mg, Ca, O, Cl, C, and on M5 30:1 and 31:1 Fe, Ca, Si, O, Cl, C. Analysis results are summarized in Table 4-17 - Table 4-18

Table 4-17. Analysis summary of cast iron insert close to hole, M4 30:1.

Exposure to air before analyses	Method	M4 30:1 iron insert at position of hole
None	Raman	C, iron oxide
Short period	FTIR	OH/H_2O, H_2O, SO_4^{2-}, possibly β-FeOOH
Extended period	SEM/EDS	C, O, Na, Mg, Al, Si, S, Cl, K, Ca, Ti, Fe
Extended period	XRD	Fe, NaCl, SiO_2, Na_2SiO_3
Likely compounds on surfaces before exposure to air		Carbon, iron oxide, chloride, silicates (from bentonite)

Table 4-18. Analysis summary M5 30:1 and M5 31:1.

Exposure to air before analyses	Method	M5 30:1 iron insert at hole	M5 31:1 iron insert at hole
None	Raman	C (graphite and amorphous)	C, iron oxide
Short period	FTIR	H_2O/OH, H_2O, SO_3^{2-}, SO_4^{2-}	H_2O, SO_3^{2-}, SO_4^{2-}, possibly β-FeOOH
Extended period	SEM/EDS	C, O, Na, Mg, Al, Si, P, S, Cl, Ca, Cr, Fe, Ni, Cu, Zn	C, O, Na, Mg, Al, Si, P, S, Cl, Ca, Ti, Fe, Cu
Extended period	XRD	Sample lost during XPS analysis	Fe, FeO(OH)
Likely compounds on surfaces before exposure to air		Carbon (graphite), iron sulphides, chloride	Carbon, iron oxide, iron sulphides, chloride

4.7.7 Loose products

This section presents analysis of deposits from the inner surface of the stainless steel cage (M5 12:1), and on the outer wall of the copper canister, facing the stainless steel cage (M5 35:1) in MiniCan 5. The sandwich specimen for MiniCan5, see Section 4.5.4, could not be separated in the glove box, instead a sample of the corrosion products from the iron part was collected (M5 13:1). The specimens analysed are shown in photos in Figure 4-61 Figure 4-63.

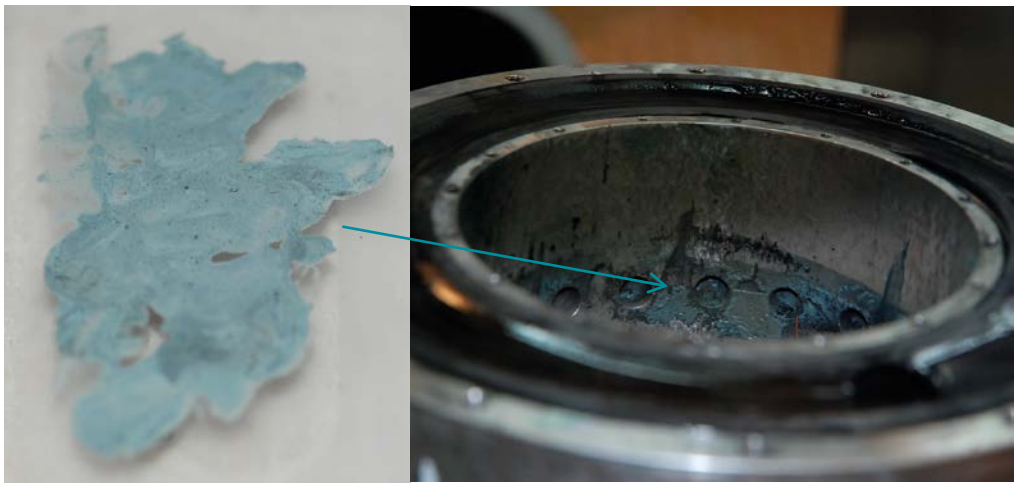

Figure 4-61. *Sample M5 12:1 green coloured corrosion products taken from the stainless steel cage.*

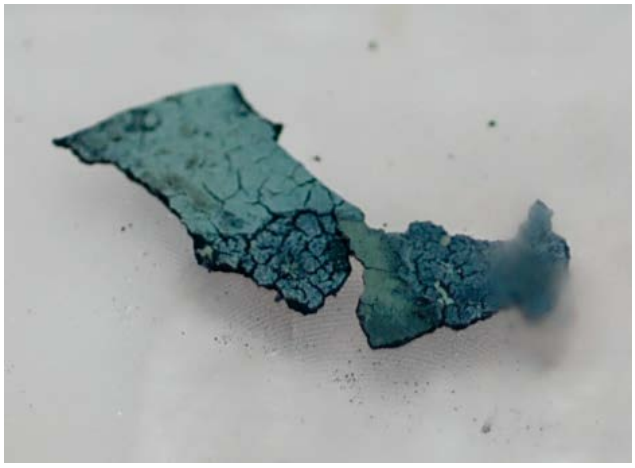

Figure 4-62. *Sample M5 35:1 corrosion products taken from outside of copper canister.*

Figure 4-63. *Sample M5 13:1 corrosion products from the iron part of the iron-copper sandwich.*

Raman analysis of the loose corrosion products revealed peaks of magnetite and carbon for M5 12:1, and calcite and possibly sulphates on M5 13:1. M5 35:1 did not produce any clear Raman peaks. No further analyses were carried out on these samples.

A summary of results from the analyses is shown in Table 4-19.

Table 4-19. Analysis summary for loose corrosion products from stainless steel cage (M5 12:1), from outside of copper canister (M5 35:1) and from the iron part of the sandwich specimen (M5 13:1).

Exposure to air before analyses	Method	M5 12:1 SS cage	M5 35:1 Cu canister	M5 13:1 Fe sandwich
None	Inspection	Green	Green	Black
None	Raman	Magnetite, C	No clear peak	Calcite, sulphate
Likely compounds in loose products before exposure to air		Magnetite, carbon	Contamination from steel cage	Calcite, Cu-sulphate

4.8 Bentonite samples from MiniCan 4

Bentonite samples were taken from the surface of the MiniCan 4 canister close to the ∅1 mm holes. Raman analysis and SEM/EDS were carried out on the samples and the results are shown in Table 4-20. In the Raman analyses only fluorescence was detected from the samples, and in the SEM/EDS analyses mainly O, Si, and Al were found with smaller amounts of C and Fe along with traces of other elements. The results are summarized in Table 4-20.

Table 4-20. Analysis summary of bentonite samples M4 28:1 and M4 28:2.

Exposure to air before analyses	Method	M4 28:1 bentonite sample	M4 28:2 bentonite sample
None	Raman	Fluorescence	Fluorescence
Extended period	SEM/EDS	C, O, Na, Mg, Al, Si, S, Cl, K, Ca, Ti, Fe	C, O, Na, Mg, Al, Si, S, Cl, K, Ca, Ti, Fe

5 Discussion

5.1 Corrosion of iron

The presence of precipitated iron sulphides indicates iron corrosion due to sulphide in the ground water and the possibility of microbiologically influenced corrosion (MIC) has to be considered. The presence and effect of bacteria on corrosion are not discussed in detail in this report, but it is possible that sulphate reducing bacteria (SRB), known to be present in the MiniCan boreholes, affected the corrosion of the iron components in both MiniCan 4 and 5, as was also concluded during the earlier examination of MiniCan 3 (Smart, et al., 2012). Results from microbial analyses for MiniCan 4 and 5 are given in SKB report TR-16-13 (Hallbeck et al. 2017).

5.1.1 Mass loss samples

The average corrosion rates of cast iron samples intended for gravimetric analysis were 2 and 3 µm/y for MiniCan 4 and 5 respectively, thus several orders of magnitude lower than the corresponding corrosion rate estimated from MiniCan 3 (Smart, et al., 2012). The iron mass loss samples from MiniCan 4 and 5 displayed selective corrosion morphology but not as severe as was found for MiniCan 3. This opens the question as to why the iron mass loss sample had corroded to such extent in the MiniCan 3 exposure. The presence and metabolism of SRB is discussed as a possible cause in Smart et al. (2012), but this does not explain the difference to MiniCan 4 and 5.

It is possible, but unlikely, that galvanic effects had played a part in the corrosion. The samples mounted on the nylon rack were attached using polypropylene thread (see Figure 5-2), which suspended all samples vertically whilst the MiniCan assemblies were in a vertical position. Once the MiniCan was inserted into the borehole the samples could then have been free to move and possibly have come in contact with one another. This means the iron mass loss sample could in principle have been in contact with several of the other more noble experimental materials (copper, platinum, gold) which could have accelerated the corrosion of the iron sample. This could also have occurred in MiniCan 5, but not in MiniCan 4 where the samples were encased in the bentonite clay and therefore fixed in their positions. The corrosion rate from MiniCan 5 does not suggest that galvanic corrosion occurred in this particular exposure as the corrosion rate is similar to that of MiniCan 4 and two orders of magnitude lower than in MiniCan 3. Against the galvanic hypothesis stands further the fact that controlled laboratory experiments did not indicate any acceleration of corrosion of copper-iron galvanic couples under oxygen lean conditions (Smart, et al., 2005).

Another possible reason for the difference in iron corrosion rates between MiniCan 3 and 5 could be the conditions inside the support cage of the experiment, shown in Figure 5-1. Since the MiniCan packages were positioned nearly horizontally but with a slight angle it is possible that water only partially filled the space in front of the canister where the external samples were positioned. The process of water sampling from inside the support cage could also have had the effect of creating a gas bubble in the area around the external samples. The main gases dissolved in the MiniCan boreholes were N_2, He, Ar, CO_2, CH_4, and H_2 (Smart, et al., 2015). If this was the case corrosion would have been most severe on those samples exposed to the water. However, there are several observations which suggest this probably was not the case. For example, all external samples from MiniCan 3 and 5 showed signs of corrosion and/or surface deposits, and the machined defects (∅1 mm holes) in the canister positioned upwards (i.e. at the 12 o'clock position in the borehole) had led to localised corrosion of the iron insert which implies the presence of water. If water was present at the top surface of the canister then it is likely it was also present in the space around the external samples which were positioned vertically lower than this point.

5.1.2 Iron electrodes

The metal loss of the MiniCan 4 electrodes was up to 1 mm from the edges, whilst up to 2.5 mm on the MiniCan 5 electrodes. Anaerobic iron corrosion rates in groundwater have been estimated to be < 1 µm/y (Smart et al. 2005). Clearly the corrosion on the iron electrodes exceeds that expected from the exposure conditions.

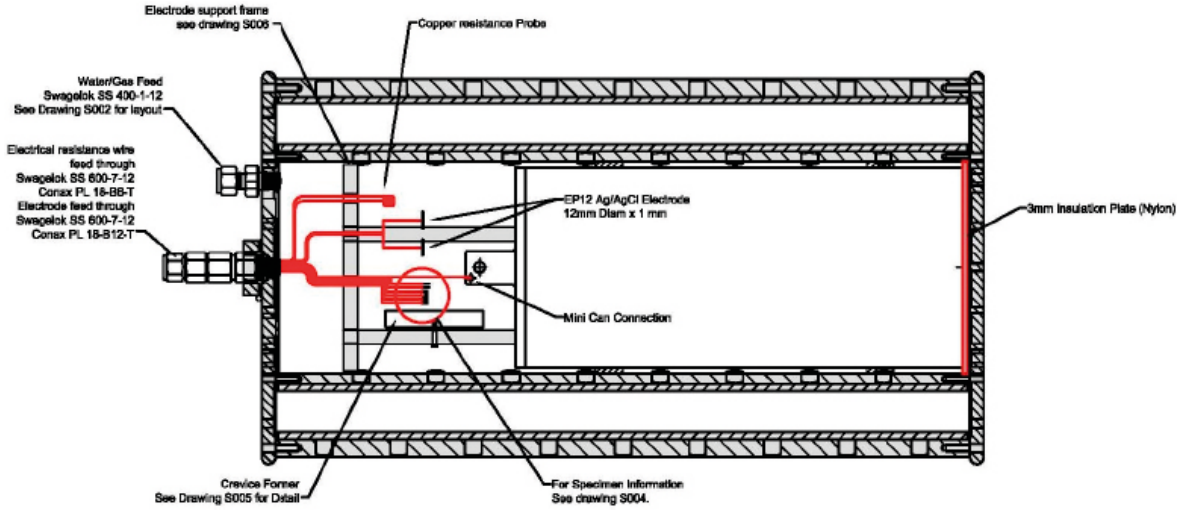

Figure 5-1. *Layout of canister and external samples inside the support cage, as it would have been positioned inside the borehole. The external samples in the space in front of the canister are positioned vertically lower than the machined defect at the top of the canister, implying corrosion at this point would mean water would have been present around all of the external samples. Note that in MiniCan 4 high density bentonite surrounded the canister and the external samples.*

The appearance of the iron electrodes also differed between MiniCan 4 and 5, similar to most of the other samples, where MiniCan 5 had a thick iron sulphide (FeS identified on some samples) surface deposit whilst MiniCan 4 had mainly bentonite attached to the electrode surfaces. However, there was corrosion of the electrodes in both experiments. The corrosion was more pronounced on the MiniCan 5 electrodes, and had signs suggesting SRB could have been involved, such as the morphology of the corrosion damage, the presence of sulphides and the results of microbial sampling which found viable SRB in the area of the electrodes (Hallbeck et al. 2017).

The iron electrodes of MiniCan 4 appeared generally less corroded but on one of the iron electrodes extensive localised corrosion was observed corresponding by geometric estimate to a corrosion rate of ca 100 µm/y locally. Iron oxides were found in the analyses suggesting presence of oxygen, possibly from the bentonite which encased the electrodes.

5.1.3 Cu-Fe sandwich specimens

The iron component of the sandwich specimen from MiniCan 5 (M5 14:1) had suffered from severe corrosion, whilst in MiniCan 4 the iron component (M4 15:1) appeared visually unaffected by corrosion. The material loss in MiniCan 5 appears to have occurred mainly on the outer surface of the iron component, although some material loss was observed near to the ∅1 mm holes on the inner surface as well as near the edges. The corrosion morphology of the iron component was similar to that observed when under deposit corrosion occurs. The observed corrosion morphology, the detection of precipitated FeS and the presence viable SRB (Hallbeck et al. 2017) thus suggests that the microbial activity has influenced the corrosion of iron.

The possibility of galvanic corrosion should in theory be low under the exposure conditions of the MiniCan5 experiment according to previous studies (Smart et al. 2005), so the significant material loss at the edges of the iron component where it had contact with the copper component is interesting. If any residual oxygen was present in the exposure conditions it is possible that galvanic corrosion could in fact occur due to the large cathode area on which the cathode reaction could take place. Without oxygen it is expected that concentration polarisation could occur due to the production of hydroxide ions as a result of the cathode reaction (reduction of water and hydrogen evolution), which would cause an increase in the pH and eventually slow down the corrosion of iron. However, due to the large cathode area, concentration polarisation would be less pronounced and corrosion could proceed furher.

Another interesting observation from the sandwich specimen from MiniCan 5 is that it was completely covered with relatively thick surface deposits, which was not the case for the sample from MiniCan 3. There seems to have been slightly different exposure conditions for these samples between the two experiments, despite the fact that groundwater was essentially able to flow around the samples in both experiments. One explanation for the difference could be the positioning of the samples relative to the vertical which would have been dependent on how the nylon support rack was placed in the support cage before it was placed in the borehole, and the water distribution around the samples as discussed in Section 5.1.1. Examining the photographs of each retrieval operation one can see a clear difference in the distribution of the black deposit over the support rack; see Figure 5-2 and Figure 5-3.

Figure 5-2. *The support table upside down immediately after removal from MiniCan 5. The copper mass loss (left) and iron mass loss (right) samples can be seen in the foreground attached to the Pt/Ti net electrode by a nylon thread. The black surface deposit can be seen to be confined to the sandwich specimen and one half of the support rack.*

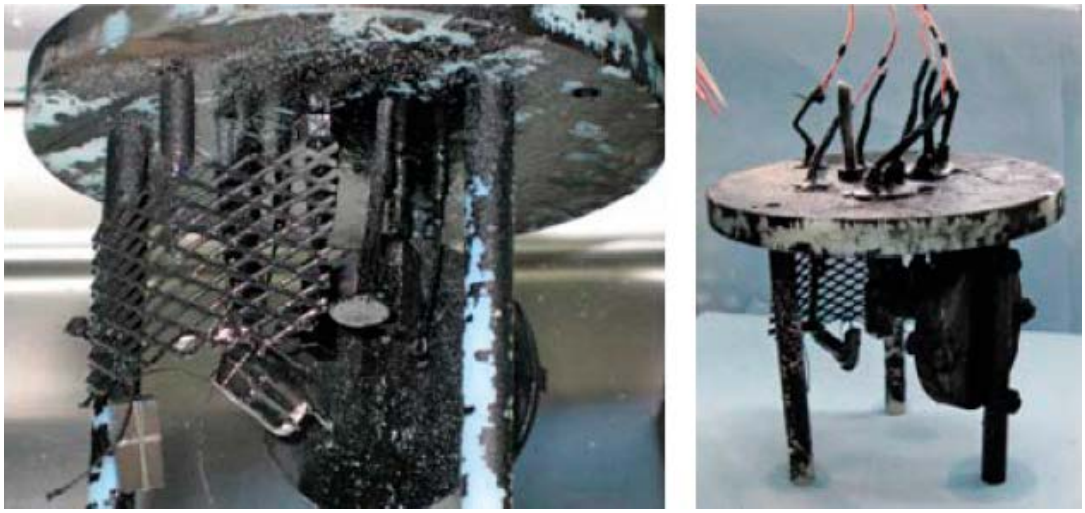

Figure 5-3. *Nylon support rack as seen directly after retrieval from MiniCan 3 with black surface deposit covered most of the surfaces (Smart et al. 2012).*

5.1.4 Cast iron inserts

Corrosion of the cast iron insert was concentrated at the locations of the machined defects on both MiniCan 4 and 5. Uneven corrosion of approximately 3–5 mm width and 0.8 mm depth was found on the edges of the iron samples. The surface analyses of these samples found mainly iron oxide but no iron sulphide. Considering the possible corrosion mechanisms it seems plausible to suggest that galvanic effects have played a part in the corrosion of the iron insert at these locations. Water would have surrounded these locations and effectively there would have been a large cathode (copper) area relative to a small anode (iron) area. This would have led to accelerated corrosion of the iron. As discussed in Section 5.1.3 the threat of galvanic corrosion is thought to be small under the experimental conditions but it appears to have occurred here.

It is interesting to note that similar corrosion features were found in MiniCan 4 despite the presence of high density bentonite clay embedding the copper canister. Analyses of bentonite from this area did not show significant numbers of bacteria, as detailed in SKB report TR-16-13 (Hallbeck et al. 2017), but the bentonite was found to be wet during the retrieval operation suggesting that water could have seeped into this area thus increasing electrolyte flow. Galvanic corrosion from the graphite in the cast iron could occur, but nodular cast iron, as used here, is not considered susceptible to this form of corrosion. Magnetite formed from corrosion could form deposits and, since being noble, could cause both under deposit and galvanic corrosion. However, as mentioned earlier, neither of these mechanisms are expected under oxygen lean conditions.

5.2 Corrosion of copper

5.2.1 Canister

In general it can be said that there was a clear difference in the appearance of the copper materials after exposure between the MiniCan 4 and 5 experiments. The presence of a black surface deposit on almost all MiniCan 5 samples was somewhat similar to what was observed during retrieval and examination of MiniCan 3 (Smart, et al., 2012). In contrast, the copper surfaces of MiniCan 4 were in general covered with bentonite clay residues that were not completely washed off during sampling, but otherwise visibly unaffected by the exposure. The black deposit was identified as a mixture of sulphides (partly iron sulphide from corroding iron parts) and carbon, similar to that found in MiniCan 3.

Visually, the canister surfaces of both MiniCan 4 and 5 appeared even, except for the ca 100 µm band structure caused by mechanical machining, visible in Figure 4-48. A closer examination of surface profiles using SEM, revealed that pits of a few µm depth occurred frequently over the canister surfaces (Figures 4-48, 4-49, and 4-53). Preliminary results indicate that these pits could be mechanical defects due to the machining and/or atmospheric corrosion that took place already before the start of the ground water exposure.

5.2.2 Mass loss samples

The gravimetrically determined integrated corrosion rate of the copper sample from MiniCan 4 (0.02 µm/y) was one about order of magnitude lower than the corresponding value for MiniCan 5 (0.11 µm/y), which was similar to that reported from MiniCan 3 (0.15 µm/y). The external samples in the MiniCan 3 exposure were not in direct contact with the low density bentonite clay, while both the canister and the samples were embedded in compact high density bentonite clay in MiniCan 4. In MiniCan 5 there was no bentonite clay. This suggests that the bentonite clay has a suppressive effect on the corrosion of copper only when the clay is highly compacted and/or adhering to the surface.

5.2.3 SCC samples

No signs of crack initiation could be found on the U-bend samples exposed in the MiniCan 4 experiment. Analysis of the WOL samples showed that there was increased amount of sulphur in the surface oxides on the fracture surfaces of the crack, and that the pre-crack had propagated along grain boundaries. There were some smaller cracks found to be emanating from the main pre-cracks on both WOL samples, in some cases perpendicular to the direction of travel of the main pre-crack.

These smaller cracks were found in areas of plastic deformation in the parent material on either side of the main pre-crack and contained branches. Such features are consistent with SCC but it is not possible to determine if these smaller cracks were due to SCC or had occurred during the fatigue loading of the specimens. In fatigue failure it is more common for the crack to propagate perpendicular to the load direction, and in some cases the smaller cracks had propagated in what would have been parallel to the direction of the load. SEM/EDS analysis of the smaller cracks detected only O and Si, but no S or Cl, suggesting corrosion had not played a part in the cracking during the exposure.

TEM analysis detected elevated amounts of sulphur at some of the grain boundaries where small particles occurred in the FIB-prepared specimen. The fracture surfaces were examined with SEM and were seen to have features consistent with fatigue failure. No evidence for SCC was found near the crack tip of the main pre-crack of the WOL samples.

5.3 Corrosion considerations from MiniCan

When the MiniCan *in situ* test was initiated there were a number of questions which were of interest, these were as follows.

5.3.1 Does water penetrate through a small defect into the annulus between the cast iron insert and the outer copper canister?

It can be concluded that the ground water surrounding MiniCan 5 did penetrate through the ∅1 mm defects in the canister wall and into the annulus between the cast iron insert and the copper canister. This is concluded from the appearance of the inner surface of the copper canister and the outer surface of the iron insert, which both had a black surface deposit. MiniCan 4 showed similar features to suggest the presence of water in the annulus such as corrosion of the cast iron insert at the position of the ∅1 mm defect, as well as some black deposits on the inner surface of the copper canister. In MiniCan 4, water would at least partially have been adsorbed by the bentonite, but the inner surfaces of the copper canister were in part covered with a black deposit similar to that of MiniCan 5. Corrosion seen on the cast iron insert at the position of the ∅1 mm defect through the copper canister would suggest the presence of water during the exposure period.

5.3.2 How do corrosion products spread around the annulus in relation to the leak point?

The spread of corrosion product throughout the annulus was evident on the MiniCan 5 samples, with a black deposit covering most surfaces. However, it is not clear from which component this deposit originated. It is likely that corrosion of the iron part of the sandwich specimen, as well as the iron electrodes produced a similar corrosion product to that of the cast iron insert. Logically however, the majority of the corrosion products found on the inner surface of the copper canister would have originated from the cast iron insert.

5.3.3 Does the formation of corrosion product in a constricted annulus cause any expansive damage to the copper canister?

The dimensions of the copper canister were taken immediately after dismantling of the experimental packages, and no increase in dimensions was detected. The amount of corrosion observed on the cast iron insert of MiniCan 5 was relatively small and the corrosion products had seemingly spread out as mentioned above, so that the threat of expansive damage appears low over the duration of the exposure period (approximately 8.5 years).

5.3.4 Is there any detectable corrosion at the copper welds?

The copper welds were inspected with LOM and SEM but no distinct areas of corrosion were detected on either MiniCan 4 or 5. Pits or indents of a few µm depth were observed in the weld of MiniCan 4, however, these were not deeper than pits/defects found on other parts of the copper canisters examined with SEM in both MiniCan 4 and 5.

5.3.5 Are there any deleterious galvanic interactions between the copper and the cast iron?

There were signs of accelerated corrosion between the cast iron insert and the copper canister at the locations of the machined defects in both MiniCan 4 and 5. The sandwich specimen from MiniCan 5 showed signs of accelerated iron corrosion, most likely due to MIC but possibly also from galvanic coupling.

5.3.6 Does corrosion lead to failure of the lid on the iron insert?

The steel lid of the cast iron insert was not seen to have suffered any damage during the exposures.

5.3.7 How is the corrosion process affected by microbial activity?

It is likely that the metabolic activity of sulphate reducing bacteria (SRB) has influenced the corrosion of iron components in MiniCan 5, the corrosion of iron is unexpectedly extensive for anoxic abiotic conditions, and viable SRB were found both in the borehole water as well as inside the experimental assembly (Hallbeck et al. 2017). The precipitated iron sulphide found on some of the iron samples supports the conclusion that MIC has occured.

5.3.8 What are the gravimetric corrosion rates of cast iron and copper in the experimental environment?

Gravimetrically determined integrated corrosion rates for copper were 0.02 μm/y and 0.11 μm/y for MiniCan 4 and 5 respectively. For the cast iron mass loss samples the corrosion rates were 2 μm/y and 3 μm/y respectively. However, estimates made from dimensional changes of the iron electrodes and iron part of the sandwich specimen in MiniCan 5 indicate that these specimens have corroded locally with a rates of ca 300 μm/y. Material loss on one of the iron electrodes from MiniCan 4 indicates a local corrosion rate of ca 100 μm/y .

5.3.9 Is there any risk of stress corrosion cracking (SCC) of copper?

The U-bend specimens from MiniCan 4 did not show any signs of crack initiation due to SCC or otherwise. The WOL specimens were examined with SEM and no signs of crack propagation from the crack tip of the original pre-crack were found. Some smaller cracks were found emanating perpendicular to the pre-crack into the cold deformation zone either side of the pre-crack but it is not possible to determine if these were due to SCC or had occurred during the original fatigue loading of the specimens. SEM/EDS analysis of the smaller cracks detected only O and Si, but no S or Cl, suggesting corrosion had not played a part in the cracking during the exposure.

5.3.10 What is the corrosion morphology of copper and is there any risk for localised corrosion (pitting)?

The copper components were in general not observed to be corroded. The mass loss specimens, despite having slightly decreased mass, did not have any local corrosion defects so it can be assumed the corrosion was generally uniform over the sample surface. The canister surfaces appeared rather even, except for the ca 100 μm band structure caused by mechanical machining. Examination of surface profiles using SEM revealed frequently occurring pits or pit-like defects of a few μm depth over the canister surfaces. Preliminary results indicate that these pits could have been caused by the machining and/or atmospheric corrosion that took place already before the start of the ground water exposure.

6 Conclusions

The compact high density bentonite clay surrounding the samples seems to have limited or retarded corrosion rather generally but with a few exceptions. This suggests that the high density bentonite has the effect of supressing microbiologically influenced corrosion (MIC), even if the reduced electrolyte flow may have had some influence as well. The exceptions were the iron mass loss sample, iron electrodes and the sample taken from the cast iron insert near the ∅1 mm defect in the copper canister which had corroded in MiniCan 4 (high density bentonite), albeit less than the corresponding samples of MiniCan 5 (no bentonite).

Extensive iron corrosion was detected on the sandwich specimen of MiniCan 5, iron electrodes as well as the iron insert of both MiniCan 4 and 5. The detection of viable sulphate reducing bacteria (SRB), precipitated iron sulphide and the corrosion morphology of the sandwich specimen of MiniCan 5 suggest that MIC has occurred. Galvanic effects have also possibly accelerated the corrosion of the iron component of the sandwich specimen from MiniCan 5 as well as the iron insert samples taken from near the defects in the copper canisters on both MiniCan 4 and 5.

Corrosion of copper parts was generally low. The integrated corrosion rate was about one order of magnitude lower for the mass loss coupon embedded in high density bentonite clay (MiniCan 4), as compared to the coupons exposed directly to the ground water (MiniCan 5) or to ground water in contact with low density bentonite clay (MiniCan 3).

By sampling the MiniCan components in an inert gas atmosphere and sealing them in transparent sample holders, it was attempted to preserve the surface deposits formed during the exposure conditions for surface analysis in the laboratory. Raman spectroscopy was carried out on the samples whilst they were still in the sample holders and the results confirm that the method worked.

Subsequent analyses with XRD for example were carried out on the samples after the sample holders were opened to the atmosphere and the results suggest that the surface deposits altered rapidly. For example, more oxides of copper and iron were observed, and sulphates were detected instead of sulphides.

A wide array of elements were detected in the SEM/EDS analyses of the surfaces, reflecting the composition of the construction materials, as well as the groundwater chemistry and the bentonite clay (in the case of MiniCan 4). The main corrosion products found on copper surfaces were cuprite and sulphide (iron or mixed iron and copper sulphides), while both iron sulphides and magnetite was detected on iron components. Chloride containing green rust was detected on the outer surfaces of the cast iron insert.

Samples for investigating stress corrosion cracking were exposed in MiniCan 4 and subjected to microscopy and metallographic examination after exposure. The U-bend specimens did not appear damaged by the exposure, i.e. showed no crack initiation, but did include some defects in the form of continuous porosity in the bulk material. The wedge open loaded (WOL) specimens were examined with SEM and no signs of crack propagation from the original pre-crack were found, however, smaller cracks were found emanating perpendicular from the original pre-crack.

References

SKB's (Svensk Kärnbränslehantering AB) publications can be found at www.skb.com/publications.

Aggarwal S, Addepalli V, Smart N, 2015. Further metallographic analysis of MiniCan SCC test specimens. SKB R-15-11, Svensk Kärnbränslehantering AB.

Frost R L, Keeffe E C, 2009. Raman spectroscopic study of the sulfite-bearing minerals scotlandite, hannebachite and orschallite: implications for the desulfation of soils. Journal of Raman Spectroscopy 40, 244–248.

Hallbeck L, Edlund J, Eriksson L, 2011. Microbial analyses of groundwater and surfaces during the retriveal of experiment 3, A04, in MiniCan. SKB P-12-01, Svensk Kärnbränslehantering AB.

Hallbeck L, Johansson L, Edlund J, Pedersen K, 2017. Microbial analyses of groundwater, bentonite and surfaces, post-test analysis of packages 4 (A05) and 5 (A06), retrieved from the MiniCan experiment at Äspö laboratory. SKB TR-16-13, Svensk Kärnbränslehantering AB.

Hua Y, Barker R, Neville A, 2015. The influence of SO_2 on the tolerable water content to avoid pipeline corrosion during the transportation of supercritical CO_2. International Journal of Greenhouse Gas Control 37, 412–423.

Martinsson Å, Sandström R, Lilja C, 2013. Hydrogen in oxygen-free, phosporous-doped copper: charging techniques, hydrogen contents and modelling of hydrogen diffusion and depth profile. SKB TR-13-09, Svensk Kärnbränslehantering AB.

Minceva-Sukarova N G C, Najdoski M, Grozdanov I, Chunnilall C J, 1997. Raman spectra of thin solid films of some metal sulfides. Journal of Molecular Structure 410–411, 267–270.

Mo W, Liu H, Xiong H, Li M, Li G, 2007. Preparation of CuCl/1,10-phenanthroline immobilized on polystyrene and catalytic performance in oxidative carbonylation of methanol. Applied Catalysis A: General 333, 172–176.

Rebollo-Plata B, Lozada-Morales R, Palomino-Merino R, Dávila-PintLe J A, Portillo-Moreno O, Zelaya-Angel O, Jiménez-Sandoval S, 2005. Amorphous carbon thin films prepared by electron-gun evapouration. AZojomo 1. doi:10.2240/azojomo0157

RRUFF database, n.d. Available at: http://rruff.info/ [February 2016]

SKB, 2010. Design, production and initial state of the canister. SKB TR-10-14, Svensk Kärnbränslehantering AB

Smart N, Rance A, 2009. Miniature canister corrosion experiment – results of operatons to May 2008. SKB TR-09-20, Svensk Kärnbränslehantering AB.

Smart N R, Rance A P, Fennell P A H, 2005. Galvanic corrosion of copper-cast iron couples. SKB TR-05-06, Svensk Kärnbränslehantering AB

Smart N, Rance A, Reddy B, Lydmark S, Pedersen K, Lilja C, 2011. Further studies of *in situ* corrosion testing of miniature copper-cast iron nuclear waste canisters. Corrosion Engineering Science and Technology 46, 142–147.

Smart N, Rance A, Reddy B, Fennell P, Winsley R, 2012. Analysis of SKB MiniCan. Experiment 3. SKB TR-12-09, Svensk Kärnbränslehantering AB.

Smart N, Rose S, Nixon D, Rance A, 2013. Metallographic analysis of SKB MiniCan Experiment 3. SKB R-13-35, Svensk Kärnbränslehantering AB.

Smart N, Reddy B, Nixon D, Rance A, Johansson A J, 2015. Miniature Canister (MiniCan) Corrosion experiment. Progress report 5 for 2008–2013. SKB P-14-19, Svensk Kärnbränslehantering AB.

Tahir D, Tougaard S, 2012. Electronic and optical properties of Cu, CuO and Cu_2O studied by electron spectroscopy. Journal of Physics: Condensed Matter 24, 175002.

Taxén T, Lundholm M, Persson D, Jakobsson D, Sedlakova M, Randelius M, Karlsson O, Rydgren P, 2012. Analyser av koppar från prototypkapsel 5 och 6. SKB P-12-22, Svensk Kärnbränslehantering AB. (In Swedish.)

Thuvander M, 2015. Investigation of the distribution of phosphorus in copper. Research Report 2015:11, Strålsäkerhetsmyndigheten (Swedish Radiation Safety Authority).

Troland F, Génin J-M R, Abdelmoula M, Bourrié G, Humbert B, Herbillon A, 1997. Identification of a green rust mineral in a reductomorphic soil by Mössbauer and Raman spectroscopies. Geochimica et Cosmochimica Acta 61, 1107–1111.

Appendix 1

Sample holders

Design of sample holders

In order to maintain the low oxygen environment that the MiniCan and its associated samples had been exposed to during the experiment, a design of sample holders was proposed to be used, similar to that used for the analyses of MiniCan 3 (see Smart et al. 2012). The design was tested for air-tightness by submerging in water for several days and monitoring for leakage. No leaks were found and the design was deemed acceptable for the project.

The design consisted of a PMMA (also known as acrylic glass) box with space enough for the sample and a lid with a microscope glass slot in order to allow analysis by Raman spectroscopy. The samples would be prepared in an inert gas glovebox and placed into the sample holders, the lid would then be fixed in place using epoxy-based adhesive and allowed to cure. The sample holders could then be removed from the glovebox and transported to the laboratory for analysis.

Once the Raman spectroscopy was completed the sample holders would be opened using a saw to cut an opening in the side to allow removal of the samples.

The sample holders were designed in three sizes to allow for the varying size of samples anticipated to be obtained from the MiniCan experiments. The different dimensions can be seen in the following figures.

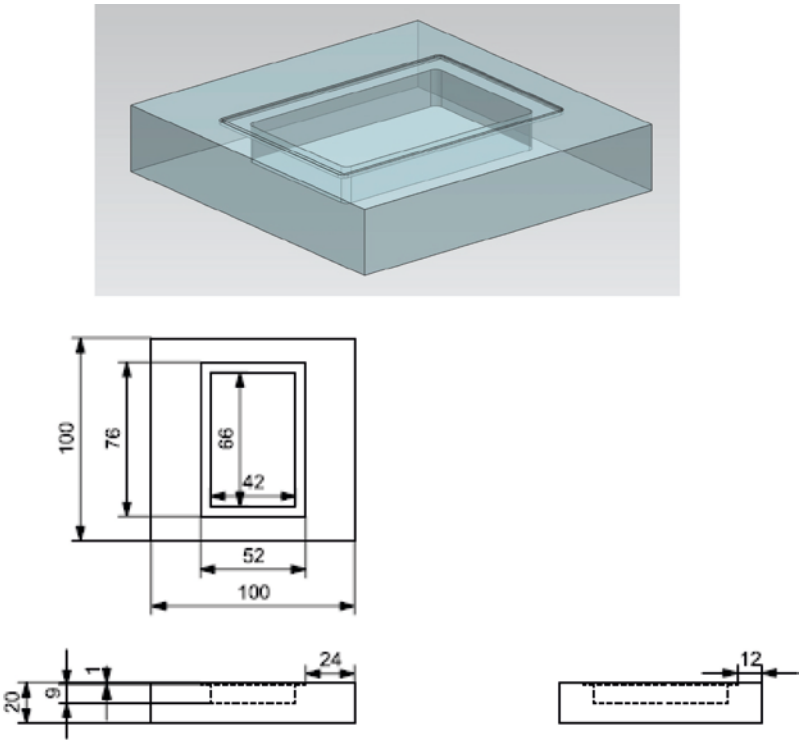

Figure A1-1. *Sample holder type 1.*

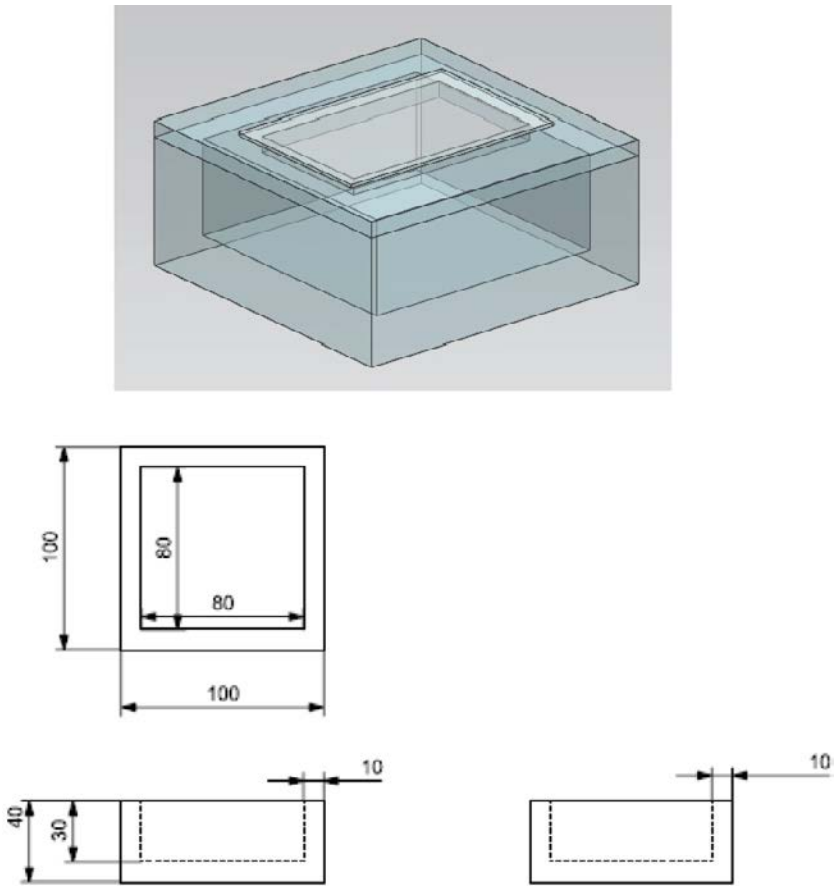

Figure A1-2. *Sample holder type 2.*

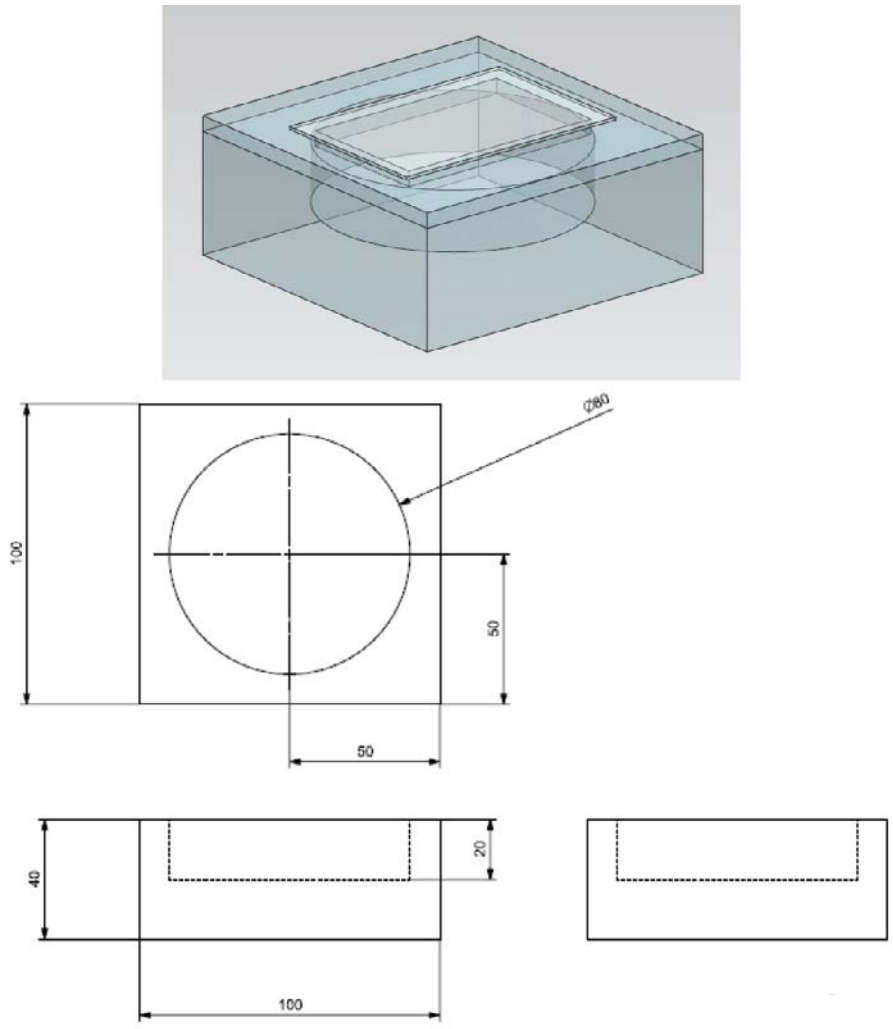

Figure A1-3. *Sample holder type 3.*

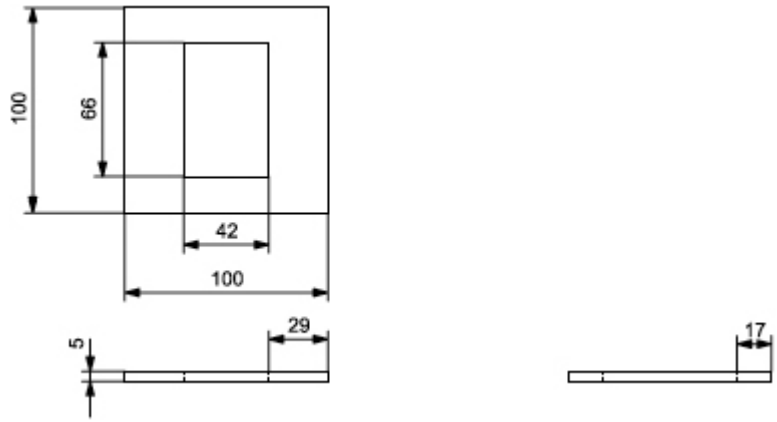

Figure A1-4. *Lid design for sample holder type 2 and 3.*

Appendix 2

Sample preparation

Sample preparation

The samples taken from the copper canister and cast iron insert were sectioned as detailed below. Some samples were taken in duplicate, with the second sample sealed in an aluminium bag. The circle saw was modified between the sampling of MiniCan 5 and MiniCan 4, with an extra saw being added and the vice arrangement altered to accommodate the larger stainless steel cage of the MiniCan assembly. The cutting blades did not last long when cutting the stainless steel, and required lubricating with ground water when cutting the copper and cast iron components.

MiniCan 4

Canister material hydrogen content samples were taken first and placed into liquid nitrogen as fast as possible. Cutting temperature was monitored using a hand-held infra-red thermometer as it was considered a threat to the results if the temperature of the copper reached too high a temperature during the cutting operations as any hydrogen contained in the material could possibly diffuse out. The highest temperature measured during cutting was 30 °C.

The copper canister was measured using calibrated callipers. Original dimensions were:

Outer ∅145 mm.

Inner ∅130 mm.

Wall thickness 7.5 mm.

Height (not including welded lid) 300 mm, with welded lid and bottom 330 mm.

Measured dimensions after exposure:

∅bottom 145.0 mm, ∅middle 145.05 mm, ∅top 145.0 mm (height at the top approximately corresponding to the hole in the canister).

Measurements taken at 90° to first measurements:

∅bottom 145.0 mm, ∅middle 145.05 mm, ∅top 145.00 mm.

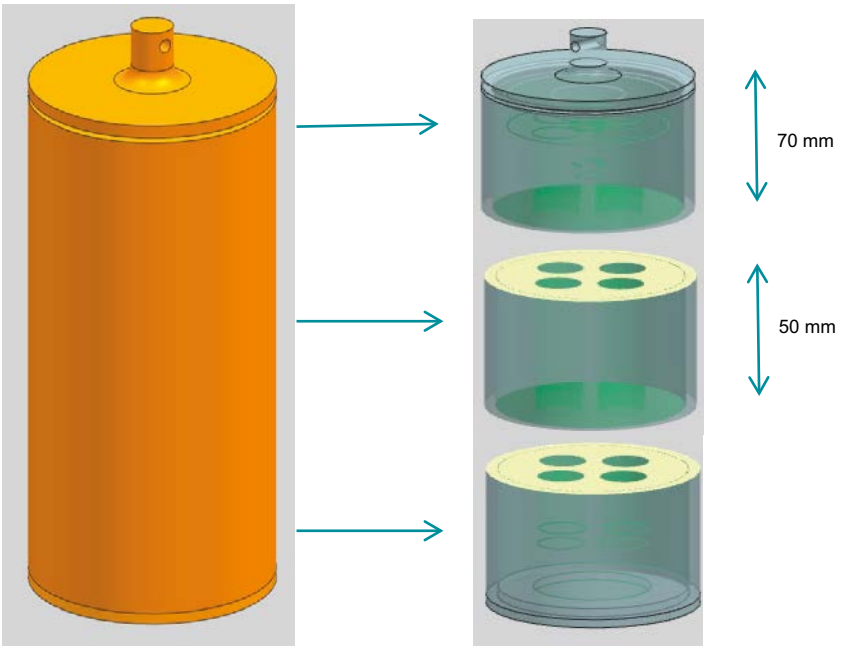

Figure A2-1. *Cutting of the canister started as shown in the figure, with the canister being cut into sections.*

The machined defect (∅1 mm hole) in the canister was identified and clearly marked with a pen. The canister was then cut into three sections, top, middle and bottom. It was intended to collect any water that was inside the canister, but no water was found inside of the cast iron insert of MiniCan 4.

Middle section

Firstly, three samples were cut out for hydrogen content analysis, with maximum dimensions of 20 × 20 × 50 mm. The samples were then removed from the glovebox and placed in a thermos containing liquid nitrogen. Three further samples of the canister with a width of approximately 70 mm were then cut and taken as samples of the inner and outer surfaces of the canister.

Table A2-1. Sample numbering copper canister MiniCan 4.

Sample	Sample ID	Sample holder type	Dimensions
Wall of copper canister for H-analyses	21:1, 22:1, 23:1	N_2 thermos	7.5 × 20 × 50 mm
Inner surface of copper canister	24:1	2	max 70 × 70 × 25 mm
Outer surface of copper canister	25:1	2	max 70 × 70 × 25 mm
Surfaces of copper canister	24:2, 25:2	Al-bag	max 70 × 70 × 25 mm

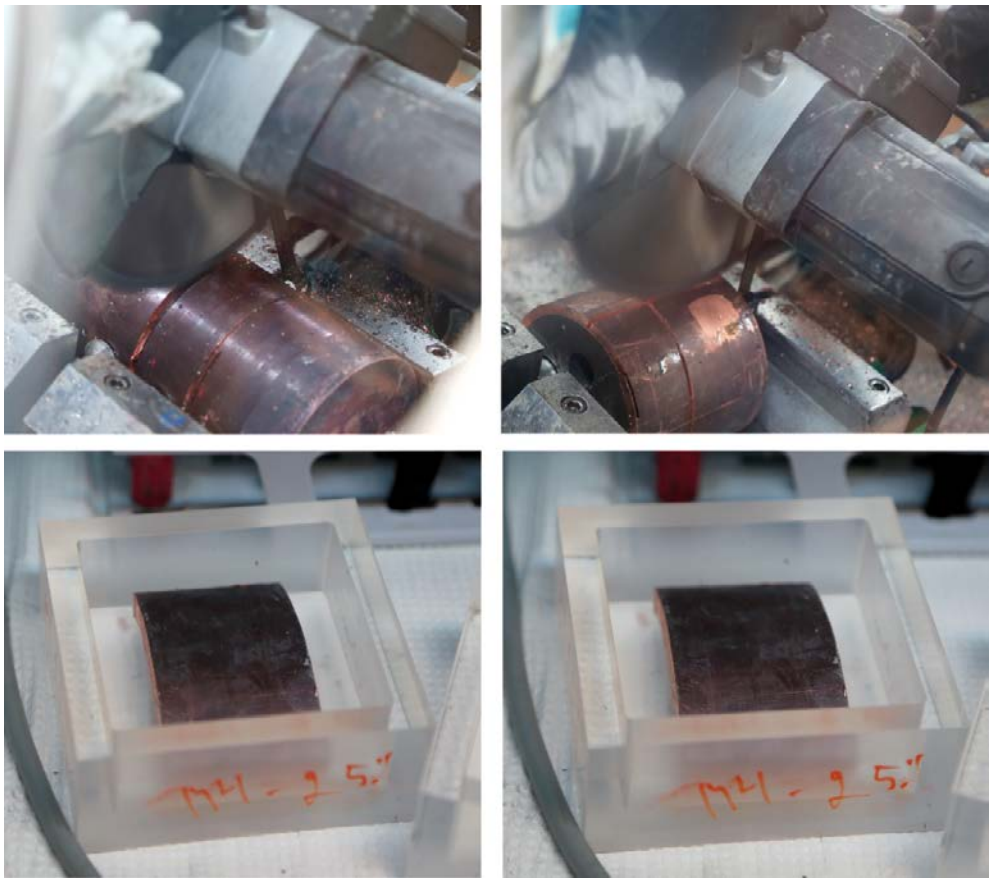

Figure A2-2. *cutting of copper canister samples MiniCan 4.*

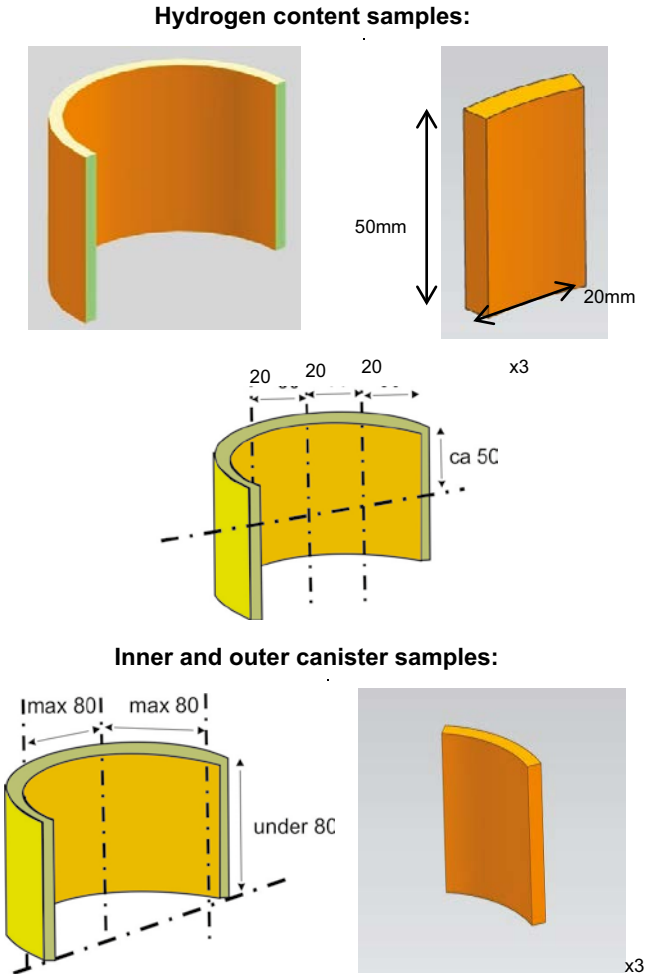

Figure A2-3. *Cutting of the hydrogen samples (M4 21, 22, 23) and canister samples (M4 24 and 25).*

Top section

The top section was cut so that the machined defect (hole) was preserved.

No loose corrosion products were found on the samples, however a sample of bentonite was taken from the vicinity of the hole. The inner surface of the canister near the defect was noted to be black in colour at first but after a while it changed to a green colour whilst still inside the glovebox.

All samples were then sluiced over to the smaller chamber of the glovebox ready to be sealed in their sample holders. All remaining material was saved in sealed aluminium bags.

Table A2-2. Sample numbering for copper canister MiniCan 4.

Sample	Sample ID	Sample holder type	Dimensions
Welds in copper shell	26:1	2	max 70 × 70 × 25 mm
	26:2	Al-bag	–
Inner surface around hole in copper shell	27:1	2	max 70 × 70 × 25 mm
Bentonite with corrosion products close to hole	28:1	1	–
Bentonite with corrosion products at hole	28:2	1	–

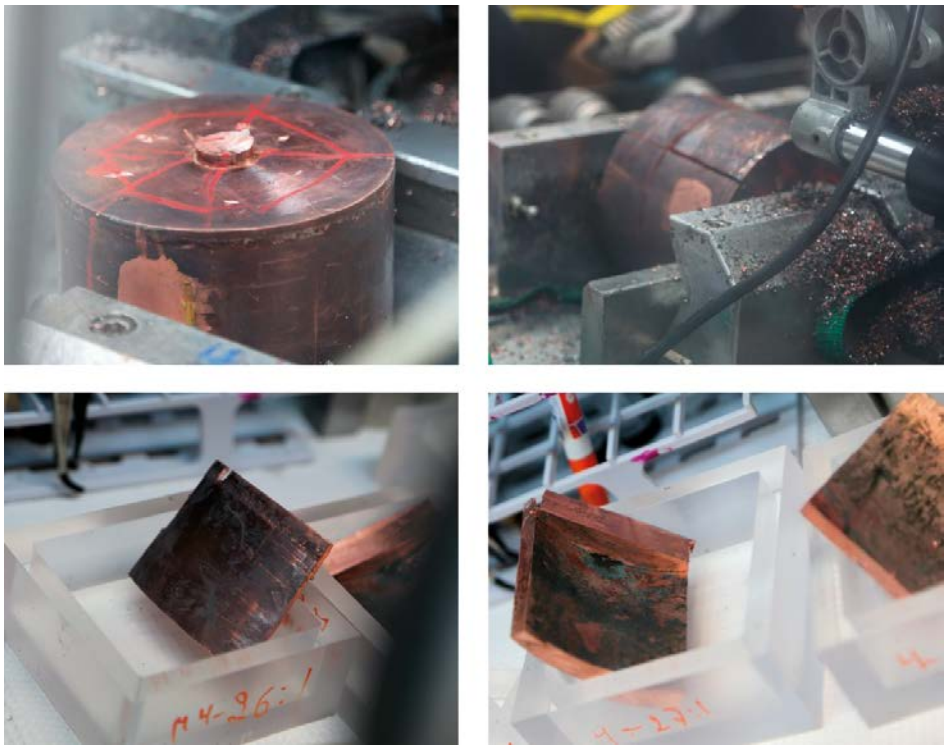

Figure A2-4. Cutting of copper canister MiniCan 4.

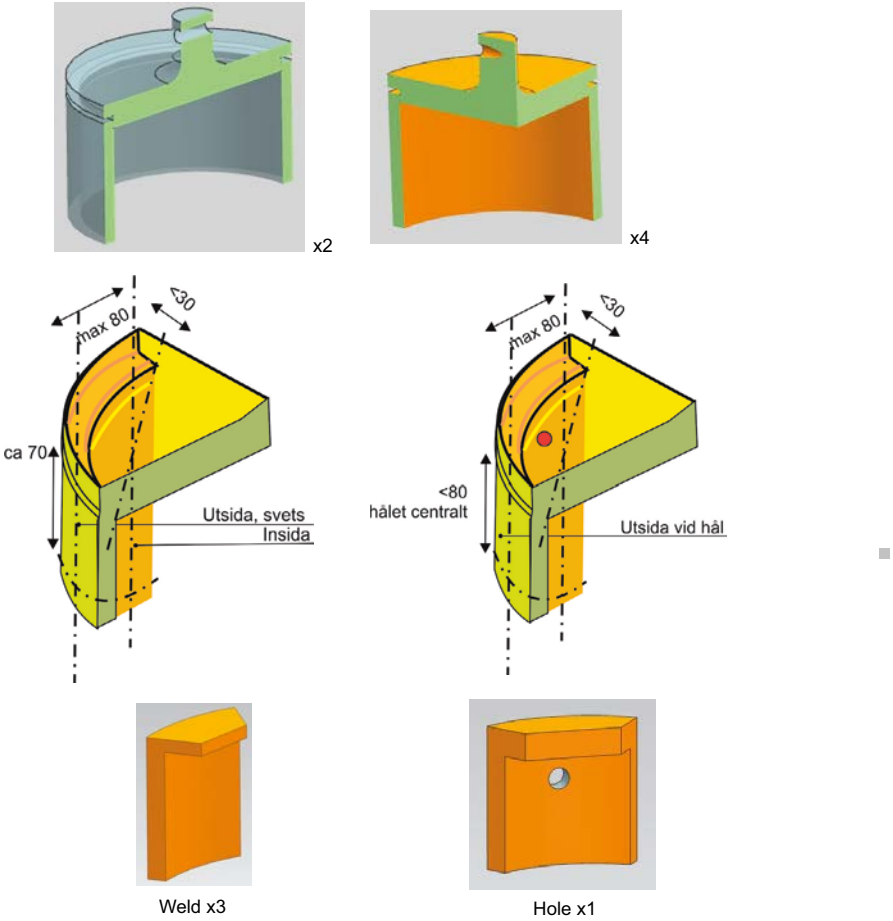

Figure A2-5. Sampling of the top section of the canister.

Bottom section

No samples were taken from the bottom section of the canister. SKB retained this piece of the MiniCan 4 canister.

Cast iron insert

The steel lid component was noted to be shiny instead of green, as it was with MiniCan 5, see Figure A2-7 and Figure A2-9.

The top third of the cast iron insert was cut so that the area near the through hole in the copper canister was in the middle of the sample. This sample was cut so that it was approximately 80 mm wide and 70 mm long. Three further samples were taken to represent the outer and inner surfaces of the cast iron insert, with dimensions of approximately 50 × 50 mm

Table A2-3. Sample numbering for cast iron insert from MiniCan 4.

Sample	Sample ID	Sample holder type	Dimensions
Outer surface of cast iron insert	29:1	2	max 70 × 70 × 25 mm
Inner surface of cast iron insert	29:2	2	max 70 × 70 × 25 mm
Wall of cast iron insert	29:3	Al-bag	–
Surface of cast iron insert at position of hole through copper shell	30:1	2	max 70 × 70 × 25 mm

Figure A2-6. *Bottom section of sectioned MiniCan 4, iron particles contaminated the surface during cutting and began to oxidise on the surface after the glovebox was opened.*

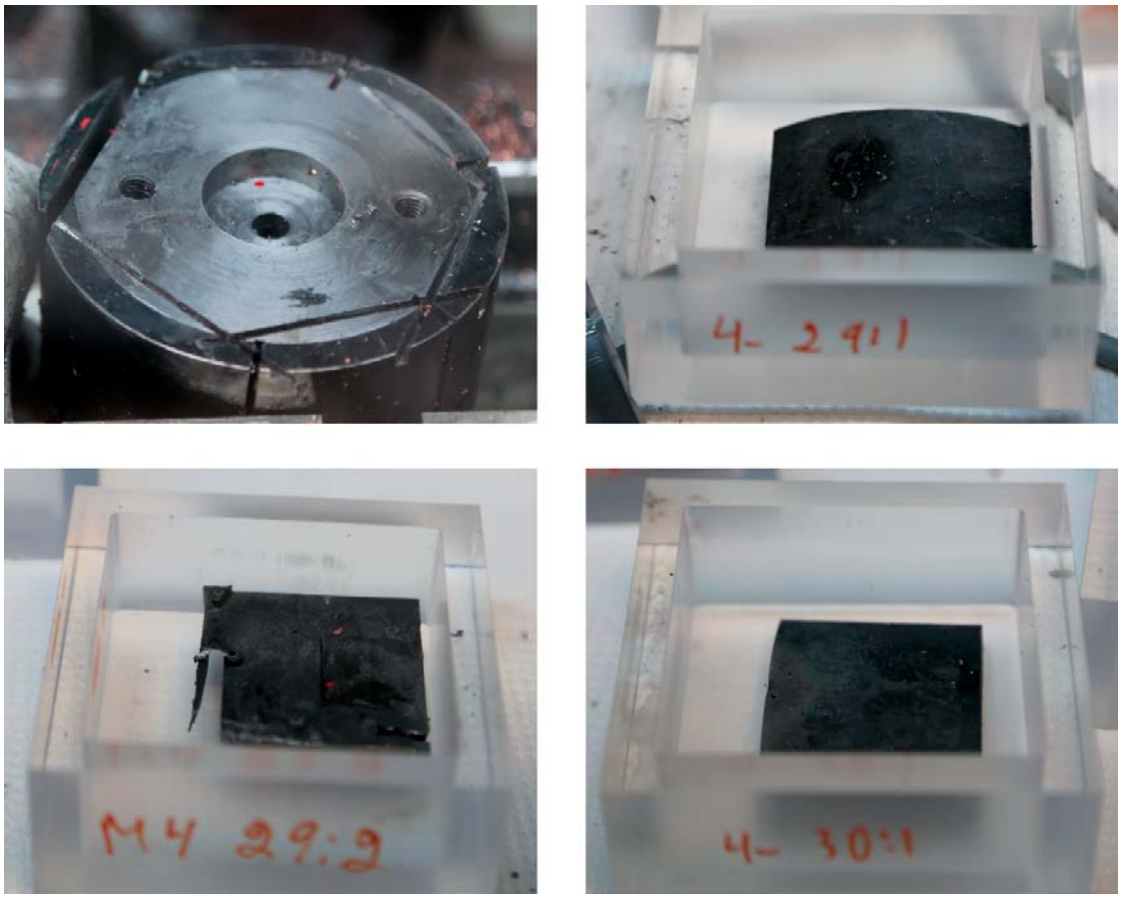

Figure A2-7. *Cutting and sampling of cast iron insert MiniCan 4, top left photo showing the shiny steel lid on top of the cast iron insert.*

MiniCan 5

MiniCan 5 was sampled in a similar way as described above for MiniCan 4, first into three sections then with samples of the copper canister and cast iron insert cut from the top and middle sections. The hydrogen content samples were taken first, and the temperatures measured during cutting were as follows:

21:1 over 120 °C, 22:1 and 23:1 approx. 50 °C.

The copper canister was measured using calibrated callipers. Original dimensions were:

Outer ∅ 145 mm.

Inner ∅ 130 mm.

Wall thickness 7.5 mm.

Height (not including welded lid) 300 mm, with welded lid and bottom 330 mm.

Measured dimensions after exposure:

Bottom 145.00 mm, middle 144.90 mm, top 145.00 mm (height at the top approximately corresponding to the hole in the canister).

Measurements taken at 90° to first measurements:

Bottom 145.0 mm, middle 144.9 mm, top 145.0 mm.

Table A2-4. Numbering of MiniCan 5 samples.

Sample	Sample ID	Sample holder type	Dimensions
Wall of copper canister for H-analyses	21:1, 22:1, 23:1	N_2 thermos	7.5 × 20 × 50 mm
Inner surface of copper canister	24:1	2	max 70 × 70 × 25 mm
Outer surface of copper canister	25:1	2	max 70 × 70 × 25 mm
Wall of copper canister	24:2, 24:3	Al-bag	–
Welds in copper shell	26:1	2	max 70 × 70 × 25 mm
	26:2	Al-bag	–
Surface around hole in copper shell (top hole)	27:1	2	max 70 × 70 × 25 mm
Outer surface of cast iron insert	29:1	2	max 70 × 70 × 25 mm
Inner surface of cast iron insert	29:2	2	max 70 × 70 × 25 mm
Surface of cast iron insert at position of hole through copper canister (top hole)	30:1	2	max 70 × 70 × 25 mm
Surface of cast iron insert at position of copper specimen with damaged hole	31:1	2	max 70 × 70 × 25 mm

Samples 29:1 and 29:2 were taken from the middle section of the cast iron insert, which is where the water sample was also taken from (see Appendix 11). It was noted that the surface of these samples were green in colour and became more black and slightly redder in appearance when moved to the smaller chamber in the glovebox. Photos when still wet and after some drying in the humid large chamber are shown in Figure A2-9; after moving to the cleaner and dryer smaller chamber, with known low oxygen level, the samples turned more black. However, iron chips did not oxidise in the smaller chamber until it was opened suggesting the oxygen level was low during the sampling of the Minican. One of the holes of the copper canister was accidently cut through.

As with MiniCan 4 the bottom section of MiniCan 5 was not sampled and was retained by SKB.

Figure A2-8. *Cutting of MiniCan 5 canister.*

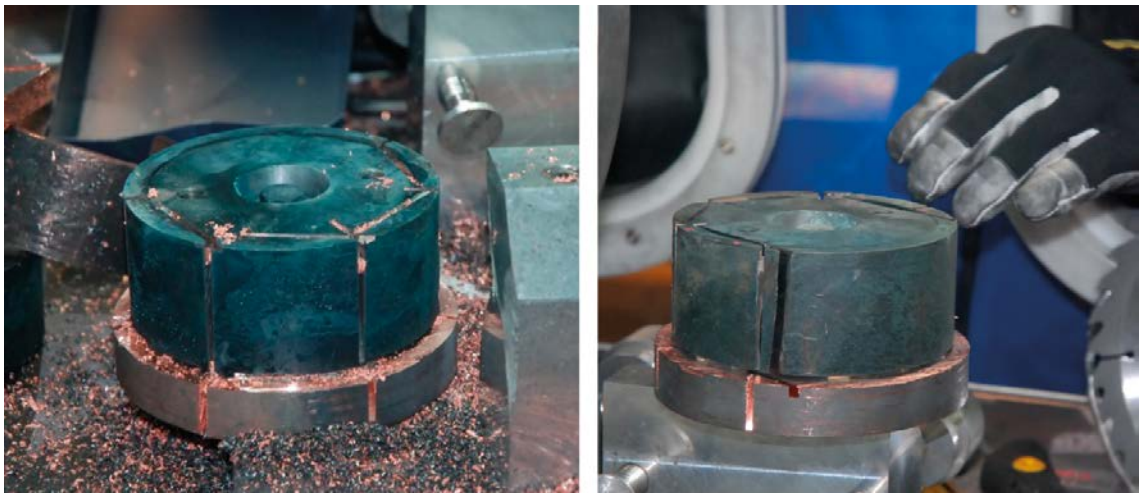

Figure A2-9. *Cast iron insert of MiniCan 5 during sampling, still wet to the left, after a few hours in the large chamber to the right. The steel lid differed in appearance to the same component in the MiniCan 4 assembly, see Figure A2-7.*

Appendix 3

Stress corrosion cracking

Stress corrosion cracking specimens

In MiniCan 4 there were four samples which were intended to be used to investigate the possibility of SCC of copper in under disposal conditions. The samples have been denoted as follows in this report:

Sample	Sample ID
U-bend 1	M4 1:1
U-bend 2	M4 2:1
Wedge open load 1	M4 3:1
Wedge open load 2	M4 4:1

The U-bend samples consisted of a strip of copper canister material bent 180° into a U shape with a bolt attached through the two free ends and tensioned, as shown in Figure A3-1.

Figure A3-1. *U-bend sample M4 1:1.*

Figure A3-2. *U-bend sample M4 2:1.*

The wedge open load (WOL) samples consisted of a piece of copper canister material machined into compact tension specimen form which was pre-cracked by fatigue. The specimen also had a bolt threaded into the side to facilitate tensioning perpendicular to the machined groove as shown in the figures below. The U-bend samples were first examined under a microscope and photographed as show in Figure A3-5 and Figure A3-22.

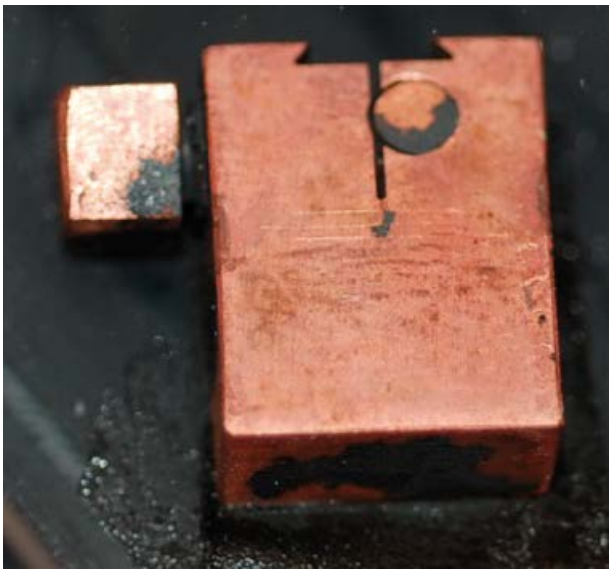

Figure A3-3. *WOL sample M4 3:1.*

Figure A3-4. *WOL sample M4 4:1.*

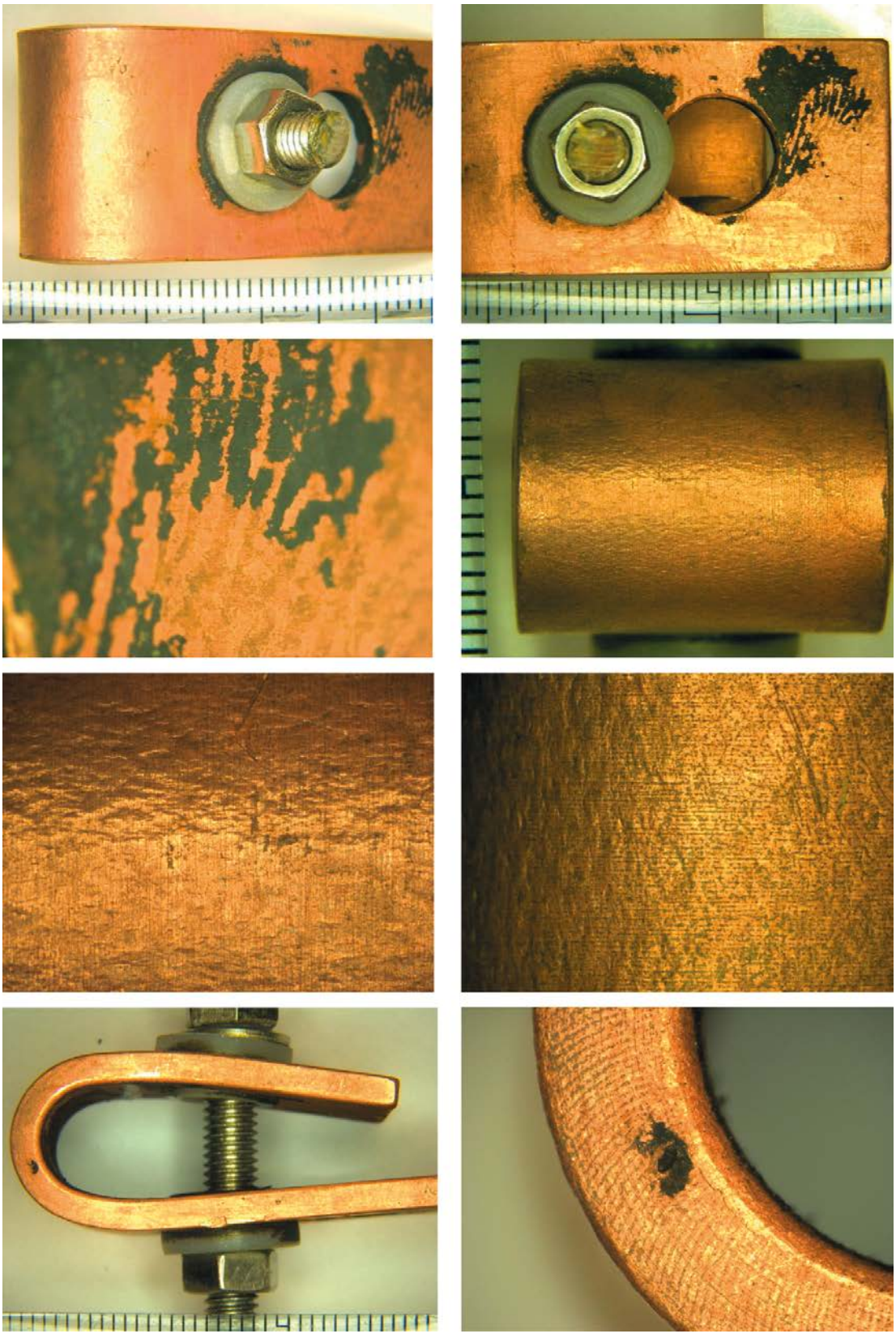

Figure A3-5. *Microscope images of U-bend sample M4 1:1. From top left to bottom right: outer surface side of sample; opposite side of sample; detail of black deposit on side surface of sample; outer surface of bend at top of sample; detail of outer surface sample at bend; detail of outer surface of sample at 45° from top; side of sample; detail of side of sample with black deposit.*

U-bend sample M4 1:1

The distance between the bolt holes was measured both before and after the bolt was removed, but there was no change in dimension, implying that there was no elastic load present in the sample due to the bolt. The samples were then sectioned as show in the Figure A3-7, before being polished to a 1 µm finish and examined again under the microscope. Several areas with porosity were found; some where the pores seemed to be oriented in lines, along grain boundaries, as shown in the figures below.

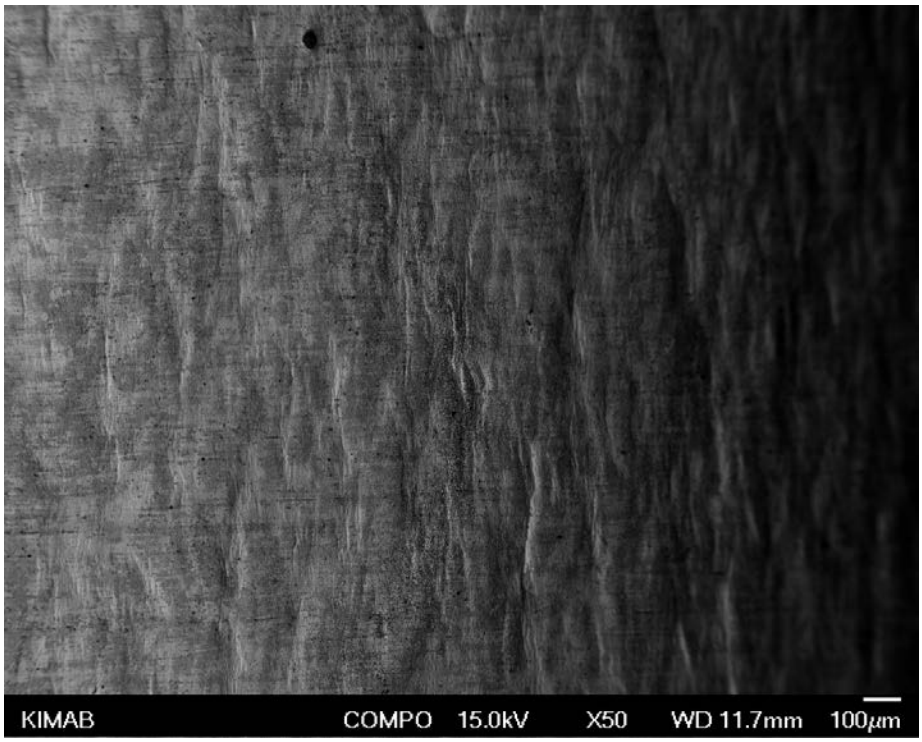

Figure A3-6. *SEM image of the top of the bend surface of U-ben sample M4 1:1, showing the relief created on the surface due to deformation, sometimes referred to as "orange peel" effect.*

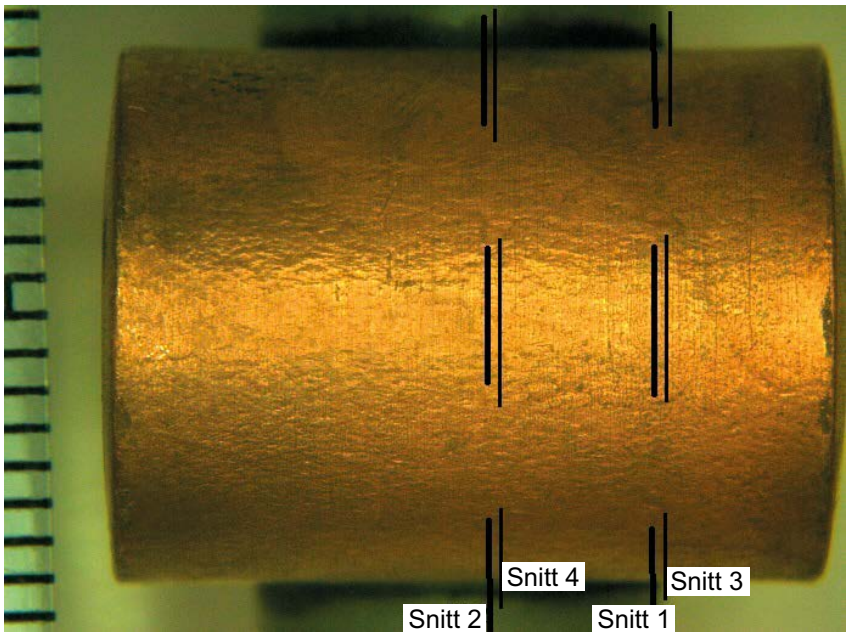

Figure A3-7. *Positions of sections taken from sample M4 1:1.*

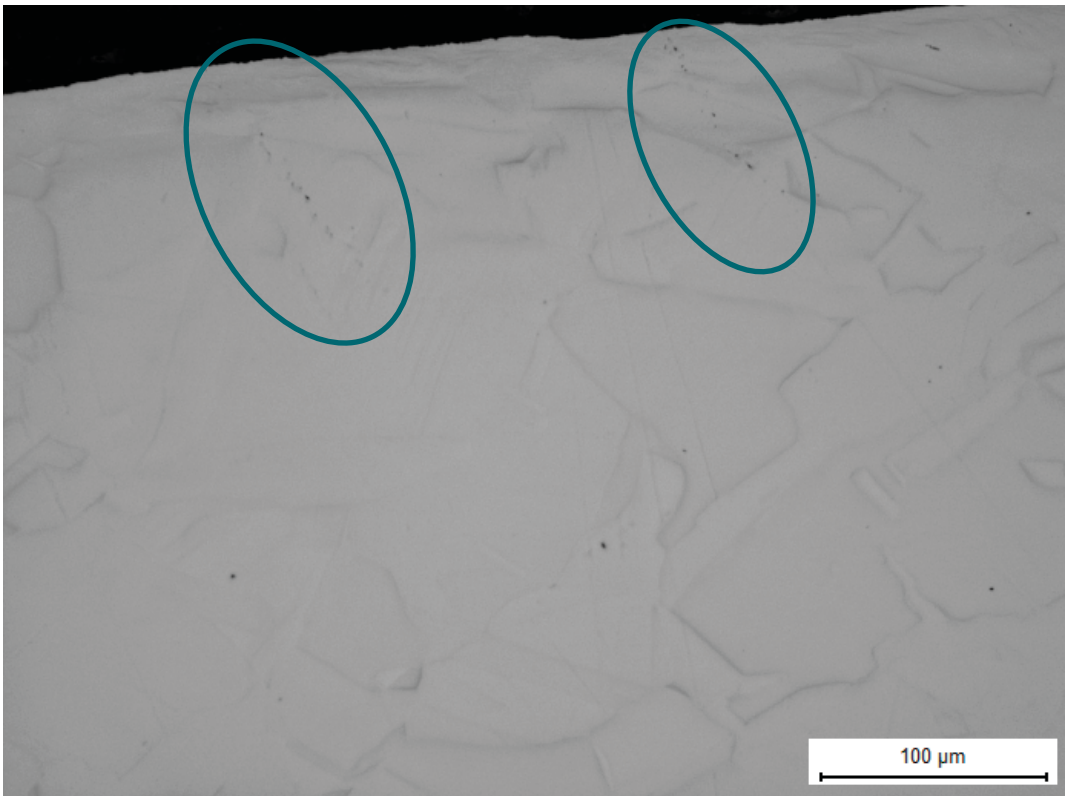

Figure A3-8. *Cross section 3 ("snitt 3"), showing two rows of pores that start form the outer surface of sample M4 1:1.*

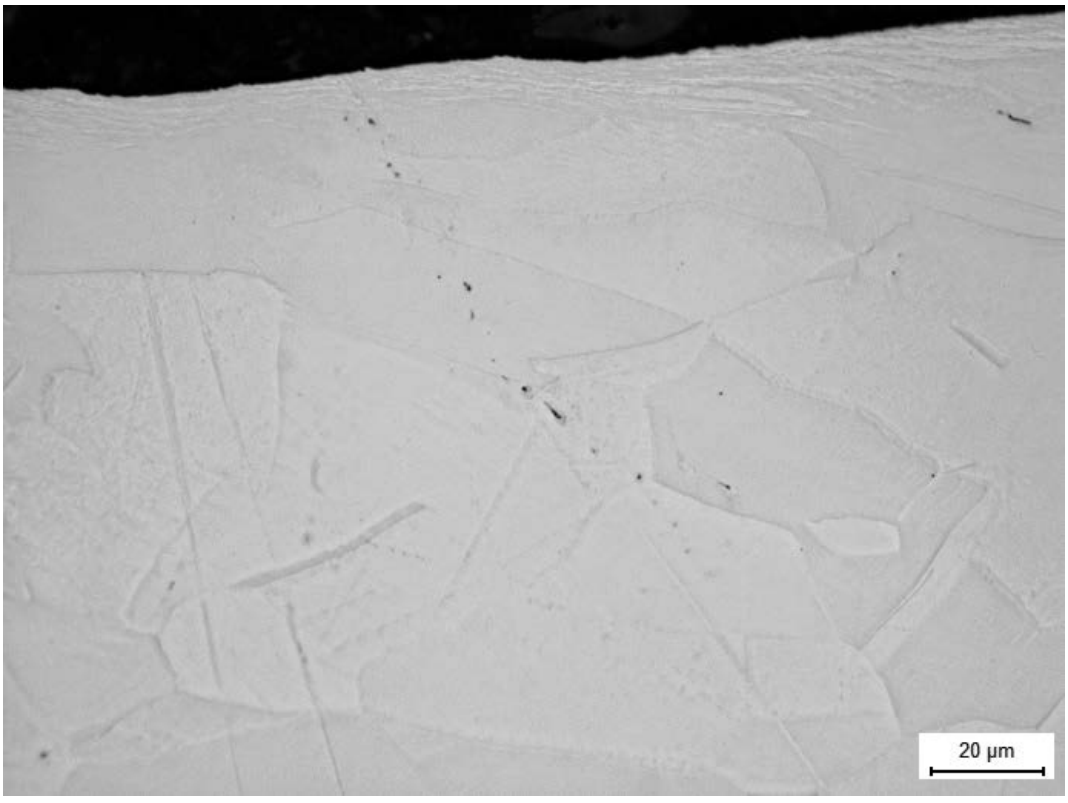

Figure A3-9. *Detail of Figure A3-8.*

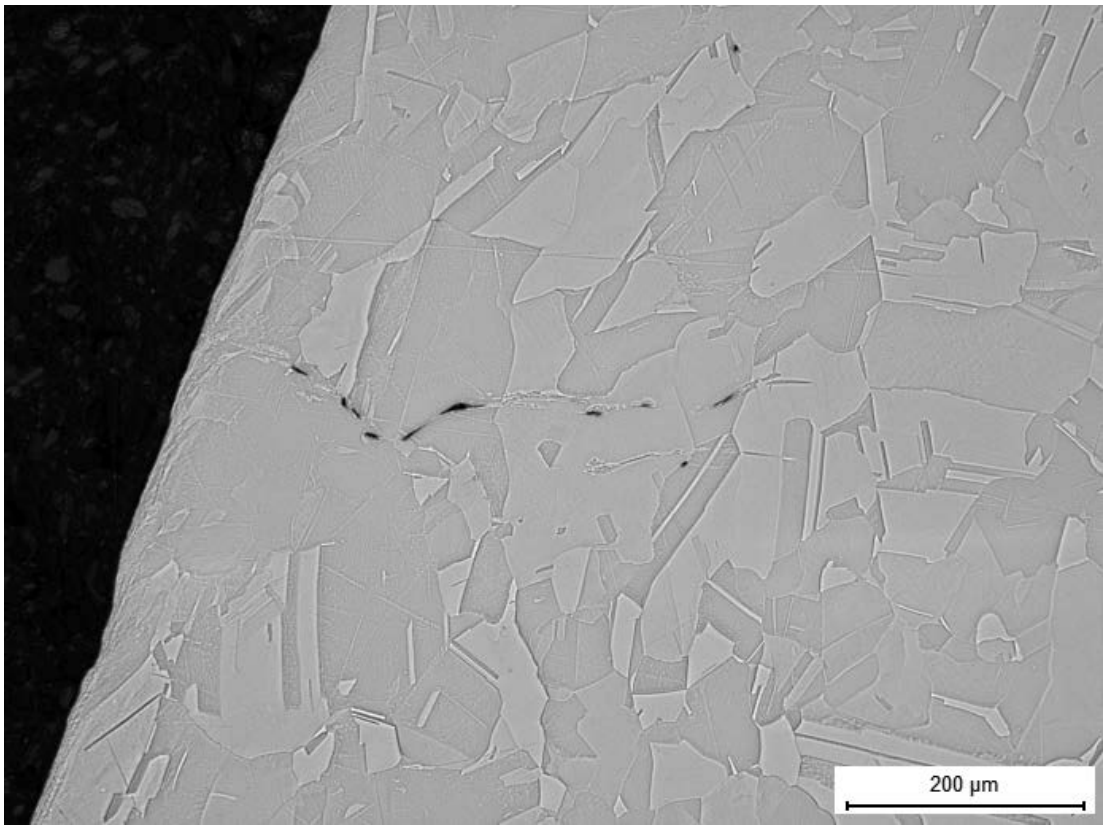

Figure A3-10. *A row of pores that start from the outer surface of sample M4 1:1.*

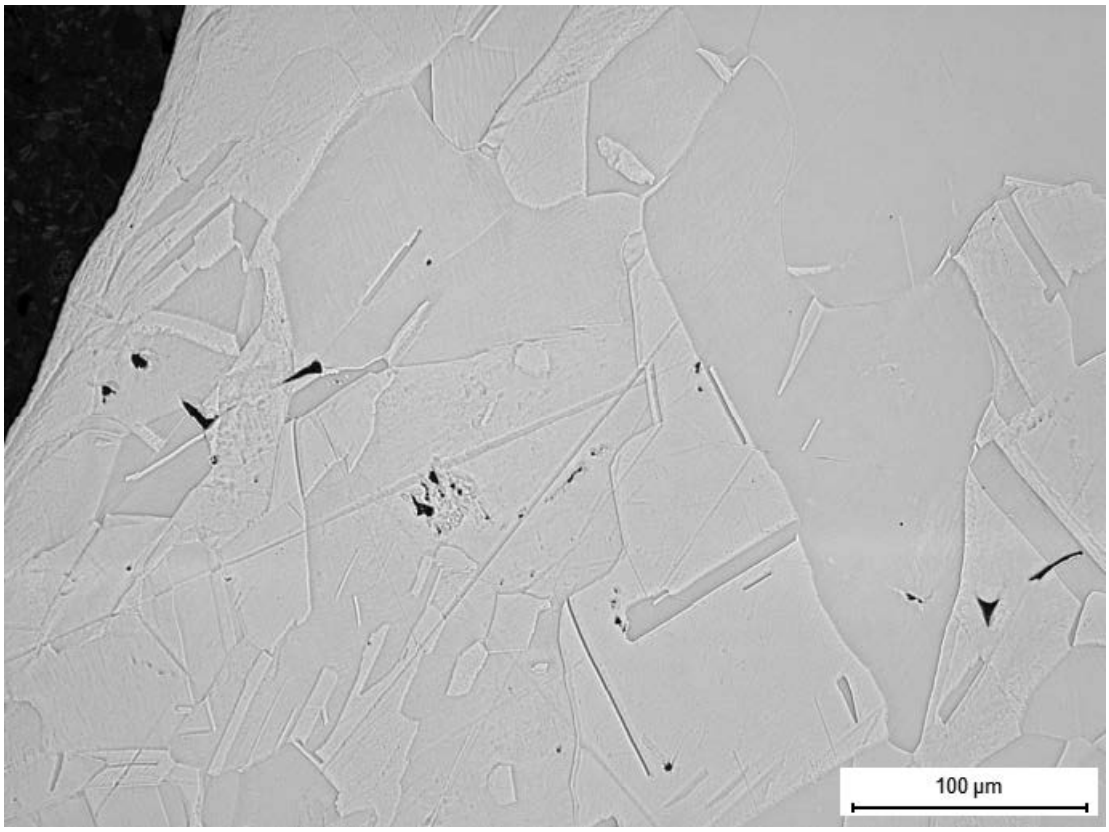

Figure A3-11. *Porosity in the material of sample M4 1:1.*

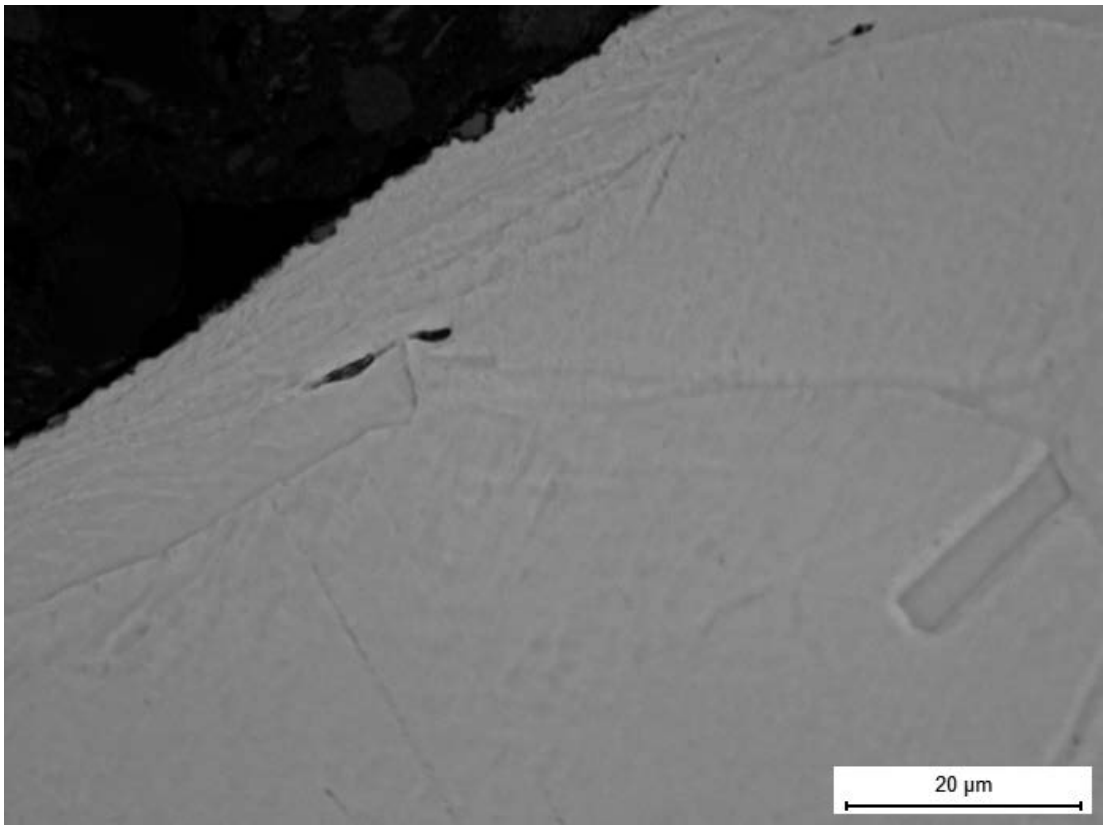

Figure A3-12. *Pores found near the cold-worked area near the outer surface of sample M4 1:1.*

The pores were examined in the SEM and EDS was carried out to determine if there were any differences to the surrounding parent material compared to the bulk of the sample. The following figures detail the analyses that were carried out on sample M4 1:1 at various points on “cross section 3”.

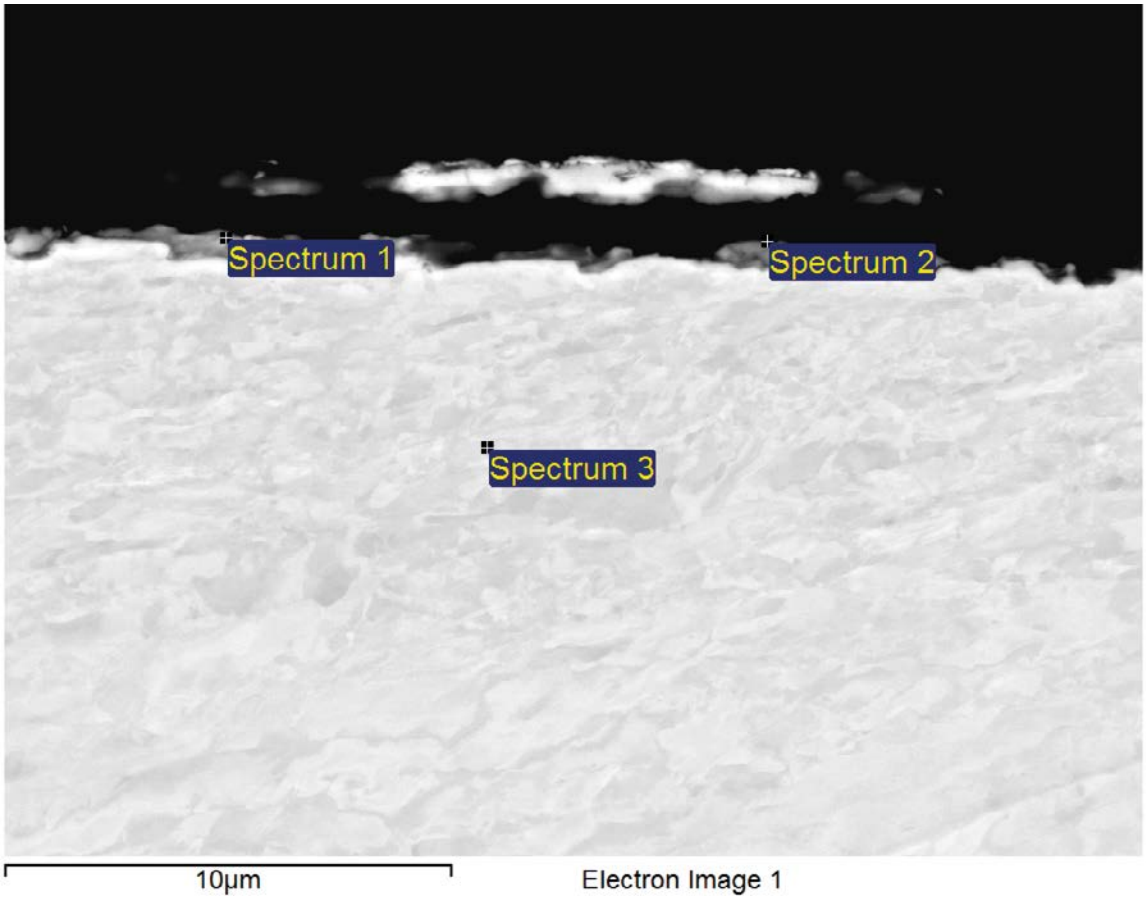

Spectrum	O	Si	S	Cl	Ca	Cu
Spectrum 1	9.84	0.77		0.88	0.30	88.21
Spectrum 2	6.76	1.96	0.99	4.49	1.54	84.26
Spec trum 3						100.00
Max.	9.84	1.96	0.99	4.49	1.54	100.00
Min.	6.76	0.77	0.99	0.88	0.30	84.26

All results in atomic%

Figure A3-13. *Copper WOL sample M4 1:1 section 3 analysis 1 – bulk material and exposed surface.*

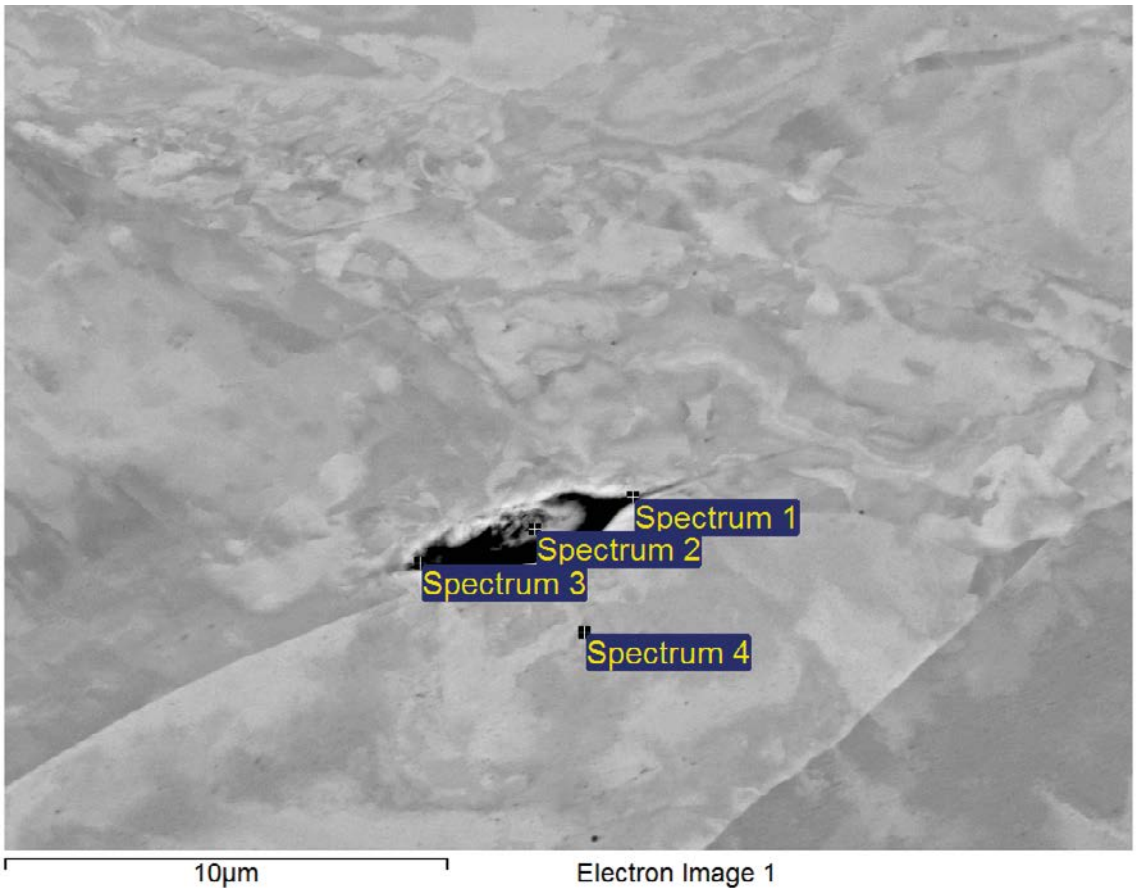

Spectrum	C	O	Si	Cu
Spectrum 1		1.94	0.36	97.69
Spectrum 2	15.32	3.30	0.59	80.79
Spectrum 3	42.60	4.60	1.70	51.09
Spectrum 4				100.00

All results in atomic%

Figure A3-14. *Copper WOL sample M4 1:1 section 3 Analysis 2 – pore at grain boundary.*

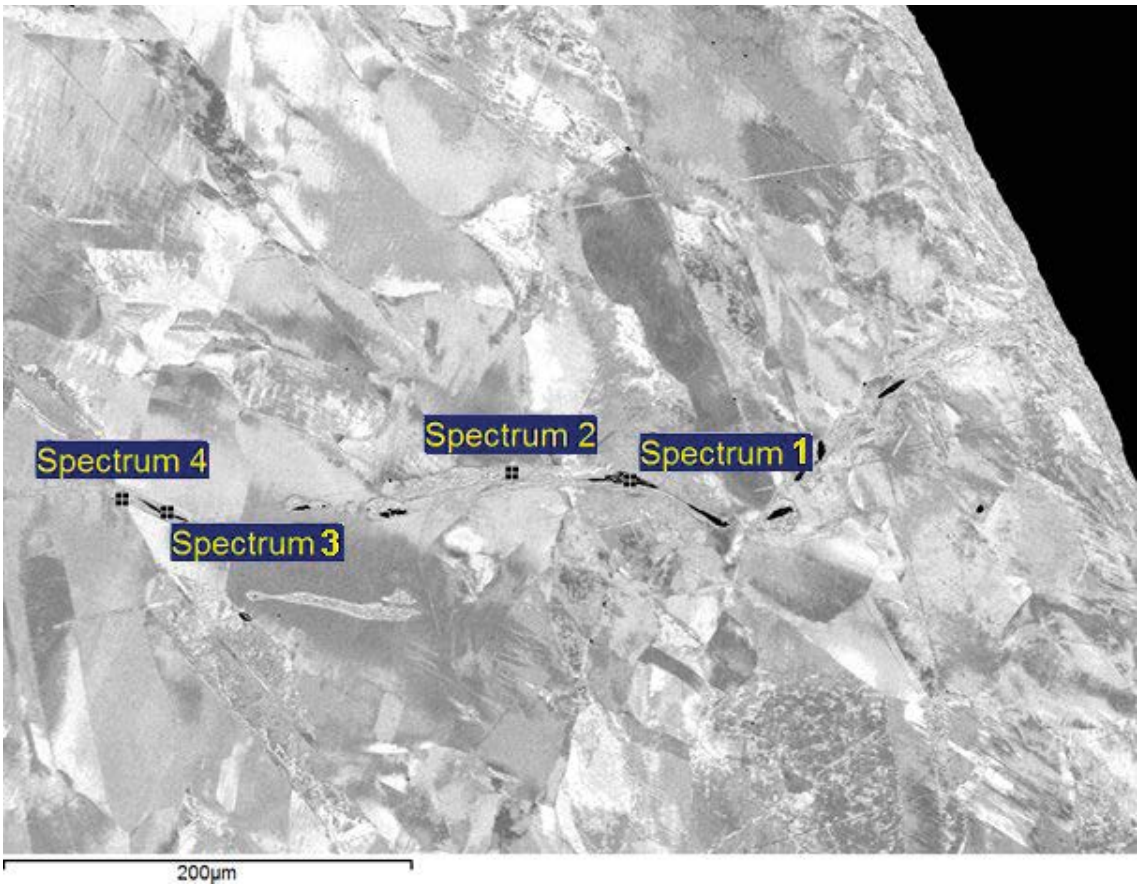

Spectrum	C	O	Si	Cu
Spectrum 1		12.65	4.54	82.81
Spectrum 2		0.96		97.80
Spectrum 3	18.88	2.36		78.76
Spectrum 4		0.83		99.17
Max.	18.88	12.65	4.54	99 .17
Min.	1.24	0.83	4.54	78.76

All results in atomic%

Figure A3-15. *Copper WOL sample M4 1:1 section 3 Analysis 2 – pores at grain boundaries.*

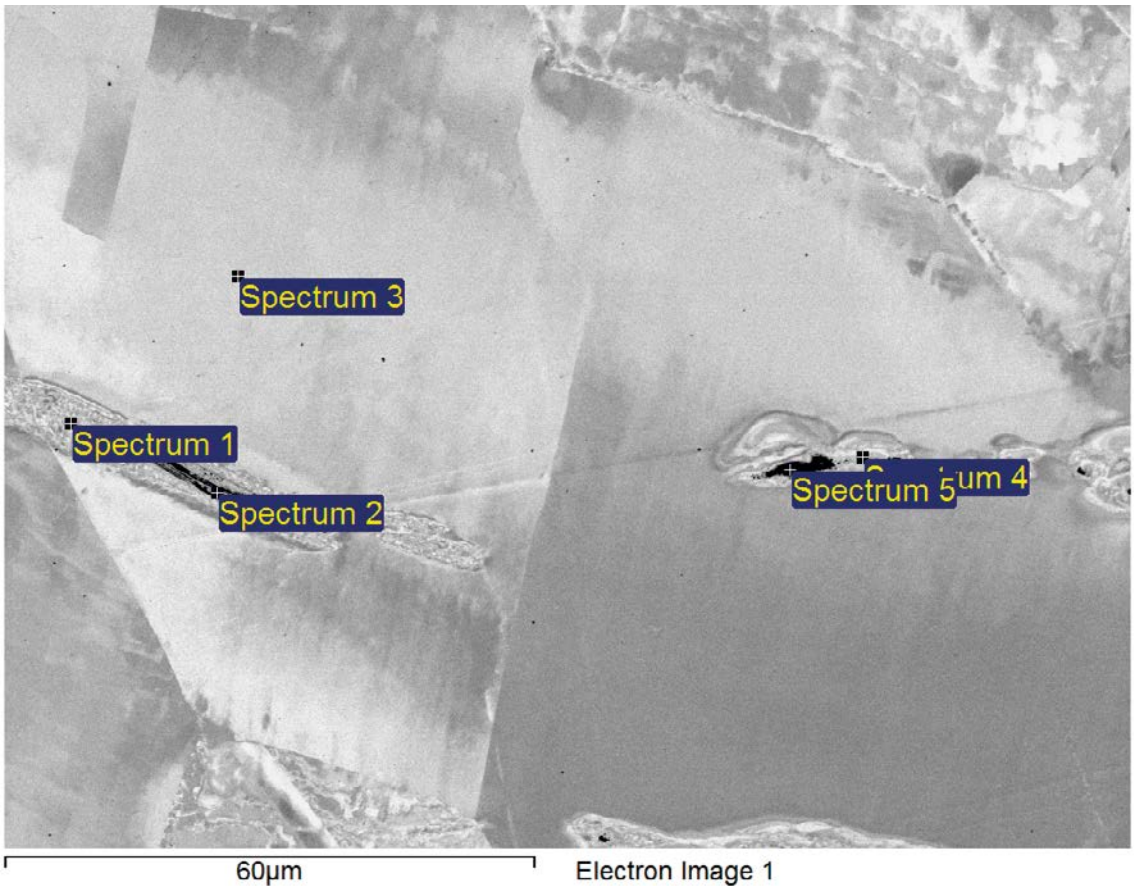

Spectrum	C	O	Si	Cu
Spectrum 1				98.58
Spectrum 2	13.87	1.81		84.31
Spectrum 3		0.98		99.02
Spectrum 4		2.24		94.68
Spectrum 5	33.91	8.15	2.87	55.07

Figure A3-16. *Copper WOL sample M4 1:1 section 3 Analysis 4 – material near pores.*

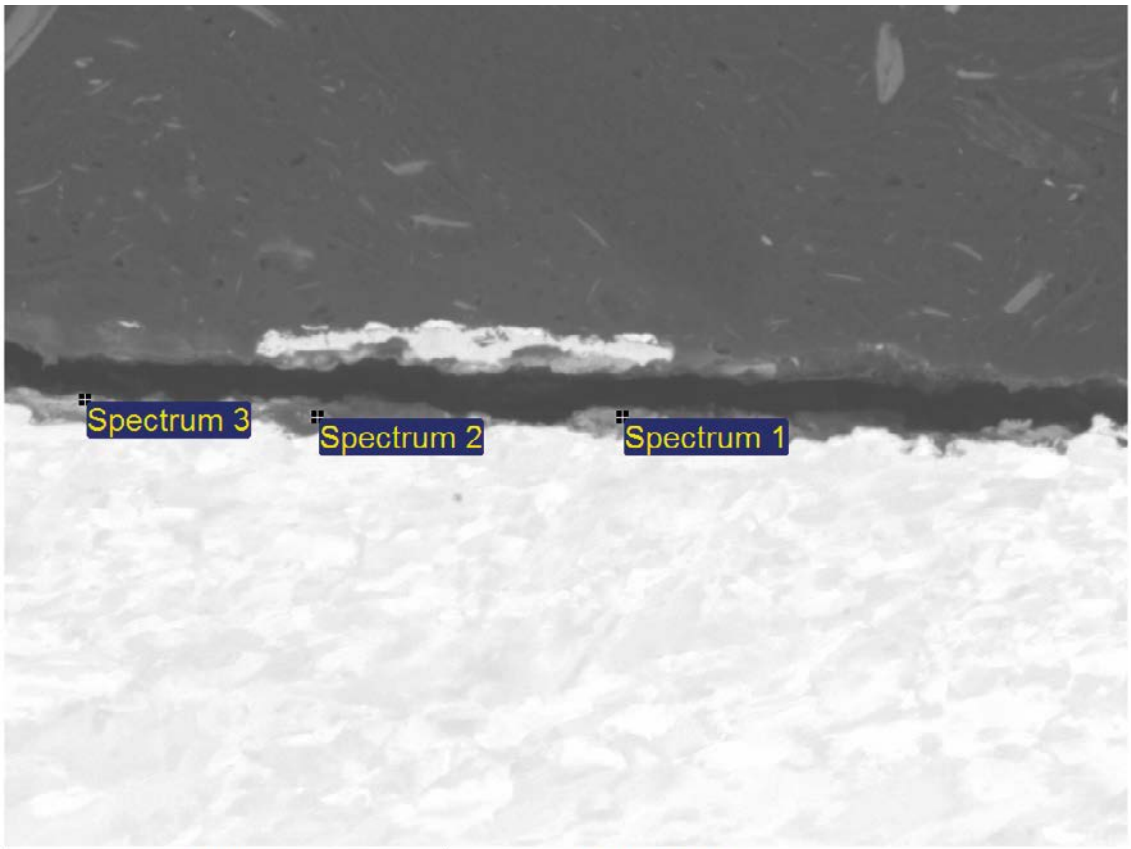

Spectrum	N	O	Si	S	Cl	Ca	Cu
Spectrum 1		10.52	4.52				84.96
Spectrum 2	12.24	15.49	1.38		2.57		68.32
Spectrum 3		5.94	2.97	3.94		50.45	36.69
Max.	12.24	15.49	4.52	3.94	2.57	50.45	84.96
Min.	12.24	5.94	1.38	3.94	2.57	50.45	36.69

All results in atomic%

Figure A3-17. *Copper WOL sample M4 1:1 section 3 Analysis 5 – surface oxide.*

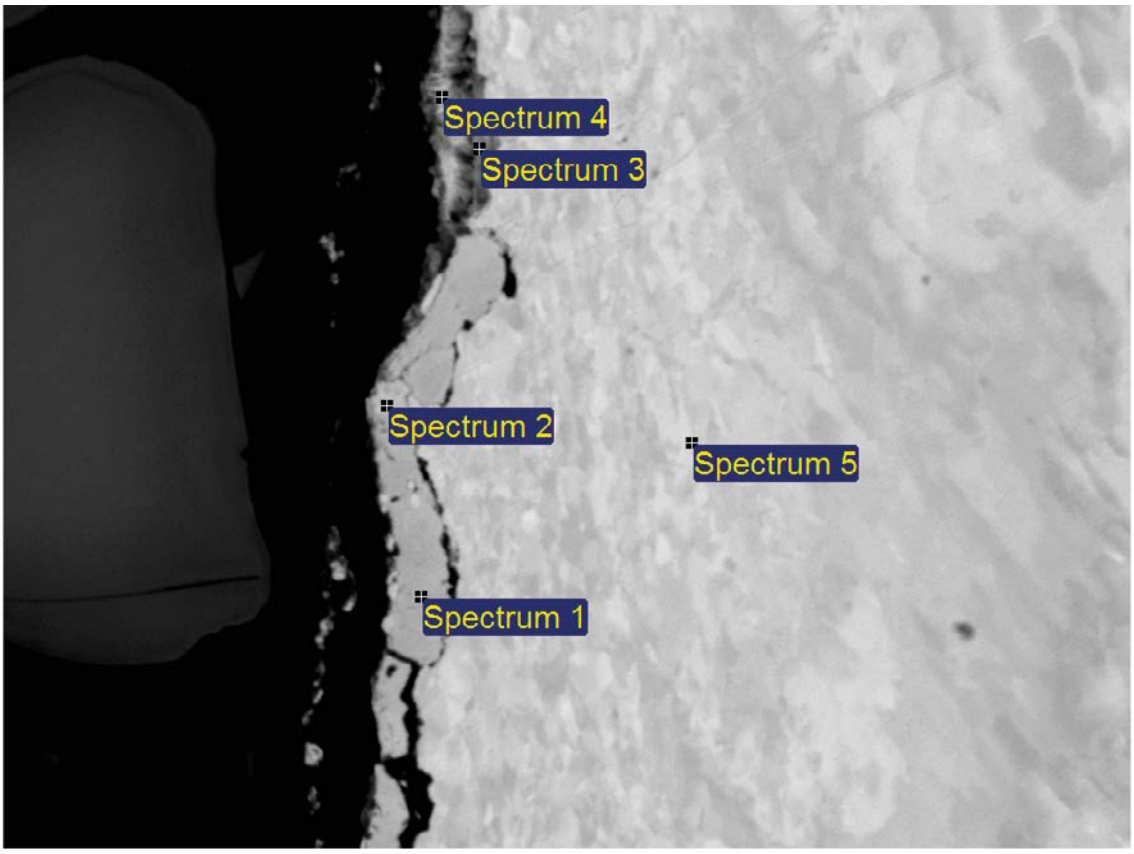

Spectrum	O	Si	Cl	Cu
Spectrum 1	26.75		3.98	69.27
Spectrum 2	29.17	0.83	2. 43	67.56
Spectrum 3	26.46		2.61	70.93
Spectrum 4	7.97	5.69	14.98	71.36
Spectrum 5				100.00

All results in atomic%

Figure A3-18. *Copper WOL sample M4 1:1 section 3 Analysis 5 – surface oxide.*

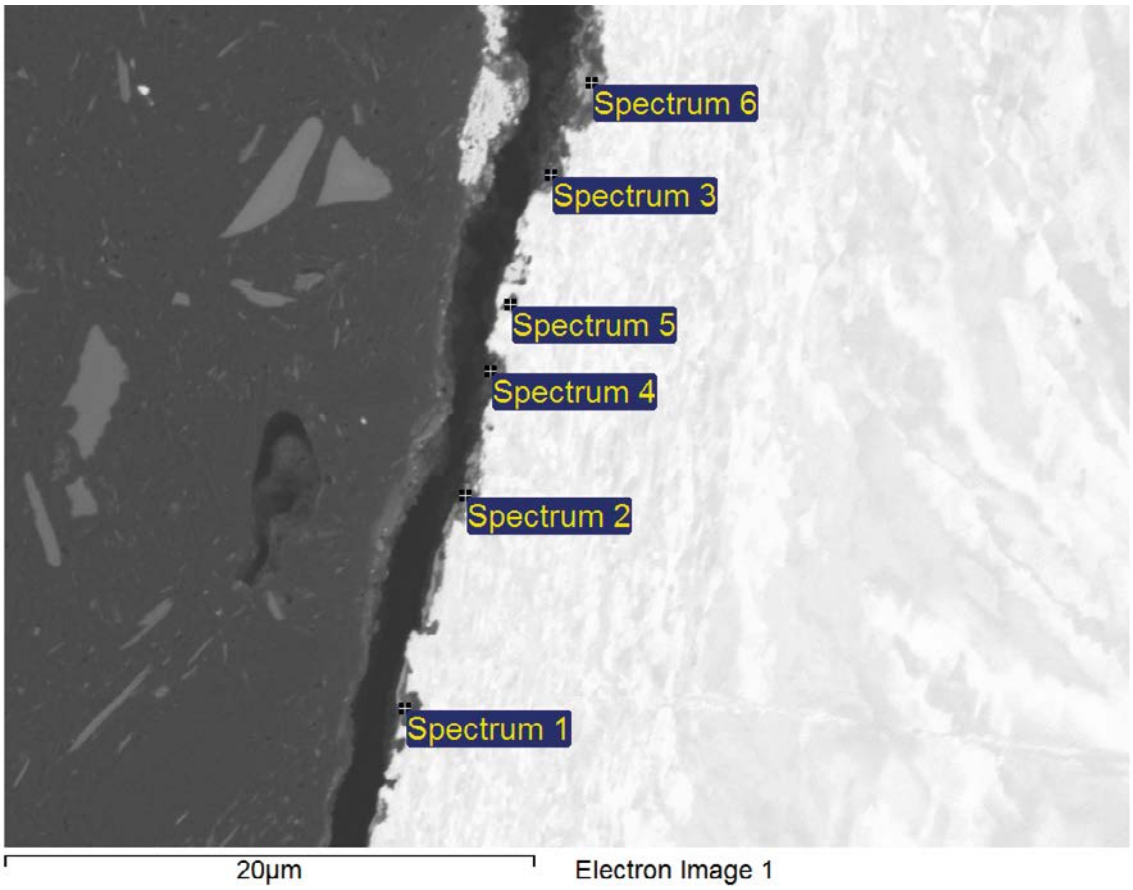

Spectrum	N	O	Mg	Si	S	Cu
Spectrum 1		20.83	0.33	2.26	1.18	75.40
Spectrum 2		17.02		11.81	3.05	68.12
Spectrum 3	15.78	17.44		4.86		61.92
Spectrum 4		4.82	6.18	18.79		70.21
Spectrum 5		9.90		7.17		82.93
Spectrum 6	8.60	16.31		2.77		72.32

All results in atomic%

Figure A3-19. *Copper WOL sample M4 1:1 section 3 Analysis 5 – surface oxide.*

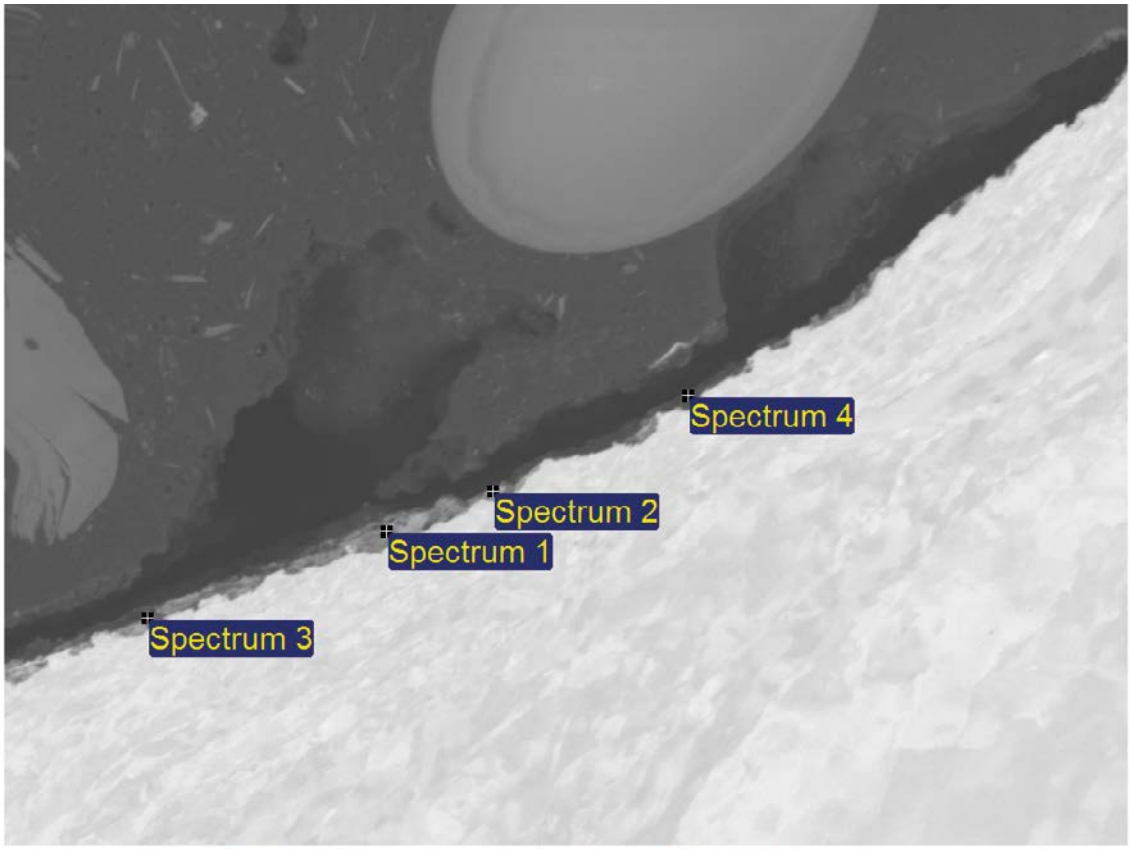

Spectrum	O	Si	Cl	Ca	Cu
Spectrum 1	8.40	0.43			91.16
Spectrum 2	20.42	27.46		33.87	18.25
Spectrum 3	2.84	29.05		23.61	44.50
Spectrum 4	42.77	22.54	17.70		17.00
Max.	42.77	29 .05	17.70	33.87	91.16
Min.	2.84	0.43	17.70	23.61	17.00

All results in atomic%

Figure A3-20. *Copper WOL sample M4 1:1 section 3 Analysis 5 – surface oxide.*

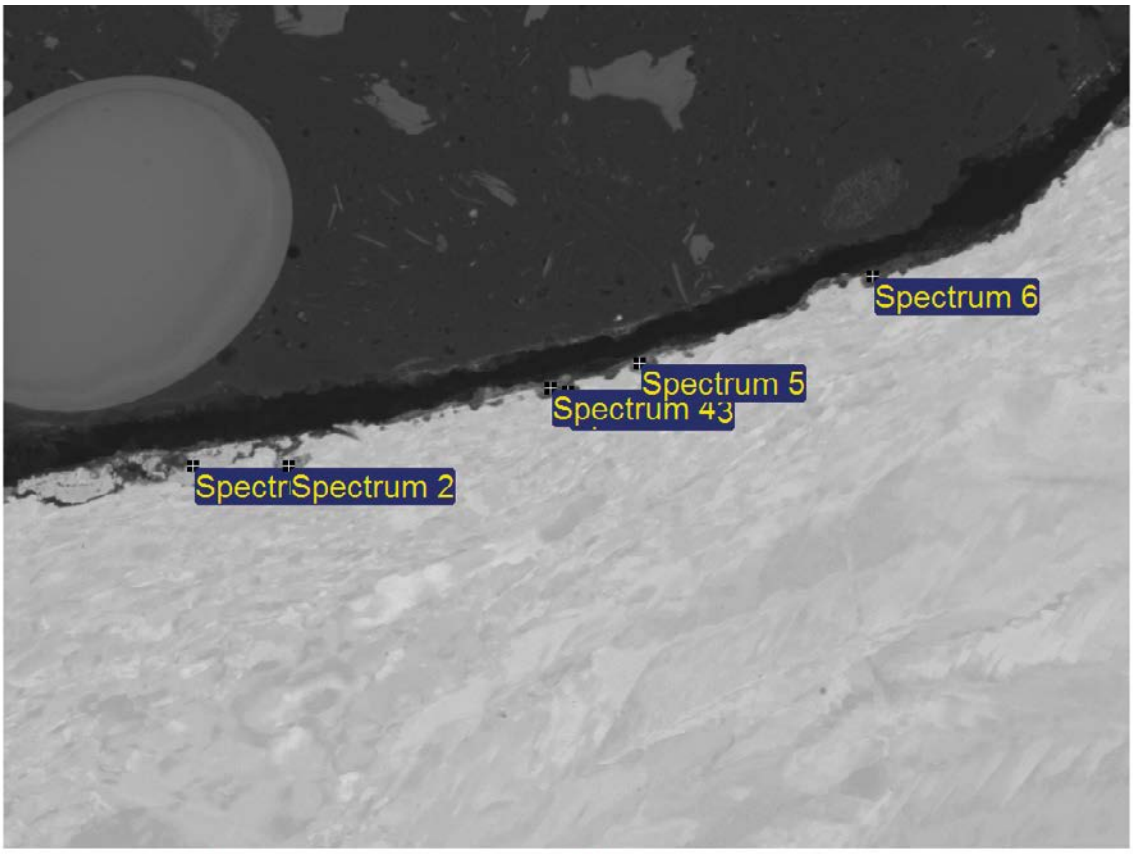

Spectrum	O	Mg	Al	Si	S	Cl	Ca	Cu
Spectrum 1	27.77					2.03		70.20
Spectr um 2	3.25							96.75
Spectrum 3	22.70	0.42	0.62	2.87			4.24	69.14
Spectrum 4	4.11		4.70	18.73	4.50		38.20	29.75
Spectrum 5	15.97		3.06	23.70	9.25			48.03
Spectrum 6	8.74	2.21		13.64			36.24	39.17

All results in atomic%

Figure A3-21. *Copper WOL sample M4 1:1 section 3 Analysis 5 – surface oxide.*

U-bend sample M4 2:1

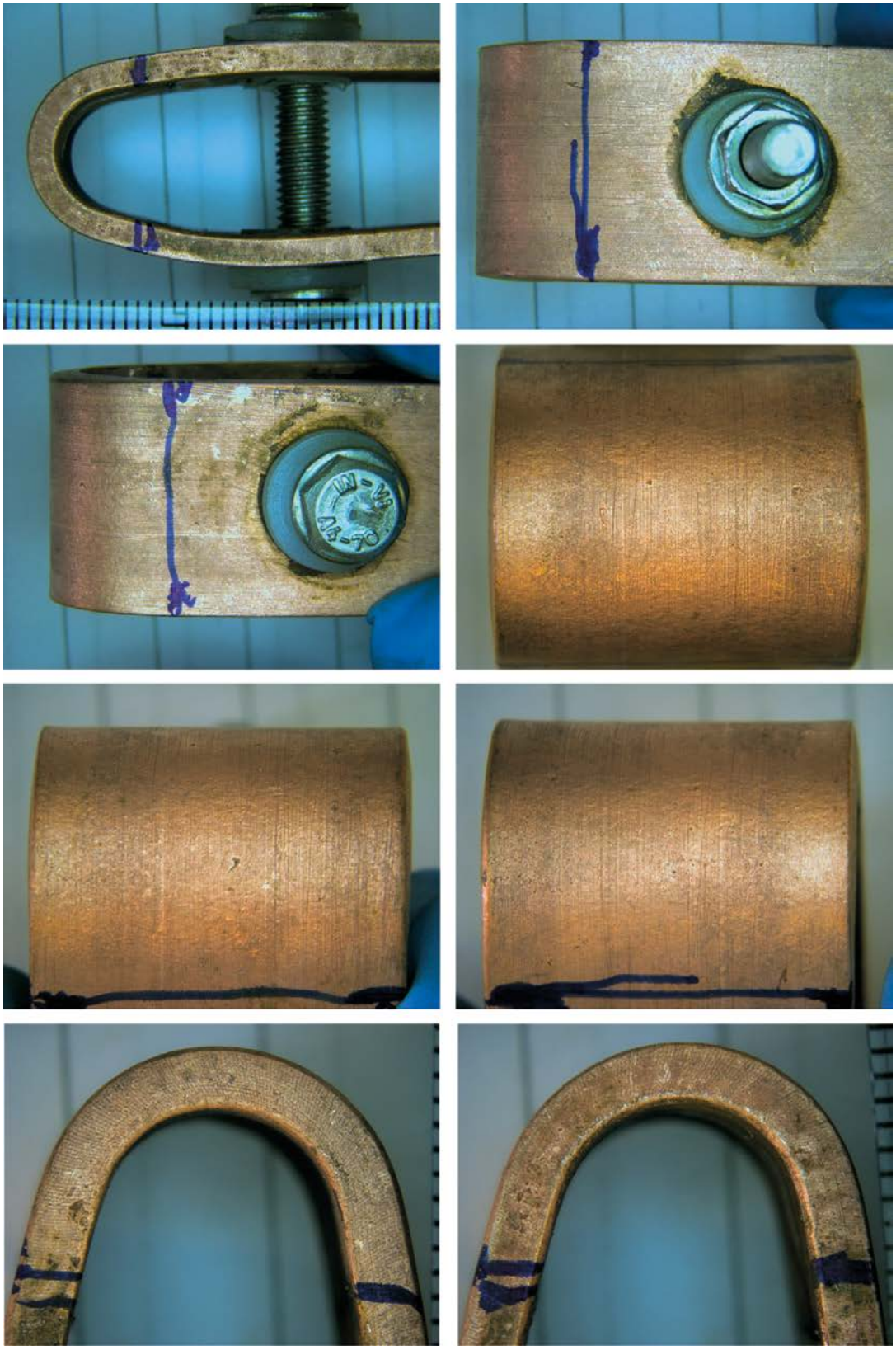

Figure A3-22. *Microscope images of U-bend sample M4 2:1. From top left to bottom right: edge of sample; side of sample marked before sectioning; opposite side of sample marked before sampling; outer surface of bend at top of sample; outer surface of bend side of sample; outer surface of bend opposite side of sample; edge of sample marked before sectioning; opposite edge of sample marked before sectioning.*

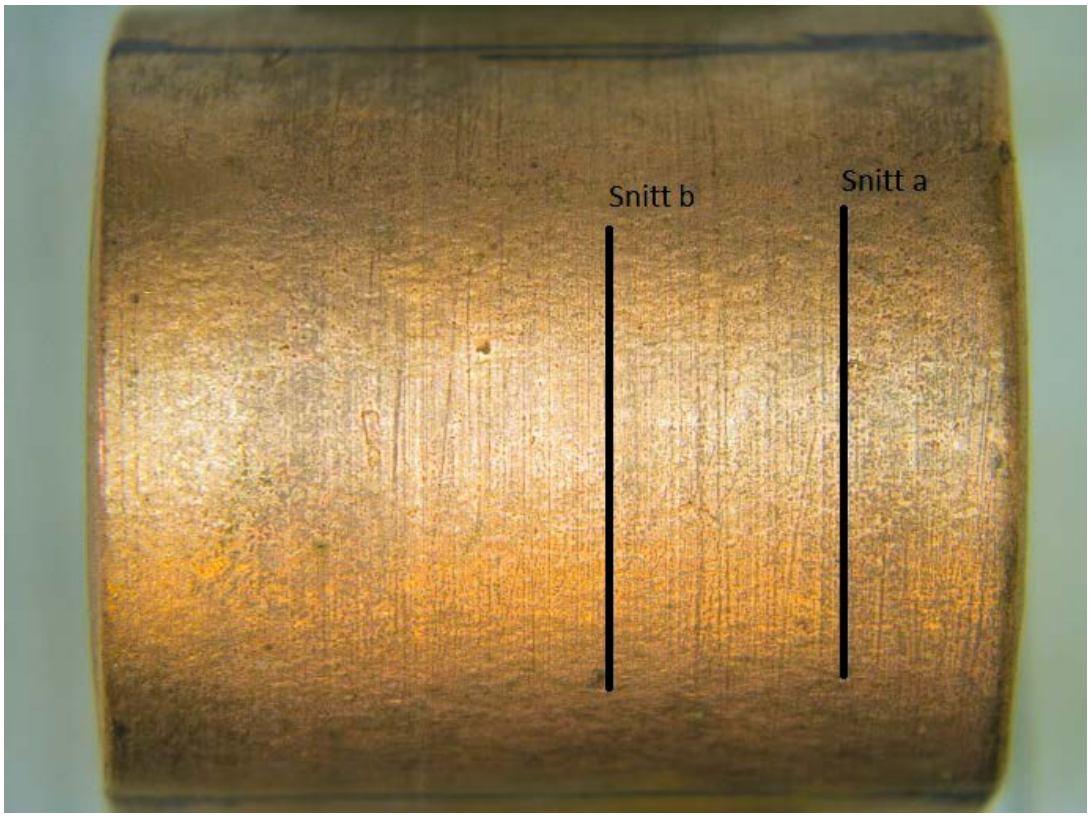

Figure A3-23. *U-bend sample M4 2:1 with approximate locations of sections taken for further analysis. Section a is 4.1 mm from the edge of the sample (right hand side of image), and section b is 9.1 mm from the edge of the sample.*

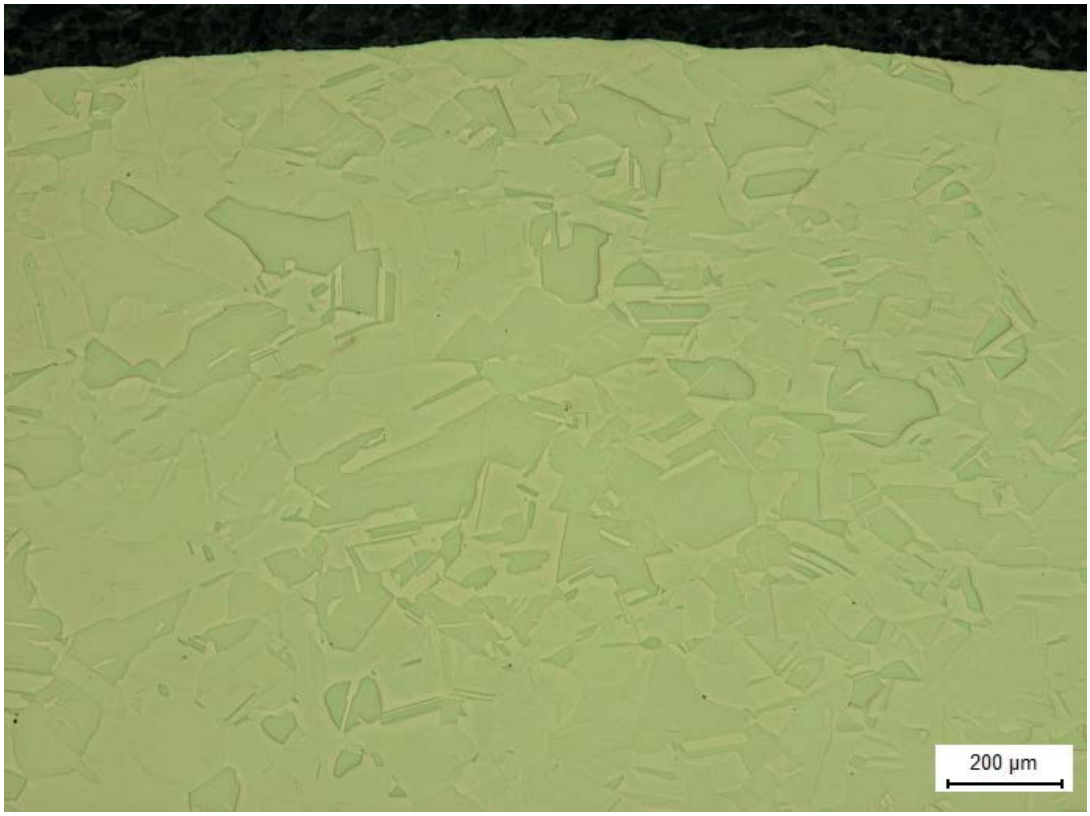

Figure A3-24. *Microscope image of section a showing microstructure.*

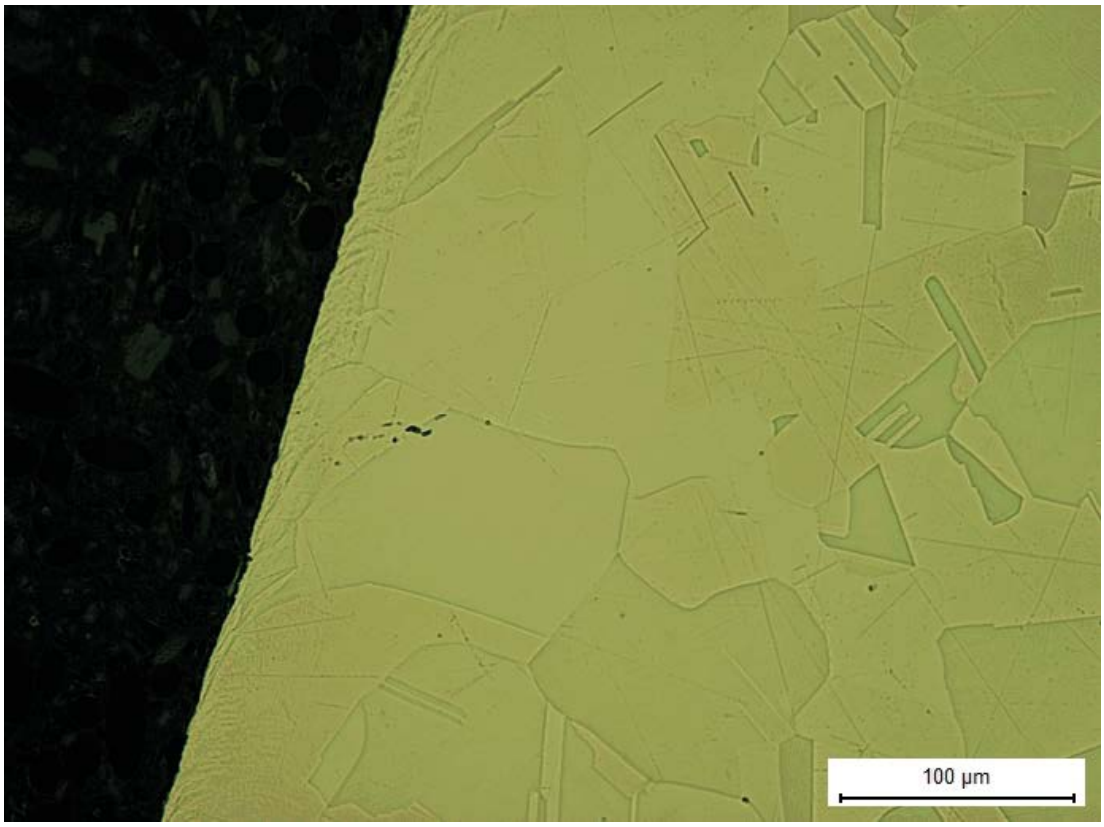

Figure A3-25. *Microstructure of section a. Defects/pores found on section a, near to grain boundaries.*

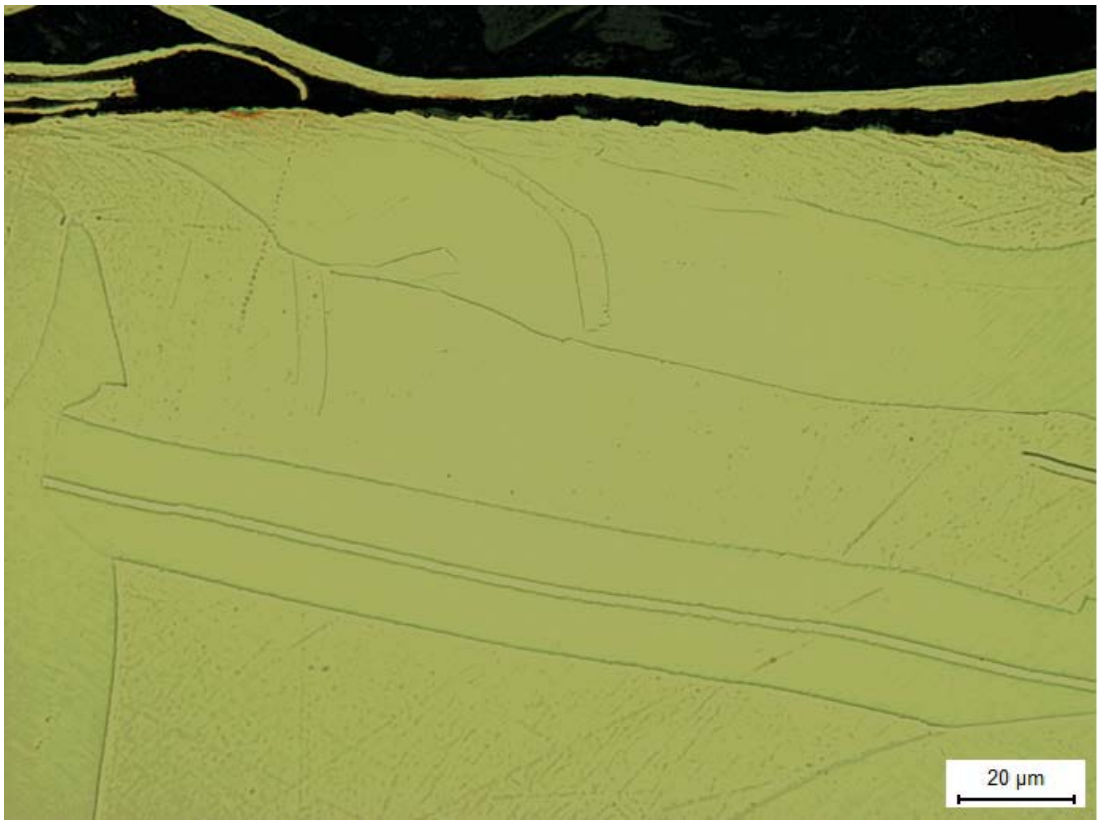

Figure A3-26. *Detail of Figure 25 showing cold-worked region of material near to the outer surface of the sample.*

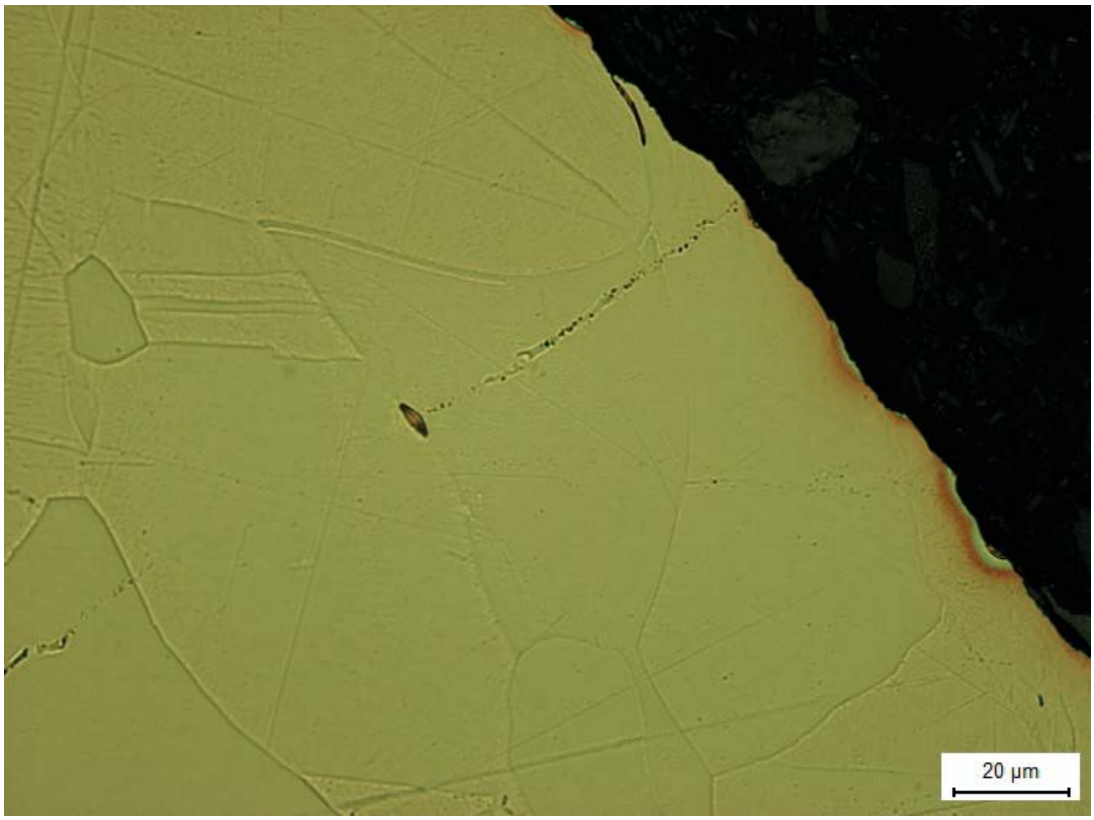

Figure A3-27. *A line of pores emanating from the outer surface of the sample in towards a pore in the material, as seen on section b.*

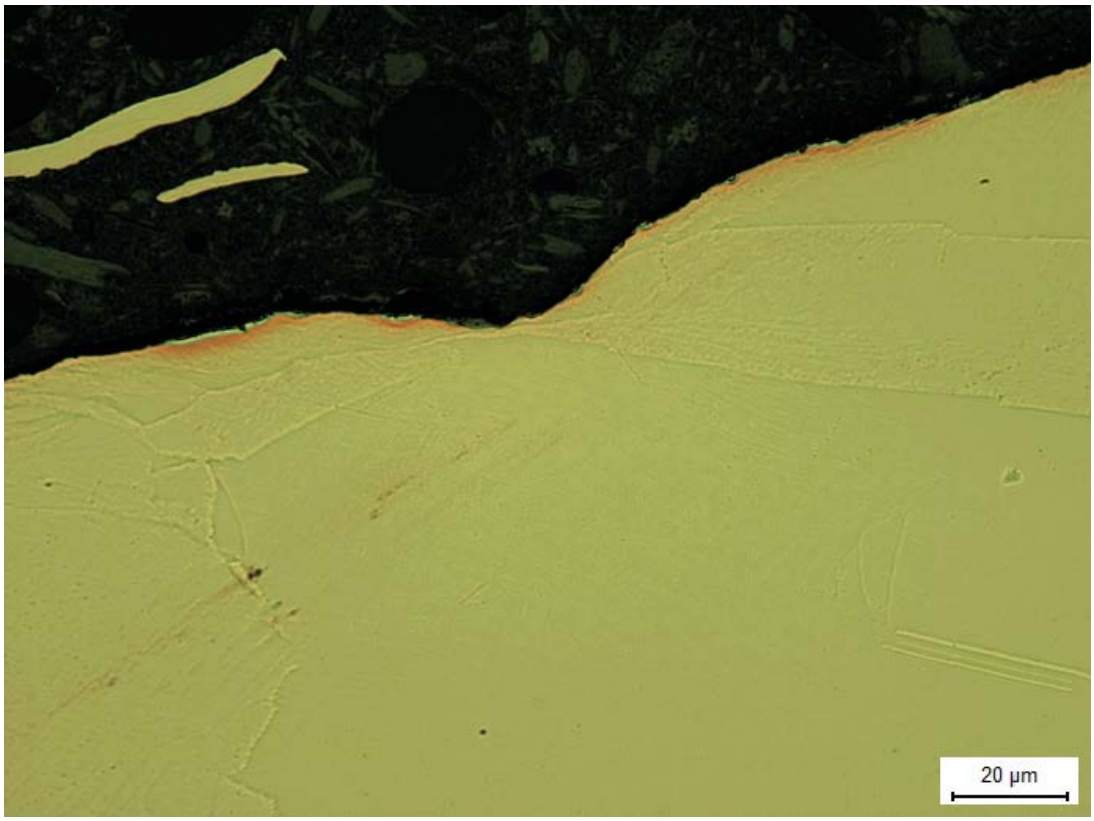

Figure A3-28. *A pit found on the outer surface of the sample on section b, which was the deepest of all pits seen on both sections a and b.*

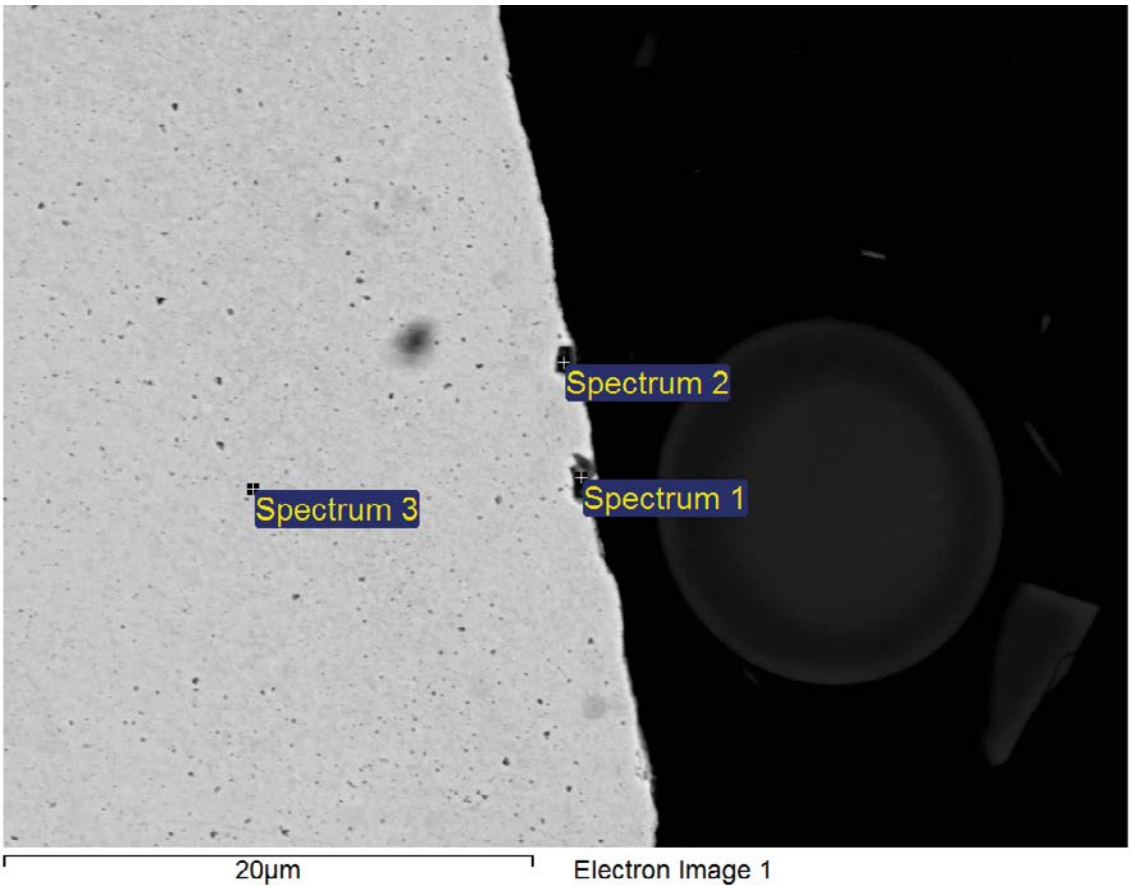

Spectrum	O	Al	Si	S	Ca	Cu
Spectrum 1	15.71	3.69	0.95	0.83	1.45	77.36
Spectrum 2	26.66	1.69	0.88	1.15	2.48	67.14
Spectrum 3	0.49					99.51
Max.	26.66	3.69	0.95	1.15	2.48	99.51
Min.	0.49	1.69	0.88	0.83	1.45	67.14

All results in atomic%.

Figure A3-29. *EDS analysis on 2 corrosion pits found on the surface of U-bend sample M4 2:1.*

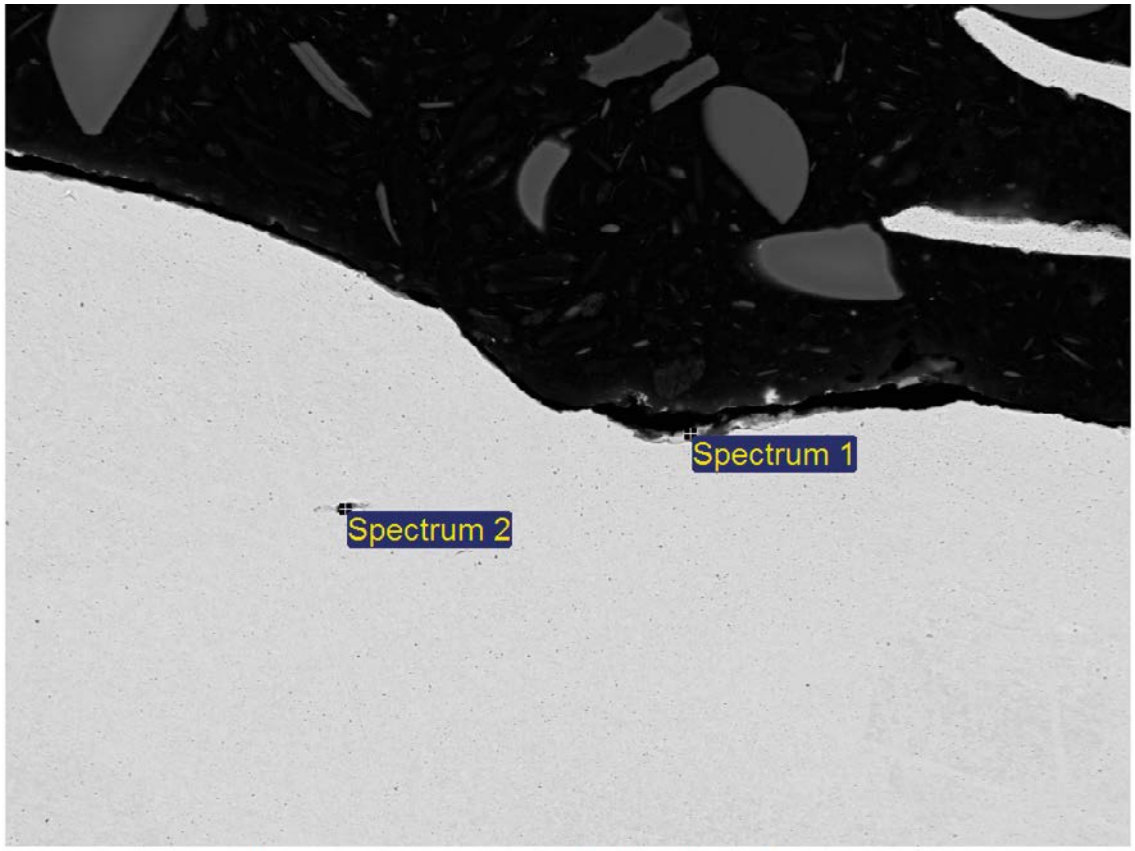

Spectrum	C	O	Al	Si	S	Cl	Ca	Cu
Spectrum 1	31.26	24.12		0.20	0.39	2.21	0.21	41.59
Spectrum 2	6.45	19.43	13.02		0.78			60.32
Max.	31.26	24.12	13.02	0.20	0.78	2.21	0.21	60.32
Min.	6.45	19.43	13.02	0.20	0.39	2.21	0.21	41.59

All results in atomic%.

Figure A3-30. *EDS analysis of U-bend sample M4 2:1 at surface pit/defect (spectrum 1) and at pore in material (spectrum 2).*

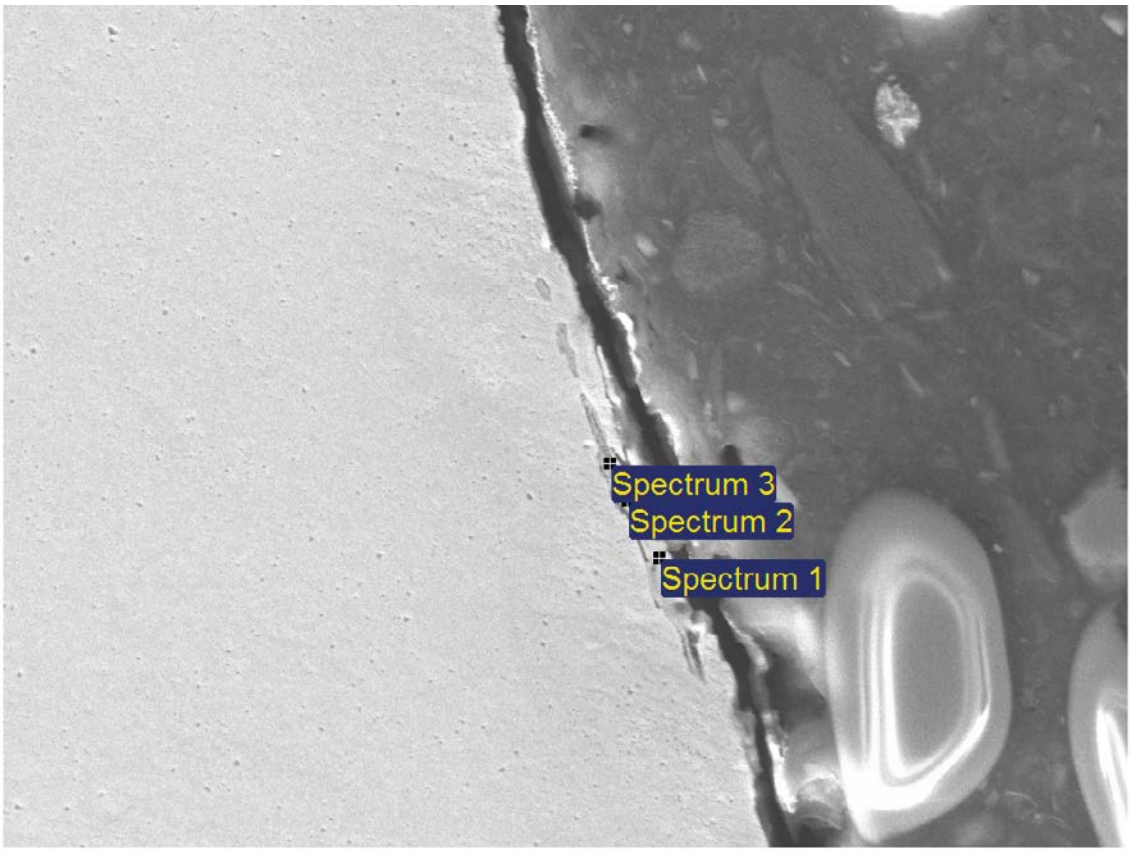

Spectrum	O	S	Cl	Ca	Cu
Spectrum 1	28.67	1.05	5.66	0.45	64.16
Spectrum 2	28.04	1.76	3.42	0.40	66.38
Spectrum 3	26.86	1.31	2.78	0.31	68.75
Mean	27.85	1.37	3.95	0.39	66.43
Std. deviation	0.92	0.36	1.52	0.07	2.29
Max.	28.67	1.76	5.66	0.45	68.75
Min.	26.86	1.05	2.78	0.31	64.16

All results in atomic%.

Figure A3-31. *EDS analysis of surface oxide layer on U-bend sample M4 2:1.*

WOL sample M4 3.1

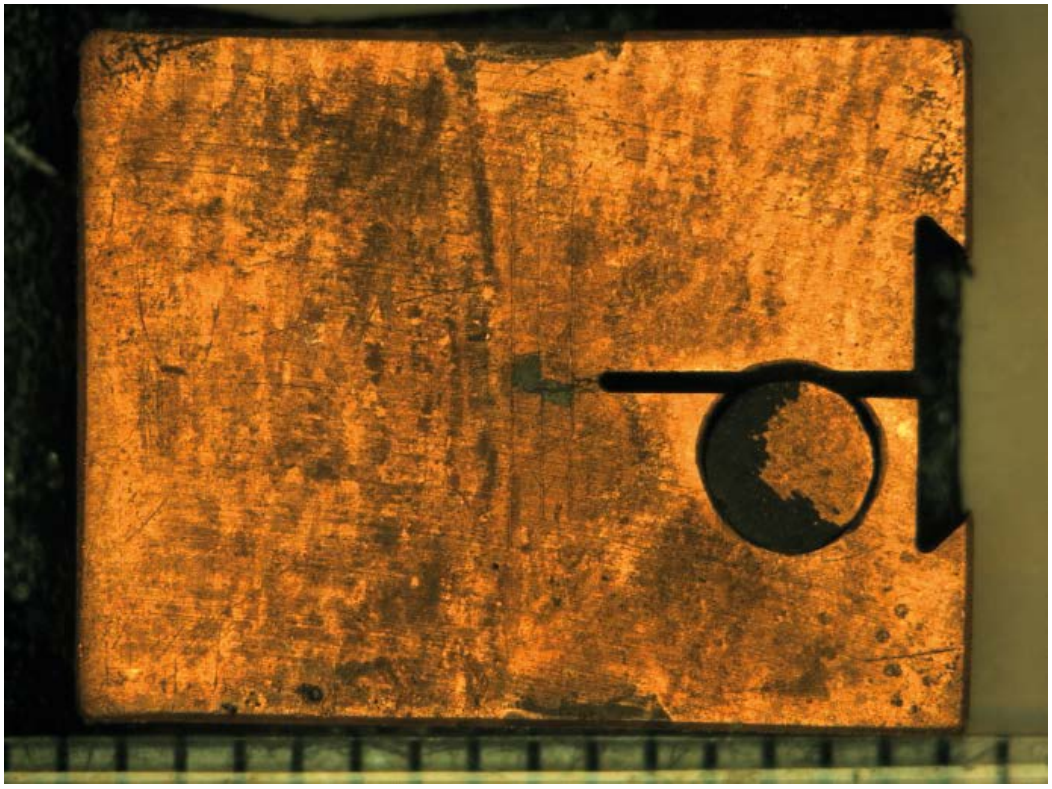

Figure A3-32. *Microscope image of WOL sample M4 3:1 after exposure. Black deposits can be seen in the notch and around the pin.*

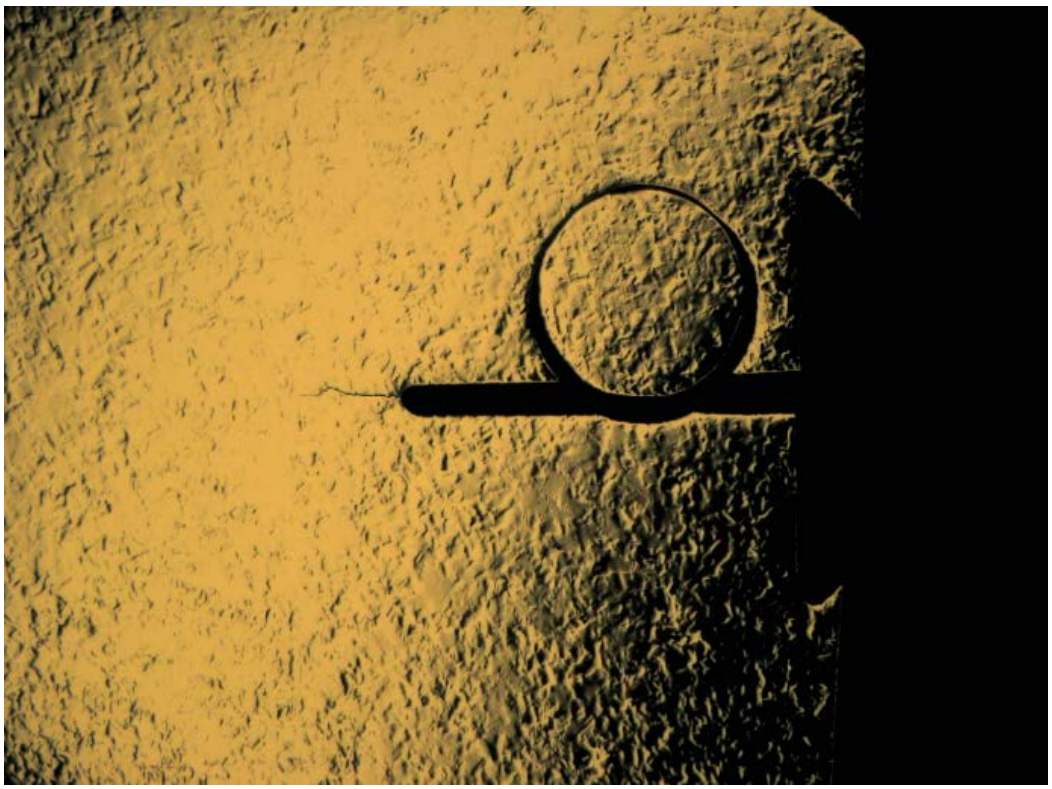

Figure A3-33. *Pre-crack at the end of notch of WOL sample M4 3:1.*

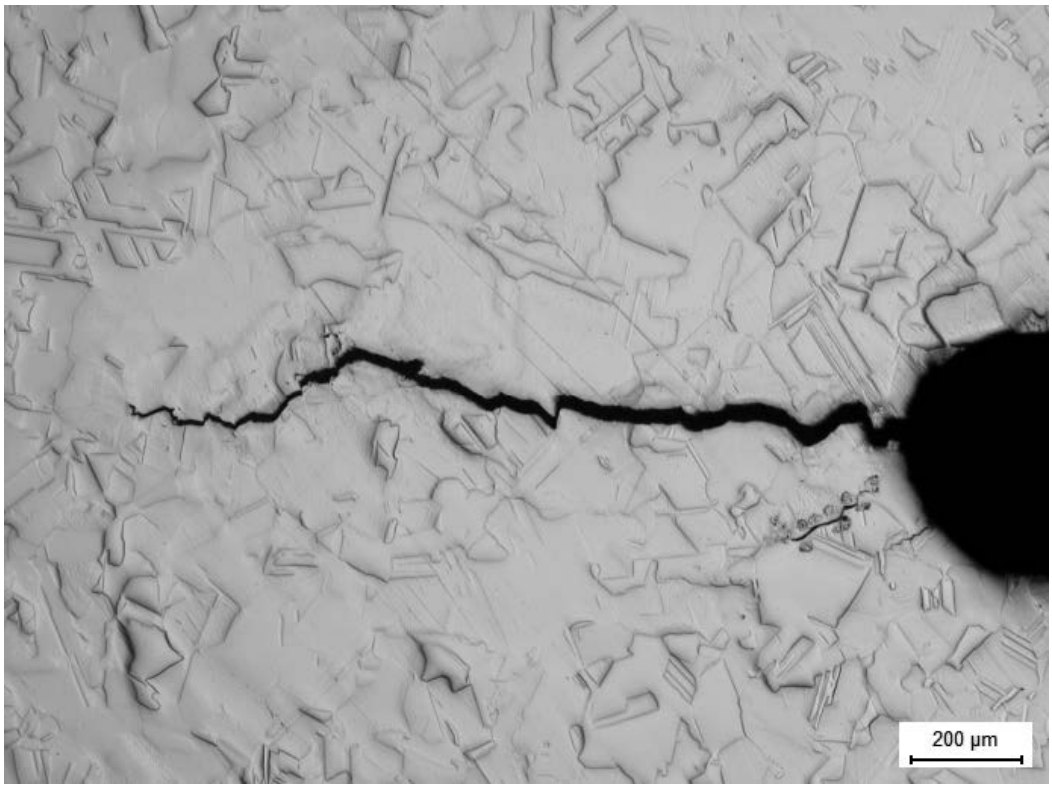

Figure A3-34. *Detail of pre-crack of WOL specimen M4 3:1 after polishing.*

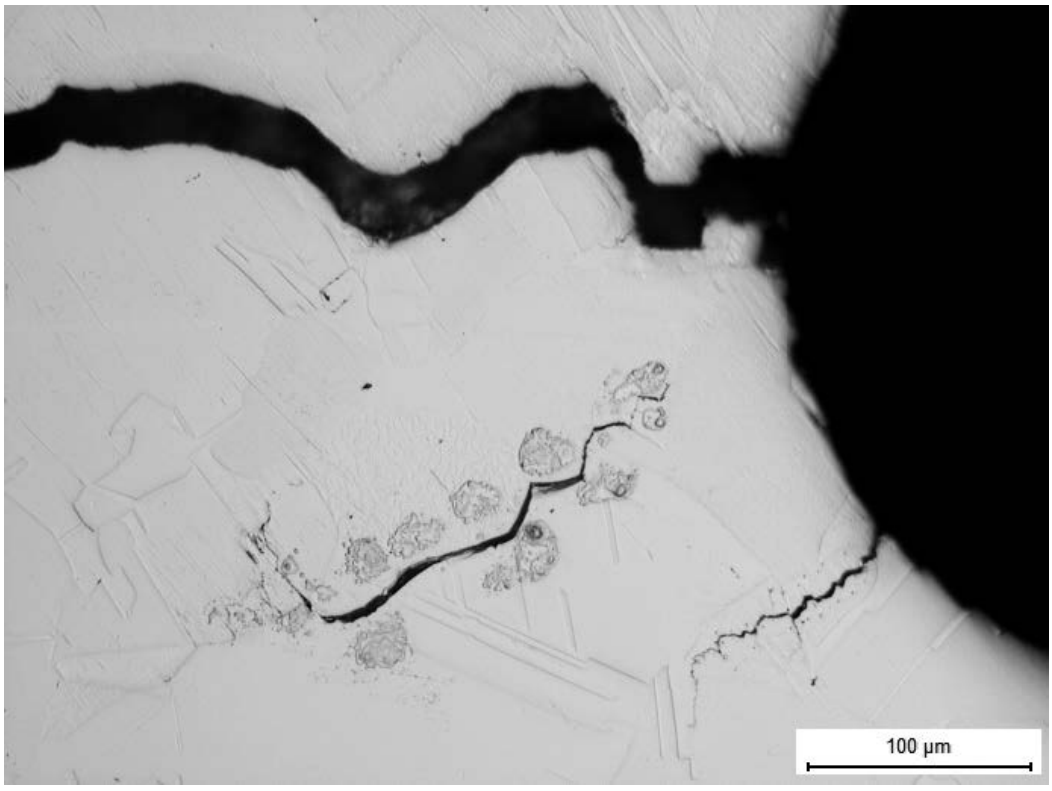

Figure A3-35. *Detail of Figure A3-34, smaller cracks seen near end of the notch of WOL specimen M4 3:1.*

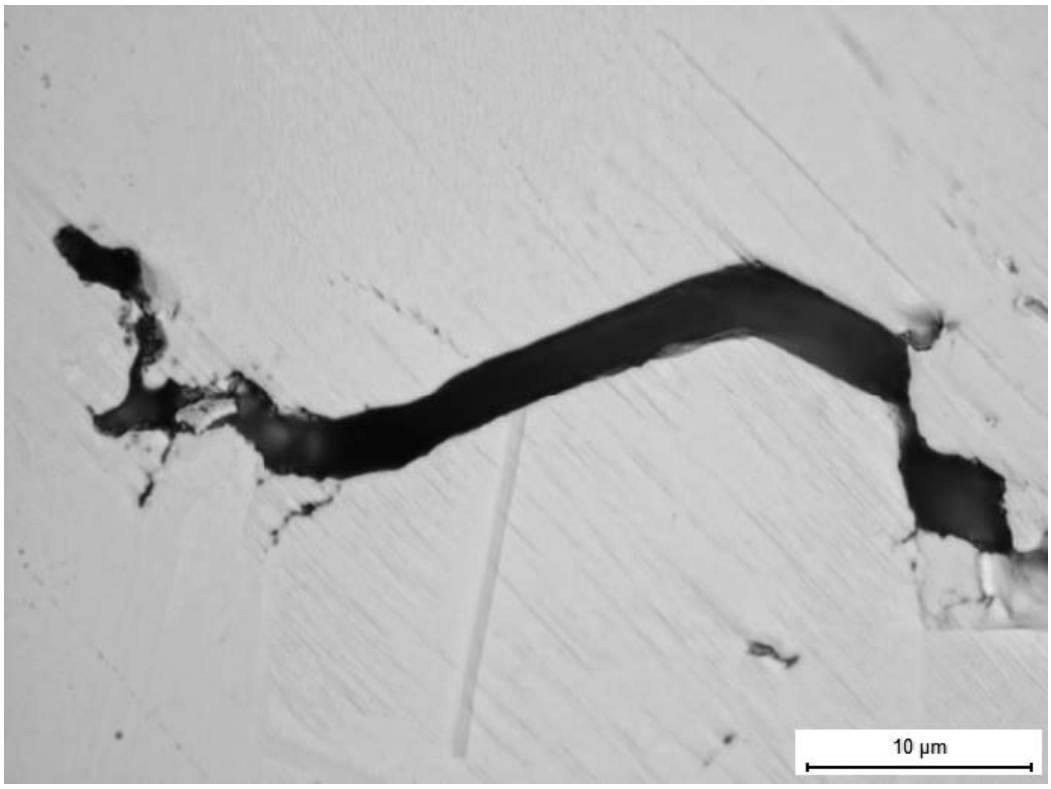

Figure A3-36. *Detail of Figure A3-34, crack tip of WOL specimen M4 3:1.*

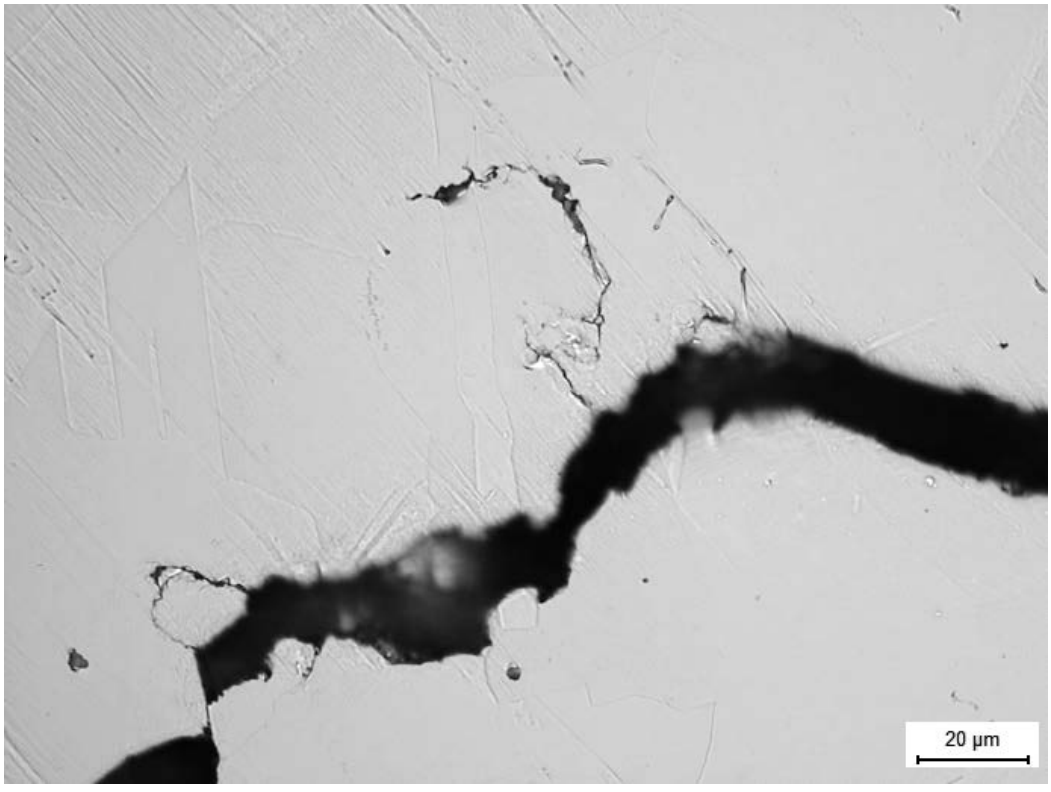

Figure A3-37. *Detail of Figure A3-34, mid crack of WOL specimen M4 3:1, with smaller cracks travelling perpendicular to the main crack.*

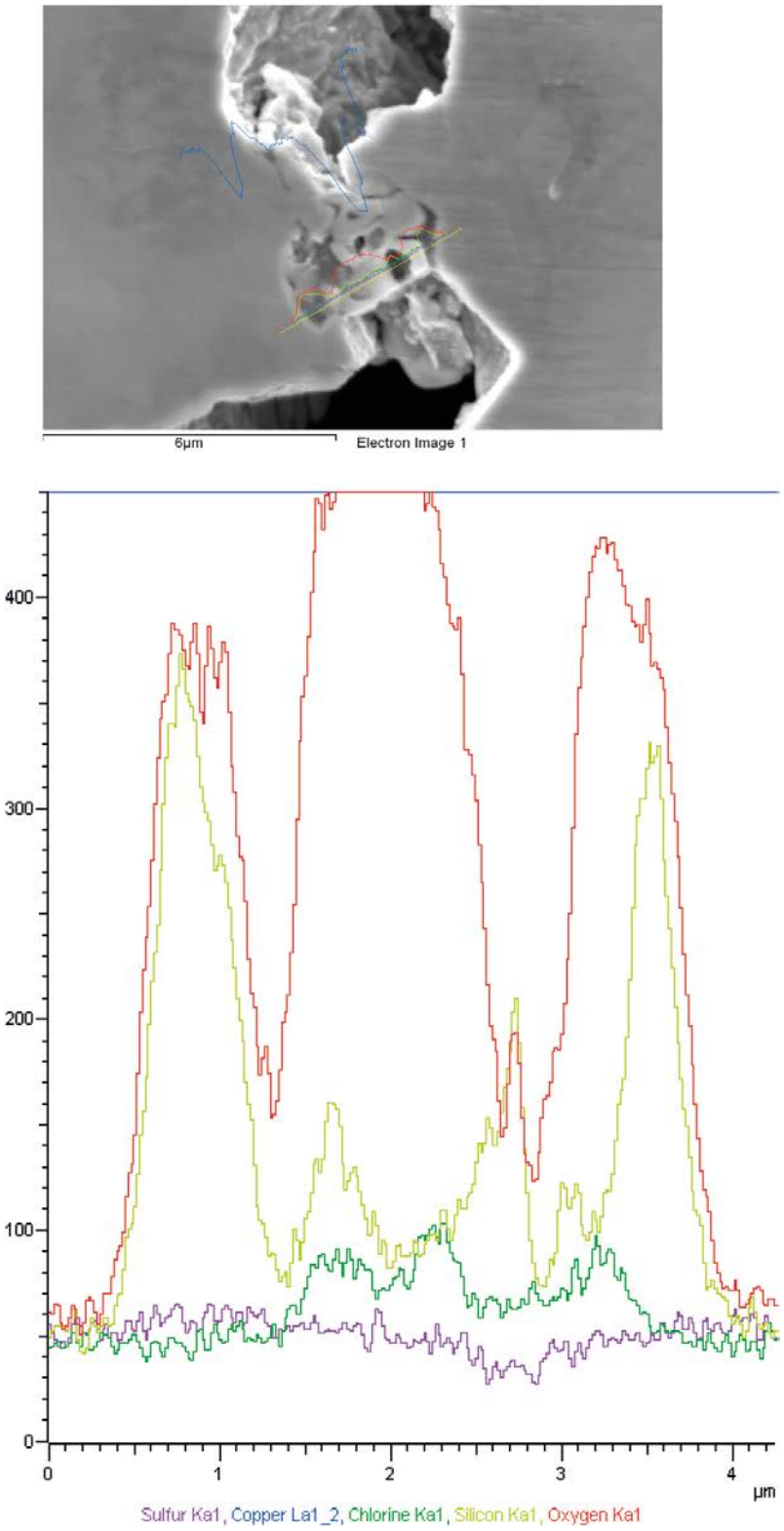

Figure A3-38. *EDS linescan of crack tip on WOL sample M4 3:1. Oxygen, silicon and chlorine vary across the crack area.*

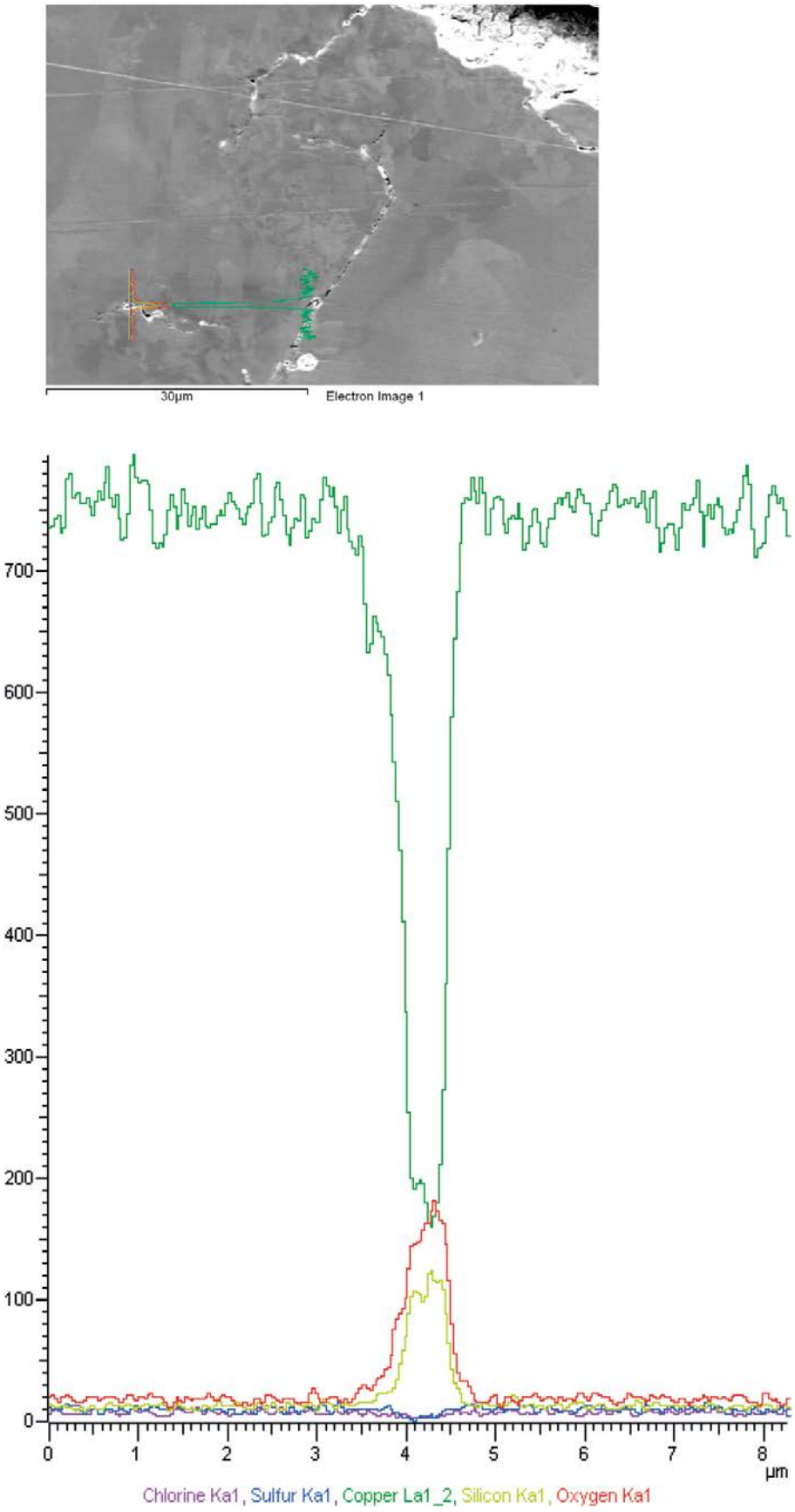

Figure A3-39. *EDS linescan of a secondary crack located near middle position of main crack. Oxygen and silicon vary over the area of the scan.*

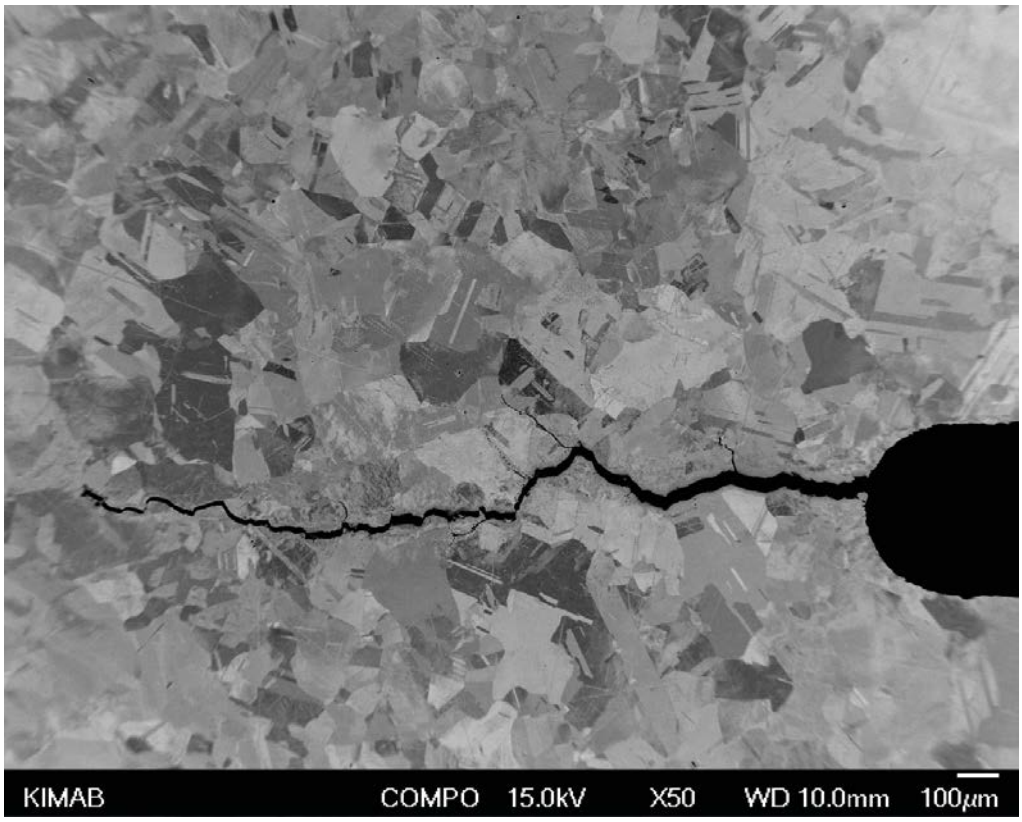

Figure A3-40. *SEM image of WOL sample M4 3:1, polished 1.24 mm from exposed surface. Several smaller cracks can be seen emanating from the pre-crack perpendicular to the direction of the pre-crack.*

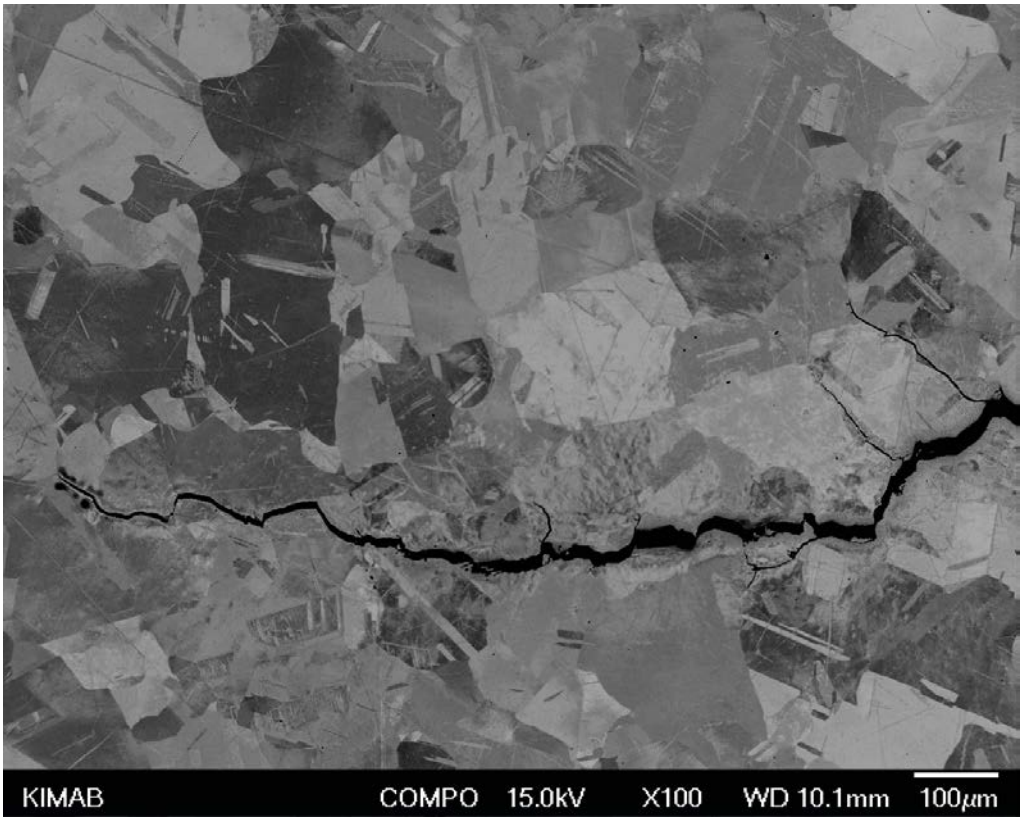

Figure A3-41. *SEM image of WOL sample M4 3:1 showing the cold deformation in the parent material at the sides of the pre-crack.*

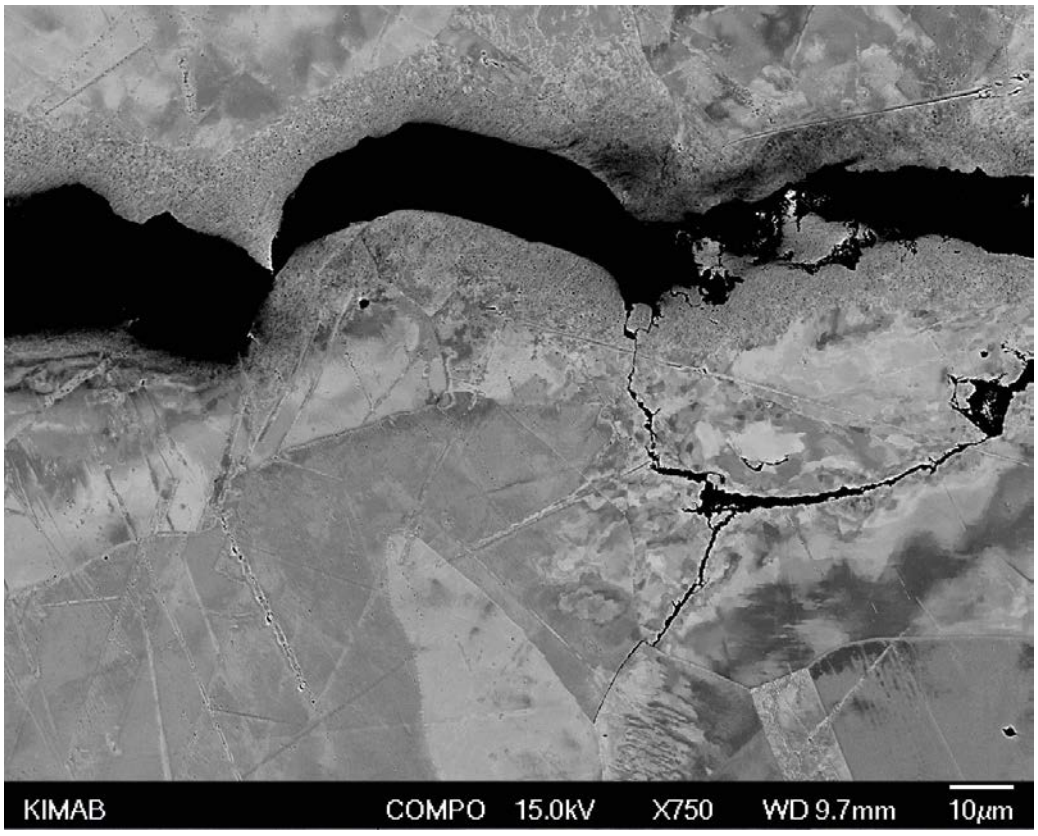

Figure A3-42. *SEM image of WOL sample M4 3:1, detail of the cold deformation in the material near the pre-crack due to the fatigue loading of the sample in producing the pre-crack.*

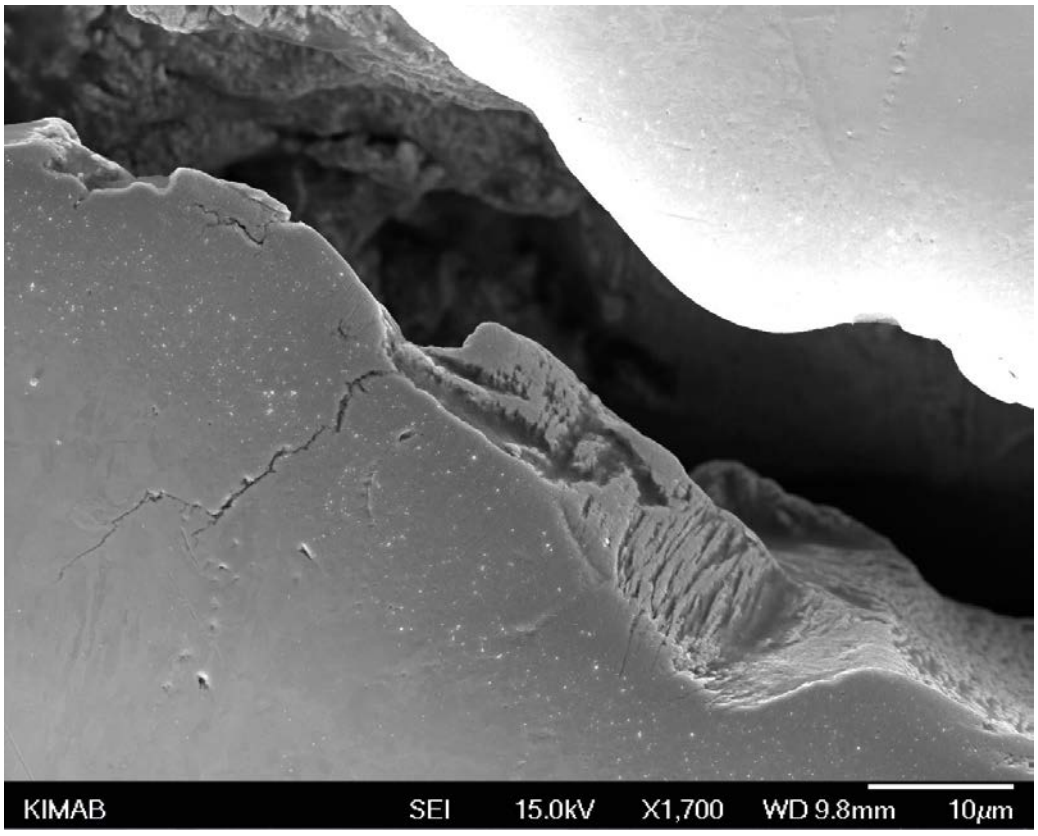

Figure A3-43. *Detail of the pre-crack of WOL sample M4 3:1 showing the oxidised fracture surface and a smaller secondary crack seen on the left hand side of the image.*

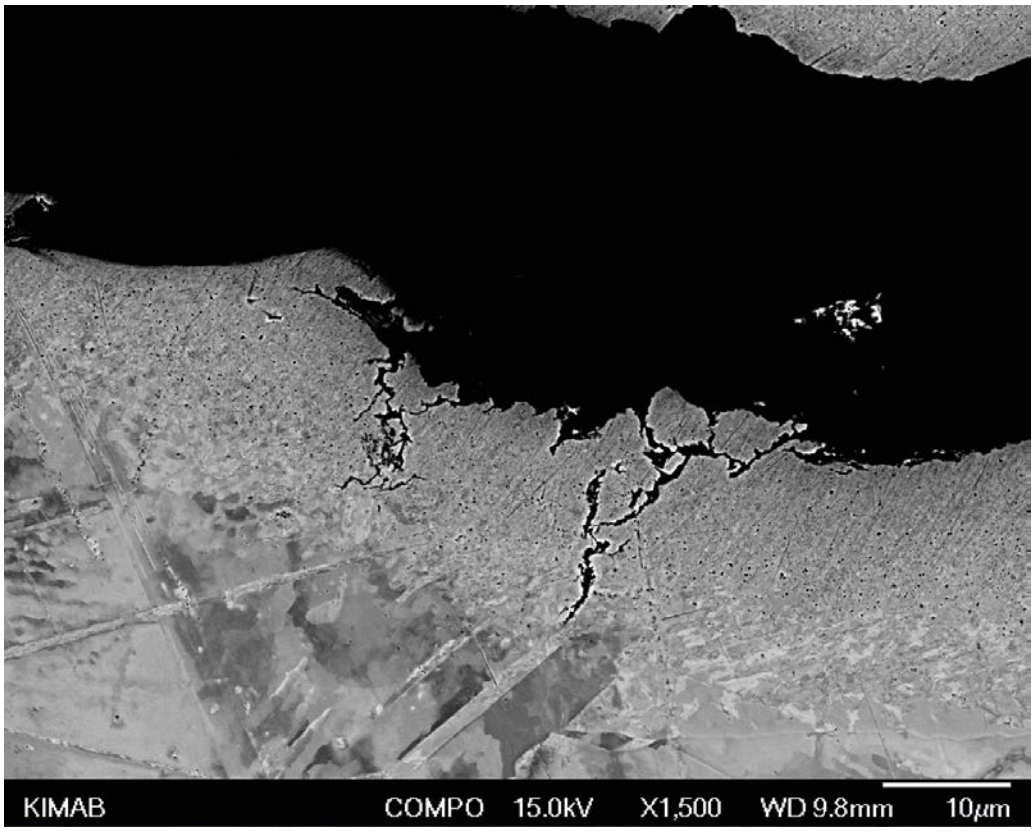

Figure A3-44. *Detail of the pre-crack of WOL sample M4 3:1 showing smaller secondary cracks in the cold deformed area of the material.*

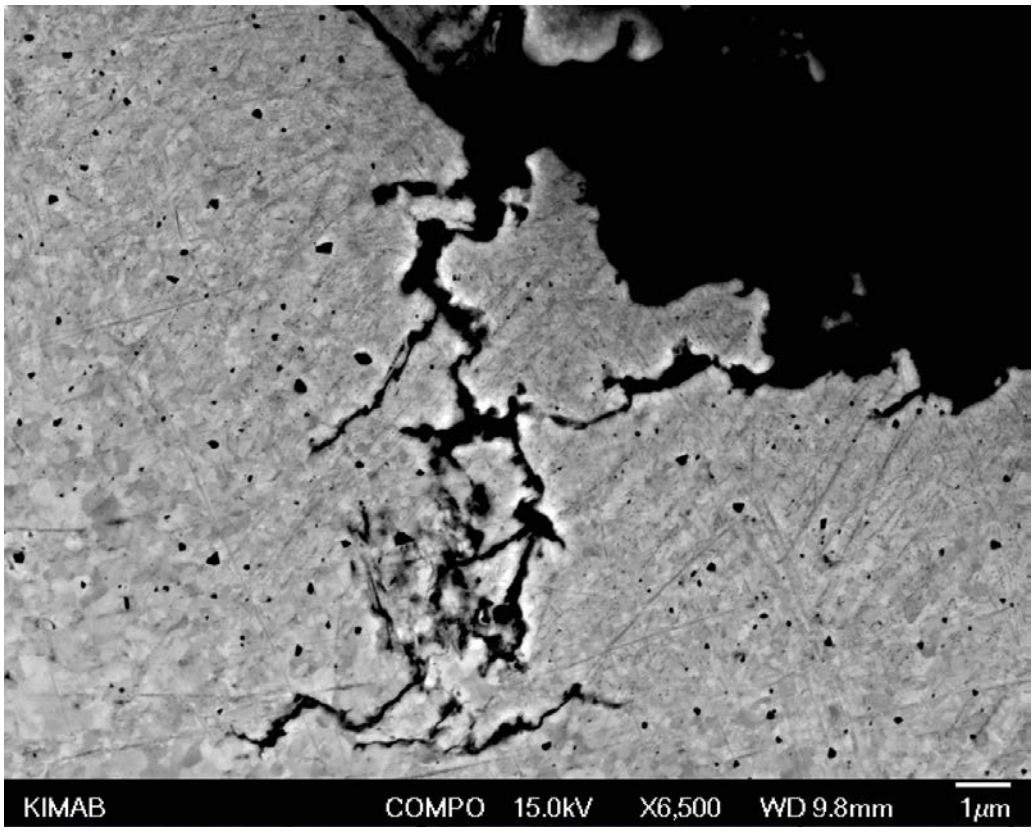

Figure A3-45. *Detail of Figure A3-44 showing WOL sample M4 3:1 and a smaller crack in the cold deformed zone near the pre-crack.*

Figure A3-46. *Detail of the crack tip of WOL sample M4 3:1.*

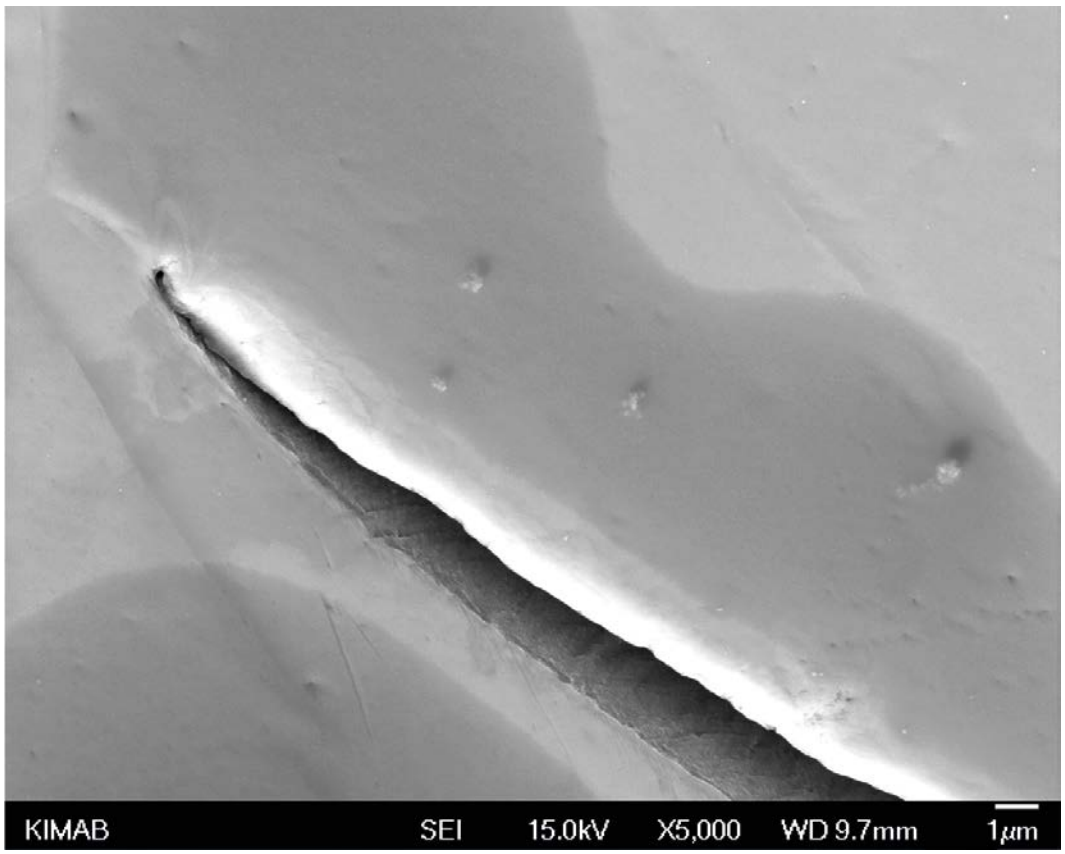

Figure A3-47. *WOL sample M4 3:1 detail of Figure A3-46. The darker areas seen on the sample surface are contamination from sample preparation.*

The sample was opened up along the fracture face by first cutting a groove from the bottom of the sample up towards the crack but without disturbing the crack, and then applying a tensile load perpendicular to the crack.

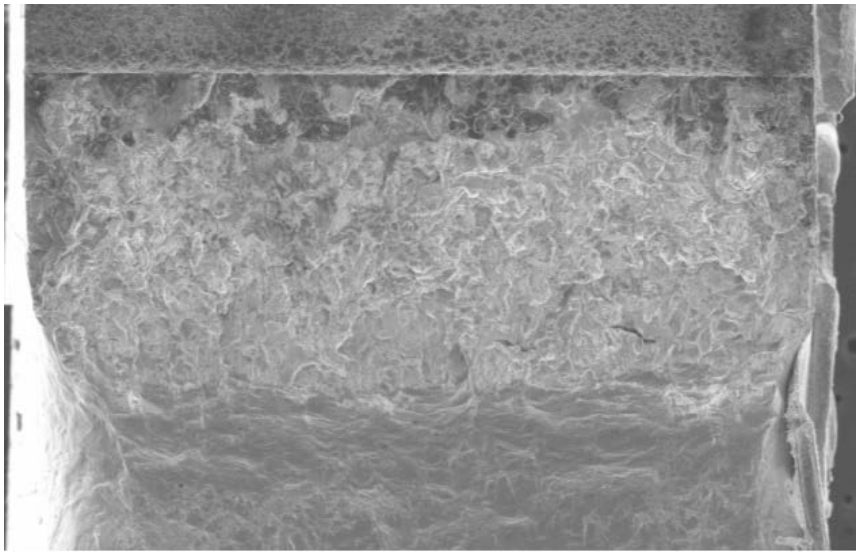

Figure A3-48. *Fracture face of WOL sample M4 3:1 after opening with a tensile load. The start of the crack is at the top of the image with the overload fracture face at the bottom of the image.*

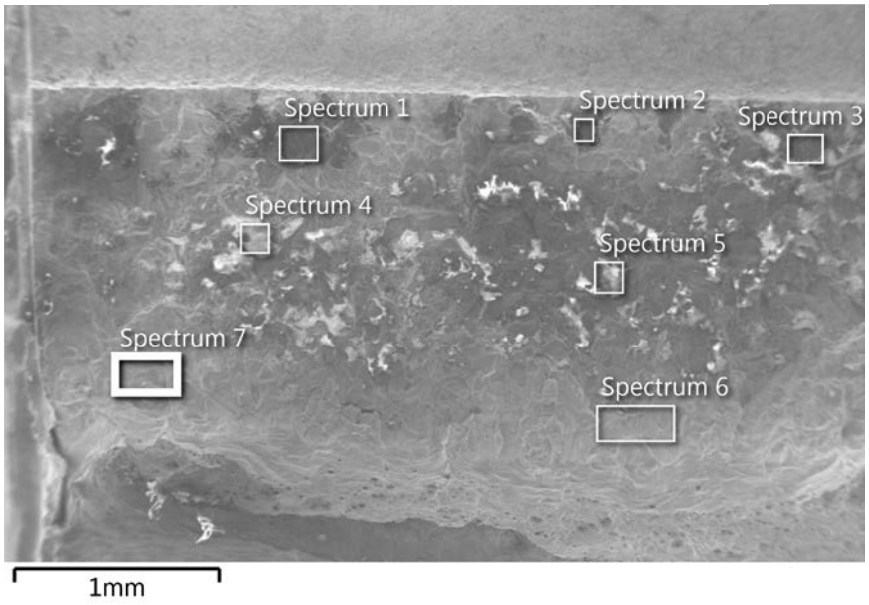

Spectrum Wt%	O	Mg	Al	Si	S	Ca	Cu	Total
Spectrum 1	53.20	1.22	5.91	19.75	1.45	1.70	16.77	100.00
Spectrum 2	43.62		1.99	33.33	0.91	0.93	19.21	100.00
Spectrum 3	47.37	0.73	2.26	27.97	0.65	2.28	18.75	100.00
Spectrum 4	46.87			35.46			17.67	100.00
Spectrum 5	42.07			30.82		1.27	25.84	100.00
Spectrum 6	13.28			4.21			82.52	100.00
Spectrum 7	10.06				0.63		89.31	100.00

Figure A3-49. *EDS analysis of fracture face of WOL sample M4 3:1. Elements associated with bentonite were detected along with copper oxide which was expected.*

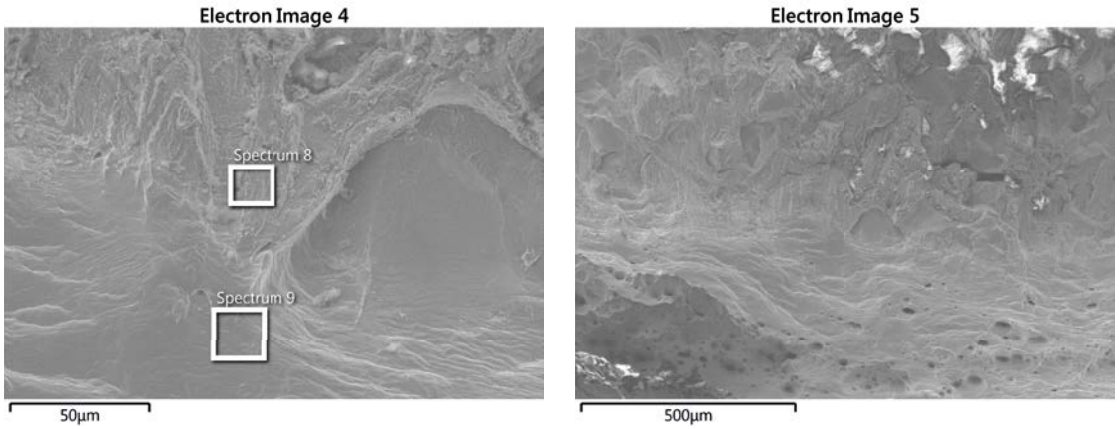

Spectrum Wt%	O	Si	Cu	Total
Spectrum 8	11.36	6.84	81.80	100.00
Spectrum 9	0.65		99.35	100.00

Figure A3-50. *Detail images of Figure A3-49 with EDS analysis of the surface. The area corresponding to spectrum 8 had particles and other foreign matter on the surface suggesting it was an older fracture surface, whilst the area corresponding to spectrum 9 was relatively clear and consisted mainly of copper. The image on the right hand side shows the same area at a lower magnification, with the ductile overload area of fracture at the bottom of the image.*

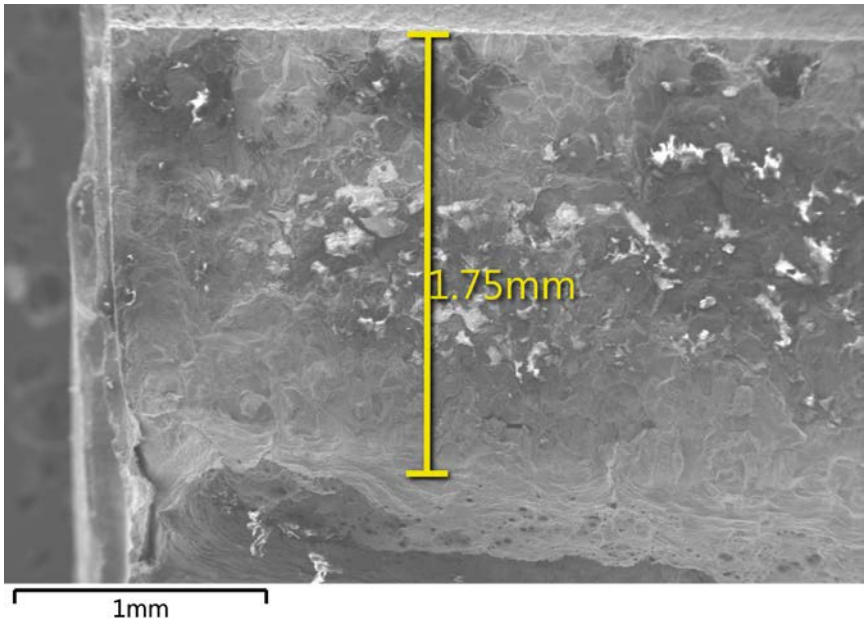

Figure A3-51. *The length of the fracture surface was measured using the SEM at 1.75 mm. This is in agreement with the estimated original pre-crack length of 1.5 mm ± 0.3 mm.*

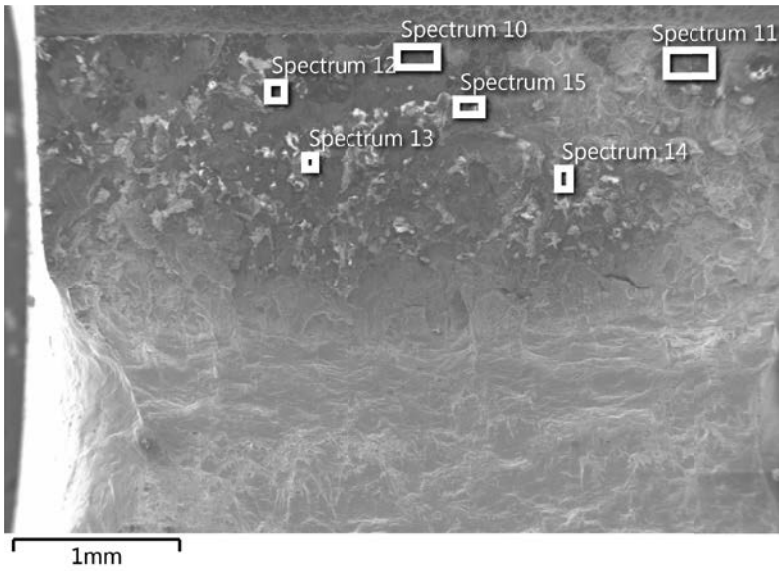

Spectrum Wt%	O	Mg	Al	Si	S	Ca	Cu	Total
Spectrum 10	40.97		4.20	13.50	1.67	2. 17	37.49	100.00
Spectrum 11	41.93		2.53	25.56	2.41		27.58	100.00
Spectrum 12	49.70	1.0 8	3.07	23.88		0.93	21.35	100.00
Spectrum 13	51.33			38.42			10.25	100.00
Spectrum 14	44.48			29.61		0.38	25.53	100.00
Spectrum 15	44.04			36.11			19.85	100.00

Figure A3-52. *EDS analysis of opposite fracture face to that shown in Figure A3-49 of WOL sample M4 3:1. The analysis shows elements associated with bentonite near to the notch along with Cu and O.*

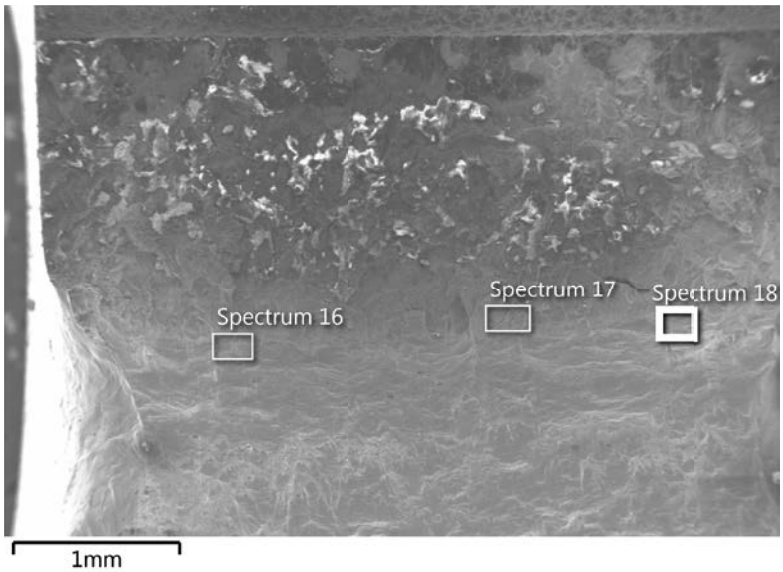

Spectrum Wt%	O	Si	Cu	Total
Spectrum 16	0.97		99.03	100.00
Spectrum 17	14.02	5.36	80.62	1 00.00
Spectrum 18	1.77		98.23	1 00.00

Figure A3-53. *EDS analysis of fracture face further away from notch of WOL sample M4 3:1, the elements detected were mainly Cu and O.*

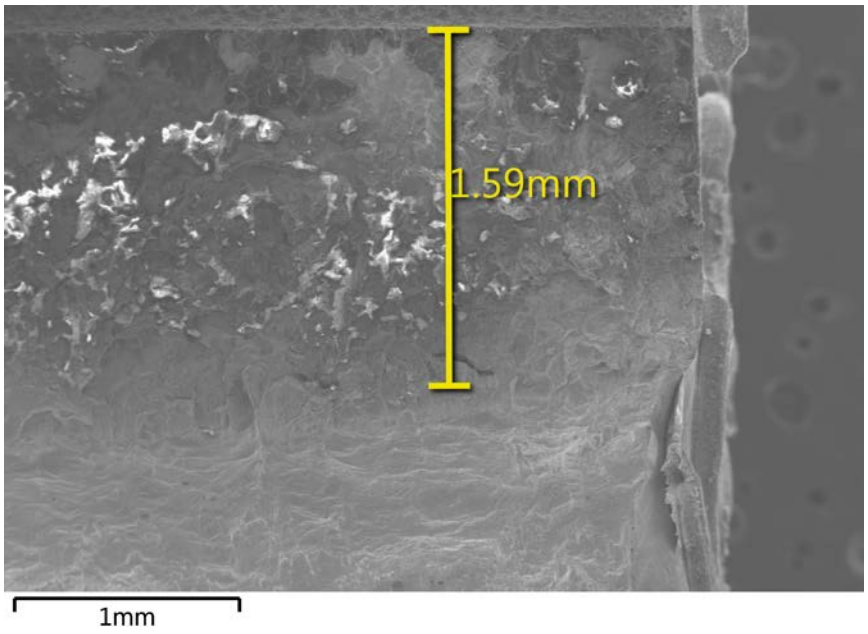

Figure A3-54. *The length of the opposite fracture surface to that shown in Figure A3-51 was measured using the SEM at 1.59 mm. This is in agreement with the estimated original pre-crack length of 1.5 mm ± 0.3 mm.*

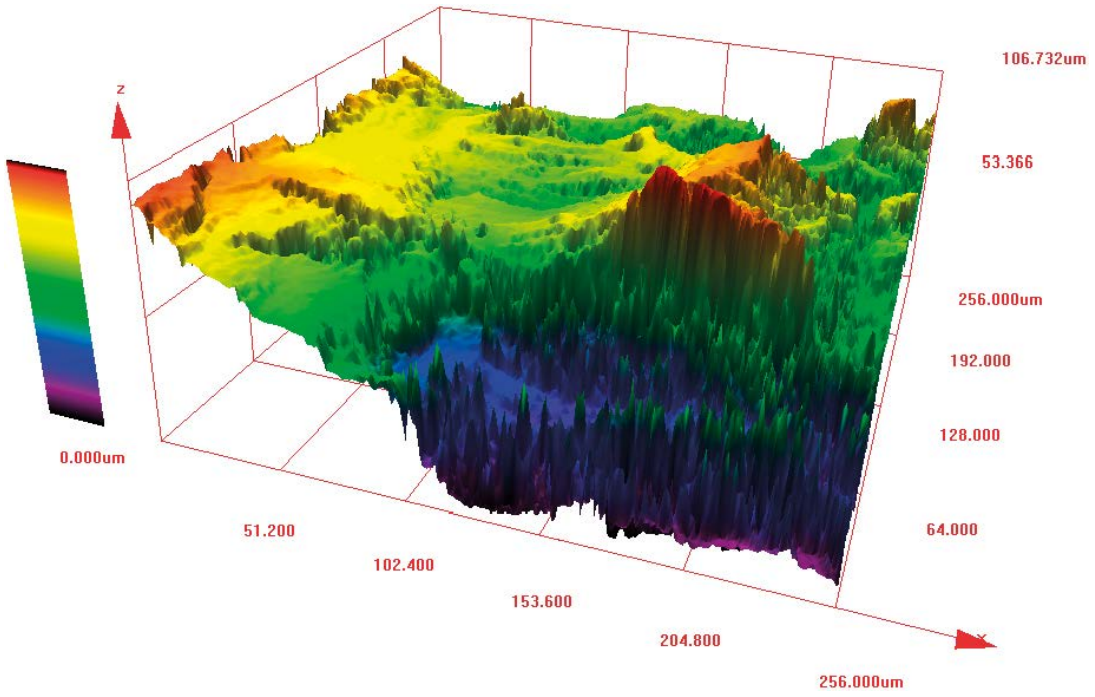

Figure A3-55. *Confocal microscope image of the fracture face of WOL sample M4 3:1 showing the pre-crack surface rising up towards the ductile fracture surface on the left hand side of the image.*

WOL sample M4 4:1

Figure A3-56. *Microscope image of WOL sample M4 4:1 after exposure.*

Figure A3-57. *Microscope image of opposite side of WOL sample M4 4:1.*

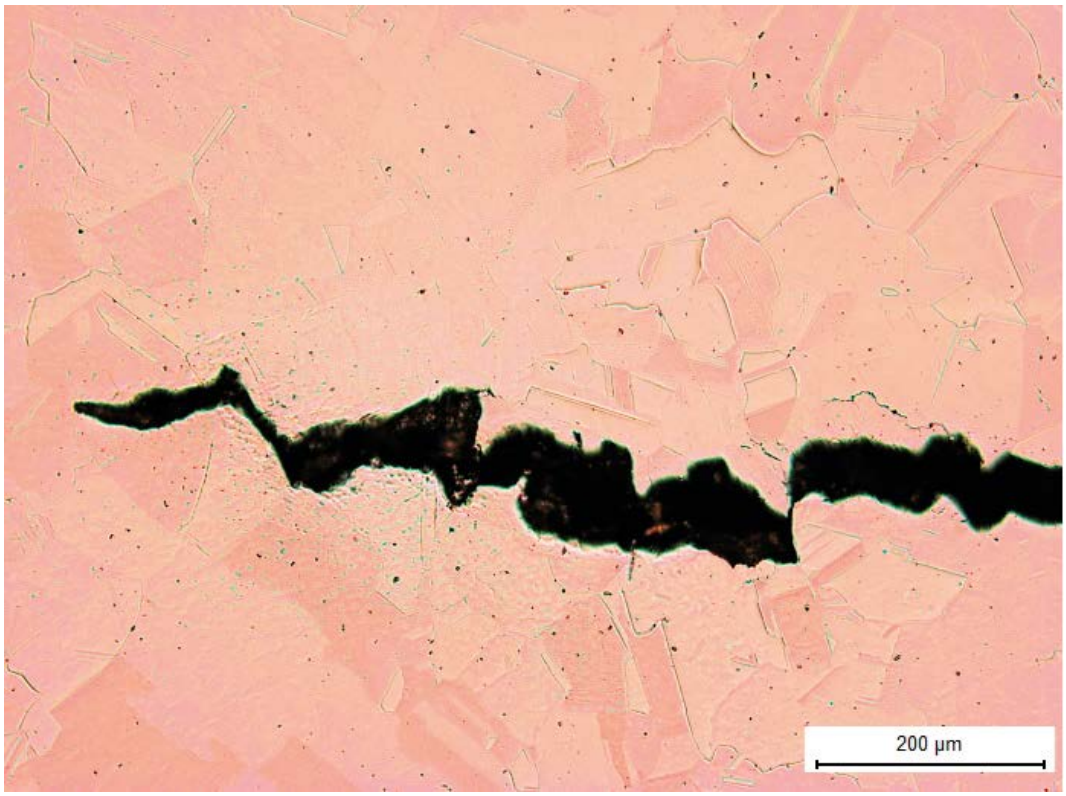

Figure A3-58. *Microscope image of the crack tip of WOL sample M4 4:1. The crack appears to be following the grain boundaries.*

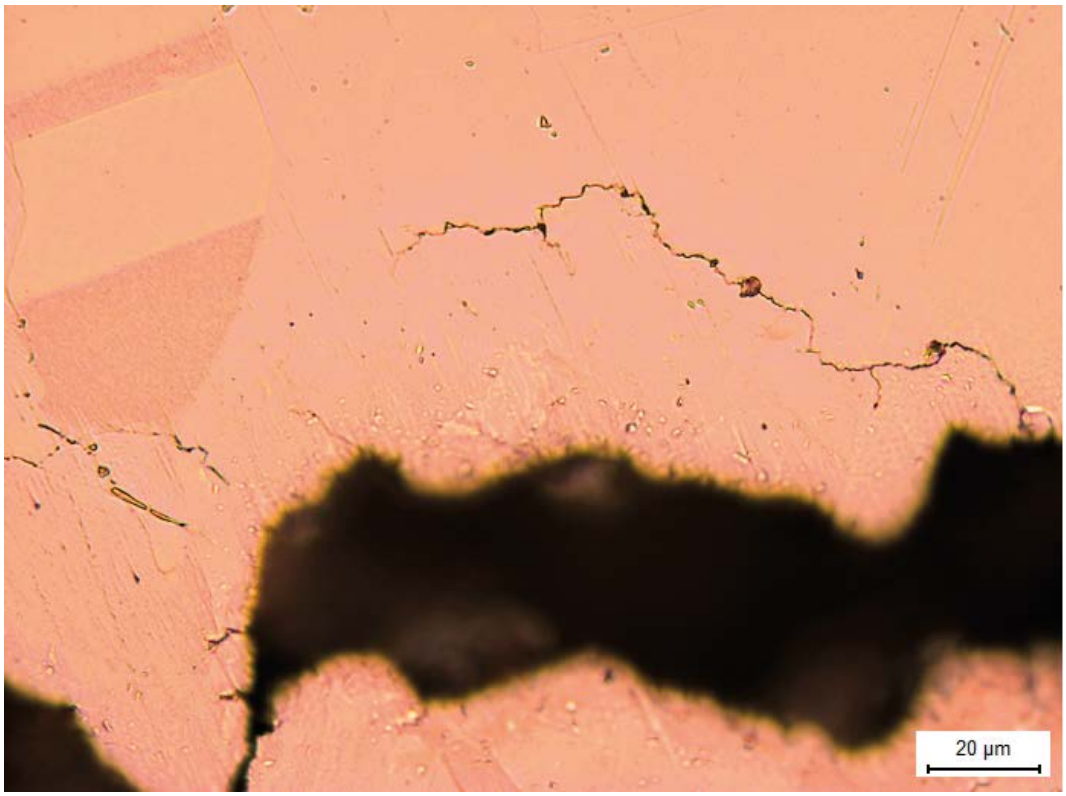

Figure A3-59. *Secondary cracks found emanating from the pre-crack of WOL sample M4 4:1.*

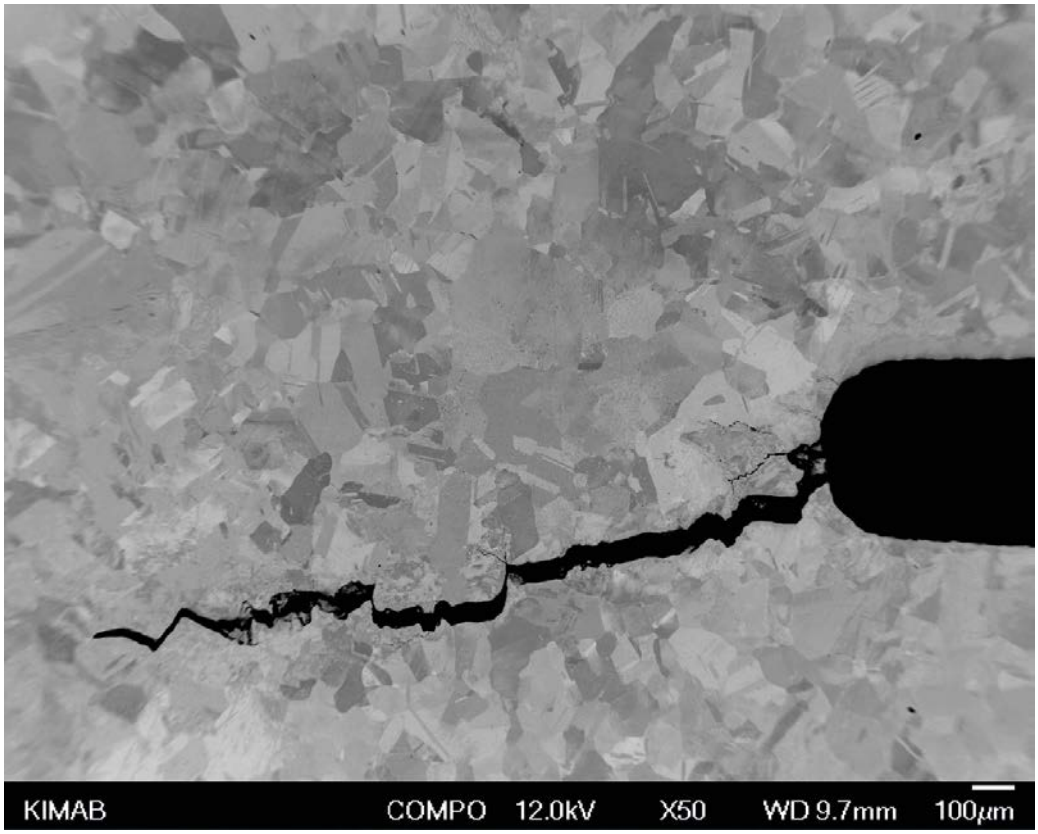

Figure A3-60. *SEM backscattered electron (BEI) image of WOL sample M4 4:1 showing the pre-crack emanating from the notch.*

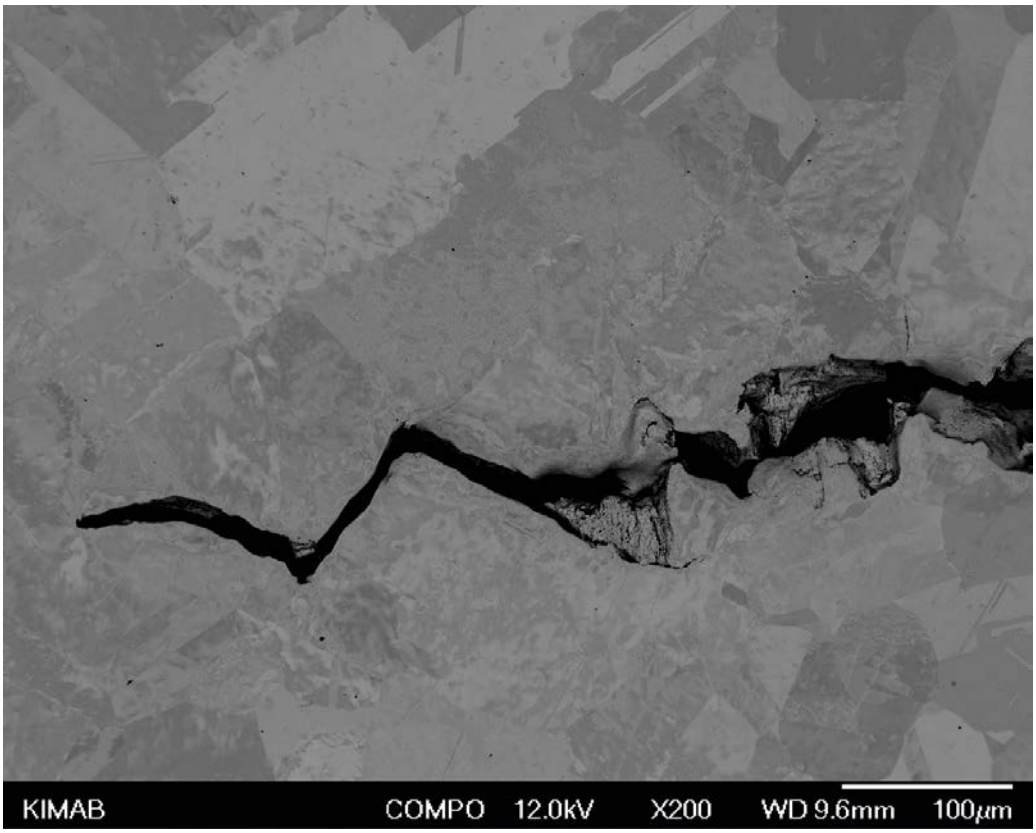

Figure A3-61. *Forward part of the pre-crack of WOL sample M4 4:1.*

Figure A3-62. *Crack tip of WOL sample M4 4:1.*

Figure A3-63. *Detail of middle section of pre-crack of WOL sample M4 4:1, with smaller cracks emanating from the pre-crack into the cold deformed zone.*

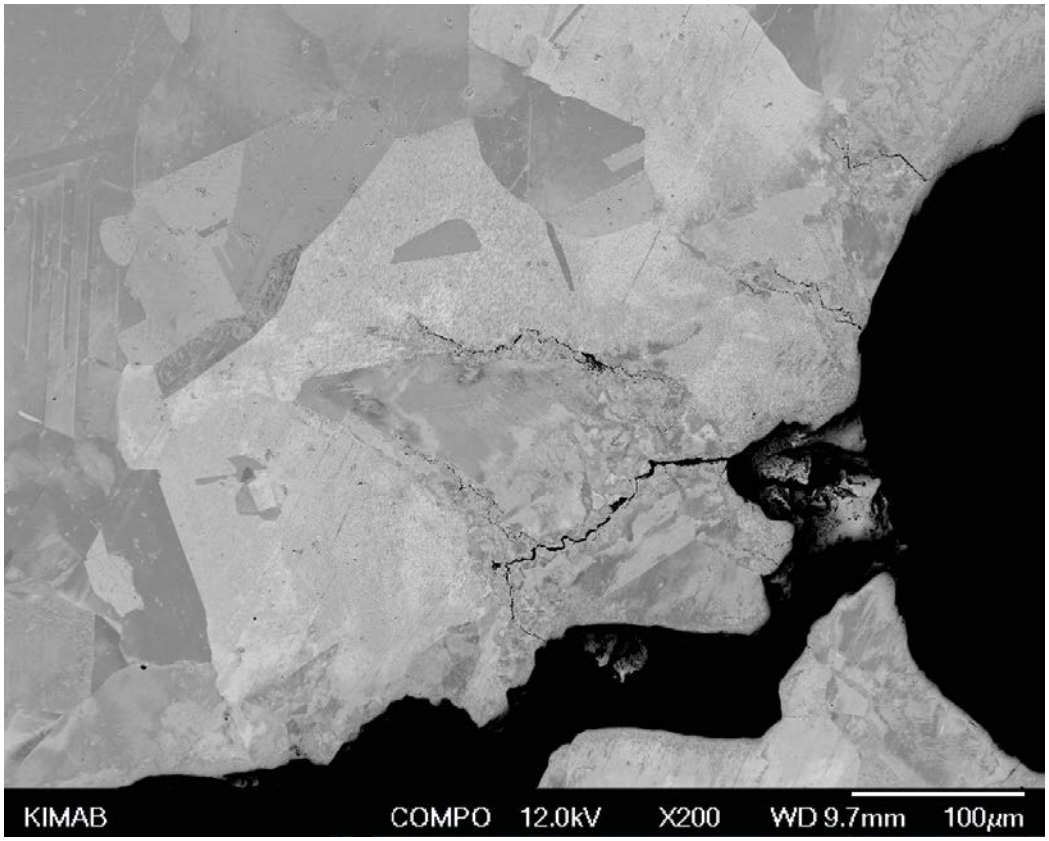

Figure A3-64. *Detail of pre-crack emanating from notch on WOL sample M4 4:1.*

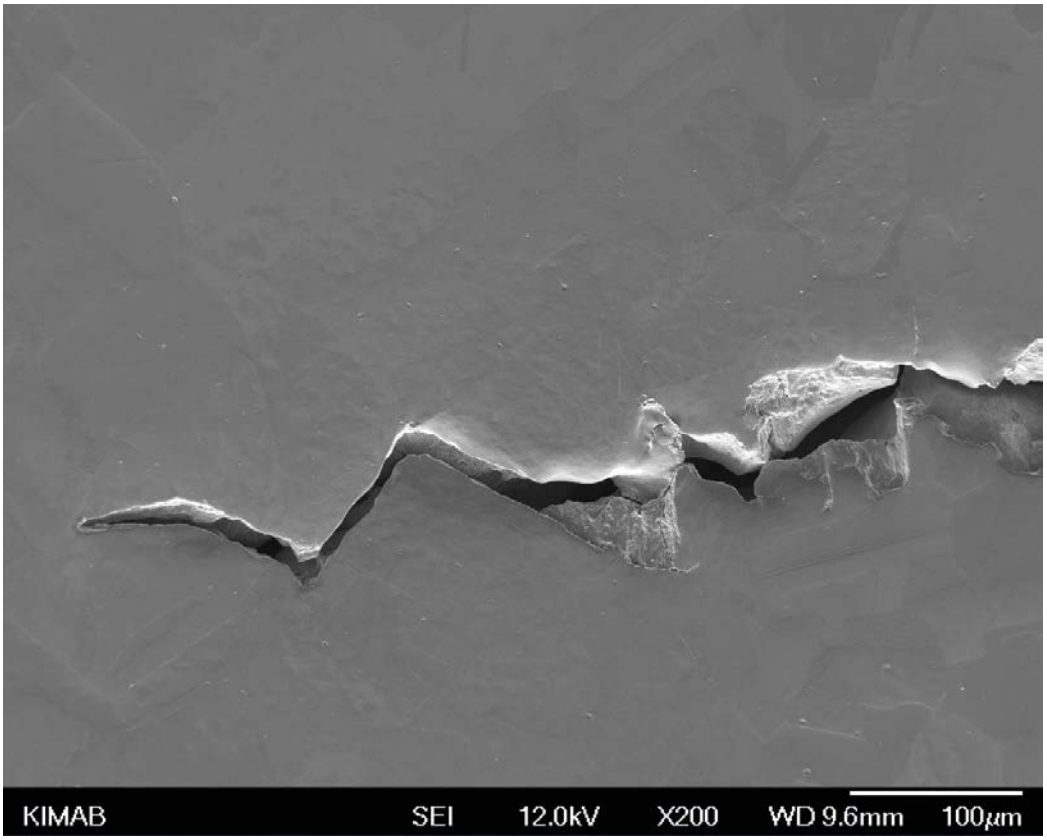

Figure A3-65. *Secondary electron image (SEI) of forward part of pre-crack of WOL sample M4 4:1.*

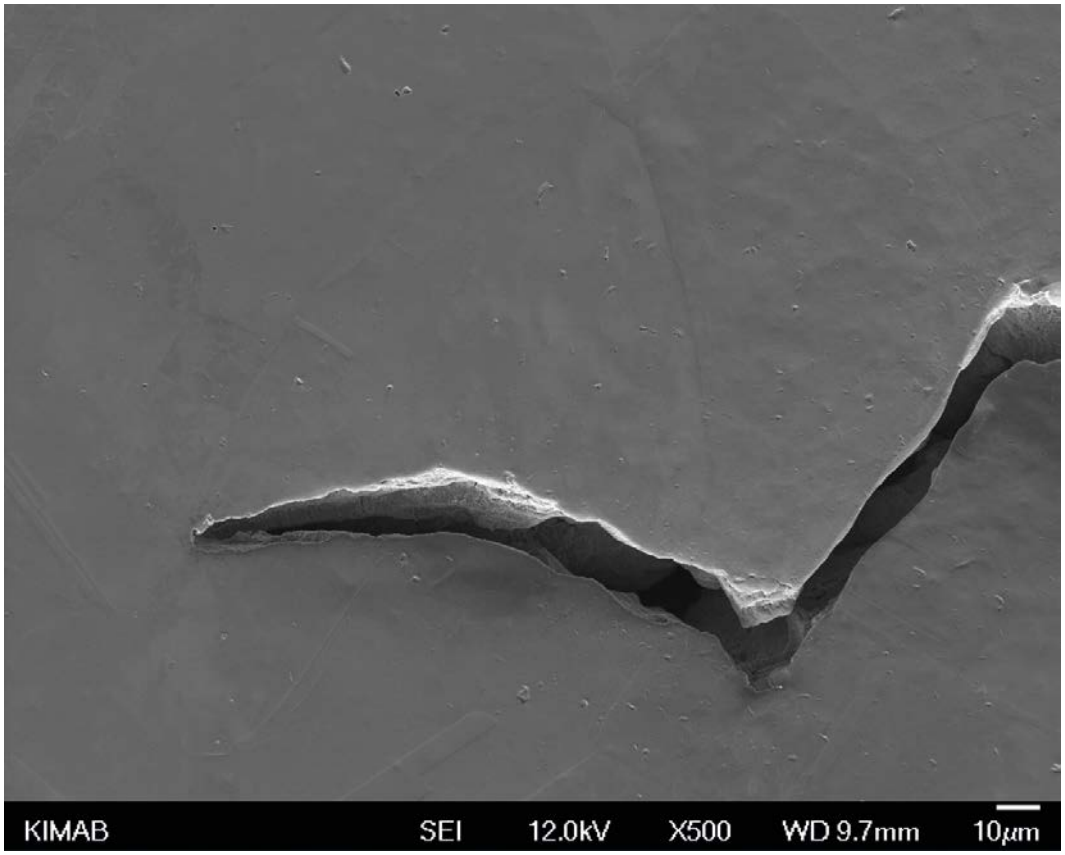

Figure A3-66. *SEI image of crack tip of WOL sample M4 4:1.*

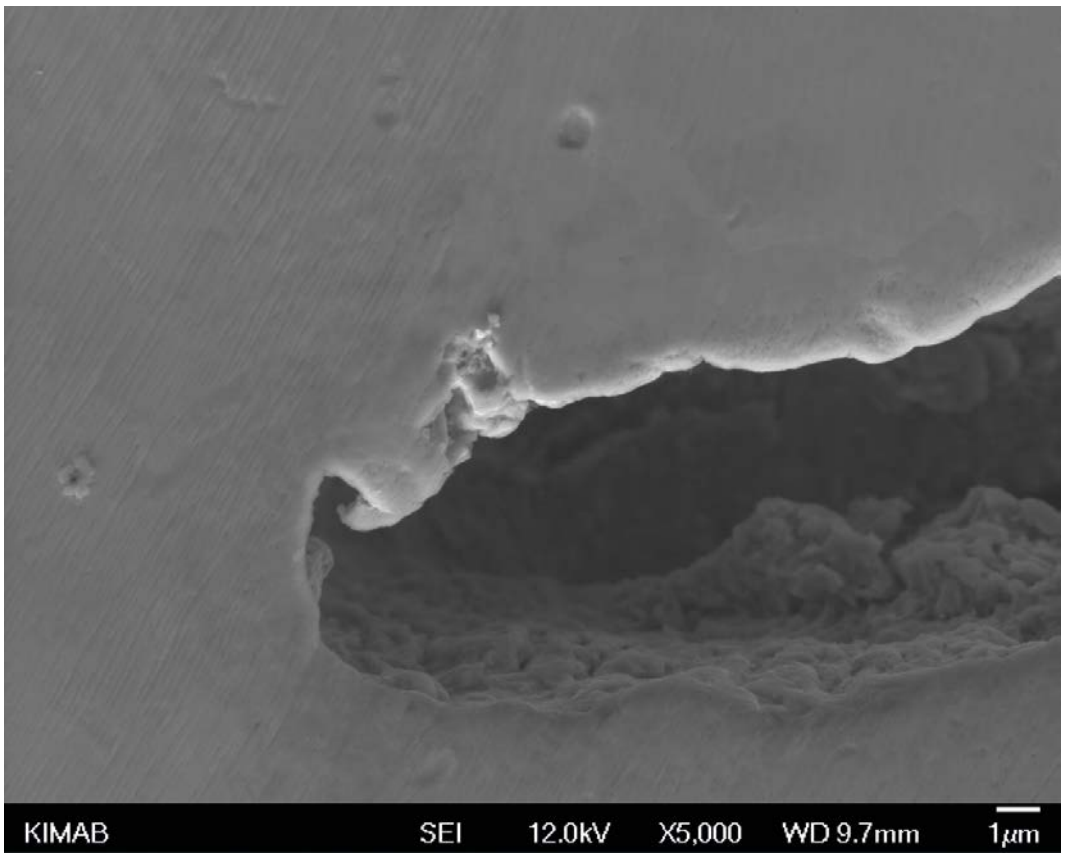

Figure A3-67. *SEI detail of crack tip ×5 000 magnification of WOL sample M4 4:1.*

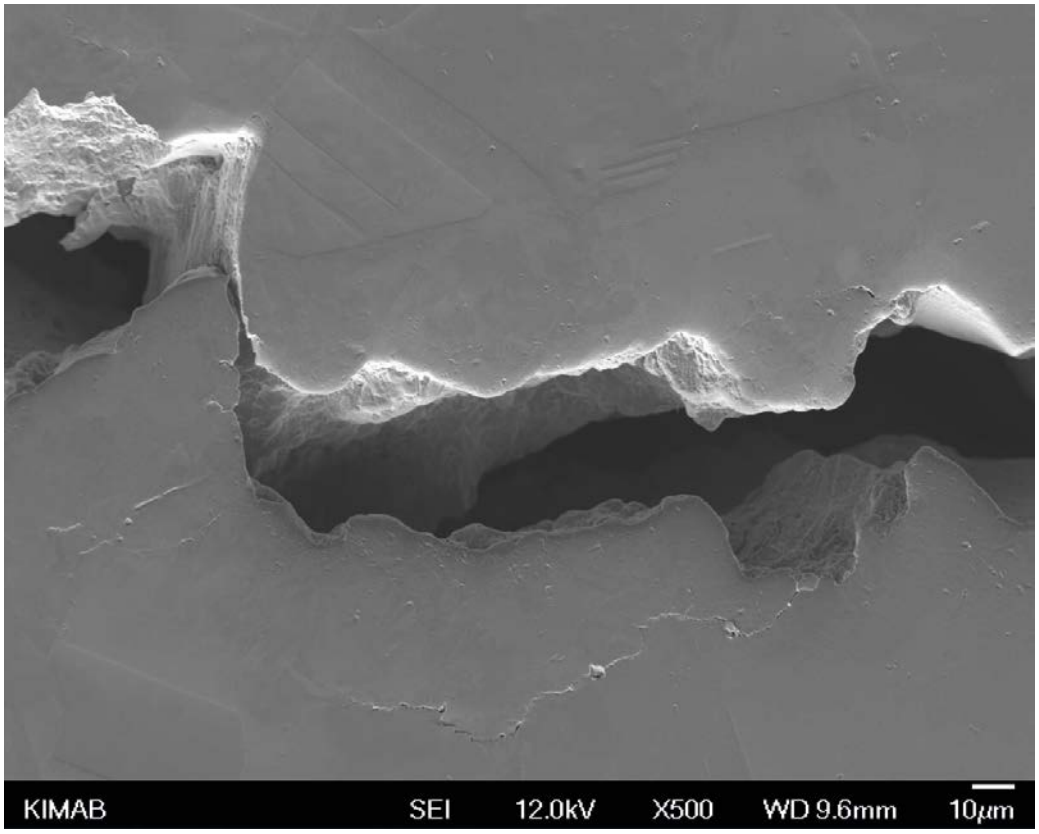

Figure A3-68. *Detail of pre-crack of WOL sample M4 4:1 approximately at middle position, showing smaller secondary cracks.*

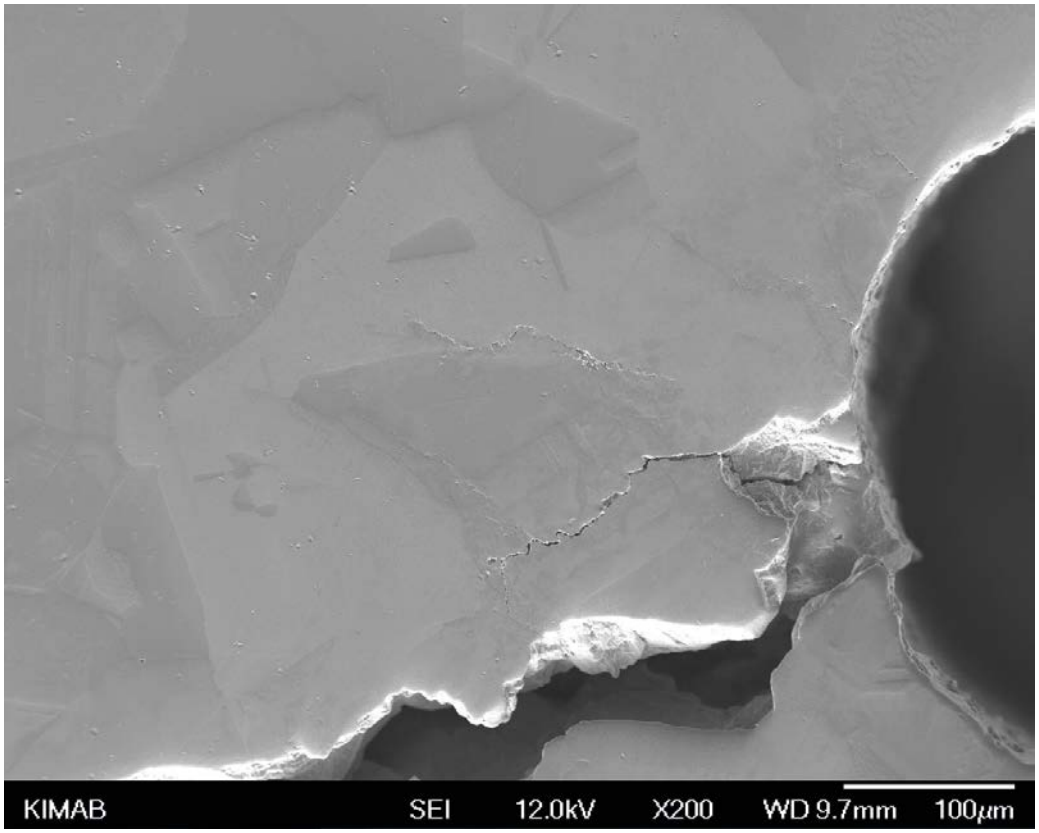

Figure A3-69. *Detail of start of pre-crack from notch of WOL sample M4 4:1.*

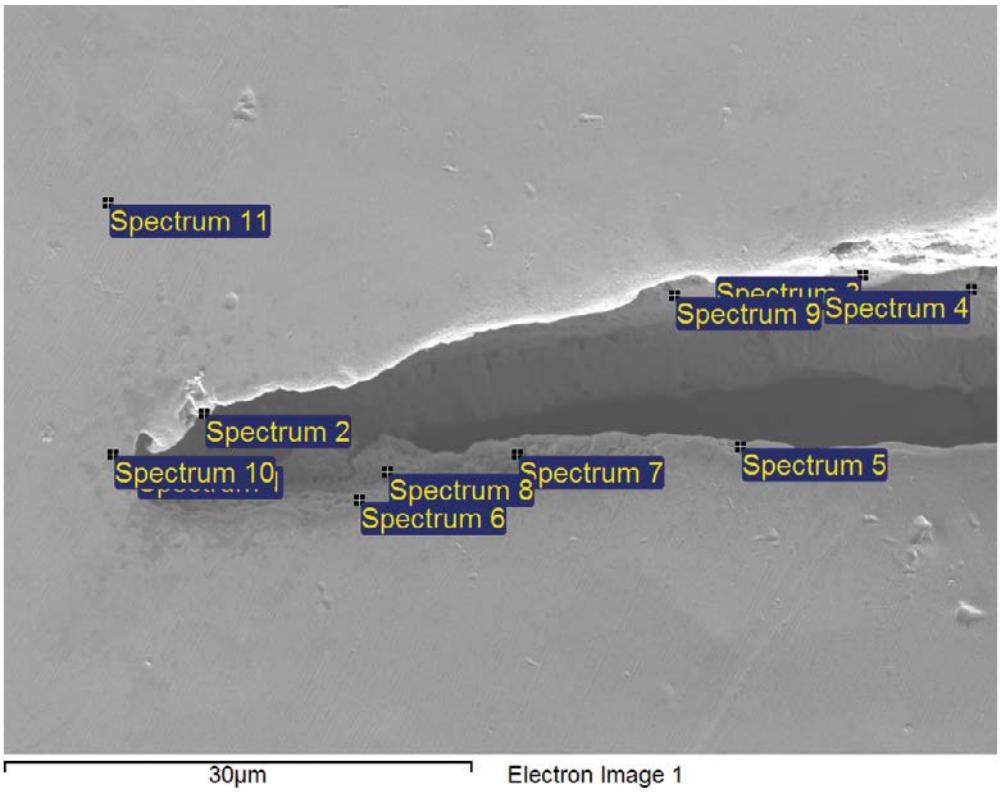

Spectrum At%	O	S	Cu
Spectrum 1	3.42	1.22	95.37
Spectrum 2	0.82	2.46	96.72
Spectrum 3	2.52	0.88	96.60
Spectrum 4	1.25	1.57	97.18
Spectrum 5	1.74	1.23	97.03
Spectrum 6	1.94	1.89	96.18
Spectrum 7	1.85	1.46	96.69
Spectrum 8	4.73	1.23	94.04
Spectrum 9	4.37	0.8 0	94.83
Spectrum 10	0.67	0.12	99.21
Spectrum 11	0.70	1.13	98.17

Figure A3-70. *EDS analysis of WOL sample M4 4:1 at the crack tip. Sulphur is present along with the copper-oxide layer.*

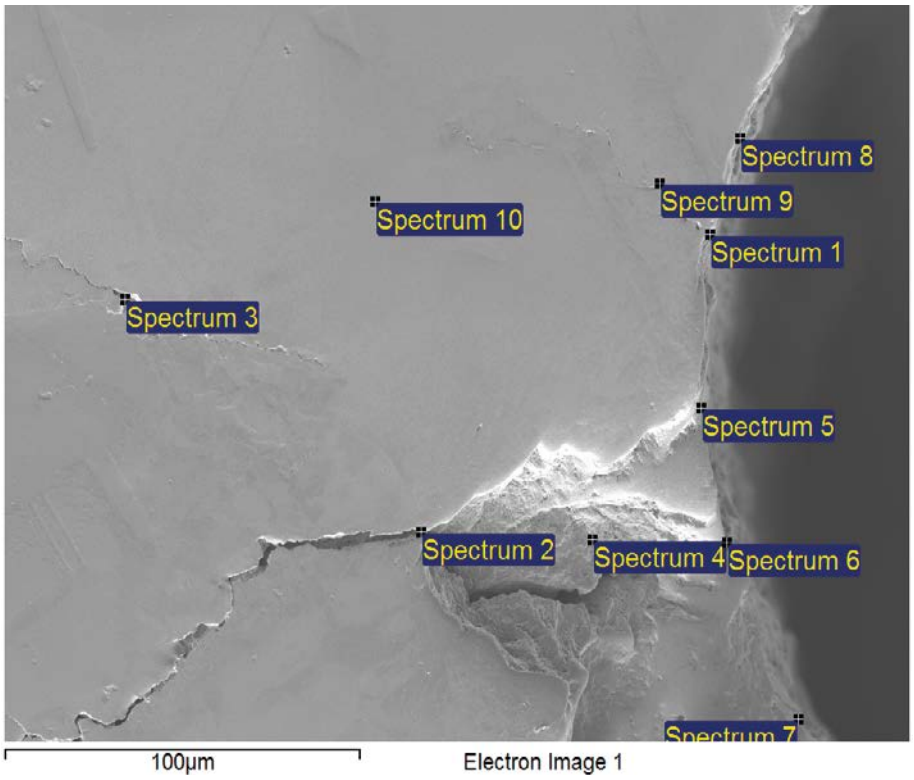

Spectrum At%	O	S	Cu
Spectrum 1	13.64	3.43	82.92
Spectrum 2	5.36	3.36	91.28
Spectrum 3	0.78	1.87	97.34
Spectrum 4	10.08	2.65	87.26
Spectrum 5	13.54	3.15	83.31
Spectrum 6	16.14	4.38	79.48
Spectrum 7	15.84	2.83	81.34
Spectrum 8	14.21	2.67	83.12
Spectrum 9	1.83	1.23	96.94
Spectrum 10	1.0 5	1.09	97.86
Mean	9.25	2.67	88.08
Std. deviation	6.35	1.02	7.18
Max.	16.14	4.38	97.86
Min.	0.78	1.09	79.48

Figure A3-71. *EDS analysis of WOL sample M4 4:1 at the crack opening near the notch. Sulphur is present along with the copper-oxide layer.*

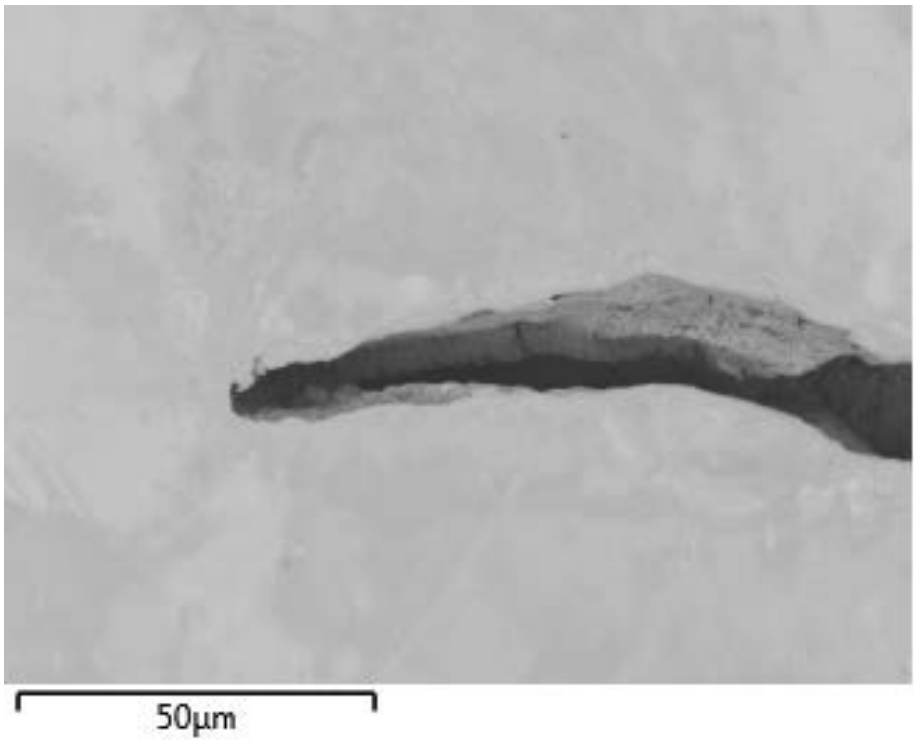

Figure A3-72. *BEI image of WOL sample M4 4:1 at the crack tip, showing the oxide and/or corrosion products on the edges of the fracture surface.*

Appendix 4

Mass loss

Mass loss analyses

Mass loss analyses of copper and iron samples from MiniCan 4 and 5 were performed according to the method contained in SS-EN ISO 8407:2014 Section 2.2. This involves removal of corrosion products using a reagent, which in the case of the copper samples was sulfamic acid (H_3NSO_3) (SS-EN ISO 8407:2014 C.2.1 Table A.1) and for the iron samples hydrochloric acid (HCl) with hexamethyltetramin (HMTA) (SS-EN ISO 8407:2014 C.3.1 Table A.1).

The samples are placed in the reagent for set periods of time whilst being agitated using an ultrasonic bath. After each pickling period the samples are weighed, and when the mass loss between each pickling process becomes steady and comparable to a reference sample the pickling is stopped.

The mass losses between each pickling period are plotted on a graph versus pickling time, and where the curve plateaus a line is extrapolated back to the mass loss axis, which then gives the total mass loss due to the corrosion exposure when compared to the original mass of the sample. This mass loss divided by area and exposure period of samples gives the corrosion rate. The dimensions for the samples were taken as being those given from the start of test as $20 \times 10 \times 5$ mm, and the exposure time was set at 8.73 years for MiniCan 4 and 8.81 years for MiniCan 5 (exposure periods 06.02.2007 to 26.10.2015 for MiniCan 4 and 11.12.2006 to 28.09.2015 for MiniCan 5). Densities used for copper and iron were 8.94 and 7.8 kg/m^3 respectively.

Table A4-1. Copper mass loss samples M4 7:1 and M5 7:1.

Sample	Original mass g	Mass after exposure (before pickling) g	Mass loss calculated from pickling g	Corrosion		
				g/m^2	g/m^2, a	µm/a
M4 7:1	8.75500	8.75387	0.0010	1.4171	0.1623	0.0182
M5 7:1	8.92523	8.92650	0.0059	8.4000	0.9535	0.1067

Table A4-2. Iron mass loss samples M4 11:1 and M5 11:1.

Sample	Original mass g	Mass after exposure (before pickling) g	Mass loss calculated from pickling g	Corrosion		
				g/m^2	g/m^2, a	µm/a
M4 11:1	6.54500	6.47790	0.1010	144.2619	16.5248	2.1186
M5 11:1	6.61189	6.54690	0.1514	216.2347	24.5442	3.1467

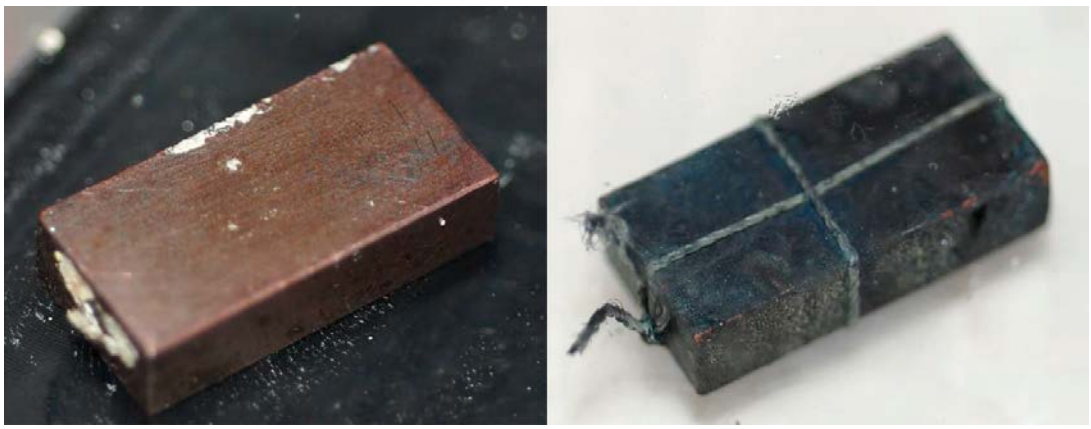

Figure A4-1. *Copper mass loss samples M4 7:1 to the left hand side and M5 7:1 after exposure, before pickling.*

Figure A4-2. *Copper mass loss sample M4 7:1 on the left hand side, and M5 7:1 on the right hand side, after pickling was completed. M4 7:1 was grey in colour after pickling.*

After pickling the copper mass loss sample M4 7:1 appeared grey in colour compared to M5 7:1, see Figure A4-2. The reason for this is unclear at the time of writing, but SEM/EDS analysis was carried out on the sample in order to see what was on the surface (see Figure A4-3). The analysis showed that the surface consisted mainly of copper but with a sulphur compound layer of about 100 nm thickness, as well as some carbon. The surface deposit was not removed entirely by a droplet of HCl that was placed on the surface as a test, suggesting that it is not a loosely adhering corrosion product but a thin film of a very stable copper-sulphide. This surface deposit introduces some error in the corrosion rate because 0.1 µm of the surface is not copper. Taking this into account the corrosion rate can be recalculated as being up to 0.1 µm / 8.73 years = 0.01 µm/a more than the given 0.0182 µm/a in Table A4-1.

Figure A4-5 and Figure A4-6 show the appearance of sample M4 11:1 and M5 11:1 after pickling was complete. Both samples shows signs of material loss, particularly on one end (see Figure A4-6, and detail in Figure A4-7). The appearance of the material loss was that of selective corrosion, which is typical of cast iron corrosion, whereby the iron corrodes leaving behind a matrix of graphite.

SEM analysis of the iron mass loss sample M4 11:1 shows the typically nodules of carbon found in ductile iron, see Figure A4-8.

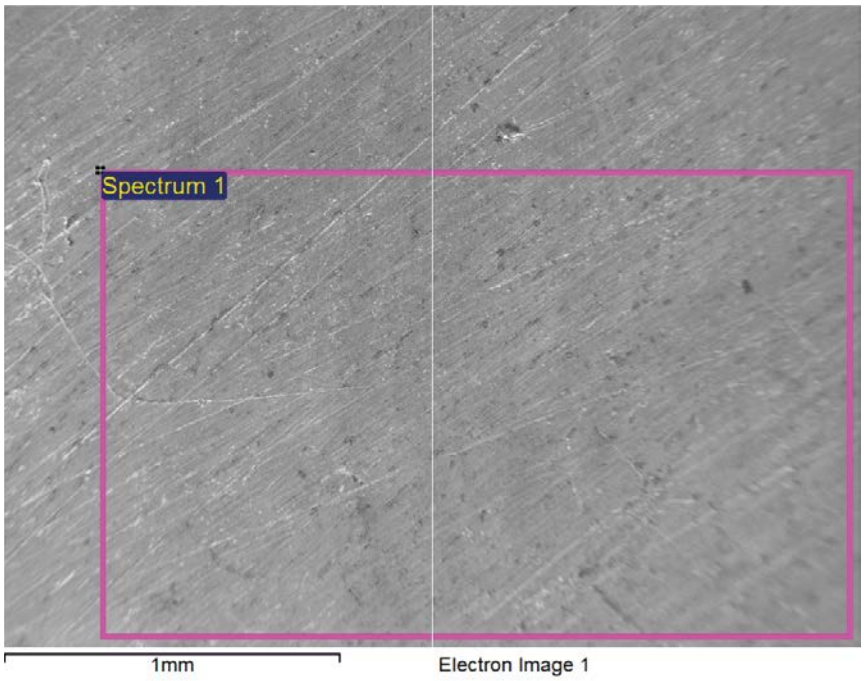

Element	Weight%	Atomic%
C	9.29	32.06
O	1.91	4.95
Al	0.10	0.16
Si	1.76	2.60
S	5.45	7.05
Cu	81.49	53.18
Totals	100.00	

Figure A4-3. *SEM image of copper mass loss sample M4 7:1, and associated EDS analysis results.*

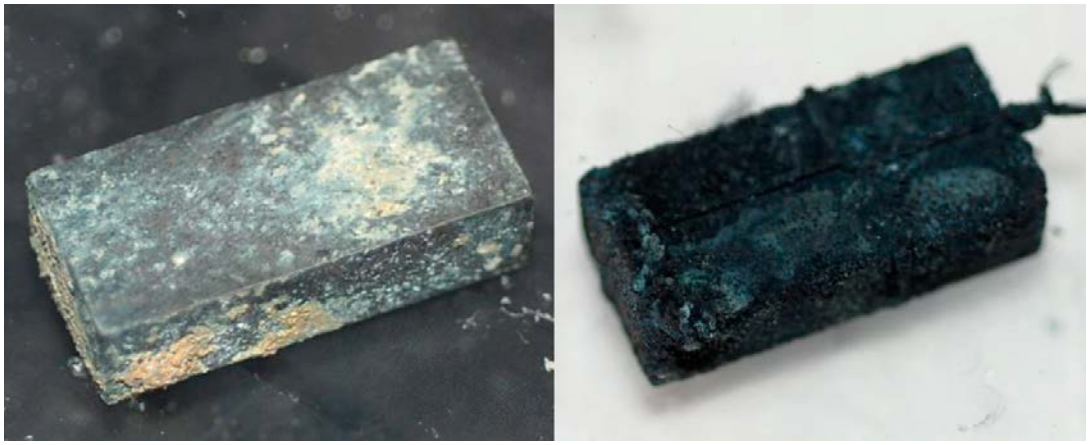

Figure A4-4. *M4 11:1 and M5 11:1 iron mass loss samples after exposure before pickling.*

Figure A4-5. *Iron mass loss samples, M4 11:1 to the left hand side, and M5 11:1 after pickling was completed.*

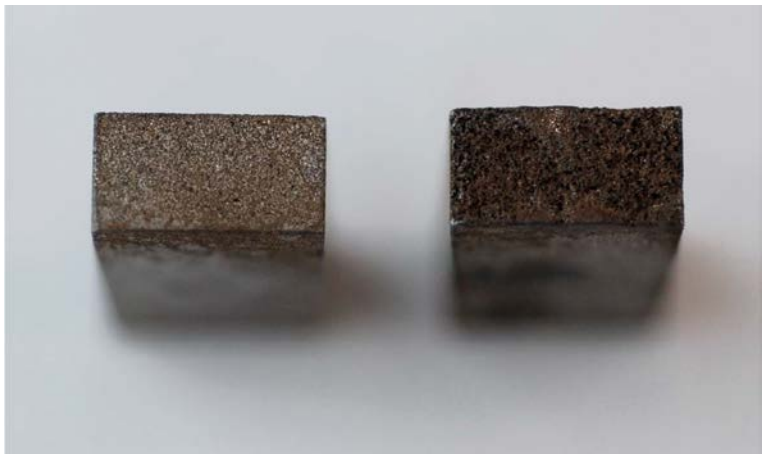

Figure A4-6. *Iron mass loss samples, M4 11:1 to the left hand side, and M5 11:1 with more corrosion loss on one end.*

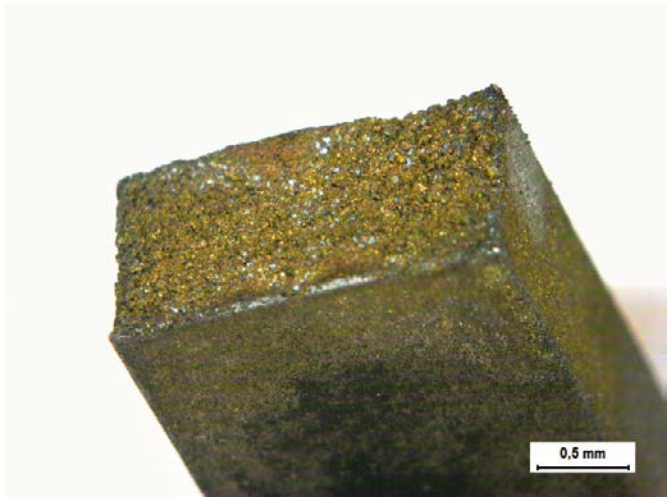

Figure A4-7. *Detail of corrosion on end of iron mass loss sample M5 11:1.*

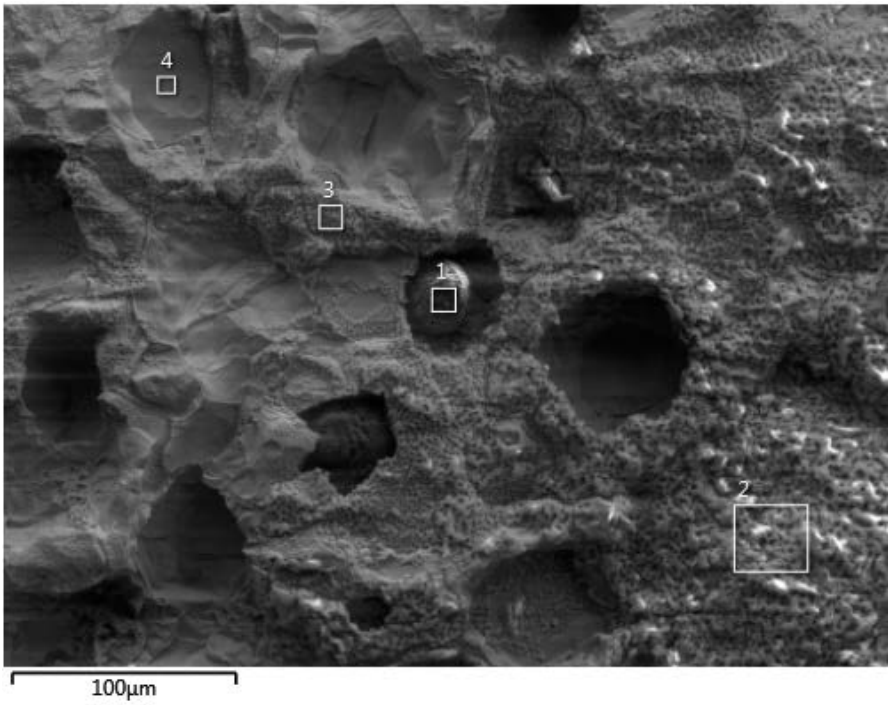

Element (Wt%)	1	2	3	4
C	93.33	5.77	3.91	1.87
O	4.05	29. 56	22.01	1.84
Na	0.06	2.03	1.77	0.09
Mg	0.14		0.04	0.10
Al		0.06	0.04	
Si	0.07	1.58	2.08	2.11
P		0.12		
S	0.11	0.44	0.26	0.26
Cl	0.09	1.01	0.57	0.03
Ca	0.09		0.09	
Fe	2.07	59.43	69.23	93.69
Total:	100.00	100.00	100.00	100.00

Figure A4-8. *Corroded area of iron mass loss sample M4 11:1 from SEM analysis. A nodule of carbon can be seen at point 1. Points 2 and 3 consisted of mainly Fe and O, whilst point 4 was mainly Fe.*

Appendix 5

Hydrogen content

Hydrogen content analyses

Hydrogen content determination with melt-extraction

Since 2007 KIMAB has used a Leco Rhen 602 melt-extraction instrument for the determination of bulk hydrogen in steel and metals. Melt-extraction is the conventional method of measuring hydrogen and is based on samples (of approx. 1 g) that are melted in a flow-through graphite crucible under Ar atmosphere. The light elements are removed as gases and after purification of the gas mixture of CO, CO_2, H_2O, N_2, etc. hydrogen is detected by its effect on the thermal conductivity of Ar/H_2 mixture. This method can be very sensitive and the instrument is capable of an accuracy of about 0.1 ppm. Calibration is done with reference samples with known concentrations provided by Leco with several suppliers. The instrument is used both for research and for external measurement assignments.

For the MiniCan tests, in total eight 1 g samples from each piece of canister material were tested. Figure 1 below shows schematically how the samples were prepared from each canister sample.

To minimize the hydrogen on the surface, immediately before the analyses, the samples were wet grinded with SiC paper and degreased in ethanol with ultrasound agitation. There is however no guarantee that this procedure will eliminate all hydrogen on the surface, part of the hydrogen detected in the analysis may still come from the surface.

The results of the tests show that there was variation in hydrogen content through the thickness of the canister wall. Sample 21:1:2 from MiniCan 4 had an anomalous result, and this was deemed to be due to a surface deposit that was noted on the sample prior to analysis. For MiniCan 5 there was a slight tendency for higher hydrogen content from the samples positioned towards the surfaces of the canister wall, see Figure A5-4. This pattern was not as clear for the samples analysed from MiniCan 4, see FigureA5-3. The amount of hydrogen measured in the tests is deemed to be representative of reference material tested previously of approximately 0.6 ppm (Martinsson and Sandström, 2013) but higher than that detected of approximately 0.4 ppm in (Taxen, et al., 2012). For MiniCan 4 the average (mean) hydrogen content measured was 0.76 ppm with a minimum value of 0.58 ppm and maximum value of 1.37 ppm measured. For MiniCan 5 the average hydrogen content measured was 0.87 ppm with a minimum value of 0.60 ppm and maximum value of 1.78 ppm.

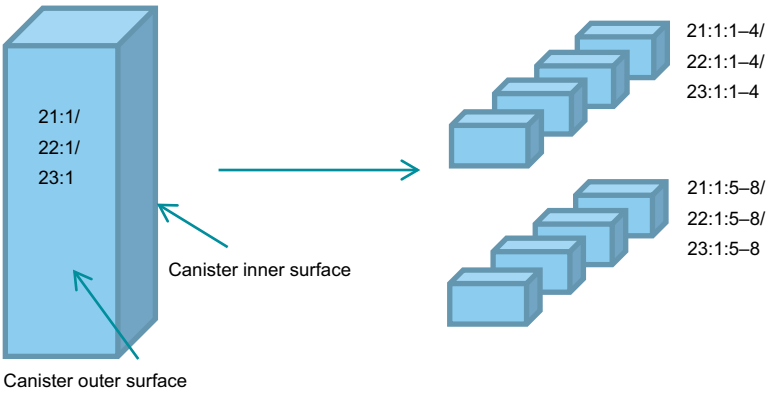

Figure A5-1. *Three pieces of canister material were sampled in the glovebox, 21:1, 22:1 and 23:1, each piece measured approximately 50 × 15 × 7.5 mm, before being sectioned at Swerea KIMAB into eight 1 g (approx.) samples for the hydrogen tests.*

Table A5-1. Hydrogen content results from MiniCan 4 samples (high density bentonite).

Sample ID	Position of sample	Mass of sample (g)	H bulk ppm
21:1:1	Outer surface	1.689	1.37
21:1:2	Middle	2.1755	8.27
21:1:3	Middle	1.2216	0.83
21:1:4	Inner surface	2.4717	0.98
21:1:5	Outer surface	2.1508	1.02
21:1:6	Middle	1.4576	0.72
21:1:7	Middle	1.7907	0.63
21:1:8	Inner surface	2.9637	0.63
22:1:1	Outer surface	2.1916	0.73
22:1:2	Middle	1.5681	0.58
22:1:3	Middle	1.4776	0.61
22:1:4	Inner surface	1.2315	1.07
22:1:5	Outer surface	2.2412	0.63
22:1:6	Middle	1.389	0.71
22:1:7	Middle	1.2034	0.69
22:1:8	Inner surface	1.793	0.77
23:1:1	Outer surface	2.471	0.84
23:1:2	Middle	1.8358	0.65
23:1:3	Middle	1.082	0.95
23:1:4	Inner surface	2.7659	0.72
23:1:5	Outer surface	2.3307	0.89
23:1:6	Middle	1.2924	0.77
23:1:7	Middle	1.9963	0.71
23:1:8	Inner surface	2.22	0.84

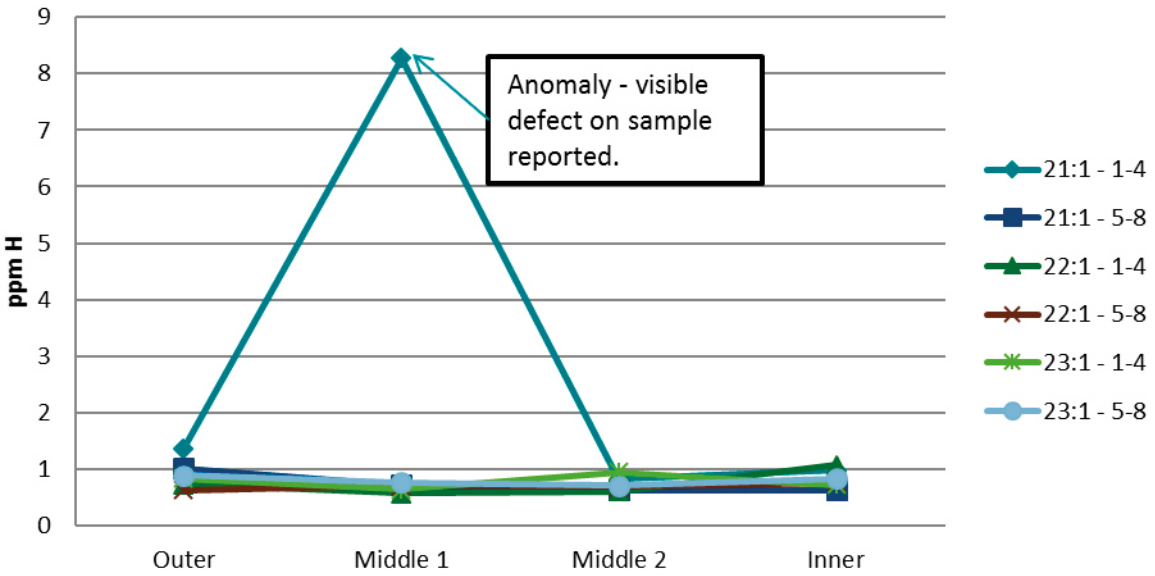

Figure A5-2. *Results from MiniCan 4 samples, hydrogen content in ppm through thickness of canister wall.*

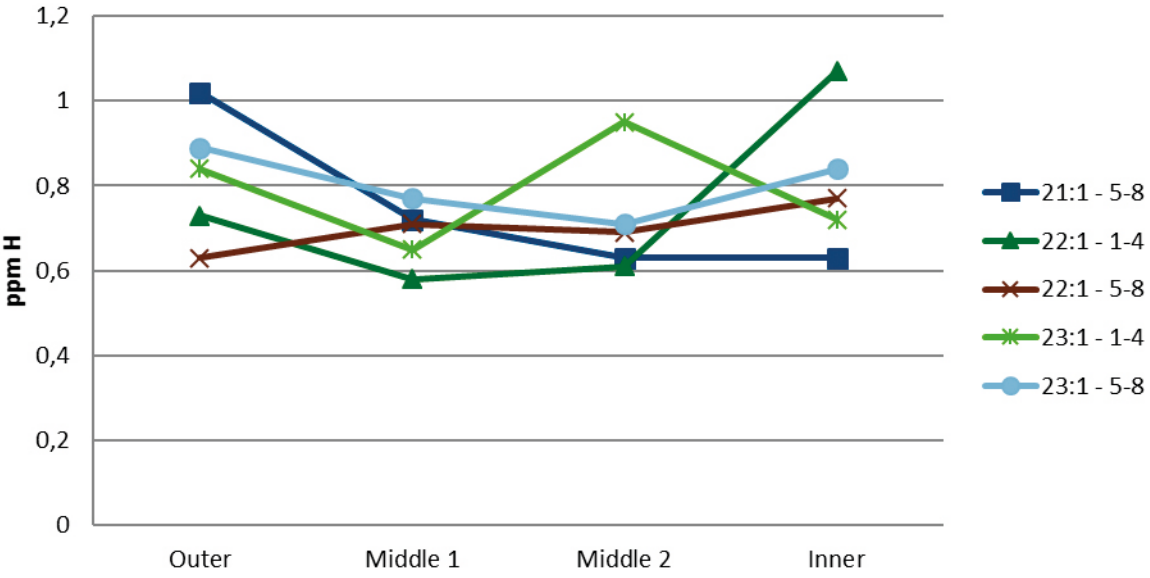

Figure A5-3. *Results from MiniCan 4 samples, hydrogen content in ppm through thickness of canister wall, with samples 21:1:1–4 removed from the diagram.*

Table A5-2. Hydrogen content results from MiniCan 5 samples (no bentonite).

Sample ID	Position of sample	Mass of sample (g)	H bulk ppm
21:1:1	Outer surface	1.2401	1.16
21:1:2	Middle	1.2688	0.83
21:1:3	Middle	1.2531	0.84
21:1:4	Inner surface	1.0801	1.06
21:1:5	Outer surface	0.6614	1.02
21:1:6	Middle	0.7731	0.8
21:1:7	Middle	0.9244	0.8
21:1:8	Inner surface	1.9279	0.78
22:1:1	Outer surface	1.7702	1.78
22:1:2	Middle	1.2289	0.86
22:1:3	Middle	1.2184	0.8
22:1:4	Inner surface	2.3252	0.72
22:1:5	Outer surface	0.5674	1.69
22:1:6	Middle	1.6507	0.62
22:1:7	Middle	1.9071	0.62
22:1:8	Inner surface	2.3741	0.92
23:1:1	Outer surface	1.7768	0.67
23:1:2	Middle	1.7663	0.67
23:1:3	Middle	1.7616	0.6
23:1:4	Inner surface	1.7095	0.73
23:1:5	Outer surface	1.4963	0.63
23:1:6	Middle	1.6121	0.62
23:1:7	Middle	1.6718	0.6
23:1:8	Inner surface	2.1996	1.15

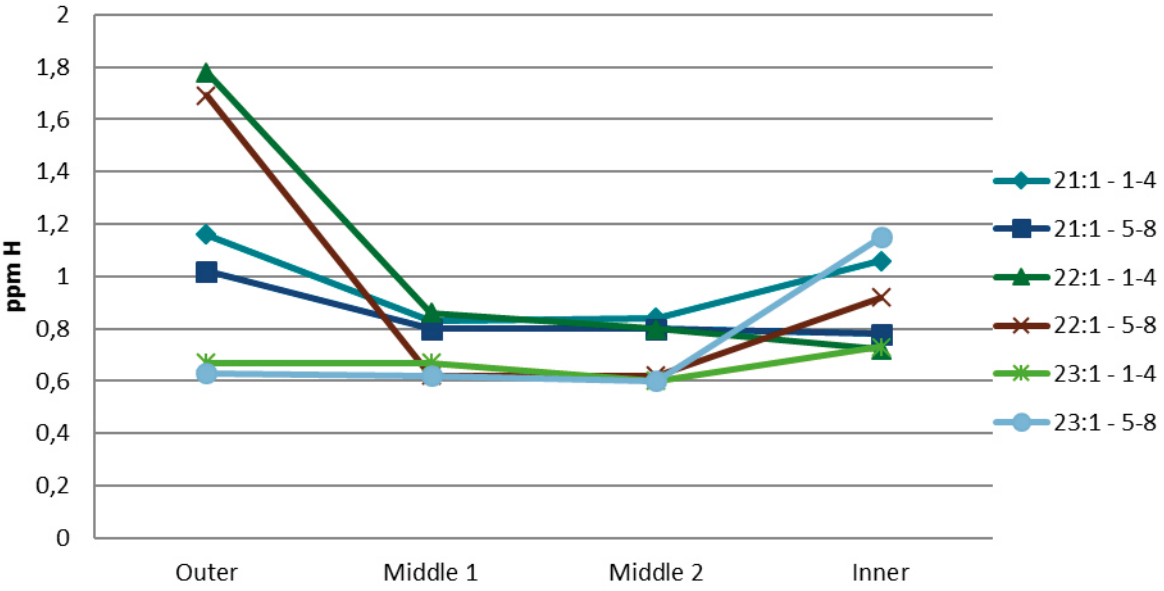

Figure A5-4. *Results of MiniCan 5 samples, hydrogen content in ppm through thickness of canister wall.*

Appendix 6

XPS, GDOES, LAICPMS

XPS, GDOES and LAICPMS analyses

As a complement to the other surface analysis techniques selected samples were exposed to several other techniques, XPS, GDOES and LAICPMS. X-ray photoelectron spectroscopy was carried out at Dept. of Physics, Uppsala University in Sweden, as Swerea KIMAB do not have an XPS instrument.

XPS: In X-ray photoelectron spectroscopy, the surface is irradiated with a beam of X-rays and the intensity and energy of electrons escaping from the surface is measured simultaneously. The XPS spectra include peaks from electrons ejected both due to the photoelectric effect (electrons ejected by incident photons, i.e. X-ray) and due to the Auger effect (electrons ejected from excited atoms after a series of internal events). The XPS characterizations were performed using a PHI 5500 spectrometer (Physical Electronics) using monochromatic Al Kα radiation (1 468.8 eV). Spectra were recorded with a pass energy of 23.5 eV giving an overall instrumental resolution of 0.6 eV as determined from the broadening of a Ag Fermi edge. XPS is used to characterise the molecular surface chemistry of a sample. The analysis depth is about 1 nm, thus it is a very surface sensitive method.

GDOES: Glow discharge optical emission spectroscopy uses a plasma gas to melt the top 5 µm of the sample and then analyses the resulting gas for content. The instrument used was a LECO GDS 850A. For the profile measurements performed, the detection limit is estimated as 0.1 % and the accuracy would be one or a few percent.

LAICPMS: Laser ablation inductively coupled mass spectroscopy uses laser radiation to sputter a sample and then analyses the resulting gas for content, with a detection limit of low ppm. Air is used in the analysis so that it is not possible to obtain values for oxygen or nitrogen.

XPS analyses

XPS was performed on two samples of copper canister material from MiniCan 5, sample M5 24:1 and M5 25:1. This method characterises the top 1 nm of the sample surface, so that the information is very surface sensitive. The results are presented as spectra. The X-axis represents the binding energy of the electron from each element, and the Y-axis shows the intensity corresponding to each binding energy. The spectra generated are element as well as chemical state specific.

Overview spectra for Minican 5 samples 24:1 and 25:1 are shown in Figure A6-1.

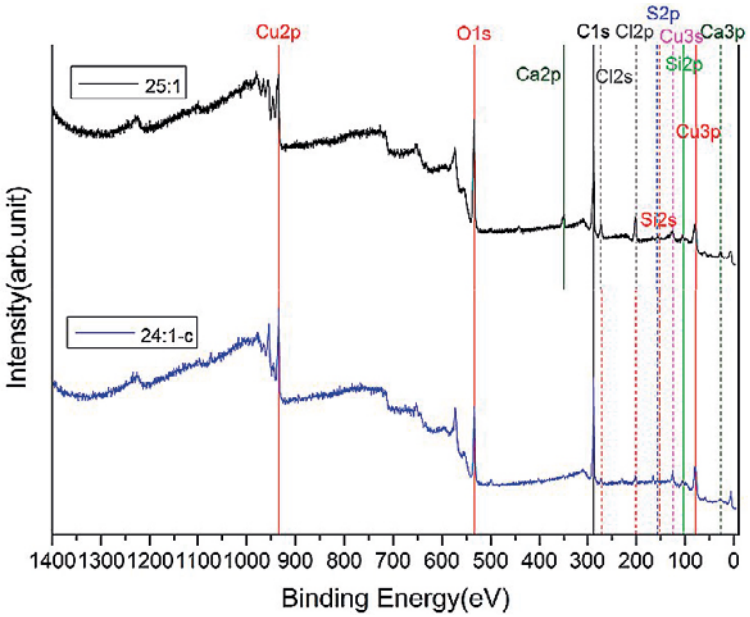

Figure A6-1. *Overview spectra from M5 24:1 and M5 25:1 (Cu2p, O1s etc. refer to electron orbitals for the different elements).*

Cu, O, Ca, C, Cl, S and Si were all found on the samples. The spectra are normalized to the background, making comparisons of the relative intensities of specific elements possible. Comparing the relative intensities, it is evident that the amounts of S, Cl, Ca and O are higher on M5 25:1 than on M5 24:1. Sample M5 25:1 represents the outer surface of the canister that would have been continuously exposed to ground water throughout the MiniCan experiment, whilst M5 24:1 represents the inner surface of the canister that would have had been exposed to ground water only from leaking in through the drilled holes and in the annulus between the canister and the cast iron insert.

In order to understand the oxidation state of Cu at the surface of the samples, additional measurements were made focusing on the signal from Cu; the Cu2p spectra from the two samples are shown in Figure A6-2. Each spectrum has two components, the $2p_{3/2}$ and $2p_{1/2}$ peaks. In both spectra, the $2p_{3/2}$ peak, found at the lower binding energy side, is composed of two peaks. This means that, for both samples, copper of at least two oxidation states is present on the surface: metallic copper or copper(I) at around 932.5 eV, and copper(II) at around 934.0 eV. The photoemission spectra from Cu(0) and Cu(I) show similar line shapes as well as very close binding energies. To distinguish between these two states, the Auger spectra Cu(LVV) can be used; these spectra are shown in Figure A6-3. From the line shapes of the Auger spectra it is clear that the peak at lower binding energy does not correspond to copper but to Cu(I) (1). The surface film of these samples is dominated by Cu in oxidation states (I) and (II).

To further investigate the copper compounds for the two oxidation states, the oxygen O1s peak is analyzed in more detail; see the spectra in Figure A6-4. Each O1s spectrum is composed of two peaks at the binding energies 532.1 and 533.6 eV respectively. The peak at the lower binding energy represents the oxygen peak from copper hydroxide and the peak at higher binding energy probably corresponds to a combination of oxides, mostly SiO_2.

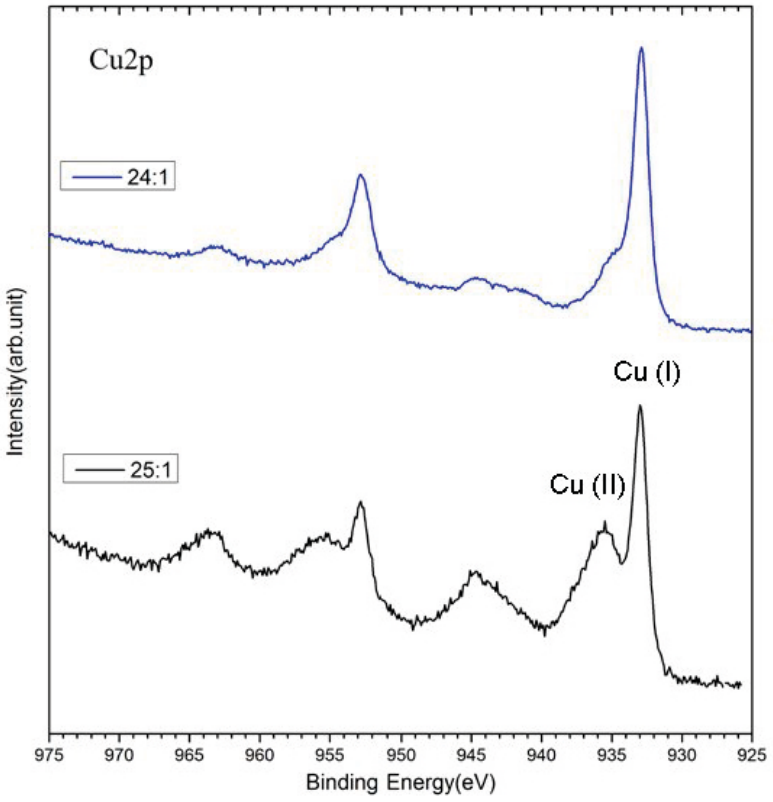

Figure A6-2. *Cu2p spectra from M5 24:1 and M5 25:1. Based on examinations of the Auger spectra, see the text above, the lower energy peak is marked Cu (I).*

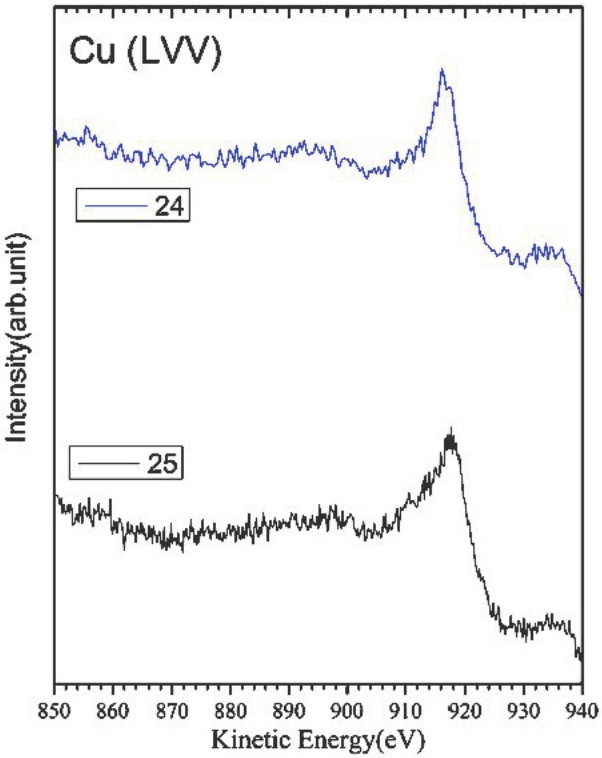

Figure A6-3. *Auger spectra Cu(LVV) from M5 24:1 and M5 25:1.*

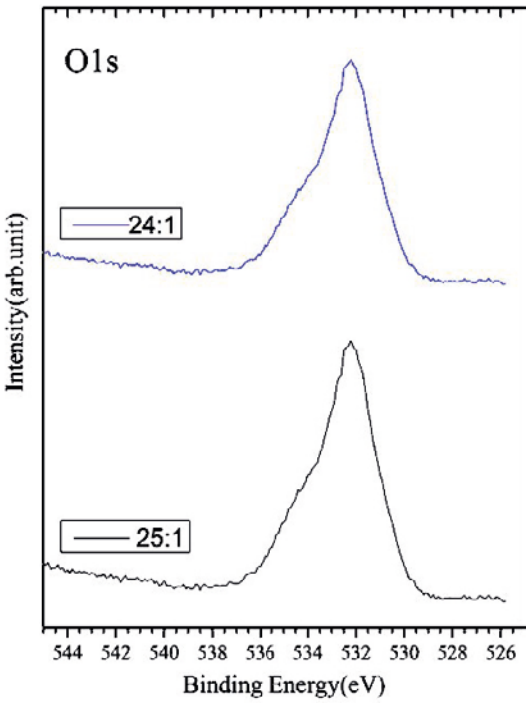

Figure A6-4. *O1s spectra from M5 24:1 and M5 25:1.*

The oxygen O1s spectra confirms the presence of $Cu(OH)_2$. Going back to the Cu2p discussion on the higher binding energy peak in the Cu2p spectra in Figure A6-2, Cu (II) is thus concluded to be $Cu(OH)_2$. This peak has contributions also from $CuCl_2$, which is in agreement with the binding energy of Cl2p at about 199.1 eV. The Cu2p peak which is found at 933 eV has contributions from CuCl having a Cu2p peak at 932.6 eV and a Cl2p peak at 199.3 eV (2).

From the analyses it is concluded that $Cu(OH)_2$, $CuCl_2$ and/or CuCl, both Cu(I) and Cu(II) species, as well as oxides, although mostly SiO_2, are present on the surfaces of both samples. A more quantitative approach reveals that the ratio between peaks of different oxidation states vary between the samples: The Cu(I) / Cu(II) ratio is smaller for M5 25:1 than for M5 24:1, indicating more severe oxidation of copper for sample M5 25:1. This is in accordance with the overview spectra in Figure A6-1 showing higher amounts of oxygen on the surface of 25:1.

GDOES analyses

Calibration was carried out using reference materials (RM) initially of aluminium (1257), brass (2161-5), titanium-hydride (TiH_2), ceramic (Ker1), stainless steel (SDN-71), aluminium-silicon (ST4), and cast iron (C1145A). Thereafter a final calibration was carried out using several copper RM's of varying qualities (Cu0X, Cu Hög, C1253). The concentration of hydrogen, sulphur and oxygen were H: 0–4.31 %, S: 0.0006–0.191 % and O: 0.0001–32.4 % respectively. By means of the calibration the depth profiles are quantified to mass fractions vs. depth. A sample of copper canister material from MiniCan 5 was analysed which represented the outer surface (sample M5 25:1), which can be seen in Figure A6-5. On the surface of the sample in the first tenths of a µm deep, some elements were clearly enriched; see Figure A6-6 to Figure A6-8.

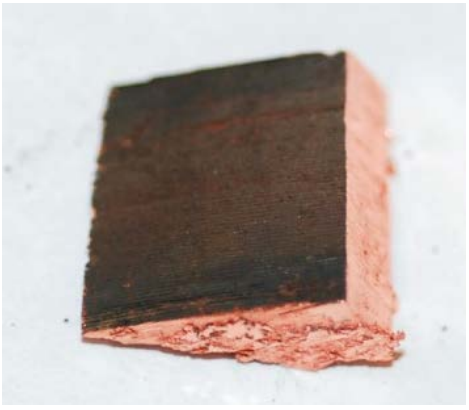

Figure A6-5. *Sample M5 25:1 outer surface of copper canister used for GDOES analysis.*

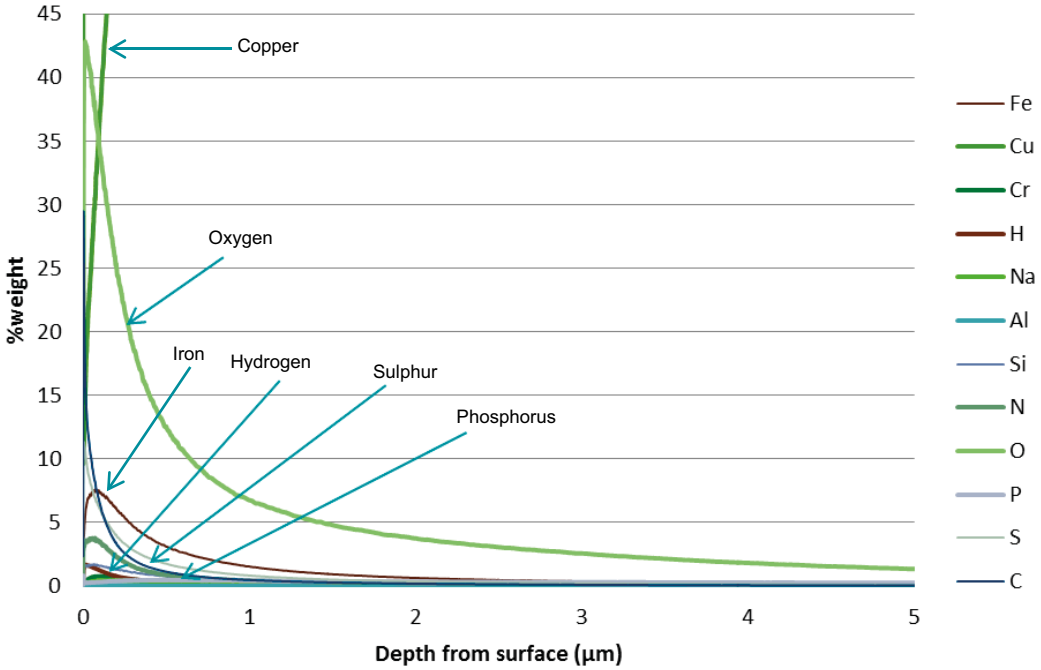

Figure A6-6. *M5 25:1, GD-OES, element profile, concentration (weight%) vs. depth (µm).*

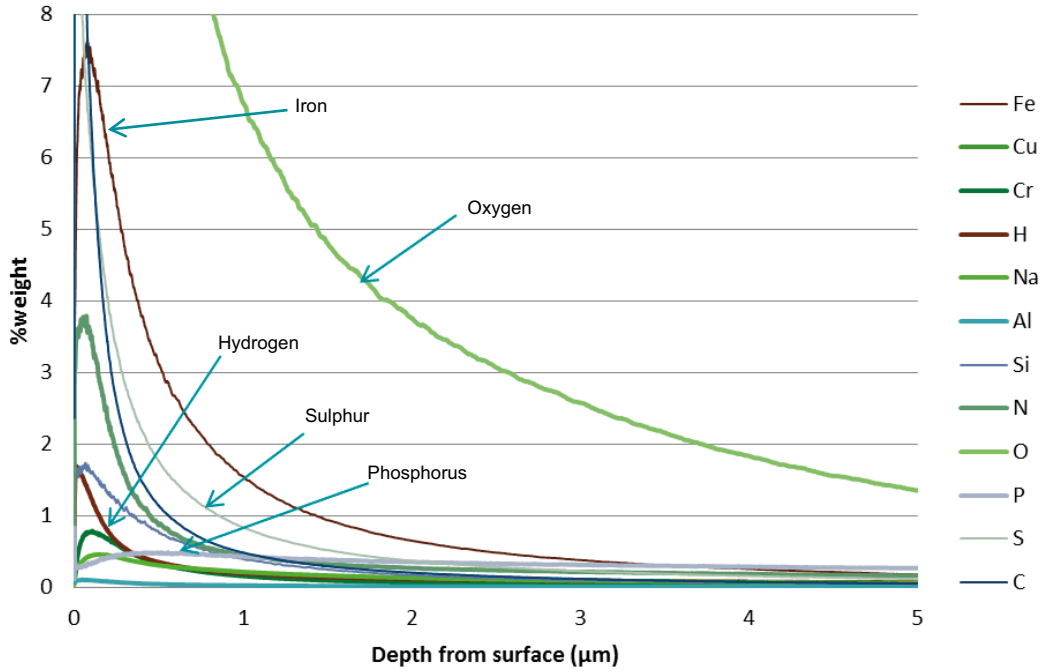

Figure A6-7. *Detail of Figure A6-6, with decreased Y axis scale. GD-OES, element profile, concentration (weight%) vs. depth (µm).*

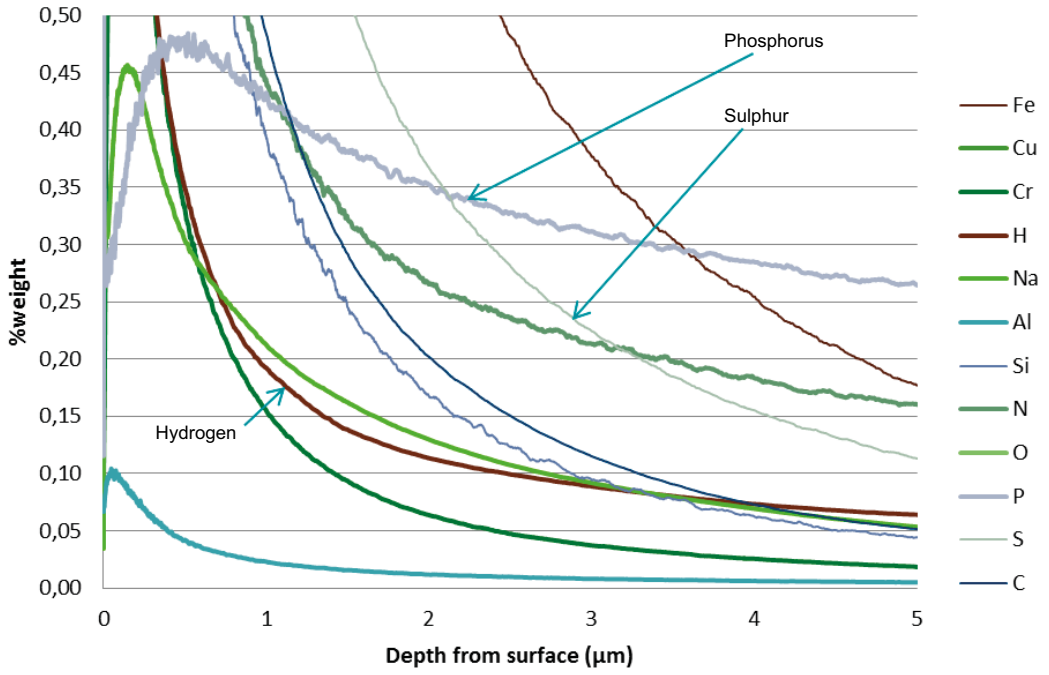

Figure A6-8. *Detail of Figure A6-7, with decreased Y axis scale. GD-OES, element profile, concentration (weight%) vs. depth (µm) (Oxygen is off the Y-axis scale).*

The oxygen profile in Figure A6-6 indicates an oxide layer of approximately 0.2 µm thick. The long "tail" of the oxygen profile is normal in GDOES analysis. Cu can be seen to increase beyond the scale of the Y-axis vs. depth as to be expected. In Figure A6-7 the elements Fe, S, C, N and Si show increased concentrations in the surface layers, approximately < 1 µm. Finally, in Figure A6-8 the elements Cr, P, Na and Al also showed increased concentrations in the surface layers, approximately < 1 µm.

LAICPMS analyses

The samples analysed with LAICPMS were representative of the outer surfaces of the canister material from both MiniCan 4 (M4) and 5 (M5) experiments. Two different methods of analysis were used, pre-burned and not pre-burned. The pre-burn ranges in depth from 10 µm to 17.5 µm on the surface of the sample. The analysis technique has a depth of about 20 µm into the sample surface. Table A6-1 shows the difference in profile of a pre-burned and non-pre-burned sample. In general the M5 sample had higher concentrations of all elements other than Cu and Al than M4 in the pre-burned analysis. From the non-pre-burned analysis the results show a clear difference between the MiniCan 4 and MiniCan 5 samples, especially with respect to the Al, Fe, Mg, Ni, S, and Si content.

Table A6-1. Results from LAICPMS analysis.

	M4 pre-burned (%)	M5 pre-burned (%)	M4 (%)	M5 (%)
Al	0.178	0.068	5.353	0.611
Ca	0.133	0.270	3.474	3.490
Cl	0.128	0.754	2.681	3.061
Cu	99.235	97.564	76.967	76.311
Fe	0.031	0.438	0.811	6.666
Mg	<0.01	0.056	0.522	1.057
Na	0.017	0.079	0.958	1.326
Ni	<0.01	0.093	<0.01	0.239
S	0.037	0.306	0.737	1.674
Si	0.148	0.266	7.863	3.977
Ti	<0.01	0.017	0.157	0.261
Zn	<0.01	<0.01	0.150	0.103

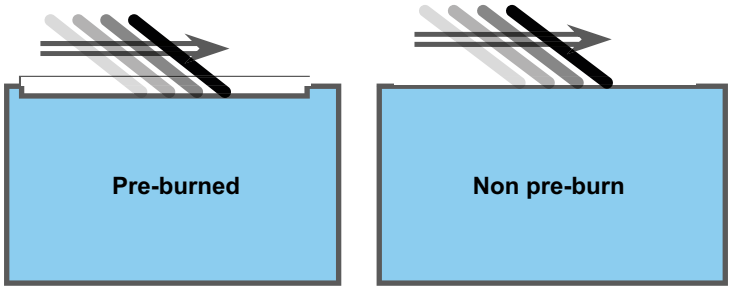

Figure A6-9. *Schematic illustration of pre-burn on LAICPMS sample. Direct application gives an information depth of less than 20 µm, while pre-burn gives an information depth of 30–37 µm. The arrow and greyscale lines represent the direction of travel of the laser as it carries out the analysis on the surface.*

Appendix 7

Raman

Raman analyses

Raman spectroscopy is used to characterise the molecular surface chemistry of a sample, with an analysis depth of about 1 μm into the surface. Raman analyses were carried out using a Horiba Labram HR 800 with an objective lens of working distance 35 mm and laser wavelength of 532 nm. This is significant as the first attempt to use a laser of 785 nm wavelength and 20 mm working distance objective was not successful, and no results could be obtained using this set-up. This was due to the working distance of the objective which was restricted by the geometry of the sample holder.

Reference materials were analysed, as well as using data from the literature when analysing the results. Cuprite (Cu_2O) has peaks at 200–230 cm^{-1} and weaker peaks at 420 cm^{-1} and 640 cm^{-1}, with fluorescence detected from the reference material sample. The fluorescence seen from most samples was thought to be from copper oxide (cuprite) due to the colour of the light emitted. It is also possible that the fluorescence was from a different copper oxide or possibly an iron oxide.

Reference spectra

If not referring explicitly to a journal article, reference spectra discussed in this section are taken from the RRUFF mineralogical database. These spectra are denoted by their RRUFF id which starts with a capital "R", followed by a six digit number.

Reference spectra for cuprite, single crystal Cu_2O (111), show two strong peaks around 200–230 cm^{-1}, a weak peak at 420 cm^{-1}, a peak at 640 cm^{-1} and strongly increasing intensity at higher wave numbers from fluorescence (R050384, R050374).

Spectra for synthetic tenorite (CuO), show peaks around 300 cm^{-1} and 650 cm^{-1} (R120076), while there is an additional peak slightly over 800 cm^{-1} for the mineral sample (R060978).

Reference spectra of iron oxides, iron hydroxide and goethite FeO(OH), with hydrolysed iron oxides have peaks between 200 cm^{-1} and 900 cm^{-1}, as well as a strong peak at 1 300 cm^{-1} (Troland et al. 1997). The spectrum from FeO (black line) has a much weaker profile than the other samples. Fe_3O_4 (magnetite) has a peak at approximately 670 cm^{-1} which is similar to the magnetite and goethite spectra taken from the RRUFF database (R061111, R050142).

The spectrum from a CuS reference sample is dominated by a peak just below 500 cm^{-1} (R060129). For deposited thin films, the Raman spectrum for Cu_2S is very similar to that of CuS (Minceva-Sukarova et al. 1997), while the spectrum for the mineral differs (R120090).

Comparing the Raman spectra of CuS (R060129) and FeS (R070242), shows that FeS has weaker peaks at 300 cm^{-1}, 410 cm^{-1}, approximately 700 cm^{-1}, 1 050 cm^{-1} and a broader peak between 1 200 cm^{-1} and 1 700 cm^{-1}. Troilite (FeS) has peaks at 200 cm^{-1}, 275 cm^{-1}, 475 cm^{-1} and 680 cm^{-1} while Fe_7S_8 (pyrrhotite) has two peaks at 340 cm^{-1} and 380 cm^{-1} (R060440).

Mixed copper and iron sulphides, $Cu_xFe_yS_z$, from the RRUFF database are dominated by peaks around 300 $cm^{-1}$with some variation (see for example R050322, R050018, and R090050).

Silver sulphide shows peaks at around 250 and 450 cm^{-1} (R070578).

The spectra of copper (II) sulphates have various peaks depending on the exact compound, but have in common that their strongest peak appear at around 1 000 cm^{-1} (see for example R050212, R070398, R060117, R060139, and R050292).

Not many Raman spectra were found for sulphites in the RRUFF database; one example with the sulphite peak at 935 cm^{-1} was found for $PbSO_3$ (R060764). For other compounds, more relevant to this work, peaks close to this location are reported: For hannebachite $(CaSO_3)_2 \cdot H_2O$ these bands are observed at 1 005, 969 and 655 cm^{-1} (Frost and Keeffe, 2009). For orschallite, a mixed sulphite sulphate compound $Ca_3(SO_3)_2SO_4 \cdot 12H_2O$, sulphite stretching bands at 971 and 984 cm^{-1} and sulphate

bands at 1 005, 1 096 and 1 215 cm^{-1} are reported (Frost and Keeffe, 2009). In a laboratory study on pipeline corrosion Hua et. al. (2015) report a sulphite peak at 954 cm^{-1} for iron (II) sulphite $FeSO_3$.

Carbonates, as for example calcite (R040070), show a strong peak at 1 085 cm^{-1}. Malachite, $Cu_2CO_3(OH)_2$, has numerous peaks up to 550 cm^{-1} and carbonate bands around 750 and at 1 090 cm^{-1} (R050531).

As for copper sulphates, Raman spectra of iron sulphates also show peaks at around 1 000 cm^{-1} (see for example R060638, R061076, and R060238).

Carbon has different peaks depending on what form it is in, with diamond having a peak at 1 300 cm^{-1} (R050204) and graphite at 1 600 cm^{-1} (R050503). Amorphous carbon has a broad peak from 1 200 cm^{-1} to 1 700 cm^{-1} (Rebollo-Plata et al, 2005).

Spectra for MiniCan 5 samples

Sample M5 5:1 was measured at four points on the surface, as shown in Figure A7-1 along with their respective spectra. Point 1 had a strong sulphate peak seen at 1 000 cm^{-1} (see reference spectra in Figure A7-8). All points had a double peak at 240–320 cm^{-1}. All points had fluorescence from cuprite, which can also produce peaks in the same area (250–320 cm^{-1}) but with a different intensity. Another alternative for peaks in this range is mixed sulphides, but not sulphate.

Sample M5 6:1 was measured at three points on the surface. Fluorescence dominates all points, but sulphate was detected (1 000 cm^{-1}) and the peaks at 200–400 cm^{-1} could be a mixture of copper oxide and iron oxide.

Sample M5 7:1 was measured at three points on the surface, with peaks detected at 250–320 cm^{-1} for points 1 and 2 which could be cuprite or sulphide. Carbon was detected at point 1. Fluorescence from cuprite dominated point 3.

The two points measured on sample M5 9:1 were similar to troilite (FeS).

Sample M5 10:1 had peaks for troilite (FeS) and sulphate.

Sample M5 11:1 iron mass loss had varying peaks detected at three different points on the surface. At point 1, iron oxide resembling FeO and C were detected, whilst at point 2, C and FeS, and at point 3, a strong peak for FeS.

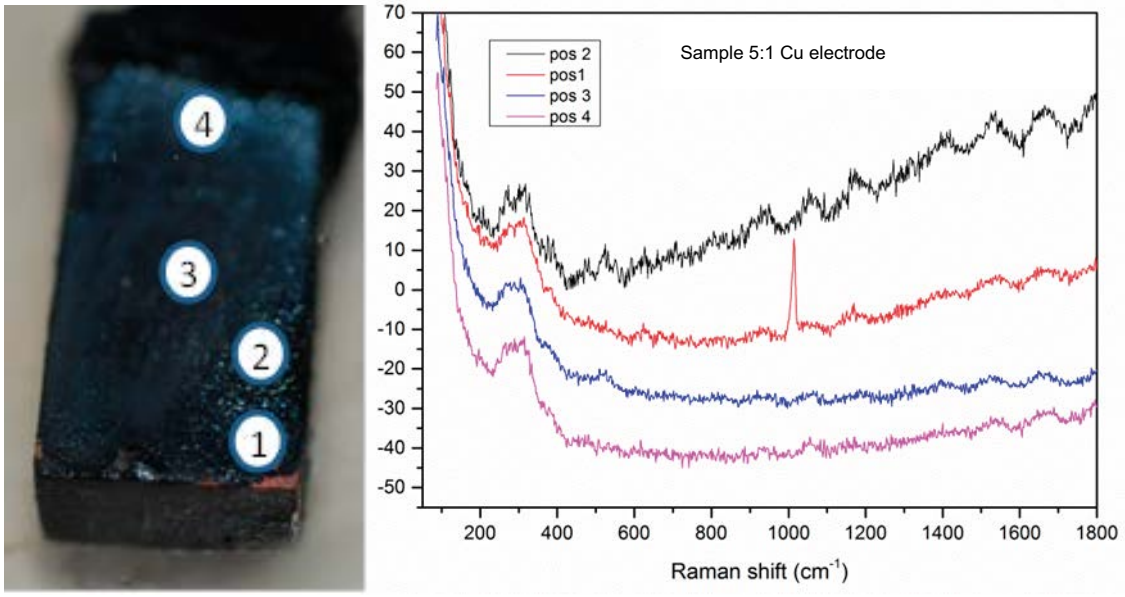

Figure A7-1. *Sample M5 5:1 copper electrode.*

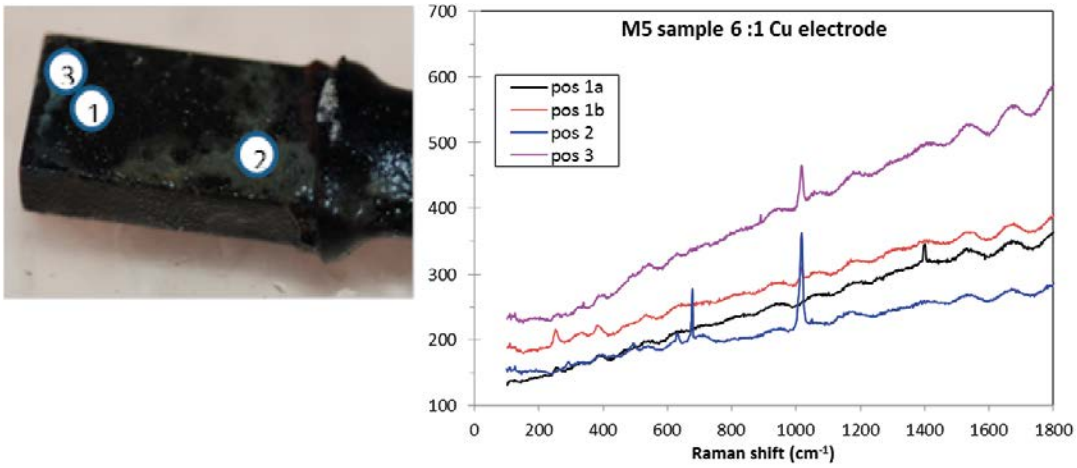

Figure A7-2. *Sample M5 6:1 copper electrode.*

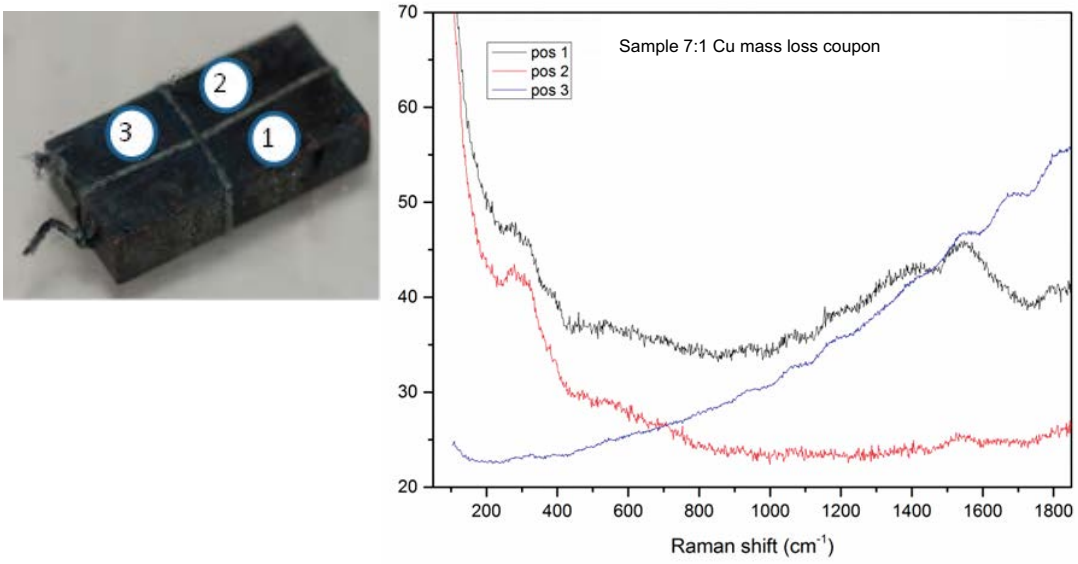

Figure A7-3. *Sample M5 7:1 copper mass loss.*

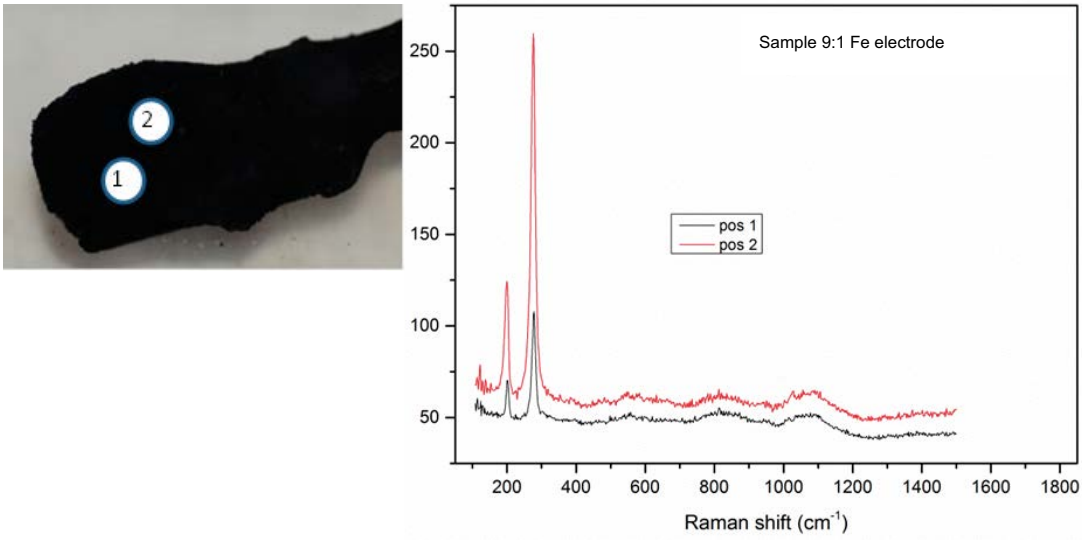

Figure A7-4. *Sample M5 9:1 iron electrode.*

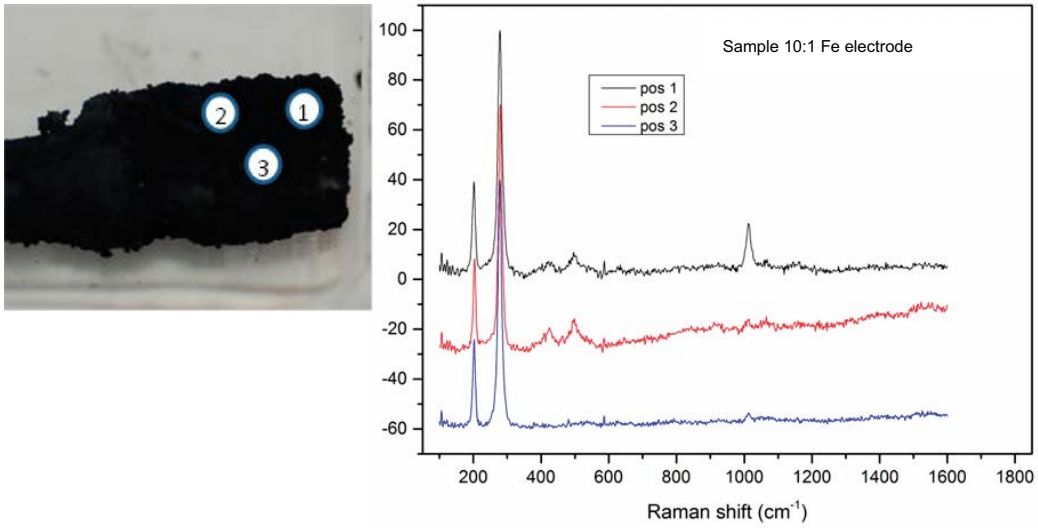

Figure A7-5. *Sample M5 10:1 iron electrode.*

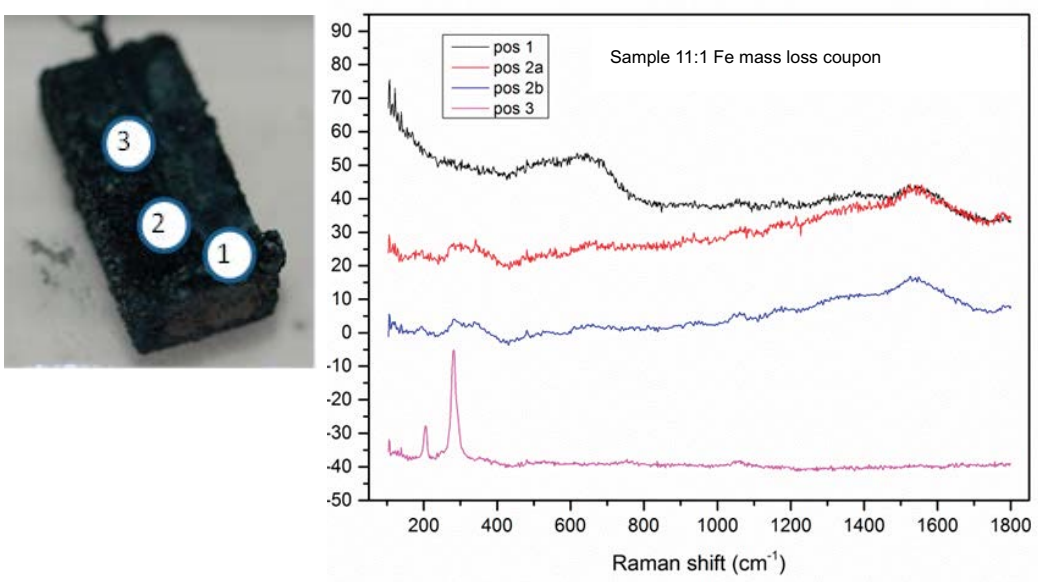

Figure A7-6. *Sample M5 11:1 iron mass loss.*

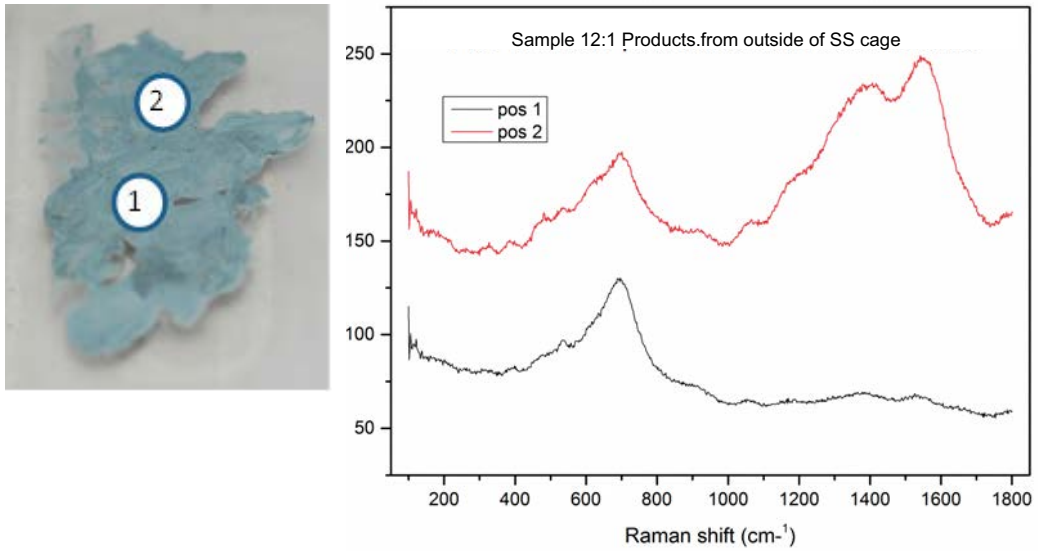

Figure A7-7. *Sample M5 12:1 corrosion products from outer surfaces of stainless steel cage.*

Products taken from outside of the stainless steel cage, sample M5 12:1 had magnetite detected at point 1 and Fe_3O_4 (magnetite) and carbon detected at point 2. The green colour suggests Cu(II) products, which is supported by them still being green after exposure to air but this is still unlikely since no films on copper surfaces were green. The source of the carbon is unknown. The most likely explanation would be contamination.

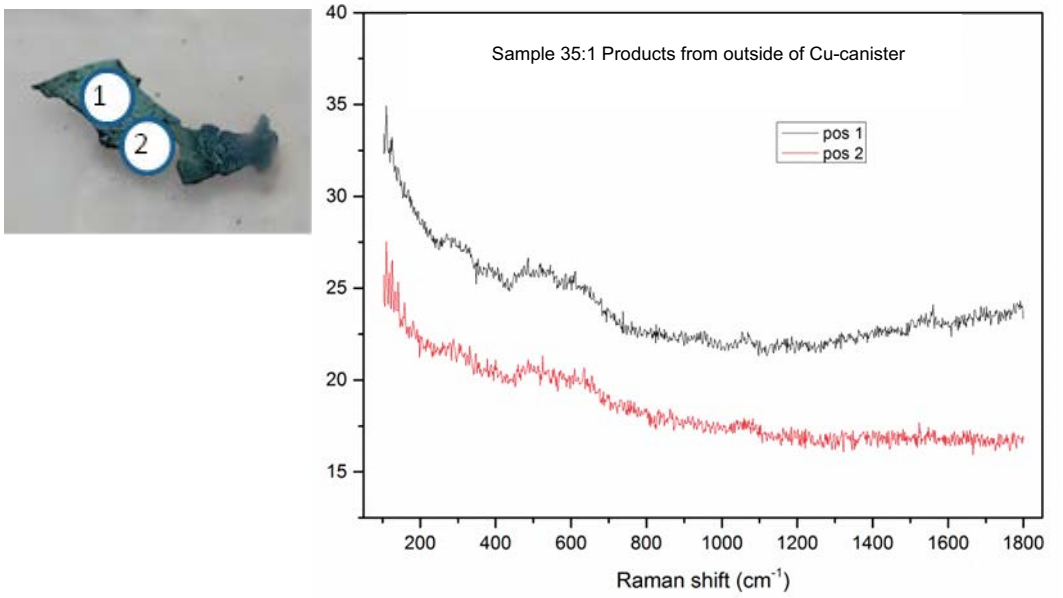

Figure A7-8. *Sample M5 35:1 corrosion product taken from outer surface of copper canister.*

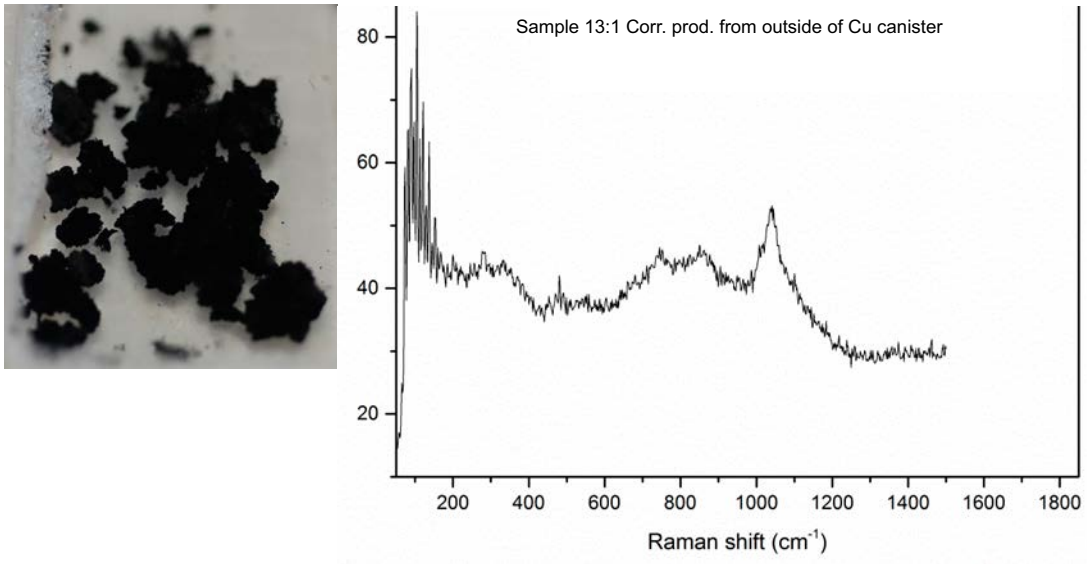

Figure A7-9. *Sample M5 13:1 corrosion products from iron part of the sandwich sample.*

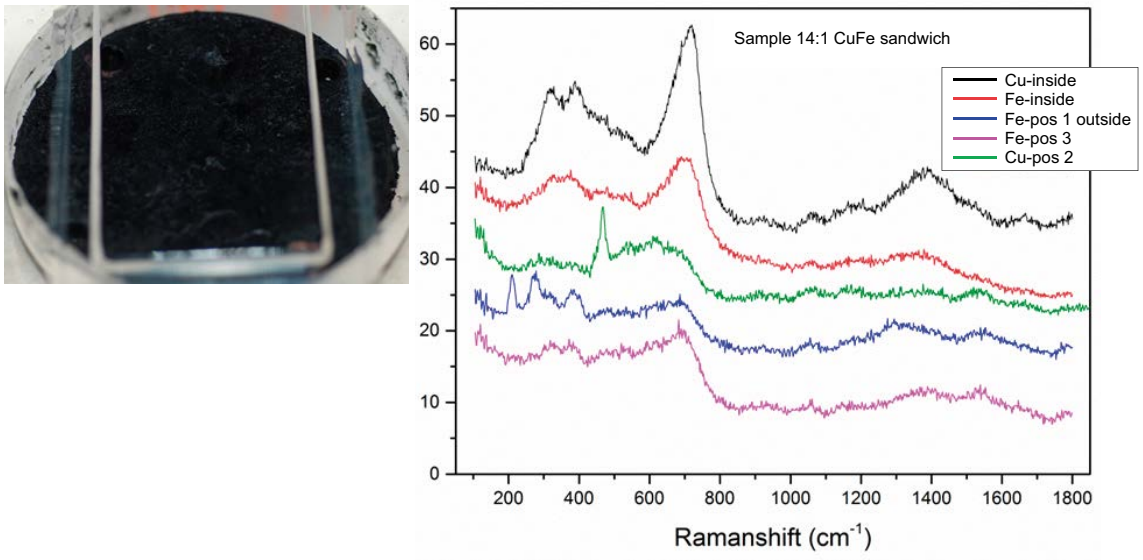

Figure A7-10. *Sample M5 14:1 copper-iron sandwich specimen.*

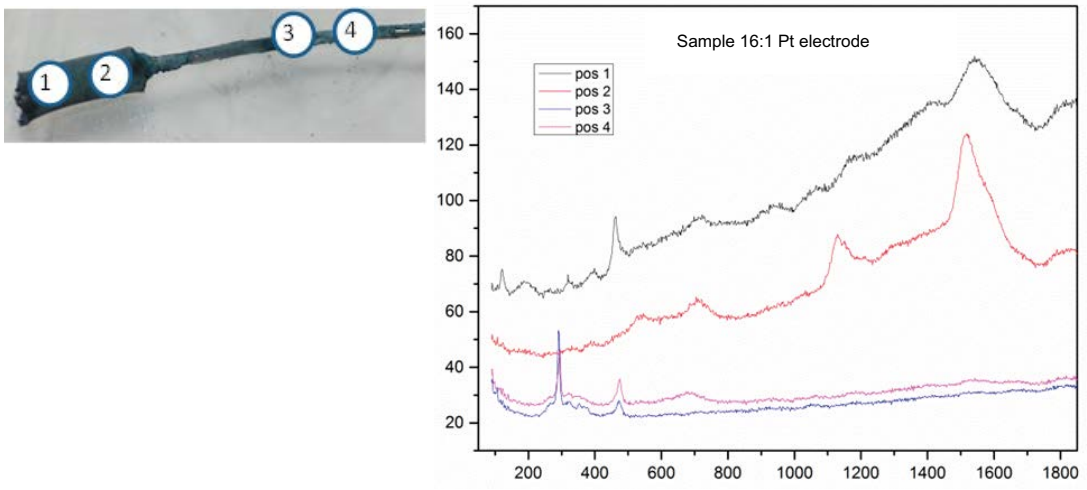

Figure A7-11. *Sample M5 16:1 platinum electrode.*

Sample M5 35:1, products taken from the outer surface of the copper canister, did not have any distinct peaks. From the appearance and the area from which the sample was taken, a composition similar to that of sample M5 12:1 (Figure A7-7) is expected, however this is contradicted by small remains of the product turning brownish yellow after exposure to air, indicating iron corrosion products.

Sample M5 13:1 which was corrosion products from the outside of the iron part of the copper-iron sandwich had peaks resembling FeS as well as $CaCO_3$ (calcite) and/or a mixture of calcite and sulphate detected but no indications of carbon.

The internal and external surfaces of sample M5 14:1 copper-iron sandwich specimen were analysed at several points; as the lid of the sample holder was accidentally opened prior to Raman analysis it was possible to analyse all sides of the components, but the sample had been exposed to oxygen before analyses. In the spectra obtained, magnetite Fe_3O_4 and sulphides dominate both on the copper and the iron components. There is some resemblance with the spectrum for sample M5 13:1, the iron corrosion products (Figure A7-10), indicating transfer of corrosion products.

Sample M5 16:1 is the platinum electrode and had carbon detected at points 1 and 2, and probably sulphide at points 3 and 4.

The gold electrode, sample M5 17.1 had carbon and iron oxide detected at point 1 and sulphide detected at points 2 and 3.

Sulphide (silver sulphide) was detected on sample M5 18.1 the Ag/AgCl electrode.

The platinum counter electrode net, sample M5 20:1, had carbon detected and fluorescence, possibly cuprite.

Sample M5 24:1 which represents the inner surface of the copper canister, had peaks characteristic of magnetite and cuprite fluorescence detected at two points on the surface.

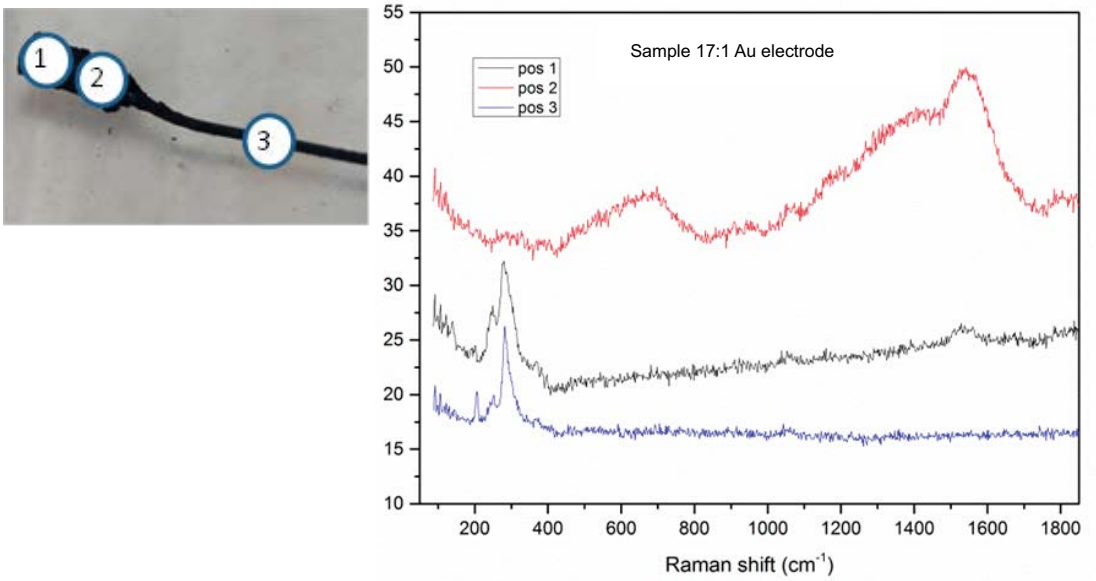

Figure A7-12. *Sample M5 17:1 gold electrode.*

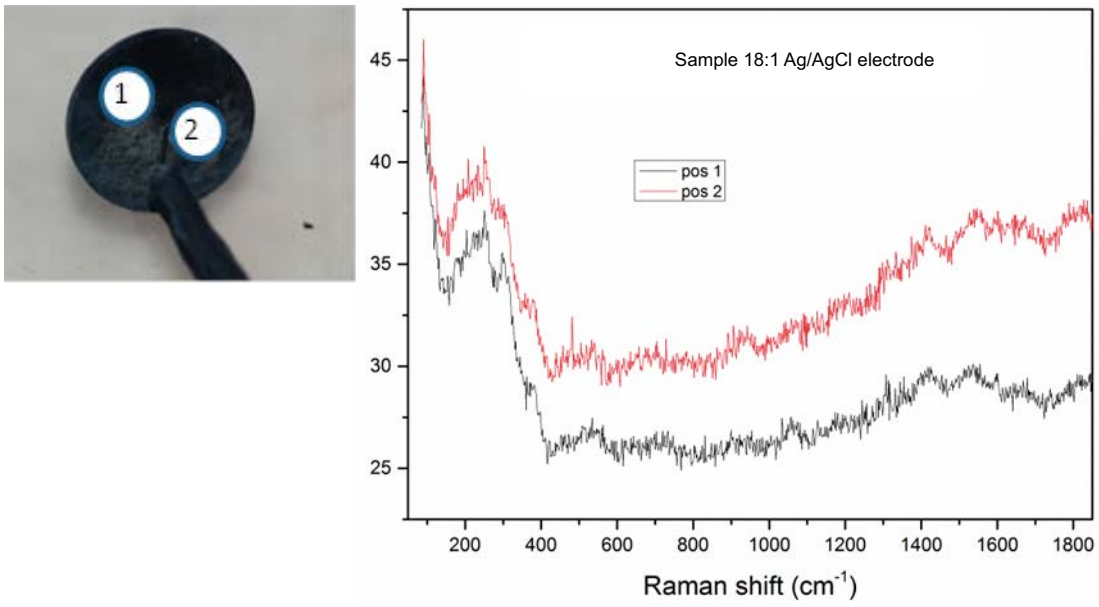

Figure A7-13. *Sample M5 18:1 Ag/AgCl electrode.*

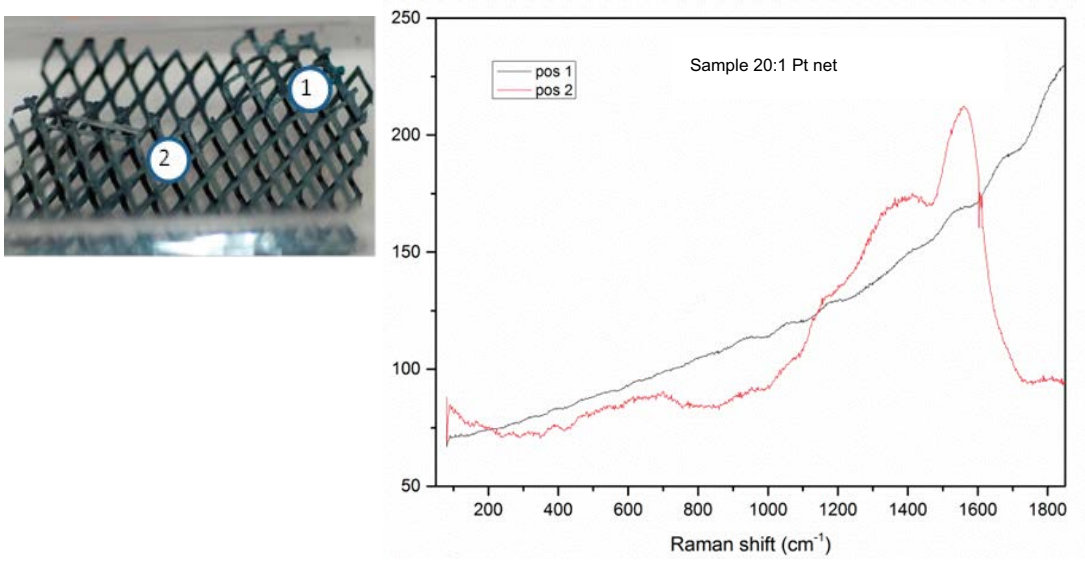

Figure A7-14. *Sample M5 20:1 platinum counter electrode.*

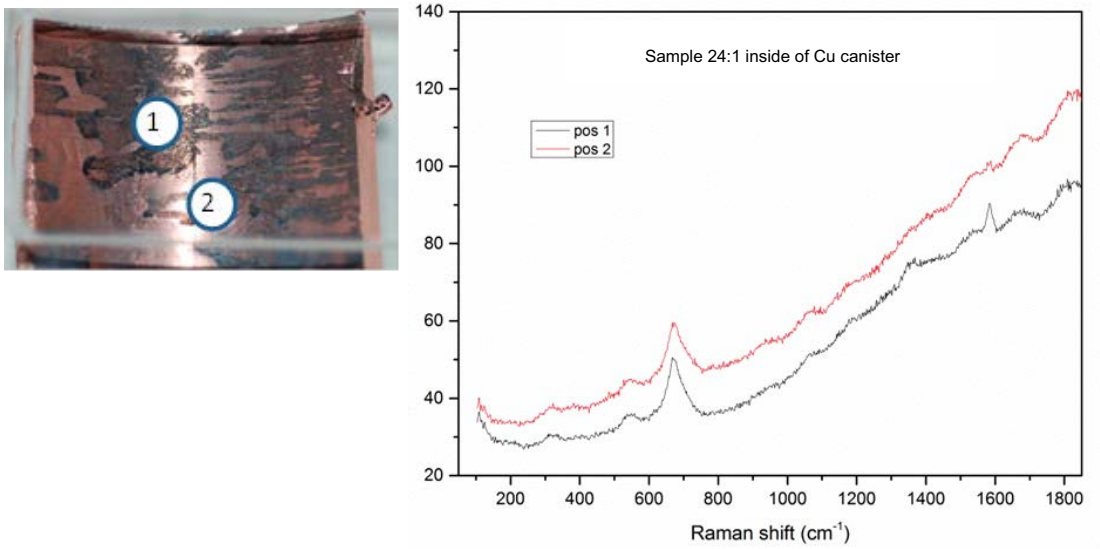

Figure A7-15. *Sample M5 24:1 inner surface of canister.*

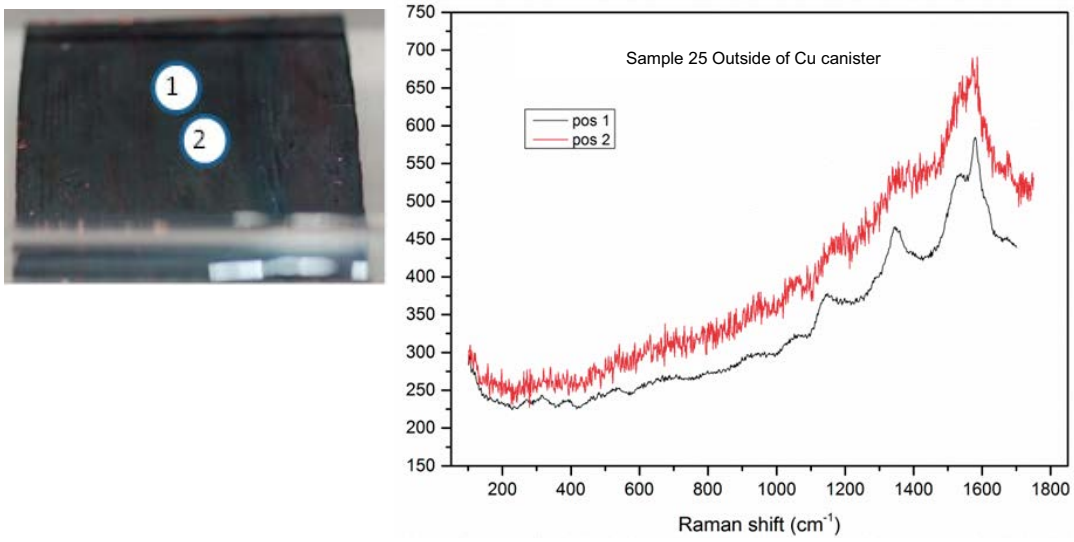

Figure A7-16. *Sample M5 25:1 outer surface of copper canister.*

On sample M5 25:1, the outer surface of the copper canister, carbon and fluorescence from cuprite were detected.

Sample M5 26:1, the weld from the copper canister, had carbon detected with a possible contribution from sulphate or calcite at point 1, whilst cuprite fluorescence was detected at point 2.

Sample M5 27:1, the inner surface of the copper canister where the machined hole was positioned, was difficult to analyse due to the geometry. Points 3 and 4 had cuprite fluorescence detected but the spectrum from point 1 was deemed unreliable.

Fe_3O_4 and carbon were detected on the points analysed on sample M5 29:1, the outer surface of the cast iron insert.

On sample M5 30:1 which was the area of the cast iron insert near the hole through the copper canister, had carbon detected, both graphite and amorphous.

Sample M5 31:1 which was similar to sample M5 30:1, had carbon detected but also possibly some iron oxide.

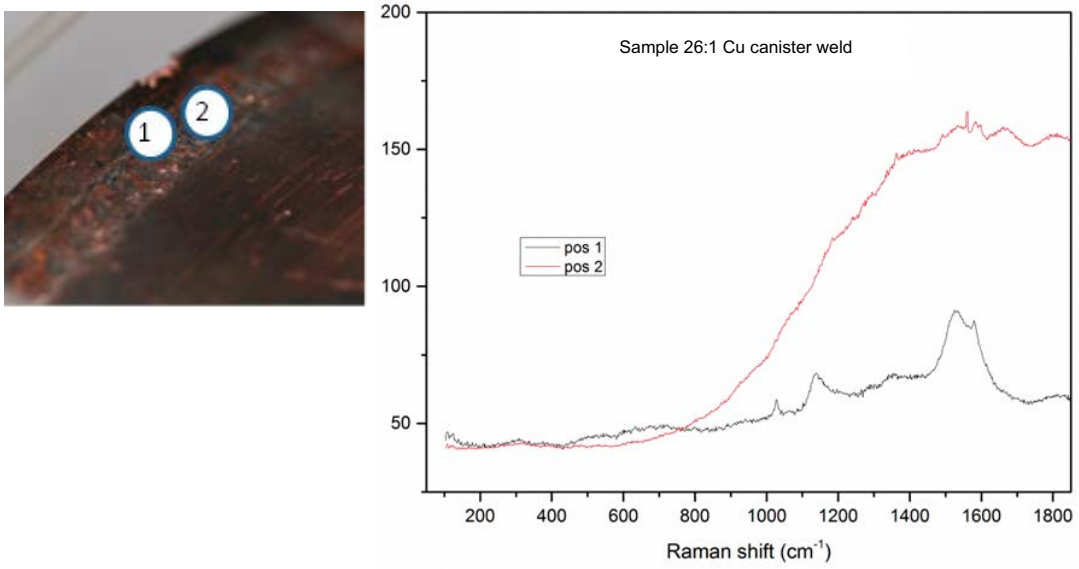

Figure A7-17. *Sample M5 26:1 weld of copper canister.*

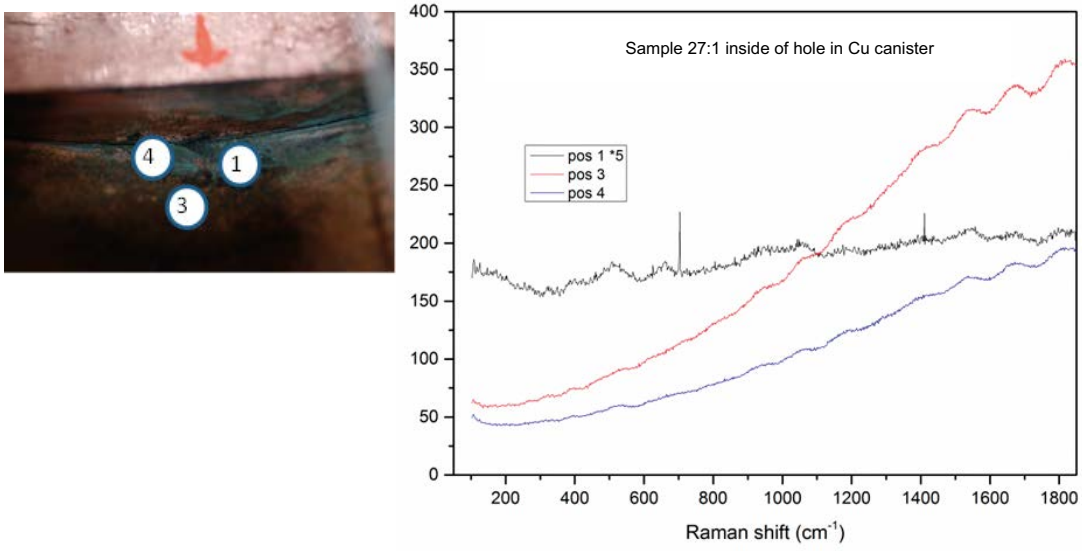

Figure A7-18. *Sample M5 27:1 hole through copper canister.*

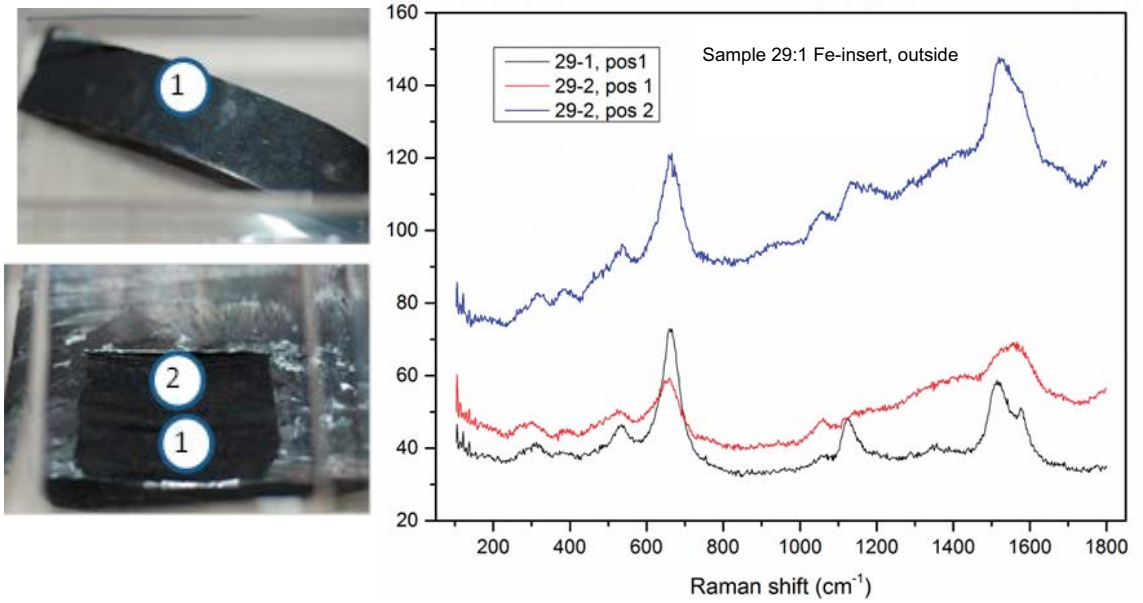

Figure A7-19. *Sample M5 29:1 outer surfaces of cast iron insert.*

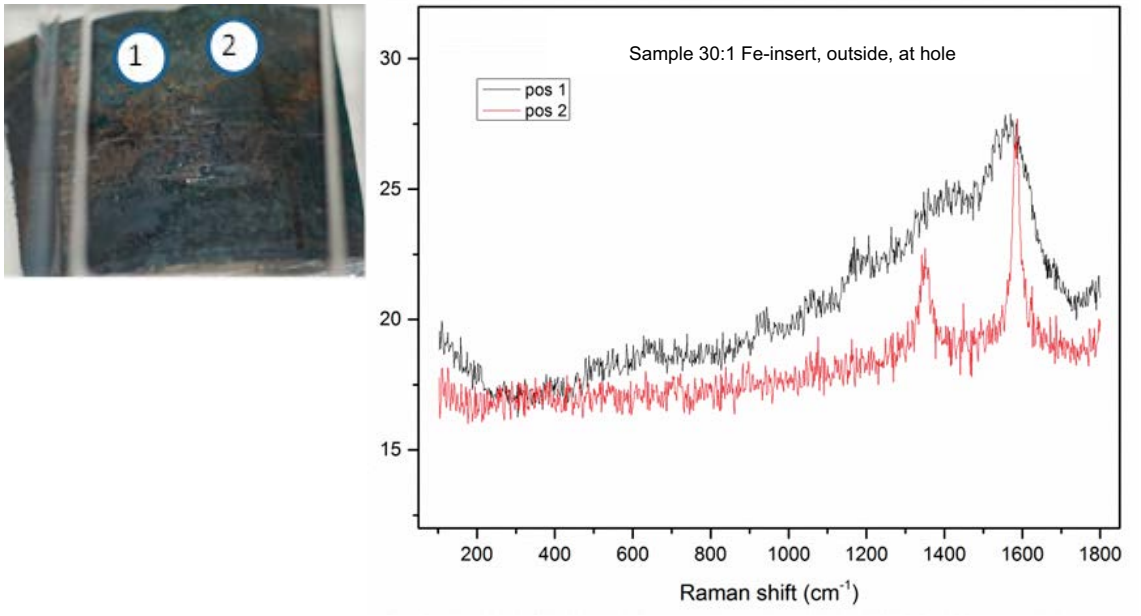

Figure A7-20. *Sample M5 30:1 surface of cast iron insert near position of hole through copper canister.*

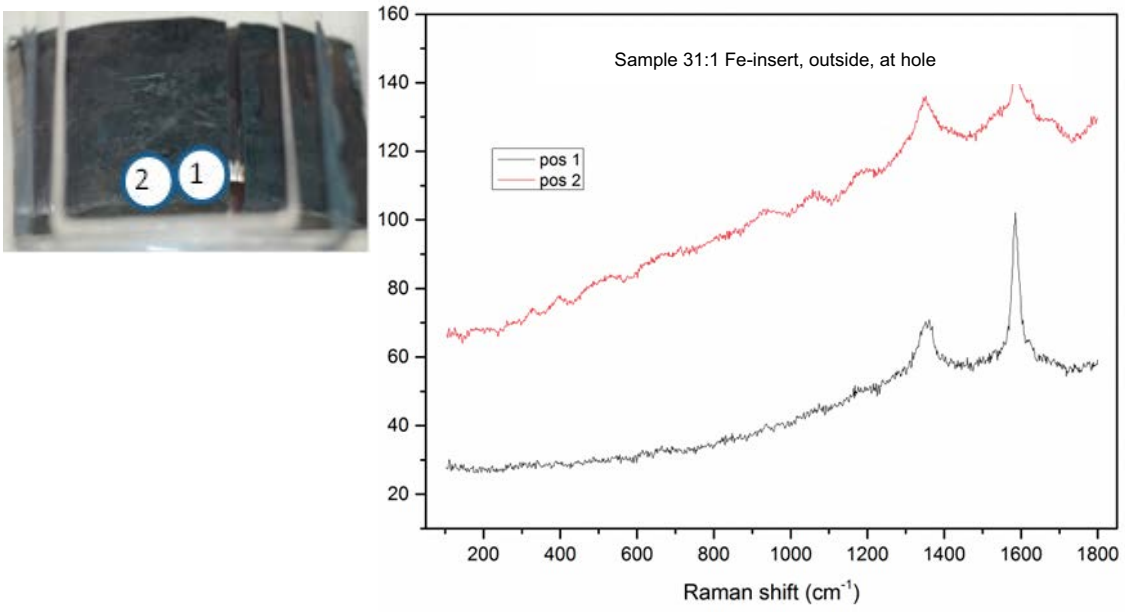

Figure A7-21. *Sample M5 31:1 surface of cast iron insert near position of the hole through the copper canister.*

Spectra for MiniCan 4 samples

With many of the MiniCan 4 samples the surfaces were covered with a layer of bentonite from the exposure, and only fluorescence (probably from cuprite) was detected during the Raman analysis. Sample M4 1:1 showed typical cuprite fluorescence, see Figur A7-22.

Sample M4 3:1 had two peaks detected at point 1, but it was unclear what these were due to. Point 2 showed only cuprite fluorescence.

Sample M4 5:1 with sulphide and cuprite detected on the surface.

Sample M4 9:1, iron electrode, had fluorescence detected, but this could have been to the bentonite that covered the surface, or less likely from cuprite. Weak peaks may be from sulphides.

Sample M4 11:1, the iron mass loss sample had calcite and fluorescence detected at point 1, and carbon and sulphide at points 3 and 4 respectively.

Sample M4 26:1 the weld from the copper canister, had only fluorescence detected.

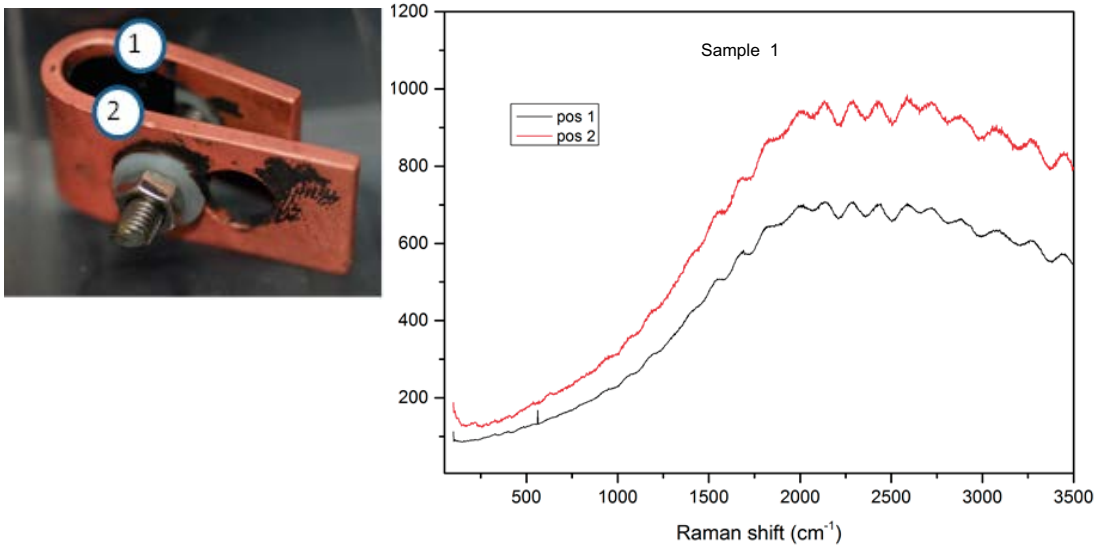

Figure A7-22. *Sample M4 1:1 u-bend specimen.*

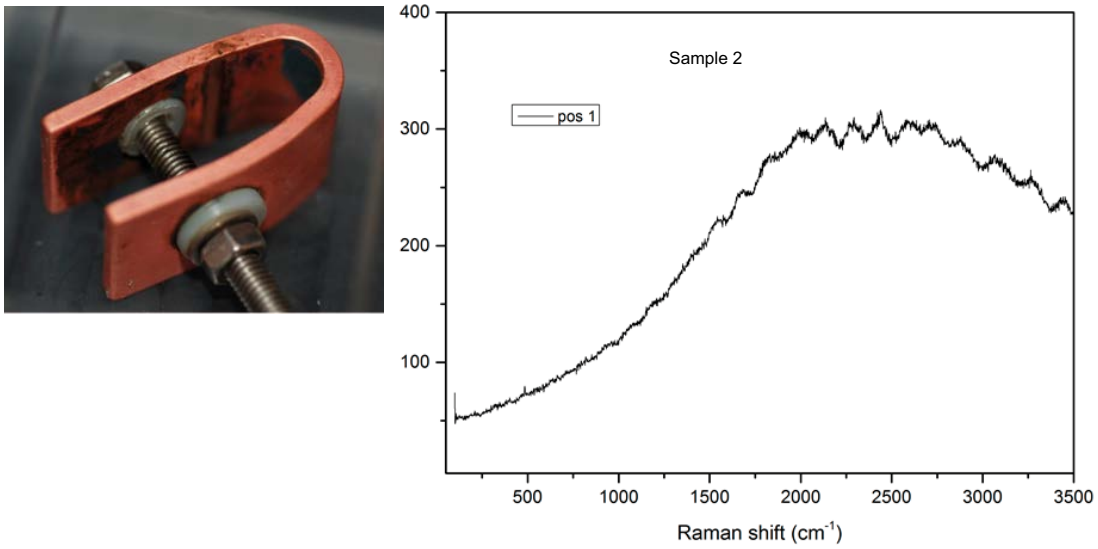

Figure A7-23. *Sample M4 2:1 u-bend specimen, with fluorescence from cuprite.*

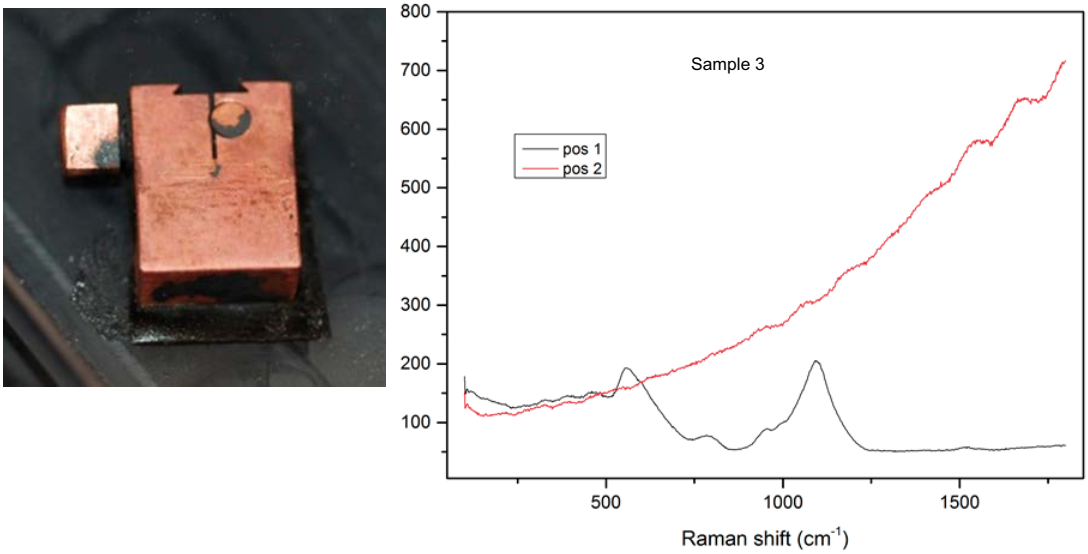

Figure A7-24. *Sample M4 3:1 WOL specimen.*

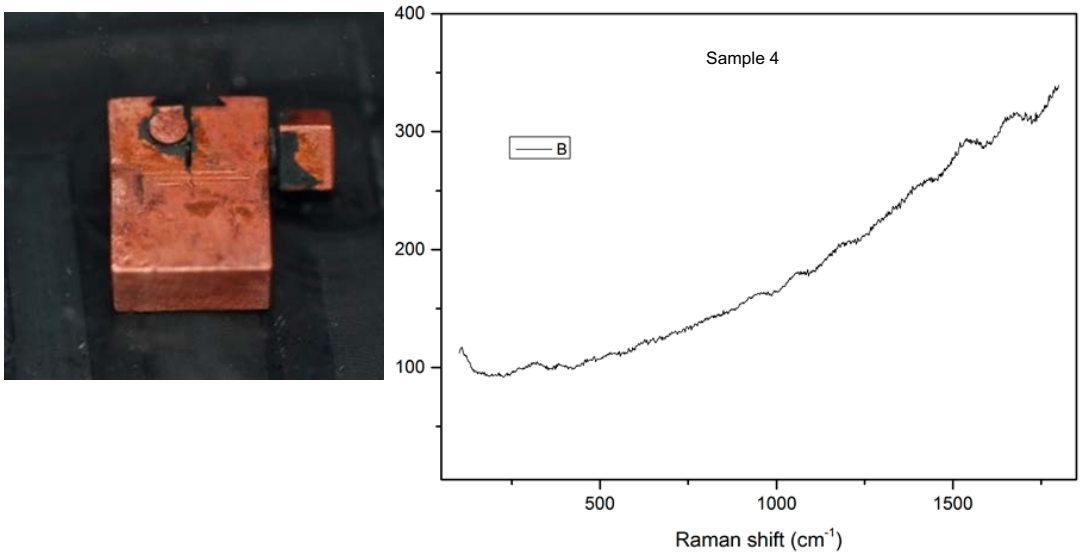

Figure A7-25. *Sample M4 4:1 WOL specimen, with fluorescence from cuprite.*

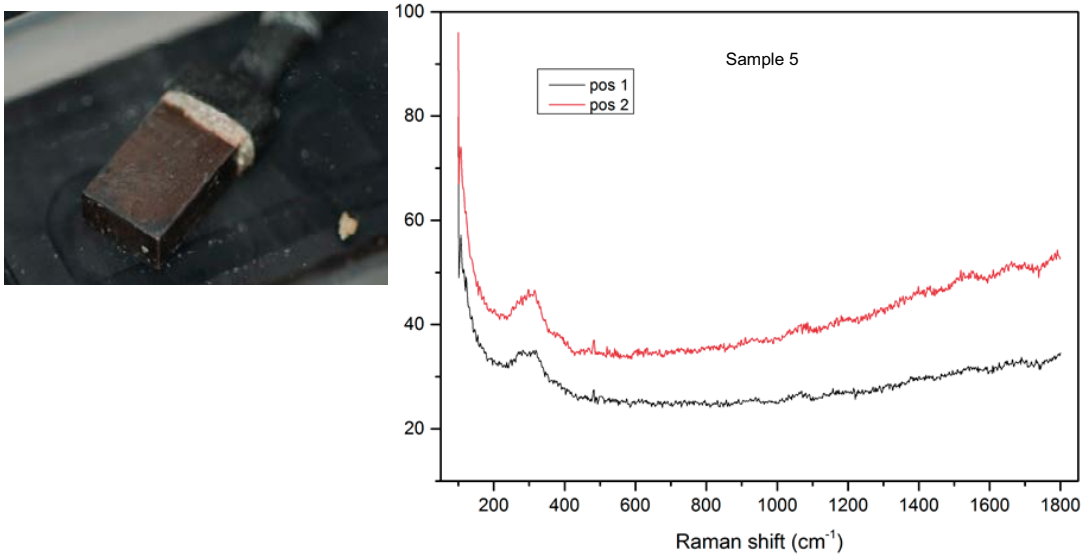

Figure A7-26. *Sample M4 5:1 copper electrode.*

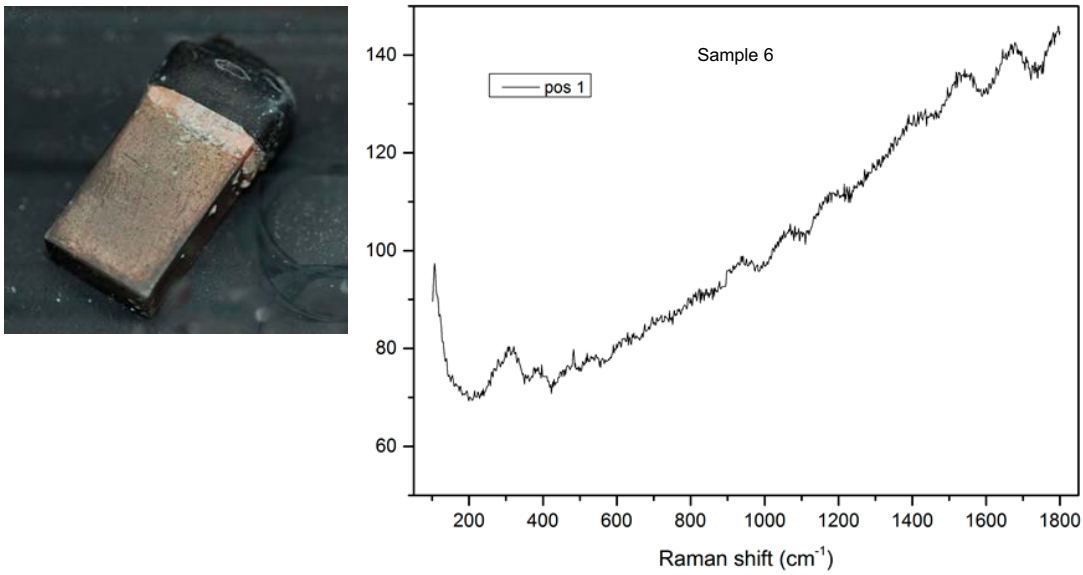

Figure A7-27. *Sample M4 6:1 copper electrode with cuprite and sulphide detected.*

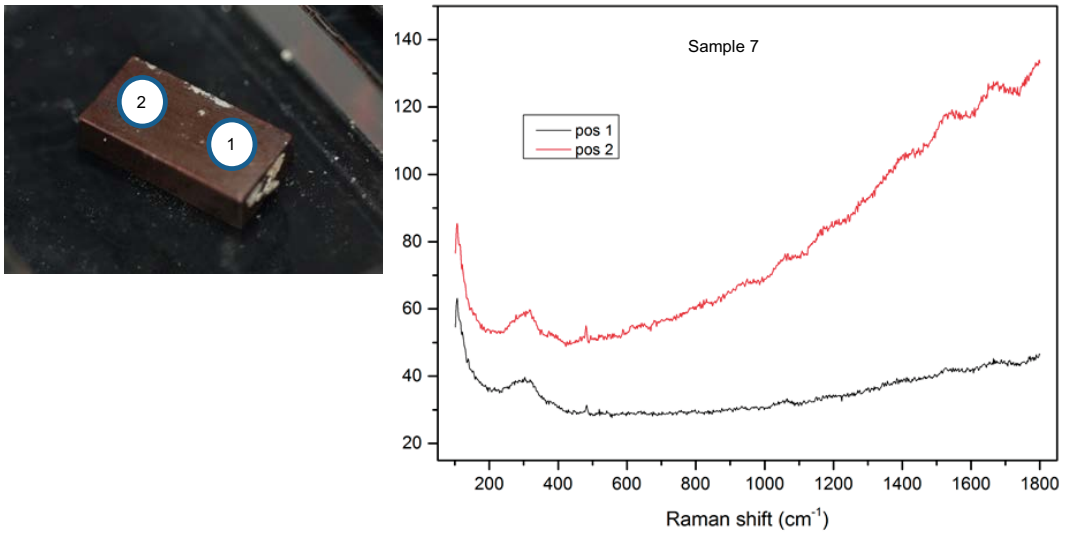

Figure A7-28. *Sample M4 7:1 copper mass loss with cuprite and sulphide detected.*

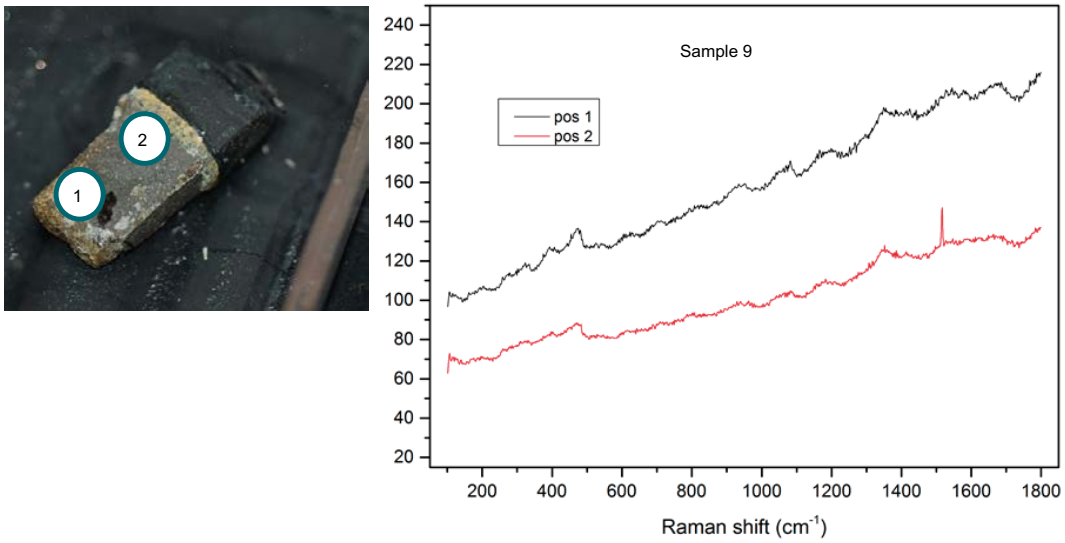

Figure A7-29. *Sample M4 9:1 iron electrode.*

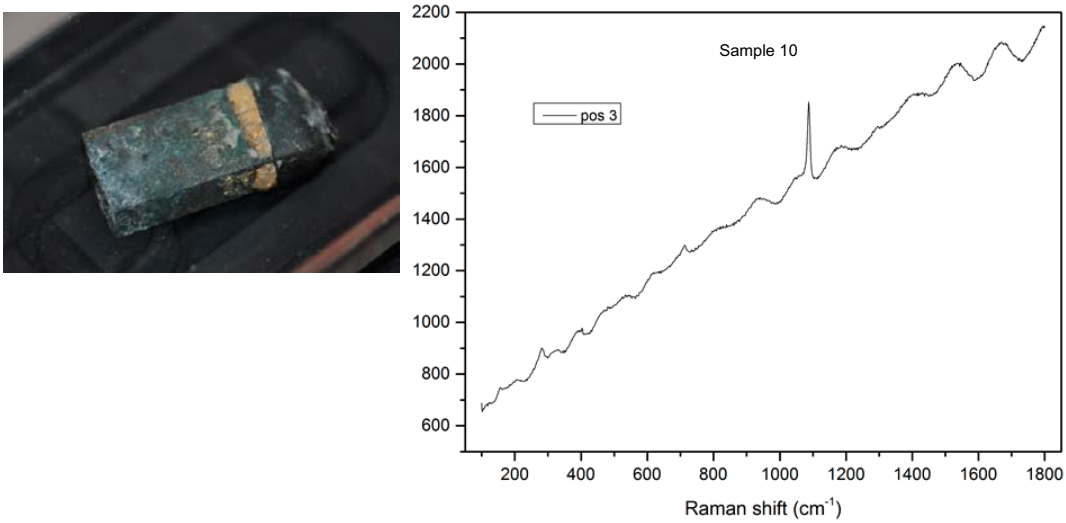

Figure A7-30. *Sample M4 10:1 iron electrode with calcite and fluorescence detected.*

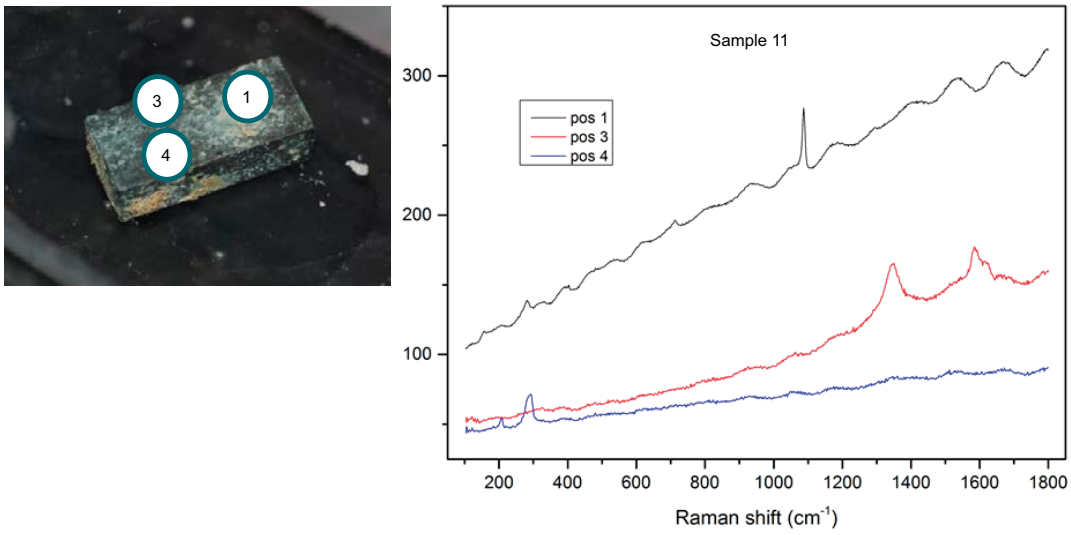

Figure A7-31. *Sample M4 11:1 iron mass loss.*

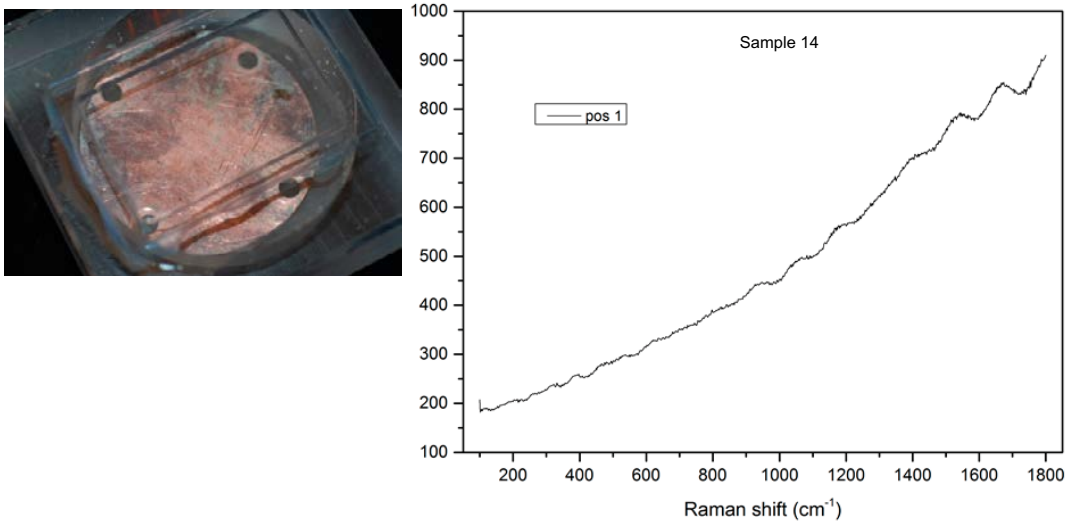

Figure A7-32. *Sample M4 14:1 copper sandwich sample with cuprite fluorescence detected.*

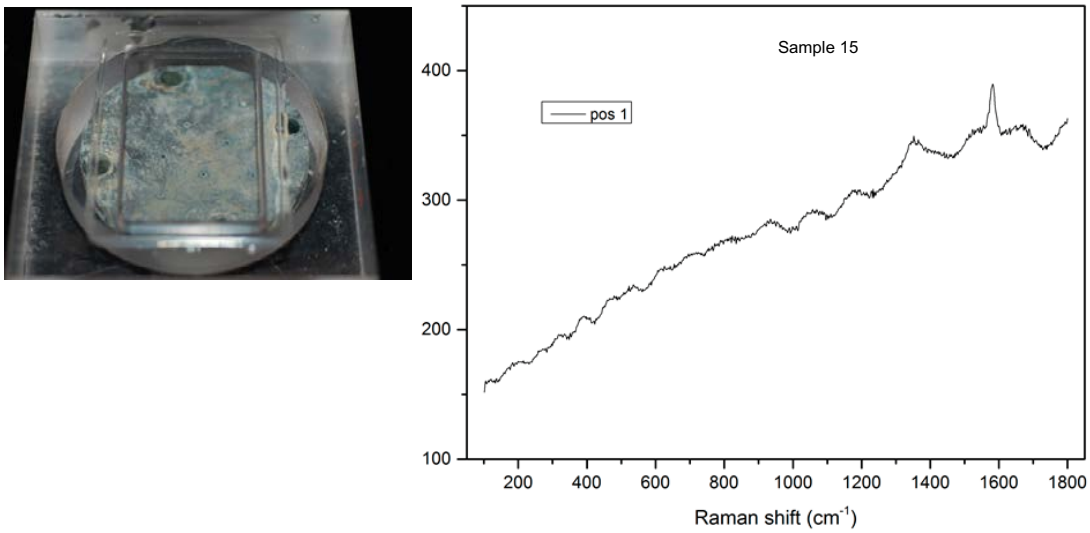

Figure A7-33. *Sample M4 15:1 iron sandwich specimen, with carbon and fluorescence detected.*

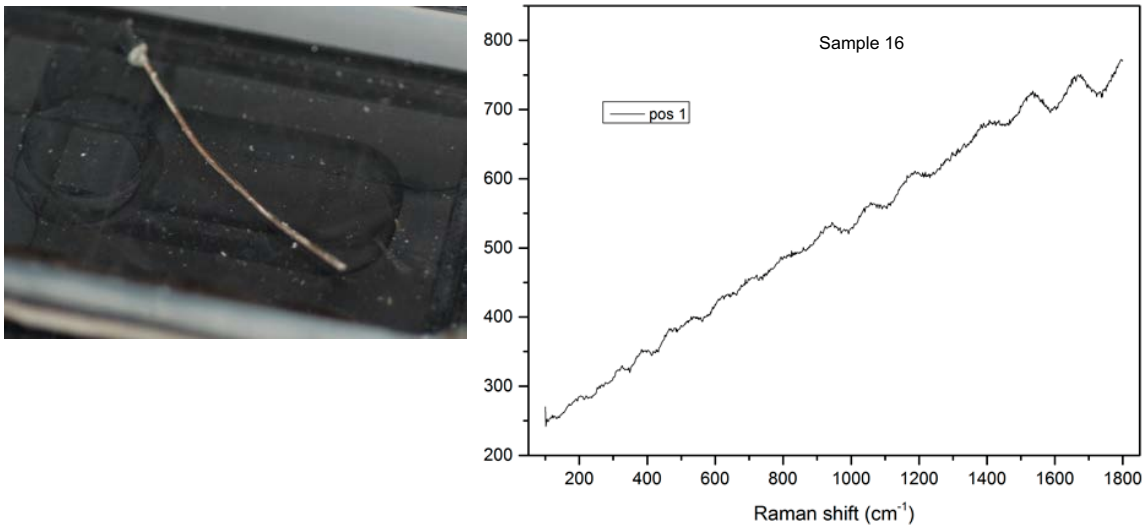

Figure A7-34. *Sample M4 16:1 platinum electrode, with fluorescence detected.*

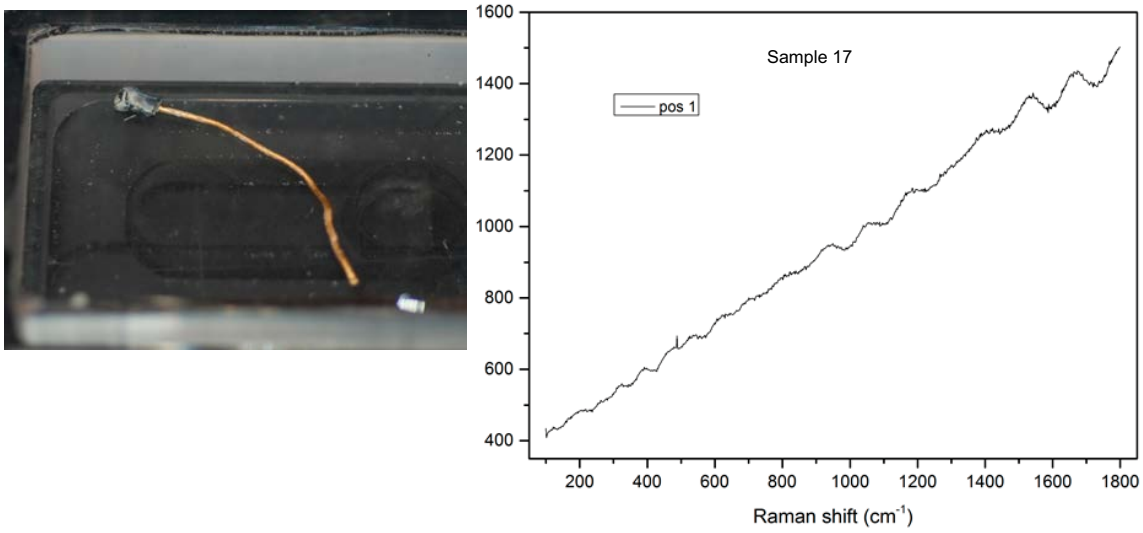

Figure A7-35. *Sample M4 17:1 gold electrode, with fluorescence detected.*

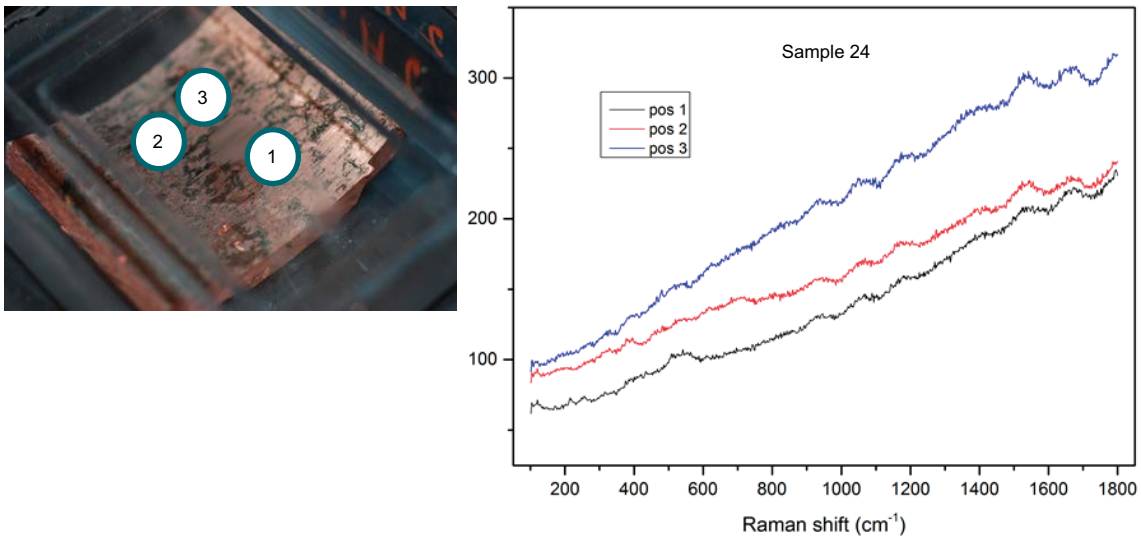

Figure A7-36. *Sample M4 24:1 inner surface of copper canister, with cuprite fluorescence detected at 3 points.*

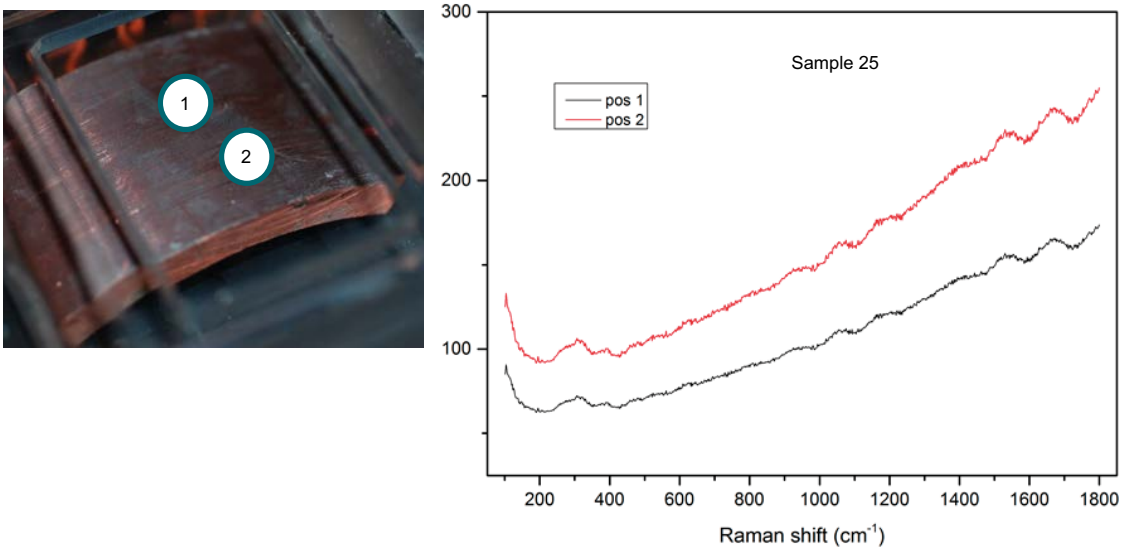

Figure A7-37. *Sample M4 25:1 outer surface of copper canister, with fluorescence and sulphide detected.*

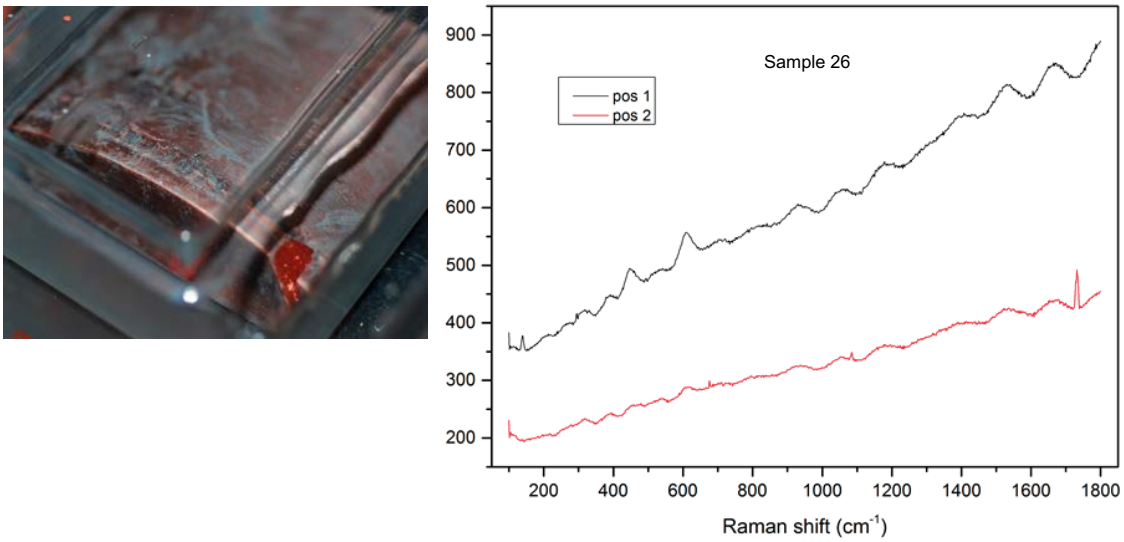

Figure A7-38. *Sample M4 26:1 weld from copper canister.*

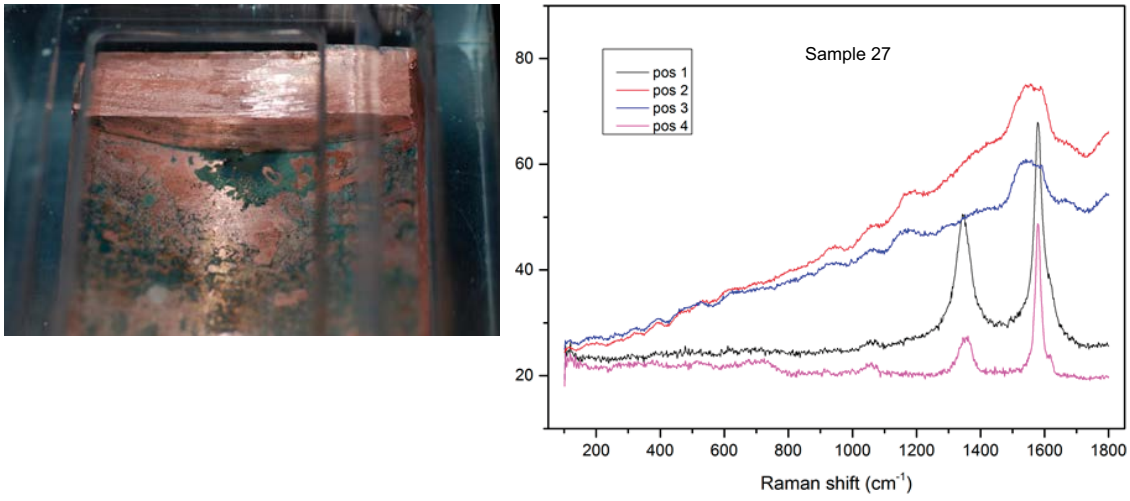

Figure A7-39. *Sample M4 27:1 inner surface of copper canister at position of machined hole. Carbon and fluorescence detected at several points on the surface.*

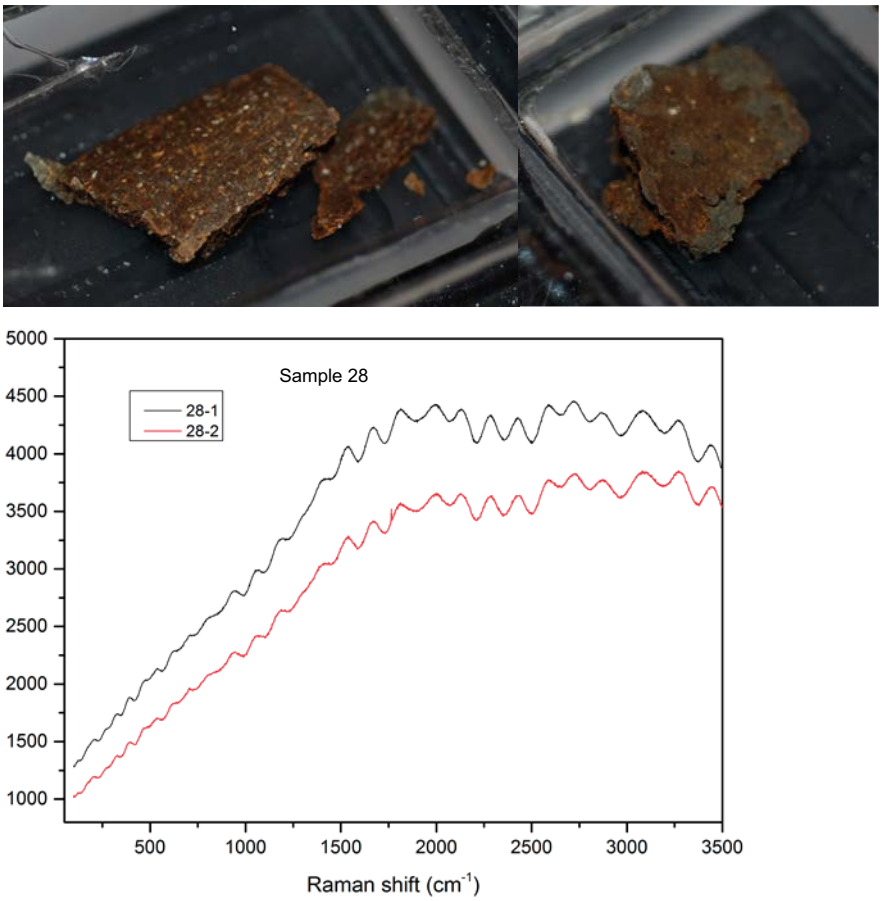

Figure A7-40. *Sample M4 28:1 and 28:2 bentonite samples taken from near hole through copper canister, with fluorescence detected.*

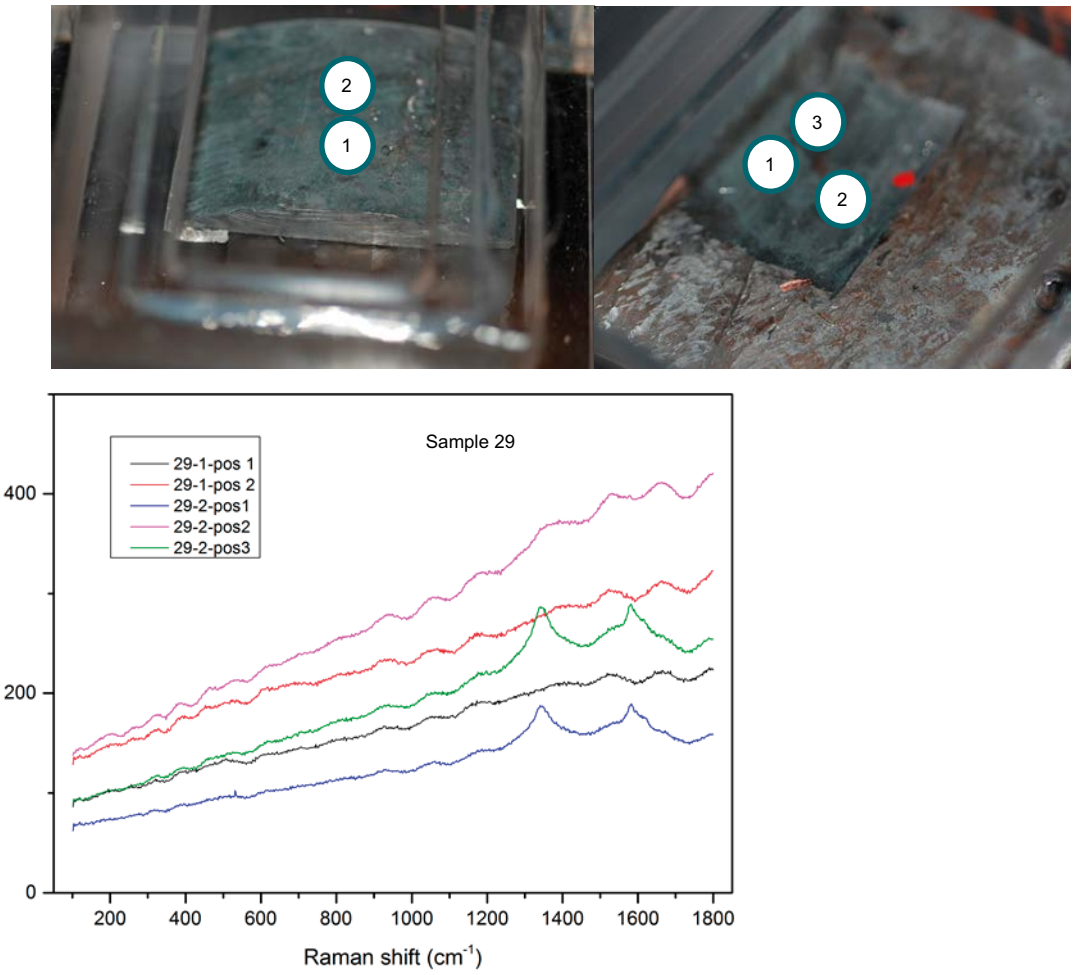

Figure A7-41. *Sample M4 29:1 and 29:2, outer surface of cast iron insert, with carbon and fluorescence detected.*

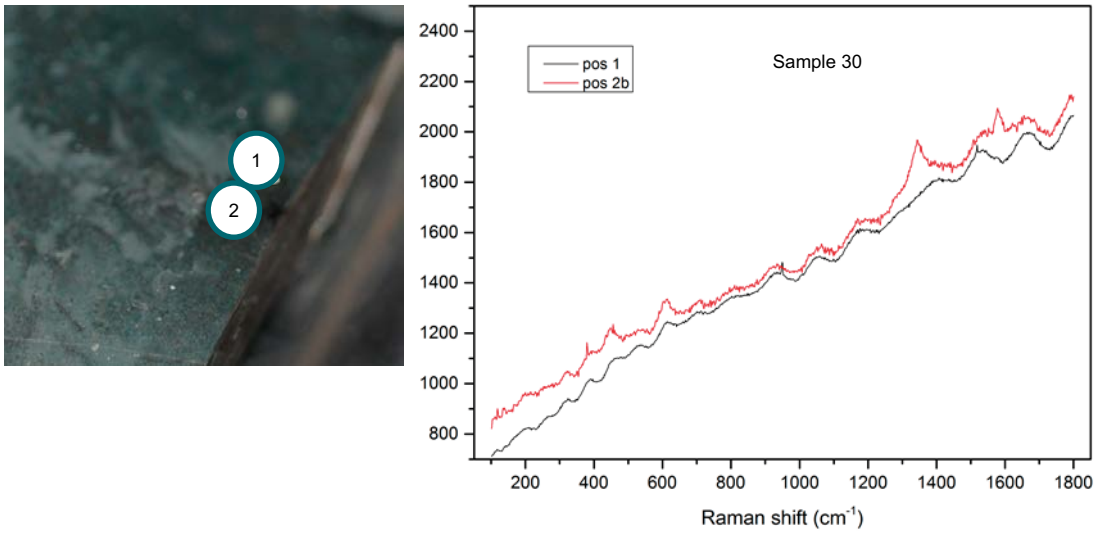

Figure A7-42. *Sample M4 30:1 cast iron insert at position of hole through copper canister, with carbon and possibly iron oxide, detected.*

Appendix 8

FTIR

FTIR analyses

Fourier Transform Infrared spectroscopy is used to characterise the molecular surface chemistry of a sample, with an analysis depth of about 1 µm into the surface. FTIR-microscopy was performed using a Perkin-Elmer Spotlight 200 FTIR microscopy system. Several areas (up to 6 points) were analysed on each sample using a 100 µm (micron) aperture. The spectra were recorded using 16 scans with a resolution of 8 cm^{-1}. A gold mirror was used to record background spectra. The instrument cannot detect below approximately 550–600 cm^{-1}, which is a region where both oxides and sulphides can usually be found. For this reason the results should be read alongside the Raman results given in Appendix 7.

MiniCan 4

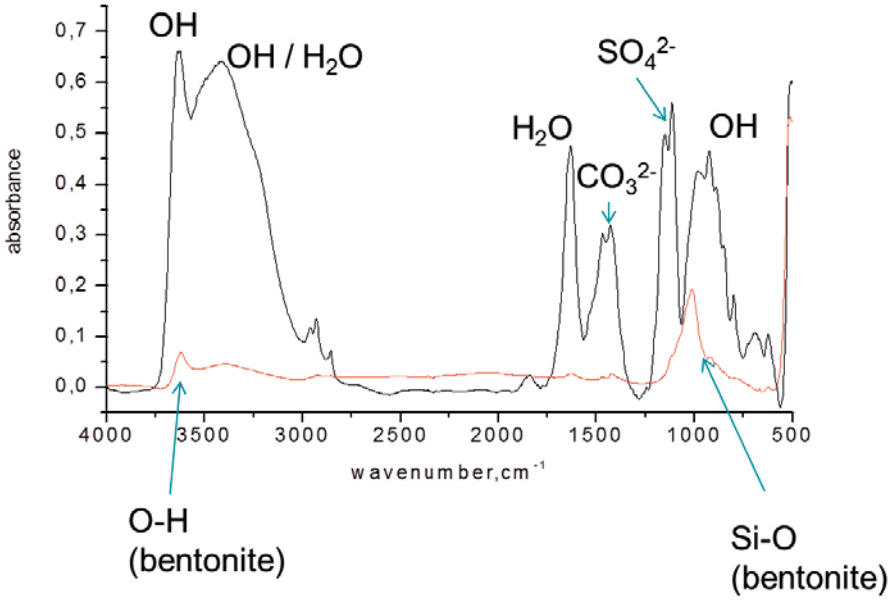

Figure A8-1. *Sample M4 5:1 spectrum representative for the copper electrode, several points on surface measured with copper hydroxy sulphate and carbonate detected.*

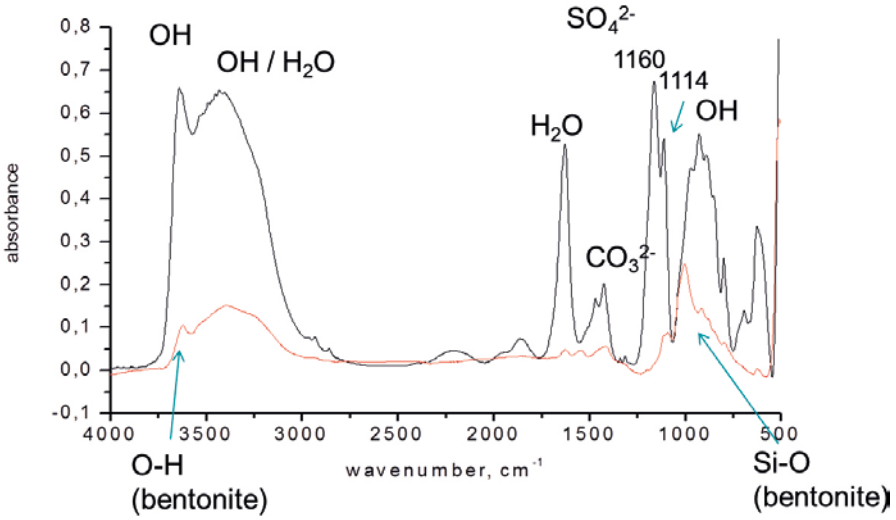

Figure A8-2. *Sample M4 6:1 spectrum representative for the copper electrode, several points on surface measured with copper hydroxy sulphate and carbonate detected.*

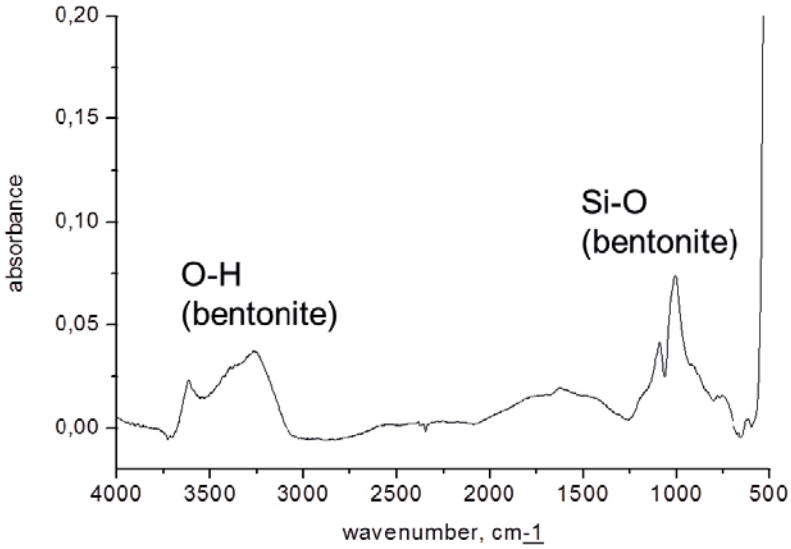

Figure A8-3. *Sample M4 7:1 copper mass loss, mainly bentonite detected.*

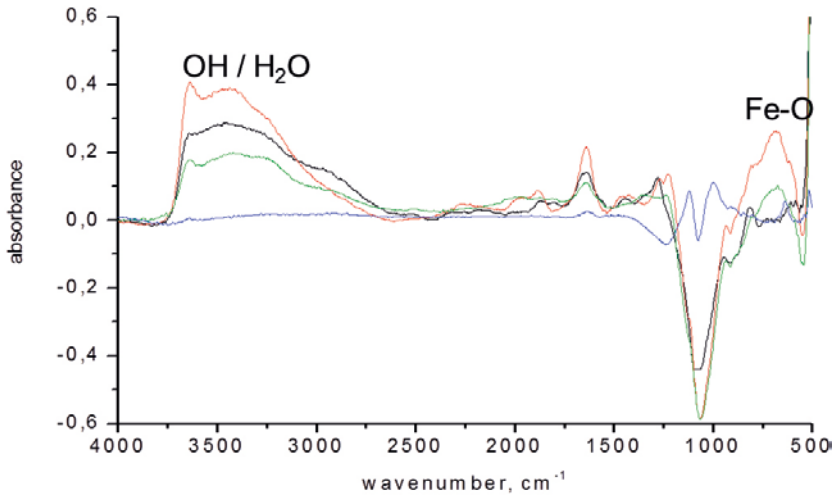

Figure A8-4. *Sample M4 9:1 spectrum representative for the iron electrode, several points on surface measured, with inverted bands due to the thick nature of the surface deposits. Bentonite and Fe corrosion products detected.*

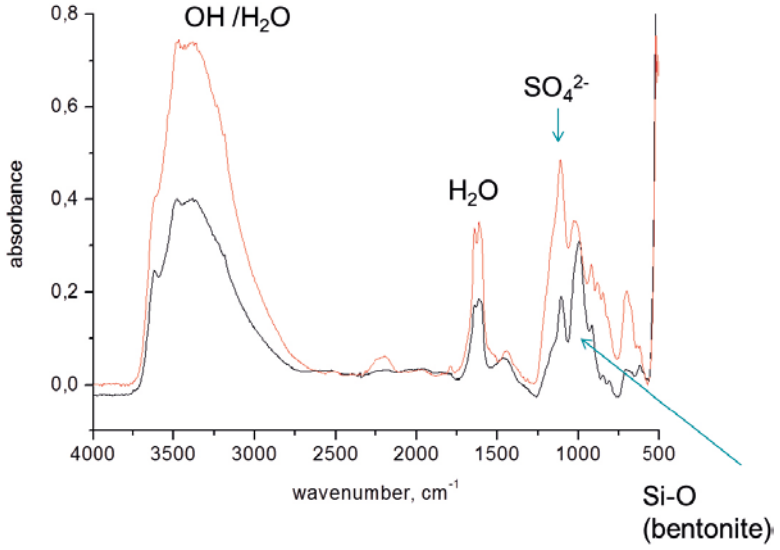

Figure A8-5. *Sample M4 10:1 iron electrode, with bentonite, sulphate and water detected ($FeSO_4 \cdot H_2O$).*

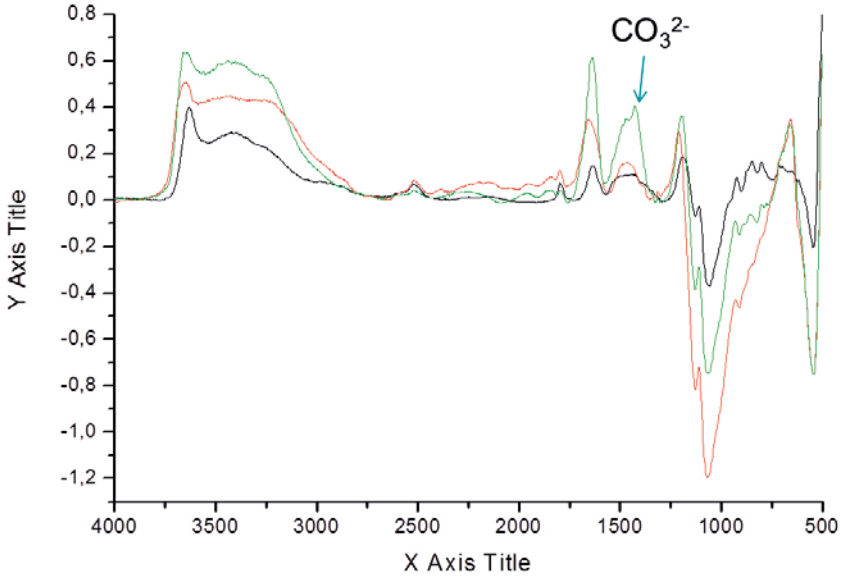

Figure A8-6. *Sample M4 11:1 iron mass loss, with mainly bentonite detected.*

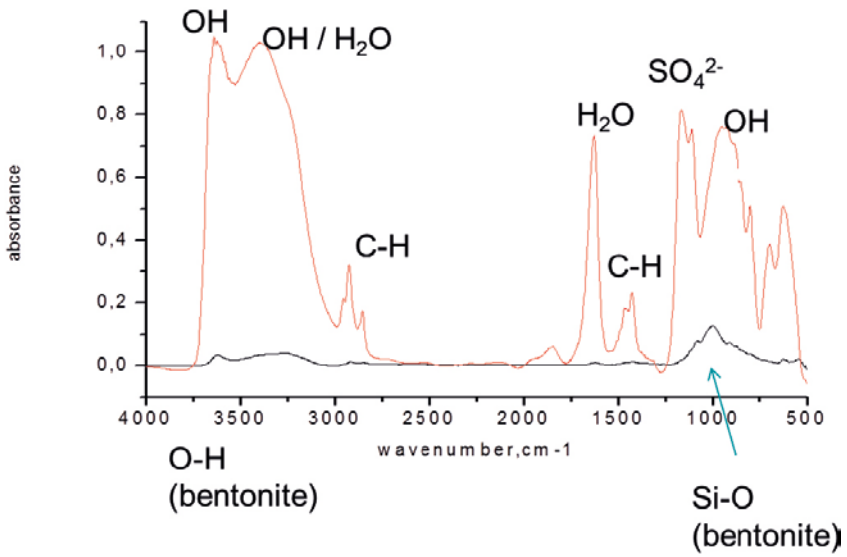

Figure A8-7. *Sample M4 14:1 copper sandwich specimen, with copper hydroxy sulphate and bentonite detected.*

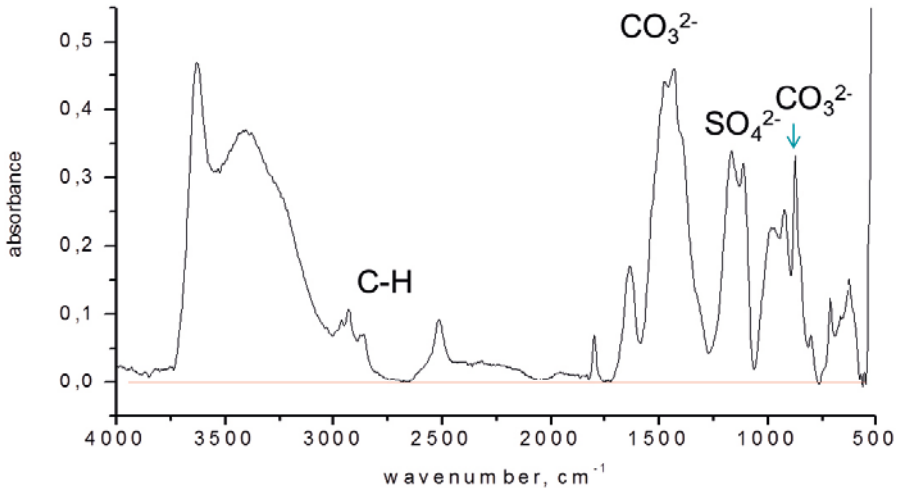

Figure A8-8. *Sample M4 15:1 iron sandwich specimen, with carbonate and sulphate peaks, as well as water and OH bands detected.*

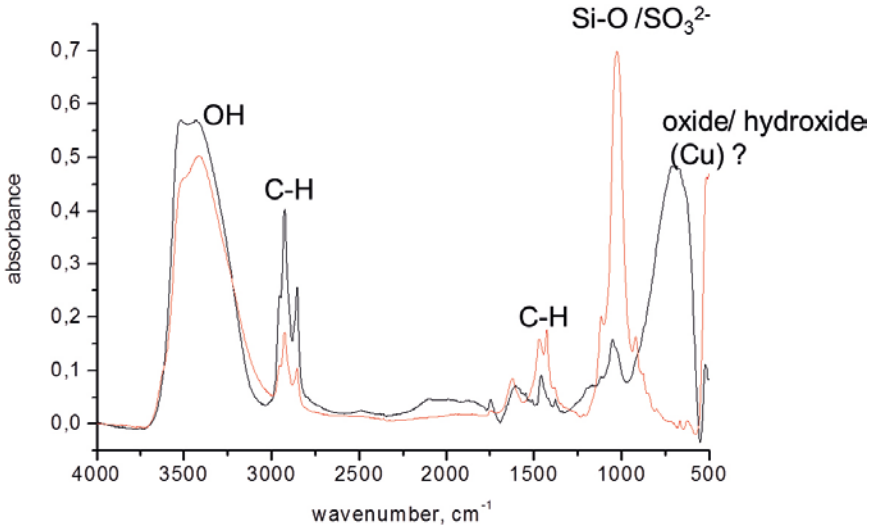

Figure A8-9. *Sample M4 24:1 inner surface of copper canister, with Si-O/SO_3^{2-} peaks, OH bands and peaks, and organic C-H peaks.*

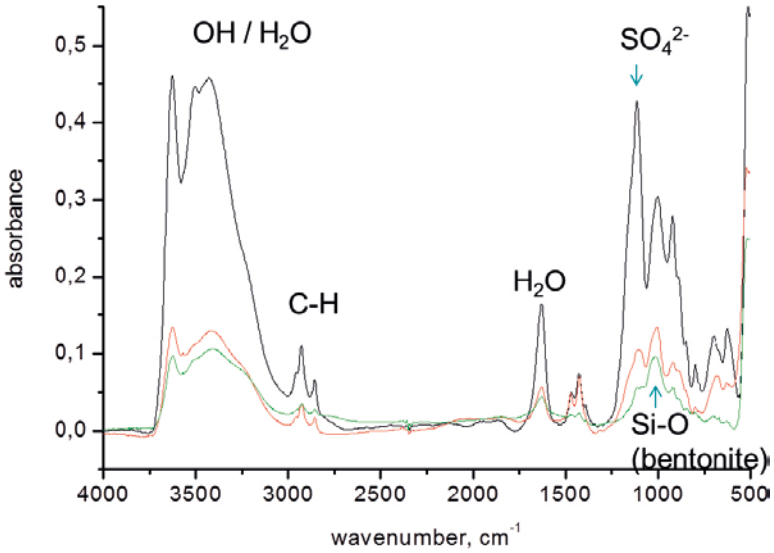

Figure A8-10. *Sample M4 25:1 outer surface of copper canister, copper hydroxy sulphate and bentonite detected.*

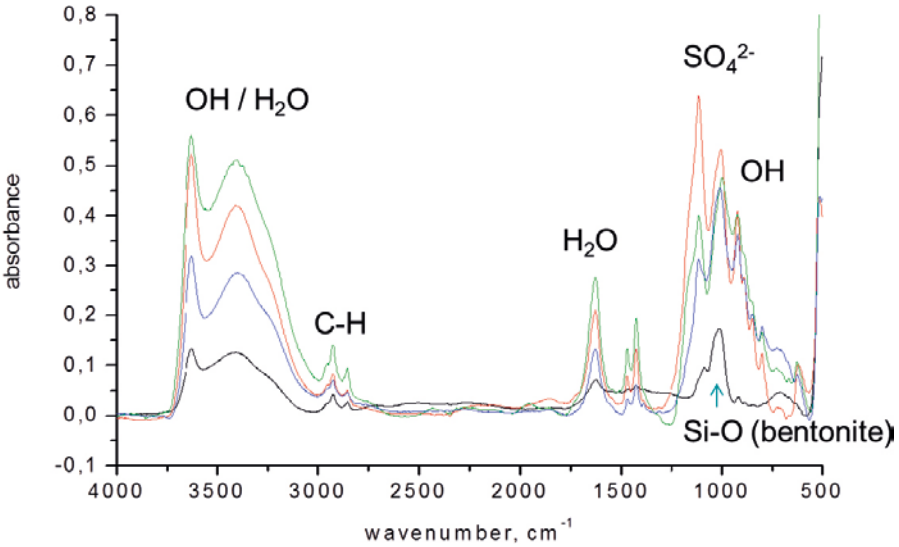

Figure A8-11. *Sample M4 26:1 weld of copper canister, copper hydroxy sulphate and bentonite detected.*

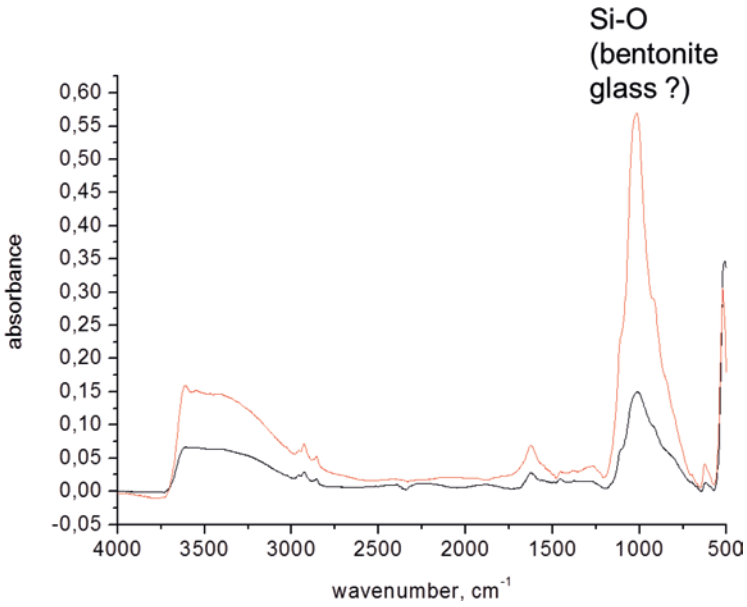

Figure A8-12. *Sample M4 27:1 inner surface of copper canister near through hole, with SiO peak, possibly from bentonite or possibly from glass particle emanating from the sample holder when it was opened.*

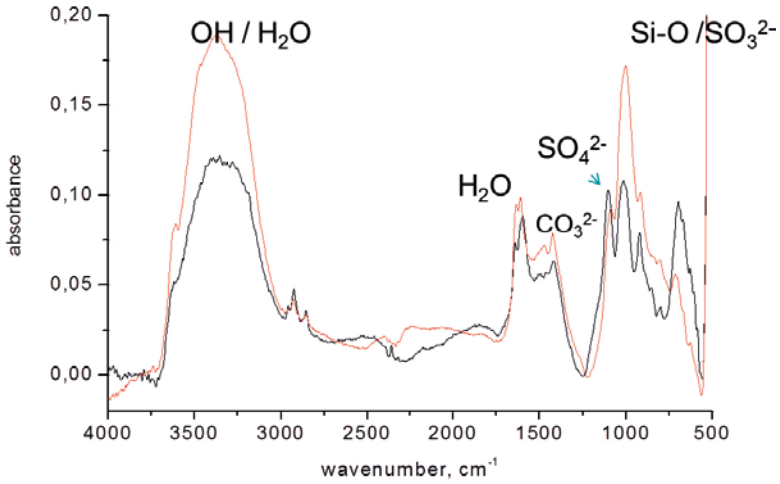

Figure A8-13. *Sample M4 29:1 cast iron insert with bands due to sulphate and water ($FeSO_4.xH_2O$) detected, with contributions from carbonate and bentonite.*

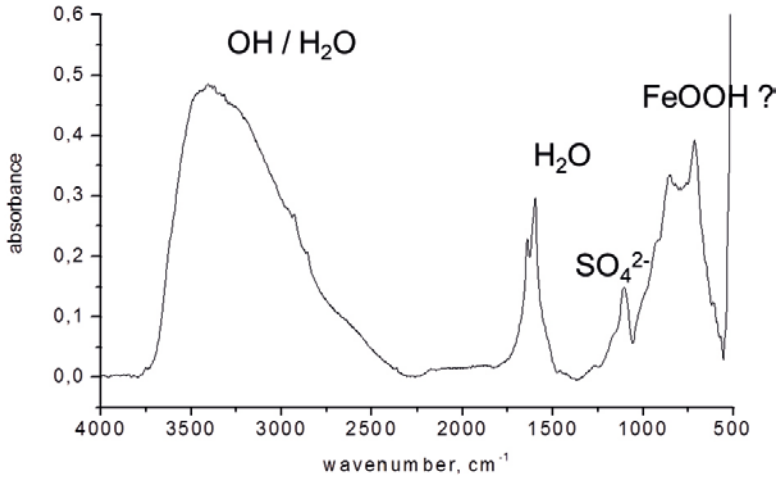

Figure A8-14. *Sample M4 30:1 cast iron insert at position near hole through copper canister, with bands due to sulphate and water ($FeSO_4.xH_2O$) detected, and possibly FeOOH.*

MiniCan 5

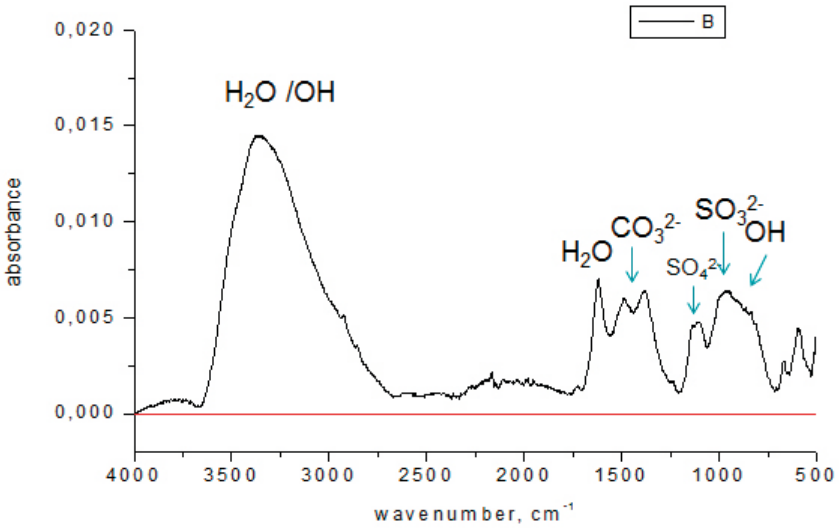

Figure A8-15. *Sample M5 5:1 copper electrode, with bands due to water, carbonate, sulphite, sulphate and hydroxy groups identified. Copper hydroxy sulphate and copper hydroxy carbonate could be present.*

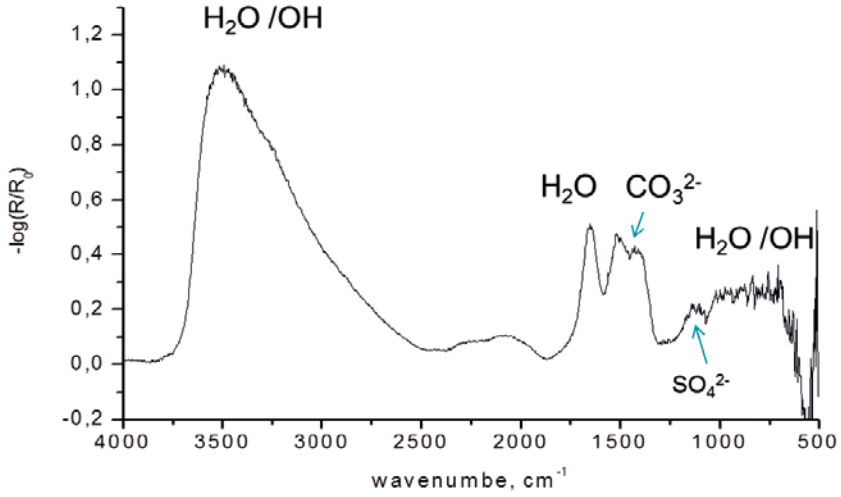

Figure A8-16. *Sample M5 6:1 copper electrode, with bands due to water, carbonate, and hydroxy groups identified. Weak bands possibly due to sulphate. Carbonate could be due to copper carbonate (malachite).*

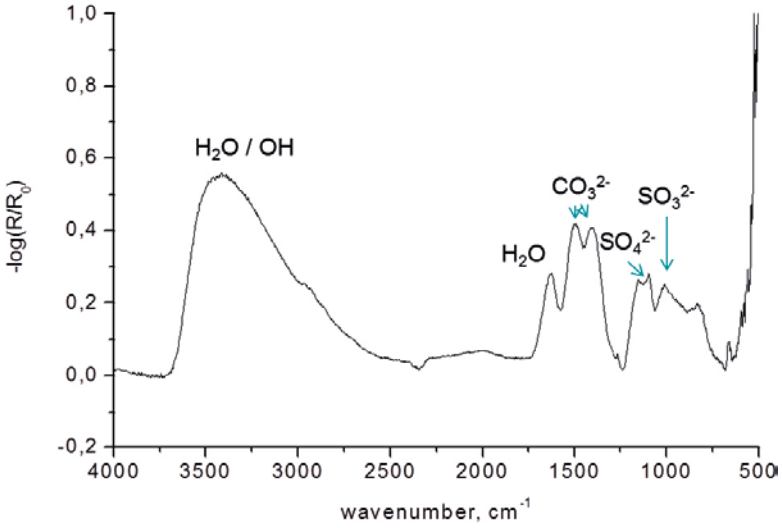

Figure A8-17. *Sample M5 7:1 copper mass loss, sulphite and carbonate varied over the surface.*

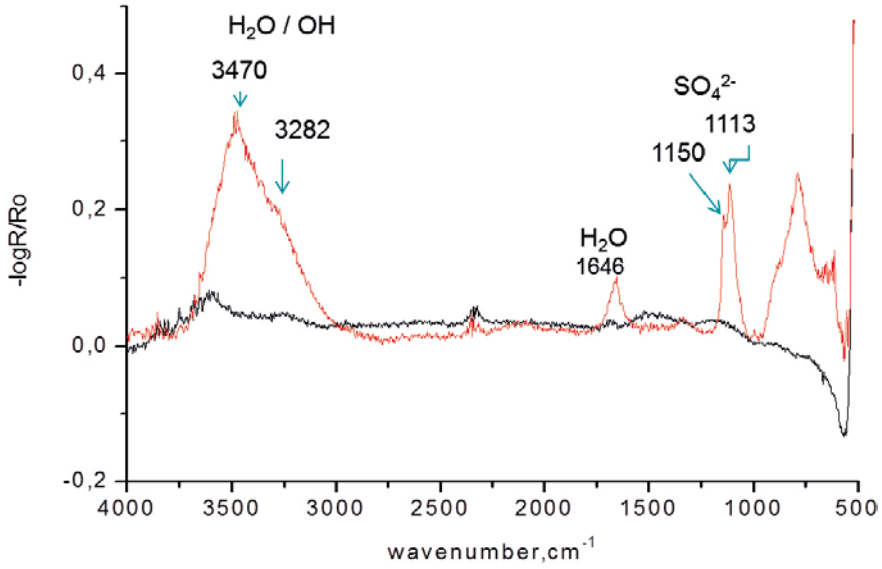

Figure A8-18. *Sample M5 9:1 iron electrode, with sulphate and water bands detected, possibly Fe(III) $SO_4 \cdot xH_2O$.*

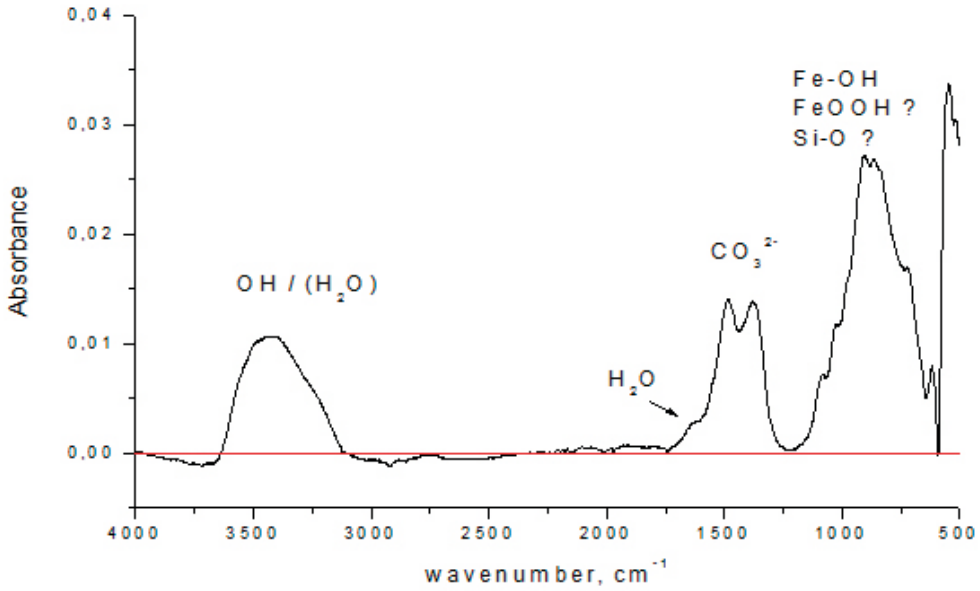

Figure A8-19. *Sample M5 10:1 iron electrode, with carbonate and hydroxy detected. Iron hydroxy carbonate could be a possibility or SiO from glass fragments from the sample holder. FTIR-analyses not using the microscope.*

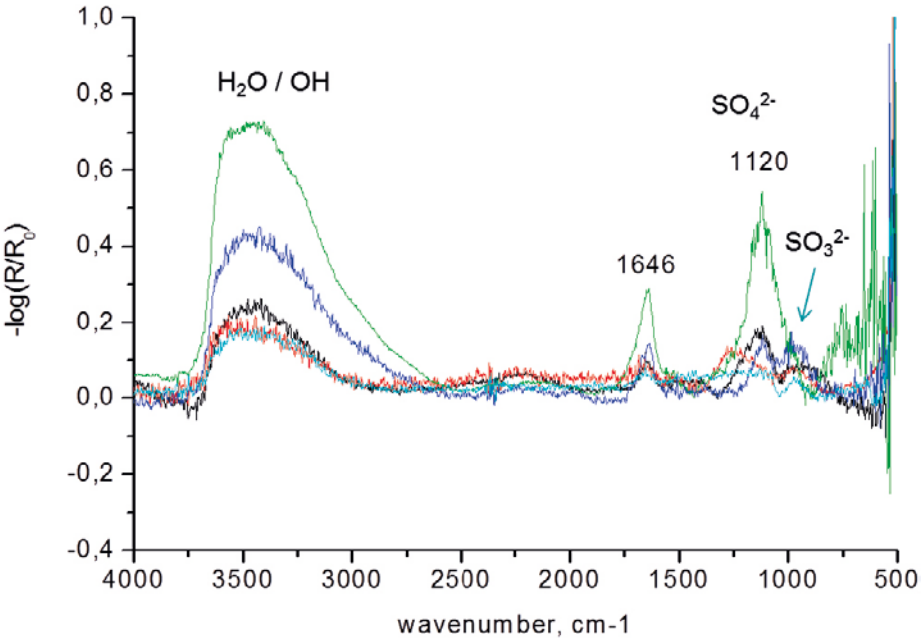

Figure A8-20. *Sample M5 11:1 iron mass loss, with sulphate, sulphite and water detected.*

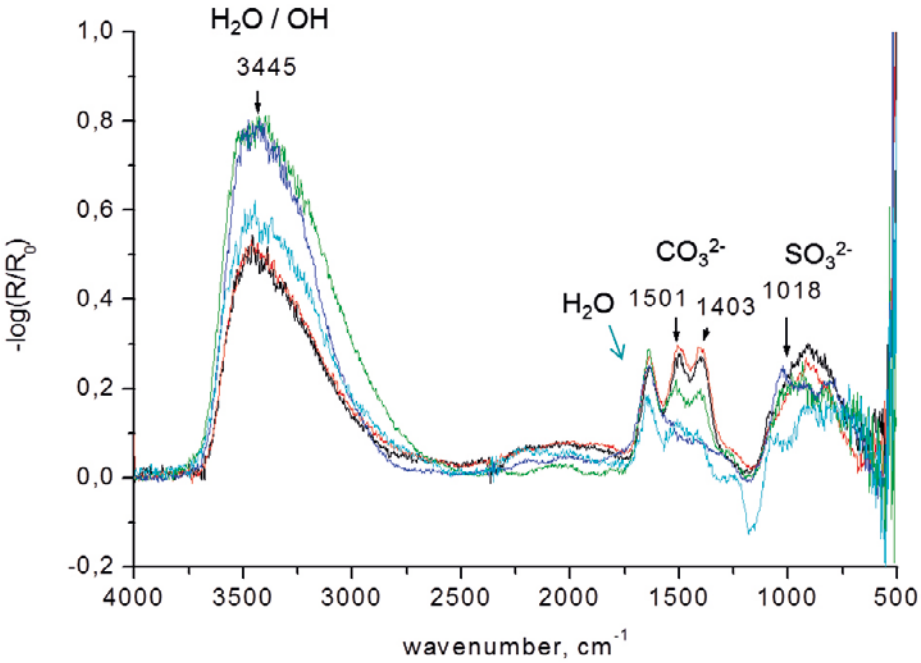

Figure A8-21. *Sample M5 14:1 copper sandwich specimen, with carbonate, water and hydroxy dominating, and some sulphite detected.*

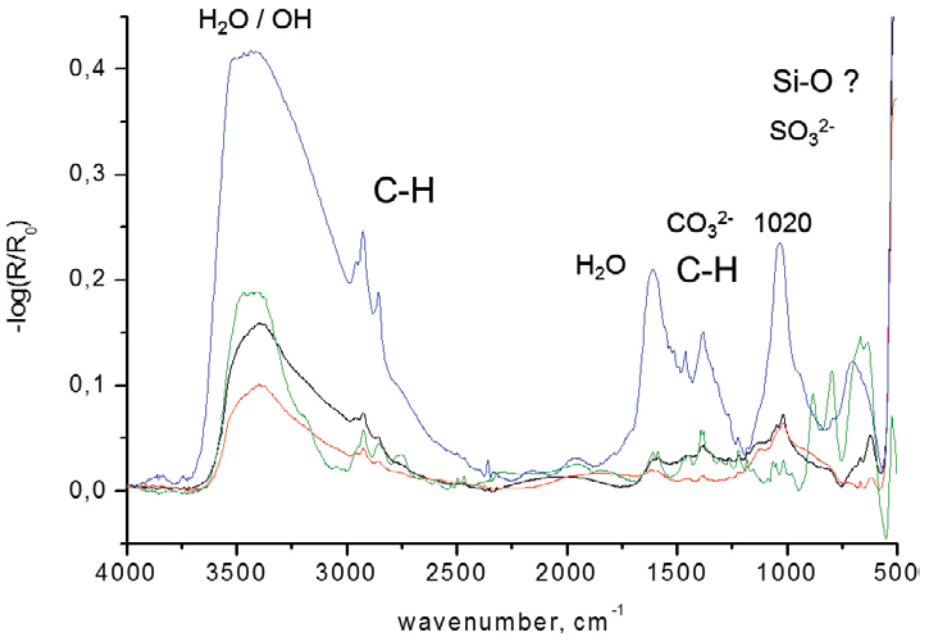

Figure A8-22. *Sample M5 24:1 inner surface of copper canister, water and sulphite detected at some points, as well as carbonate and organics C-H.*

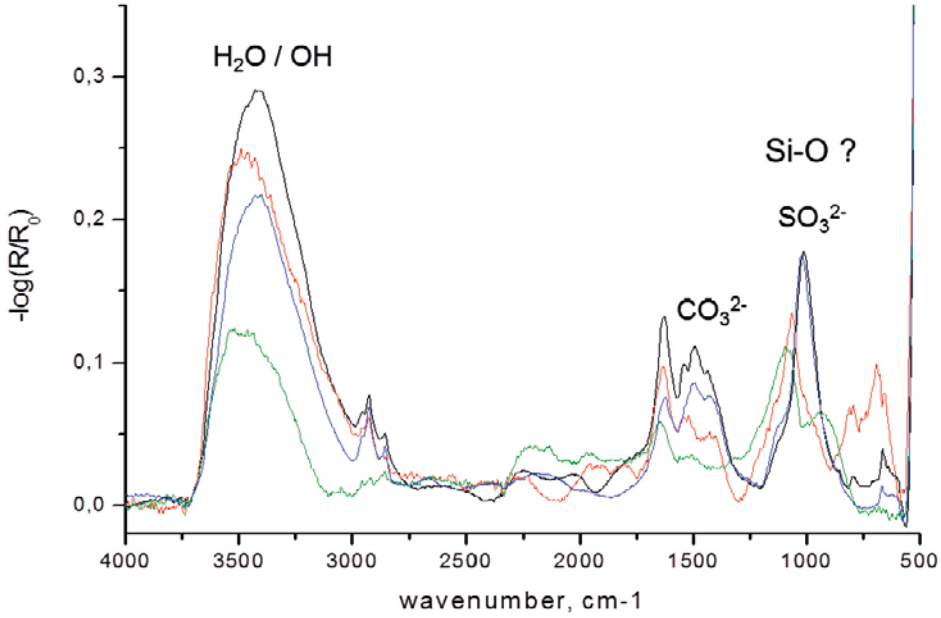

Figure A8-23. *Sample M5 25:1 outer surface of copper canister, water and sulphite along with bands of carbonate detected. Some organics C-H also detected.*

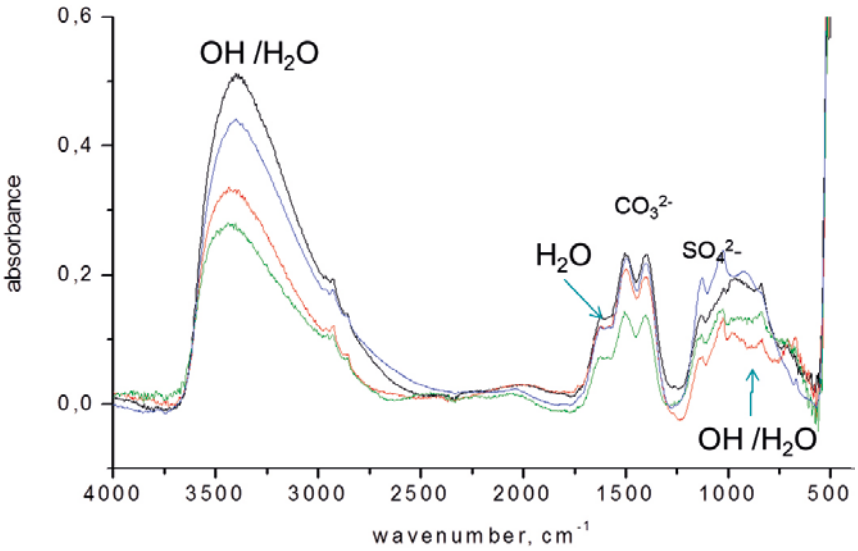

Figure A8-24. *Sample M5 26:1 weld on copper canister, with water, OH and carbonate dominating. Copper carbonate with OH and H_2O. Sulphate also detected.*

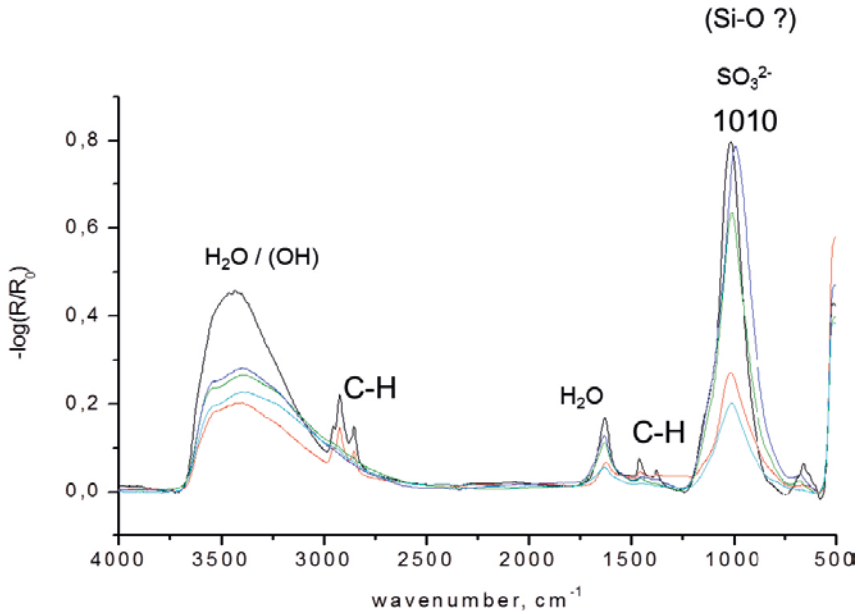

Figure A8-25. *Sample M5 27:1 inner surface of copper canister near through hole, with sulphite and water bands detected, as well as some organics C-H and contributions from SiO, which occurs at a similar position as sulphite.*

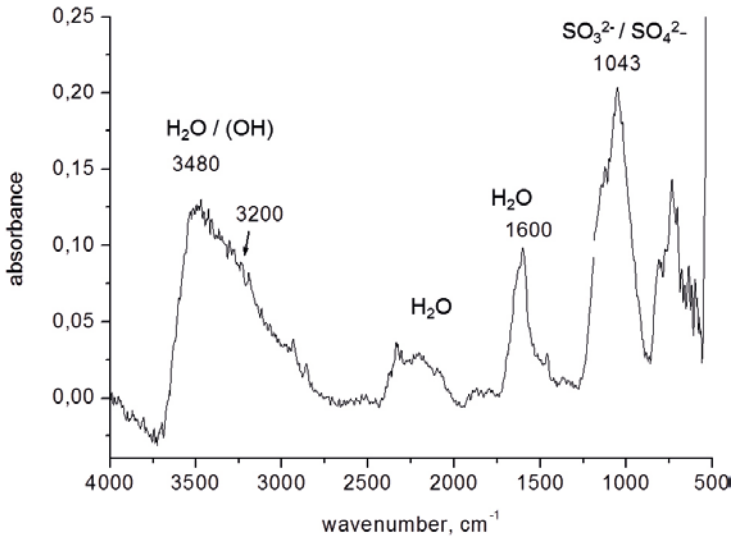

Figure A8-26. *Sample M5 29:1 cast iron insert, with water, sulphite and sulphate detected. Iron sulphite with water.*

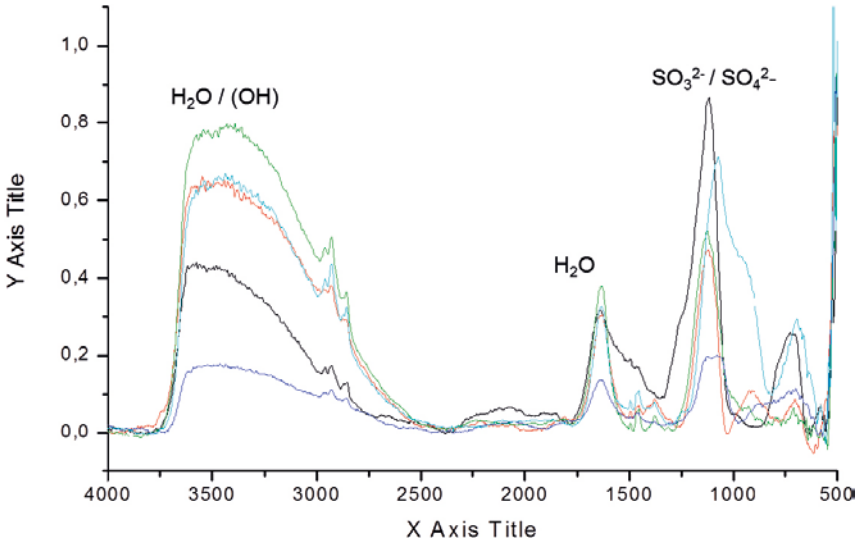

Figure A8-27. *Sample M5 30:1 surface of cast iron insert at position near to hole through copper canister. Water, sulphite and sulphate detected. Iron sulphite with water.*

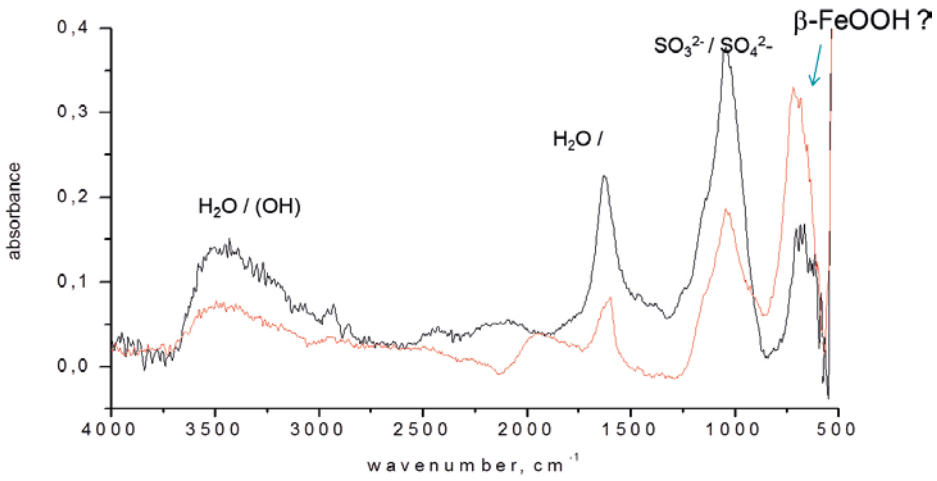

Figure A8-28. *Sample M5 31:1 surface of cast iron insert at position near to hole through copper canister. Water, sulphite and sulphate detected. Iron sulphite with water. Possible β-FeOOH.*

Reference spectra

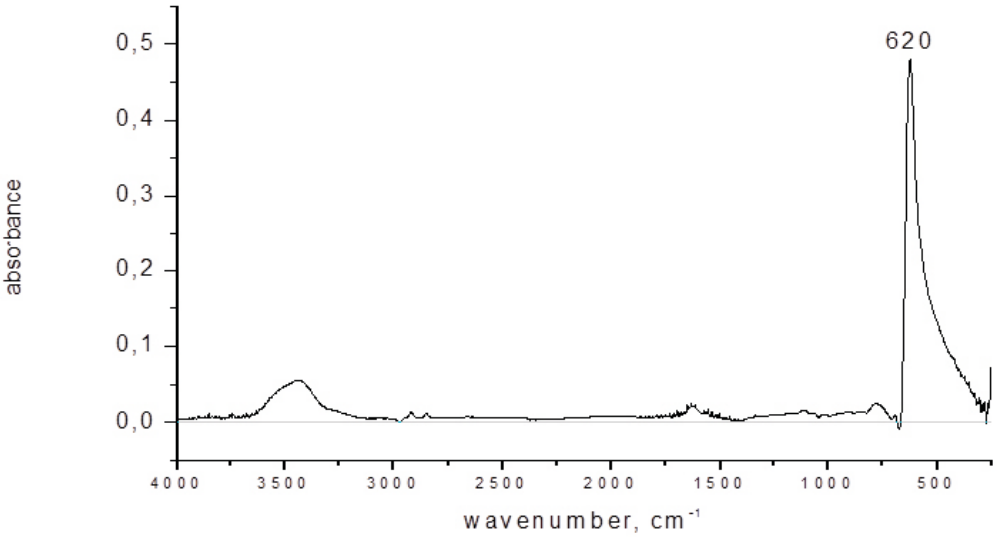

Figure A8-29. *Cuprite (Cu_2O) transmission spectrum (KBr).*

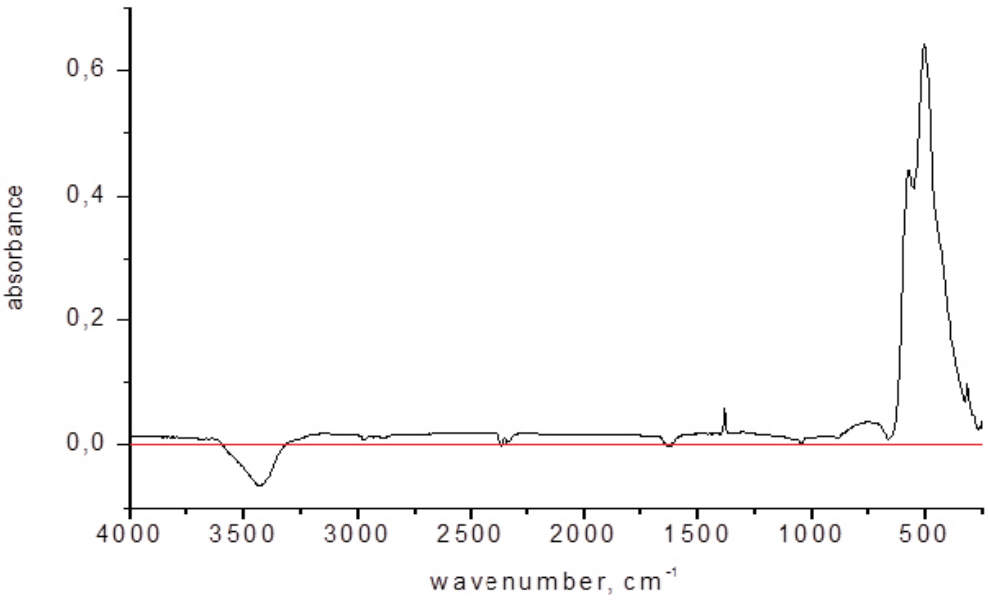

Figure A8-30. *Tenorite (CuO) transmission spectrum (KBr).*

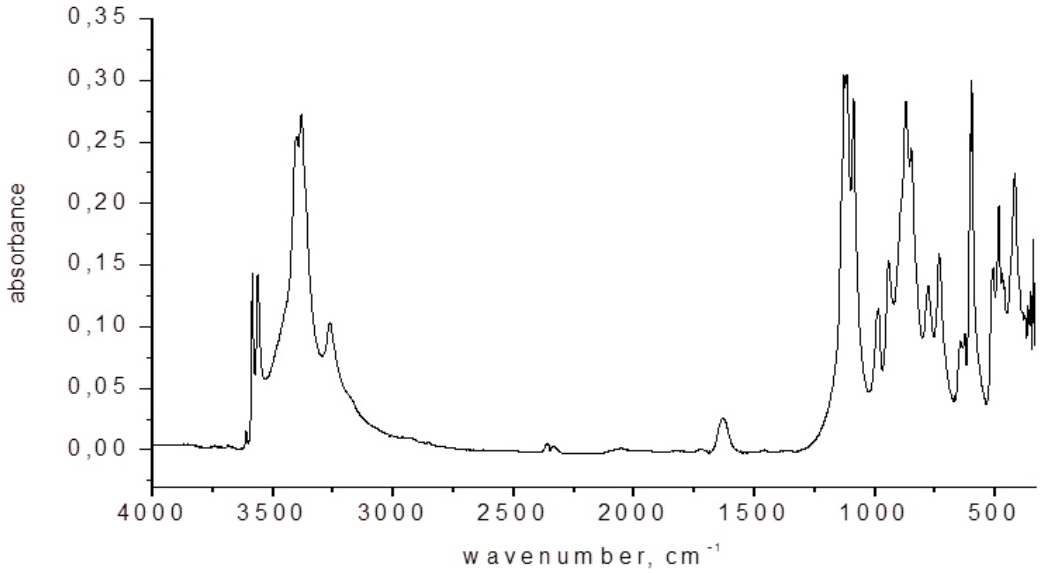

Figure A8-31. *Brochantite, $Cu_4(OH)_6SO_4$.*

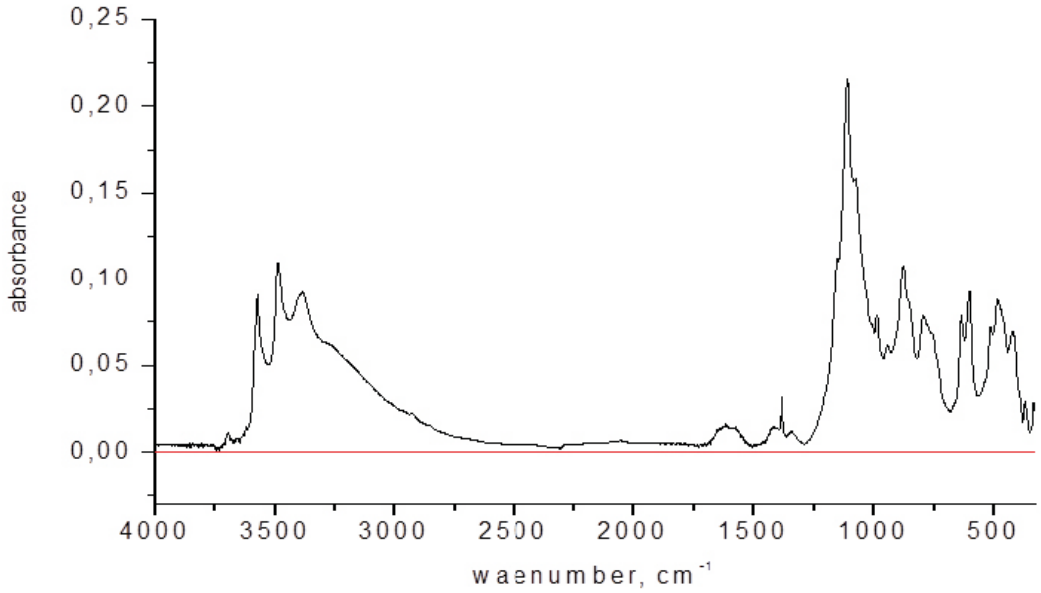

Figure A8-32. *Anthlerite, $Cu_3(OH)_4SO_4$.*

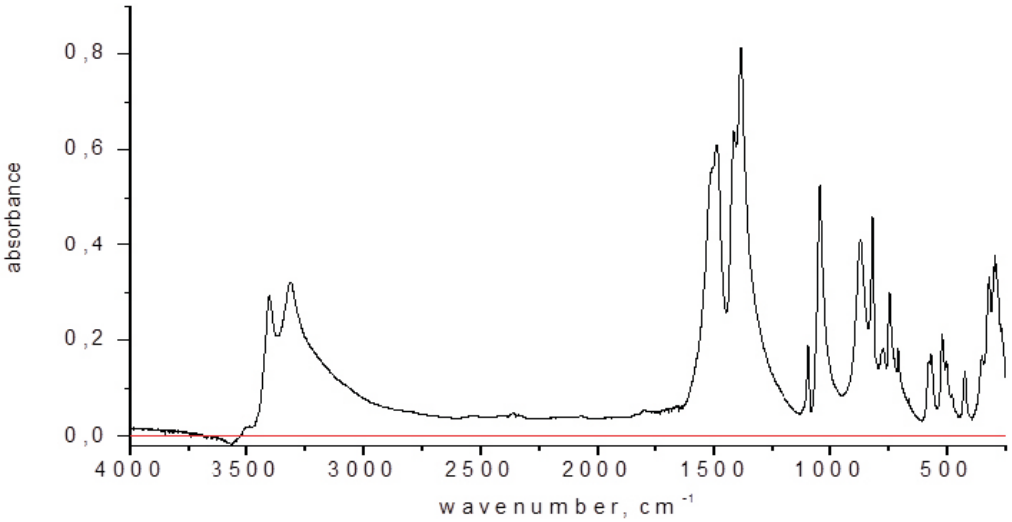

Figure A8-33. *Malachite, $Cu_2(OH)_2CO_3$.*

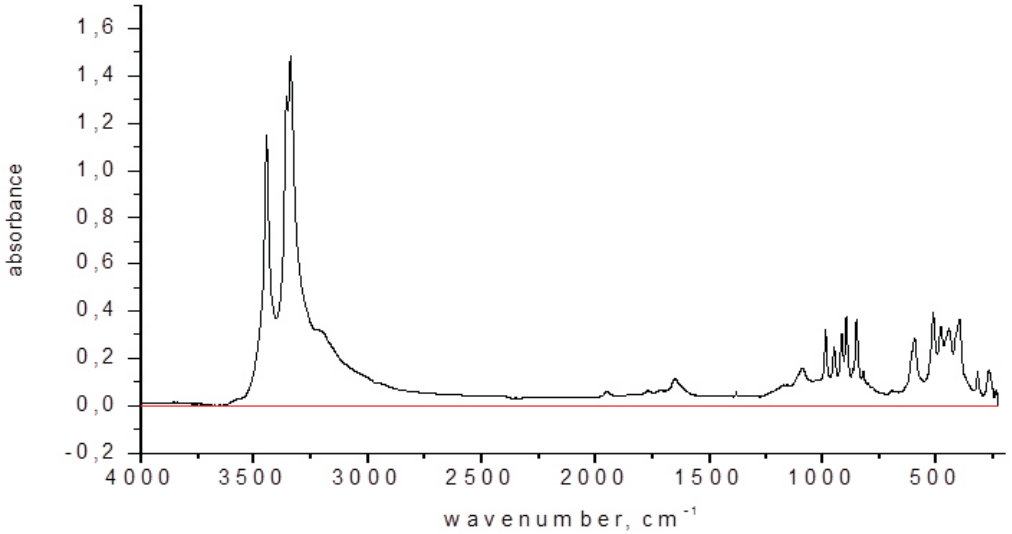

Figure A8-34. *Atacamite, $Cu_2(OH)_3Cl$.*

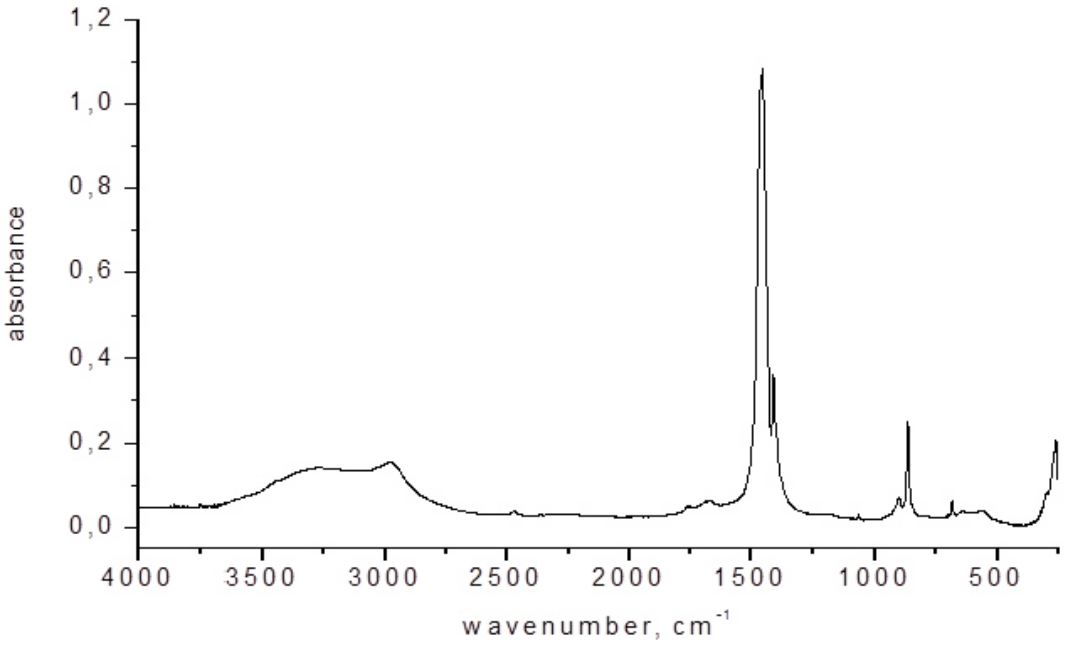

Figure A8-35. *$Na_2CO_3 \cdot xH_2O$.*

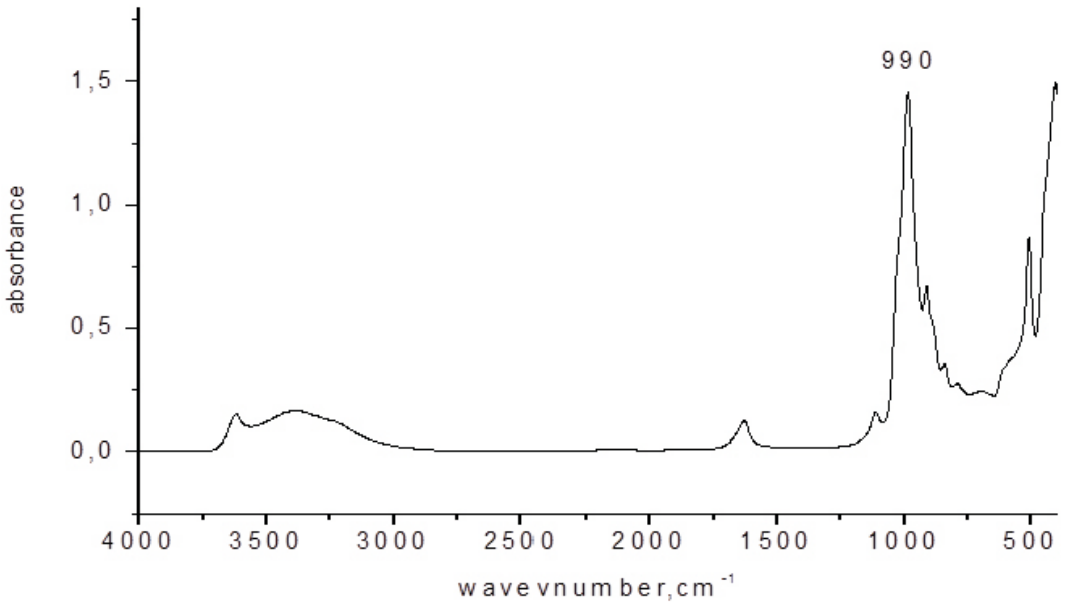

Figure A8-36. *Bentonite (ATR spectrum).*

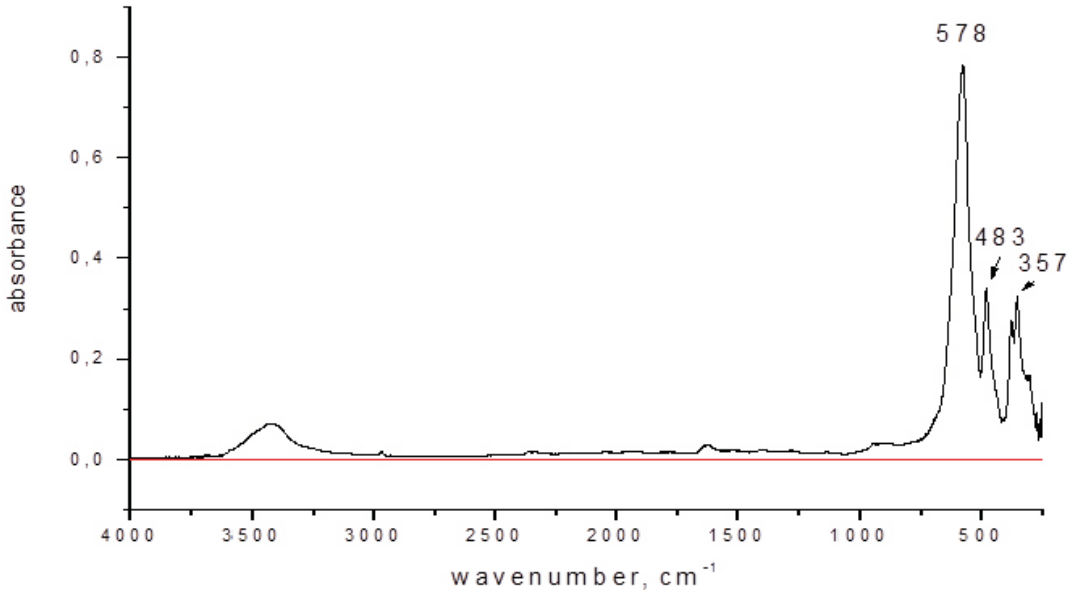

Figure A8-37. *Hematite, α-Fe_2O_3.*

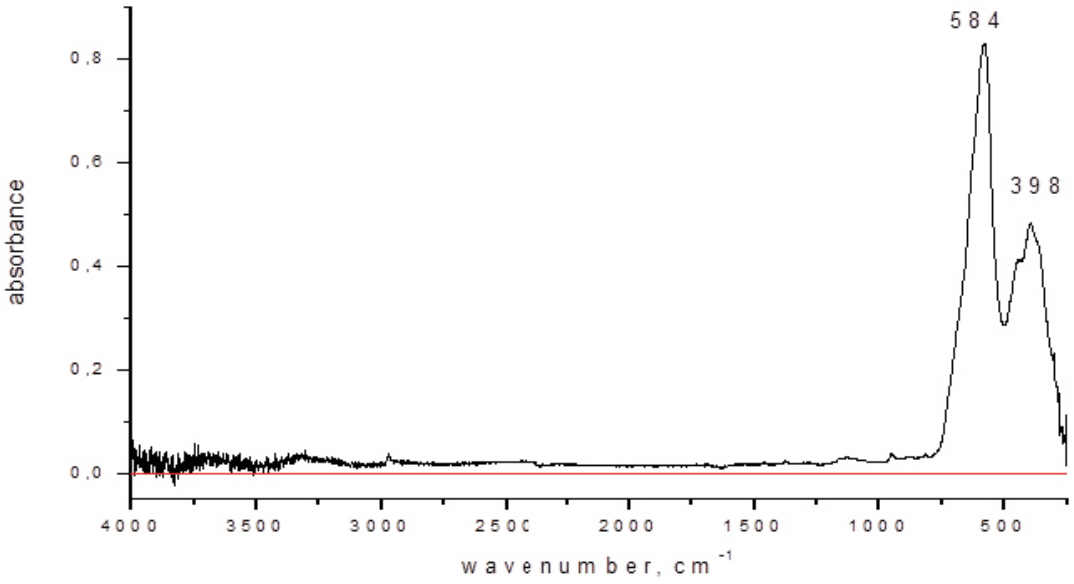

Figure A8-38. *Magnetite, Fe_3O_4.*

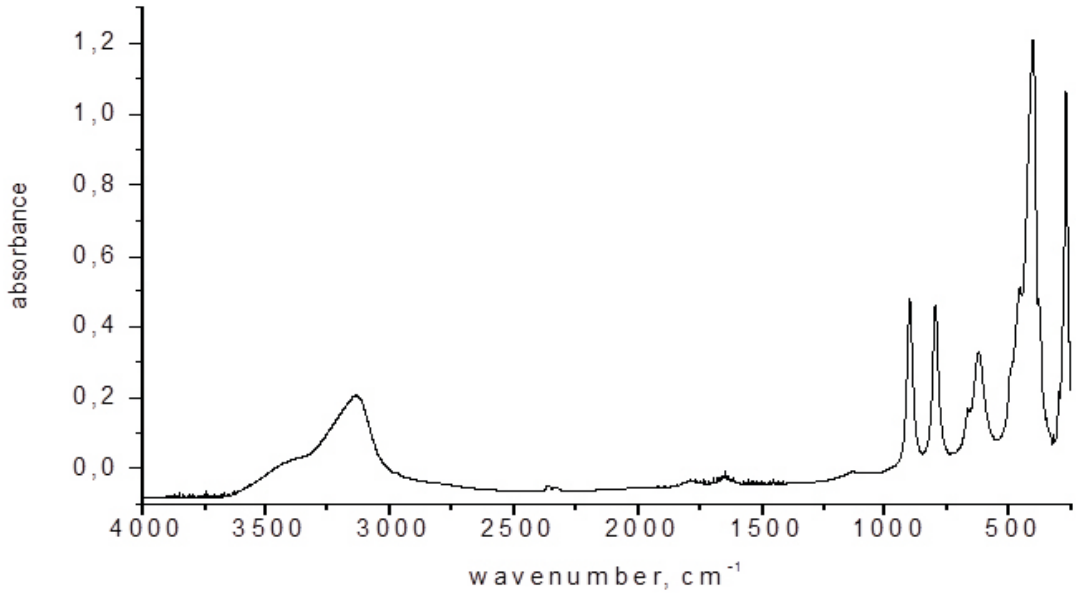

Figure A8-39. *Goethite, α-FeOOH.*

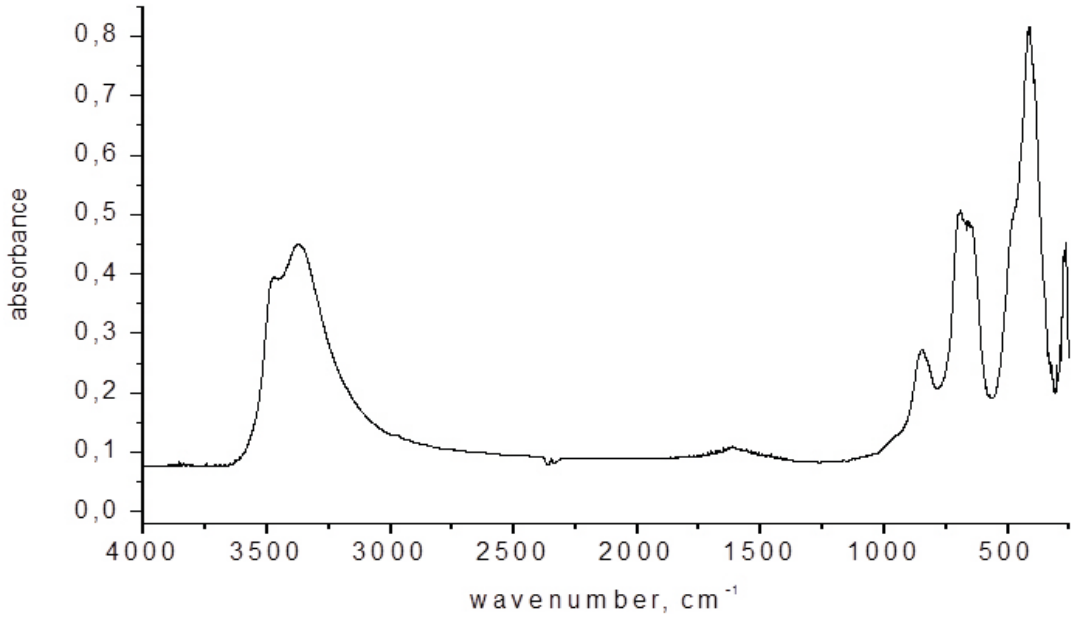

Figure A8-40. *Akaganeite, β-FeOOH.*

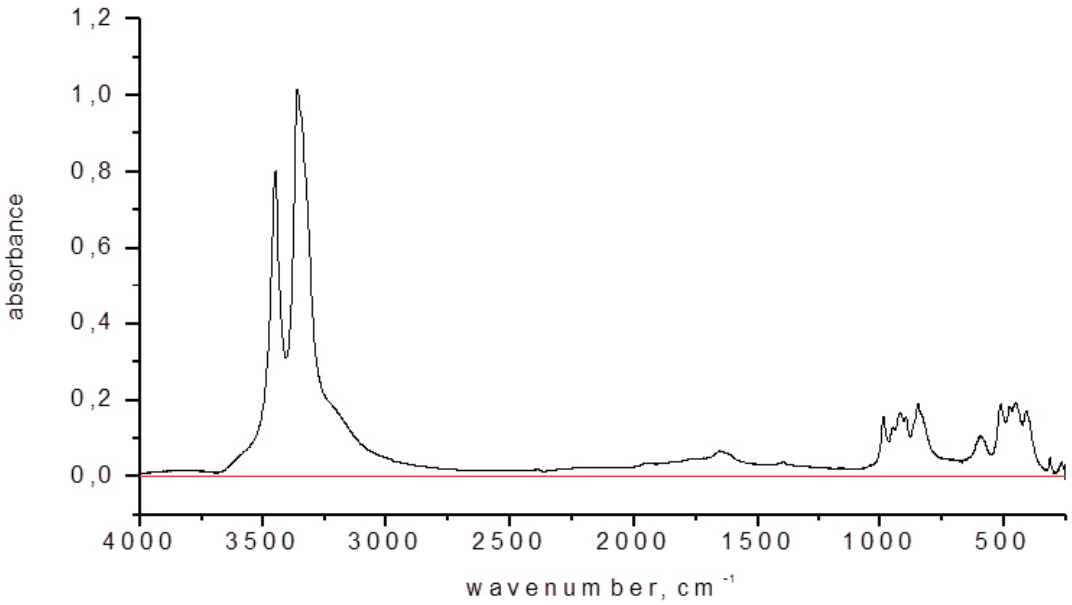

Figure A8-41. *Paratacamite, $Cu_2(OH)_3Cl$.*

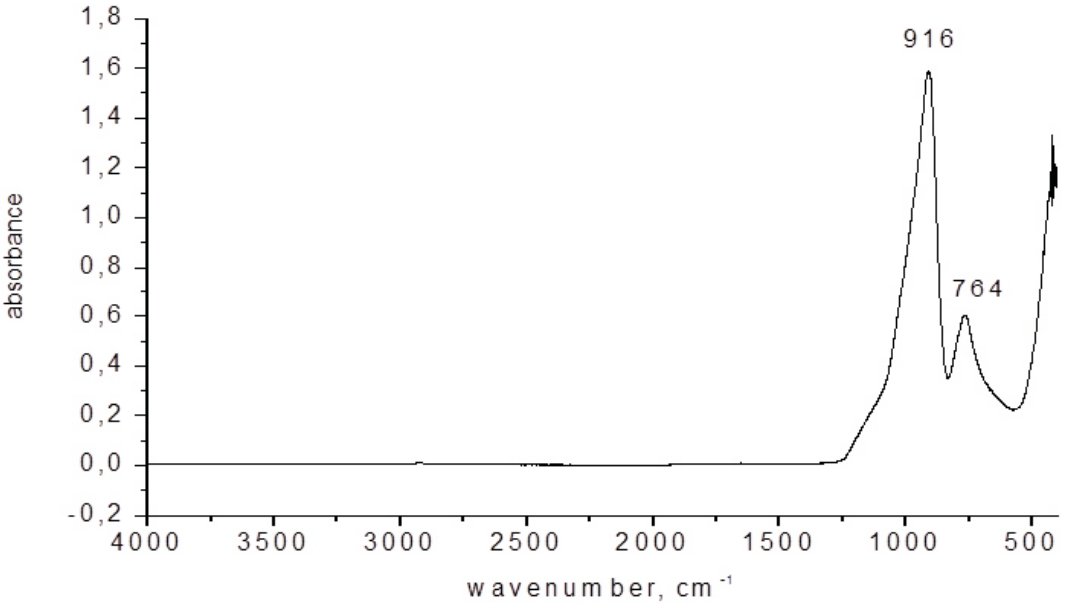

Figure A8-42. *Glass slide (ATR-spectrum).*

Appendix 9

XRD

XRD analyses

X-ray diffraction is used to identify crystalline phases present on a sample, with an analysis depth of about 1 µm into the surface. Analyses were carried out on a Bruker D8 Discover instrument, with Kα beam (1.54 Å), which can obtain measurements approximately 5 µm deep into the surface with an accuracy of 1 %weight of phases detected. The peak identification is according to best match by the analysis software. The %weight values presented in the tables below are approximations based on reference spectra contained within the analysis software.

MiniCan 5

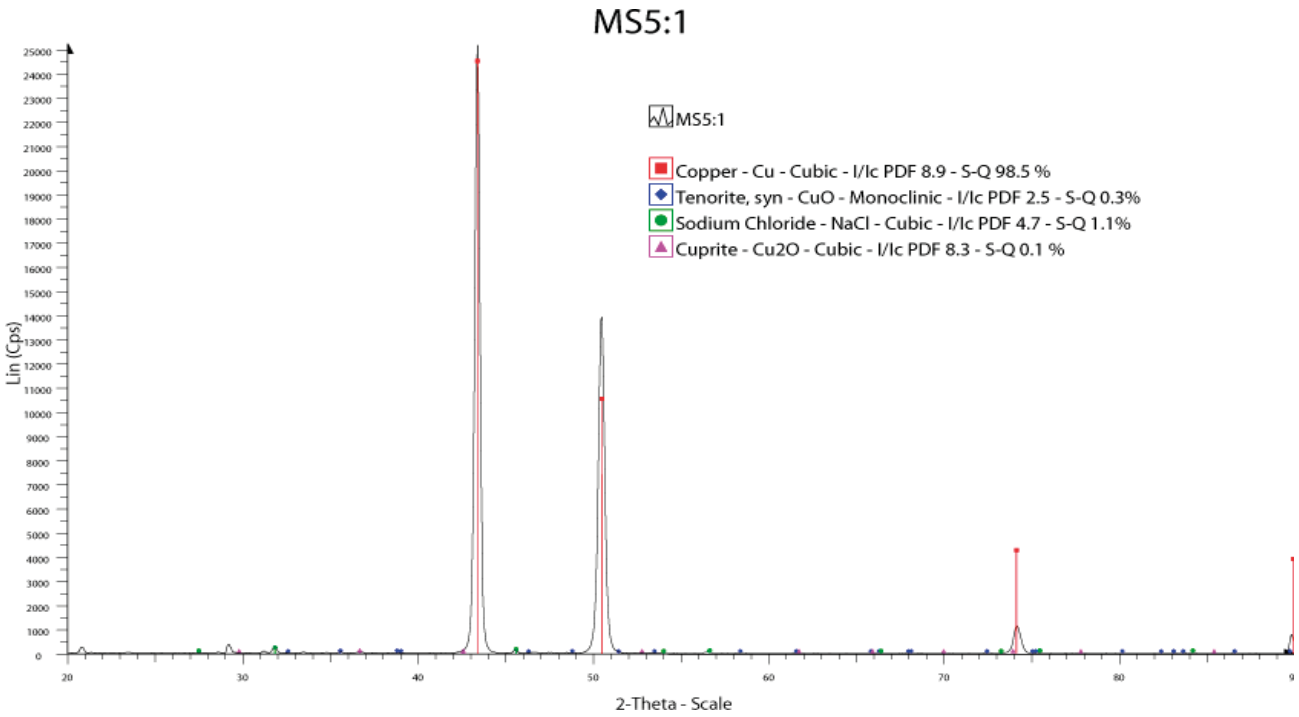

Compound name in powder database	Formula	%weight
Cuprite	Cu_2O	0.1 %
Tenorite	CuO	0.6 %
Halite	NaCl	1.1 %
Copper	Cu	98.5 %

Figure A9-1. *Sample M5 5:1 copper electrode.*

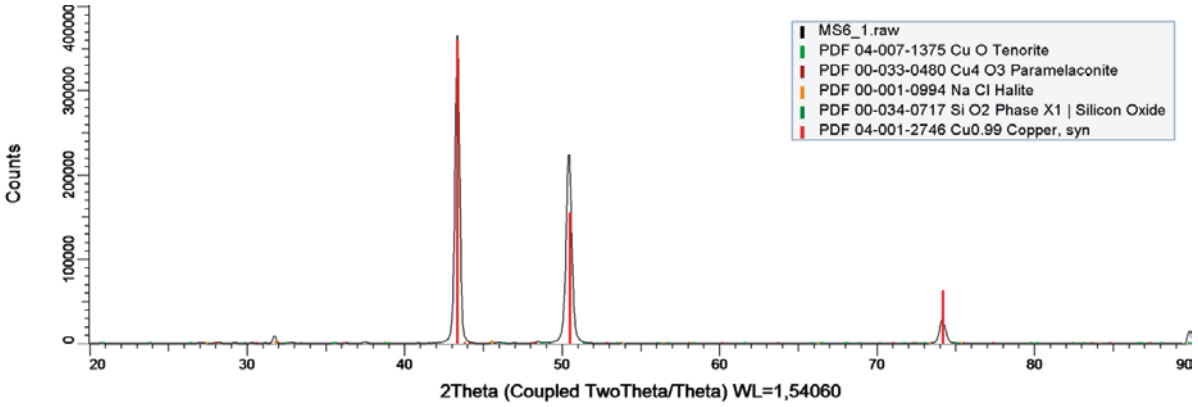

Compound name in powder database	Formula	%weight
Tenorite	CuO	0.5 %
Paramelaconite	Cu_4O_3	0.2 %
Halite	NaCl	9.0 %
Phase X1 | Silicon Oxide	SiO_2	2.1 %
Copper	Cu	88.1 %

Figure A9-2. *Sample M5 6:1 copper electrode.*

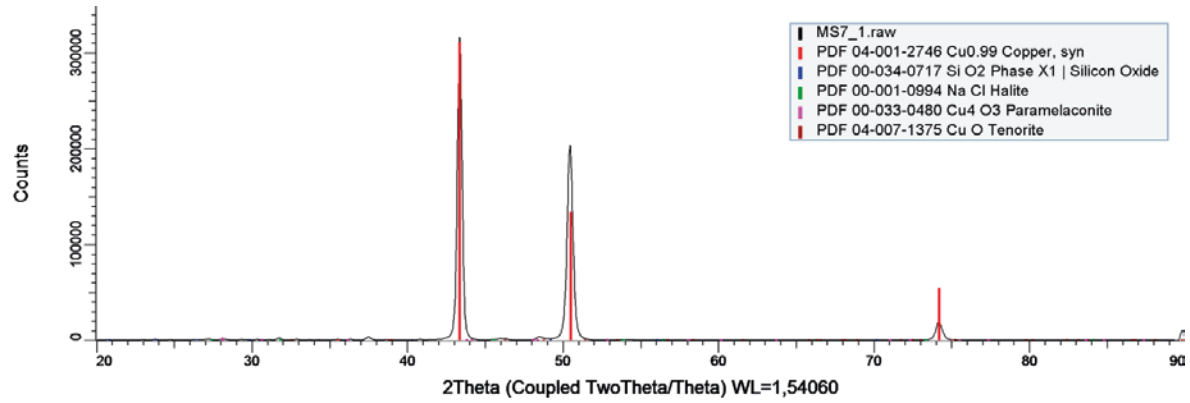

Compound name in powder database	Formula	%weight
Copper	Cu	92.4 %
Phase X1 | Silicon Oxide	SiO_2	1.9 %
Halite	NaCl	4.5 %
Paramelaconite	Cu_4O_3	0.3 %
Tenorite	CuO	0.8 %

Figure A9-3. *Sample M5 7:1 copper mass loss.*

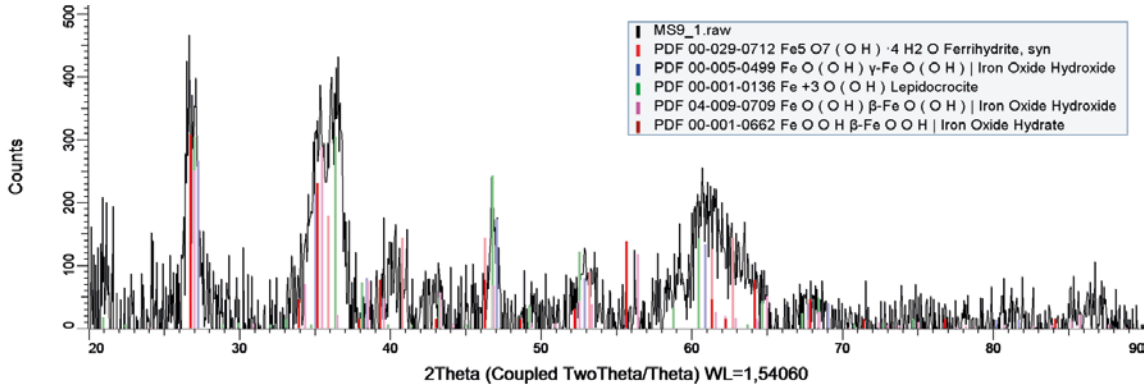

Compound name in powder database	Formula	%weight
Ferrihydrite	$Fe_5O_7(OH) \times 4\ H_2O$	15.1 %
γ-FeO(OH) | iron oxide hydroxide*)	FeO(OH)	22.4 %
Lepidocrocite*	FeO(OH)	25.6 %
β-Fe O (O H) | iron oxide hydroxide	FeO(OH)	11.2 %
β-Fe O O H | Iron Oxide Hydrate	FeO(OH)	25.8 %

*) Other γ-FeO(OH) phase(s) than Lepidocrocite.

Figure A9-4. *Sample M5 9:1 iron electrode (red rust detected).*

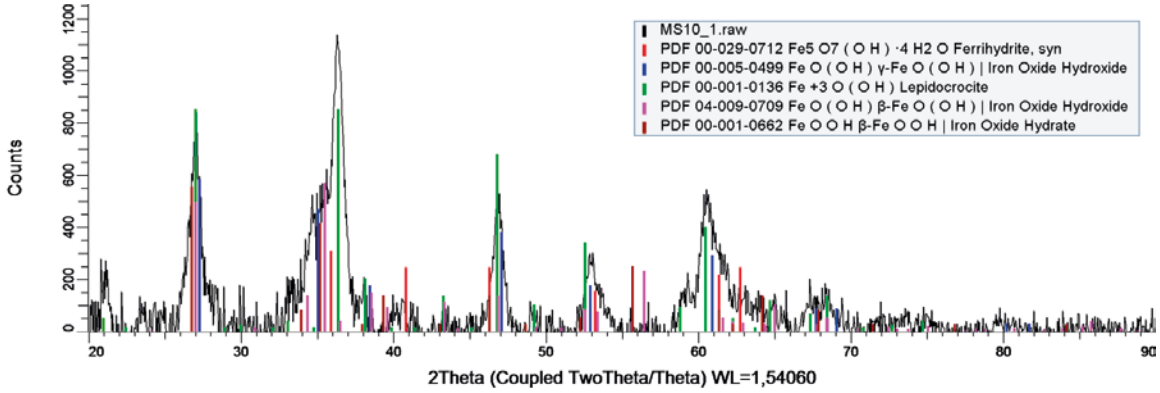

Compound name in powder database	Formula	%weight
Ferrihydrite	$Fe_5O_7(OH) \cdot 4\ H_2O$	12.1 %
γ-Fe O (O H) | Iron Oxide Hydroxide*)	FeO(OH)	22.8 %
Lepidocrocite	FeO(OH)	33.2 %
β-Fe O (O H) | Iron Oxide Hydroxide	FeO(OH)	10.3 %
β-Fe O O H | Iron Oxide Hydrate	FeO(OH)	21.6 %

*) Other γ-FeO(OH) phase(s) than Lepidocrocite.

Figure A9-5. *Sample M5 10:1 iron electrode (red rust detected).*

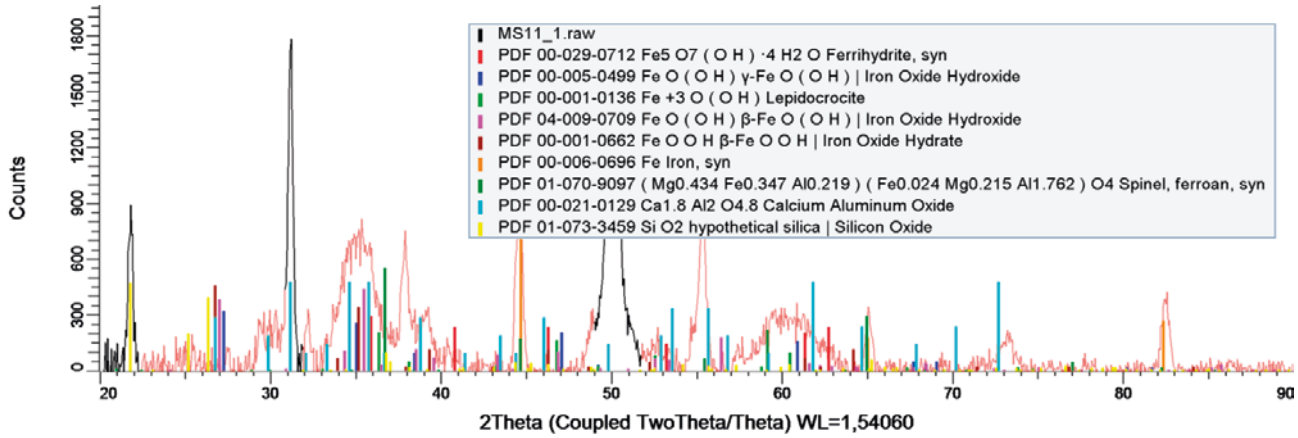

Compound name in powder database	Formula	%weight
Ferrihydrite	$Fe_5O_7(OH) \cdot 4\ H_2O$	8.8 %
γ-Fe O (O H) | Iron Oxide Hydroxide*)	FeO(OH)	9.7 %
Lepidocrocite	FeO(OH)	6.2 %
β-Fe O (O H) | Iron Oxide Hydroxide	FeO(OH)	6.1 %
β-Fe O O H | Iron Oxide Hydrate	FeO(OH)	13.7 %
Iron, syn	Fe	26.8 %
Spinel, ferroan	$(Mg_{0.434}Fe_{0.347}Al_{0.219})\ (Fe_{0.024}Mg_{0.215}Al_{1.762})O_4$	7.5 %
Calcium Aluminum Oxide	$Ca_{1.8}Al_2O_{4.8}$	14.4 %
hypothetical silica | Silicon Oxide	SiO_2	6.9 %

*) Other γ-FeO(OH) phase(s) than Lepidocrocite

Figure A9-6. *Sample M5 11:1 iron mass loss (mainly red rust detected).*

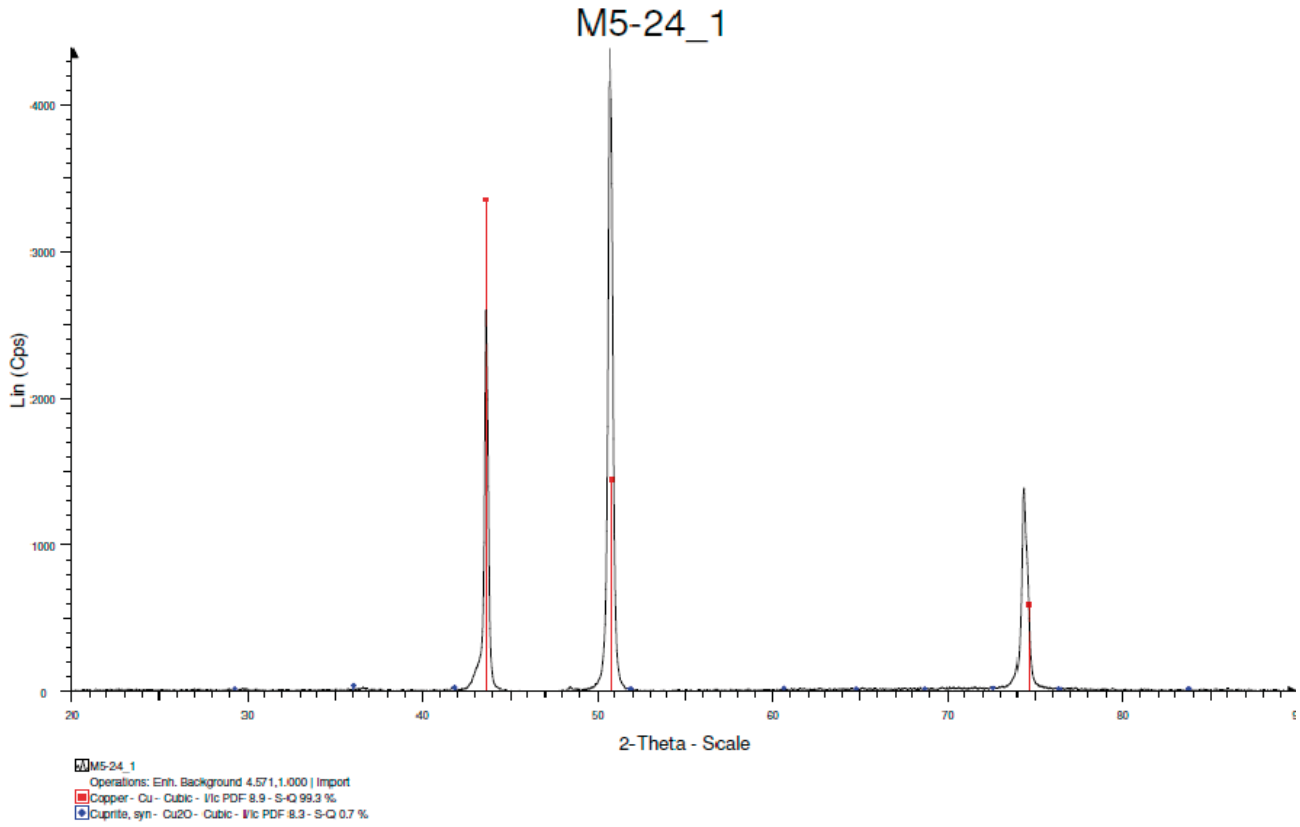

Compound name in powder database	Formula	%weight
Copper	Cu	99.3 %
Cuprite	Cu_2O	0.7 %

Figure A9-7. *Sample M5 24:1 inner surface of copper canister.*

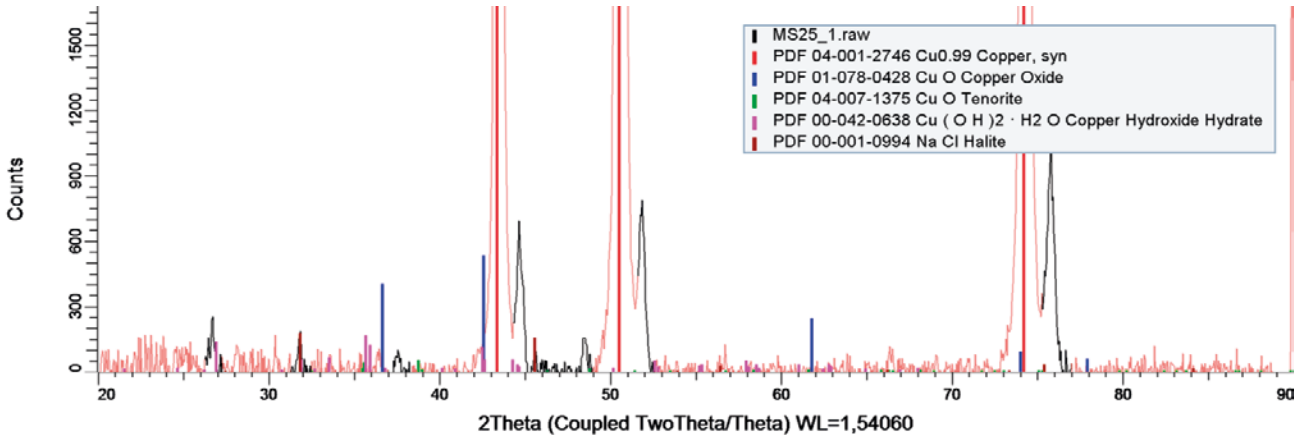

Compound name in powder database	Formula	%weight
Copper	Cu	78.0 %
Copper Oxide	CuO	2.7 %
Tenorite	Cu_2O	0.4 %
Copper Hydroxide Hydrate	$Cu(OH)_2 \cdot H_2O$	14.0 %
Halite	NaCl	4.9 %

Figure A9-8. *Sample M5 25:1 outer surface of canister.*

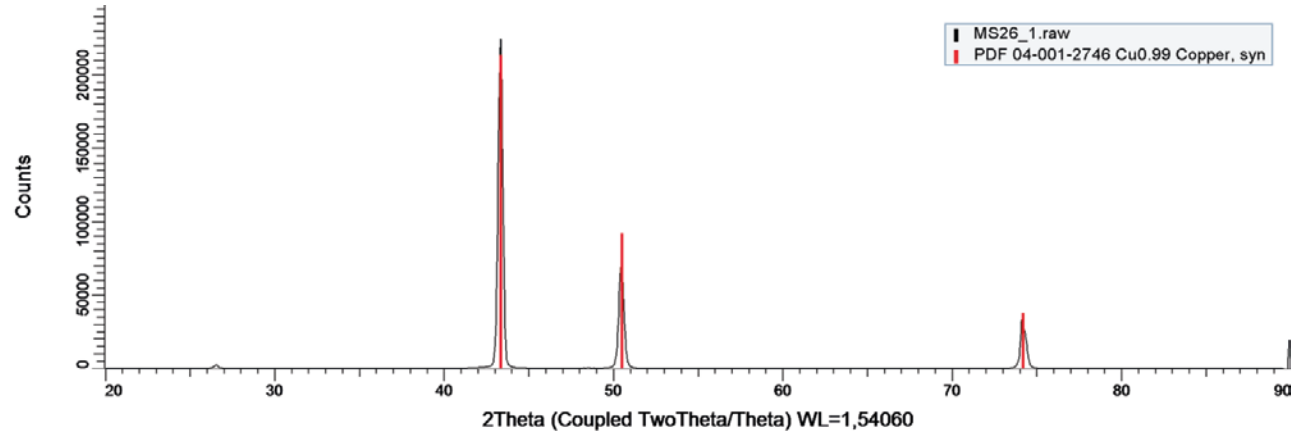

Compound name in powder database	Formula	%weight
Copper	Cu	NA

Figure A9-9. *Sample M5 26:1 weld of copper canister.*

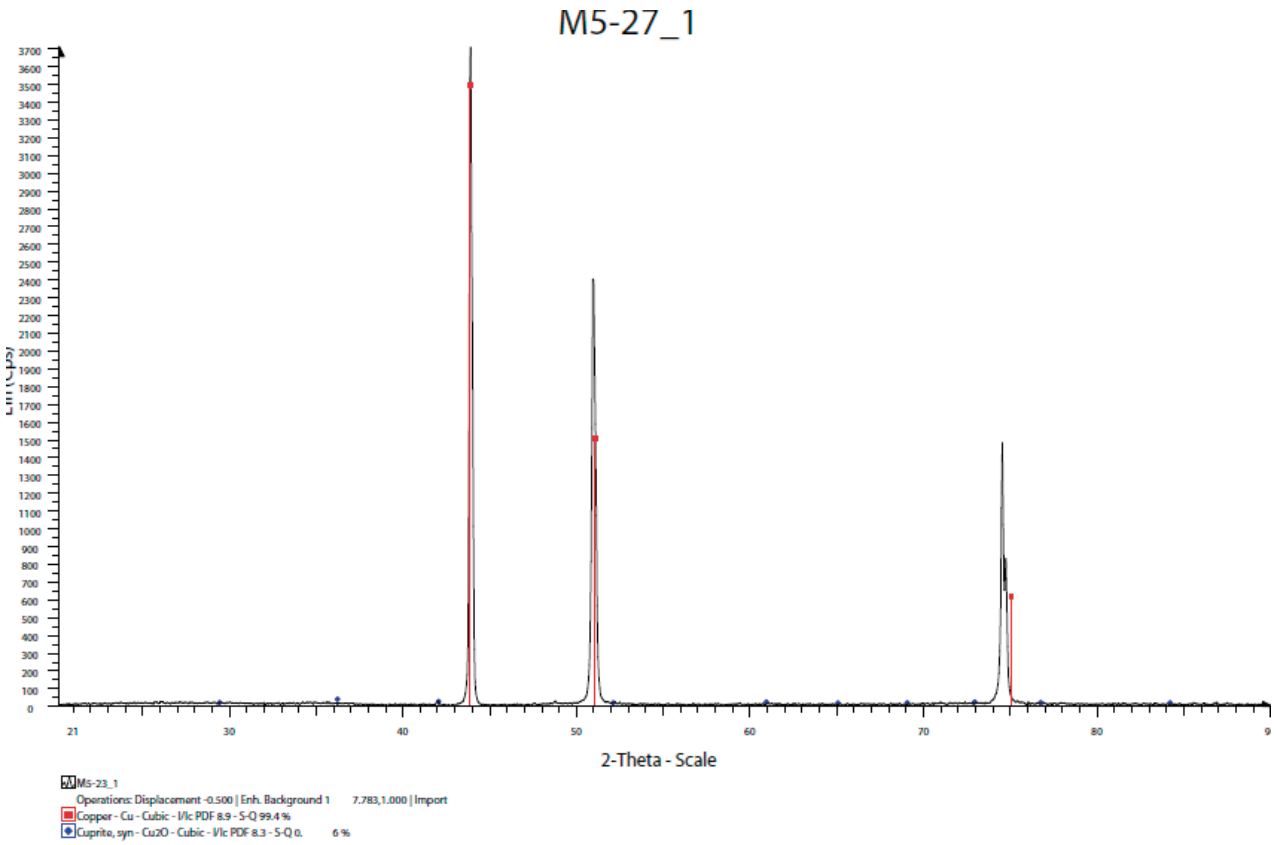

Compound name in powder database	Formula	%weight
Copper	Cu	99.4 %
Cuprite	Cu 2O	0.6 %

Figure A9-10. *Sample M5 27:1 inner surface of copper canister near through hole.*

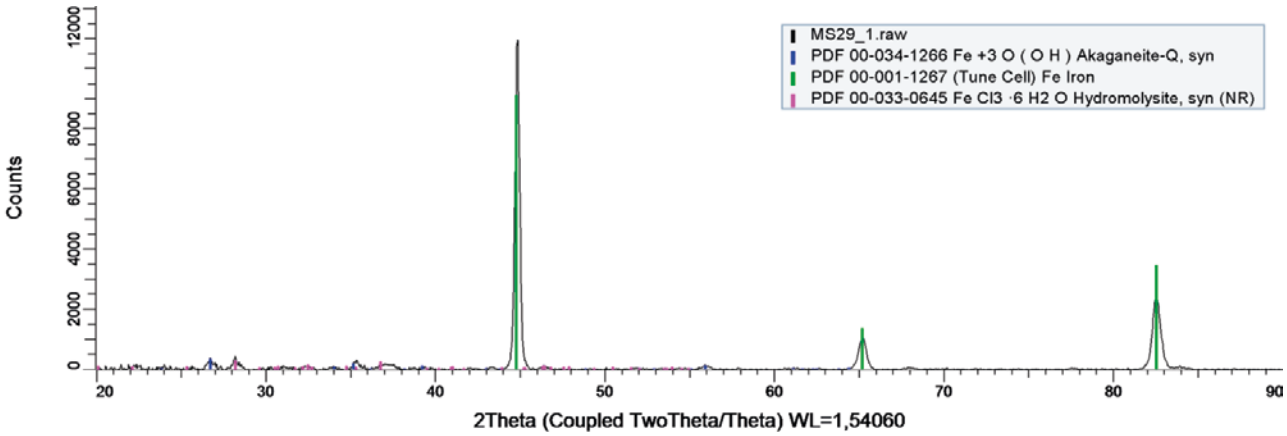

Compound name in powder database	Formula	%weight
Akaganeite	FeO(OH)	17 %
Iron	Fe	74.7 %
Hydromolysite	$FeCl_3$ $6H_2O$	8.3 %

Figure A9-11. *Sample M5 29:1 cast iron insert.*

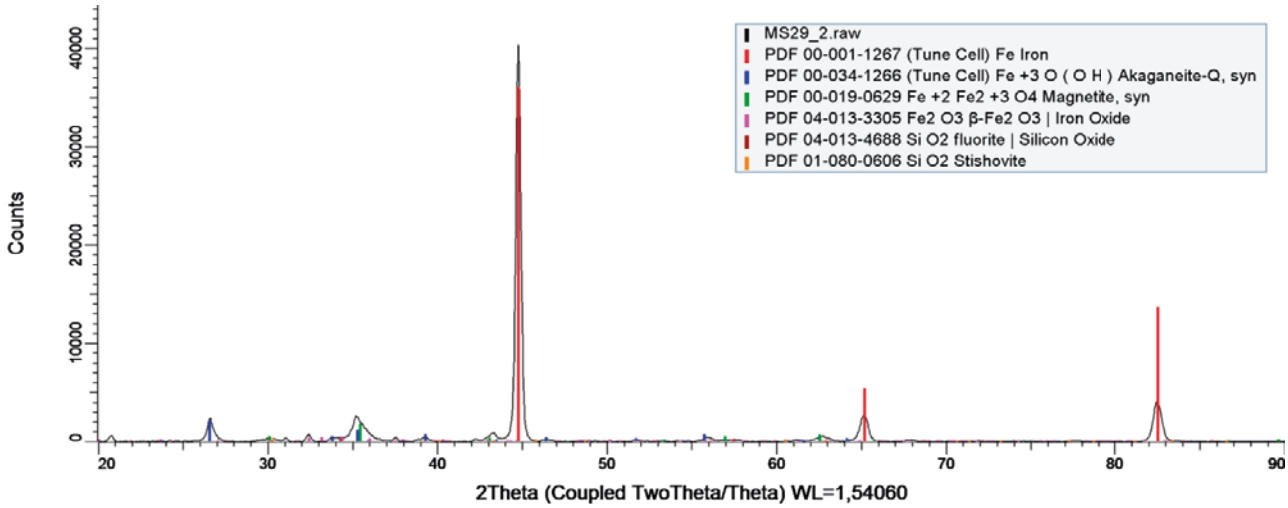

Compound name in powder database	Formula	%weight
Iron	Fe	92.1 %
Akaganeite-Q	FeO(OH)	5.3 %
Magnetite	Fe_3O_4	0.9 %
Hematite	Fe_2O_3	1.0 %
Fluorite | Silicon Oxide	SiO_2	0.3 %
Stishovite	SiO_2	0.3 %

Figure A9-12. *Sample M5 29:2 cast iron insert.*

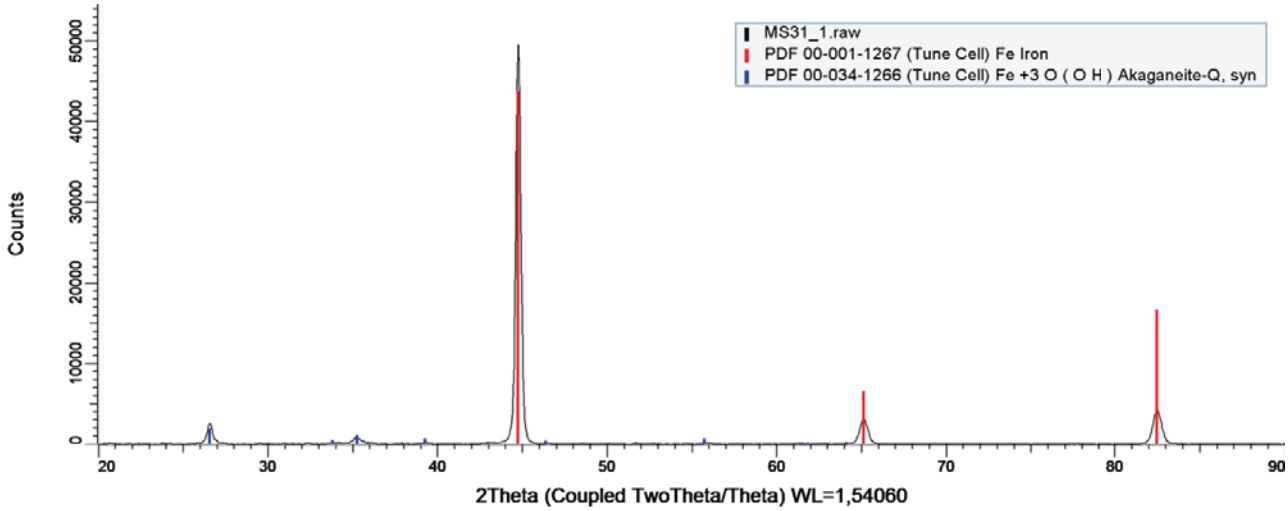

Compound name in powder database	Formula	%weight
Iron	Fe	97.4 %
Akaganeite-Q	FeO(OH)	2.6 %

Figure A9-13. *Sample M5 31:1 cast iron insert at position near hole through copper canister.*

MiniCan 4

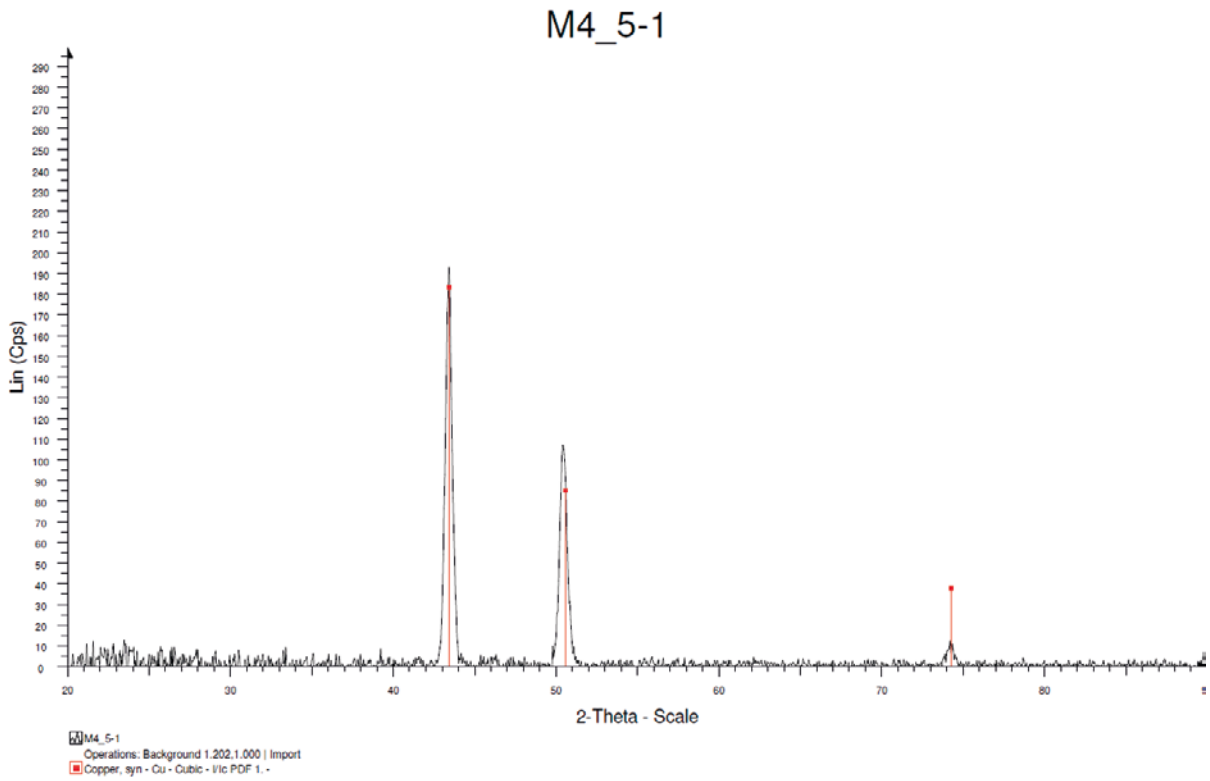

Compound name in powder database	Formula	%weight
Copper	Cu	NA

Figure A9-14. *Sample M4 5.1 copper electrode.*

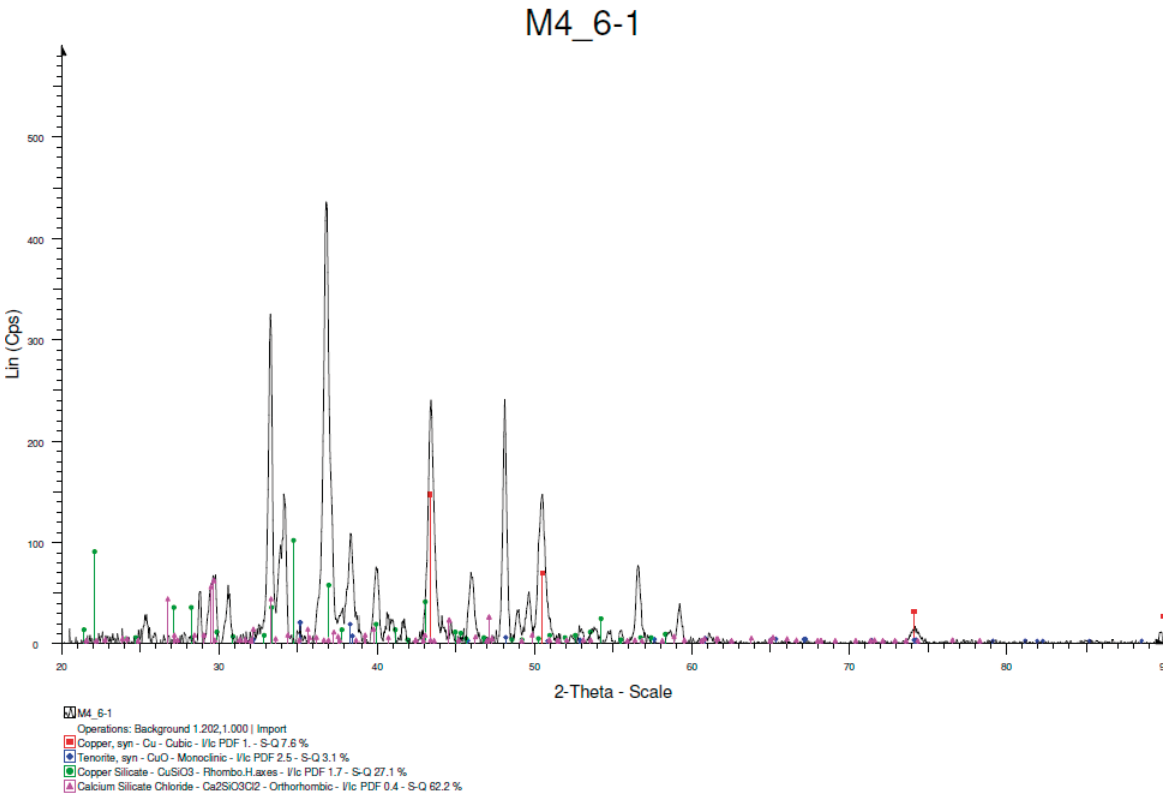

Compound name in powder database	Formula	%weight
Copper	Cu	7.6 %
Tenorite	CuO	3.1 %
Copper silicate	$CuSiO_3$	27.1 %
Calcium silicate chloride	$Ca_2SiO_3Cl_2$	62.2 %

Figure A9-15. *Sample M4 6:1 copper electrode (silicates likely from bentonite not complete washed off the samples).*

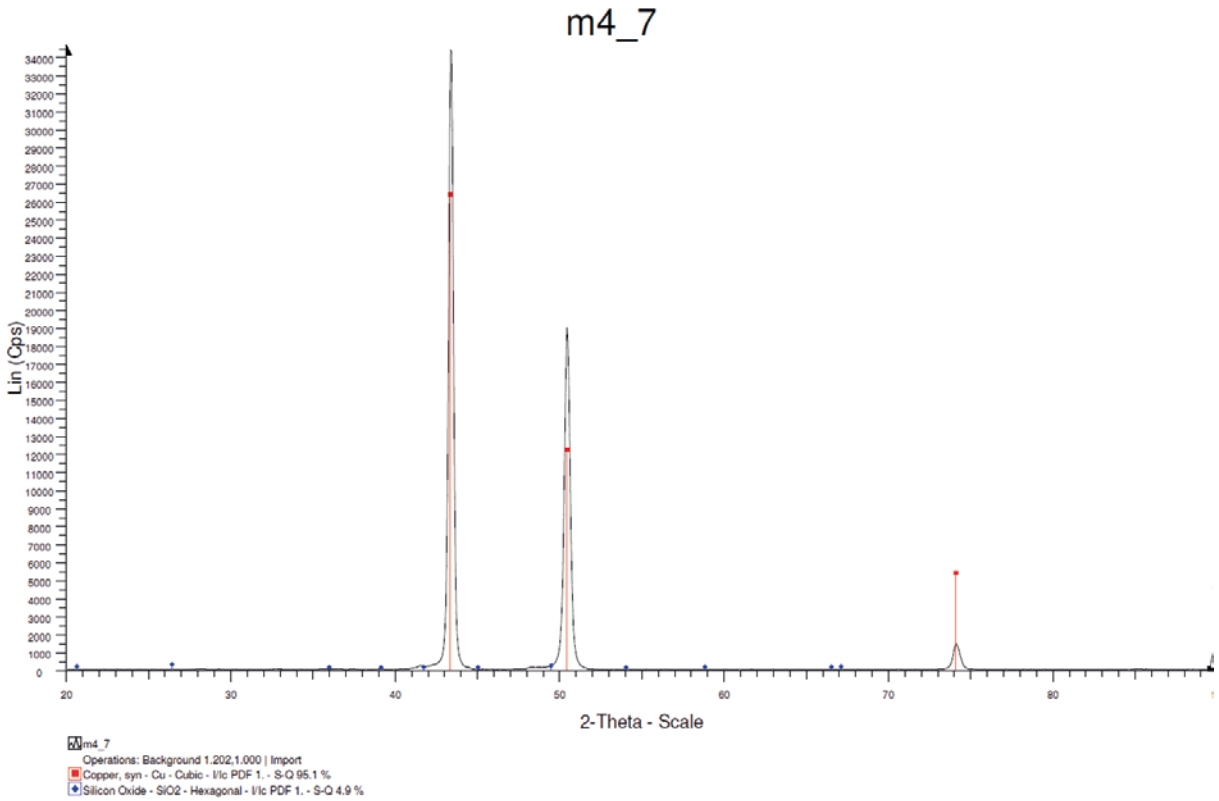

Compound name in powder database	Formula	%weight
Copper	Cu	95.1 %
Silicon oxide	SiO_2	4.9 %

Figure A9-16. *Sample M4 7:1 copper mass loss.*

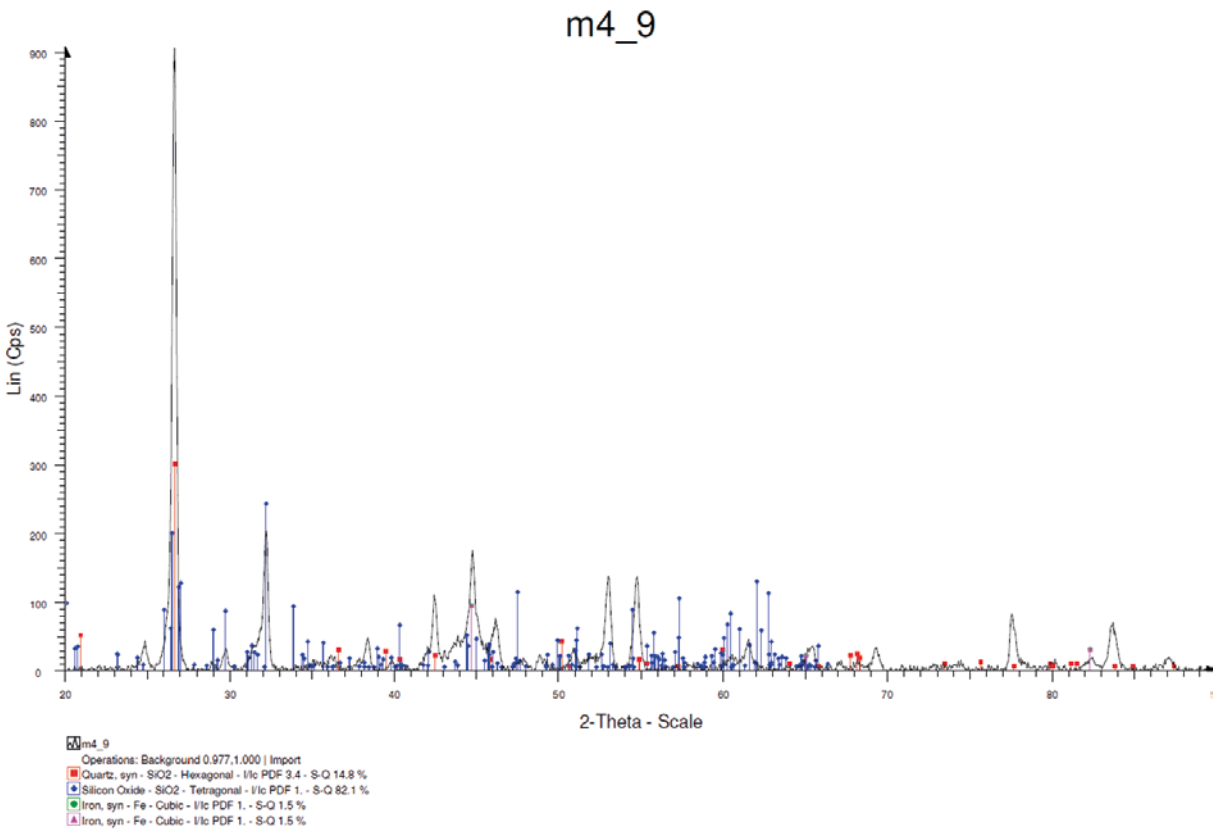

Compound name in powder database	Formula	%weight
Quartz	SiO_2	14.8 %
Silicon oxide	SiO_2	82.1 %
Iron	Fe	1.5 %
Iron	Fe	1.5 %

Figure A9-17. *Sample M4 9:1 iron electrode.*

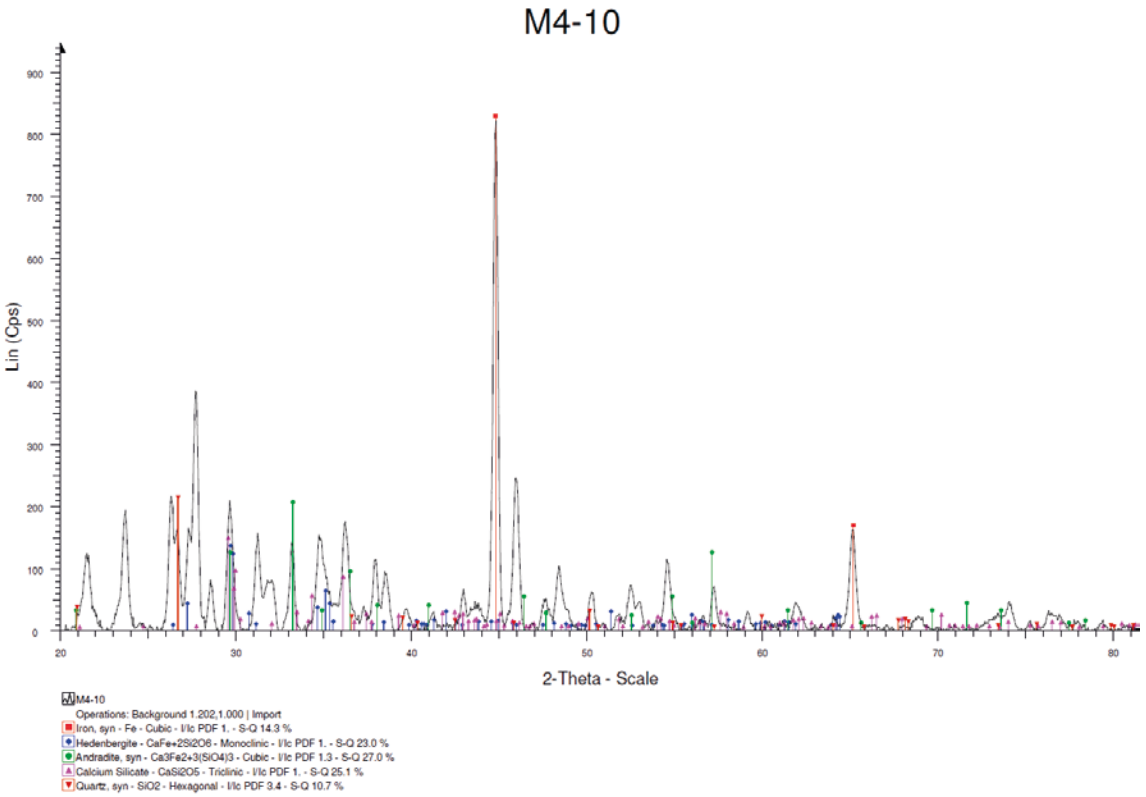

Compound name in powder database	Formula	%weight
Iron	Fe	14.3 %
Hedenbergite	$CaFeSi_2O_6$	23.0 %
Andradite	$Ca_3Fe_2(SiO_4)_3$	27.0 %
Calcium silicate	$CaSi_2O_5$	25.1 %
Quartz	SiO_2	10.7 %

Figure A9-18. *Sample M4 10:1 iron electrode (silicates likely due to bentonite not complete washed off the samples).*

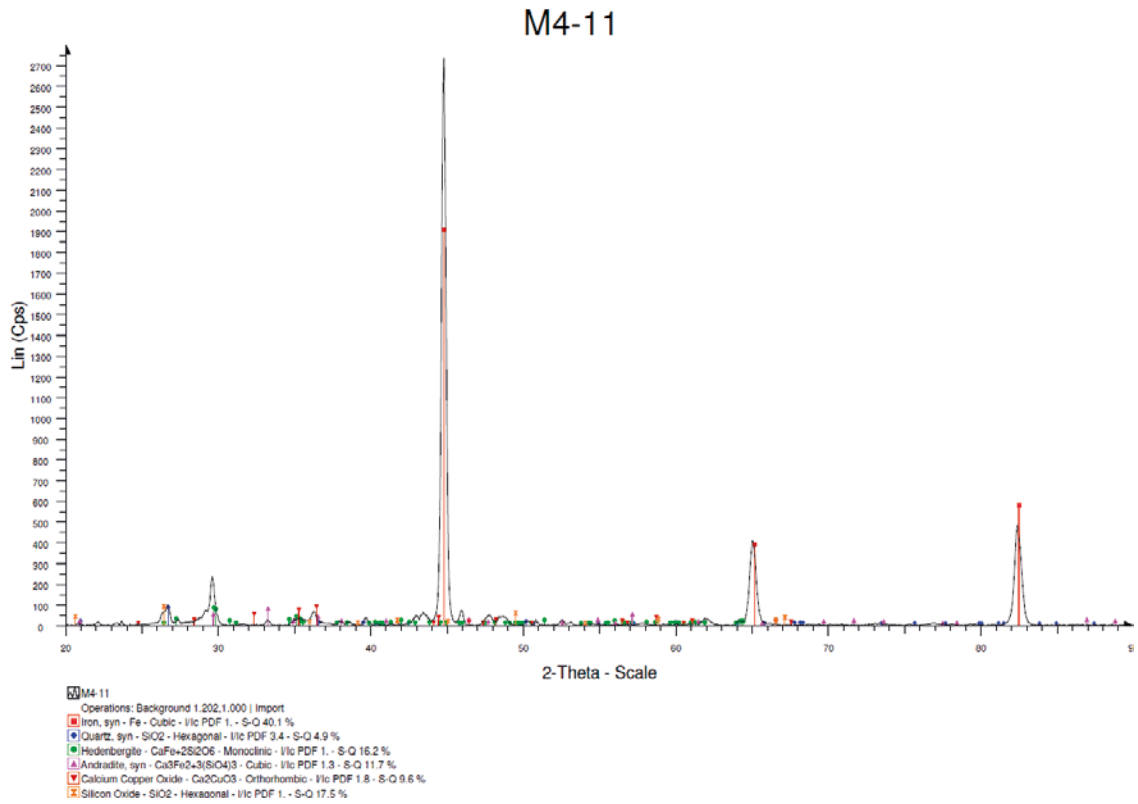

Compound name in powder database	Formula	%weight
Iron	Fe	40.1 %
Quartz	SiO_2	4.9 %
Hedenbergite	$CaFeSi_2O_6$	16.2 %
Andradite	$Ca_3Fe_2(SiO_4)_3$	11.7 %
Calcium copper oxide	Ca_2CuO_3	9.6 %
Silicon oxide	SiO_2	17.5 %

Figure A9-19. *Sample M4 11:1 iron mass loss.*

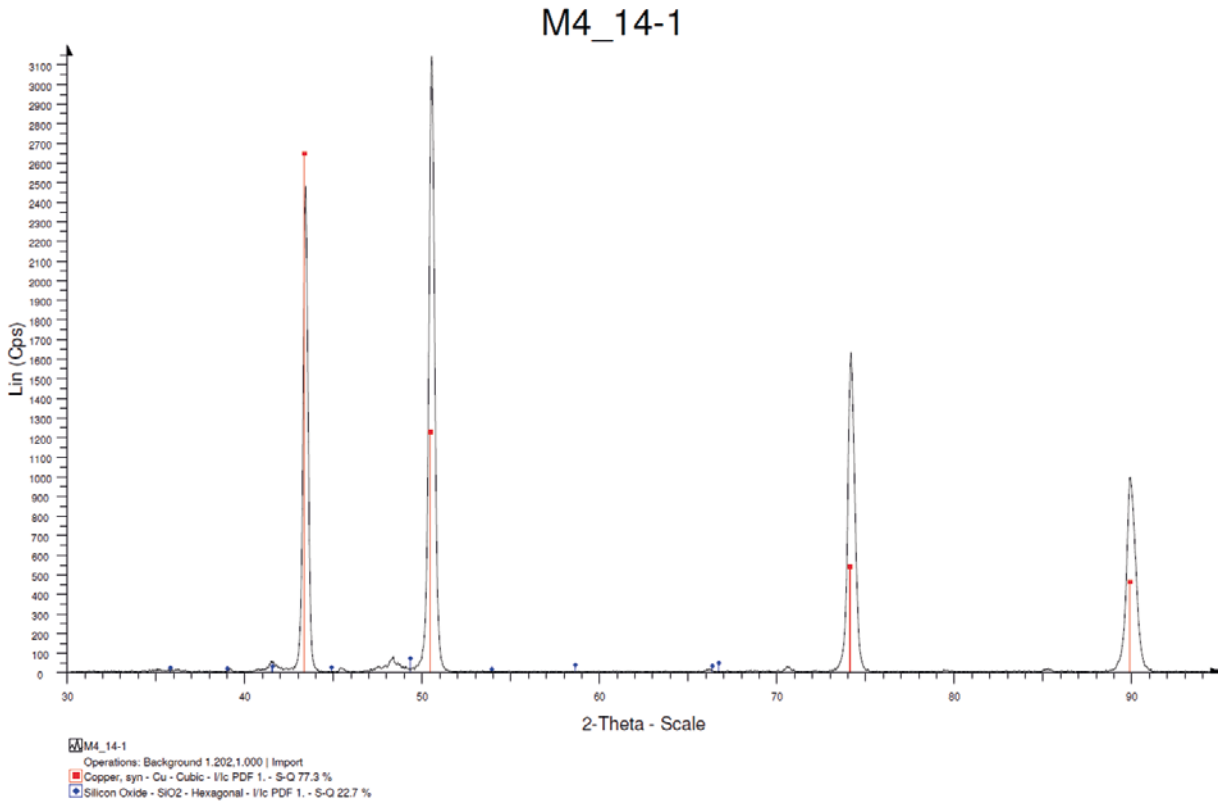

Compound name in powder database	Formula	%weight
Copper	Cu	77.3 %
Silicon oxide	SiO_2	22.7 %

Figure A9-20. *Sample M4 14:1 copper sandwich specimen.*

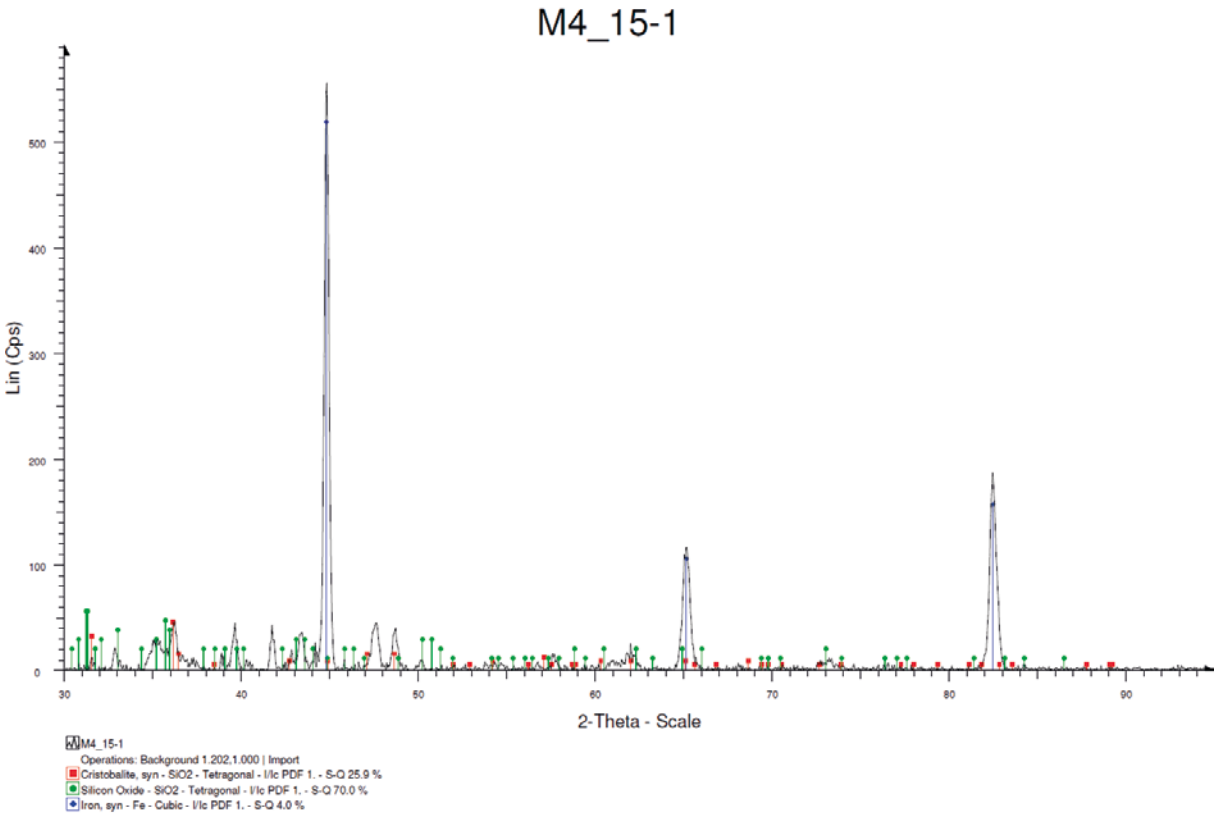

Compound name in powder database	Formula	%weight
Cristobalite	SiO_2	25.9 %
Silicon oxide	SiO_2	70.0 %
Iron	Fe	4.0 %

Figure A9-21. *Sample M4 15:1 cast iron sandwich specimen.*

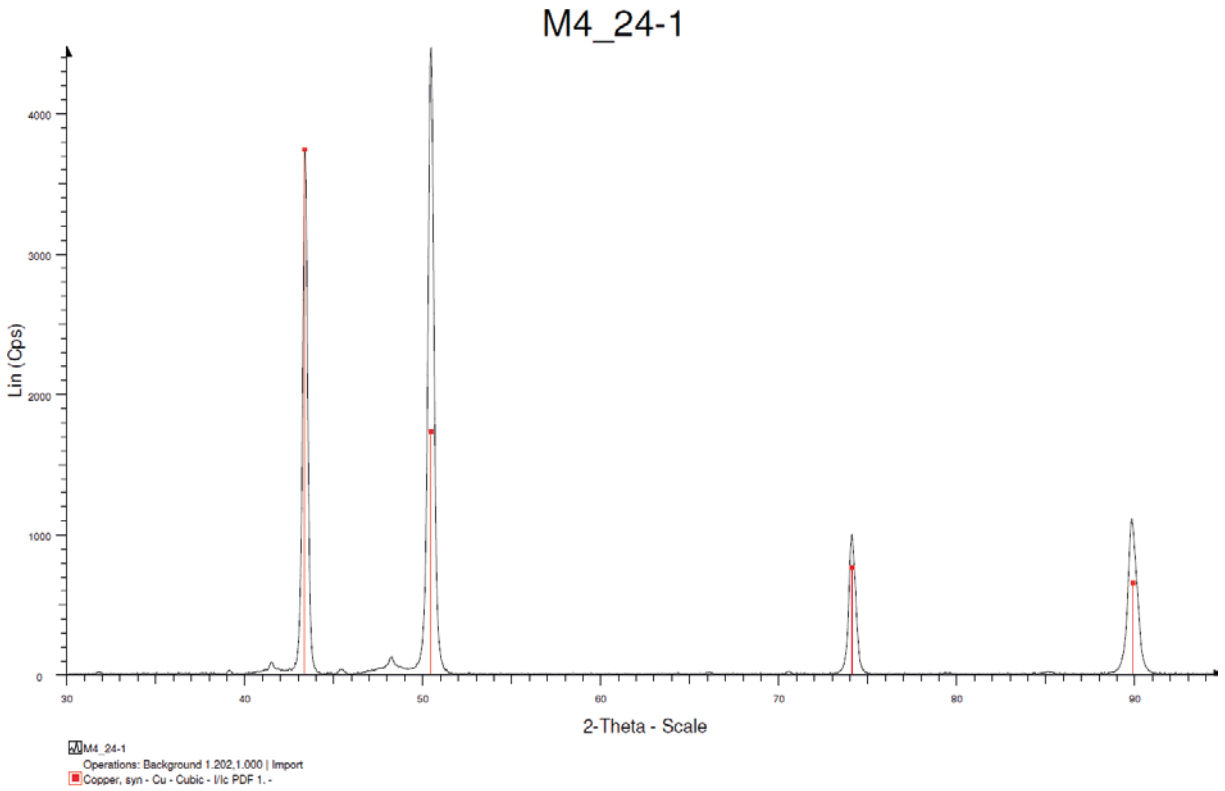

Compound name in powder database	Formula	%weight
Copper	Cu	NA

Figure A9-22. *Sample M4 24:1 inner surface of copper canister.*

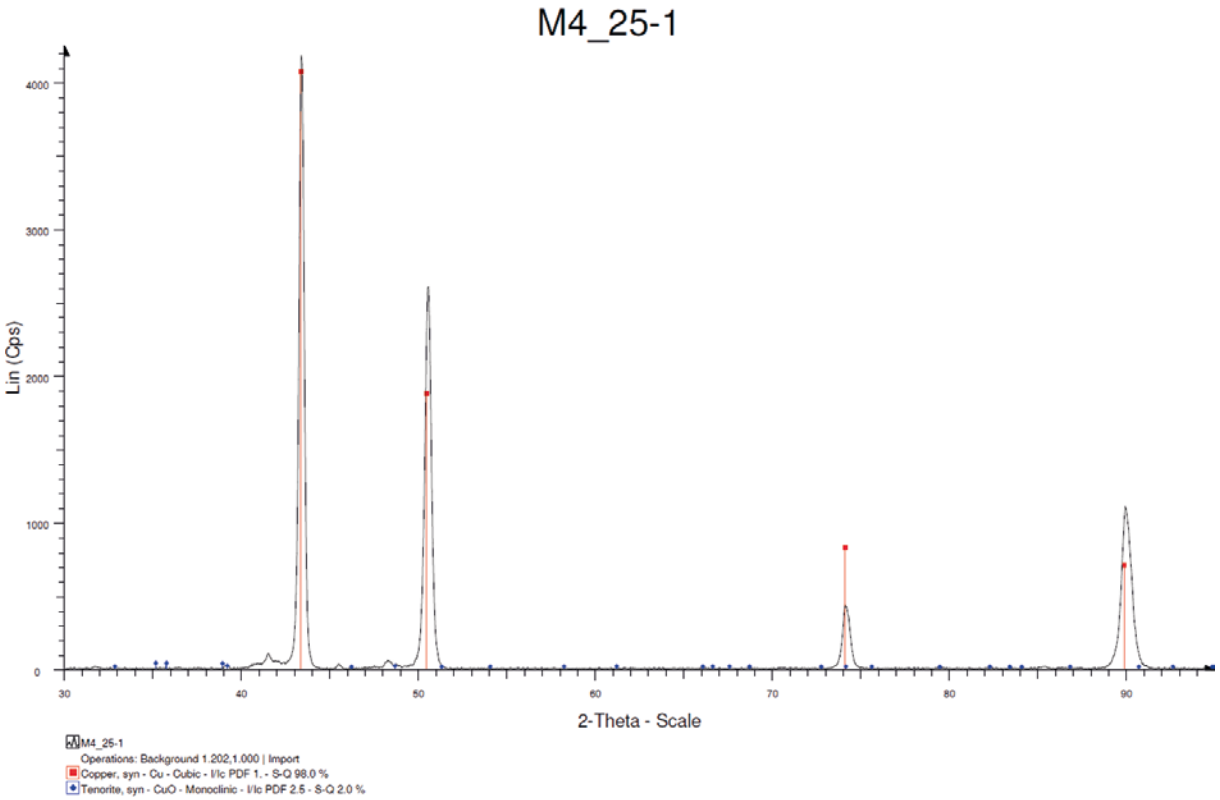

Compound name in powder database	Formula	%weight
Copper	Cu	98.0 %
Tenorite	CuO	2.0 %

Figure A9-23. *Sample M4 25:1 outer surface of copper canister.*

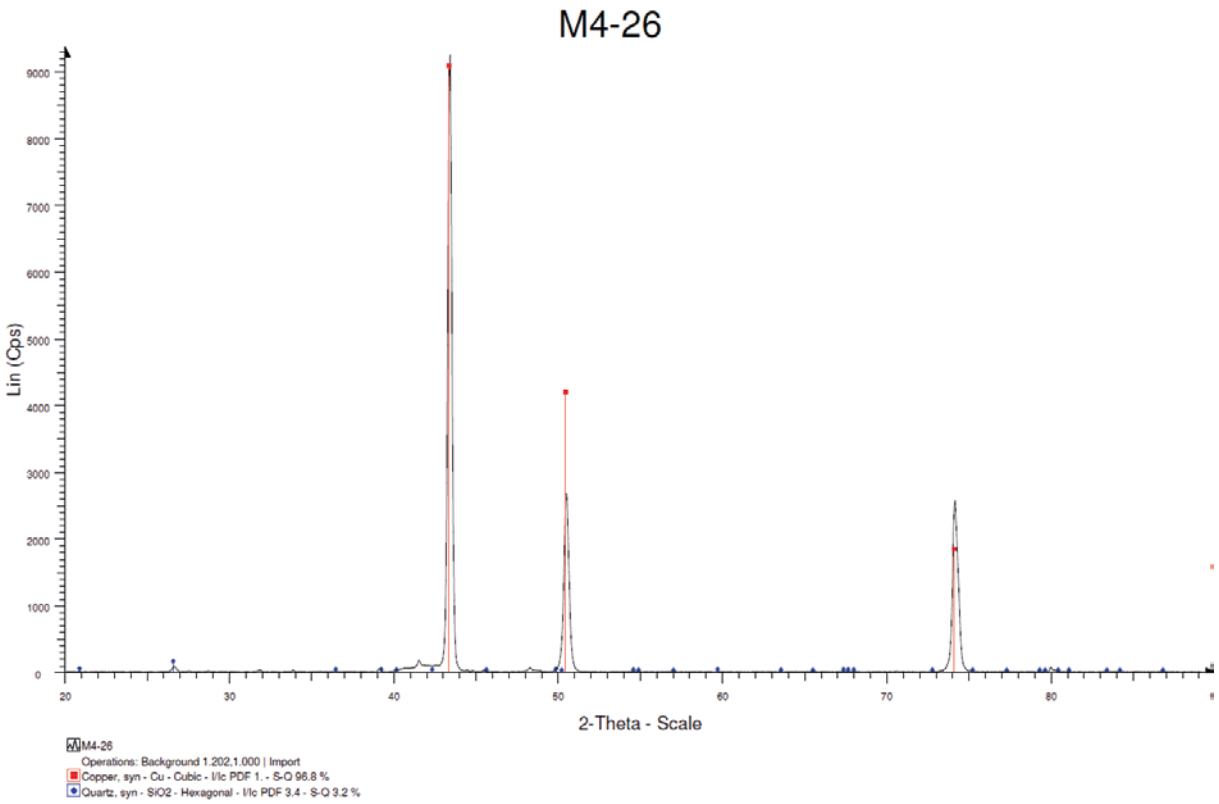

Compound name in powder database	Formula	%weight
Copper	Cu	96.8 %
Quartz	SiO_2	3.2 %

Figure A9-24. *Sample M4 26:1 weld of copper canister.*

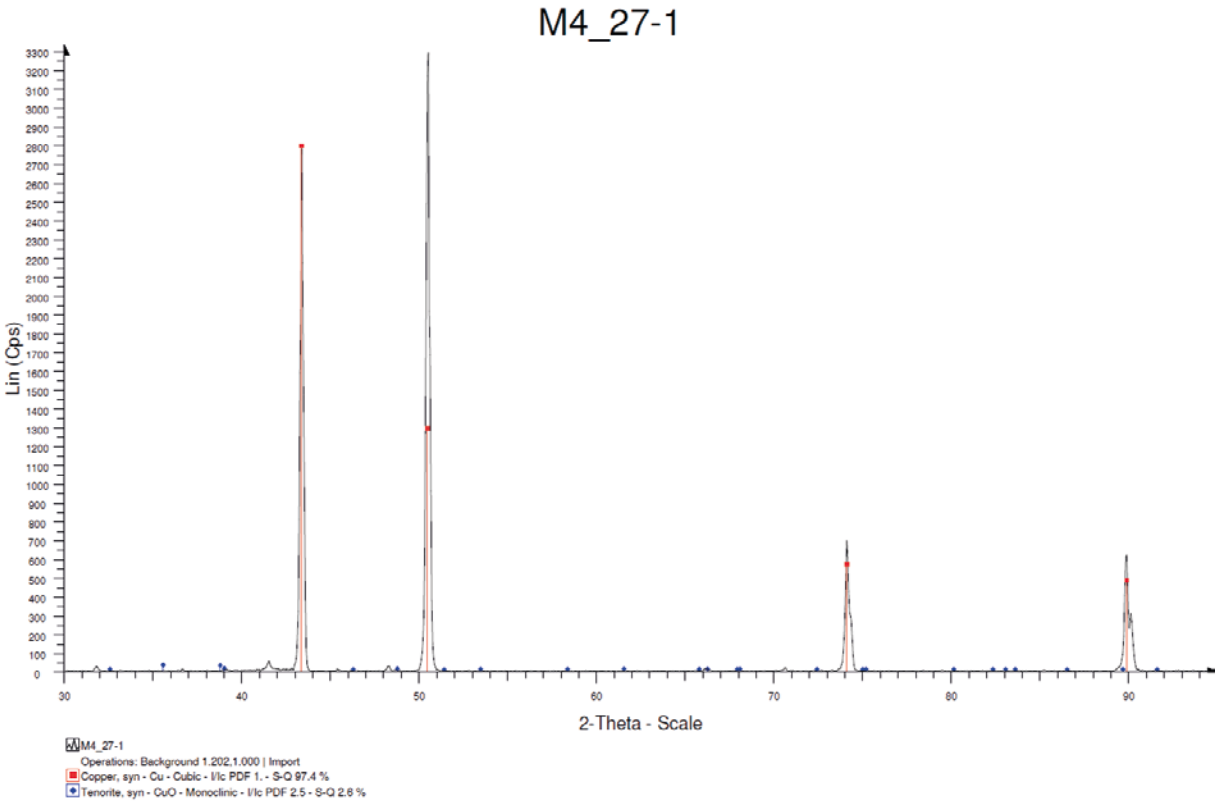

Compound name in powder database	Formula	%weight
Copper	Cu	97.4 %
Tenorite	CuO	2.6 %

Figure A9-25. *Sample M4 27:1 inner surface of copper canister near through hole.*

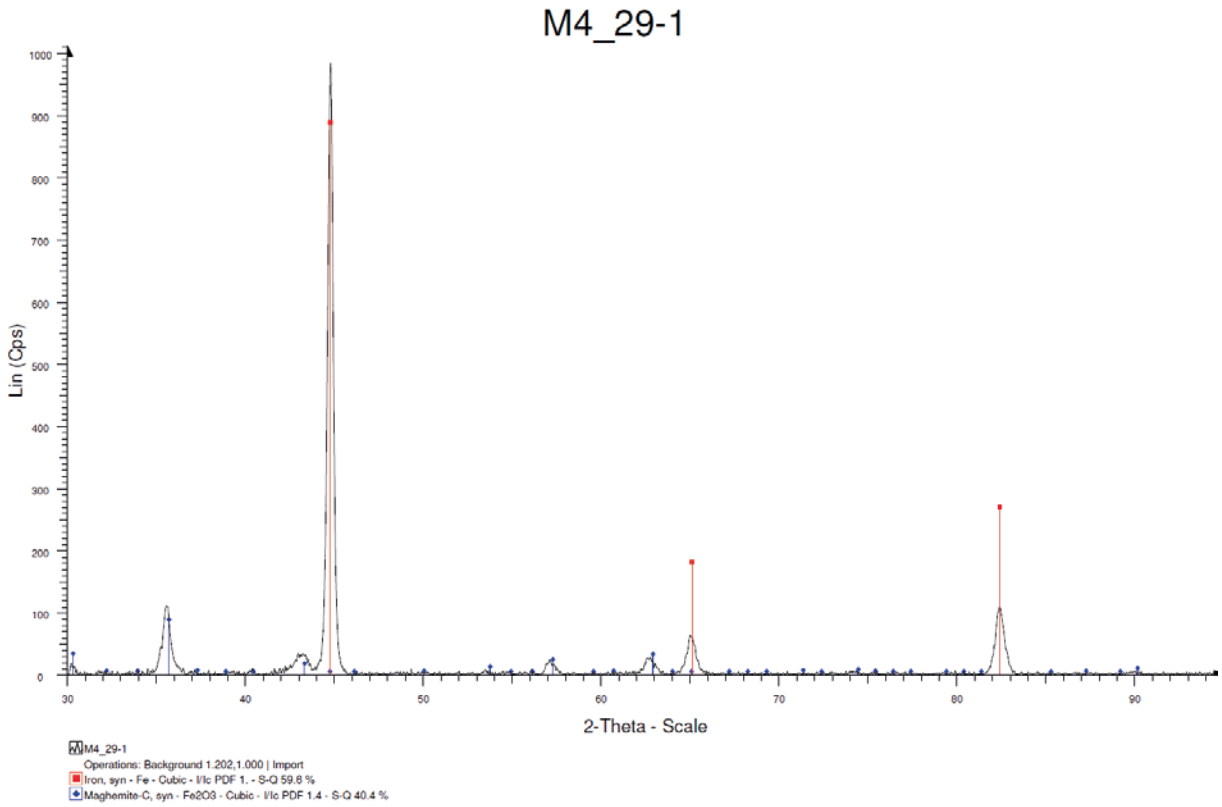

Compound name in powder database	Formula	%weight
Iron	Fe	59.6 %
Maghemite-C	Fe_2O_3	40.4 %

Figure A9-26. *Sample M4 29:1 cast iron insert.*

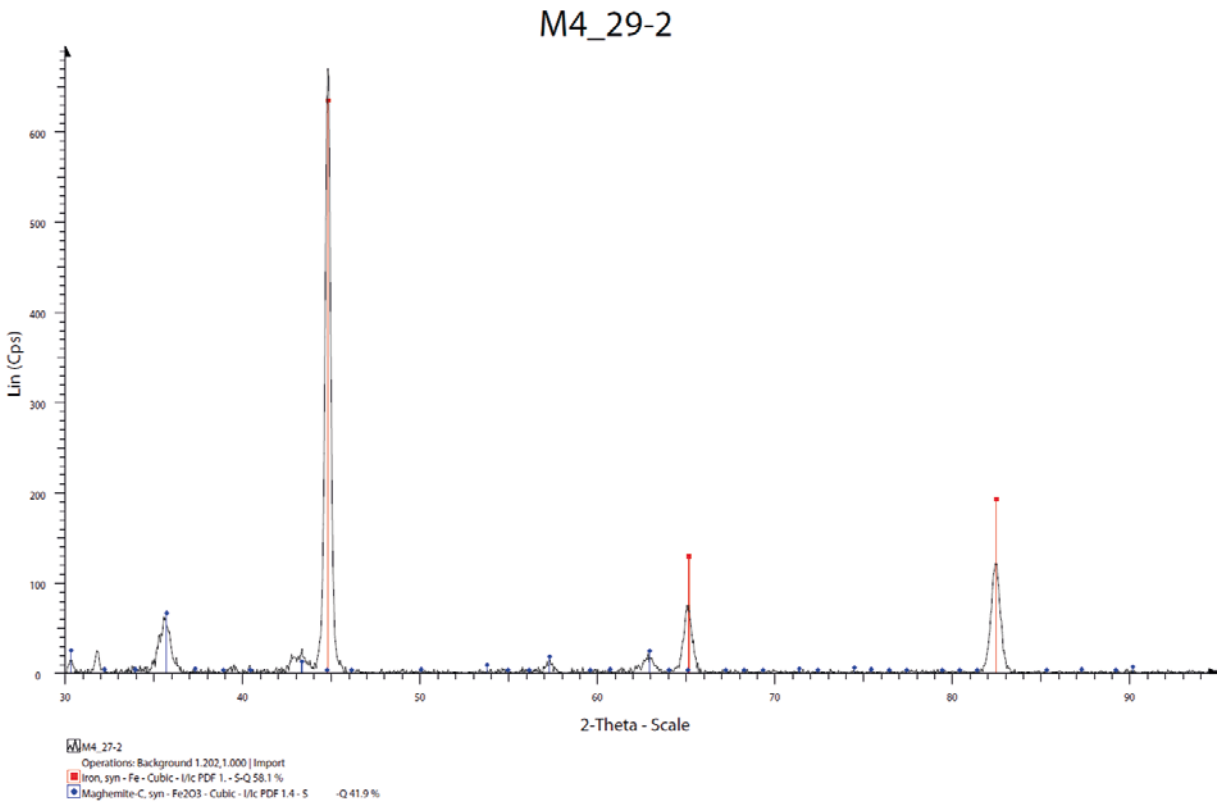

Compound name in powder database	Formula	%weight
Iron	Fe	58.1 %
Maghemite-C	Fe_2O_3	41.9 %

Figure A9-27. *Sample M4 29:2 cast iron insert.*

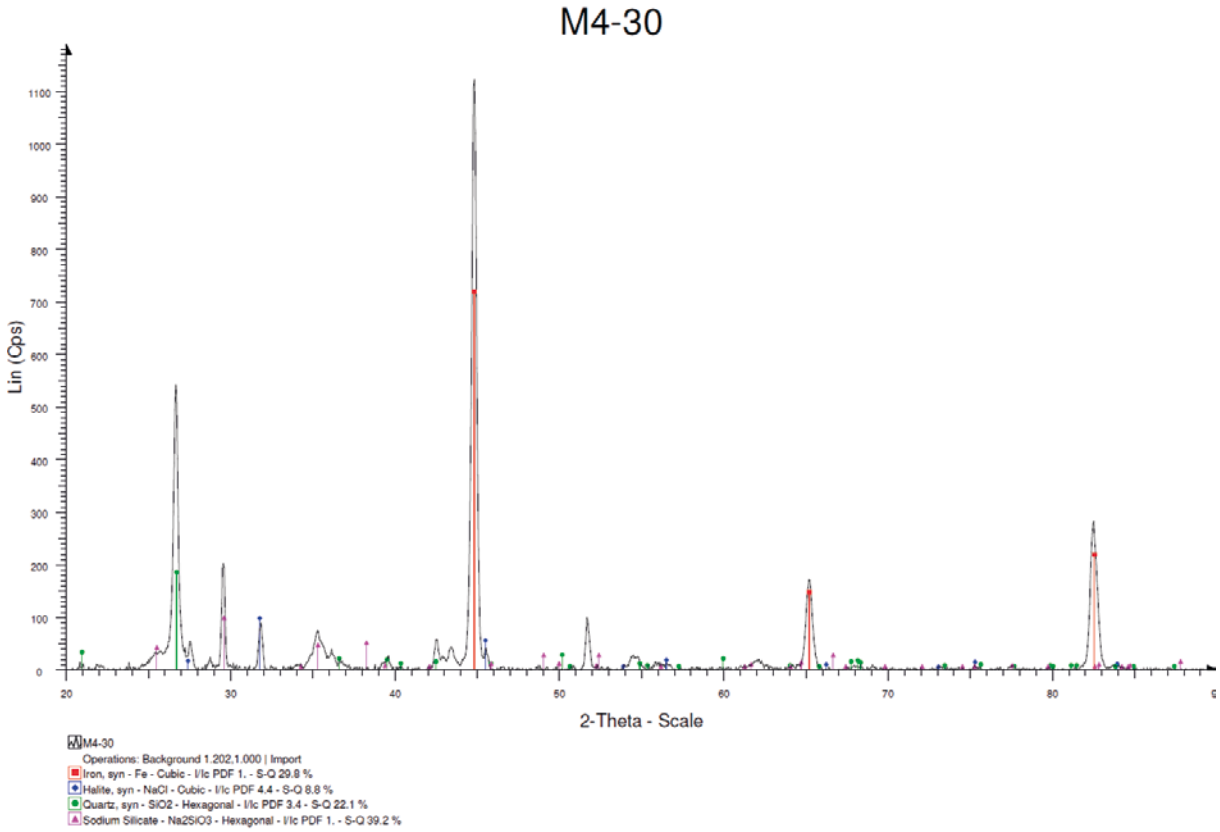

Compound name in powder database	Formula	%weight
Iron	Fe	29.8 %
Halite	NaCl	8.8 %
Quartz	SiO_2	22.1 %
Sodium silicate	Na_2SiO_3	39.2 %

Figure A9-28. *Sample M4 30:1 surface of cast iron insert near hole through copper canister (silicates likely from bentonite not complete washed off the samples).*

Appendix 10

SEM/EDS

SEM EDS analyses

Scanning Electron Microscopy (SEM) with Energy Dispersive X-ray Spectroscopy (EDS) is used to characterise the morphology and elemental composition of the surface of a sample, with the chemical analyses carried out to a depth of about 1 µm into the surface. SEM work was carried out on a JEOL 7000F field emission instrument which gives a high spatial resolution in pictures, ca. 1 nm. The SEM is equipped with EDS with very high sensitivity, with a window area of 20 mm^2. The SEM also has a detector for back scattered electrons which gives contrast based on atom size and different grain crystal orientations. Deformation of grains can also be seen using the back scatter detector.

The samples were analysed using EDS and the results are presented below as weight% of element detected at different points on the surface. In general the samples were analysed at areas deemed representative of the majority of the surface as well as any areas which appeared different, such as with surface deposits and/or particles. The sample identification codes as given in the main body of the report are given in the figure captions, "M4 5:1" thus represents MiniCan 4 sample 5:1.

Figure A10-1. *MiniCan 4 samples positioned on plinth ready for SEM analysis. From left to right: Copper electrode M4 5:1, copper electrode M4 6:1, copper mass loss sample M4 7:1, iron electrode M4 9:1, iron electrode M4 10:1, iron mass loss sample M4 11:1.*

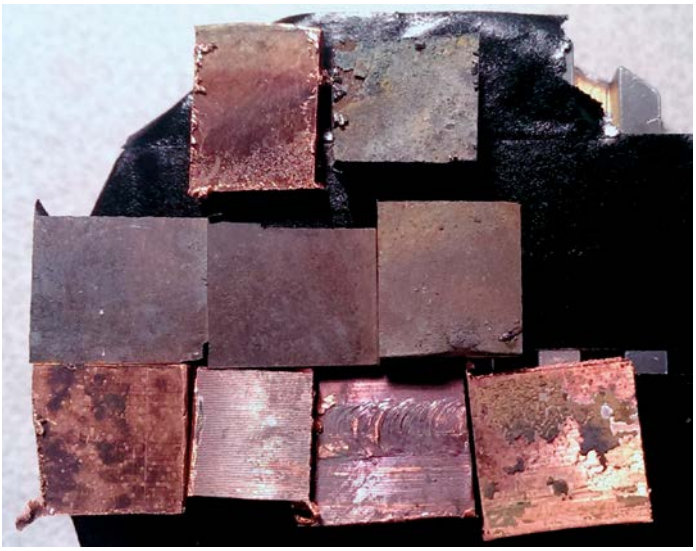

Figure A10-2. *MiniCan 4 canister and insert samples ready for SEM analysis. From top left to bottom right: Copper sandwich specimen M4 14:1, iron sandwich specimen M4 15:1, iron insert samples M4 29:1 and 29:2, iron insert sample from near canister hole M4 30:1, copper canister inner surface M4 24:1, copper canister outer surface M4 25:1, copper canister weld surface M4 26:1, copper canister inner surface near hole M4 27:1.*

MiniCan 4 copper electrode 5:1

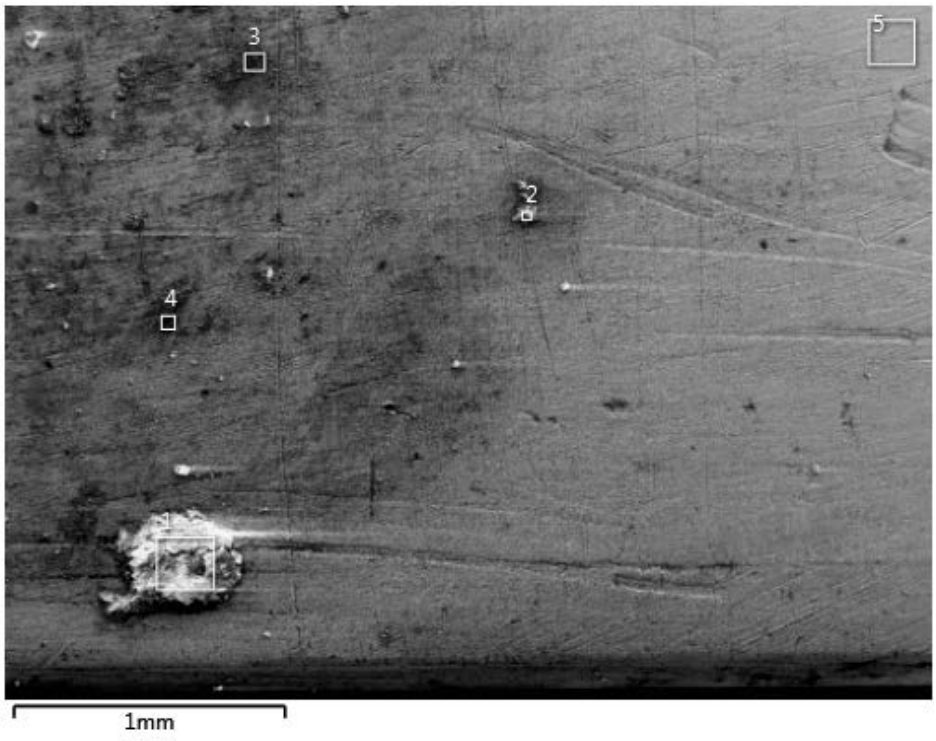

Element (Wt%)	1	2	3	4	5
C	7.25	5.94	4.97	6.41	5.54
O	43.35	37.88	31.55	31.42	1.80
Na	0.31	0.52	0.30	0.67	0.14
Mg	1.22	1.06	1.07	1.23	0.16
Al	8.59	7.89	6.23	5.84	0.28
Si	22.32	21.93	15.21	14.91	1.20
S	0.94	0.75	3.53	4.11	4.33
Cl	2.37	2.87	3.15	3.43	0.15
Ca	3.60	4.55	2.78	3.39	0.10
Fe	2.70	2.10	1.38	1.20	0.12
Cu	7.35	14.51	29.84	27.40	86.17
Total:	**100.00**	**100.00**	**100.00**	**100.00**	**100.00**

MiniCan 4 copper electrode 6:1, analysis 1

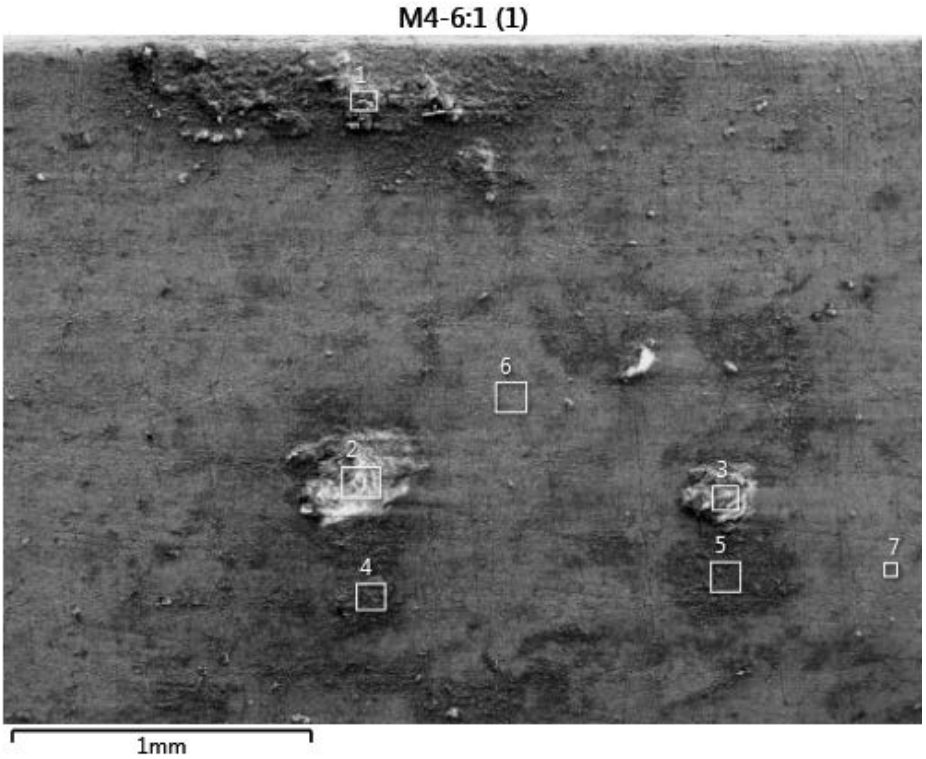

Element (Wt%)	1	2	3	4	5	6	7
C	19.07	9.78	16.10	9.59	3.92	2.84	3.55
O	31.09	32.02	30.40	28.41	32.18	6.16	7.37
Na	0.90	1.66	0.80	0.27	0.03	0.30	0.33
Mg	0.92	0.97	0.74	1.04	0.92	0.56	0.34
Al	5.70	6.45	5.05	4.49	6.21	0.73	1.06
Si	13.86	17.01	13.32	12.79	15.99	2.80	2.80
S	0.31	0.09	0.30	0.33	0.12	4.92	4.88
Cl	6.05	8.21	7.56	9.93	8.48	0.87	1.08
K	0.30	0.09	0.06		0.12		
Ca	3.30	4.07	4.38	4.91	4.33	0.76	0.81
Fe	1.85	2.00	2.09	1.46	1.79	0.18	0.22
Cu	16.65	17.66	19.21	26.77	25.91	79.52	77.57
Sn						0.36	
Total:	**100.00**	**100.00**	**100.00**	**100.00**	**100.00**	**100.00**	**100.00**

MiniCan 4 copper electrode 6:1, analysis 2

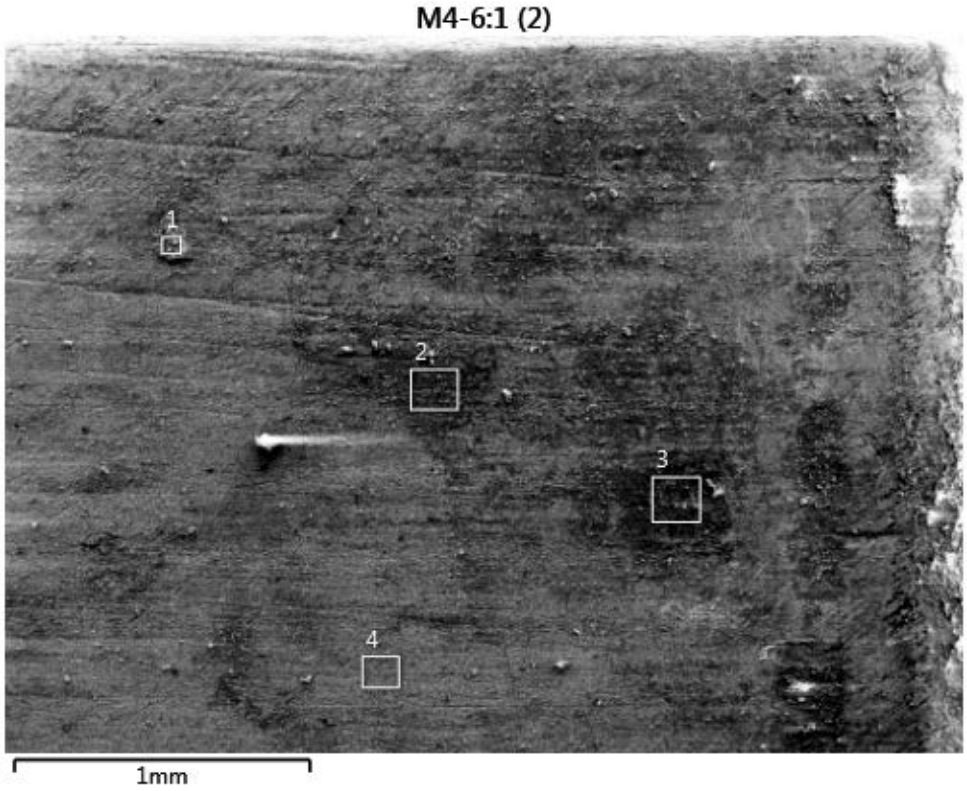

Element (Wt%)	1	2	3	4
C	14.15	4.60	4.46	4.15
O	29.24	23.20	25.24	5.48
Na	6.16	5.23	1.42	2.64
Mg	0.67	0.56	0.68	0.19
Al	5.05	1.91	3.32	0.64
Si	12.52	4.73	8.17	2.06
S	0.57	4.72	5.40	5.45
Cl	12.50	7.95	4.23	2.15
K	0.30			
Ca	3.43	10.37	7.11	0.76
Fe	1.59	0.97	1.81	0.24
Cu	13.84	35.75	38.15	76.25
Total:	**100.00**	**100.00**	**100.00**	**100.00**

MiniCan 4 copper mass loss sample 7:1

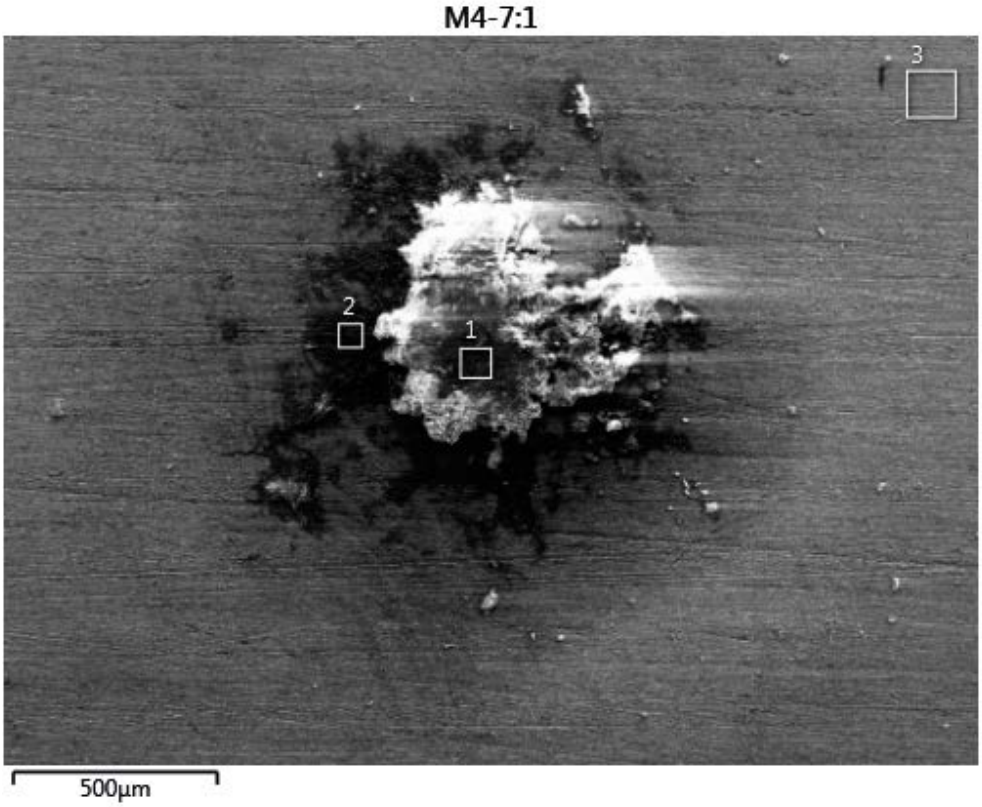

Element (Wt%)	1	2	3
C	9.42	7.19	3.34
O	48.91	42.15	2.98
Na	0.55	0.43	
Mg	1.39	1.33	
Al	8.63	7.64	0.34
Si	24.72	20.40	2.41
S	0.28	1.76	5.59
Cl	0.22	0.49	0.10
K	0.20		
Ca	2.94	4.49	0.13
Fe	1.76	1.70	0.07
Cu	0.99	12.40	85.03
Total:	**100.00**	**100.00**	**100.00**

MiniCan 4 iron electrode 9:1

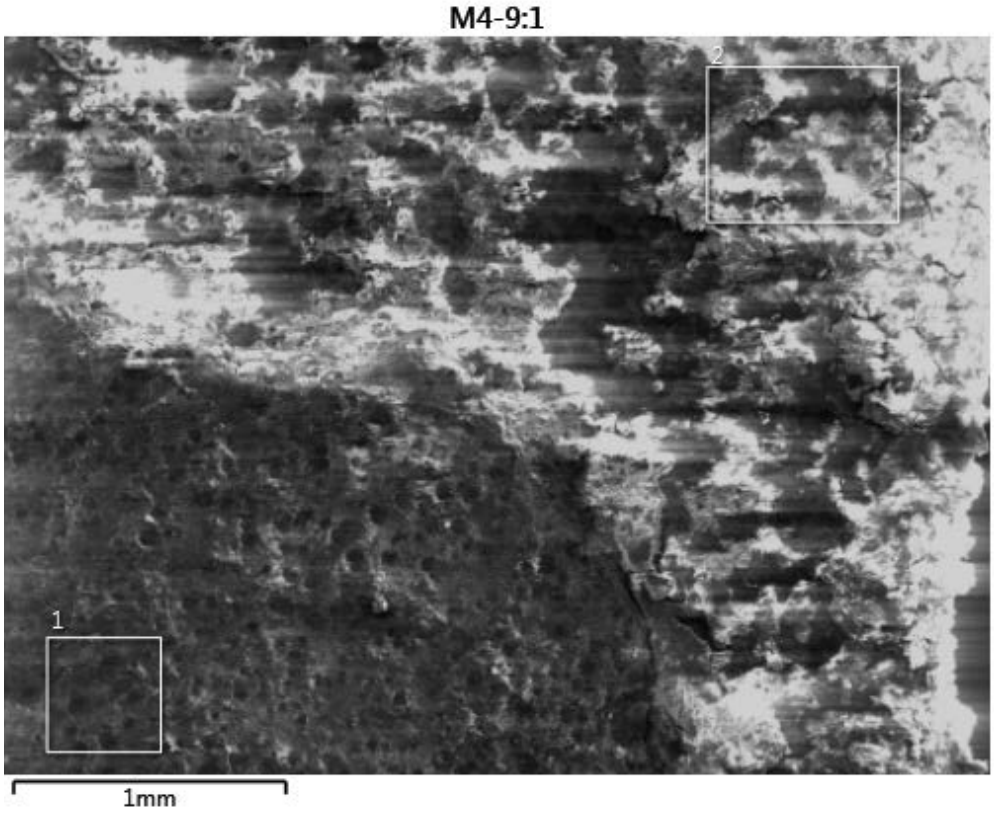

Element (Wt%)	1	2
C	22.78	5.47
O	40.78	36.10
Na	0.57	1.63
Mg	0.43	0.94
Al	2.10	6.48
Si	24.82	18.36
P	0.07	0.07
S	1.47	0.23
Cl	1.62	4.51
K	0.15	0.13
Ca	2.21	2.51
Ti		0.12
Fe	1.80	23.45
Ni	0.49	
Cu	0.71	
Total:	**100.00**	**100.00**

MiniCan 4 iron electrode 10:1, analysis 1

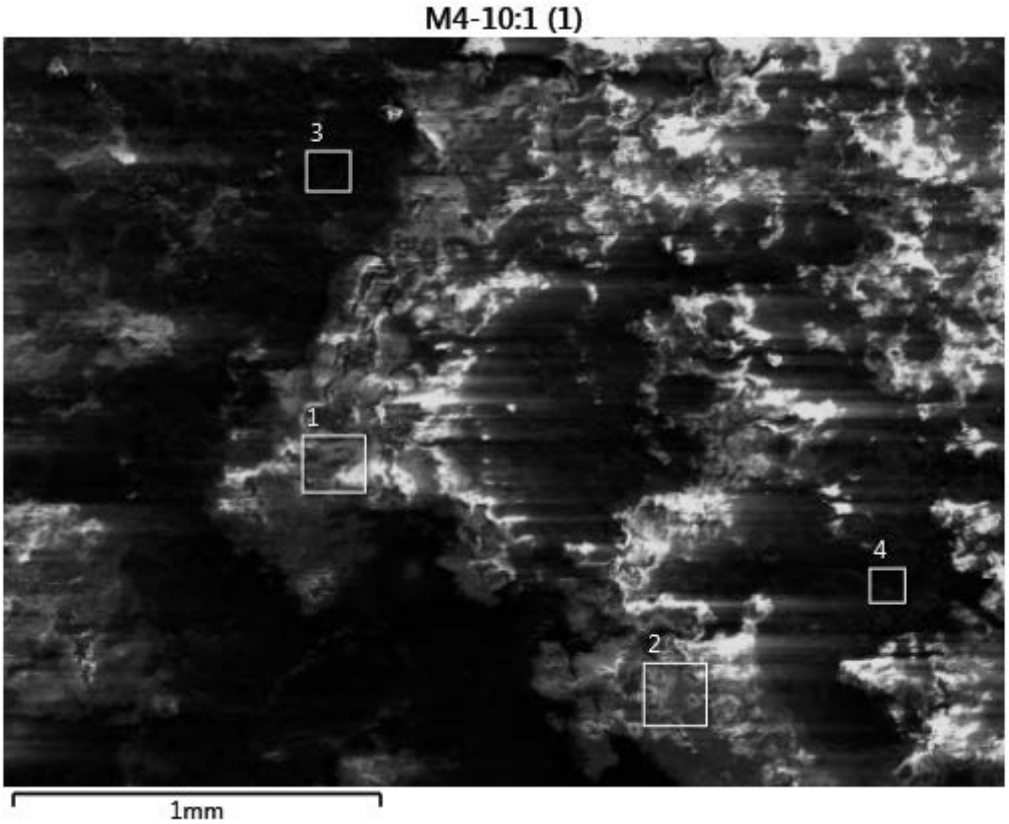

Element (Wt%)	1	2	3	4
C	5.64	5.13	19.49	7.41
O	50.61	50.24	34.82	43.29
Na	0.81	0.62	0.47	0.61
Mg	1.13	1.09	0.13	0.46
Al	8.08	7.45	0.44	1.68
Si	20.46	18.77	1.24	4.51
S	0.08	0.20	1.66	0.54
Cl	0.11	0.84	0.12	0.49
K	0.10	0.18		
Ca	8.48	11.71	24.88	22.65
Fe	4.51	3.78	15.52	17.08
W			1.25	1.28
Total:	**100.00**	**100.00**	**100.00**	**100.00**

MiniCan 4 iron electrode 10:1, analysis 2

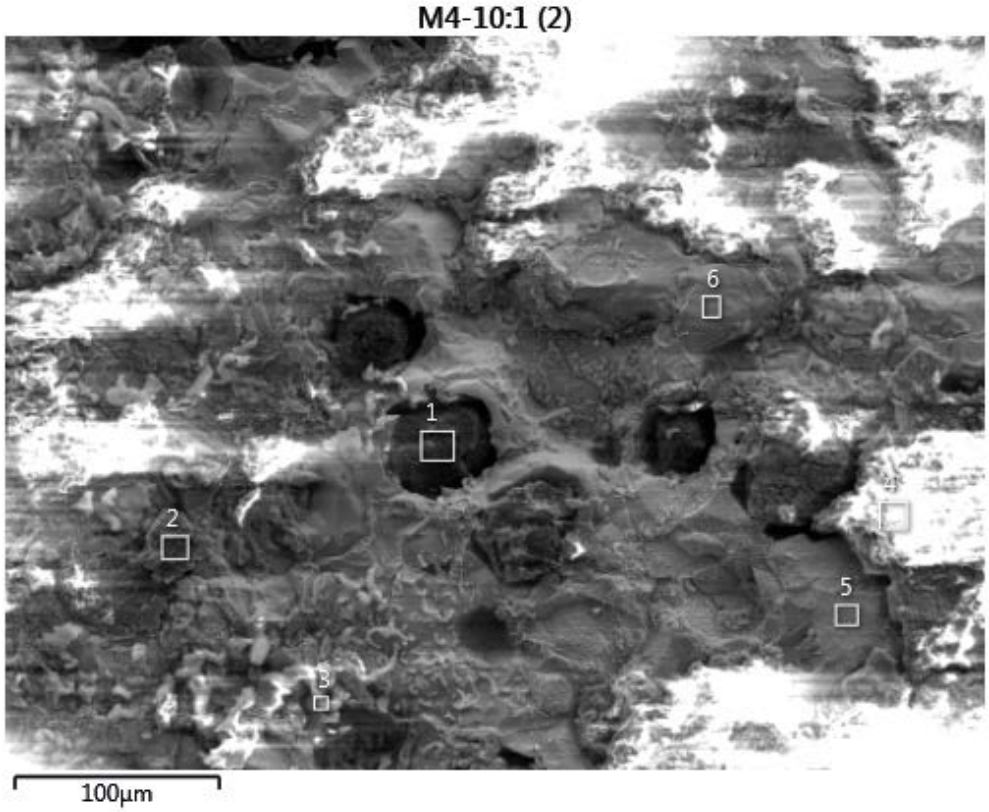

Element (Wt%)	1	2	3	4	5	6
C	76.89	46.97	4.07	5.20	3.13	2.39
O	11.51	29.03	26.41	49.66	11.45	1.38
Na	0.41	1.20	0.21	1.42	1.45	
Mg	0.14	0.38		1.06		
Al	0.38	2.08	0.16	6.27	0.11	0.09
Si	1.15	8.17	1.70	17.06	2.64	2.77
S	1.64	0.96	0.91	0.20	0.59	0.43
Cl	0.74	0.77	5.29		0.75	0.10
Ca	0.53	0.91	0.50	14.02	0.24	0.07
Ti			0.44			
Cr			0.27		0.05	0.17
Fe	6.60	9.52	60.05	5.10	79.58	92.60
Total:	**100.00**	**100.00**	**100.00**	**100.00**	**100.00**	**100.00**

MiniCan 4 iron mass loss sample 11:1, analysis 1

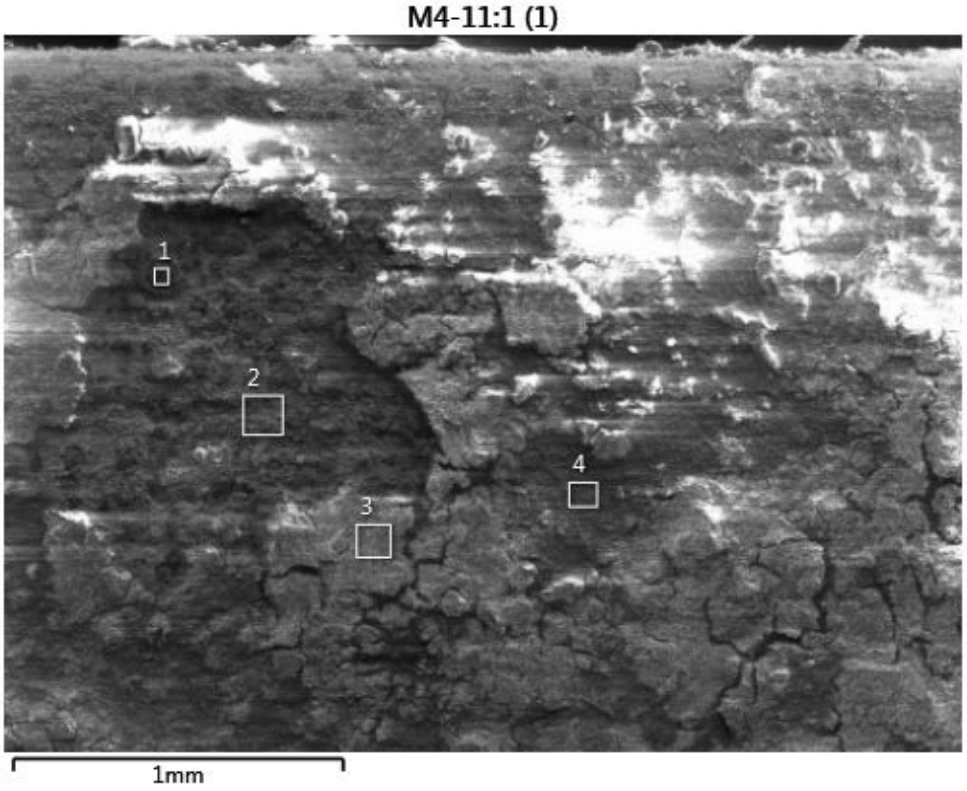

Element (Wt%)	1	2	3	4
C	35.38	3.68	3.53	3.55
O	29.94	19.28	47.53	47.37
Na	0.48	0.86	0.96	0.81
Mg	0.38	0.26	1.52	1.29
Al	2.65	1.47	11.13	9.52
Si	10.54	5.28	28.48	25.01
S	0.34	0.93	0.09	0.26
Cl	1.76	2.08	0.85	0.64
K			0.18	0.12
Ca	2.32	0.34	1.95	4.59
Cr	0.62	0.15		
Fe	15.59	65.10	3.79	6.83
Ni		0.57		
Total:	**100.00**	**100.00**	**100.00**	**100.00**

MiniCan 4 iron mass loss sample 11:1, analysis 2

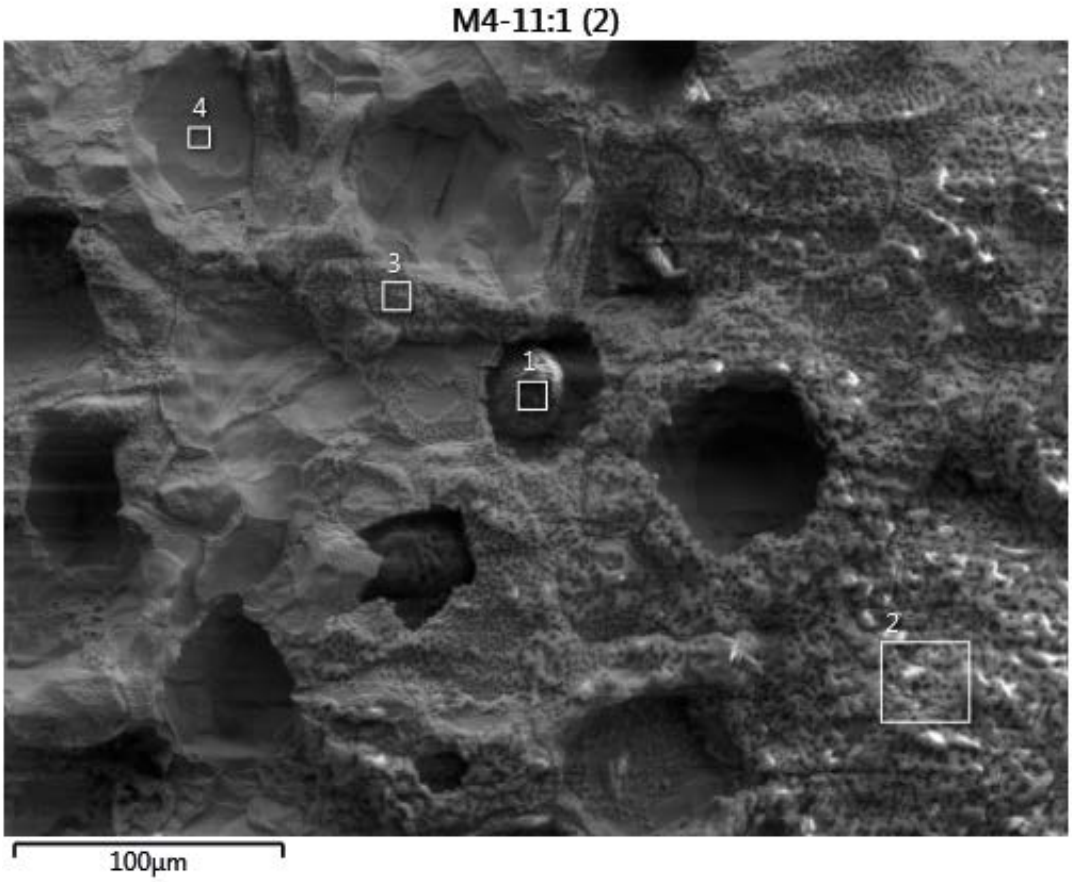

Element (Wt%)	1	2	3	4
C	93.33	5.77	3.91	1.87
O	4.05	29.56	22.01	1.84
Na	0.06	2.03	1.77	0.09
Mg	0.14		0.04	0.10
Al		0.06	0.04	
Si	0.07	1.58	2.08	2.11
P		0.12		
S	0.11	0.44	0.26	0.26
Cl	0.09	1.01	0.57	0.03
Ca	0.09		0.09	
Fe	2.07	59.43	69.23	93.69
Total:	**100.00**	**100.00**	**100.00**	**100.00**

MiniCan 4 copper sandwich sample 14:1, analysis 1

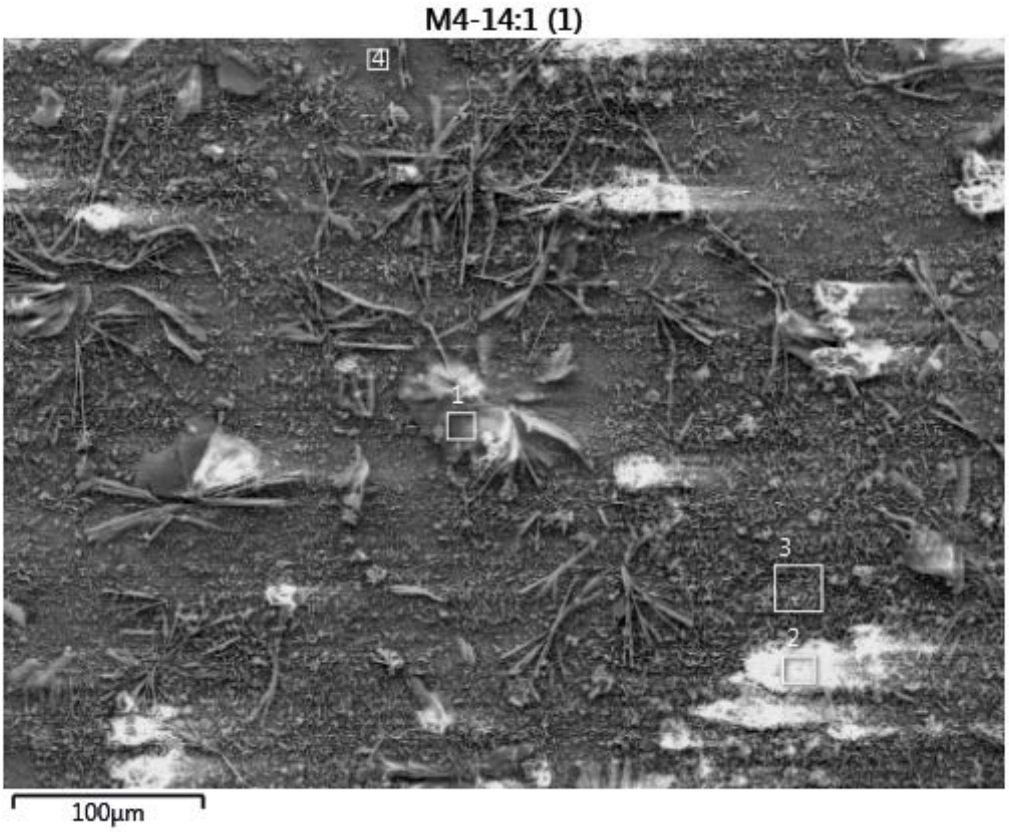

Element (Wt%)	1	2	3	4
C	4.05	3.81	3.76	6.09
O	32.73	25.75	23.82	13.14
Na	1.24			
Mg	0.69	0.62	0.52	0.25
Al		0.15		
Si	0.55	0.64	0.58	2.97
S	2.17	0.18	0.20	0.41
Cl	1.64	2.33	3.55	0.38
Ca	0.67	0.42	0.27	0.20
Fe	45.99	52.24	39.29	8.62
Cu	10.27	13.85	28.00	67.96
Total:	**100.00**	**100.00**	**100.00**	**100.00**

MiniCan 4 copper sandwich sample 14:1, analysis 2

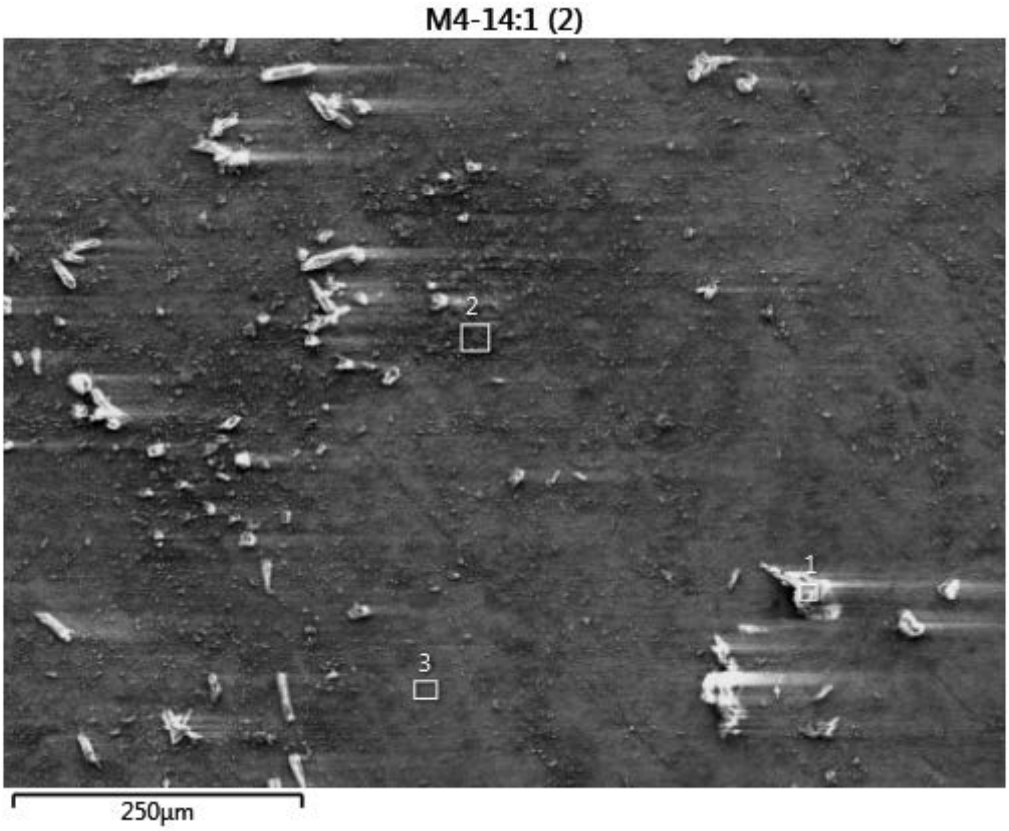

Element (Wt%)	1	2	3
C	9.03	6.43	6.80
O	18.59	27.53	12.58
Na	0.53	0.50	0.12
Mg	0.39	0.46	0.31
Al	0.30	0.59	0.22
Si	4.26	4.50	2.39
S	0.54	0.49	0.19
Cl	1.59	3.16	0.87
Ca	0.56	0.87	0.28
Fe	13.37	34.60	8.07
Cu	50.83	20.87	68.17
Total:	**100.00**	**100.00**	**100.00**

MiniCan 4 copper sandwich sample 14:1, analysis 3

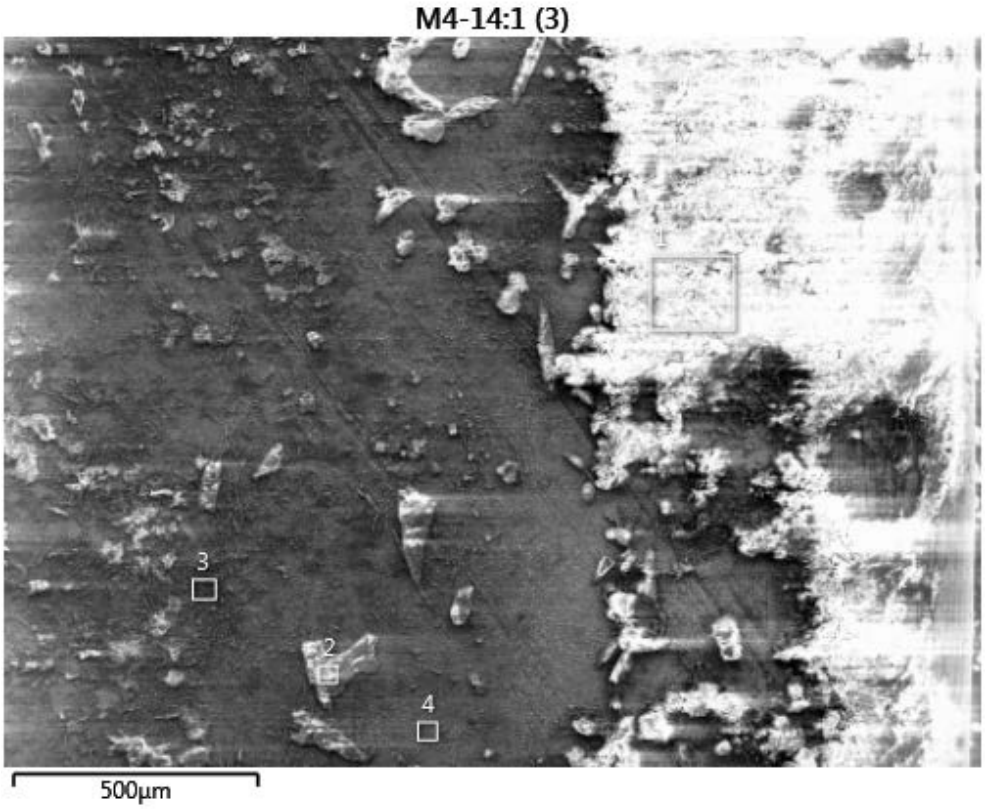

Element (Wt%)	1	2	3	4
C	7.63	8.64	11.59	7.84
O	41.05	37.25	30.82	19.16
Na	0.69	0.55	0.74	0.25
Mg	1.33	0.50	0.61	0.51
Al	6.53	1.10	0.94	0.56
Si	20.17	12.13	15.70	6.42
S	0.29	0.83	0.45	0.99
Cl	0.96	1.39	0.93	1.36
K	0.16			
Ca	4.28	7.15	0.89	0.68
Fe	15.86	26.27	26.38	9.97
Cu	1.06	4.19	10.95	52.27
Total:	**100.00**	**100.00**	**100.00**	**100.00**

MiniCan 4 iron sandwich sample 15:1, analysis 1

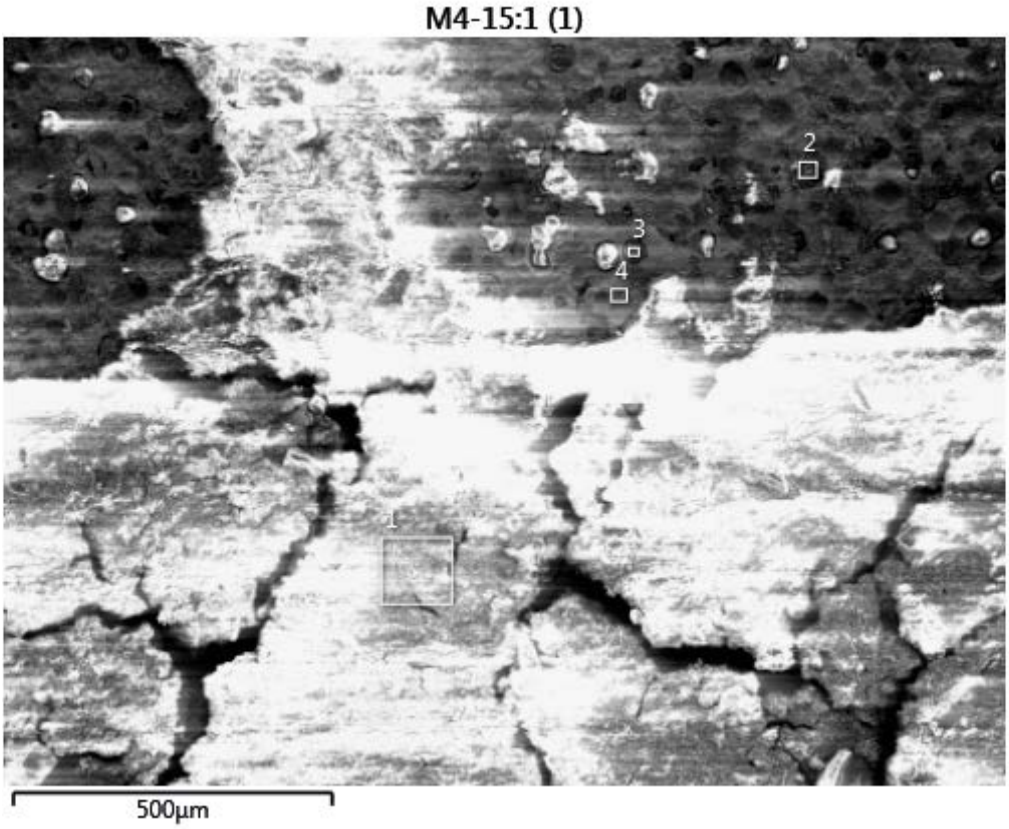

Element (Wt%)	1	2	3	4
C	6.94	20.03	45.81	2.61
O	46.66	39.54	24.65	3.73
Na	0.38	0.42	0.38	0.01
Mg	1.28	0.99	0.33	0.38
Al	7.94	5.48	0.40	0.47
Si	21.78	14.58	7.58	3.25
S	0.76	0.30	0.64	0.32
Cl	0.57	0.31	0.23	0.11
K	0.12	0.06		0.07
Ca	7.00	9.30	1.31	2.06
Fe	6.56	8.99	18.68	86.98
Total:	**100.00**	**100.00**	**100.00**	**100.00**

MiniCan 4 iron sandwich sample 15:1, analysis 2

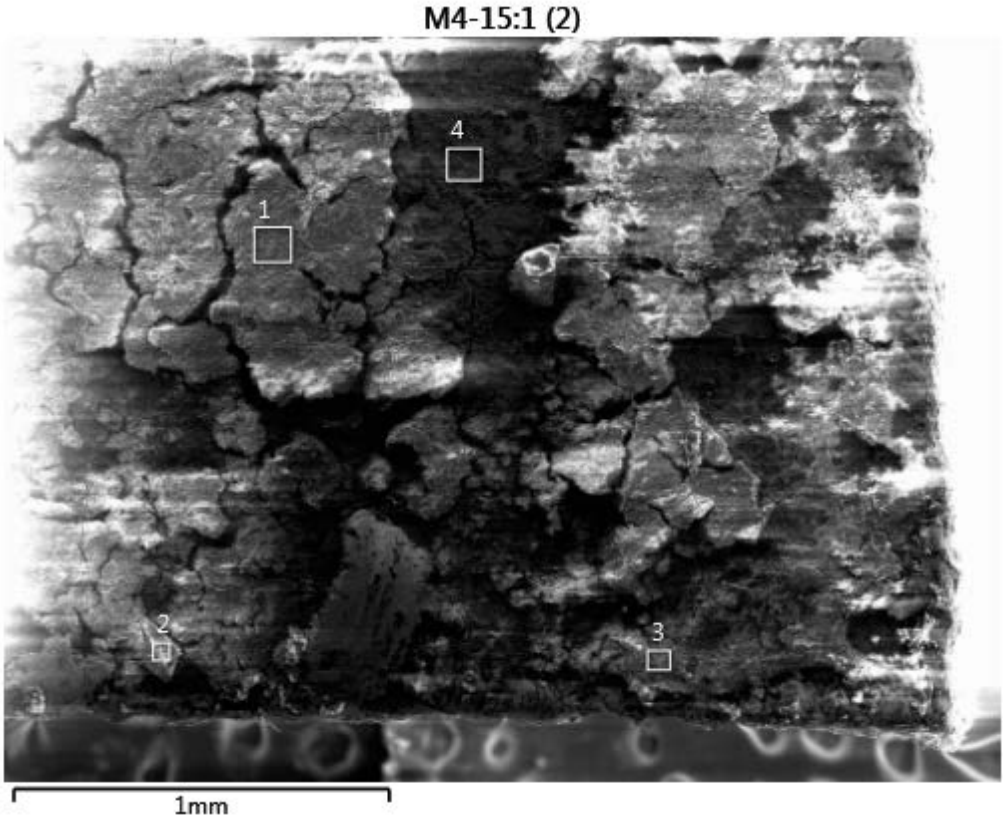

Element (Wt%)	1	2	3	4
C	5.52	11.69	16.94	6.07
O	50.52	46.19	43.50	44.52
Na	0.71	4.03	0.67	0.52
Mg	1.43	0.52	1.09	0.94
Al	9.75	9.44	7.33	6.14
Si	25.72	23.50	22.28	16.55
S	0.37	0.08	0.19	0.43
Cl	0.49	0.29	0.36	0.44
K	0.13	0.60	0.31	0.10
Ca	1.89	2.20	3.59	10.37
Fe	3.47	1.47	3.74	13.91
Total:	**100.00**	**100.00**	**100.00**	**100.00**

MiniCan 4 copper canister inner surface 24:1

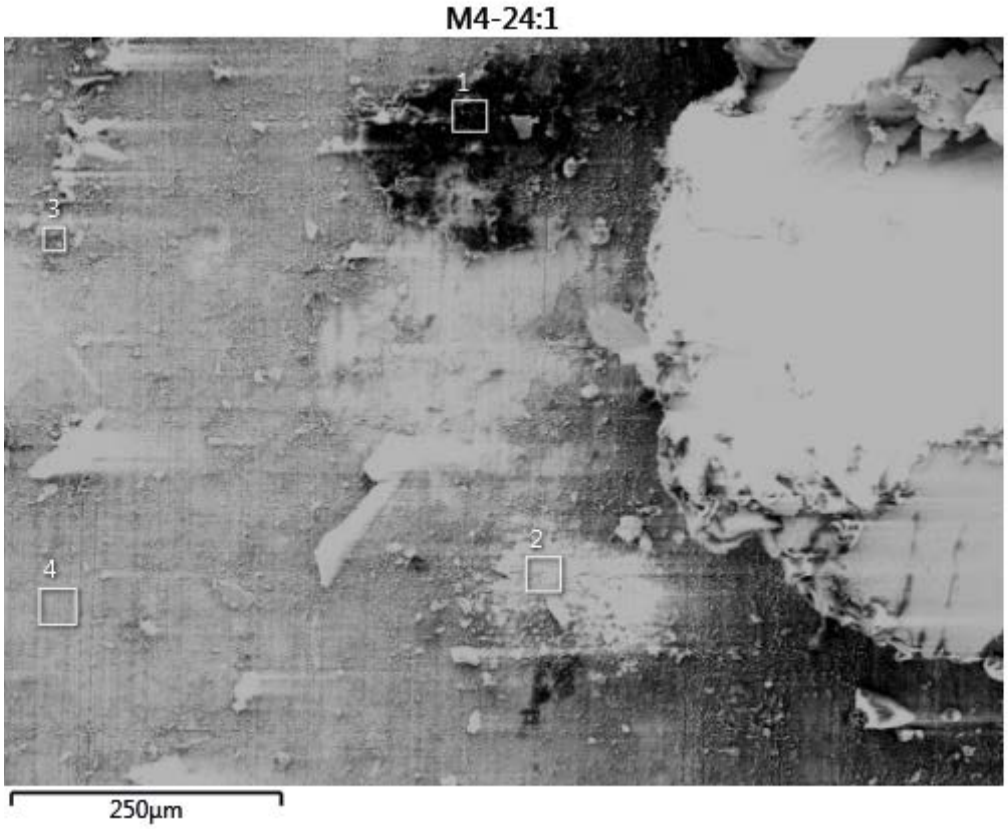

Element (Wt%)	1	2	3	4
C	73.74	10.75	13.52	14.88
O	5.23	36.49	17.35	20.91
Na	0.52	0.53	1.42	0.67
Mg	0.08	1.05	0.40	0.10
Al	0.31	7.00	1.91	0.45
Si	1.00	17.36	4.91	1.45
P	0.04	0.07		0.08
S	0.17	0.39	0.23	0.19
Cl	2.25	5.39	7.81	1.51
Ca	0.96	4.01	1.58	0.85
Fe	9.40	4.55	27.10	23.70
Cu	6.31	12.40	23.79	35.20
Total:	**100.00**	**100.00**	**100.00**	**100.00**

MiniCan 4 copper canister outer surface 25:1, analysis 1

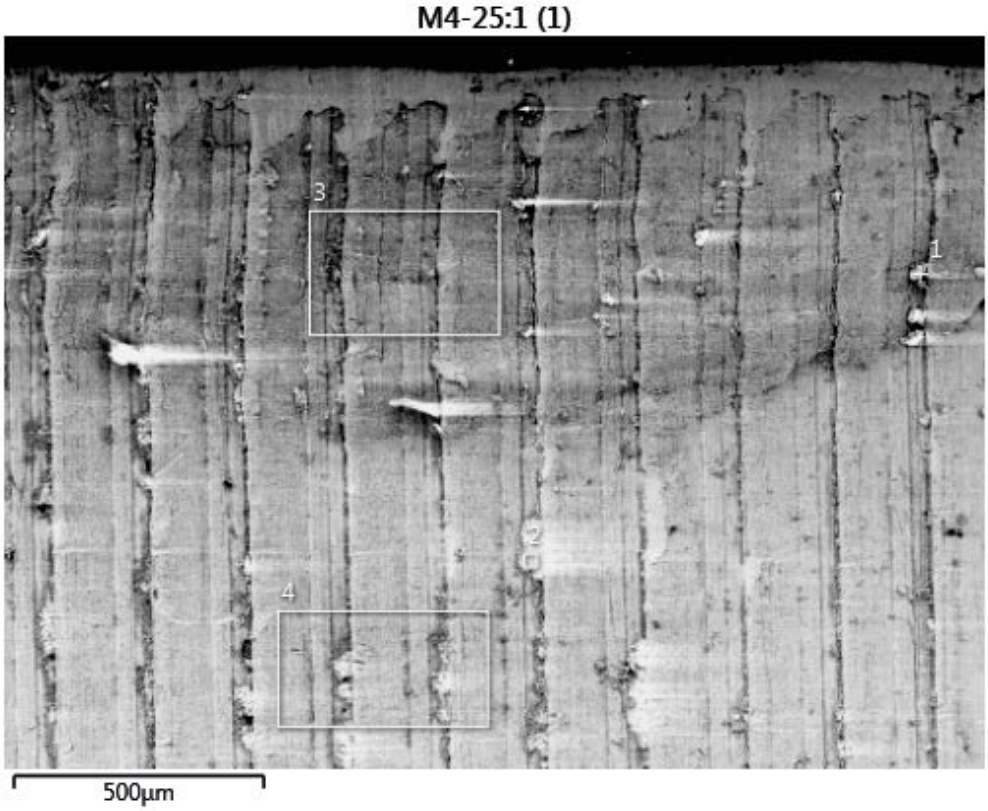

Element (Wt%)	1	2	3	4
C	21.06	13.92	6.97	6.74
O	13.78	34.14	5.12	10.55
Na	10.15	0.06	1.53	1.14
Mg	0.03	0.94	0.13	0.43
Al	0.34	6.43	0.78	1.96
Si	0.60	15.38	1.70	4.28
P		0.20		
S	0.12	0.08	2.53	2.29
Cl	20.45	5.81	2.61	2.89
Ca	2.33	3.00	1.13	1.39
Ti		0.46		
Mn		0.49		
Fe	1.20	5.56		0.44
Cu	29.95	13.54	77.50	67.89
Total:	**100.00**	**100.00**	**100.00**	**100.00**

MiniCan 4 copper canister outer surface 25:1, analysis 2

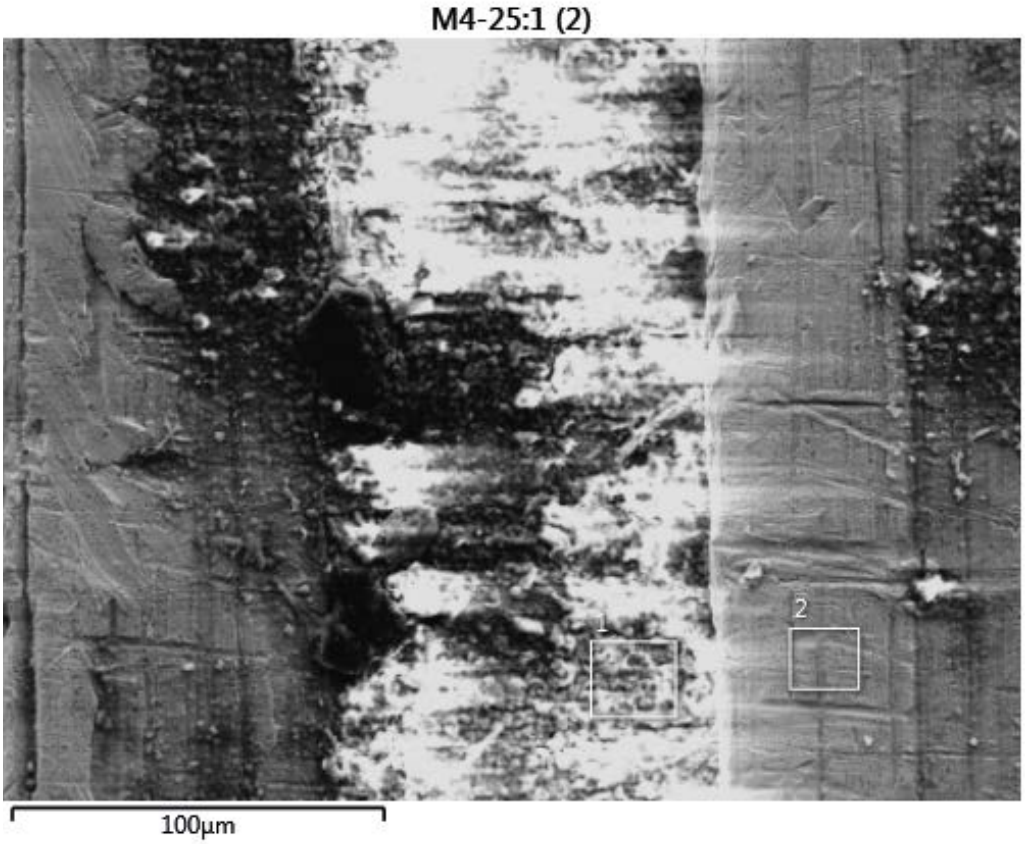

Element (Wt%)	1	2
C	5.53	5.11
O	36.25	3.50
Na	1.25	0.18
Mg	1.18	0.12
Al	7.94	0.49
Si	19.47	1.07
S	0.69	2.71
Cl	6.00	0.49
Ca	3.56	0.15
Ti	0.37	0.07
Fe	1.94	0.08
Cu	15.81	86.03
Total:	**100.00**	**100.00**

MiniCan 4 copper canister outer surface 25:1, cross sections of surface defects

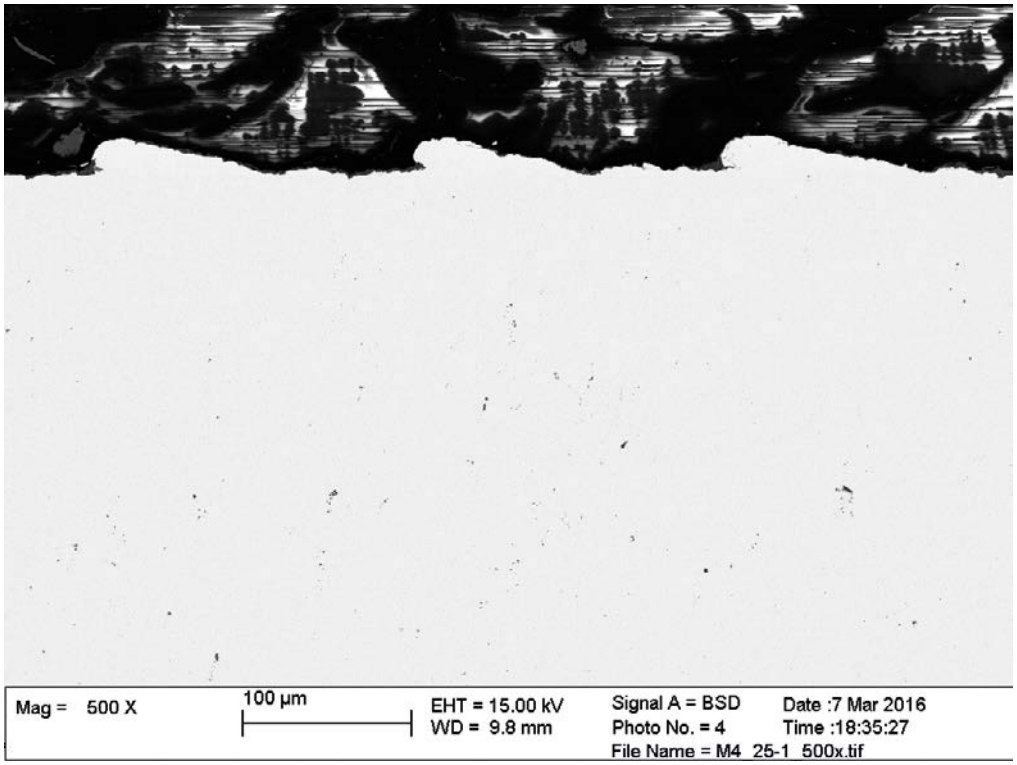

Machining marks.

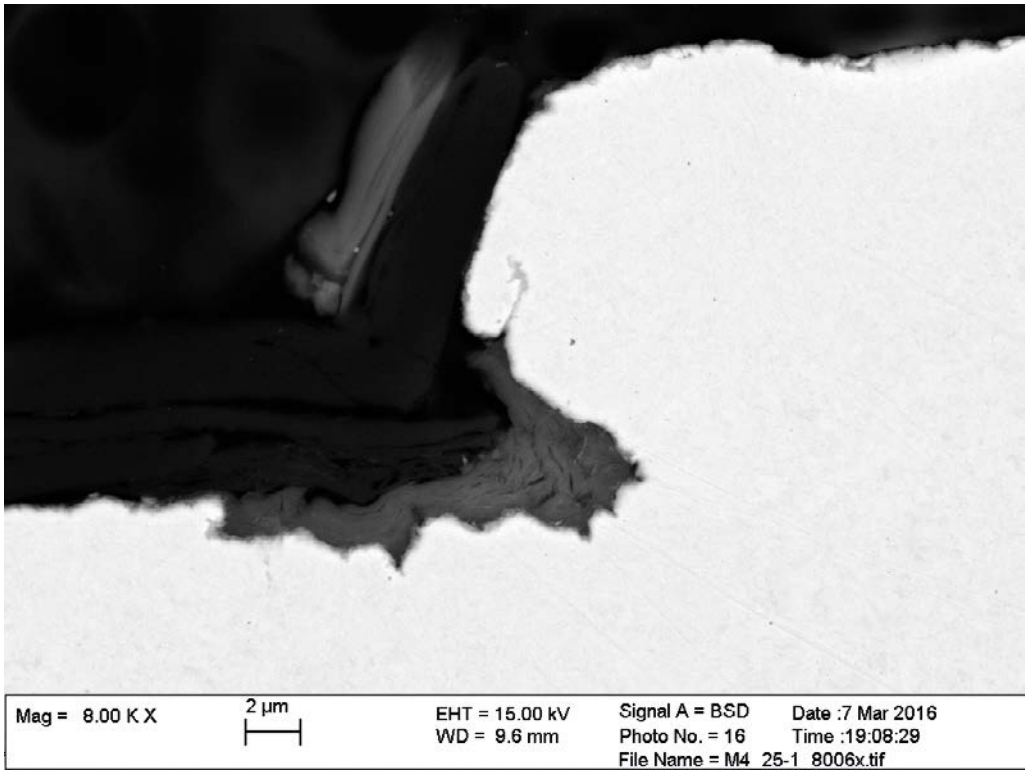

Detail of area at machining mark.

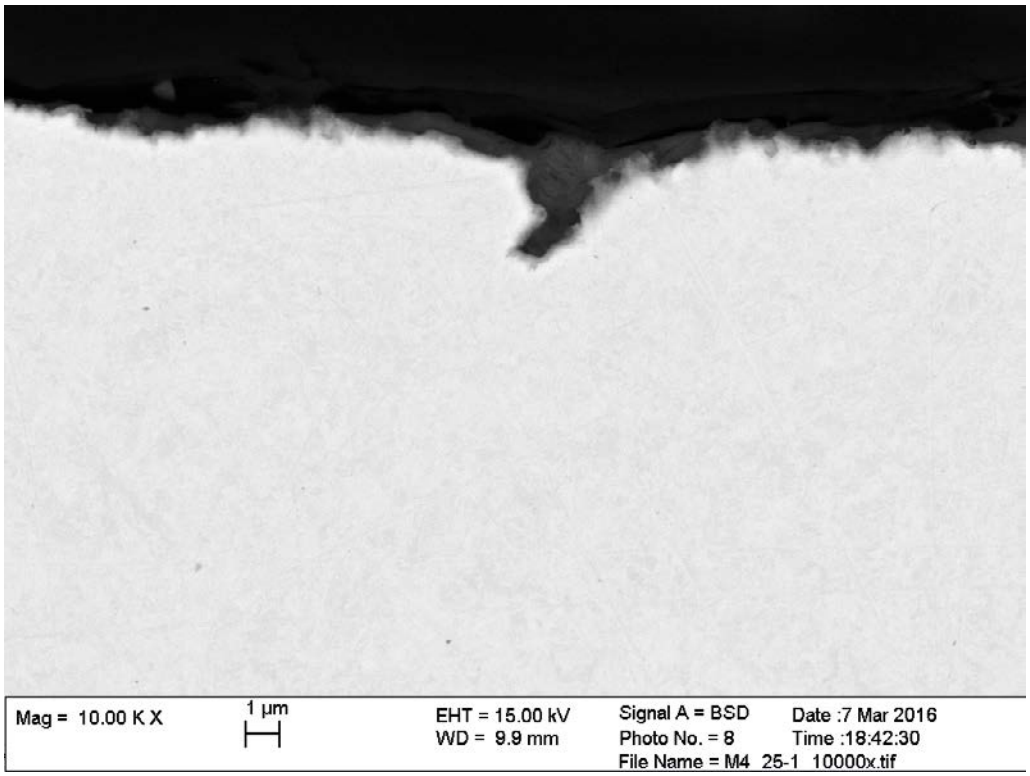

Small pit in surface, about 3 µm deep.

MiniCan 4 copper canister outer surface 25:1, cross section 1

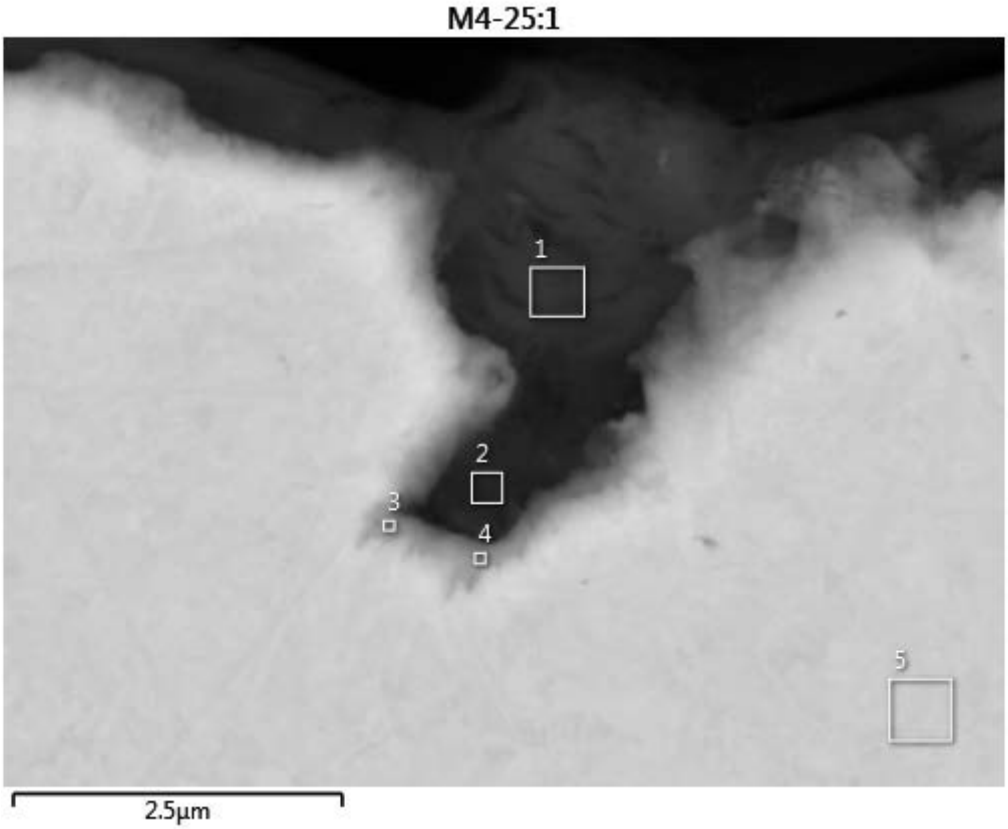

Element (Wt%)	1	2	3	4	5
C	16.49	7.68	5.43	9.22	4.88
O	36.68	31.55	8.08	13.38	
Mg	1.51	1.26	0.57	0.56	
Al	10.10	8.73	2.06	3.28	
Si	26.40	21.69	4.98	7.86	
S	0.24	1.69	5.64	5.75	
Cl	0.17	1.16	0.36	0.64	
K	0.19	0.13			
Ca	0.61	1.04	0.37	0.52	
Fe	3.28	2.89	1.16	0.94	0.75
Cu	4.34	22.17	71.36	57.84	94.37
Total:	**100.00**	**100.00**	**100.00**	**100.00**	**100.00**

MiniCan 4 copper canister outer surface 25:1, cross section 2

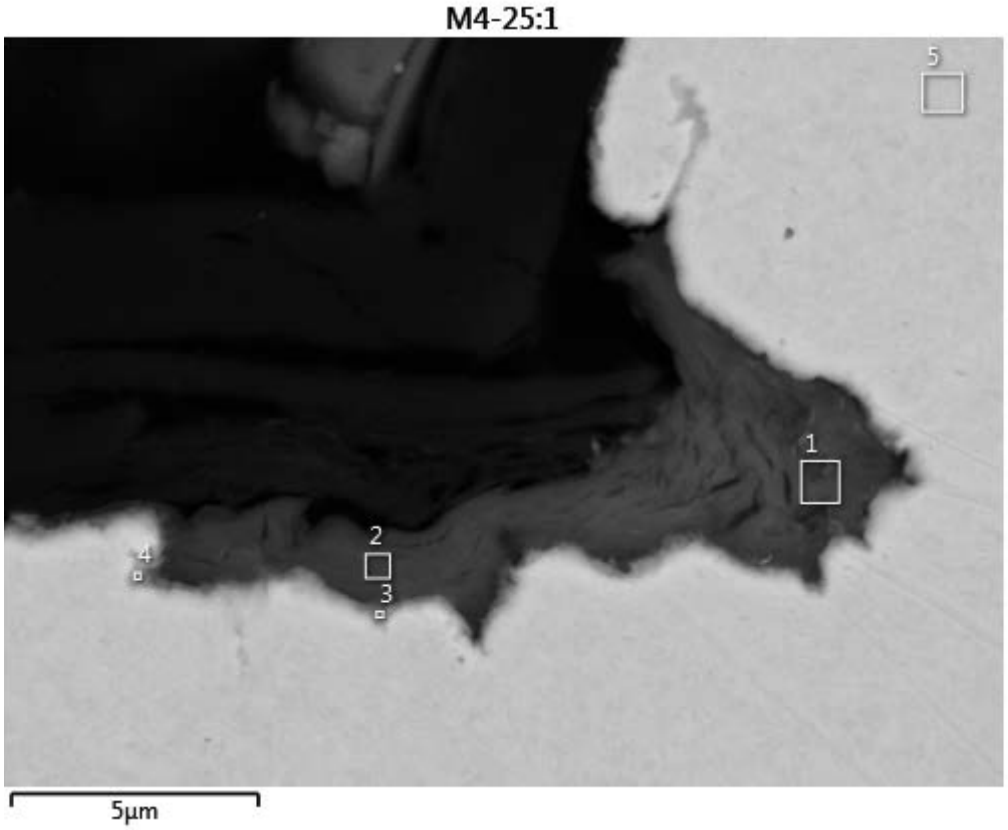

Element (Wt%)	1	2	3	4	5
C	7.78	30.98	10.31	6.27	4.35
O	35.57	30.47	17.63	7.41	
Mg	1.23	1.24	0.84	0.36	
Al	8.89	6.92	4.88	1.80	
Si	21.05	17.56	10.54	3.61	
S	0.08	0.14	2.41	5.98	
Cl	2.79	1.20	1.75	0.38	
K	0.20	0.10			
Ca	1.27	0.55	0.53	0.42	
Fe	3.52	2.08	1.22	0.69	0.93
Cu	17.62	8.77	49.88	73.08	94.72
Total:	100.00	100.00	100.00	100.00	100.00

MiniCan 4 copper canister weld surface 26:1

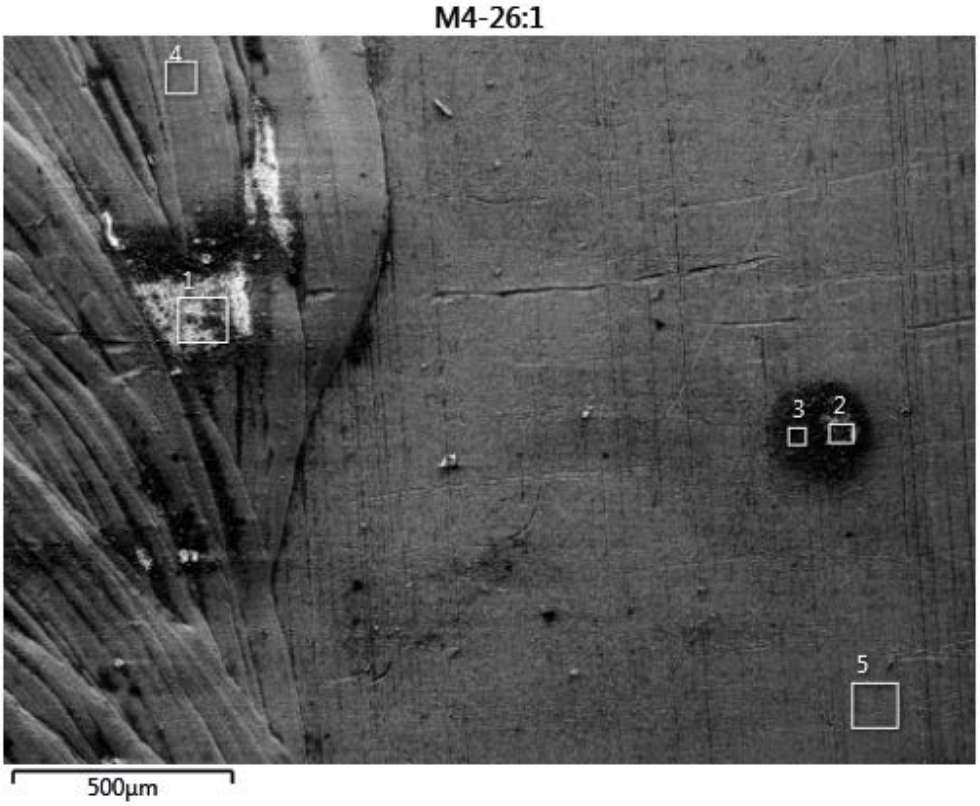

Element (Wt%)	1	2	3	4	5
C	12.59	10.11	6.84	5.34	3.88
O	37.05	34.62	31.79	3.02	2.64
Na	1.44	1.32	1.57	0.40	0.78
Mg	1.46	1.27	1.18	0.25	0.07
Al	8.00	7.89	7.22	0.50	0.55
Si	20.42	19.14	16.59	0.83	0.90
S	0.63	0.73	1.55	6.31	2.57
Cl	4.09	5.90	4.75	0.69	0.34
Ca	2.62	3.18	2.98	0.35	0.11
Ti	0.79	0.53	0.80	0.11	0.06
Fe	3.20	3.04	2.41	0.18	0.18
Cu	7.72	12.26	22.30	82.01	87.93
Total:	**100.00**	**100.00**	**100.00**	**100.00**	**100.00**

MiniCan 4 copper canister weld surface 26:1, cross section

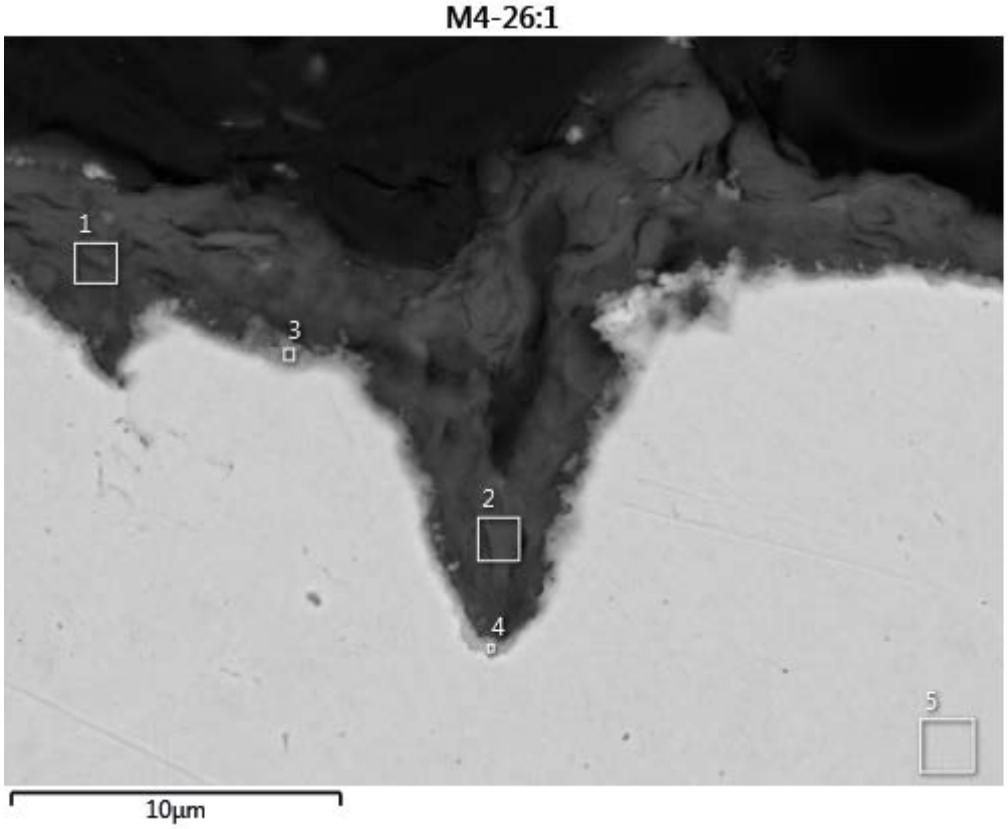

Element (Wt%)	1	2	3	4	5
C	11.53	8.92	8.81	5.32	3.15
O	38.09	42.16	25.46	9.42	
Mg	3.46	1.44	1.23	0.30	
Al	9.29	10.07	7.05	2.15	
Si	23.45	24.84	16.62	4.31	
S	0.69	0.08	0.97	8.77	
Cl	0.29	0.83	0.51	0.63	
Ca	1.15	1.39	0.83	0.45	
Fe	3.80	3.03	2.11	0.44	
Cu	5.81	7.24	36.42	68.21	96.85
Ba	2.45				
Total:	**100.00**	**100.00**	**100.00**	**100.00**	**100.00**

MiniCan 4 copper canister inner surface near hole 27:1, analysis 1

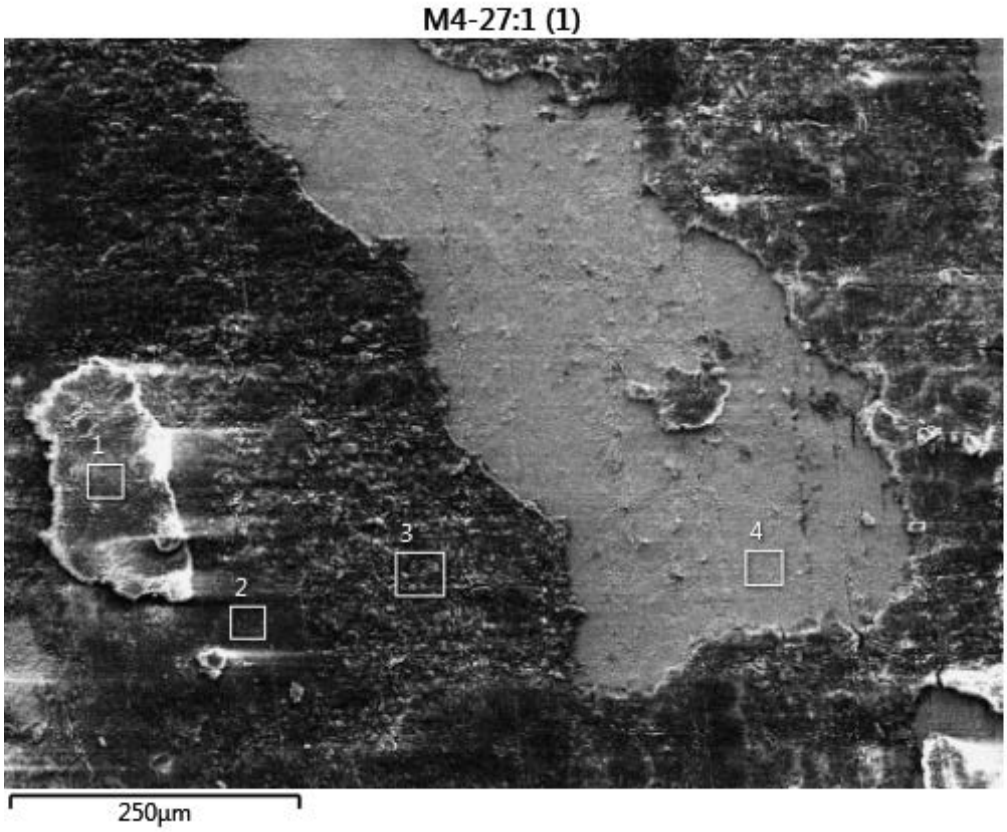

Element (Wt%)	1	2	3	4
C	3.14	2.67	6.08	3.29
O	41.13	42.37	40.15	0.88
Na	0.15	0.19	0.33	0.03
Mg	0.86	1.07	1.26	0.07
Al	7.00	8.57	8.95	0.19
Si	18.78	21.70	25.57	0.28
S	0.17		0.09	
Cl	0.47	0.05	0.18	
K		0.06	0.08	
Ca	0.20	0.55	1.12	0.08
Ti			0.21	
Fe	26.37	20.76	11.23	0.27
Cu	1.74	2.00	4.76	94.90
Total:	**100.00**	**100.00**	**100.00**	**100.00**

MiniCan 4 copper canister inner surface near hole 27:1, analysis 2

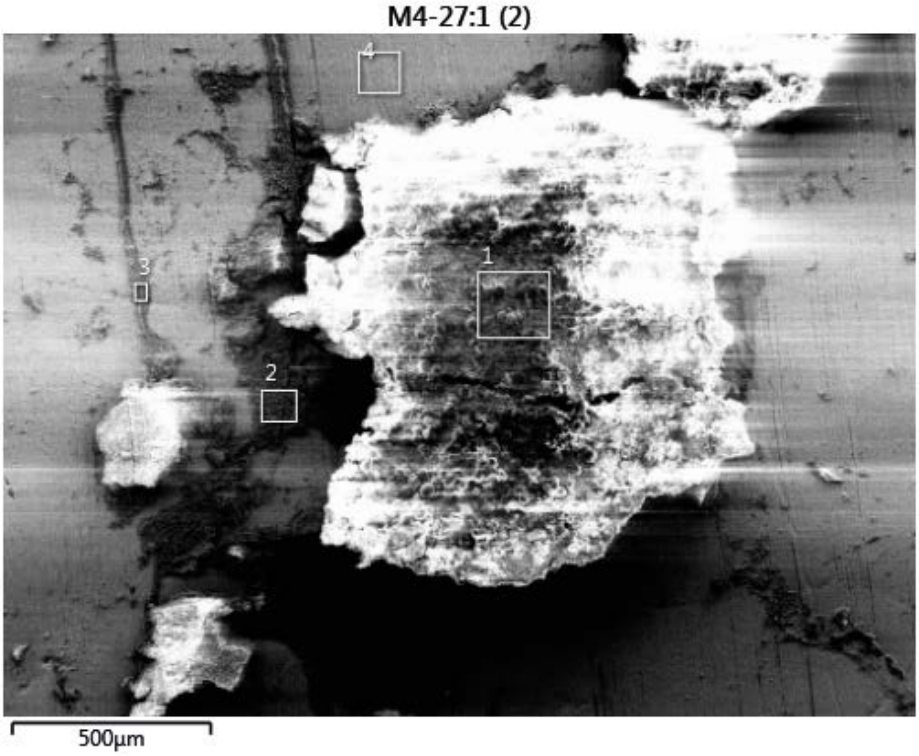

Element (Wt%)	1	2	3	4
C	41.62	5.00	4.98	4.73
O	23.18	38.57	17.02	3.26
Na		0.68	0.31	
Mg	0.29	0.94	0.36	
Al	1.84	7.18	2.05	0.37
Si	6.92	23.25	10.83	0.81
P	0.88		0.12	0.20
S	1.04	0.14	0.03	0.09
Cl	1.80	0.95	1.50	1.41
K		0.10		
Ca	0.68	1.12	0.31	
Ti	0.98			
Cr	0.48			
Fe	16.84	14.96	4.55	0.66
Ni	1.38			
Cu	2.06	7.11	57.93	88.48
Total:	**100.00**	**100.00**	**100.00**	**100.00**

MiniCan 4 copper canister inner surface near hole 27:1, analysis 3

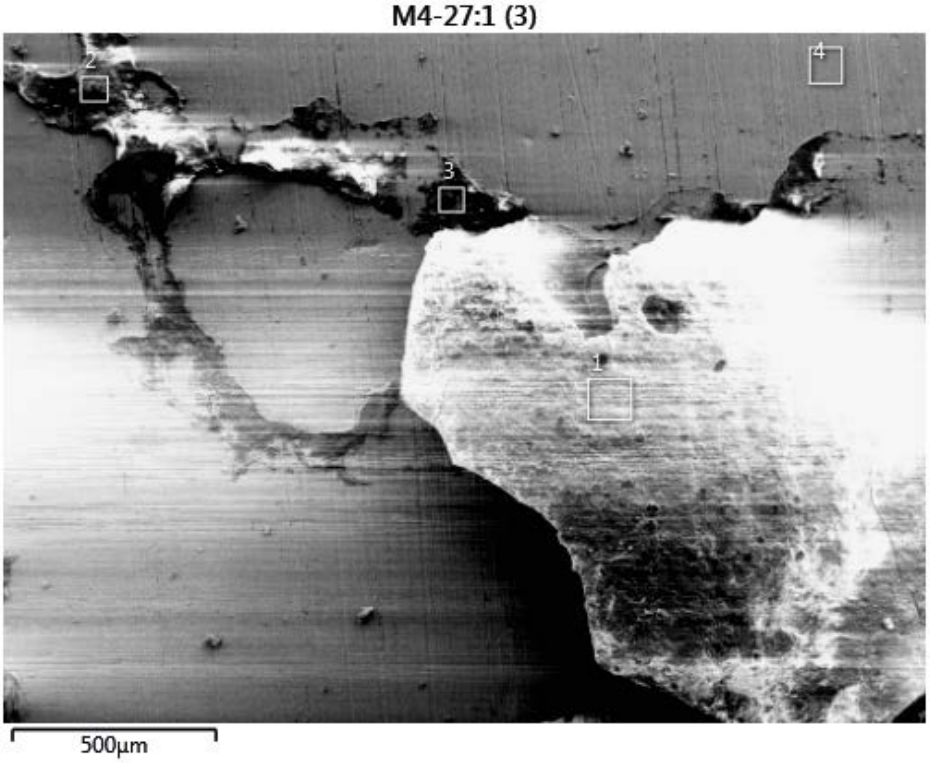

Element (Wt%)	1	2	3	4
C	11.18	12.80	11.04	4.44
O	42.06	37.29	30.41	1.11
Na	0.40	0.14	0.22	
Mg	0.09	0.34	0.32	
Al	1.03	2.20	1.92	0.10
Si	15.01	18.89	15.30	0.25
P	0.18	0.12	0.06	
S	1.62	0.20	0.31	
Cl	0.43	0.30	0.50	
Ca	1.69	0.42	0.42	0.10
Ti	0.12			
Cr	0.21			
Fe	25.59	25.24	20.59	0.68
Cu	0.38	2.04	18.91	93.32
Total:	**100.00**	**100.00**	**100.00**	**100.00**

MiniCan 4 copper canister inner surface near hole 27:1, analysis 4

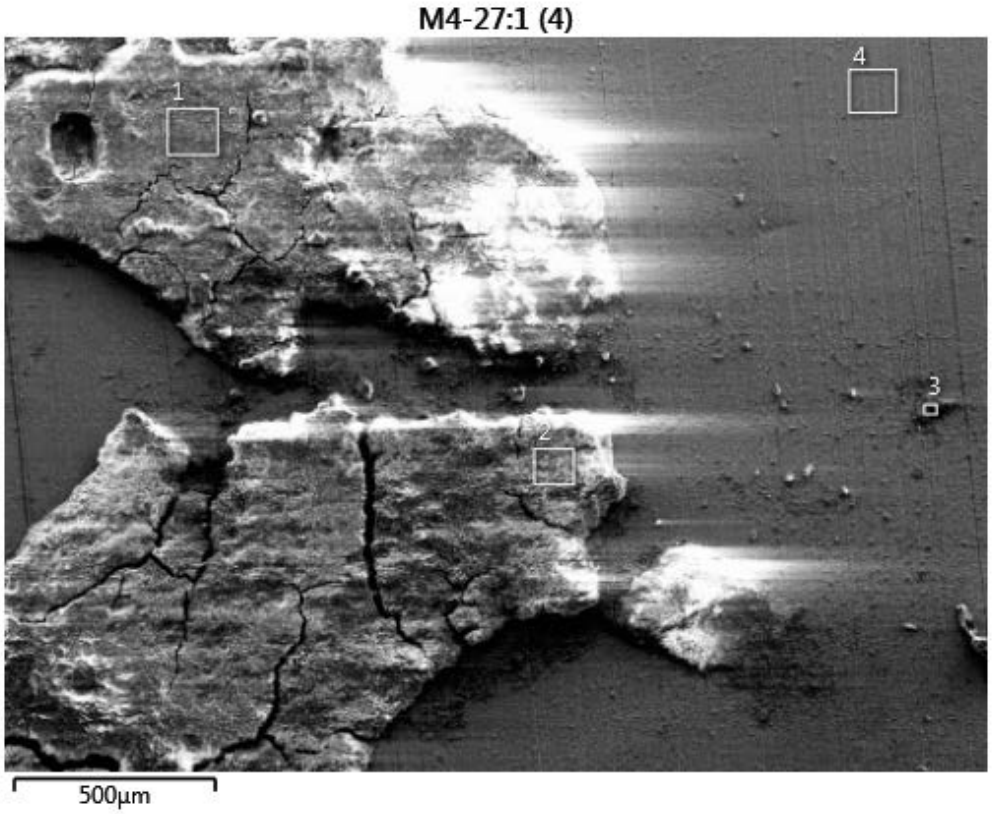

Element (Wt%)	1	2	3	4
C	5.31	5.37	8.64	5.19
O	40.66	39.00	23.31	3.17
Na	0.58	1.13	1.32	0.25
Mg	0.65	0.79	0.17	
Al	4.27	3.90	0.43	0.15
Si	15.22	12.23	5.25	0.59
P			0.16	0.06
S	0.56	1.70	1.72	0.14
Cl	1.32	4.67	5.38	0.48
Ca	0.43	2.38	2.37	0.16
Fe	29.80	24.46	44.75	1.40
Cu	1.20	4.36	6.51	88.41
Total:	**100.00**	**100.00**	**100.00**	**100.00**

MiniCan 4 bentonite sample from near canister hole 28:1

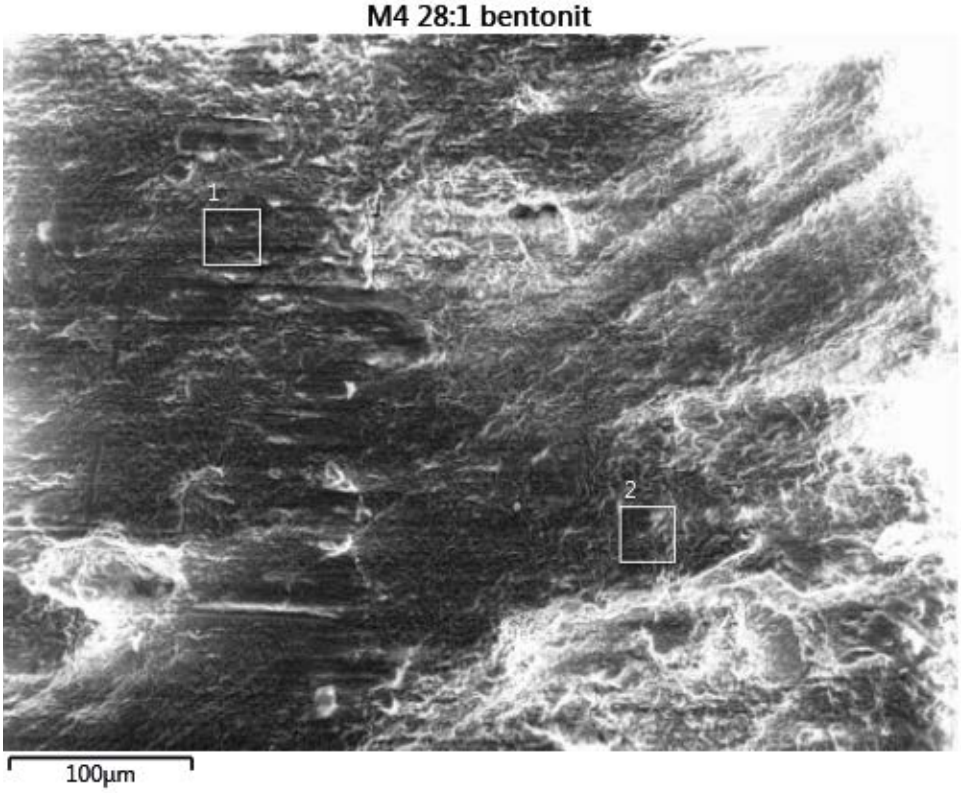

Element (Wt%)	1	2
C	5.32	3.37
O	46.61	48.15
Na	0.50	0.56
Mg	1.47	1.41
Al	11.66	10.70
Si	28.86	30.94
S	0.08	0.08
Cl	0.15	0.07
K	0.12	0.14
Ca	1.46	1.39
Ti	0.13	
Fe	3.63	3.18
Total:	**100.00**	**100.00**

MiniCan 4 bentonite sample from near canister hole 28:2

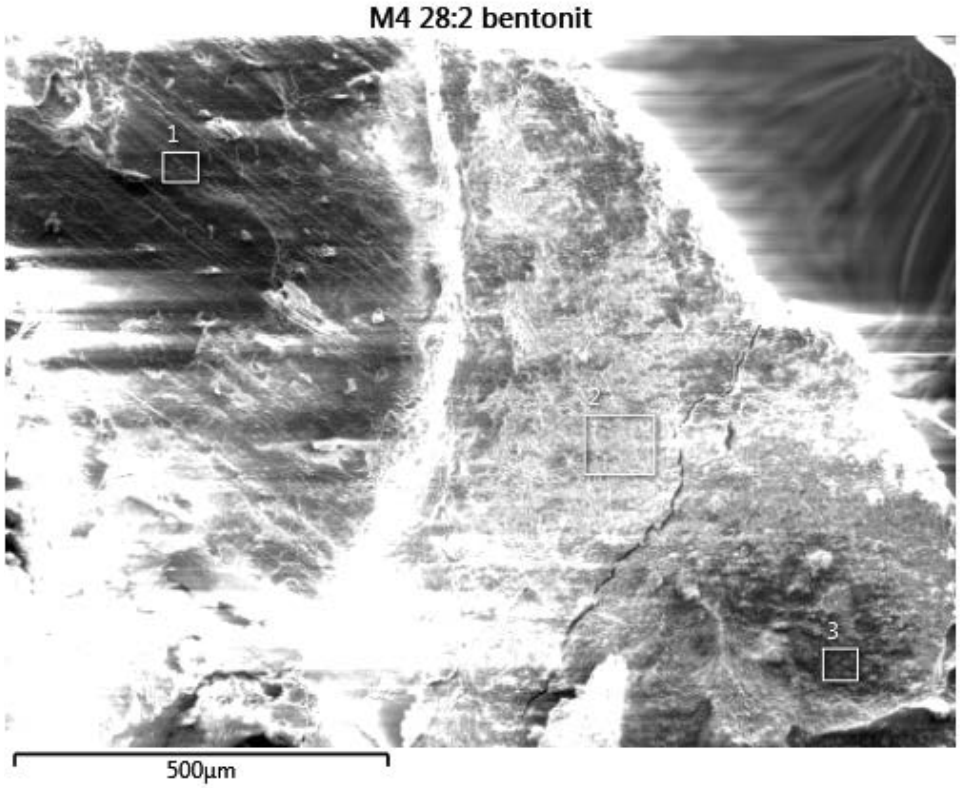

Element (Wt%)	1	2	3
C	5.11	6.75	5.81
O	49.48	50.17	48.83
Na	0.67	0.66	0.65
Mg	1.48	1.61	1.50
Al	10.68	10.07	10.67
Si	27.40	25.74	27.25
S	0.11	0.19	0.14
Cl	0.31	0.38	0.51
K	0.11	0.17	0.18
Ca	1.34	1.43	1.30
Ti	0.07	0.13	
Fe	3.24	2.71	3.12
Total:	**100.00**	**100.00**	**100.00**

MiniCan 4 iron insert outer surface sample 29:1

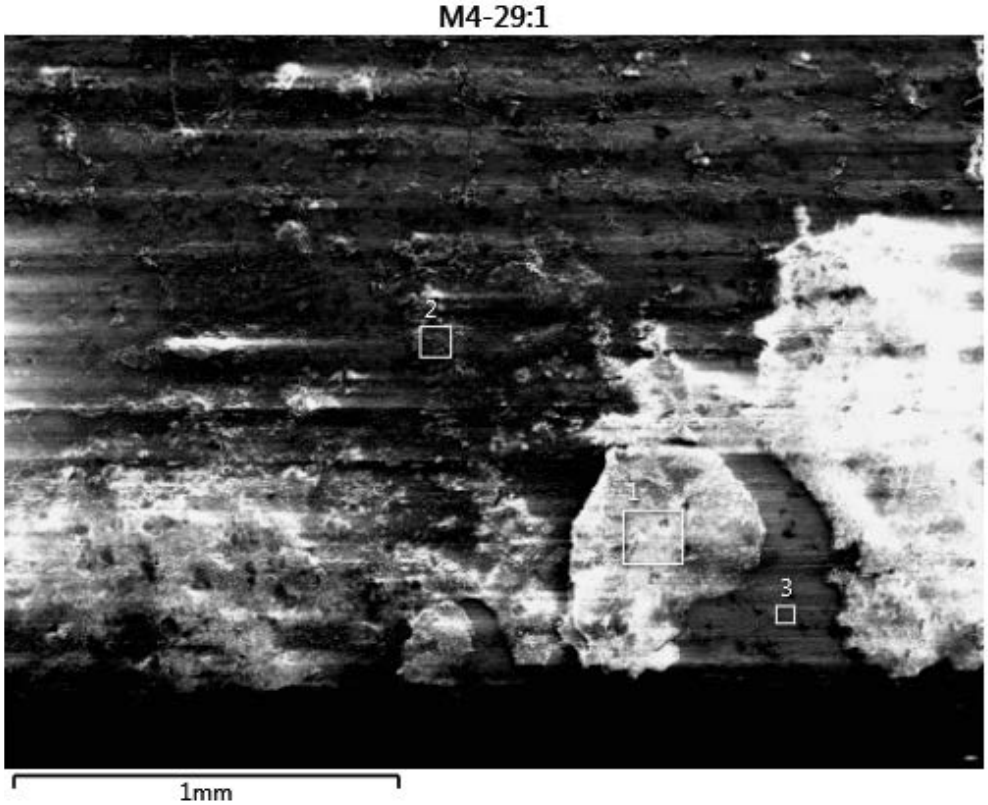

Element (Wt%)	1	2	3
C	23.17	14.81	7.20
O	35.64	39.28	8.08
Na	0.26	1.48	0.18
Mg	0.98	1.23	
Al	6.93	8.31	0.20
Si	17.56	21.04	2.73
S	0.33	0.48	
Cl	1.31	1.66	1.21
K		0.17	
Ca	1.82	1.88	0.16
Ti	1.00	1.18	
Fe	10.99	8.48	80.25
Total:	**100.00**	**100.00**	**100.00**

MiniCan 4 iron insert outer surface sample 29:2

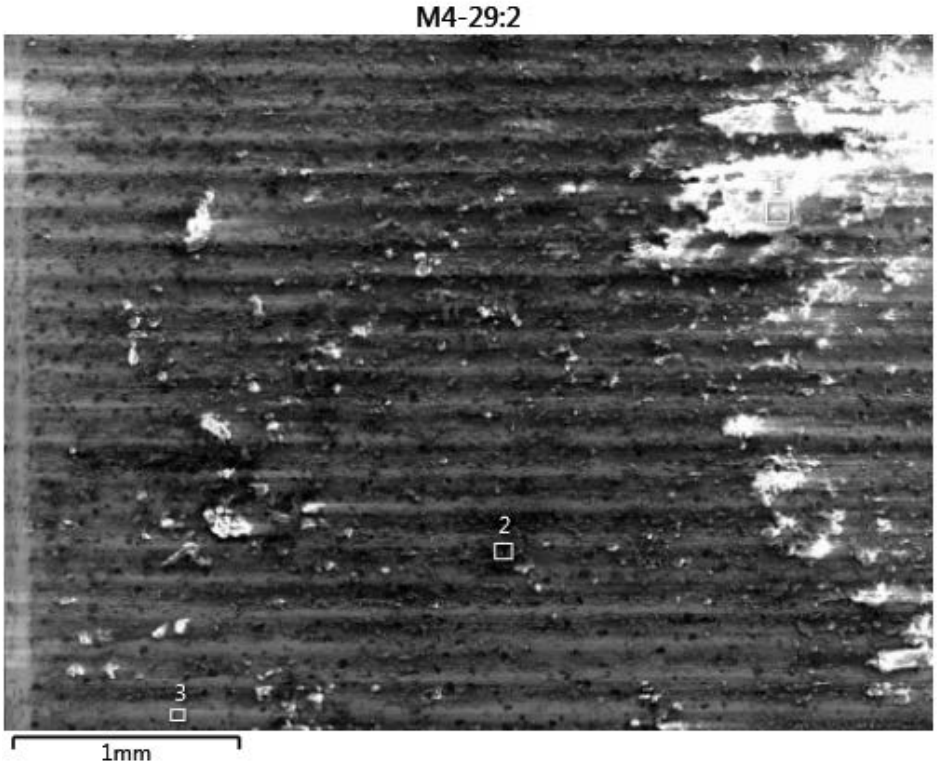

Element (Wt%)	1	2	3
C	28.93	41.15	7.05
O	34.29	11.98	11.64
Na	0.31	3.03	1.26
Mg	0.93	0.76	0.10
Al	6.93	0.96	0.47
Si	16.91	3.44	2.62
S	0.20	0.32	0.24
Cl	1.08	5.56	1.60
K	0.36	0.07	
Ca	1.53	1.79	0.65
Ti	0.96	0.10	
Fe	7.58	30.40	73.07
Cu		0.43	1.32
Total:	**100.00**	**100.00**	**100.00**

MiniCan 4 iron insert sample from near canister hole 30:1

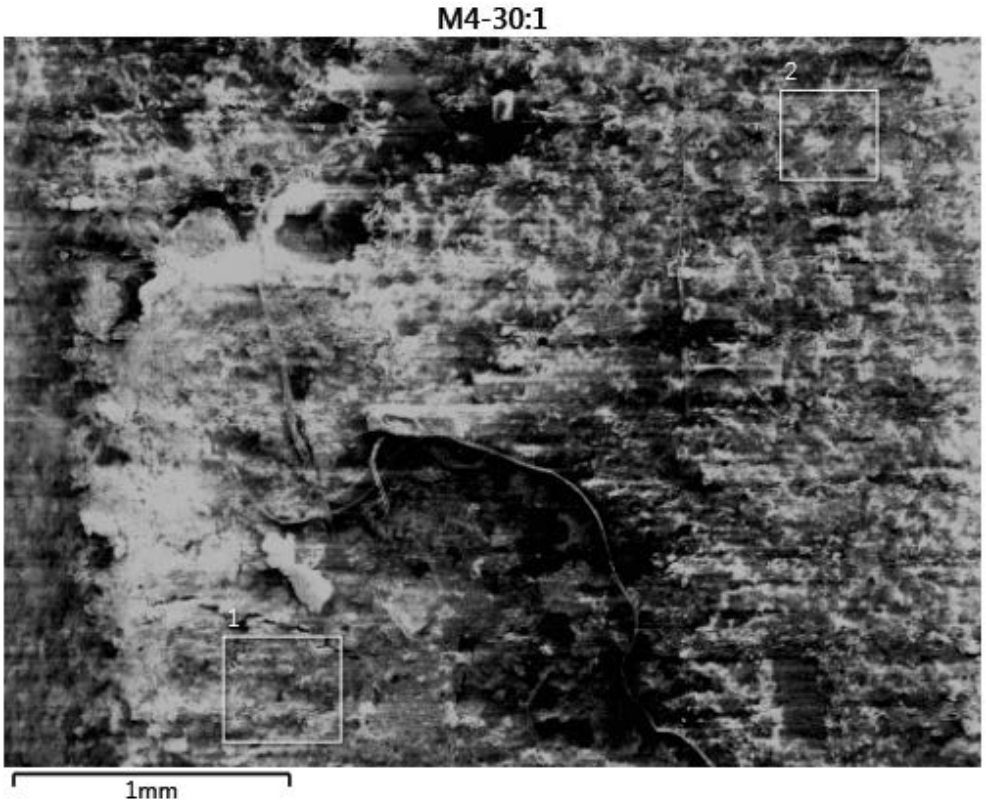

Element (Wt%)	1	2
C	14.14	10.86
O	41.75	38.46
Na	0.32	0.43
Mg	1.25	1.15
Al	7.26	7.47
Si	19.89	19.23
S	0.76	0.82
Cl	1.44	1.93
K	0.07	0.16
Ca	2.45	2.81
Ti	0.94	1.21
Fe	9.73	15.46
Total:	**100.00**	**100.00**

MiniCan 5 copper electrode 5:1, analysis 1

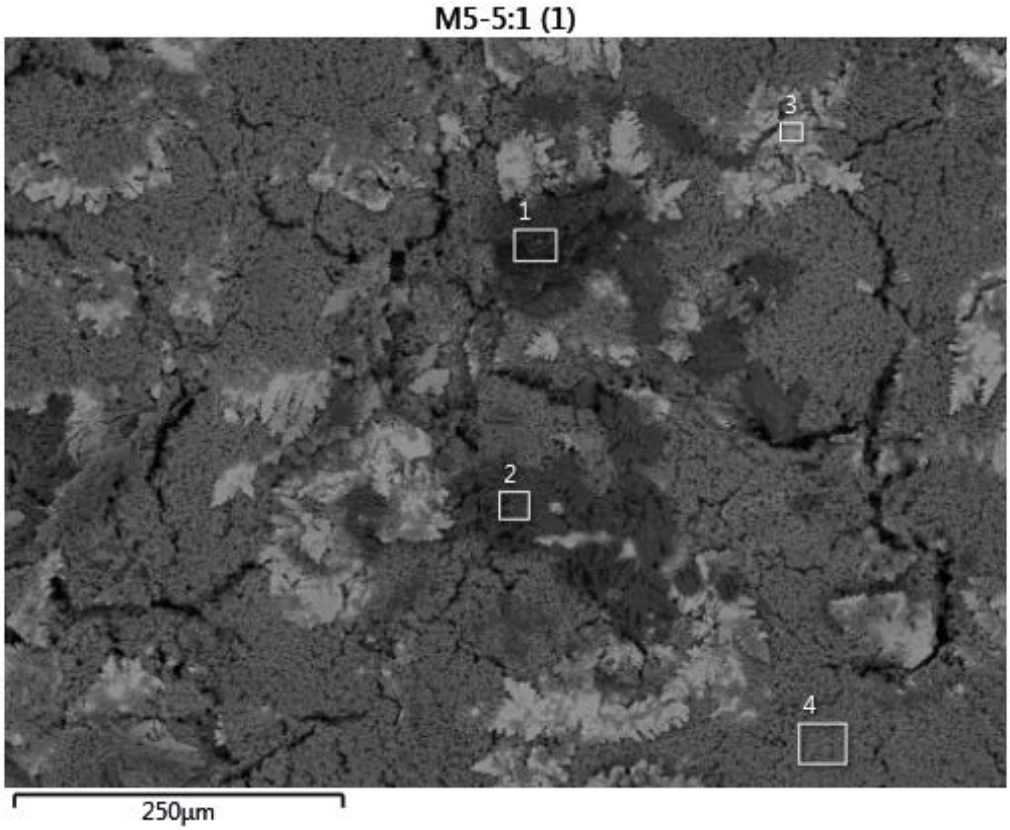

Element (Wt%)	1	2	3	4
C	25.18	3.04	3.46	6.01
O	17.28	51.64	1.44	26.56
Na	2.98			1.28
Al	0.17			
Si	0.33	0.08	0.06	1.69
S	1.20	17.61	15.67	1.00
Cl	23.57	0.44	0.61	13.11
Ca	8.42	21.49	0.59	4.20
Cr	0.90	0.21	0.83	8.88
Fe	7.44	1.75	1.56	18.76
Ni	1.06	0.41	0.35	1.32
Cu	11.46	3.33	75.43	17.17
Total:	**100.00**	**100.00**	**100.00**	**100.00**

MiniCan 5 copper electrode 5:1, analysis 2

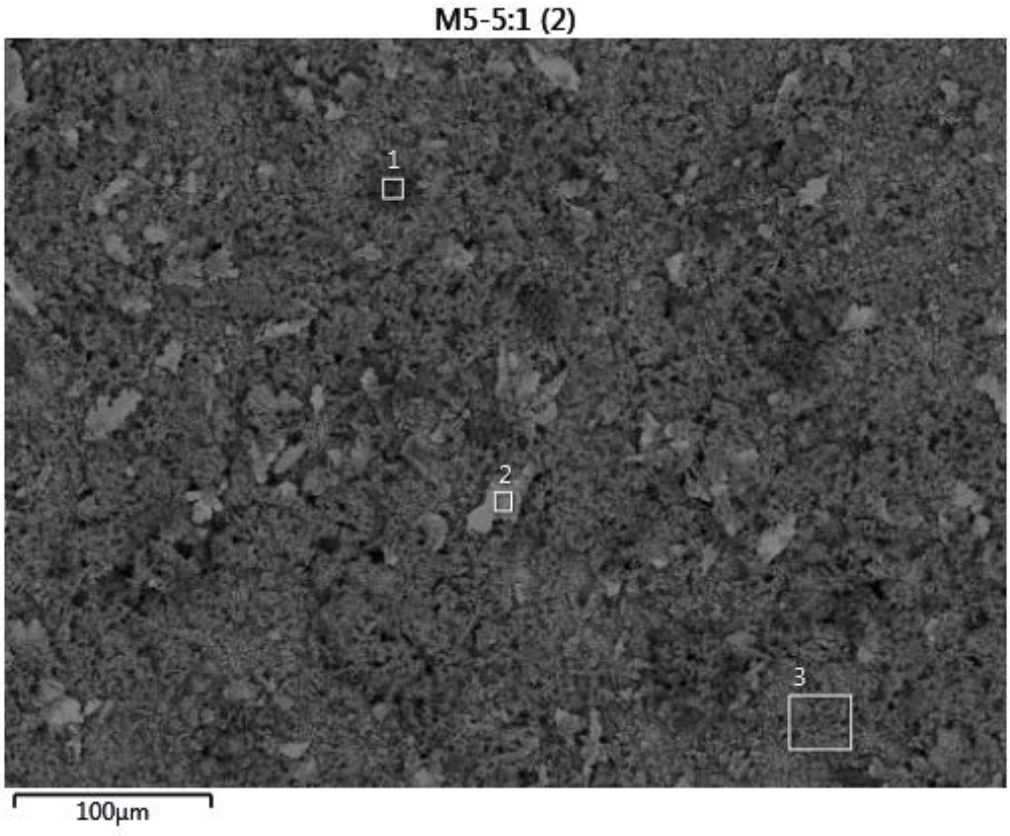

Element (Wt%)	1	2	3
C	2.76	4.13	3.88
O	38.55	2.87	6.31
Na			11.05
Si		0.16	0.35
S	18.95	16.45	6.98
Cl	0.82	0.69	16.73
Ca	22.67	0.44	1.69
Cr	0.20	0.60	1.14
Fe	3.08	1.13	2.41
Ni	0.79	0.00	0.57
Cu	12.18	73.54	48.90
Total:	**100.00**	**100.00**	**100.00**

MiniCan 5 copper electrode 5:1, analysis 3

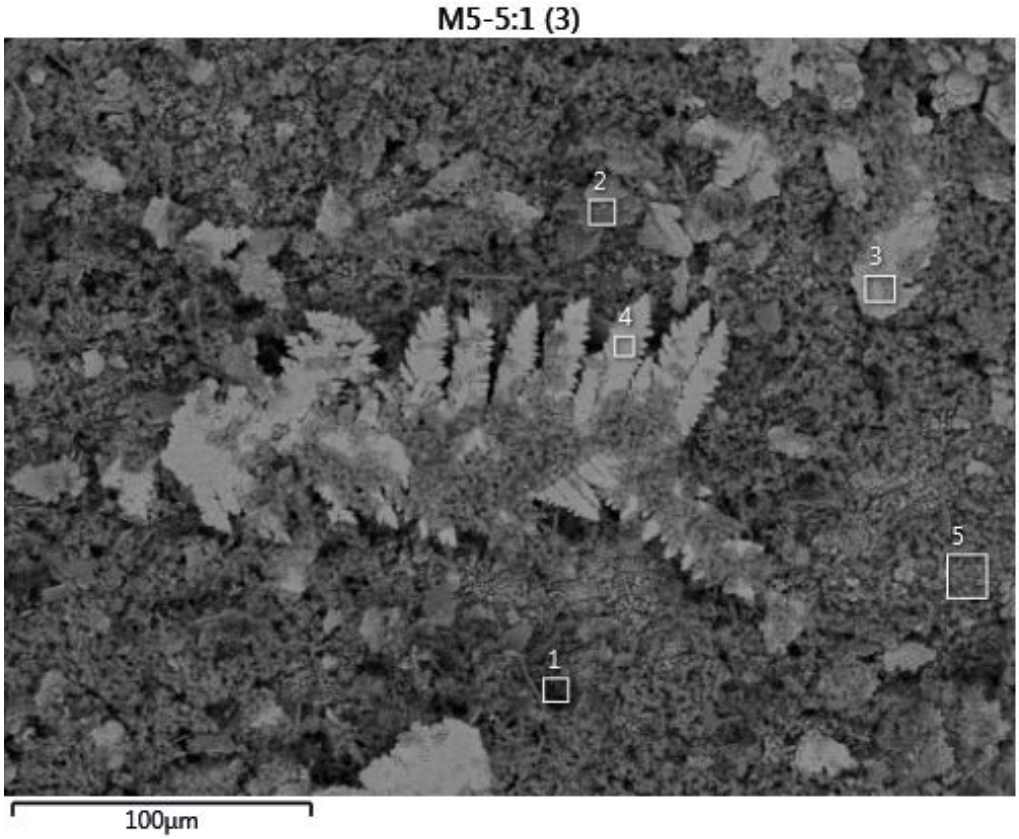

Element (Wt%)	1	2	3	4	5
C	3.95	3.88	4.17	3.92	3.26
O	6.69	4.03	4.54	1.85	9.08
Al			0.10		0.14
Si	0.31	0.23	0.24	0.15	0.43
S	10.47	10.94	13.46	16.91	8.44
Cl	5.46	1.69	1.66	0.71	3.99
Ca	2.36	1.32	1.07	0.40	2.96
Cr	2.13	1.71	1.19	0.28	3.51
Fe	1.95	2.04	1.71	0.54	4.09
Ni		0.24			0.58
Cu	66.68	73.92	71.85	75.24	63.53
Total:	**100.00**	**100.00**	**100.00**	**100.00**	**100.00**

MiniCan 5 copper electrode 6:1, analysis 1

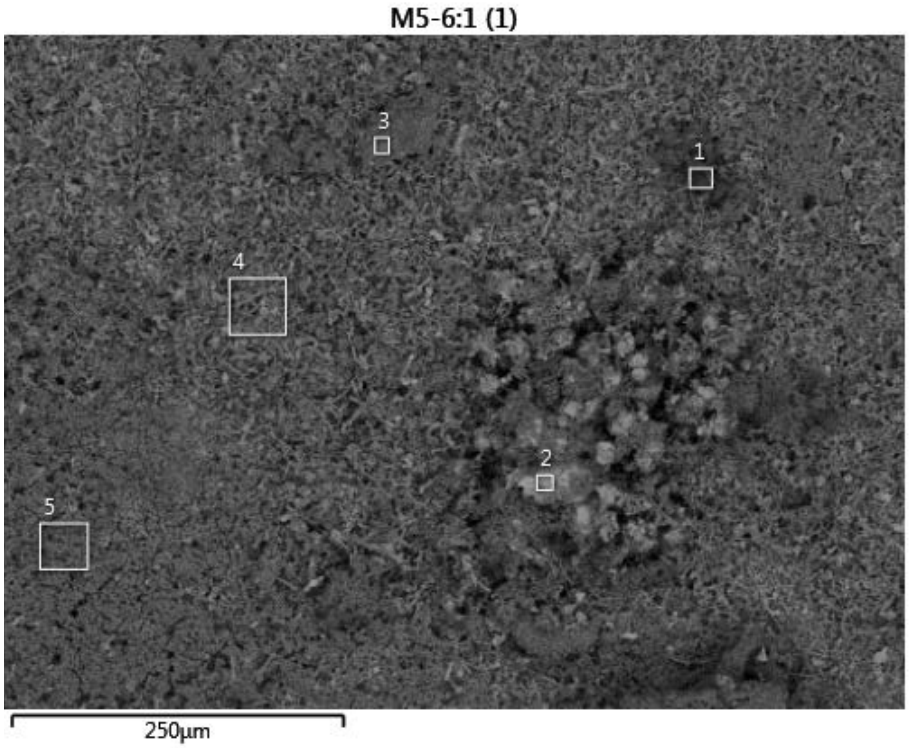

Element (Wt%)	1	2	3	4	5
C	35.70	0.58	5.08	3.28	3.16
O	21.53	1.11	17.14	4.29	18.03
Na	0.99	0.17	0.15		3.75
Mg				0.20	
Al	0.45			0.08	0.11
Si	0.61	0.16	0.99	0.02	0.56
S	2.49	0.34	0.35	9.98	1.98
Cl	2.66	1.04	5.37	3.34	16.21
Ca	2.42	1.20	4.30	3.14	7.91
Cr	5.97	21.67	4.62	2.50	15.77
Mn		2.90	0.44		0.21
Fe	5.83	61.71	51.68	1.19	6.58
Ni	2.19	3.99	0.68	5.72	0.79
Cu	19.16	4.96	9.18	66.25	24.31
Sn		0.16			0.62
Total:	**100.00**	**100.00**	**100.00**	**100.00**	**100.00**

MiniCan 5 copper electrode 6:1, analysis 2

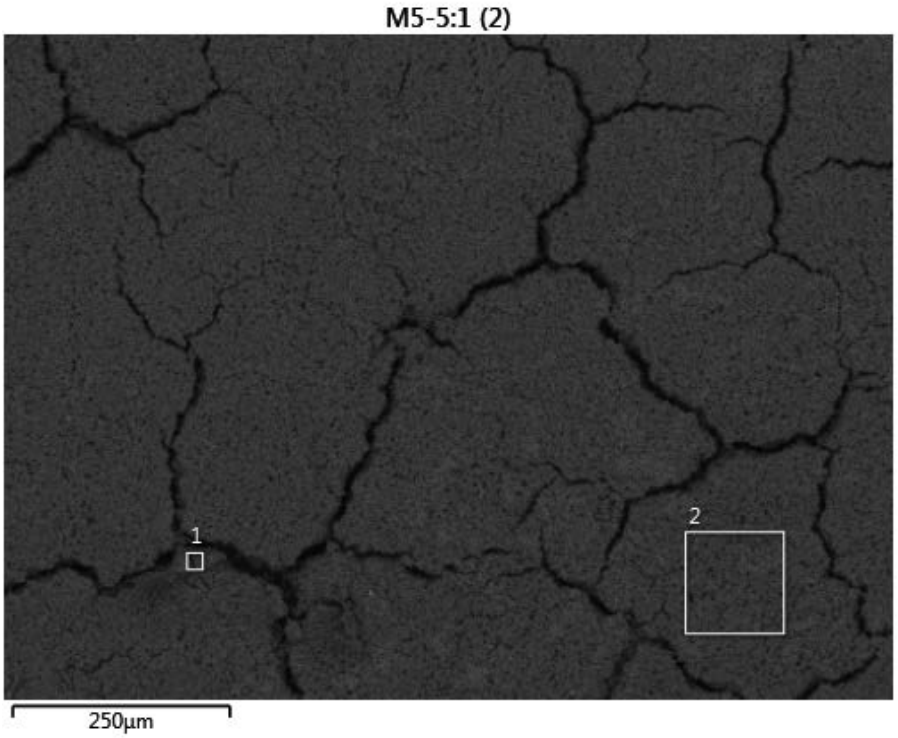

Element (Wt%)	1	2
C	2.37	4.55
O	31.78	30.66
Na	5.06	0.18
Mg	1.13	0.09
Al	0.16	0.04
Si	13.14	0.93
S	0.44	0.56
Cl	5.74	10.42
K	0.14	0.07
Ca	7.06	7.60
Cr	21.51	28.71
Fe	5.40	10.41
Ni	0.31	0.20
Cu	5.77	5.58
Total:	**100.00**	**100.00**

MiniCan 5 copper mass loss sample 7:1, analysis 1

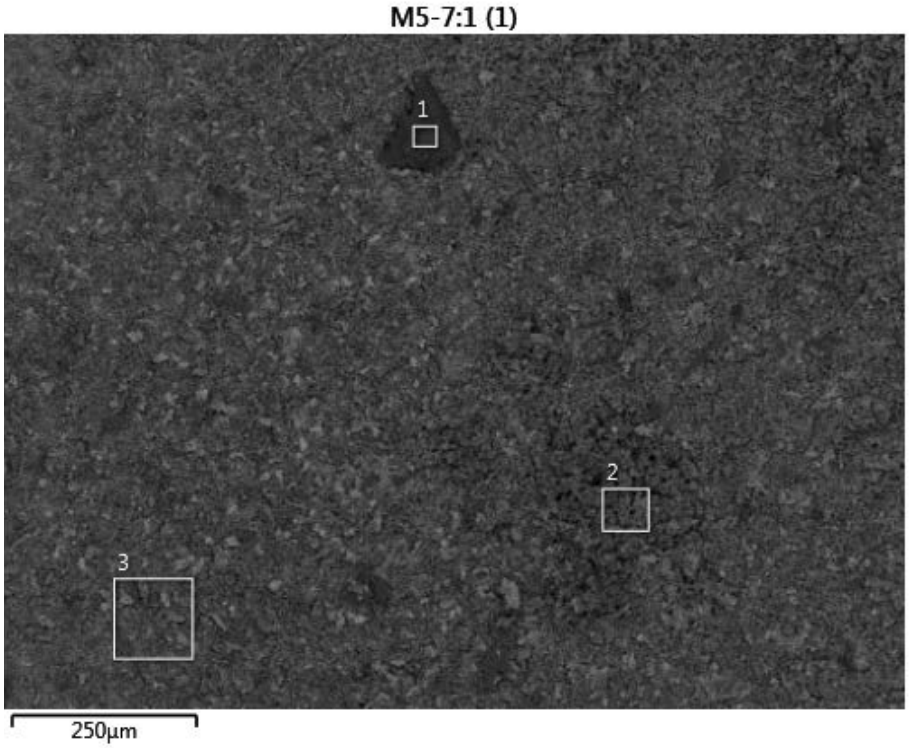

Element (Wt%)	1	2	3
C	2.11	4.10	3.65
O	43.30	13.09	19.27
Na	9.79	2.09	2.49
Mg	2.65	0.07	0.10
Al	0.26	0.05	0.06
Si	33.87	0.82	1.14
S	0.14	5.61	5.19
Cl	0.22	8.03	8.24
K	0.35	0.09	0.09
Ca	5.87	3.49	4.42
Cr	0.24	15.25	15.50
Fe	0.06	8.36	8.15
Ni	0.17	1.99	1.80
Cu	0.99	36.99	29.90
Total:	**100.00**	**100.00**	**100.00**

MiniCan 5 copper mass loss sample 7:1, analysis 2

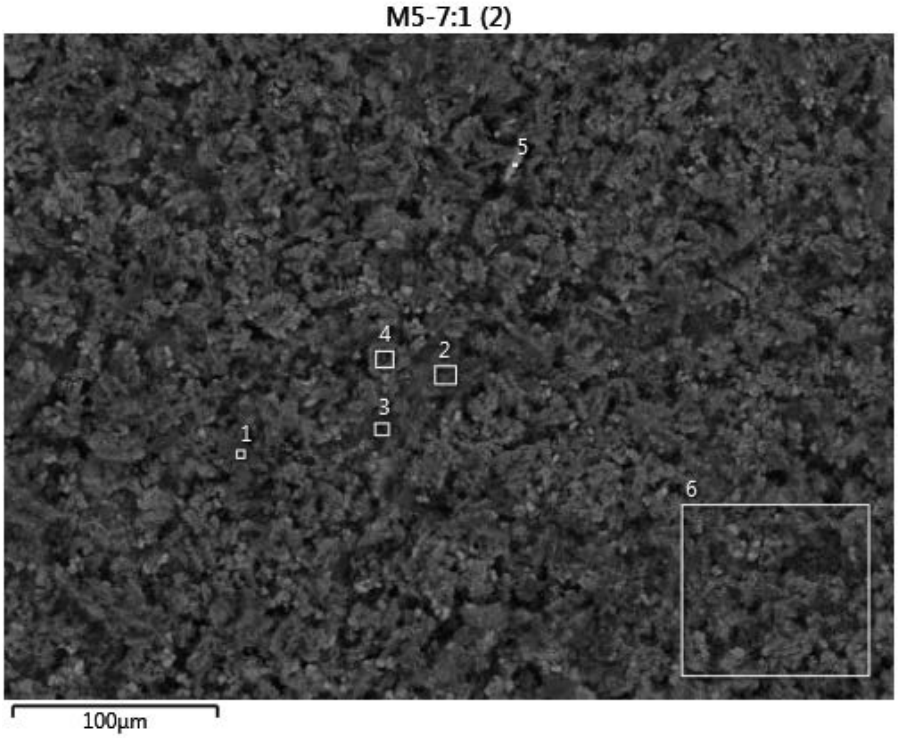

Element (Wt%)	1	2	3	4	5	6
C	3.62	3.84	0.85	5.53	5.54	4.17
O	45.32	10.34	2.50	13.42	2.77	10.53
Na	10.06	2.63	0.36	3.06	0.18	1.84
Mg	2.55					
Al	0.20					
Si	28.92	1.27	0.20	0.67	0.20	0.95
S	0.43	6.89	1.73	11.21	15.94	7.33
Cl	0.27	6.75	2.39	4.89	1.00	4.81
K	0.30					
Ca	4.97	3.49	3.52	5.43	0.60	3.41
Cr	0.46	13.95	21.57	8.40	2.08	12.58
Fe	0.25	8.42	13.84	3.15	1.57	7.00
Ni	0.02	0.71	1.64	0.17	0.16	0.94
Cu	2.63	41.71	51.40	44.05	69.95	46.44
Total:	**100.00**	**100.00**	**100.00**	**100.00**	**100.00**	**100.00**

MiniCan 5 iron electrode 9:1, analysis 1

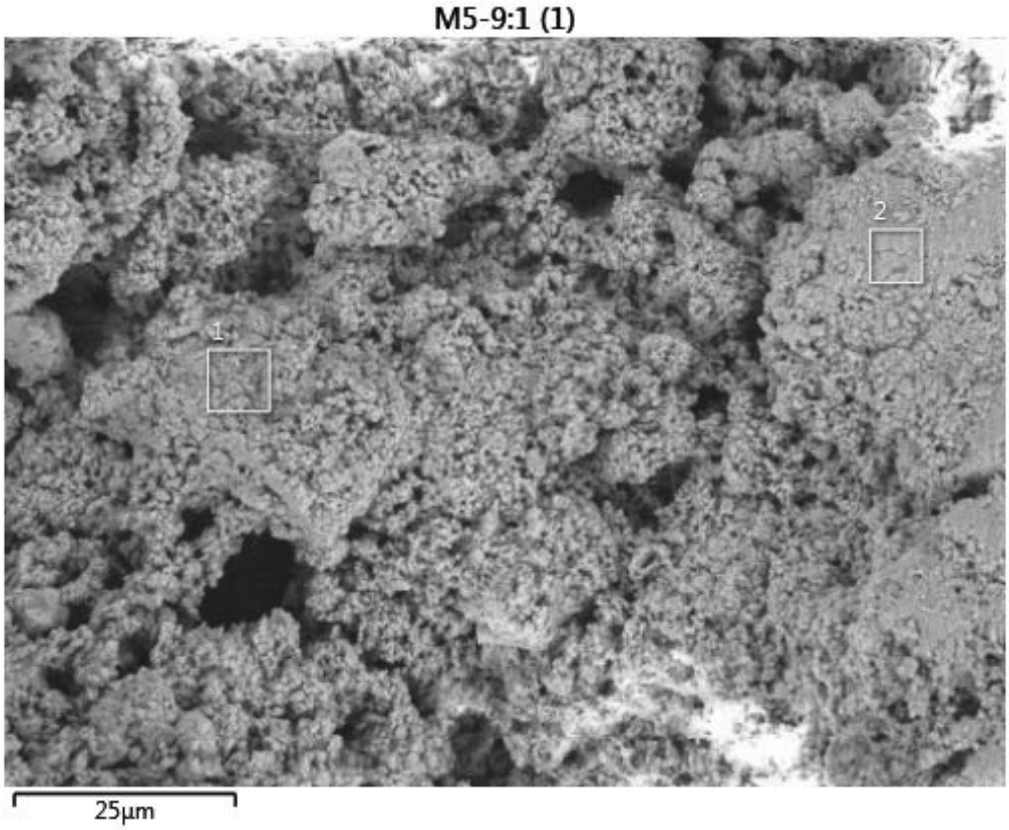

Element (Wt%)	1	2
C	24.34	23.23
O	67.07	70.57
Na	1.28	1.30
Mg		0.18
Al	0.15	0.24
Si	4.42	2.56
S	1.21	1.24
Cl	0.88	0.50
Ca	0.45	
Fe	0.21	0.18
Total:	**100.00**	**100.00**

MiniCan 5 iron electrode 9:1, analysis 2

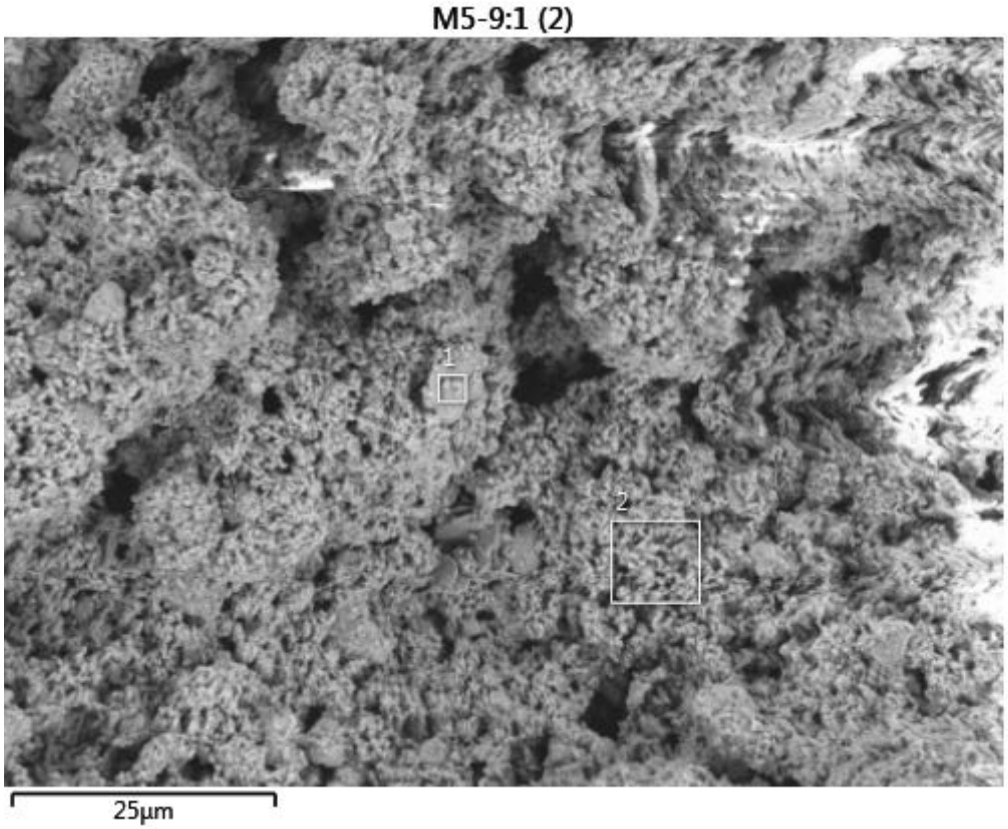

Element (Wt%)	1	2
C	11.61	19.99
O	66.90	70.89
Na	1.49	1.21
Al	0.18	
Si	6.35	5.14
S	5.73	1.73
Cl	2.90	0.86
Ca	0.73	0.05
Cr	2.08	0.00
Fe	2.04	0.12
Total:	**100.00**	**100.00**

MiniCan 5 iron electrode 10:1, analysis 1

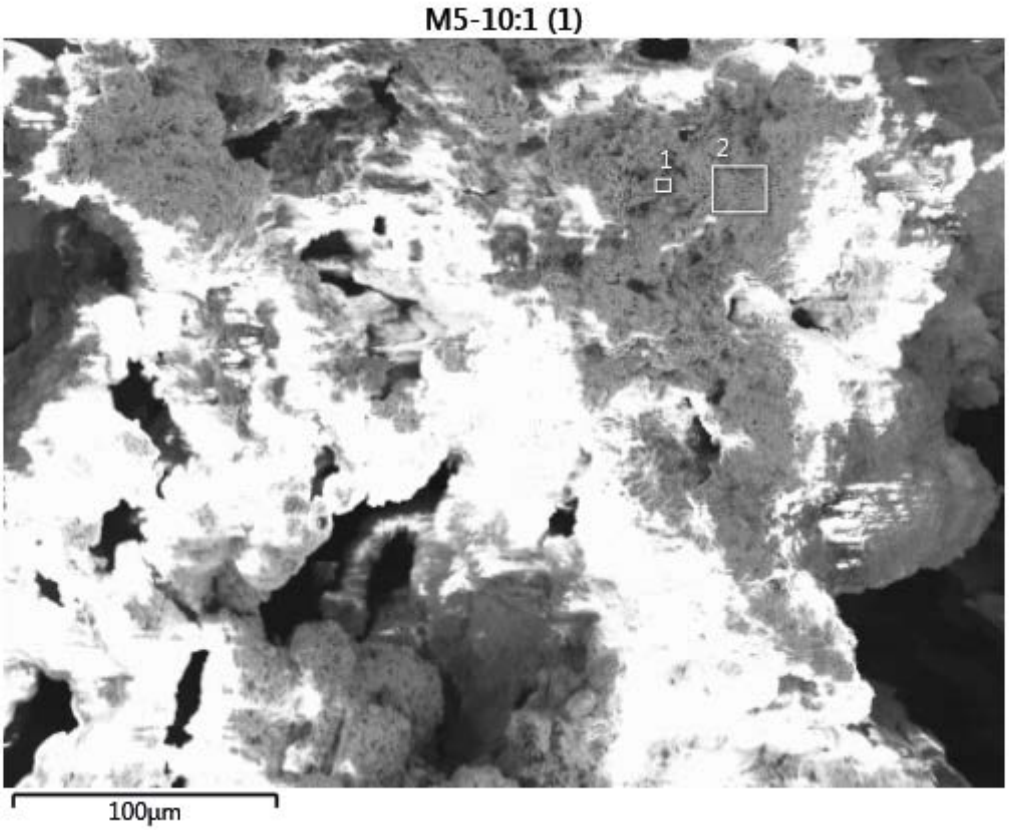

Element (Wt%)	1	2
C	18.09	20.90
O	61.55	66.75
Na	0.30	0.24
Mg	0.12	
Al	0.10	0.28
Si	2.61	1.84
S	1.78	2.42
Cl	4.04	3.43
Ca	0.42	0.13
Cr	0.20	0.35
Fe	10.78	3.66
Total:	**100.00**	**100.00**

MiniCan 5 iron electrode 10:1, analysis 2

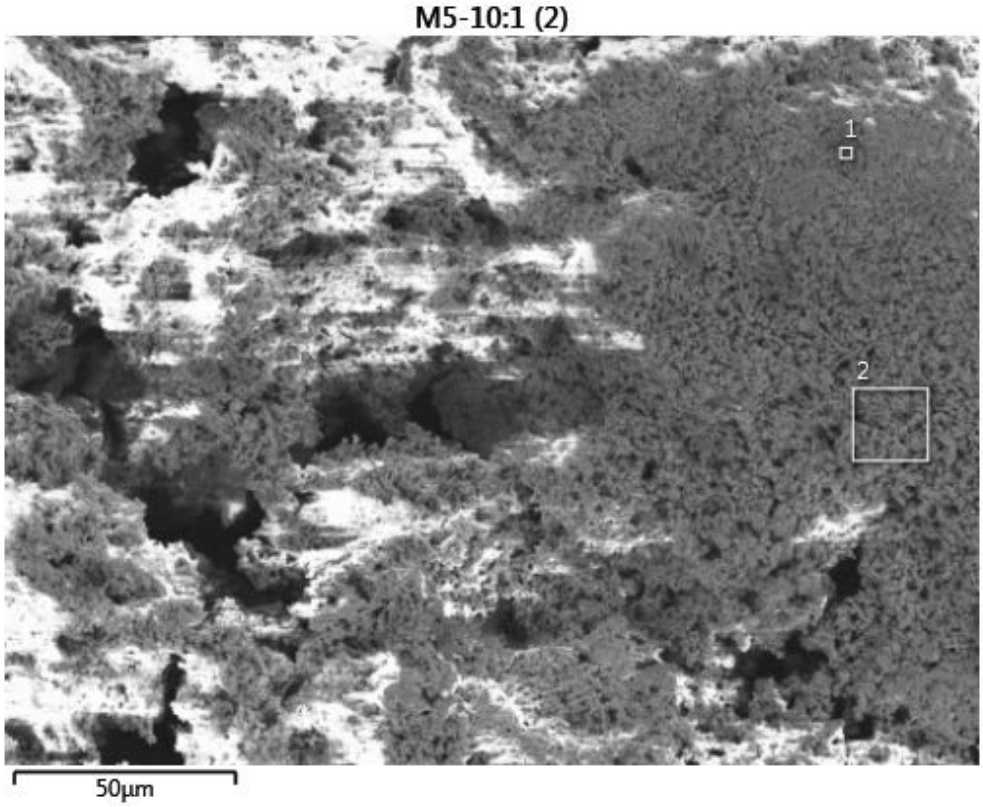

Element (Wt%)	1	2
C	15.29	11.05
O	55.26	33.66
Na	0.43	0.42
Mg	0.07	0.20
Al	0.11	0.04
Si	4.19	5.94
S	3.44	9.82
Cl	3.31	2.74
Ca	0.46	0.73
Cr	0.61	1.44
Fe	16.67	31.54
Ni	0.18	2.43
Total:	**100.00**	**100.00**

MiniCan 5 iron mass loss sample 11:1, analysis 1

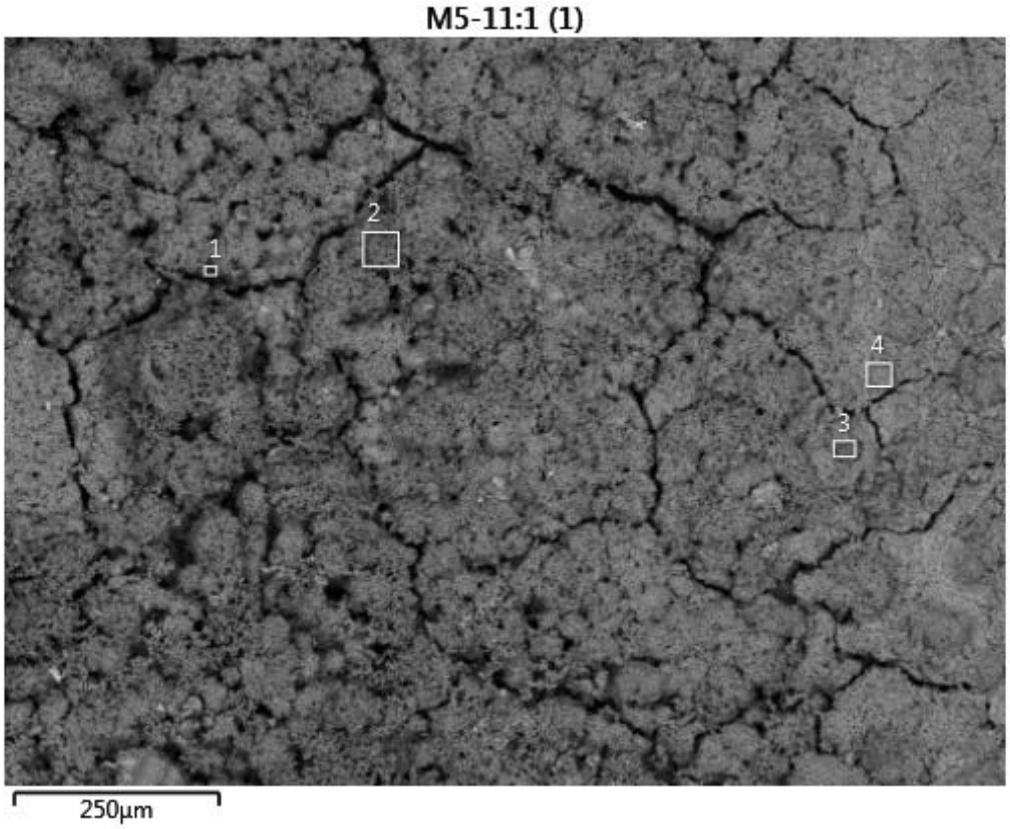

Element (Wt%)	1	2	3	4
C	2.07	7.01	6.01	7.67
O	5.39	29.79	25.02	21.48
Na	0.24	0.80	0.34	0.20
Si	1.91	8.44	7.25	5.15
S	2.42	4.15	6.86	12.14
Cl	0.24	2.22	2.01	1.44
Ca	0.87	2.69	2.53	1.71
Cr	0.12	5.19	2.10	0.65
Fe	80.15	36.87	47.29	44.91
Ni	6.60	2.84	0.60	4.65
Total:	**100.00**	**100.00**	**100.00**	**100.00**

MiniCan 5 iron mass loss sample 11:1, analysis 2

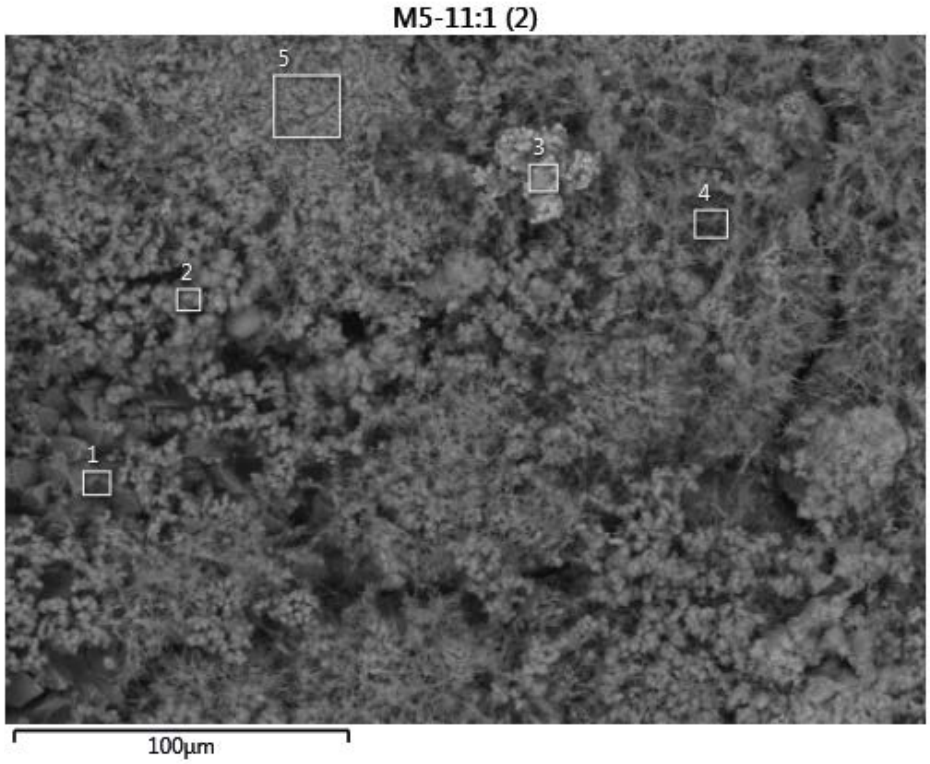

Element (Wt%)	1	2	3	4	5
C	2.42	4.05	5.53	2.35	4.95
O	20.77	31.24	18.15	21.57	34.94
Na	0.35	1.12	0.20	1.78	1.80
Mg	0.04	0.06			
Si	5.47	12.72	1.92	14.82	14.95
S	0.54	5.05	13.83	0.52	0.89
Cl	1.08	1.75	1.59	0.80	1.11
Ca	28.85	2.10	4.64	2.71	2.68
Cr		0.34	10.24	0.03	1.26
Fe	40.47	35.22	11.09	55.43	37.43
Ni		6.35	0.58		
Cu			32.24		
Total:	**100.00**	**100.00**	**100.00**	**100.00**	**100.00**

MiniCan 5 copper sandwich sample 14:1

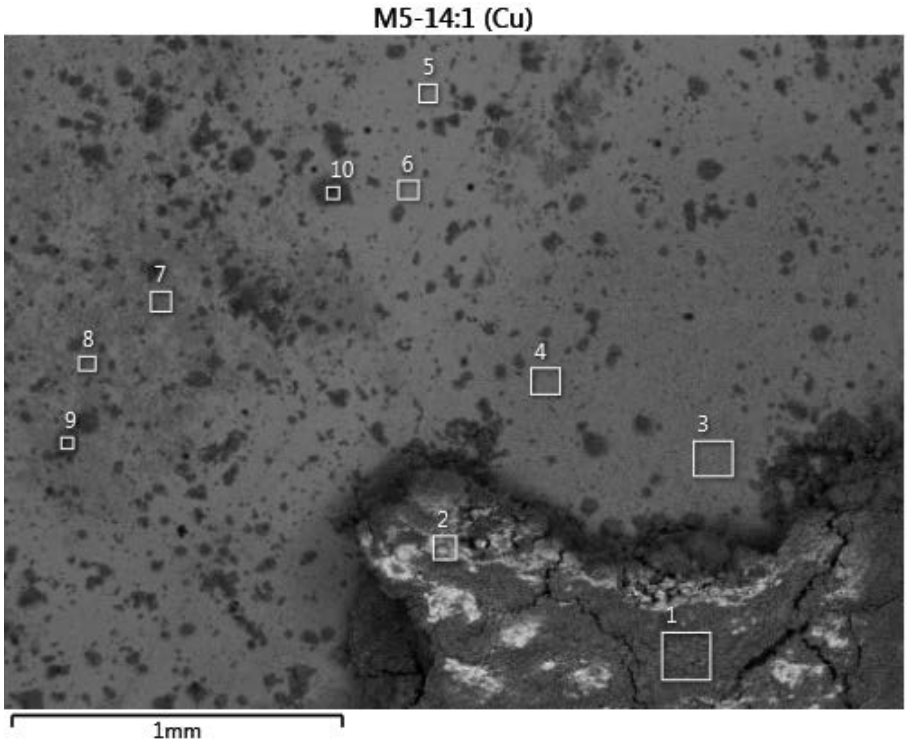

Element (Wt%)	1	2	3	4	5	6	7	8	9	10
C	8.25	8.93	5.07	5.40	4.57	4.37	5.12	4.43	5.02	8.11
O	49.90	47.11	2.28	1.63	1.08	0.90	12.09	11.47	23.24	29.99
Na	0.67	0.32								
Mg	0.15	0.14								
Al							0.13	0.15	0.07	0.04
Si	7.10	6.45	0.41	0.20	0.12	0.08	0.13	0.07	1.89	4.11
S	2.17	1.79	21.39	22.18	2.05	2.06	0.89	1.76	7.15	1.09
Cl	1.41	1.46					10.06	9.14	1.01	1.47
Ca	0.68	0.61							0.48	0.35
Cr									0.69	0.19
Fe	29.67	33.19	1.71	1.28	0.25	0.49	0.56	0.39	56.24	50.88
Ni									0.92	
Cu			69.13	69.31	91.95	92.10	71.03	72.59	3.29	3.78
Total:	**100.00**	**100.00**	**100.00**	**100.00**	**100.00**	**100.00**	**100.00**	**100.00**	**100.00**	**100.00**

MiniCan 5 copper canister inner surface 24:1, analysis 1

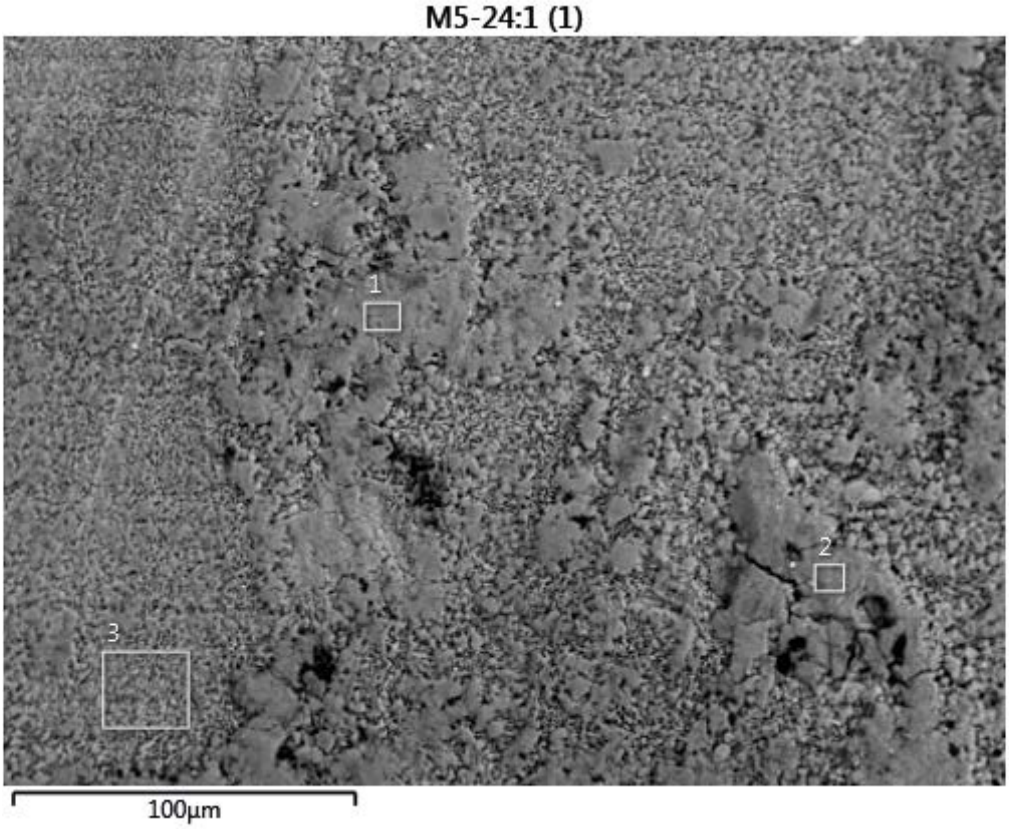

Element (Wt%)	1	2	3
C	5.90	6.78	6.47
O	20.77	22.93	20.84
Na	0.29	0.53	0.25
Al	0.09	0.04	0.05
Si	0.17	1.26	0.28
S	0.11	0.55	0.27
Cl	6.52	2.84	7.45
Ca	0.18	0.89	0.63
Fe	52.13	54.89	43.11
Cu	13.84	9.29	20.66
Total:	**100.00**	**100.00**	**100.00**

MiniCan 5 copper canister inner surface 24:1, analysis 2

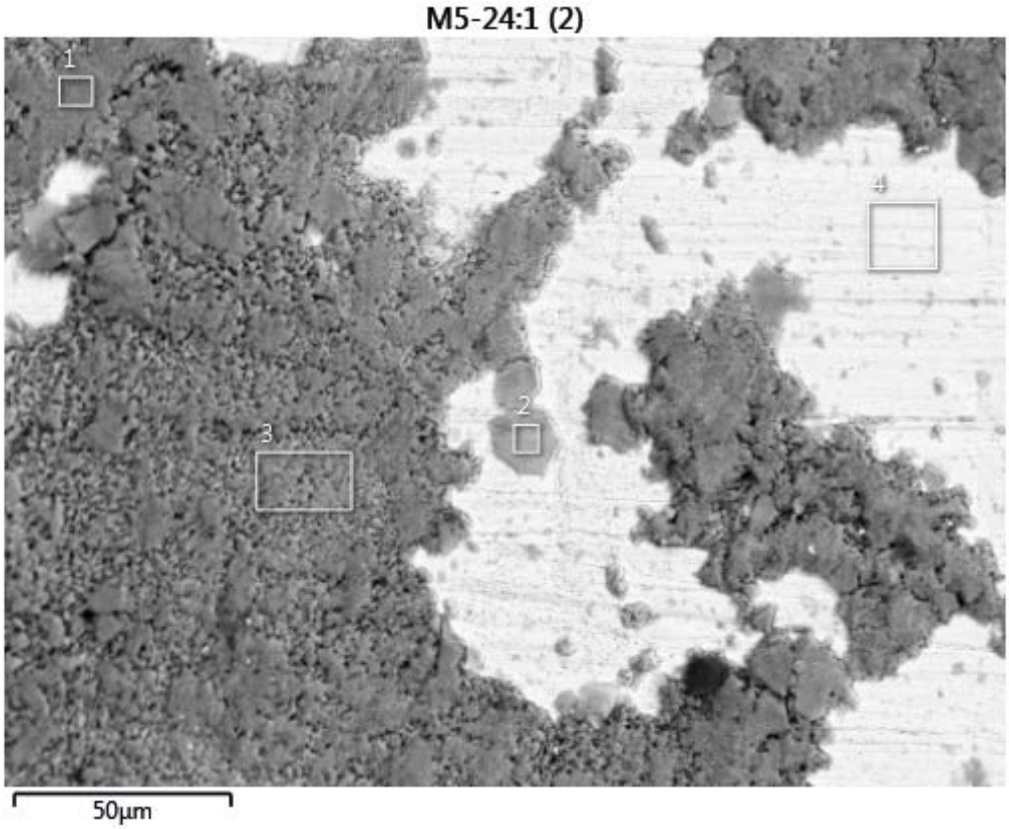

Element (Wt%)	1	2	3	4
C	9.62	3.93	11.21	3.03
O	21.12	17.47	19.42	1.33
Na	0.20		0.15	
Al			0.12	
Si	0.39		0.28	
P				0.12
S	0.14	0.06	0.28	0.09
Cl	7.98	5.75	8.25	0.29
Ca	0.50	0.06	0.42	
Fe	47.56	27.08	42.26	0.71
Cu	12.48	45.65	17.61	94.42
Total:	**100.00**	**100.00**	**100.00**	**100.00**

MiniCan 5 copper canister outer surface 25:1, analysis 1

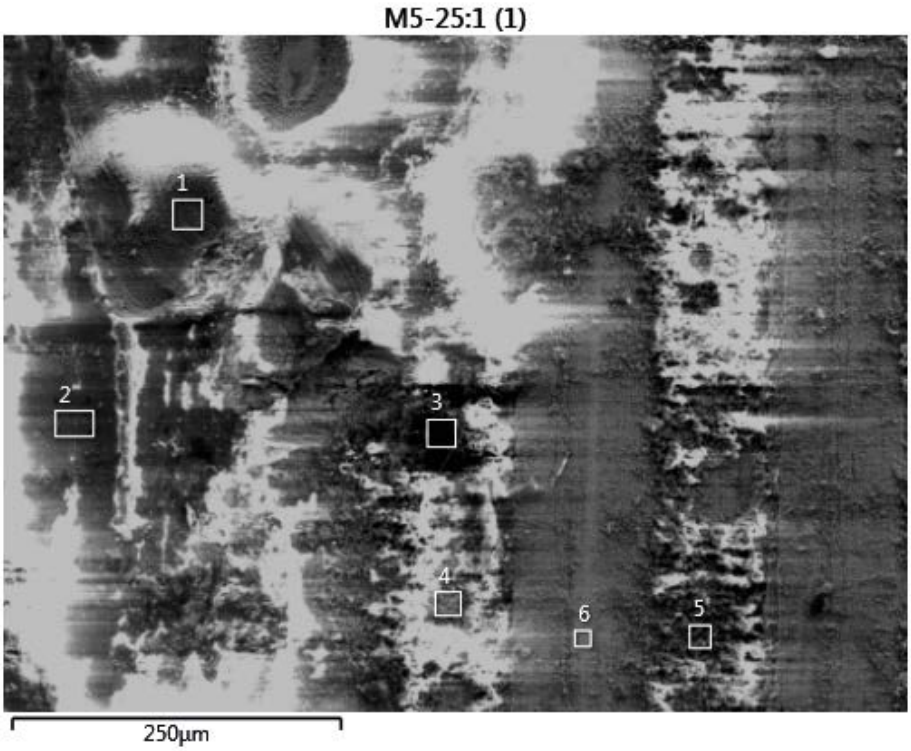

Element (Wt%)	1	2	3	4	5	6
C	12.81	26.40	85.37	27.27	36.51	8.99
O	36.50	29.24	4.06	17.02	19.56	3.17
Na		0.64	0.23	4.41	0.31	
Mg		0.60	0.11	0.53	0.78	0.15
Al	1.55	1.03	0.12	0.26	0.28	
Si	0.10	2.50	0.50	3.43	3.91	0.36
S		0.79	0.29	3.07	2.49	1.36
Cl	0.19	1.44	1.45	9.32	4.32	0.98
Ca	0.08	0.60	0.78	2.43	3.11	0.33
Ti	47.09	27.22	0.21			
Cr		0.61	0.37	1.08	0.99	
Fe	0.14	6.37	3.59	9.78	8.40	0.29
Cu	1.55	2.56	2.93	21.40	19.36	84.37
Total:	**100.00**	**100.00**	**100.00**	**100.00**	**100.00**	**100.00**

MiniCan 5 copper canister outer surface 25:1, analysis 2

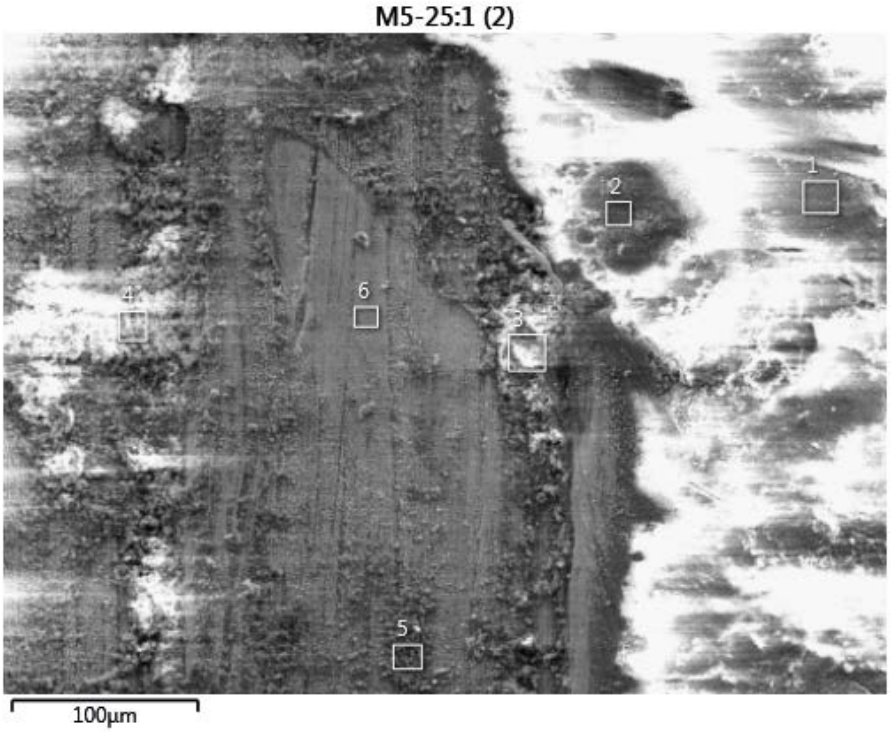

Element (Wt%)	1	2	3	4	5	6
C	9.99	13.78	19.93	15.56	16.72	6.72
O	39.73	31.07	28.47	26.64	28.47	4.81
Na			0.94	0.52	1.23	0.48
Mg		0.23	0.45	0.94	0.95	0.32
Al	1.44	1.42	0.77	0.50	0.74	
Si	0.30	0.65	4.31	7.59	5.22	0.84
S	0.10	0.38	0.67	1.20	1.69	4.51
Cl	0.30	0.79	4.94	5.26	3.78	1.18
Ca	0.15	0.38	2.00	3.51	2.01	0.51
Ti	46.37	45.90	19.56	7.82	16.49	0.12
Cr		0.49	1.43	1.74	0.80	
Fe	0.45	1.69	9.06	17.20	9.69	0.87
Ni			0.29	0.36	0.17	0.63
Cu	1.17	3.22	7.19	11.14	12.04	79.00
Total:	**100.00**	**100.00**	**100.00**	**100.00**	**100.00**	**100.00**

MiniCan 5 copper canister outer surface 25:1, cross sections of surface defects

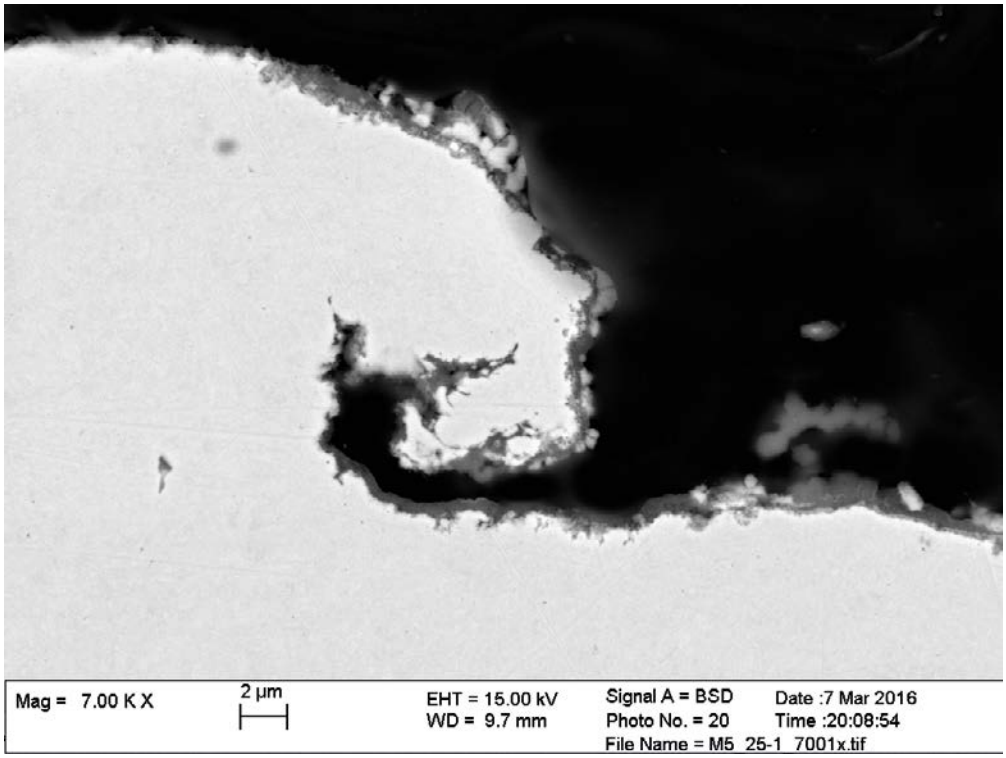

Detail of machining mark.

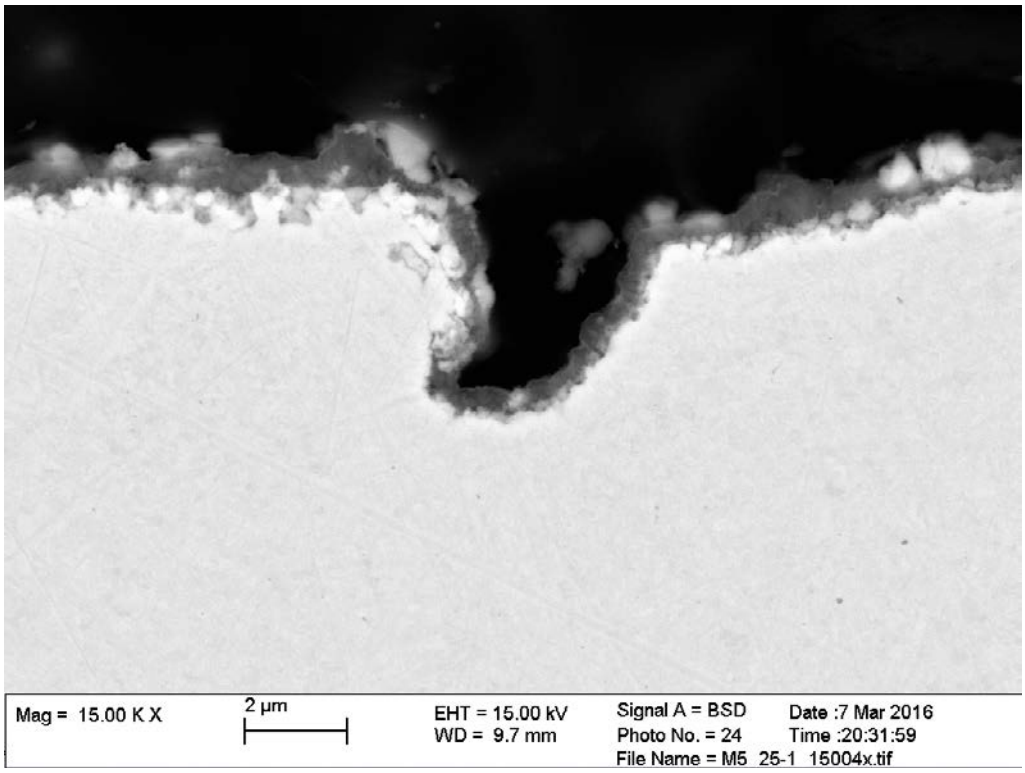

Pit, about 4 µm deep.

MiniCan 5 copper canister outer surface 25:1, cross section

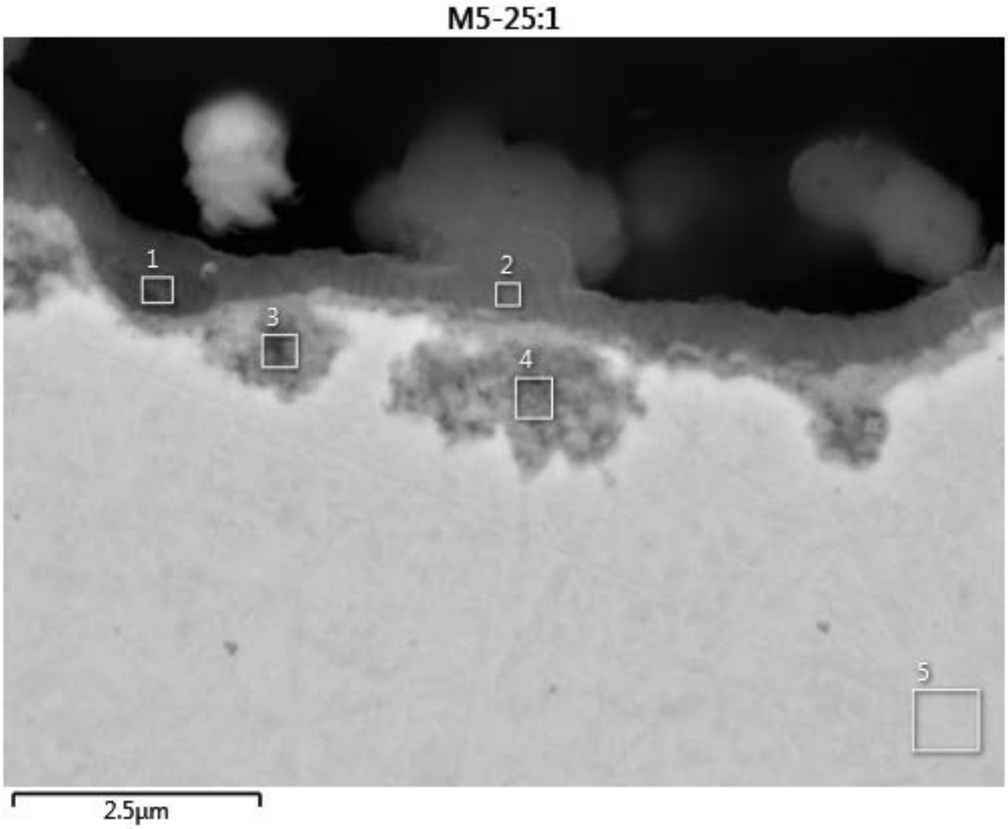

Element (Wt%)	1	2	3	4	5
C	30.41	23.37	12.93	8.10	4.12
O	18.29	17.53	10.43	10.87	
Mg	0.99	1.19	0.16	0.33	
Al	0.33	0.43	0.12	0.14	
Si	7.08	9.79	3.47	3.16	
S	0.83	1.04	2.77	2.85	
Cl	1.32	2.22	0.74	0.84	
Ca	2.65	3.53	0.86	0.62	
Fe	13.67	17.01	6.01	4.96	
Cu	24.44	23.88	62.50	68.13	95.88
Total:	**100.00**	**100.00**	**100.00**	**100.00**	**100.00**

MiniCan 5 copper canister weld surface 26:1, analysis 1

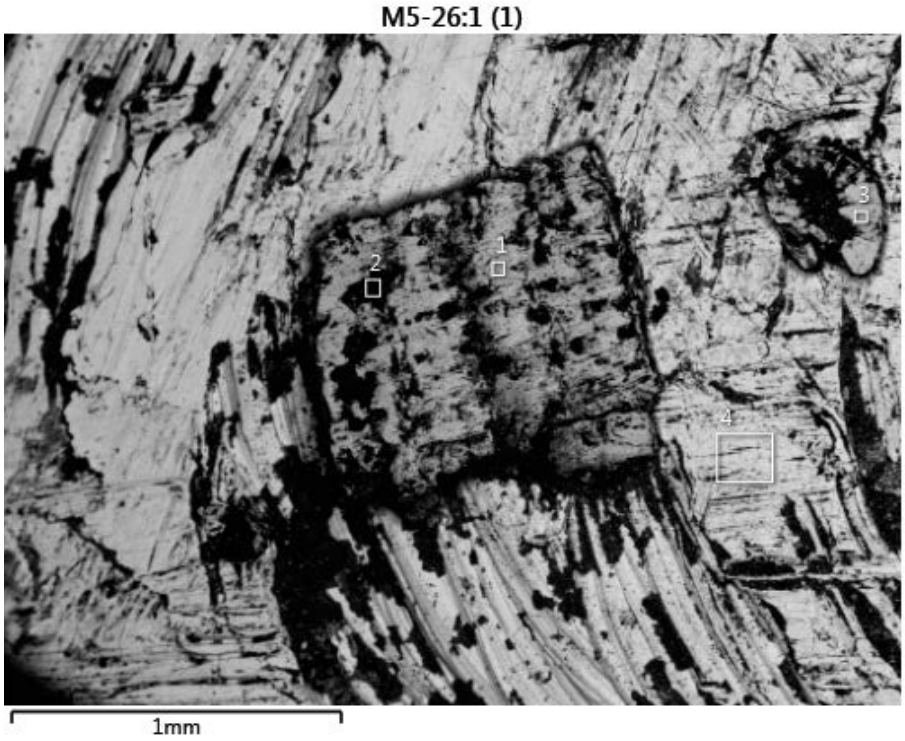

Element (Wt%)	1	2	3	4
C	8.48	19.58	5.10	6.83
O	1.92	18.63	2.24	3.60
Na		0.15		
Mg		3.06		0.37
Al	0.38	51.14	2.83	2.56
Si	2.21	0.35	2.41	0.39
S	0.18	0.54	0.04	0.52
Cl	0.15	0.99	0.08	0.28
Ca		0.38		
Cr		0.49		0.44
Mn		0.31		
Fe	86.42	2.80	87.24	0.97
Ni		0.36		
Cu	0.26	1.21	0.05	84.05
Total:	**100.00**	**100.00**	**100.00**	**100.00**

MiniCan 5 copper canister weld surface 26:1, analysis 2

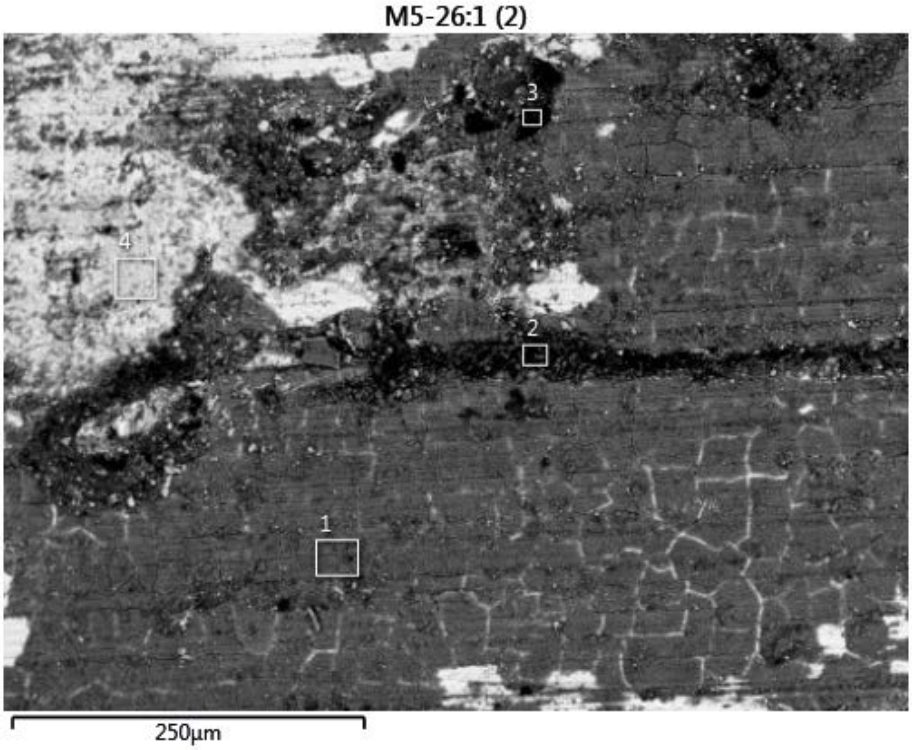

Element (Wt%)	1	2	3	4
C	14.34	43.84	84.47	8.69
O	28.90	21.68	6.36	4.41
Na	1.07	0.95	0.77	0.63
Mg	0.33	0.31	0.11	0.16
Al	0.22	0.65		0.09
Si	1.17	1.40	0.41	0.36
S	2.48	2.15	0.73	11.39
Cl	3.71	3.40	1.19	0.96
K	0.03	0.16	0.21	
Ca	2.85	2.41	0.92	0.34
Ti	0.24	0.92		
Cr	20.69	6.70	0.76	0.49
Fe	6.28	8.60	1.52	1.11
Ni	0.47	0.23		
Cu	17.22	6.60	2.55	71.35

MiniCan 5 copper canister inner surface near hole 27:1, analysis 1

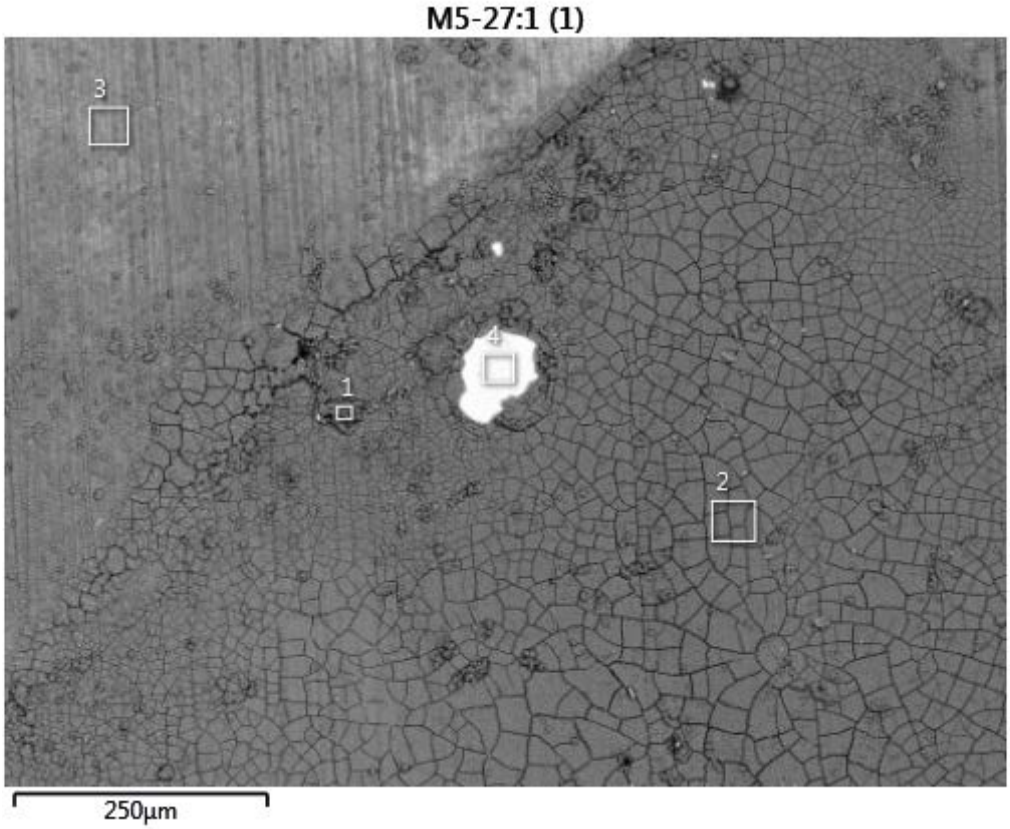

Element (Wt%)	1	2	3	4
C	6.28	5.80	5.48	3.84
O	36.63	36.05	30.36	1.80
Na	0.16			
Si	16.34	16.65	11.74	0.46
S	0.15	0.20	0.17	
Cl	0.27	0.04	0.24	0.14
Ca	0.32	0.27	0.16	
Fe	37.70	31.91	22.56	1.11
Cu	2.16	9.08	29.29	92.64
Total:	**100.00**	**100.00**	**100.00**	**100.00**

MiniCan 5 copper canister inner surface near hole 27:1, analysis 2

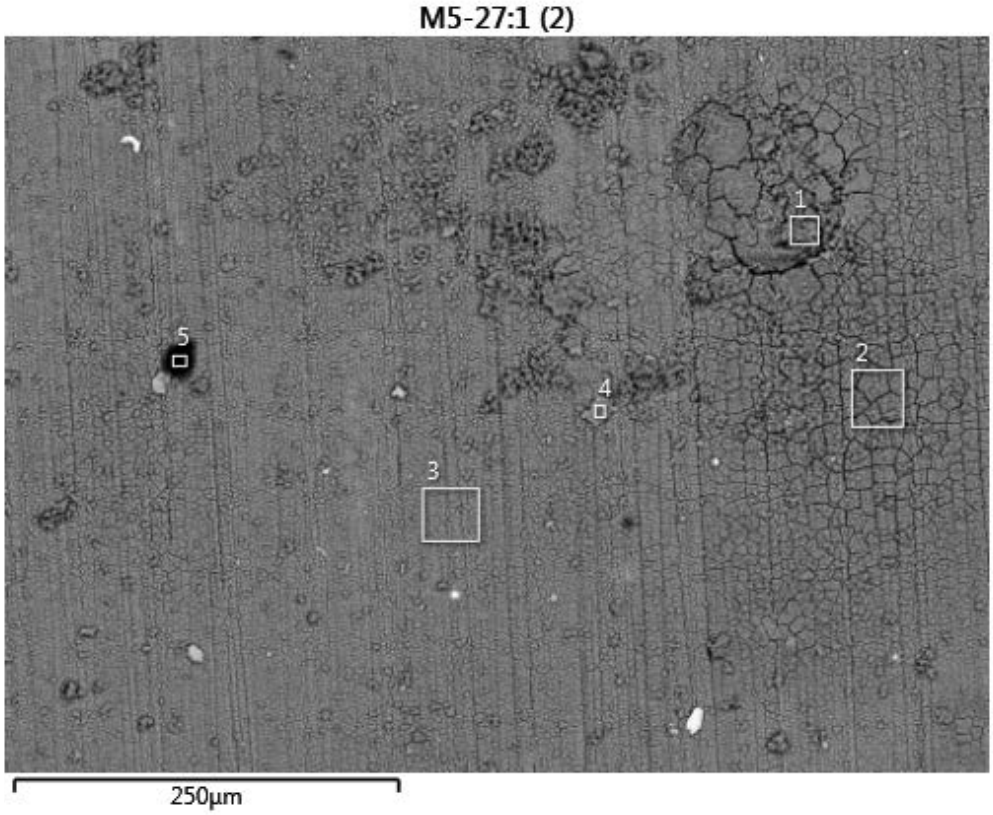

Element (Wt%)	1	2	3	4	5
C	11.77	6.79	6.04	5.58	59.32
O	39.18	34.66	34.23	35.35	28.66
Na					1.34
Al	0.09	0.05	0.13		
Si	14.29	15.10	14.14	16.08	2.37
P					0.19
S	0.28	0.18	0.25	0.16	1.12
Cl	0.21	0.27	0.14	0.20	1.41
K					1.03
Ca	0.10	0.36	0.20	0.10	0.29
Fe	32.22	34.56	31.42	39.49	2.60
Cu	1.87	8.04	13.46	3.03	1.66
Total:	**100.00**	**100.00**	**100.00**	**100.00**	**100.00**

MiniCan 5 iron insert outer surface sample 29:1

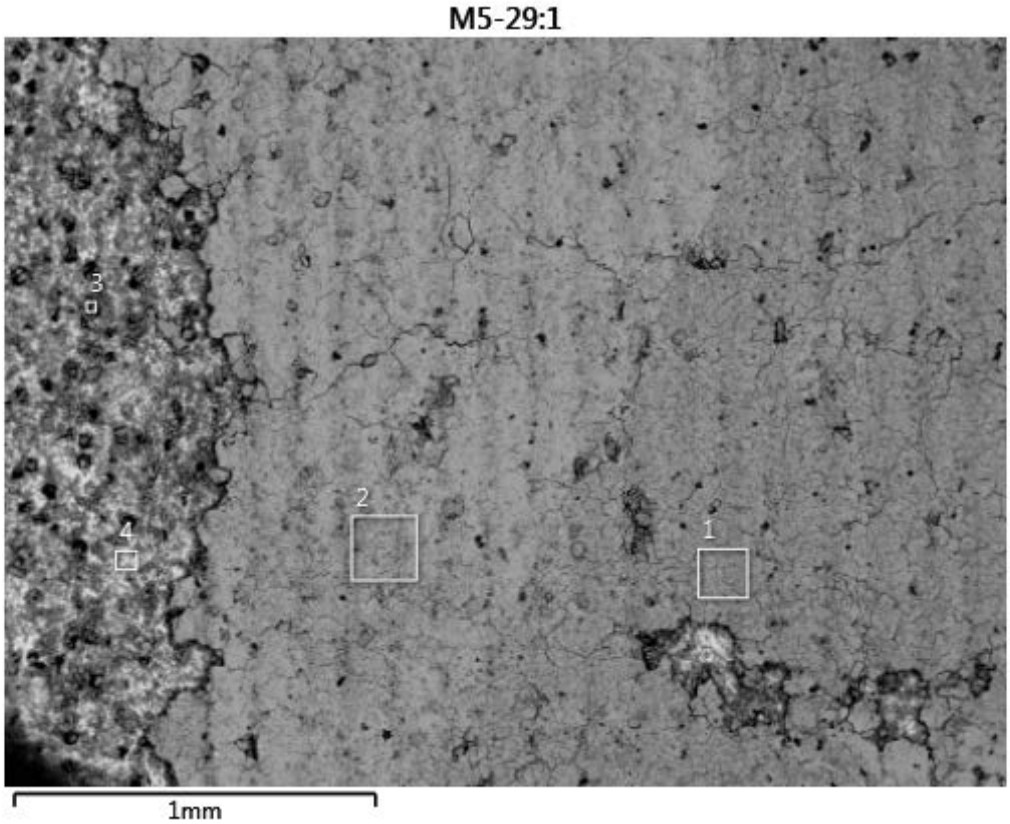

Element (Wt%)	1	2	3	4
C	5.65	6.16	26.37	3.98
O	25.01	26.06	21.14	12.68
Mg		0.26	0.13	
Al	0.12	0.20	0.05	0.06
Si	0.31	0.46	1.28	2.04
S	0.28	0.27	0.06	0.06
Cl	2.57	2.61	5.02	3.22
Ca	0.22	0.26	0.09	
Fe	65.84	63.73	45.87	77.95
Total:	**100.00**	**100.00**	**100.00**	**100.00**

MiniCan 5 iron insert sample from near canister hole 30:1

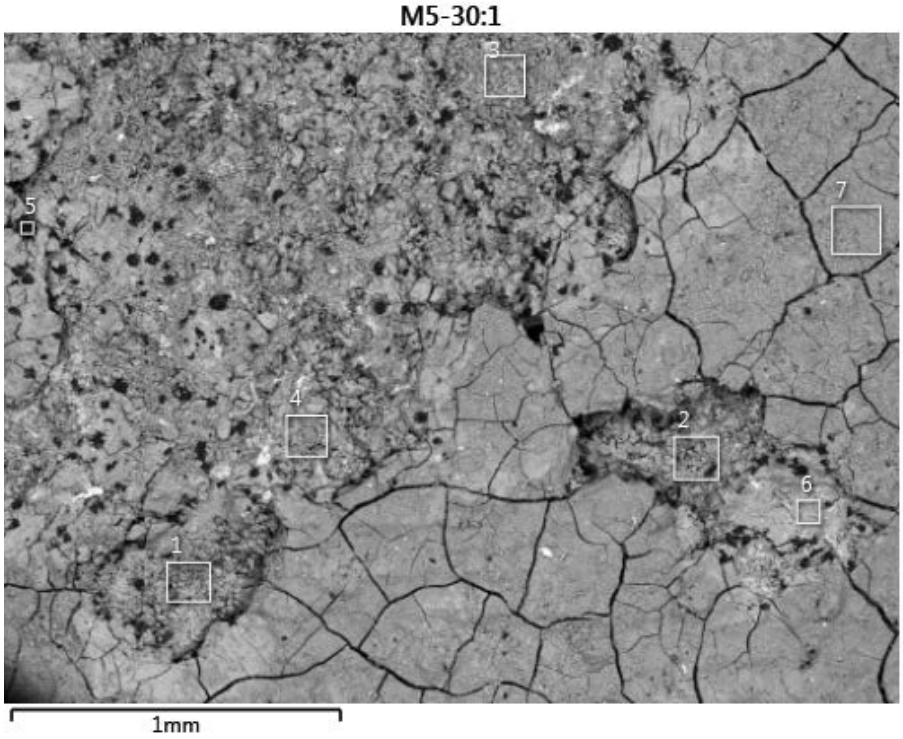

Element (Wt%)	1	2	3	4	5	6	7
C	10.13	22.36	8.45	12.48	88.62	11.72	14.19
O	24.97	26.81	32.09	31.09	7.07	29.55	33.42
Na	0.27	0.37	0.09	0.42		0.21	0.51
Mg	0.14						
Al	0.06	0.16	0.12	0.21		0.12	
Si	11.64	9.94	15.27	12.95	0.77	12.08	13.22
P	0.26	0.07	0.06	0.18		0.07	
S	0.80	0.21	0.22	0.27	0.06	0.52	0.72
Cl	1.46	0.78	0.93	1.12	0.06	1.47	1.19
Ca	1.38	0.48	0.53	0.56		1.02	1.17
Cr	0.24	0.22	0.15	0.06		0.11	0.69
Fe	46.46	38.60	42.11	40.40	3.42	42.65	34.18
Ni	0.91						
Cu	1.29			0.26		0.49	0.09
Zn							0.61
Total:	**100.00**	**100.00**	**100.00**	**100.00**	**100.00**	**100.00**	**100.00**

MiniCan 5 iron insert sample from near canister hole 31:1

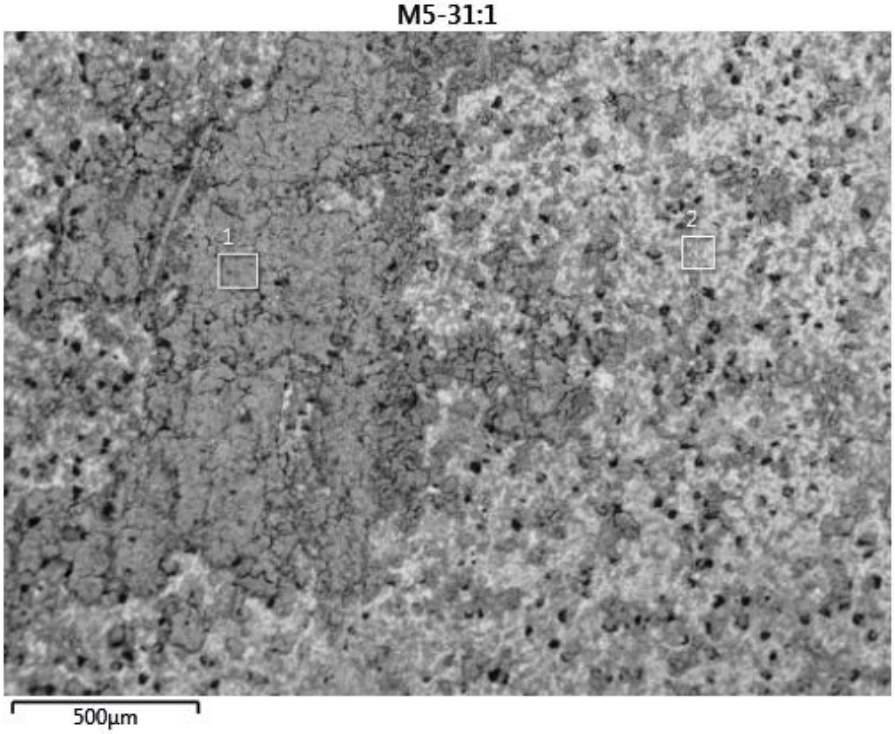

Element (Wt%)	1	2
C	8.94	5.63
O	21.89	14.92
Na	1.46	0.22
Mg	0.29	
Al	0.10	0.12
Si	1.39	2.20
P	0.14	0.14
S	0.61	0.17
Cl	4.15	3.65
Ca	1.60	0.12
Ti	0.17	
Fe	58.47	72.83
Cu	0.79	
Total:	**100.00**	**100.00**

Appendix 11

Water composition

Water sample analyses

A water sample was collected from the inside of MiniCan 5 whilst it was being sectioned inside the glovebox. The sample was then sealed in a glass bottle and taken to Swerea KIMAB for analysis with induced coupled plasma mass spectroscopy (ICP-MS). The results of the analysis are given below in Table 1. Results less than 1 µg/l are not included in the table. Accuracy of the results is ±30 % as the method used is semi-quantitative.

Table A11-1. ICP-MS results from MiniCan 5 water sample (mg or µg/L).

Element	mg/L	µg/L
Li	2.3	
B	2.7	
Na	3256	
Mg	47	
Al		15
Si	3.6	
Ca	3561	
Sc		3.6
Ti		23
V		57
Cr		40
Mn	3.5	
Fe	208	
Co		16
Ni		57
Cu		79
Zn	1.9	
Ga		6.6
Ge		9.0
As		1.9
Se		29
Rb		47
Sr	74	
Mo		364
Rh		1.3
Cd		1.8
Sn		1.1
Te		1.7
Cs		3.5
Ba		132
La		2.9
Ce		3.8
W		5.3
Hg		3.2

Appendix 12

Electrode potentials

Electrode potential measurements

The potential of each electrode was measured whilst still inside the glovebox using an Ag/AgCl (3M KCl) external reference electrode ("Ref A" or "Ref B"). For Minican 5 all electrodes were placed in a container of ground water where they could be identified. For Minican 4 the measurements were performed with the electrodes still embedded in bentonite soaked in groundwater in the transport flask. The reference electrodes were comparable to one another, varying by < 5 mV.

The potentials measured for MiniCan 5 (see Table 1) are in the same order of magnitude as the on-line measurements, potential estimated from figures 5-22 and 4-23 in the SKB report P-14-19 (Smart et al. 2015), although lower for the Eh probe, but quite different to those measured during the retrieval of MiniCan 3 (Smart et al. 2012) against the "Silvion" electrode, several hundreds of mV higher. It was reported that the Silvion electrode had probably failed during the retrieval of MiniCan 3, which could explain the difference seen in the results. Electrode potentials measured for MiniCan 3 with the SHE at the Culham laboratory at a later date are, for three out of four electrodes, of the same order of magnitude as the MiniCan 5 electrode potentials, differing by 60–130 mV.

Table A12-1. Electrode potentials measured from MiniCan 5 whilst still inside the glovebox during disassembly; comparisons with published data for the same and for the MiniCan 3 experiment.

Electrode	Description	MiniCan 5		MiniCan 5 on-line 2012–2013 (Smart et al. 2015)	MiniCan 3 (Smart et al. 2012)	
		Potential vs. Ag/AgCl, mV	Potential vs. SHE, mV	Potential vs. Silvion, expressed vs. SHE mV	Potential vs. Silvion, mV	Potential vs. SHE, mV
"Cu1" vs. Ref A	Cu-electrode	−417	−212	−320	27.5	−487
"Cu2" vs. Ref A	Cu-electrode	−566.3	−361		11.3	−491.4
"Fe1" vs. Ref A	Fe-electrode	−629	−424	−430	14.0	−488.2
"Fe2" vs. Ref A	Fe-electrode	−629	−424		14.4	−486
"ΔE" vs. Ref A	Eh probe	−652	−447	−370	–	–
"Ag 2" vs. Ref A	Ag-electrode	−397.5	−192	–	–	–
Silvion Ref vs. Ref A	MiniCan 5 ref	−364.4	−159	–	–	−489.1
Silvion Ref vs. Ref B	MiniCan 5 ref	−364.2	−159	–	–	−494.7

MiniCan 4 had two cable bundles and these were denoted "4a" and "4b", but the naming was arbitrary and does not necessarily correspond to the nomenclature in Smart and Rance (2009). The measurement results for MiniCan 4a (see Table A12-2) varied but it was not possible to distinguish which cable belonged to which electrode due to the presence of the high density bentonite clay which had encapsulated all electrodes and connections, so the information is not useful for understanding the condition of the electrodes. The potentials measured from bundle 4b (see Table A12-3) were all approximately the same, indicating that the cables were not connected to electrodes but to the strain gauge sensors mounted on the copper canister in MiniCan 4. The potentials measured for bundle 4b are thus not useful for interpretation of the MiniCan experiment but are included for completeness.

Table A12-2. Electrode potentials measured from MiniCan 4 whilst still inside the glovebox during disassembly.

MiniCan 4a Identification	Potential (mV)	Comments
1 red	−290	Unstable
1 white	−125	Unstable
3 white	−795	Stable
3 red	−796	Stable
4 red	−797	Stable
4 white	−797	Stable
6 white	−210	Fairly unstable
6 red	−186	Fairly unstable
2 red	−709	Stable
2 white	−800	Stable
5 red	−740	Unstable, decreasing
5 white	−804	Stable

Table A12-3. Potentials measured from MiniCan 4b, strain gauge sensors mounted on the copper canister, whilst still inside the glovebox during disassembly.

MiniCan 4b Identification	Potential (mV)	Comments
4 red	−819	Stable
4 white	−820	Stable
2 red	−821	Stable
2 white	−821	Stable
1 white	−822	Stable
1 red	−822	Stable
5 red	−823	Stable
5 white	−823	Stable
3 red	−825	Stable
3 white	−824	Stable
6 red	−824	Stable
6 white	−824	Stable

Arkitektkopia AB, Bromma, 2017

SKB is responsible for managing spent nuclear fuel and radioactive waste produced by the Swedish nuclear power plants such that man and the environment are protected in the near and distant future.

skb.se